BOOK OF ABSTRACTS

EUROEM 2004

12 - 16 July 2004, Magdeburg, Germany

hosted by the
Otto-von-Guericke-University Magdeburg

EUROEM 2004
Book of Abstracts

Euro Electromagnetics
12 – 16 July 2004, Magdeburg, Germany

EUROEM 2004 Book of Abstracts

Published by the Institute for Fundamental Electrical Engineering and Electromagnetic Compatibility, Otto-von-Guericke-University Magdeburg, Magdeburg, Germany.
Printed by the Federal Armed Forces Institute for Protective Technologies and NBC Protection, Munster, Germany.
ISBN: 3-929757-73-7

Contents

Conference Schedule

Monday July 12, 2004							
Time	G26-H1	G22A-H2	G29-307	G22A-013	G22A-020	G22A-120	G22A-122
09:00	Welcome						
09:50	Coffee Break						
10:30	HPEM 1/1	HPEM 2/1	UWB 1/1	HPEM 3/1	HPEM 4/1	UXO 1/1	HPEM 5/1
11:50	Lunch Break						
13:30	HPEM 1/2	HPEM 2/2	UWB 1/2	UWB 2/1	HPEM 4/2	HPEM 6/1	HPEM 5/2
14:50	Coffee Break						
15:30	HPEM 1/3	UWB 3/1	UWB 1/3	UWB 2/2	HPEM 4/3	HPEM 6/2	HPEM 5/3
19:30	Opening Ceremony (Doors open at 19:00)						

Tuesday July 13, 2004							
Time	G26-H1	G22A-H2	G29-307	G22A-013	G22A-020	G22A-120	G22A-122
08:30	HPEM 7/1	UWB 4/1	HPEM 8/1	UWB 5/1	HPEM 9/1	UWB 6/1	HPEM 10/1
09:50	Coffee Break						
10:30	HPEM 7/2	UWB 4/2	HPEM 8/2	UWB 5/2	HPEM 9/2	UWB 6/2	HPEM 10/2
11:50	Lunch Break						
13:30	HPEM 7/3	UWB 7/1	HPEM 8/3	UWB 5/3	HPEM 9/3	HPEM 11/1	HPEM 10/3
14:50	Coffee Break						
15:30	HPEM 7/4	UWB 7/2	HPEM 12/1	HPEM 13/1	HPEM 9/4	HPEM 11/2	UXO 2/1
19:00	Mayor’s Reception (on Invitation only)						

Wednesday July 14, 2004							
Time	G26-H1	G22A-H2	G29-307	G22A-013	G22A-020	G22A-120	G22A-122
08:30	PLENARY						
10:00	Coffee Break						
10:30	PLENARY						
12:00	Lunch Break						
13:30	UWB 8/1	HPEM 14/1	UWB 9/1	UXO 3/1	HPEM 9/5	HPEM 11/3	HPEM 15/1
14:50	Coffee Break						
15:30	UWB 8/2	HPEM 14/2	UWB 9/2	UXO 3/2	HPEM 9/6	HPEM 11/4	HPEM 15/2
18:30	Boarding Buses at Hotels						
19:00	Banquet						

Thursday July 15, 2004							
Time	G26-H1	G22A-H2	G29-307	G22A-013	G22A-020	G22A-120	G22A-122
08:30	HPEM 16/1	UWB 8/3	HPEM 17/1 UWB 10/1	UWB 11/1	HPEM 18/1	HPEM 19/1	UWB 12/1
09:50	Coffee Break						
10:30	HPEM 16/2	UWB 8/4	HPEM 17/2 UWB 10/2	UWB 11/2	HPEM 18/2	HPEM 19/2	HPEM 20/1
11:50	Lunch Break						
13:30	HPEM 21/1	UWB 8/5	HPEM 17/3 UWB 10/3	UWB 13/1	HPEM 18/3	HPEM 19/3	HPEM 22/1
14:50	Coffee Break						
15:30	HPEM 21/2	HPEM 23/1	HPEM 24/1	UWB 13/2	HPEM 18/4	HPEM 19/4	

Friday July 16, 2004							
Time	G26-H1	G22A-H2	G29-307	G22A-013	G22A-020	G22A-120	G22A-122
08:30	UWB 14/1	HPEM 21/3	HPEM 24/2	UWB 15/1	HPEM 22/2	UWB 16/1	UWB 17/1
09:50	Coffee Break						
10:30	UWB 14/2	UXO 4/1	HPEM 24/3	UWB 15/2	HPEM 22/3		
12:20	Farewell						

Plenary Session

PS-1: "...it is now discovered and demonstrated, both here and in Europe, that the Electrical Fire is a real Element, or Species of Matter, not *created* by the Friction, but *collected* only." Thoughts on the Fundamentals of Electromagnetics

F. W. Hehl
Univ. of Cologne and Univ. of Missouri-Columbia

Illustrated by some historical examples, we point out that classical electrodynamics is based on the conservation laws of *electric charge* and *magnetic flux*. In fact, these two laws are encoded in Maxwell's equations. The latter are expressed in terms of the field strengths (E, B), the excitations $(\mathcal{D}, \mathcal{H})$, and the sources (ρ, j). Together with the constitutive laws, such as $\mathcal{D} = \mathcal{D}(E, B)$ and $\mathcal{H} = \mathcal{H}(B, E)$, they are a complete system of equations that describe the temporal development of the electromagnetic field. Modern electromagnetic engineering is drawing from these basic structures.

PS-2: New developments on integral equation based methods

T. Sarkar
Syracuse University

In conventional numerical techniques we usually choose the lowest order polynomials (either a constant or a piecewise linear function) as the expansion function for the unknowns and then try to refine the solution by subdividing the doamin of support of the basis functions through small spatial discretisations. The objective of this talk will to illustrate that instead a choice of a higher oreder basis for the unknowns will lead not only to use of large discretisation cells but the problem to be solved also will scale much better in numerical performance particularly when convergence issues are concerned. Use of higher order basis will be illustrated through the use of an electric field integral equation and in finite element techniques in the frequency domain. Finally, it will be shown that use of higher order basis may lead to the complete elimination of the Courant s criteria from a time domain methodology be it be finite element, finite difference or integral equations based techniques as the time variable can be completely eleiminated analytically from the final equations.
Examples will be presented to illustrate the various methodologies.

PS-3: JOLT: A Highly Directive, Very Intensive, Impulse-Like Radiator

D. V. Giri
Pro-Tech, 11-C Orchard Court, Alamo, CA 94507-1541

Ultra-wideband (UWB) systems that radiate very high-level transient waveforms and exhibit operating bandwidths of over two decades are now in demand for a number of applications. Such systems are known to radiate impulse-like waveforms with risetimes around 100 picoseconds (ps) and peak electric field values of 10s of kV/m. Such waveforms, if properly radiated, will exhibit an operating spectrum of over two decades, making them ideal for applications such as concealed object detection, countermine, transient radar, and communications.
In this paper, we describe a large, high voltage transient system built at the Air Force Research Laboratory, Kirtland AFB, NM, during 1997-1999. The pulsed power system centers around a very compact resonant transformer capable of generating over 1 MV at a pulse repetition frequency (PRF) of 600 Hz. This is switched via an integrated transfer capacitor and an oil peaking switch onto an 85-Ohm Half-IRA (Impulse Radiating Antenna). This unique system will deliver a far radiated field with a full-width half maximum (FWHM) on the order of 100 ps, and a field-range product (r Efar) of 5.3 MV, exceeding all previously reported results by a factor of several.

PS-4: Survey of Ultrawideband Radar

E. L. Mokole
Naval Research Laboratory, Radar Division, Washington, DC 20375 USA

The development of UWB radar over the last four decades will be summarized. A brief history of UWB-radar developments will be followed by discussions of key supporting technologies and current UWB radars. Selected UWB radars and the associated applications will be highlighted. In particular, the Naval Research LaboratoryÕs experimental, low-power, dual-polarized, short-pulse, ultra-high resolution radar will be used to address applications and issues of UWB radar. Applications that will be mentioned include detecting and imaging buried mines, detecting and mapping underground utilities, detecting and imaging objects obscured by foliage, through-wall detection in urban areas, short-range detection of suicide bombs, and the characterization of the impulse responses of various artificial and naturally occurring scattering objects. Some of the crucial issues that are problematic to UWB radar are spectral availability, electromagnetic interference and compatibility, difficulties with waveform control/shaping, hardware limitations in the transmission chain, and the unreliability of high-power sources for sustained use above 2 GHz.

PS-5: Application of HPM-Technology for Protective Measures

J. Bohl
DIEHL Munitionssysteme

Electronic systems are susceptible to electromagnetic irradiation. These waves generate unwanted currents and voltages in the circuit, which are added to the nominal signal and distort the signal processing. If the distortion level lies outside the semiconductor specification, irreversible destruction effects can take place inside the die. Irradiating with electromagnetic fields therefore enables the manipulation and the loss of functionality of electronic systems. Much effort has been invested in shielding and hardening electronic equipment and almost perfect hardening can be realized. However due to the economic pressure to use COTS products and commercial computer, networking and signal processing subunits there exists a wide range of weak or semi-hardened systems. Each new semiconductor technology reduces the size and the maximum ratings and rises the susceptibility to electromagnetic radiation.
Radio-frequency (RF) weapons (RFW) offer the promise of reduced lethality attack against electronic systems. It has been widely recognized that compact CW, UWB, WB and HPM sources provide a significant capability for the disruption, setup or destruction of all kind of electronic civil and military equipment. However the parameters like pulse width, pulse repetition rate of bursts and pulse shape has to be adopted to the irradiated electronic technology. Parameters like the center frequency and bandwidth has to be adopted to the target shape and the coupling paths to achieve a tactical relevant distance between source and target.
The maximum radiated power or energy of a source is restricted by electrical breakdown and defines the minimum source and antenna geometry after iterative optimization processes. However the breakdown limit itself depends on the defined pulse shape, pulse duration and burst behavior. Further range enhancement typically is achieved by cascading optimized single sources to arrays which also allows beam-forming when the common triggering is accomplished in an adequate manner. A size- optimized array source is shown on the picture left.
In this presentation the parameter space of electromagnetic sources and electronic target systems are discussed with the focus on susceptibility and protective measures of civil electronic infrastructure as well as the potential of HPM sources to protect this infrastructure.

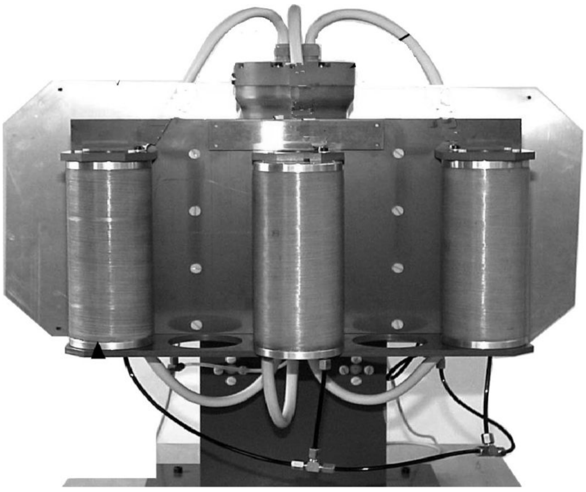

PS-6: Nonlinear Effects (Chaos) in Circuits Due to Out-Of-Band RadioFrequencies Waveforms

T. D. Andreadis
Naval Research Laboratory, Washington, DC, 20375-5000, USA

Interest of nonlinear effects (Chaos) due to radio frequency RF waveforms in circuits is stimulated primarily by the search for decreased effect thresholds from high power RF irradiation. In addition there is interest in explaining circuit response of circuits to coupled RF energy. In many analysis the contribution of RF is assumed to disappear due to rectification of the RF and it is assumed that only the envelop of the RF is removed. This assumption enables easier circuit analysis since without the RF the waveform is in-band to many circuits and their components. In some cases this assumption has been shown to be correct by experiments where injected pulsed RF waveforms have the same effect as pulsed waveform without the RF. In other cases this assumption does not hold.
If the RF is not stripped and enters a circuit, analysis becomes more complicated since circuit components parameters are not generally specified or carefully controlled by manufacturers. Values out of band may vary widely. The frequency response of even resistors at GHz frequencies may not be well represented by low frequencies.
The response of simple circuits has been examined in order to determine fundamental characteristics of such non-linear response so as to better understand the response of systems to the effects of RF. The objective of the work was to determine if chaos was useful and if we could predict when it would appear. Work by other researchers was investigated for clues relevant to the upset of systems by high power RF. Investigations were carried out on simple circuits similar to the one studied by Linsay in order in order to determine if there were ways of predicting when chaos would occur and under what circumstances.
The Linsay circuit consists of a resistor, a capacitor, an inductor, a diode, and a frequency source. Measurements were carried out in the MHz region. The circuit was also modeled with P-Spice that yielded results very similar to those in the experiments.
Experimental results will be presented showing the onset of chaotic effects and compared with simulation results. A key parameter in the response of the circuit is the reverse recovery time of the diode. The reverse recovery time is the time period after a diode is reverse biased but since there are still charge carriers in the diode, the diode is still capable of conducting current. The work shows that there is a need to investigate this parameter further and other papers presented in the conference will deal more quantitatively with this aspect of the circuit. This parameter is voltage dependent and is not well controlled by diode vendors. Diodes of the same type may have reverse recovery times that vary by an order of magnitude.
Some Conclusions obtained from this work include:

(1) Chaos regions are banded. As RF power is increased, the circuit alternates chaotic and non-chaotic states.
(2) The recombination time is a key parameter for determination of chaos onset
(3) The recombination time is voltage dependent

HPEM - High Power ElectroMagnetics

HPEM 1 - Vulnerability of Systems and Components

HPEM 1-1: A Case Study of the Impact of High Power Microwaves on Communication Systems

S. Helmers[1], **M. Löbmann**[1], **D. Hoffmann**[1], **M. Leone**[2]
[1]*Siemens AG, Center for Quality Engineering, ICN TQM QE 11, 81359 Munich (Germany)*; [2]*Siemens AG, Corporate Technology, CT PS 5, P.O.B. 3220, 91050 Erlangen (Germany)*

The threat caused by high power microwaves (HPM) plays an important role in the design of future information and communication systems. The question arises if traditional approaches of electromagnetic interference (EMI) protection measures (such as grounding, filtering, shielding etc.) still cover the higher demands of protection against HPM. Therefore, a particular communication system is analyzed systematically with respect to possible HPM electromagnetic effects (EME) which might significantly affect the system performance.
The system behaviour of the equipment under test (EUT) is investigated as follows:
1. Primarily, the hardware of the EUT is inspected to list all potential weak points of the electromagnetic compatibility (EMC) design.
2. Next, the immunity of the EUT against radiated continous wave (CW) is examined using both modulated and not modulated sources.
3. Finally, the EUT is exposed to pulsed fields originating from different HPM sources.
Regarding the complexity of the EUT, each of these steps contributes to a picture of the electromagnetic effects which might be induced by pulsed HPM fields. The aim of the analysis is to set up a basic fingerprint of the vulnerability of the EUT with respect to its communication capatibilities. The EMI analysis is enhanced by setting up transfer functions, based on experimental data and numerical field simulation.

HPEM 1-2: HPM Threat to Airborne Systems

M. Rothenhäusler
EADS Germany GmbH

Until now the risk for airborne systems such as aircraft's, drones and missiles against HPM threats, generated by HPM weapons, cannot be reliably predicted. The way how HPM penetrates into systems is not new, but the available field levels now reached dimensions, which are not covered by any military or civil specification. Hence there is a great demand of investigation.
The German Federal Office of Military Technology and Procurement (BWB) raised a programme in 1994, where EADS-Military Aircraft Division took the part to investigate the vulnerability of airborne systems. Based on the experience of EADS's EMC Team, skilled in full aircraft HIRF (High Intensity Radiated Fields) testing and the associated problems of availability of aircraft with the related costs, developed a special test-programme.
Instead of illuminating the whole aircraft system the idea of this approach is, that the path, electromagnetic energy penetrates into a system can be reproduced by simulating all the parts that are needed for full operation of the system and only the direct connected devices and cables for the device under test are built into a special area. This area should have the same dimensions as the original one, but is much more easier to handle, than the whole aircraft system. This procedure can be compared with an organic transplantation were these requirements have to be fulfilled too. The realisation of this idea is an HPM Experimental Pod which allows to study the penetration path including the operational equipment that may be disturbed. Inside the HPM Experimental Pod an equipment is installed to energise, stimulate and monitor the selected equipment boxes. The devices under test are then transplanted into the Pod and work under comparable conditions as they would do in an operational airborne system. So we fulfil all the required conditions at the equipment box boundaries and are able to investigate the vulnerability in the laboratory with much less restrictions than by using complete airborne systems. With the ability of the HPM Experimental Pod to remove or open specific parts of its structure the attenuation of the skin can be varied from 30 dB to 0 dB. By this way these results can be scaled up or down to different systems of interest, e.g. missiles, drones, if the skin attenuation is known.
The program introduced by the German Federal Office of Military Technology and Procurement (BWB) was split in two phases. Phase I was carried out from 1995-2000 and has already been presented at the EUROEM 1998 and 2000. Now the program has entered phase II which will last from 2001-2005. At the AMEREM 2002 first results of phase II have already been presented and the research on this topic is still ongoing.

HPEM 1-3: HPM PCs Susceptibility

J.-P. Percaille, **D. Chastras**, **R. Pouzalgues**
DGA/DCE/CEG Centre d'études de Gramat 46500 Gramat France

Military systems are more and more composed of standard electronic devices. The command and control units use a lot of these components on the shelves and especially PC.
To define the HPM vulnerability of systems the stresses induced must be compared to the susceptibility threshold levels.
Thus, the aim of this study was to define the susceptibility threshold levels of different generations of PC for three kinds of electromagnetic attack : narrow band threat, UWB threat, damped sines threat.
The narrow band threat has been investigated between 1GHz and tens of GHz, for pulses duration from tens of nanoseconds up to microseconds, and repetition rate between 0 Hz and 1kHz.
Studies have been performed with stirring mode chamber and anechoic chamber and with 1kW amplifiers.
The UWB shape has been realized in a Giga Transverse Eletromagnetic cell (GTEM) associated with an impulse generator. The incident electric field levels ere between hundreds of V/m to some kV/m. The frequency rate varied from 0 Hz to 1kHz.
The damped sines threats were also radiated inside the GTEM. A maximum of 1 kV/m incident electric field was provided inside the cell. The frequency varied from tens of MHz up to hundreds of Megahertz. The damping coefficient was between three and ten, and frequency rate could reach 1MHz.
Three generations of PCs have been tested (80486 DX2-66MHz, Pentium 133MHz, and Pentium 4 -3 GHz with WI-FI and bluetooth technologies.)
For each family, a software, based on an exchange of data between two same PCs was running during the test.
For each kind of threat and each family of PC several kinds of disruptions have been observed and recorded.
This study gave a relative comparison of the electromagnetic attack efficiency and also comparison of the susceptibility of different PCs generations.
Associated with coupling experiments on structures, the data issued from this analysis can offer an assessment of systems vulnerability.

HPEM 1-4: A Methodology for Statistical Characterization of Modeling Parameters for HPM/RF Effects Prediction

W. Sessions, **M. W. Baedke**
Joint Program Office for Special Technology Countermeasures

The Joint Program Office for Special Technology Countermeasures (JPO-STC) at the Naval Surface Warfare Center Dahlgren Division (NSWCDD) is currently investigating the effects of High Power Microwave (HPM) and Radio Frequency (RF) attacks on electronic infrastructure. As part of the JPO-STC mission, computational and statistical models are being developed to predict the effects from a HPM/RF attack. One ingredient for a successful prediction capability is to quantify both numerical

modelling errors, which arise in such complex problems. In every computational model of a complex system, errors arise owing to (1) the discrete nature of the algorithm, (2) the detail of model in the simulation, and (3) the approximate values of input parameters being used in a given simulation.
The focus of this paper is the development of a methodology to determine the sensitivities of model output to the uncertainty of model input, e.g. material parameters. Consideration will be given to a “generic” one-floor building with concrete walls. The material properties of the walls and source frequency are used as inputs to the model, and the output is quantified by possible effects predictors, e.g. average peak energy density throughout a region of the building. A Gaussian-derivative, plane-wave source is used so that a consistent ambient field is produced as frequency is varied. Multidimensional, nonlinear regression analysis is then used to determine the sensitivity of a given output to uncertainties/variances of a given input. Examples of these functional sensitivities will presented and discussed.

HPEM 1-5: EM Coupling to Military Hardened Systems

D. Weixelbaum, **R. H. Stark**, **J. Bohl**
Diehl Munitionssysteme GmbH & Co. KG, Fischbachstr. 16, D-90552 Röthenbach a.d. Pegnitz

Irradiation of modern electronic systems with intense EM-fields show an increased susceptibility of such systems. Interaction of the EM-field with the target system mainly depends on dimensions, geometry and the material properties, as well as the characteristics of the incoming EM-field. For hardened systems the EM-wave may penetrate into the interior by back door coupling and interacts with wiring and traces of electronics and printed circuit boards. The interaction of the EM-field induces voltages and currents in signal- and power-lines which lead to disruption or even destruction of electronic systems, subsystems or components. In both cases the system loses the functionality it was designed for.
This paper presents systematic coupling measurements and analysis of the susceptibility of military hardened systems irradiated with microwave radiation. The studies were performed at the EM- test facility WTD81 (‘Wehrtechnische Dienststelle für Informationstechnologie und Elektronik’) in Greding and at the Fraunhofer Institute FhG-INT in Euskirchen. Low power cw and pulsed microwave radiation were used to measure susceptibility of the hardened system.
In addition pulsed DS-HPM sources, which had been developed at Diehl Munitionssysteme GmbH & Co. KG, Röthenbach a.d. Pegnitz, were used. The target was irradiated at frequencies ranging from several 100 MHz up to the GHz regime. Parameters like angle of incidence, polarisation and fieldstrength were varied. Comparing the test results of the CW-measurements with pulse irradiation tests the influence of the pulsewidth can be shown clearly.
The transfer function of the outer EM-field to the interior field was determined by means of electric probes inside the target body. First results on the susceptibility of those systems and possible hardening aspects are presented.

HPEM 1-6: EMI Studies with Complex, Distributed Weapon Systems

R. H. Stark, **D. Weixelbaum**, **F. Sonnemann**, **W. Mueller**, **J. Bohl**
Diehl Munitionssysteme GmbH & Co. KG, Fischbachstr. 16, D-90552 Röthenbach a.d. Pegnitz

Modern electronic systems are susceptible to intense electromagnetic fields. Coupling of electromagnetic (EM) waves mainly depends on target size, geometry, material properties and characteristics of the incident electromagnetic radiation. Usually coupling paths are very complex. Besides front door coupling, where the EM wave couples to the system through active antennas and sensors, most systems are very sensible to back door coupling. Here coupling paths are mainly unknown, hard to determine and hardening of the system is difficult. The EM-wave panetrates through small slits, holes and feed throughs or even parasitary antennas into the interior of the system. The field amplitude is then converted into currents and voltages on the signal and power lines. Dependend on the amplitude of the induced signals disruption or even distruction of electronic systems and components occure. In both cases the system loses functionality it was designed for.
Complex, large and distributed systems usually consist of several sub-systems and components which often are seperated from each other, distributed and connected to each other via data transfer cables and power lines. Breakdown of a single component or sub-system often causes failure of the total system. Also network cables and power lines are excellent antennas for EM coupling. Hence EMI studies with complex, large and distributed weapon systems are of growing interest. Systematic studies are required in order to determine coupling paths and error mechanisms of such systems.
The paper presents EMI studies performed with an air defence system. The studies have been performed in free space at a governmental furnished proving ground as well as in an anechoic chamber at the Wehrtechnischen Dienststelle für Informationstechnologie und Elektronik, Greding (WTD81). Noval pulsed DS-HPM sources which had been developed at Diehl Munitionssysteme, Röthenbach Peg. were used to study the system. Further studies were performed with low power microwave sources in a frequency range from several hundred MHz up to the giga hertz regime. Requirements regarding support, infrastructure and test procedure will be discussed. First results will be presented.

HPEM 1-7: Analytical Estimate of Cell Phone Susceptibility to Radiated Electromagnetic Pulse

W. J. Scott, **J. McAdoo**
Mission Research Corporation

A preliminary analysis has been performed to determine the potential vulnerability of modern hand-held cell phones to a fast transient, radiated electromagnetic pulse (EMP). This analysis should be considered as a representative example, rather than a worst-case analysis. No attempt is made to bound the estimated response in either direction (maximum or minimum response), or to determine the sensitivity of the result to the physical input parameters selected.
The first part of the briefing presents a preliminary analysis used to determine potential suscptibility. Based on engineering judgment various assumptions are made to select a representative fast transient EMP waveform, coupling geometry, antenna impedance, etc. A case study is performed on a typical cell phone configuration to calculate the energy delivered to the cell phone receiver circuit.
The second part of the briefing presents a more detailed analysis to support the validity of key assumptions. It also provides additional analytical information on the calculations performed; estimates of component damage levels based on commercial device susceptibility test data; and a comparison of the EMP radiated fields with the fields produced by a nearby electrostatic discharge (ESD). Potential sources of modeling errors are discussed briefly. The analysis is limited to the front-end receiver circuit of a cell phone. Other modes of operation and/or coupling paths that may contribute to the overall susceptibility of cell phones exposed to an EMP environment were not examined. An estimate will be provided for the percentage of unprotected cell phones exposed to the representative EMP environment that are likely to be damaged.
This work was sponsored and funded through the U.S. Defense Threat Reduction Agency

HPEM 1-8: Experimental Data on Immunity of Certain Radio Systems

Y. V. Parfenov, **L. L. Siniy**, **G. V. Vodopyanov**
Research Institute of Pulse Technique

Objects of researches were:
- Radio relay station;
- Ground station of a satellite communication;
- Radio center of decameter waves.

The specified objects are widely applied in a civil infrastructure. So, for example, the tested radio relay station is applied on many Russian radio relay lines, both in northwest of the country, and in the east, for example, in Yakutia.

About fifty stations such as ”Orbit” function now on a network of a satellite communication. They are used now basically for a telecommunication. Widely also stations of decameter waves are used. Usually these stations have aerials of small diameter. Now about thousand such stations exist in Russia.

The estimation of immunity of radio equipment of these objects to high energy pulses included three stages:
- At the first stage maximum-permissible levels of the induced voltages and currents for typical semi-conductor devices and separate electronic blocks were determined;
- At the second stage characteristics of voltages and the currents induced on inputs of these devices and blocks were determined;
- At the third stage the comparing levels of the induced voltages and their maximum-permissible values was carried out.

At performing experiments by determination of characteristics of induced voltages and currents the following ways of penetration of disturbances to sensitive electronic devices have been investigated:
- External communication and power cables;
- Antennas;
- Internal power and communication wires;
- Printed-circuit-boards.

External lines and antennas were exposed to influence of the pulse with the following characteristics:
- Peak of an electric field -50 kV/m;
- Rise time – 2.5 ns;
- Pulse - 23 ns.

In experiments with internal lines and printed-circuit-boards the shielding buildings and cases was taken into account. Therefore at performing the experiments the pulse with the following characteristics was formed:
- Peak of an electric field - 15 kV/m;
- Rise time - 24 ns;
- Pulse duration - 225 ns.
- The most vulnerable are systems of communication of decameter waves;
- The basic threat is pulse voltages and the currents induced in long cables;
- Direct influence of high energy pulses on the radio equipment and on antennas (excepting the antennas of radio centers of decameter waves) does not result in failure of the equipment.

HPEM 1-9: HEMP Effects Analysis of Network Equipment

B. M. Grady, **J. Latess**, **D. C. Stoudt**
Joint Program Office for Special Technology Countermeasures

Recent HEMP simulation tests conducted by the Joint Program Office for Special Technology Countermeasures (JPO-STC) produced susceptibility data on infrastructure and networking equipment. The goal of this testing was to provide data to access the impact of HEMP to civilian infrastructure operations. The limited test volume of the HEMP simulator required that the network equipment under test be configured as a reduced scale commercial installation. Several analysis steps are required to take the simulation susceptibility data and extrapolate it to a larger scale commercial installation. This includes establishing the conduction paths for the damaging energy, computing the appropriate transfer function, modeling the coupling for the non-tested configuration of interest and estimating if the same vulnerabilities exist for commercial installations. These analysis functions have been performed on network equipment to better understand the response of this equipment to HEMP. The paper will describe the results of the HEMP simulation testing, and how these results scale to systems more representative of actual infrastructure installations.

HPEM 1-10: HEMP Susceptibility Assessments of Modern Digital Control and Communications Equipment

J. Latess, **B. M. Grady**, **D. C. Stoudt**
Joint Program Office for Special Technology Countermeasures

Concern about the impact of high-altitude nuclear electromagnetic pulse (HEMP) to modern infrastructure systems has spawned a series of HEMP effects testing on digital control and communications equipment. One of the most accepted means for determining these effects is to conduct HEMP simulation testing. The simulation testing provides an opportunity to observe the interaction of the electromagnetic energy with equipment in an operational mode. The Joint Program Office for Special Technology Countermeasures (JPO-STC) has recently conducted HEMP testing of control systems typical of those supporting infrastructure elements such as electrical power generation, transmission and distribution as well as petroleum product refineries and pipelines. Because it is difficult to adequately illuminate large test objects in HEMP simulators, the observed effects can be related to the systems response in more realistic scenarios through straightforward analysis based on coupling differences between the simulated and actual interconnections. The presentation will highlight the testing goals, and testing methodology and discuss in general terms the vulnerability of this electronic equipment and components to HEMP.

HPEM 1-11: Prediction of the Operational Readiness of EM Agressed Systems

R. Marijon[1], **C. Girard**[1], **W. Tabbara**[2]
[1]*Thalès Communications TCF/UCR/DIS*; [2]*Département de recherche en Electromagnétisme - Supélec*

I. Abstract
In EMC and hardening contexts, the ultimate goal of vulnerability studies is to evaluate the functional consequences resulting from an electromagnetic aggression, as for example in the case of an aircraft in a HIRF environment. Numerical modeling is used to assess the operational readiness of the system by means of a combination of different codes, that need to share information. A solution is described where weak hybridization between 3D EM codes and equipment vulnerability modeling are emphasized.

II. Methodology
The methodology is explained through the example of the vulnerability of the communication function of a fighter landing on a carrier, in a HIRF environment. The study is conducted through the following steps :
- Primary HIRF sources analysis and definition (aircraft carrier RADAR & communication antennas).
- Definition of the aircraft communication function by means of a fault tree or a critical list involving equipments. For example, the communication function involves, among others, an amplifier and a receiver.
- Rigorous 3D EM codes (Finite Difference Time Domain, Finite Element...) or asymptotic HF codes are used to model the electromagnetic environment around the aircraft. We define secondary EM sources placed on a Huygen’s box enclosing the aircraft (the simulations are still system independent).
- The secondary sources are then used to illuminate the fighter. Equipments and cables are represented in the aircraft numerical model by boxes and simple conductors. We compute fields around the equipments and currents induced on cable shields.
- Network and cables modeling are used to evaluate currents injected in the equipments.
- For each equipment, according to the induced fields and currents, we evaluate the perturbation and destruction probabilities.

A model of the equipment vulnerability is described in part IV.
- Fault tree or critical list solving is used to estimate the operational readiness probability of each function.
A decoupling hypothesis, inherent to weak hybridization, is used in the above mentioned approach.
III. Exchange surface for weak hybridization
Exchange surface or Huygen's box representation takes into account the following constraints :
- Generated by one code, it must fit the needs of other ones involved in the hybridization that are unknown at the generation step. Interpolation, time-frequency domain conversion steps could be needed.
- The exchanged data volume must be of reasonable size. A compromise must be found between the quality of the transferred data (after interpolation for example) and the data volume. Examples will be given to illustrate the compromise.
IV. Equipment vulnerability model
It aims at evaluating perturbation and destruction probabilities of an equipment subject to aggression fields around its enclosure and to pin currents. The model makes use of :
- The technical characteristics of its major electronic components.
- A functional fault tree description of the equipment involving these components.
- Component vulnerability models for each family (bipolar, MESFET, MOSFET).
- Description of the enclosure and protection stage filtering. These data are obtained from measurements and/or simulation.

HPEM 2 - Pulsed Power

HPEM 2-1: Solid-State Marx Bank Modulator for the Next Generation Linear Collider

J. A. Casey, F. O. Arntz, M. P. J. Gaudreau, M. A. Kempkes
Diversified Technologies, Inc.

The Next Generation Linear Collider (NLC) will require hundreds to thousands of pulse modulators to service more than 3300 klystrons. Under a recently completed Phase II SBIR contract, DTI investigated the use of a solid-state Marx switch topology for the NLC, and has transitioned this work into the development of a full-scale, 500 V solid state Marx system. These efforts, combined with recent advances in semiconductor technology and packaging, have moved the performance of the Marx pulser far ahead of early estimates. The Marx pulser has the advantage of eliminating the pulse transformer, which is associated with significant loss of performance and a 15-20% efficiency penalty in conventional modulators. The efficiency penalty alone can account for over \$100M in power costs over ten years of NLC operation, an amount comparable to the acquisition costs of the pulsed power systems.
In this paper, DTI will discuss the design and development status of the Marx Bank modulator, which is expected to deliver performance that scales to 125 ns risetime (10-90%) for either a 500 kV, 265 A pulse (for one klystron), or a 500 kV, 530 A pulse (for two klystrons). The use of a unique, common mode inductive charging system allows transfer of filament power without separate isolation transformers.

HPEM 2-2: A Compact Former of High-Power Bipolar Subnanosecond Pulses

Y. Yankelevich, A. Pokryvailo
Soreq NRC

The system comprises a nanosecond SOS-generator (see, e.g., Rukin S. N. et al., Proc. of Tenth IEEE Int. Pulsed Power Conf., 1995, pp. 1211-1214) or the RADAN SEF-303 pulsed power source (see, e.g., Mesyats G. A. et al., Proc. of Ninth IEEE Int. Pulsed Power Conf., 1993, pp. 835-838) that charges resonantly a short pulse-forming line (PFL1) through a decoupling inductor, a peaker spark gap, an active converter, a matched load and several built-in voltage probes. The active converter comprises two spark gaps (chopper and peaker), the additional 1ns pulse-forming line (PFL2) and secondary decoupling inductor for resonance charging of PFL2. The peaker spark gap and active converter are set in one body and operate in N2 at pressure up to 60 atm. Weighing less than 10kg, an active converter provides output bipolar subnanosecond pulses having peak-to-peak amplitude up to 250kV on a 50Ω load at operation with RADAN (at repetition rate of 25Hz in continuous mode) and more then 300kV on a 45Ω load at operation with SOS-generator (at repetition rate of 50Hz in continuous mode and up to 300Hz in burst mode). The pulsewidth of each half wave of bipolar pulses on FWHM is 280ps at the rise time of the first half wave of about 180ps. The peaker spark gap and the spark gaps of the active converter can be regulated without depressurizing (a technique adopted from Shpak V. et al., Izvestia Vyshikh Uchebnykh Zavedenii, Fizika, No. 12, 1996, pp. 119-127).
Circuit analysis accounting for nonlinear processes, distributed character of the components and numerous parasitic parameters is presented. Electro- and magnetostatic field simulation assisted in choice of the values for the circuit analysis and insulation design.
Voltage measurement means, including several capacitive dividers, Rogowski coils, attenuators and connection cables, were time-domain calibrated using ultrafast high voltage solid-state pulsers. Waveforms probed at different locations of the pulser systems, from the SOS-generator and from the RADAN to the load, are presented. The bipolar subnanosecond pulses had very stable rise, while the fall jitter was around 50ps. On the whole, these pulses were sufficiently stable to be recorded using broadband sampling digitizing scopes. The experimental results are in fair agreement with the simulation.
The pulser was tested with a TEM horn antenna. An effective potential of 500kV was obtained.

HPEM 2-3: Compact, Solid-State High Voltage Radar Modulators

M. A. Kempkes, M. P. J. Gaudreau, J. A. Casey, T. Hawkey, P. Brown, J. M. Mulvaney
Diversified Technologies, Inc.

As the operating life of existing transmitters is extended, switching power supplies and solid-state high voltage modulators are replacing conventional tube-type radar modulators in a range of transmitter upgrades and new designs. The new technology is a viable and cost-effective replacement for obsolete components. Further, it improves the reliability of the transmitter and delivers better protection to the RF amplifier (klystron, TWT, etc.) This paper summarizes DTI's recent ongoing work in developing solid-state components for three different radar transmitter upgrades.
AN/SPS-49 – DTI successfully demonstrated an electrical prototype of a solid-state cathode modulator for the AN/SPS-49 radar. This modulator replaces two, obsolescent switch tubes which currently drive the mod-anode of the klystron, as well as the existing crowbar in the 200+ fielded AN/SPS-49 systems. DTI has recently transitioned this prototype to a MIL-QUAL production design.
Cobra Judy and Gray Star X-Band Radar Upgrades -In 2003, DTI upgraded the X-band radar transmitters in the Cobra Judy system on the USNS Observation Island, and the Gray Star system, located onboard the USNS Invincible. In both of these U.S. Air Force data collection systems, DTI's switching power supplies and solid-state switches replace obsolescent tube technology, and significantly increase the reliability of these critical radar systems. For Cobra Judy, DTI built the complete transmitter, including all electronics required from ship power to modulating the two 100 kW average power TWTs located behind the dish itself.

Figure 1: Transmitter upgrade installed on board USNS Observation Island

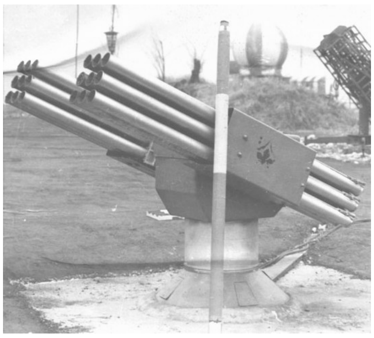

Figure 3: The sources intended for operation

HPEM 2-4: MCG - Based Electromagnetic Sources

V. A. Soshenko[1], **A. H. Adzhiev**[2], **A. S. Tishchenko**[1], **V. V. Sinkov**[1], **V. E. Novikov**[3]
[1]*The Usikov Institute of Radio Physics and Electronics of the National Academy of Sciences of Ukraine*; [2]*High-Mountain Geophysical Institute, RUSSIA*; [3]*Science and Technology Center of Electrophysics, NASU*

As known, an electromagnetic signal source consists of a generator, a feeder and an antenna. MCG, being used as a basis for the radiator, enables one to preserve the traditional energy dependence. However, there are some complex problems in the way of developing of such sources. These are the conversion of the MCG current into high-frequency oscillations, and improvement of the matching between antennas.
We have designed some basic variants of RF MCG, which are used in similar sources. The circuit of these generators is shown in Fig. 1. The basic difference of these circuits from the previous variants consists in a partitioning of the MCG coil. Each section is an oscillatory circuit. The time-dependent voltage in the loading is shown in Fig. 2. Such partitioning allows to use efficiently the potential energy of explosive substances. The MCG design and the feed circuits essentially differ from the traditional spiral MCG. A magnetic coupling provides the coordination between the generator and antenna. The coupling ratio is the most important factor, determining the voltages in the MCG devices and the signal spectrum). In the suggested design, the winding voltage was restricted by 30 kV. Such restriction is necessary to ensure a reliable operation of the radiator in high atmosphere layers. The sources intended for operation in high atmosphere layers are shown in Fig. 3. In such devices, two types of antennas are used. These are plasma and linear antennas.
The oscillation frequency of MCG reaches 85 MHz. The plasma antennas added nonlinearity to the source operation. The spectrum of a signal sources belongs to the microwave region. The circuit of plasma jet excitation determines the frequency band and the amplitude components of the spectrum. The tests have proven the rich application perspectives of such sources

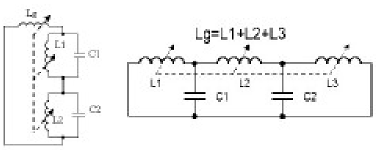

Figure 1: The circuit of generators

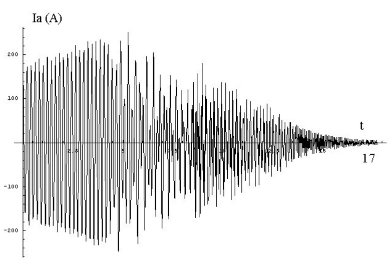

Figure 2: The time-dependent voltage in the load

HPEM 2-5: High-Voltage Pulse Generator of Average Power up to 40 kW and Pulse Repetition Frequency up to 1000 Pulses per Second

M. I. Boyko, **A. V. Bortsov**, **L. S. Evdoshenko**, **A. I. Zarochentsev**, **V. M. Ivanov**
RDI "Molniya" NTU "KhPI"

Generator of high-voltage pulses with amplitude on load up to 120 kV, average power, consumed from mains, up to 40 kW has been developed, manufactured and tested.
In generator, principle of decreasing of recovery time of electrical strength, improving of operation stability, decreasing of erosion of electrodes of high-current spark gaps as consequence of shortening of front of high-voltage pulses applied to them and leading to gap breakdown, was applied. On the base of this effect, pulse repetition frequency up to 1000 pulses per second was achieved. Besides, principle of forming of high-voltage pulses with steep front (in nanosecond range) on the load by means of pulse transformer (in Tesla circuit), that ensures maximal transformation ratio at minimal overall dimensions and full exploitation of spark discharge properties in sharpening of pulse front, was applied.
Generator includes power low-voltage thyristor source of pulses, two high-voltage pulse transformers with systems of forming and sharpening of pulses, having common load, and control unit. Generator load impedance can be from 10 Ω to 10000 Ω. In testing of generator, the load was working chamber with running tap water. Modes of energy releasing in working chamber, both without discharges and with underwater spark discharges, were successfully tested.
Systems of forming, on which high-voltage windings of pulse transformers were loaded, are made on the base of low-inductance capacitive stores (capacitors) and multigap multichannel air spark dischargers. Pulse front on the generator load is less 10 ns. Magnetic cores of pulse transformers are made strip-wound from thin electrotechnical steel. Each sharpening system has two stages. In the first sharpening stage, capacitor has capacitance 4 nF, in the second – 1 nF. High-voltage part of generator is placed in soundproof enclosure, which is electromagnetic shield at the same time.
Forced air cooling of high-voltage and power low-voltage units of generator was provided.
Mass of generator on the whole (including power low-voltage pulse source) is 500 kg.

HPEM 2-6: Testing of Solid Dielectrics with Application to Compact Pulsed Power

E. Schamiloglu, **J. A. Gaudet**, **C. J. Buchenauer**, **P. Castro**, **M. Roybal**
University of New Mexico

In our ongoing effort to develop transmission lines with higher energy storage capabilities for compact pulsed power applications we have been developing and studying ceramic dielectrics and their electrical breakdown strength (BDS). Results of research to-date show that dense titania ceramics with nanocrystalline grain size (200 nm) exhibit significantly higher BDS as compared to ceramics made using coarse grain materials when tested under DC conditions. We have performed pulsed testing under similar electric field stresses and found comparable behavior. However, we also found that these ceramics tend to breakdown at lower electric fields under pulsed conditions compared to DC conditions (approximately 25% lower). This is opposite from the behavior of liquid dielectrics, but has also been shown in our studies to be the case with ordinary dielectrics such as Mylar.

This presentation will describe our testing methodology, present our results, review the statistics that are used to analyze the data, and relate our understanding to what has been accumulated in the literature to-date in the context of dielectric breakdown. Our progress in developing a pulser to test large ceramics under higher energy conditions will also be discussed.

This work was supported by an AFOSR/DoD MURI grant on compact pulsed power.

HPEM 2-7: Renaissance of the Transmission Line Transformer with Modern Cable Technology

A. Lindblom[1], **H. Bernhoff**[1], **A. Larsson**[2], **P. Appelgren**[2], **J. Isberg**[1]

[1]*Division for Electricity and Lightning Research, Ångströmlaboratoriet, Uppsala University*; [2]*Grindsjön Research Centre, Swedish Defence Research Agency*

A practical implementation of the transmission-line transformer (TLT) is presented. A voltage step-up TLT is made of a coaxial cable where the inner conductor acts as the secondary winding and the screen as the primary winding. The cable insulation is one limiting property of the TLT since it must withstand the full output voltage. Modern high-voltage cables are equipped with a resistive layer (semicon) on the inner conductor and on the inside of the outer conductor, which increases their dielectric performance substantially. Thus, using this kind of cable in a TLT, the voltage levels of the TLT can be increased. The construction of such a TLT is presented in this conference communication together with equivalent electric circuit simulations. The coupling factor for the single layer transformer is 0.8. This high coupling factor is achieved due to the coaxial structure.

The transformer was tested in an existing pulse conditioning system, and the operating principle for that system is illustrated in Figure 1: The primary energy storage is discharged through the primary winding of the transformer by closing the first switch. When the second switch is opened the current is abruptly interrupted and the magnetically stored energy in the transformer is discharged into the load. The opening switch is based on electrically exploding copper wires. Figure 2 (left) shows the high voltage results when the opening switch was equipped with 18 and 37 copper wires, respectively, and the right figure shows an electric circuit simulation. The electric circuit model of the transformer consists of distributed capacitance, resistance and inductance in order to resemble a transmission line. The high voltage cable with PEX insulation proved to withstand very high stress (85 MV/m). This type of transformer is useful in applications where weight is an important factor. The simple design ensures low cost manufacture.

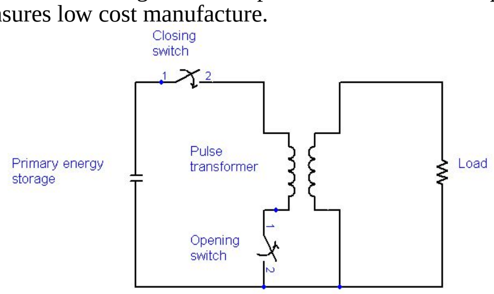

Figure 1: Simplified electric circuit of the pulse transformer in the pulse conditioning system.

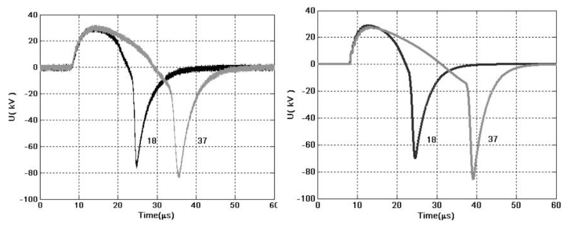

Figure 2: Measured (left) and simulated (right) load voltage of the transformer for two different numbers of wires in the opening switch.

HPEM 2-8: Study of a Laboratory Pulsed-Power Conditioning System for HPM Applications

S. E. Nyholm, **P. Appelgren**, **G. Bjarnholt**, **T. Hultman**, **A. Larsson**

Swedish Defence Research Agency - FOI

A comparatively slow high current pulse can be converted to a fast high voltage pulse suitable for powering an HPM source by using simple switch technology. The pulsed power conditioning system presented contains an electrically exploded opening switch (copper wire fuse), a spark gap as a closing switch, and a resistive 15 Ω dummy load. The system is fed with a 60 kA peak current pulse from a 30 kJ (67 uF, 30 kV) pulsed power supply usually charged to 20 kV. The system has been used in two configurations, one with an intermediate storage inductor (cf. figure 1) and one with a transmission line transformer (cf. Lindblom et al., "Renaissance of the transmission line transformer with modern cable technology", this session). In the inductor configuration, the maximum voltage obtained across the load was 150 kV with a rise time of about 270 ns. The diagnostics used consisted of an integrated capacitive voltage probe and in-house made Rogowski probes for current measurements. Experiences and results from an experimental parameter study, electric equivalent circuit simulations, and an energy efficiency analysis are presented (cf. figure 2).

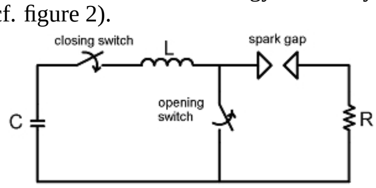

Figure 1: Pulsed-power conditioning system based on inductive intermediate storage of electric energy, where C represents the primary energy storage, L the storage inductor and R the load.

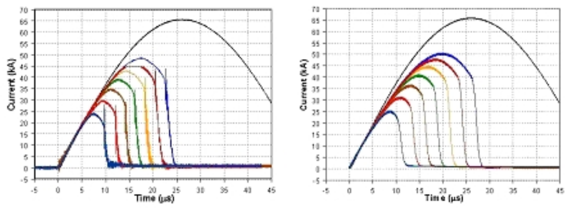

Figure 2: Measured (left) and simulated (right) storage inductor current for different configurations of the electrically exploded opening switch.

HPEM 2-9: High Voltage Switching Tubes with a Small Voltage Drop on the Anode

V. Perevodchikov, **A. Murashov**, **V. Shapenko**, **P. Stalkov**

All Russian Electrotechnical Institute (VEI), Moscow

Development of powerful electromagnetic radiation applications increased the interest to various types of high voltage, high speed switching devices. High-voltage switching tubes have a number of important advantages such as high electric strength, high operation speed, full controllability, i.e. ability to change current or to disconnect a circuit at the full applied voltage.The main deficiency of high-voltage vacuum tubes is rather big voltage drop on the anode. Researches and development of high-voltage switching tubes with a small voltage drop on the anode are carried out for many years in VEI. The effect of reducing of anode voltage drop and anode losses has been reached because of careful formation of an electron beam and its deceleration on the anode. Such tubes were named "electron beam valves" (EBV). In EBV the accelerating electrode is located near to the cathode, it has the high positive potential to provide a high current. The anode potential is 3-4 time lower comparing potential of accelerating electrode. Deceleration of electron beam at the anode provides small power losses and high efficiency of such tubes.

Problems of an intensive electron beams deceleration by a small current return to the accelerating electrode are examined. There are two ways for creation of such optimal electron systems. The first way is the use of the anode having a concave surface, which prevents the electron return. This way is more convenient for high voltage tubes with a relativity small current. As for high current tubes, the second way is more convenient - the use of multiple tape beams, which electrons trajectories are orthogonal to the anode surface. The important advantage of vacuum switching tubes is resistance to breakdowns and an opportunity to dissipate high anode power losses. The EBV voltage-current characteristic has weak dependence of a current on an anode voltage that allows to use them in a current regulation mode in view of a high dissipated power possibilities at the anode.

The EBV with a switching voltage up to 60 kv, switching continuous current 8 A and short pulse current to 50 A is presented. The anode voltages at such currents are 1.2 kV and 3 kV accordingly. This type of EBV is used in radar modulators. The EBV for switching voltage 100-120 kV, continuous current 50 A and pulse current 300-500 A has been also developed. This tube is intended for gyratrons power supply and for corona discharge devise for atmosphere cleaning.

A new idea will be proposed for developed a high efficiency high frequency generator pentode with electron deceleration on the anode. On our mind it is one of the possible ways to create pulse generator tubes with rated power of tens MW.

HPEM 3 - EMP Phenomenology, Propagation, Source Region

HPEM 3-1: Calculation of Energy Evolved in the Loads of Strip Transmission Line in Action of Pulse Electromagnetic Field

S. A. Podosenov, K. Y. Sakharov, A. A. Sokolov

The excitation of linear strip transmission line by external pulse electromagnetic field at matched loads is considered on the basis of transmission line equations derived in (Podosenov S.A., Sokolov A.A., Linear Two-Wire Transmission Line Coupling to an External Electromagnetic Field, Part I: Theory, IEEE Trans. Electromagn. Compat. 1995. V. 37, N 4. P. 559-566, Podosenov S.A., Sakharov K.Yu., Svekis Ya.G., and Sokolov A.A., Linear Two-Wire Transmission Line Coupling to an External Electromagnetic Field, Part II: Specific cases, experiment, IEEE Trans. Electromagn. Compat. 1995. V. 37, N 4. P. 566-574). Transmission line consists of linear parallel wires divided by the dielectric layer. The energy evolved in the loads by the field is calculated. The calculations have been carried out directly in time domain. The energy Q evolved as a result of electromagnetic pulse action of arbitrary shape in the load is determined by the obvious formula

$$Q = \int_0^\infty i(t)^2 W \, dt,$$

where $i(t)$ is the current in the load, W is the load resistance equal to the line characteristic impedance, the line is matched at both sides. It is obvious from general considerations that for arbitrary pulse with duration T at specified length l of the strip line the some optimal value T exists. This value corresponds to the maximum evolved energy. Really at very small $T \ll l/c$ the energy is small because of small action time. On the other hand when T tends to infinity the energy tends to zero so far as the strip line does not respond to static fields. Specific value of optimal duration depends on pulse shape. Either one period of the sinusoid with duration T or unipolar sinusoid half-period with period $2T$ is accepted as the calculation signal shape. Thus, in interval T two pulses with identical duration – two-polar and unipolar are considered. The calculation results at strip line length 0.2 m and typical problem parameters are present in Fig. 1, where energy Q evolved in the load of the strip line at action of unipolar and two-polar signals is presented as T function. One can see from the presented figure that maximal energy emission in the strip line load takes place at definite duration of effected pulse for both field pulses. At specified problem parameters the two-polar pulse energy emission is 2.6 times greater than unipolar one but at pulse
duration increase 1.68 times. Thus, the optimal pulse duration corresponding maximum energy emission exists for each strip line length and for each pulse shape. This reminds the resonance phenomenon. Presented simplest calculation model permits to evaluate the action efficiency of different shape electromagnetic pulses on radio electronic equipment containing strip transmission lines.

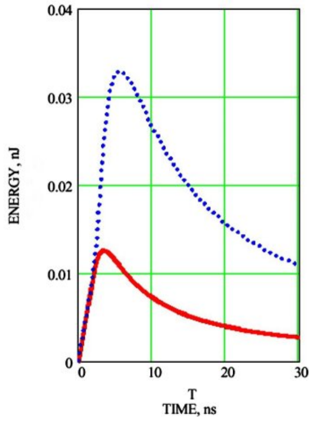

Figure 1: Energy evolved in the load, – unipolar pulse, ... two polar pulse.

HPEM 3-2: Influence of Earth Surface on TEM Horn Array Transient Radiation

S. A. Podosenov, K. Y. Sakharov, A. A. Sokolov

In the work the pulse radiation in time domain for TEM horn array taking into account earth reflection is calculated. Radio wave reflection is influenced by the earth surface relief, electric parameters of the surface and polarization of radiated waves. The problem when the center of radiating antenna and receiving antenna are removed from the earth on height h_1 and h_2 is considered. The problem geometry is presented in Fig. 1. The results obtained (Mikheev, O. V., Podosenov, S. A., Sakharov, K. Y., Sokolov, A. A., and Turkin, V. A.; Approximate Calculation Methods for Radiation of a TEM-Horn Array, IEEE Trans. Electromagn. Compat. 2001. V. 43, N 1. P. 67-74, Podosenov, S. A., Potapov, A. A., Sokolov, A. A.; Pulse electrodynamics of wideband radio systems and fields of bound structures, Moscow: Radiotekhnica, 2003.- 720 p.) have been used for the calculation.

In the work the heights of tolerance irregularities for mirror reflection satisfying to the Reley's criterion are determined:

$$h \le \frac{\lambda}{16 \sin \beta}, \quad (1)$$

where β is the angle of slide and λ is the wave length. For pulse radiation wave length may be determined as $2c\tau$, where c is the light velocity, τ is the signal duration.

It is shown that for small heights of radiator and receiver the earth influence to sum signal one can take into account in accordance with the formula

$$E = \frac{Sh_1h_2}{\pi r^2 c}\frac{d^2E_s(t)}{dt^2}, \quad (2)$$

where S is the array area and $E_s(t)$ is the electric field in its aperture. Formula (2) is valid for any radiated signal. In particular for harmonic signal it coincides with well-known square-law Vvedensky formula (Vvedensky B.A., Arenberg A.G., Problems of ultra-short waves propagation, Moscow: Sovetskoe radio, 1938.- 284 p.).

It is follows from formula (2) that at small grazing wave angles the field decreases with the distance inverse to distance number squared and increases directly proportional to product of earth heights of radiator and receiver. Such rapid decrease of field with distance r and height diminishing is accounted for the circumstance that the fields of direct and reflected pulses are approximately equal in magnitude but they are opposite on sign. The calculation of horn system field taking into account the reflection by earth surface has been carried out. The calculation results are presented in Fig. 2.

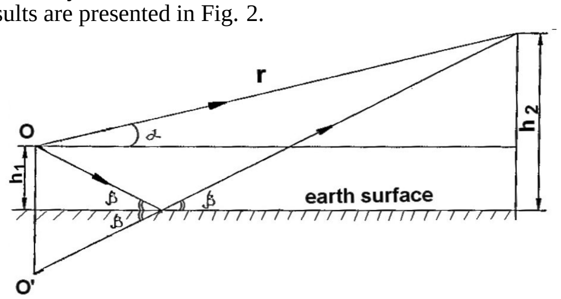

Figure 1: The problem geometry; O and O' are the centers of real and reflected radiators.

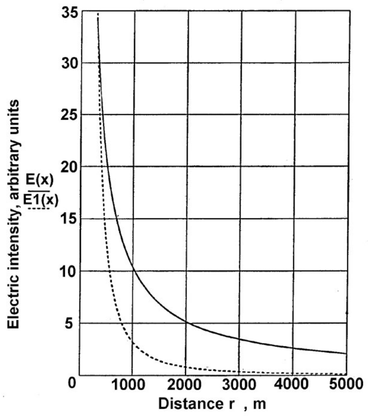

Figure 2: Dependence of electric intensity on distance: $E(x)$ is the field intensity in a free space, $E_1(x)$ is the field intensity taking into account earth action.

HPEM 3-3: Effect of a Cylindrical Density Enhancement on Electromagnetic Wave Radiation from a Modulated Electron Spiral Beam in a Magnetoplasma

T. Zaboronkova, **C. Krafft**
Radiophysical Research Institute, N. Novgorod, Russia

Electromagnetic wave emission from spiral thin modulated beam injected in a homogeneous anisotropic plasma medium have been studied extensively in many works during past decades (see, C.Kraft, A.Volokitin, and G.Matthieussent, Phys.Plasmas, 1996, 3, p.1120, and references therein). Our motivation for continuing research work in this realm is that no detailed fullwave treatment has yet been performed for the case of beam injection in anisotropic open waveguides such as magnetic-field-aligned plasma channels (so called density ducts), for example. Recent space experiments and model laboratory experiments provide evidence that ducts with enhanced density can be formed in a magnetoplasma due to various nonlinear effects (I.G.Kondrat'ev, A.V. Kudrin, and T.M. Zaboronkova, Electromagnetis of Density Ducts in Magnetized plasmas, Gordon and Breach, amsterdam, 1999). Since the study of nonlinear effects connected with the beam-plasma interaction in the presence of plasma nonuniformities seems imposible without a preliminary analysis in the linear approximation, we assume that the beam is given and consider the case of cylindrical channel with a step-shaped radial density profile. We consider electromagnetic radiation from a thin modulated beam of finite length injected oblique to the external magnetic field. In additional we assume that the Larmor radius of the beam is smaller than the duct size, and that the beam density is so small that its contribution to plasma dispersion properties can be neglected.

The mathematical solution for the excited field is obtained by taking the Laplace transform in time and the Fourier transform in space of Maxwell's equatios and beam current, and then taking the inverse transforms of the resulting field. The formulas for the power lost by the beam in the presence of the channel is examined. The power emitted from the beam in the presence of a channel are derived as a function of the beam and channel parameters. A significant deference between the whistler wave emission in the presence of a channel and in the case of a homogeneous unbounded plasma is revealed, due to the excitation of guided whistler mode by the beam in the whistler frequency range.

Acknowledgments. This work was supported by the Centre National de la Recherche Scientifique (CNRS, PICS 1310, France).

HPEM 3-4: Electromagnetics Associated with Laser Pulse Propagation and Ionization

W. E. Page[1], **W. Zimmerman**[1]
[1]*Air Force Research Laboratory / DELS*; [2]*ITT-AES*

Ultra short lasers pulses propagating in air have been observed by many investigators to produce filaments or narrow ionization channels (A. Braun et al, Optics Letters, Vol. 20, No. 1, January, 1995). Near field and far field measurements of the electromagnetic fields produced by these filaments have been made by researchers (A. Proulx et al, Optical Communications Vol. 174 Jan 15 2000, and S. Tzortzakis et al, Optics Letters, Vol. 27, No.21, November 2002). A theory of RF generation from laser filaments has been proposed (C. C. Cheng et al, Phys. Rev. Lett., Vol. 87, No. 21, November 2001). The proposed mechanisms were challenged (N. Carron, 2002) with an analysis predicting a propagating coulomb field with no radiation. Presently there is a dearth of quantitative data for RF radiation from these filaments. In addition a satisfactory theory for the observed RF radiation does not exist.

In this paper the experimental evidence for RF radiation from ultra short pulse laser induced ionization channels in air will be reviewed. We have attempted a direct numerical calculation of Maxwell's equations for the optical fields and their ionization. The numerical problem is daunting due to the temporal and spatial scales involved. Initial results appear to be consistent with Carron. Current analytic and numerical models for this laser propagation and ionization are based on the production of very intense optical electromagnetic fields due to non linear compression of the propagating pulse. These models will be reviewed along with their advantages and shortcomings. These models will include the nonlinear Schrödinger equation (P. Sprangle et al, Physical Review E 66, 06418 2002) and self consistent Finite Difference Time Domain/Particle techniques in real and retarded time (Zimmerman, 2003). Methods for incorporating frequency dependent dielectric constants into time domain numerical calculations will be discussed. Recommendations for further analysis and near field/far field RF experiments needed to better understand RF radiation from ionization channels will be discussed. The current status of suggested experimental measurements designed to help elucidate these phenomena will also be reviewed.

HPEM 3-5: Excitation and Propagation of Nonlinear Waves of Volume Charge in Metall Conductors

S. V. Adamenko[1], **V. E. Novikov**[2], **A. V. Paschenko**[3], **I. M. Shapoval**[3]
[1]*Electrodynamic Laboatory "Proton-21", Kyiv, Ukraine*;
[2]*Science & Technology Center of Electrophysics, NASU*;
[3]*National Science Center "Kharkov Institute of Physics and Technology"*

In our report, there is very important factor, realizable from the very beginning evolution of pulse relativistic electron beams interference on the condensed medium - the uncompensated volume charge. In the traditional experiments on electron beam coupling with targets, the beam electrons, that strike the metal and impart their kinetic energy, diffuse over the metal, not creating the volume charge. At high enough currents and growth speed, the beam volume charge in metal exceeds the fluctuation value, producing a non-linear electron wave of volume charge, which propagates following the ion flow. As a result of the specific target compression.
The problem of volume charge wave creation in metal is not trivial owing to the presence of high conduction electron density. In the experiment, this problem was solved after creation of the regime of controlled current transfer all over the system. In this regime, the e-beam delivers, as part of the electric circuit, a quantity of electrons to the target (anode) that is larger than the quantity that can be carried away by electron current in the circuit.
In our report is shown, that the collective processes in the targets occur at such a level of influence on the condensed media that the system can neither be considered equilibrium nor ideal, nor non-equilibrium.
Theoretical investigation is shown that as a result of evolution of the electron wave, its leading edge steepens and, in certain depth inside of the target, the wave collapses. The collapse brings about appearance of a very thin layer on its leading edge with a very high density of the electron volume charge, huge electric fields and extreme states of matter.

HPEM 3-6: The Contribution of Hydrodynamics to the Evolution of the Lightning Source Region

R. L. Gardner

The lightning source region is one of the most energetic electrically driven events that we study in the electromagnetic compatibility community. Near ground effects for a cloud-to-ground event can include substantial physical as well as electrical damage. Electrical parameters can exceed hundreds of kiloamps, hundreds of kilovolts and charge transfers of several coulombs. Near ground processes can be quite fast emitting higher frequencies than those observed in far field observations.
The picture we have of the initiation of cloud-to-ground return stroke is that of upward and downward traveling leaders joining a few meters above the ground and discharging the charge stored in the channel. The time development of the early time current, hence the high frequency development, depends critically on the details of that joining process and the electrical parameters describing the first few meters of the discharge channel.
Observations of the joining process are limited because of the hostile environment around the strike and point and the unpredictable strike point. Triggered lightning measurements are available but the triggering distorts the early development of the channel.
If we think of the lower section of the channel as a transmission line then the post-switch-closure propagation of the current depends on the diameter and conductivity of the inner channel and the surrounding charge stored in the corona. These physical characteristics are described in the nonlinear, time dependent and length-dependent capacitance, inductance, conductance and resistivity per unit length of the channel. These parameters, in turn, depend on the conductivity and size of the conducting current channel. The development of the channel is described by the radial hydrodynamic equations and the electrical and thermal transfer mechanisms that drive them.
In this paper we will look directly at the first few meters of the lightning source region channel and describe the physical and electrical evolution of that region in terms of the hydrodynamic and radiation transport equations. It will be shown that the evolution of the transmission line variables will limit the high frequency emissions of the channel to within 100m of the channel initiation point.

HPEM 4 - Hardening and Protection

organized by the German URSI Commission E

HPEM 4-1: Investigation of Limiters for HPM Front Door Protection

T. Nilsson, **R. Jonsson**
Swedish Defence Reserch Agency

The threat from high power microwave (HPM) weapons is steadily gaining importance. Both civilian and military electronic equipment are vulnerable to this threat. A typical component that needs to be protected is a MMIC front-end receiver. Depending on the level of threat and the damage level of the receiver different types of protection circuits can be used to limit the power delivered to the sensitive circuitry. The growing use of array antennas has also increased the demands on miniaturization of the protection devices.
We present pulsed power measurements on several types of commercial limiter and ESD/NEMP protection devices as well as in-house designed MMIC limiter circuits (T. Nilsson, R. Jonsson, HPM Front-door Coupling and Protections Progress Report 2003, FOI-R–1020–SE)
The measurement setup seen in figure 1 is used to characterize the limiters; it allows measurements of input power, reflected power and transmitted power in the frequency range of 0.5 to 18 GHz, in both CW and pulsed mode. The maximum output power level is 33 dBm when solid-state amplifiers are used. Recently additional microwave amplifiers (TWT, Traveling Wave Tube) were installed, with these can the maximum output power level reach 53 dBm, for the lower frequencies, 1 to 4 GHz. The power level of the injected signal is stepwise increased until the component starts to limit or the maximum input power level is reached. S-parameter measurements have also been done using a HP 8510C Network analyzer. Some examples of the measurement results are shown in figure 2 and 3.
The tested commercial limiters are not primarily intended for HPM protection, some are for NEMP (Nuclear Electro Magnetic Pulse), ESD (Electro Static Discharge) or lightning protection. The technology used in these limiters is mainly gas discharge tubes or diodes. Also a commercial MMiC limiter/LNA from MA/COM is tested. The work consists of evaluating these limiters, to see which ones that also can be suitable for HPM protection. Limiters from several different component suppliers, mainly from M/A-Com, Huber+Suhner and Littlefuse have been tested
The most compact solution would be to integrate the final stage protection with the receiver LNA it is aimed to protect. Therefore we have initiated an effort to study the feasibility of limiters made in a process that is already in use for making various receiver circuitry (the OMMIC ED02AH MMIC -process). Five limiters and test structures were processed to evaluate different kinds of possible limiting circuit elements.

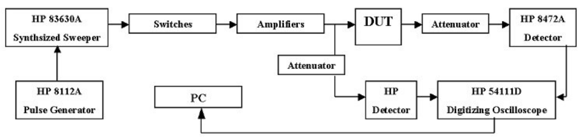

Figure 1: Block diagram of the measurement setup.

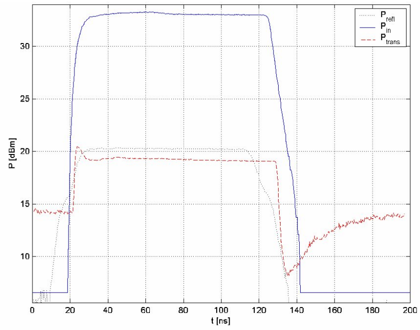

Figure 2: Time resolved large signal measurements on the MA01502D.

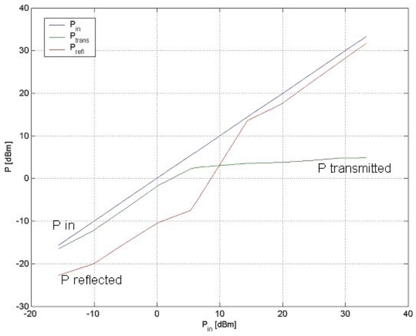

Figure 3: The Reflected and the transmitted power as a function of the input power for a measurement on the Microsemi GG-77314-04.

HPEM 4-2: Considerations Regarding Reduced Shielding Effectiveness of C4I Enclosures

M. Nyffeler[1], **F. M. Tesche**[2]

[1]*Armasuisse, NEMP-Laboratory, Spiez, Switzerland*; [2]*EMC Department, Saluda, NC, USA*

Electronic warfare is increasing in complexity, while military budgets are decreasing in most countries. As a consequence, the use of commercial, off the shelf (COTS) equipment for intelligent systems is becoming commonplace. Electromagnetic (EM) immunity of commercial products is normally guaranteed by requiring conformity to EMI standards. As C4I equipment are generally required to be the most reliable systems of an Army, civilian and military standards require an electric shielding effectiveness of at least 80 dB up to a frequency of 1 GHz for enclosures containing such COTS technology. This requirement is for protection against high- altitude nuclear electromagnetic pulses (HEMP) or other external EM environments. In addition to the external EM threats to a system, another aspect of required system hardening is the electro static discharge (ESD). The peak amplitudes of the internal EM fields due to an ESD occurring within a shielded room can be significantly larger than the residual HEMP fields. We have recently examined the ESD-produced EM fields within a shielded enclosure and performed a comparison with the internal HEMP fields. (Tesche, F. M., "Calculation of ESD-Generated Fields in Shielded Enclosures", Report for armasuisse, October 17, 2003.) The findings of this study are summarized in this paper.

For an ESD discharge from a peak static voltage of 5 kV onto a wire extending across the volume of the room (see Fig. 1), the radiated E and H fields have been computed using an FDTD approach. The peak values of the internal EM fields vary with changes of the observation location. To summarize these results, the peak amplitudes of all E and H field components at 1-million internal observation points were computed, and cumulative probability distributions were determined. It was found that an E-field amplitude of 300 V/m and an H-field amplitude of 1 A/m corresponded to a probability of 0.5 . That is to say, 50% of the interior points have field values greater than these levels, and 50% have values less. Measurements of the described installation have confirmed these computations.

By applying the shielding specifications for an enclosure specified by MIL-STD-188-125, the internal H-field for a NEMP excitation was estimated using standard H-field shielding models. It was found that the peak amplitude of this field was on the order of 0.04 A/m. This value is significantly smaller than the ESD-produced field.

This difference between the NEMP and ESD H-field levels suggests that there should be a better coordination of the EM hardening requirements given by the various specification documents. It is evident that the HEMP shielding requirement of MIL-STD-188-125 provides for a very low internal field, and that this results in a well-hardened system. However, if there were an ESD event within such a shielded enclosure, the expected internal EM fields will most likely be well above these NEMP field levels. The results of this study suggest that a more cost-effective construction of enclosures for C4I equipment may be possible by reducing the shielding effectiveness requirements for external EM environments. However, to best coordinate EM hardening it is important to keep in mind, that even with a high quality enclosure the EMC-aspects inside the enclosure are not at all negligible and protection against conducted transients in cables entering the enclosure remains a necessity.

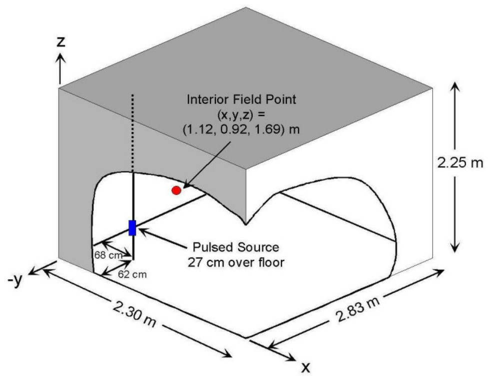

Figure 1. Illustration of the shielded enclosure with internal ESD source.

HPEM 4-3: Practical Design of Protection Circuits against Extremely Fast High Power Electromagnetics

R. Krzikalla, **J. L. ter Haseborg**

Department of Measurement Engineering and EMC, University of Technology Hamburg-Harburg, Germany

The threats of electronic systems due to high power electromagnetics have been discussed in several publications (e.g.: W. A. Radasky, et al., Intentional Electromagnetic Interference (EMI) – Test data and implications, International Zurich Symposium on EMC 2003). Especially the influence of the so called ultra wideband pulses (UWB pulses) is quite probable due to their extreme short rise times and the resulting broad frequency spectrum. Investigations have been done to examine the response behavior of traditional protection concepts, built up with spark gaps, varistors and suppressor diodes, by stressing with UWB pulses (T. Weber, et al., Hardening of electronics against transmission line coupled UWB – signals, XXVIIth General Assembly of the International Union of Radio Science, Maastricht, 2002). Due to the very steep rising edge of UWB pulses, spark gaps show no relevant effects by stressing with UWB pulses. The tested varistors and most of the common suppressor diodes show instead of nonlinear a linear behavior by stressing with UWB pulses caused by parasitic capacitances of the element and line inductivities. Furthermore suppressor diodes with extremely small parasitic capacitances ($<$5pF) have been tested as protection elements against UWB pulses, which are mainly capable against electrostatic discharges (ESD). These elements show a diode-typical nonlinear behavior, whereby the energy of the UWB pulse has been reduced, but the rising edge and the maximum voltage of the interference have not been influenced significantly.

Due to the linear behavior of most of the tested traditional

nonlinear elements, directly linear filters have been developed and tested successfully for the protection of band limited high-frequency applications. High demands on the linear filters have to be made also in voltage resistance and in the high-frequency behavior. Therefore interdigital bandpass filters in microstrip technique have been designed for different applications to provide a sufficient protection against UWB pulses (R. Krzikalla, et al., Interdigital microstrip filters as a protection device against UWB pulses, 2003 IEEE Int. Symp. Electromagn. Compat., Istanbul).
As mentioned before these diodes, which show a typical nonlinear behavior by stressing with UWB pulses, can reduce in fact the energy, but not the steep rising edge and the voltage amplitude of an UWB pulse significantly. Due to the possibility of the filtering of high voltage UWB pulses with linear microstrip filters, this investigation will focus on a combination of linear filters with nonlinear elements to provide an all-around protection against different electromagnetic interferences. In the first step the time response of UWB stressed diodes with very small parasitic capacitances will be measured with a linear pre-filtering of the interfering pulse. Therefore different lowpass filters with decreasing cutoff frequencies are used. Furthermore the same test setup is used to determine the cutoff frequency of a needed linear pre-filter where traditional nonlinear protection elements (spark gaps, varistors, diodes with comparable high parasitic capacitance) will behave again in a nonlinear way.

HPEM 4-4: Grounding Systems Frequency Response

J. Wiater
Technical University of Bialystok, Poland

Grounding system characteristic during lightning strike isn't constant. It depends on grounding resistivity, surge current value, earthing network etc. In this paper simple grounding systems was analyzed.
First configuration of grounding system (Fig. 1a) consists of simple grounding gird (ring around bouilding). Second one (Fig. 1b) consists of ring-earth electrode around bouilding, overhead transmission line and grounding system of MV/LV substation.
The MV/LV substation earth grid is used as an electrical connection to earth at zero potential reference. This connection, however, is not ideal due to the resistivity of the soil within which the earth grid is buried. During typical earth fault conditions, the flow of current via the grid to earth will therefore result in the grid rising in potential relative to remote earth to which other system neutrals are also connected. This produces potential gradients within and around the substation ground area. This is defined as ground potential rise or GPR. The GPR of a substation under earth fault conditions must be limited so that step and touch potential limits are not exceeded, and is controlled by keeping the earthing grid resistance as low as possible.
Knowledge of grounding behavior is crucial to safety standards and to overvoltage protection systems. GPR in carry out to the final user instalation comes by neutral wire, by the phase wire, by voltage difference between them. GPR with reference to the true earth can be very high and directly depend on grounding systems.
Presented calculation allows to provide behaviour of GPR in time domain. During lightning or short circuit GPR can rise high values. Indirectly can be estimate required real protection level. Real measurments are very expensive, so it's economical reason for computer simulations. The engineering program CDEGS was used to compute frequency response to the lightning surge. It was made for wide range of the frequencies – up to 100 kHz. Presented computation results describe GPR in frequency domain for two cases: simple grounding system (Fig. 2) and complex grounding system (Fig. 3). In theoretical model implemented into CDEGS the following assumptions were made:
- ground resistivity ρ=100 $\Omega \cdot m$,
- excitation 1A for whole range of the analyzed frequencies.

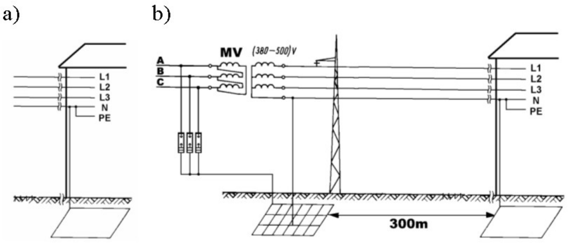

Figure 1: Grounding system view – first case (a), second one (b).

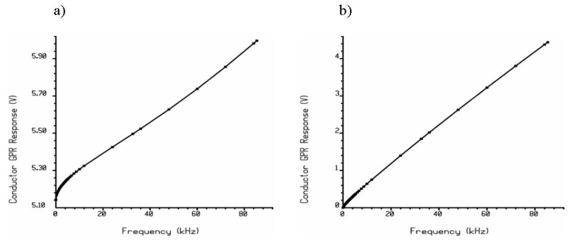

Figure 2: Ground potential rise frequency response (first case) – real part (a), imagine part (b).

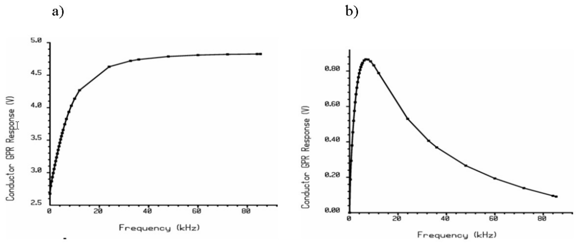

Figure 3: Ground potential rise frequency response (second case) – real part (a), imagine part (b).

HPEM 4-5: Multi-Channel Coax-EMP-Protector with Superior Performance

A. W. Kaelin
Meteolabor AG, Wetzikon, Switzerland

Antenna feed cables for modern RF-communication installations transmit various electrical signals through a single coaxial cable. A typical coaxial link between an outdoor-unit and an indoor-unit transmits multi-channel RF-signals and an AC or DC voltage for the power supply of the outdoor unit. In addition to that, in some cases there is also a digital data channel of up to several Mbit/s superimposed to the other signals.
Whilst the lightning protection for such an installation is usually accomplished by gas tube surge arresters, the protection against much faster rising voltage pulses, such as in the case of HEMP (High-Altitude Nuclear Electromagnetic Pulse), is much more challenging, since the attenuation for the signals should be negligible and the attenuation of the overvoltage as high as possible. In this paper we present an EMP-Protector transmitting all the above mentioned signals with low attenuation and provides very low residual voltages, even under HEMP conditions.
The principle of the protection circuit is shown in the block diagram in figure 1. A coarse protector, typically a gas tube arrester, blocks the majority of the energy. However, since it has a finite response time, a steep front voltage pulse will pass unattenuated through the arrester during a few nanoseconds. This let-through voltage may destroy sensitive electronics, although once the arrester has fired the let-through energy is relatively small. For further attenuation of the let-through voltage pulse the signal path is split into two or more paths. Each path consists of a frequency selective filter and nonlinear protection elements such as transient voltage suppressor diodes (TVS). One path is consists of a non-linear low-pass filter, which transmits DC. The filter is designed in such a way, that it will also transmit digital data of several Mbit/s. One or several other paths transmit the RF-

signals and are designed as non-linear bandpass filters. Special care must be taken, because TVS have a rather large capacitance and also a parasitic inductance. There are design limits, because intermodulation distortion by the non-linear elements must be avoided. Finally the filtered and limited signals are combined again into a single coaxial line.
By splitting the signal into several channels having separate fine protection and recombining them, very low residual voltage levels can be achieved. More details will be presented during the paper.

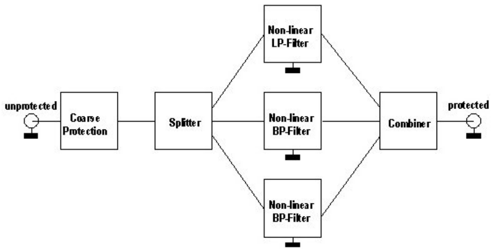

Figure 1: Block Diagram of EMP-Protector with superior protection levels.

HPEM 4-6: EMC and Surge Protection Concept for Mobile Power Generators

G. K. Wolff
Phoenix Contact GmbH & Co. KG, Blomberg, Germany

Mobile power generators have to ensure the availability of electricity for outdoor usage equipment and systems without interrupt. Influences like given from lightning strokes or surge voltages can lead to malfunction, to interrupt or to breakdown of significant system functions. A modern EMC and surge protection concept for mobile power generators provides protection means against the dangerous threats given from those risks. The concept introduced in this paper considers as well internal as external loads powered via power outlets. It includes means against overload and electrical shock. The surge protection devices are designed in a way, that they neither corrupt the means against overload and electrical shock in the generator unit itself nor the protection means given by an external standby power supply, e.g. a temporary connection to a local power distribution network. The protection means support single and three phase systems as well as 24 V DC systems including a battery charging unit. The EMC and surge protection concept has been realised in decontamination system containers. The mobile power generator unit is an implemented part of the container. The system passed a field test in combination with a NEMP-, EMC- and lightning protection test. The protection concept increases the system function availability of generator powered equipment.

HPEM 4-7: The Protection of Ordnance and its Electronic Subsystems against the Threat Imposed by CW and Pulsed Electromagnetic Fields

H. Herlemann[1], **M. Koch**[1], **A. Bausen**[2], **F. Sabath**[2]
[1]*Institute of Electrical Engineering and Measurement Science, University of Hannover, Germany*; [2]*Armed Forces Scientific Institute for Protection Technologies, Munster, Germany*

In recent years there has been an increasing threat that military electronic equipment may be influenced or damaged by high frequency electromagnetic fields. This is especially critical in case of ordnance because the performance of modern weapon systems is based on the extensive use of electronic devices covering the broad range from control systems containing microprocessors to electrically initiated devices (EID).
Destruction effects on semiconductors caused by pulsed electromagnetic fields were investigated recently. In contrast, short pulses are normally not considered to be a threat to EID since it takes some time for the EID to heat up. It has to be considered however that some RF sources like radar and some types of directed energy weapons radiate repetitive pulses. After several pulses the heating may be sufficient to initiate the EID. The disturbance may occur in storage, in transit or in operation. If the disturbance occurs in storage or transit, methods of shielding have to be investigated. A measure for the protective properties of a shield particularly against pulsed signals has to be found.
The question of how to determine the protective properties of a shield is a difficult one to be addressed, even in frequency domain. In general, the common definitions of shielding effectiveness do not provide a measure for the capability of a shield to protect a certain application against electromagnetic fields. This is because in most cases, only the electric- or magnetic shielding effectiveness of the empty shield is measured. Since the shield usually forms a cavity resonator with internal resonances, the shielding effectiveness breaks down at the cavity's characteristic resonance frequencies. In addition, it becomes a function of position. Due to these resonance phenomena, tests as close as possible to the actual configuration are preferred over measurements of the shield alone and a dummy load is used.
In this contribution, a measurement technique in the time domain is presented, using pulses of double exponential characteristic for the examination of electrically conductive textiles used as enclosures for different applications. At first, microprocessor boards are being exposed to these pulses while being in action. With these pulses, the susceptibility of the equipment with and without the shield is determined, while being in operation. The protective properties of the shield are determined from the different field strengths at which certain malfunctions appear. The measurement technique is based on the determination of probability rates for the breakdown or destruction of a device. Since special devices like microcontroller boards or microprocessors are used, the disadvantage may be that test results cannot easily be transferred to other systems with a completely different configuration. However, measurements of different microcontrollers or microprocessors exhibit an astonishing comparability even between different generations of devices.
Secondly, for the investigation of the threat on ordnance by high frequency electromagnetic fields, measurement results of electrically conductive pouches for the protection of ordnance during storage and transportation are presented. As an example the MILAN FIELD OVERSOCK MK 4, which is currently used by the UK Armed Forces in Afghanistan, is considered more closely. For comparison reasons, the required immunity levels for ordnance according to MIL-STD 464 and STANAG 4234 are reviewed.

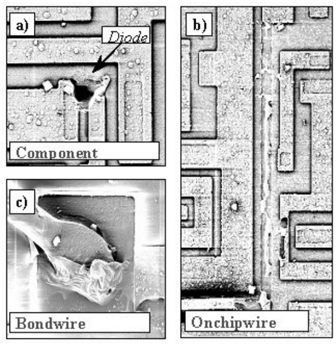

Figure 1: Destruction of semiconductors caused by electromagnetic fields.

Figure 2: Shielded and unshielded MILAN missiles during a training exercise.

HPEM 4-8: RF & Microwave Monolithic without DC Bias

J. Zbitou[1], **M. Latrach**[1], **S. Toutain**[2]
[1]*Electronic Departement, Ecole Supérieure d'Electronique de l'Ouest, Angers, France*; [2]*IRCCyN SETRA, Ecole Polytechnique de l'Université de Nantes, Nantes, France*

Microwave power limiters find widespread use in protecting sensitive RF components; the output power is reduced to a level that will not overdrive a receiver, burn out an amplifier, mixer, etc. For input power levels exceeding the limiter's threshold level, the output power tends to remain constant. Limiters can be designed by using transistors, PIN and Schottky diodes. The goal of our study is the achievement of a limiter without DC bias. Then the use of transistors and PIN diodes becomes impossible where the choice of Schottky diodes. In this paper, a new monolithic configuration, based on zero-bias diodes in antipodal configuration "two back to back diodes" (I. Bahl, P. Bhartia, Solid State Circuit Design, 1988 edition by John Wiley & Sons), is used to develop a wide-band limiter "0.5-20 GHz".The philosophy used to enlarge the frequency band is based on the pass band filter theory, thus by replacing the parallel capacitors in the filter by the antipodal topology. This monolithic limiter was achieved and fabricated (Fig. 1) using ED02AH process from OMMIC, which gives the possibility to modify and to vary the geometrics dimensions of the diodes used in the limiting operation.
Figure 2 shows a good agreement between simulation and measurements results. The limiter handles 30 dBm as a maximum input power, with a limiting threshold value equal to 10 dBm with a quasi ideal characteristic. The use of the monolithic technology permits the optimization of the geometrics dimensions which allow to obtain a monolithic wide-band limiter. The final circuit achieved has small dimensions of 1500 μm x 1286.5 μm, with quasi-ideal performances in a large frequency band "0.5-20GHz".

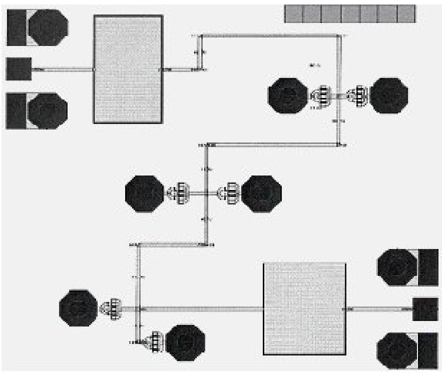

Figure 1: Layout wide band monolithic limiter.

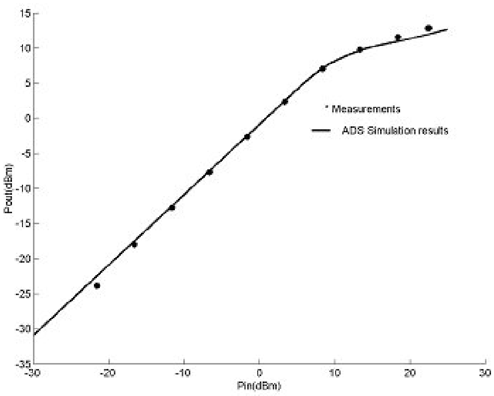

Figure 2: Measurements and simulation results of output power versus input power.

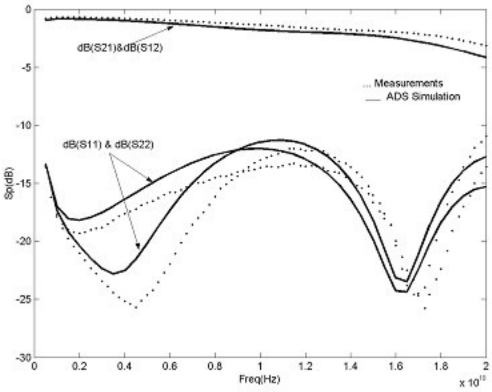

Figure 3: Small signal measurements and simulation results comparison.

HPEM 4-9: E3 Characterization Testing of Modular Conductive Tents

W. Crevier[1], **N. Wild**[1], **T. Gray**[2], **S. Colvin**[3]
[1]*Jaycor/Titan, San Diego, CA, USA*; [2]*Defense Threat Reduction Agency*; [3]*Tactical Operation Centers*

Two prototype E3 tents utilizing conductive cloth material were designed, constructed, and tested. The tents closely resemble the standard 11' x 11' modular tents used by the United States Army. Conducting bootwalls also were developed to connect the modular tents to Rigid Wall Shelters (RWS). One of the key features of the standard modular tents is the ability to connect multiple tents together to form a multi-node Tactical Operations Center (TOC). The prototype tents were required to demonstrate this capability while maintaining the integrity of the shielding.
The tents were tested in a mini-TOC configuration consisting of two E3 tents, E3 bootwalls, and RWS. The modular E3 tents successfully protected the SINCGARS radio antenna from EMI radiated by electronic equipment operating in the tent area. Much of the E3 testing involved selectively degrading the tents to determine sensitivity to the types of flaws expected in an operational environment. It was found that the level of protection was still adequate with significant degradations to the shield, such as the removal of the floor or the opening of a door. However, unprotected penetration of an electrical cable significantly reduced the level of protection.
The EMI tests were followed up with tests in HEMP and lightning simulators. Results from all three tests will be presented.
This work was sponsored by the Defense Threat Reduction Agency and the Product Manager, Tactical Operation Centers.

Figure 1: EMI testing of modular E3 tents made from conductive cloth.

HPEM 5 - EM Modeling

HPEM 5-1: Electromagnetic Simulation in Anisotropic and Inhomogeneous Media by Volume Currents in the Moment Method

C. Findeklee[1], **H.-D. Brüns**[2], **H. Singer**[2]
[1]*Philips Research Laboratories, Hamburg, Germany*;
[2]*Technical University Hamburg Harburg, Germany*

The Method of Moments (MoM) is a very efficient electromagnetic simulation technique, especially for the calculation of radiation and near fields of antennas or scattering problems. However, for modeling of field distributions and distributions of the specific absorption rate (SAR) inside human bodies other methods are frequently applied. Especially the FDTD (Finite Difference Time Domain) is commonly used at present, since the implementation of this technique is straightforward and since arbitrary, i.e., inhomogeneous and anisotropic tissue can be handled easily. The new approach to be discussed here is based on the volume equivalence principle in conjunction the MoM, using Green's function of free space. Anisotropy is taken into account by special boundary conditions.
The Method of Moments has proven to be successful for the modeling of wire and surface structures, because only those parts have to be discretized. Dielectric lossy materials, like human tissue, are usually modeled by assuming a homogeneous material. Matching the two boundary conditions for the electric and magnetic field on the inner and outer surface sides gives linear equations for equivalent surface currents.
Another existing integral equation technique uses equivalent volume currents. Both methods can be used for electric and/or magnetic materials, by applying the corresponding boundary conditions for the equivalent surface approach or equivalent electric and magnetic currents in the volume current method.
In contrast to the surface current technique the volume current method can easily handle inhomogeneous media. This technique was modified to also be able to calculate anisotropic media, using the isotropic Green's function by choosing adapted equivalent volume currents. Such a proceeding avoids complicated calculations with special Green's functions for arbitrary anisotropies. Unfortunately, the equivalent current method leads to a very high number of unknowns compared with a pure surface discretization. On the other hand the system matrix for volume currents is very well-conditioned compared with a wire- or surface problem. Coupling to wire- and/or surface structures can be handled easily using the volume MoM approach. In practical applications (human being inside an MRI-system, radiation of mobile phones), most of the unknowns are still caused by the equivalent volume currents. In this case, efficient solvers, which use preconditioning or iterative techniques, can be used to solve the overall linear equation system. If the same dielectric tissue, for example a general human body model, is used for different scattering problems, the calculated coupling quantities between the volume elements can easily be reused and the solving algorithm for the complete equation system can make use of a general LU decomposition of the volume current matrix.

HPEM 5-2: Field Excited Multiconductor Transmission Lines

F. Schlagenhaufer
Western Australian Telecommunications Research Institute (WATRI)

Coupling of external fields into transmission lines, and coupling between individual conductors are fundamental electromagnetic problems. This type of problems can often be treated with numerical methods based on transmission line theory. Transmission line solutions, while restricting the type of geometries that can be treated, usually result in very short calculation times and therefore are especially well suited for extensive parameter studies.
A basic configuration, as shown in Figure 1, is used to investigate the influence of some parameters on the induced currents in field excited multiconductor transmission lines. Some preliminary results for variants of this structure are shown in Figure 2.
A closer distance between coupled conductors could be assumed to result in higher coupling between the two lines. However, it is found that the current maximua differ only slightly with different distances. But in all cases, where all conductors are of equal length, pronounced beat frequencies can be observed; these beat frequencies depend on the mutual inductance and hence on the conductor separation.
The highest coupling occurs when all conductor lengths are equal. Modifying the length of conductor 1 (see Figure 1) reduces the current induced in observation point 2 significantly.
An artificially high resistance per unit-length is sometimes used to allow the application of Fourier and Inverse Fourier Transform for conversion between time and frequency domain. The effect of such a resistance will also be subject of an investigation.
Parameter variations for final paper will be:
Distance between conductors: d = 2 . . . 20 cm
Conductor lengths: L1/L2 = 0.1 . . . 10
L1/L3 = 0.1 . . . 10
Resistance per unit length: R' = 0 . . . 2 Ω/m

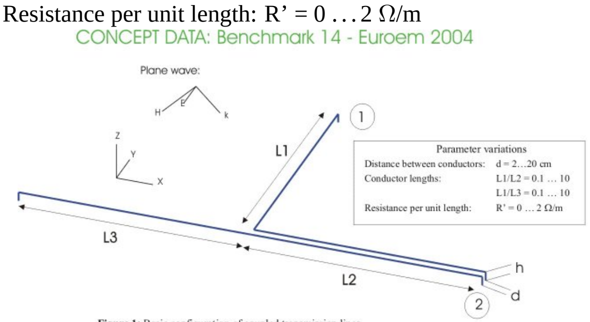

Figure 1: Basic configuration of coupled transmission lines

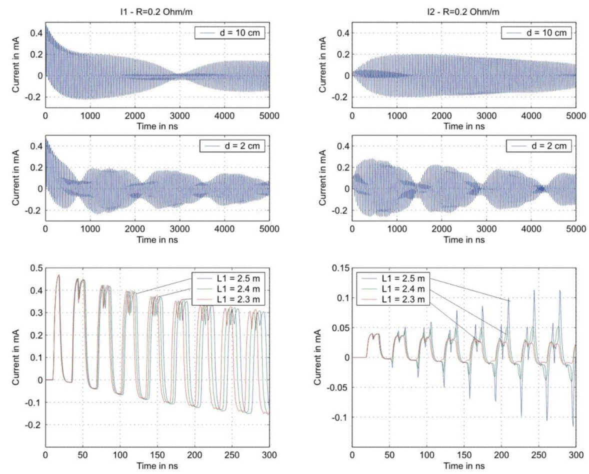

Figure 2: Induced currents for variation of conductor separation and conductor length

HPEM 5-3: Field Simulation Based EMC-Optimisation of a Converter Power Stage Design

A. Röhrich
University of Duisburg-Essen, Institute of Electrical Power- and Control Engineering

In modern motor vehicles the increasing demand on electric power offers novel applications for power electronic components and systems. Apart from the functional behaviour the Electromagnetic Compatibility (EMC) for these components has to be ensured. A common way is to investigate, if the devices comply with the limits of the applicable standards. An investigation of the electromagnetic behaviour should ideally take place in the preliminary stages of the development or during the design phase. For this purpose investigations using field simulation tools are useful, because they allow an estimation of the EMC behaviour while varying several parameters.
In this presentation the EMC performance of a power converter design for an integrated-starter-generator (ISG) for the 42 V

powernet is investigated by simulation. Here, the converter operates as a motor drive for an integrated starter generator utilizing a pulsewidth modulation (PWM) control. A typical used clock frequency of the PWM is 11 kHz. PWM switching edges mediated by unbalances are the major sources of interferences. They have to be reduced or even suppressed so that they cannot influence the on-board network and the radio receivers operated in the vicinity. This can be done on one hand by using suitable filters, on the other hand with special design features within the packaging- and interconnecting technology.

In fig. 1 a schematic view of the prototype converter components is given in detail. The bottom side of the DC link capacitor forms one electrode to be connected to the power net (positive battery potential). This electrode is contacted with the MOSFET modules via clamps at the back side of the capacitor and additional copper clamps also used as mechanical fixture. The top side of the capacitor (top electrode, ground terminal) is directly contacted to a water cooler. The top side of the water cooler forms the base plate of AlSiC for the MOSFET substrates. For the interconnection of the modules and the phase terminals bus bars of copper are used, which are installed isolated on the base plate. Driven by the PWM of the gate drive circuits the MOSFET switches generate a three-phase voltage of 42 V at the three-phase terminals for the motor mode of the ISG. The three-dimensional packaging- and interconnecting technology of the power converter eludes the common investigation practices for printed circuit boards (PCB).

The simulative investigations take place using a program based on the Method of Moment (MoM). The model for the field simulation consists of surface structures. The convenience of this surface model is the calculability of surface currents, which are vitally important for the electromagnetic emission. In simulation-based investigations measures are often taken on the basis of network analysis using suitable equivalent circuit models. In this presentation the model for the field simulation is directly used without an equivalent network. The three-dimensional model allows to recognise current loops in all directions in space. Thus a design of filter elements based on the calculated surface currents becomes possible. The preferred positions for placing filters as well as the most favourable geometric form for the set-up components can be found by means of the surface currents.

The DC link capacitor is a significant component of the converter. The structure of its simulation model has to correspond with the original prototype. Furthermore it is important that the frequency-dependent impedance of the capacitor model conforms to the original prototype. In the presentation the modelling of the DC link capacitor will be discussed.

From the point of view of EMC the MOSFET switches represent sources of high frequency disturbances. To the simulation of the electromagnetic behaviour only the direct switching respond is of interest. Without loss of generality it is sufficient to regard only one switch consisting of four chips in parallel as the source of disturbances.

The simulation is carried out with an excitation by three impressed sinusoidal currents of each 1 A at an initially frequency of 11 kHz, which is the fundamental frequency of the PWM signal. The impressed currents are positioned at the places of the MOSFET power switches in the real prototype (fig. 1).

Fig. 2 shows the calculated surface currents and the associated magnetic field strength distribution 1 cm above the model is depicted. Both results indicate a significant current flow through the machine model. Ideally the machine should be supplied with a pure low frequency current. The PWM clock signal is only relevant to the internal generation of the three-phase voltage. Therefore the aim of measures is a high concentration of the high frequency currents in smallest possible areas. Thus a near sinusoidal three-phase system can be achieved.

The magnetic field strength distribution in fig. 2 indicates also the existence of eddy currents at the top side of the structure. Since the processes at the top side of the structure are of particular interest in regard of the EMC, in the following investigations a simplified model is used. With this model the simulation time can be reduced to a hundredth or less.

Various measures and results will be shown in the presentation. As an example, the consequences of additional capacities for the surface currents are displayed in fig. 3. The capacities short-circuit the +42 V bus bars and the phase terminals to the base plate for high frequencies. Thus a distinct reduction of the current flowing through the machine model as well as a concentration of the currents in considerably smaller areas can be achieved.

In the presentation the surface currents, which are provided by the field simulation tool as an additional result, are included in the investigation. Thus the principle concept of the proposed simulation methodology is the development of measures for reducing the disturbances based on the surface currents.

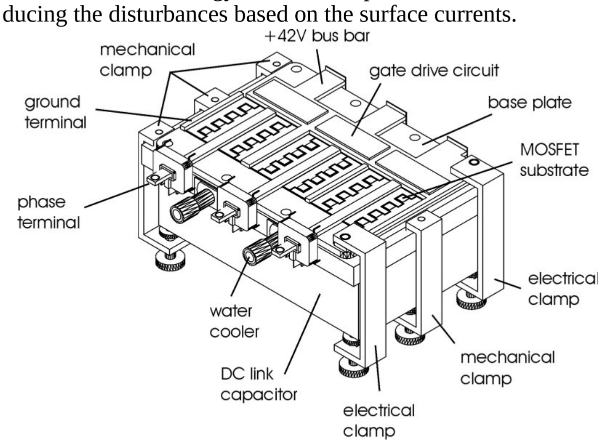

Figure 1: Schematic drawing of the analysed prototype

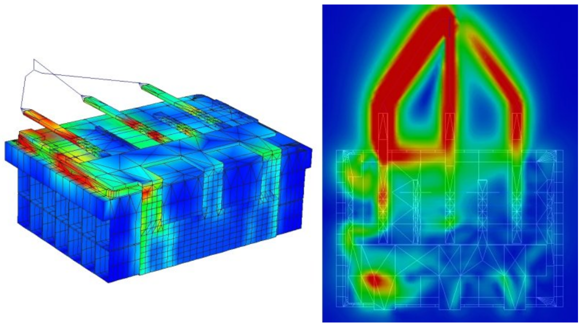

Figure 2: Calculated surface currents and magnetic field strength distribution at a frequency of 11 kHz (Complete model)

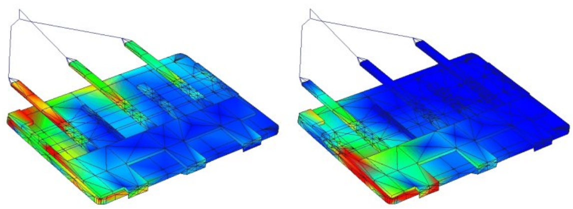

Figure 3: Calculated surface currents at a frequency of 1 Mhz. Left without, right with additional capacities (Simplified model)

HPEM 5-4: Reduction of EMI and HERP by the Use of Metal Rods for HF Screening

H.-F. Harms
Nordseewerke GmbH Emden

Introduction

At the shipyard Nordseewerke GmbH in Emden currently the resaerch and trial ship class 751 for the German Navy is under construction (figure 1). On this ship are military as well as commercial off the shelf (COTS) devices in use. Especially these COTS devices are very often the reason for EMC problems which are to be solved.

Problem

On the open bridge wings of the trial ship are additionally mounted control units. These COTS units are only specified of

10 V/m susceptibility. Close to the control units are powerful HF-rod antennas located.
Calculations with the field analyzing programm CONCEPTII have shown that the electrical field strength on both sides of the bridge wings is far above 10 V/m. Faultless and correct operation of the control devices is not guaranted any more. An other point is the exposure of the crew members to these high electrical fields and radiations (hazard of electromagnetic radiation to personel HERP).
Some simple sun sails have been planned to stay outside on the bridge wings also when the sun is shining very strong. The first idea was to use the sun sails only occasionally. Some racks made of plastics or aluminium to save weight covered by simple cloth have been proposed.
But a metallic frame would be very complicated to connect and to mass with the ships ground every time when constructing and deconstructing.
Field computations with different constructions of the sun sail have shown that a solid connection of the frame with the ship body also with relativly big openings of 130 cm $\times$ 90 cm reduces the electric fields of the HF-antennas on the bridge wings enormous (figure 2).
Figure 3 shows the field distribution without sun sail on the starport wing seen from the front.
Red colored areas are the areas with field strength above 20 V/m.
Figure 4 shows the same area but with sun sail.
Conclusion
It was shown that with relativly simply constructive provisions many possible EMC-problems can be eliminated already in advance without more efforts. Functionality, effort and EMC don´t need to be contradictionary to each other.

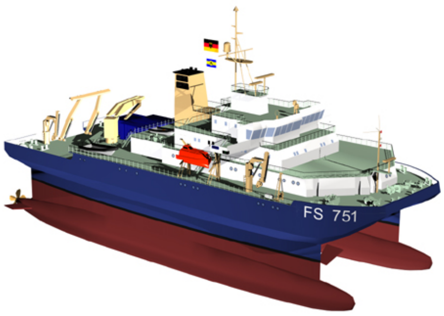

Figure 1: Research and trial ship class 751

Figure 2: Sun sail on the trial ship class 751

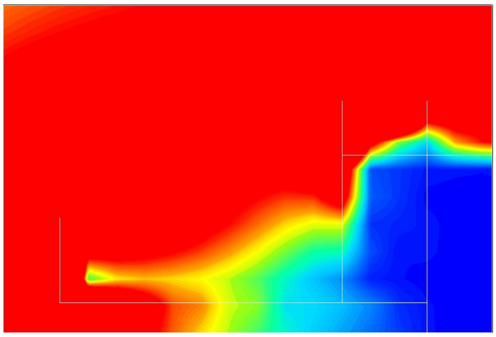

Figure 3: Bridge wing without sun sail

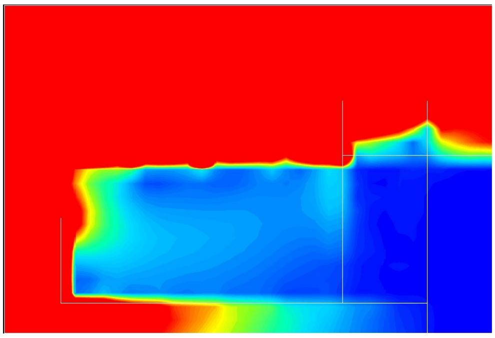

Figure 4: Bridge wing with sun sail

HPEM 5-5: Frequency Selective RF Shielding of COTS Components

H.-F. Harms
Nordseewerke GmbH Emden

1 Introduction
On modern military ships more and more low cost COTS (Commercial off the shelf) equipment will be installed in the upper deck area. Their immunity against high frequency electromagnetic fields is only specified with 10 V/m. Military components on the other hand are specified with 200 V/m.
With the multitude of transmission-antennas and high HF-power, there is nearly no place at upper deck on modern ships, where the fieldstrength is durable under 10 V/m and the COTS equipment can work interference-free.
The highest fieldstrength on ships are produced in the HF-Area from 1.5 MHz up to 30 MHz. In this frequency range the Transmitters on board have an output power of about 1000 Watts up to 1500 Watts. The wavelength is between 200 m (at 1.5 MHz) and 10 m (at 30 MHz).
In most facts the power of the transmitters and so the fieldstrength at the location of the COTS-components could not be reduced because of preconditions from the customer
However the COTS-components have to be shielded against high frequency field without impairing there function.
2 Possibilities
Most installed COTS equipment are transmitter or receiver of high frequency electromagnetic fields. Therefore a better shielding of the case (closed metal container) must be excluded. Additionally the used COTS-components should not be modified.
So, there is only the way to shield against HF from 1.5 MHz up to 30 MHz and pass higher frequencies at the same time. These higher frequency must be much higher then 30 MHz to reach a sufficient shielding.
The antennas of GPS equipment how the are installed on board in many cases are fine. There working frequency is round about 1.5 GHz (wavelength 20 cm) and consequently wide above 30 MHz.
A good shielding can only be possible with an coarsely meshed metal cage.
After a theoretical analyse an practice measurement should be done.
The analyse was done with the program CONCEPT II.
3 Shielding
The first step was to find a good shielding cage, which was build with metal rods. Because of the position on a ship, the shielding cage has to keep some values of size and weight.
The fieldstrength were observed in an Area of 10 cm $\times$ 10 cm, 10 cm above ground. This is about the size of an typically GPS-antenna. Many calculations with different cage forms (pyramids, bows, double cages,...) and sizes were done.
The best shielding reaches a cage like the cage in picture 1 with about 14 dB. The cage size is about 20 cm $\times$ 20 cm $\times$ 20 cm.
4 Radiation
The next step was to analyse the radiation diagram of the GPS-antenna inside the cage.
Naturally the cage will deform the radiation diagram, but that doesn't matter. The influence of the rods isn't vary high. When the rods are resonant, there is even a small gain.

5 Measurements
The measurements in an laboratory have to be done next to compare the analyse data with the practice. After that, the cage should be installed on a “real” ship to do some more test.
6 Summary
With a shielding cage the fieldstrength can be reduced up to 14 dB without influencing the operation of COTS equipment. This is not a large value, but the field reduction by more than four can really help to have one EMC problem less.

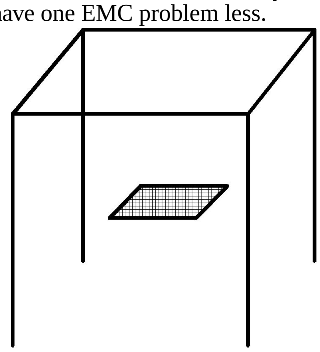

Figure 1: Shielding cage

HPEM 5-6: Practical Use of the MoM-PO Hybrid Technique in Conjunction with Feeding Structures Modelled by Impressed Current Sheets

M. Sabielny, **D. Leugner**, **H.-D. Brüns**
Technical University Hamburg-Harburg

In long-distance radio communication and high resolution radar applications antennas with high gain are necessary. In this area reflector systems are widely used as antennas. They normally achieve gains that are better than 30 dB in the microwave region. In this contribution the modelling of such antennas will be discussed. The computational method is a hybrid technique combining the Method of Moments (MoM) with the Physical Optics (PO).
For the analysis of electrically large radiators the PO has become an effective tool. Nevertheless it is inevitable to model the real physical sources exciting the reflector antennas by means of more elaborate numerical techniques such as MoM. Let us consider for example a Cassegrain reflector system. This radiating system consists of a feed horn, a hyperbolic subreflector and a parabolic main reflector. Other examples of electrically large antennas are so-called prime-focus parabolic reflector antennas. A full-wave solution of this kind of problem usually needs a lot of computer resources. Thus more advanced approaches have to be applied to predict the radiation diagrams and the gain for example.
One method of solution could be to consider the complete horn and the subreflector system as the MoM region and the rest of the structure as the PO region. However, such a simple proceeding would provide no numerical advantage, mainly because of the large MoM area interacting with the PO region (the main reflector). Taking the subreflector also as a PO region would reduce the MoM region but introduces a new difficulty. Now it is necessary to include the interaction of two PO regions, that is, the subreflector and the main reflector. At least the impact of the subreflector onto the the main reflector has to be computed. It will be shown that this can be accomplished on the basis of a pure PO approach without solving an equation system.
The number of unknowns still remains high because the simulation of the horn needs a considerable amount of unknowns. Therefore it is advantageous to introduce a further measure to reduce the computation time. In a first step solely the horn is considered in a MoM-based computation. By electric and magnetic currents in the cross-section at the back end of the horn one can generate fields of a given modal structure. The feeding waveguide does not need to be lengthened in order to suppress higher order modes. A conventional excitation, for example a small dipole at the rear part ot the waveguide feeding the horn, does not offer this possibility. Moreover a dipole in a waveguide excites fields that propagate in both directions whereas electric and magnetic sources can generate modes of a given direction.
After the MoM computation of the horn section the electromagnetic fields are computed in the aperture plane and are again converted to magnetic and electric surface currents. These equivalent currents are ready to be used as an excitation source for a pure PO simulation to be carried out in the second step. Modelling rules for analyzing reflector antennas by means of the described method will be given.

HPEM 5-7: Time Domain Model for ELF Radio Noise

A. P. Nickolaenko
Usikov Institute for Radio-Physics and Electronics, National Academy of Sciences of the Ukraine

The model for extremely low frequency (ELF) electromagnetic noise is suggested. Natural radio signal at ELF (the ELF band occupies the range from 3 Hz to 3kHz) is a composition of overlapping electromagnetic pulses arriving from the global thunderstorm activity. Owing to the small attenuation rate, all the thunderstorms worldwide contribute to the radio signal observed at arbitrary field site. The report presents a numerical model for such a signal. The model is effective being based on the direct time domain ELF solution with accelerated convergence.
The code computes the waveform of individual pulsed signal for the given source - observer distance. These individual pulses arrive to the observer from random independent lightning strokes, overlap, and thus yield the continuous ELF noise. It is supposed in the particular model that lightning activity is uniformly distributed on the globe within a given area. The amplitude distribution of pulses is the Gaussian one, and the pulses in time form a Poisson succession of a given rate. The standard software generates quasi-random numbers with the above distributions.
We demonstrate that model explains many known experimental properties of the ELF radio signal. In particular, the temporal stabilization of its spectral estimates is obtained, etc. The code itself is a useful tool for the modeling of experimental data. It enables to solve the inverse problems by comparing the experimental data with the model results computed for different sets of parameters. The waveform generated by the soft might be also used in calibrations of the experimental equipment with the noise of the fixed ’standard’ properties.

HPEM 5-8: A Network Formulation of the Power Balance Method for High Frequency Coupling Mechanisms

I. Junqua, **J.-P. Parmantier**, **F. Issac**
ONERA/DEMR/CDE

Although the coupling of an electromagnetic (EM) wave with any system can be theoretically computed thanks to Maxwell’s equations, this classic approach may become tedious and unsuited in the case of high frequency incident electromagnetic environments. To cope this problem, for a few years some articles dealing with a method, that will be called Power Balance (PWB) in this paper, have been published (references listed in Interactions Note 576 ‘A network formulation of the PWB method for high frequency coupling mechanisms’I. Junqua, J-P. Parmantier & F. Issac, November 2002). Based on macroscopic concepts of transfer of energy at high frequency, its objective consists in developing a simple approach to estimate EM constraints induced by a high frequency threat on any system. The main assumption is that the system under test must be large compared to the wavelength of the electromagnetic threat so that the internal electromagnetic environment can be modeled by probabilistic laws such as in mode stirring chambers.
Under this assumption, one will derive the fundamental equations of the PWB approach from the definition of coupling cross sections and quality factors and the conservation law, saying that the power transmitted in a cavity is equal to the sum of dissipated powers.
After introducing the concepts of combined waves (as a linear relation between dissipated power and power density), we show

how the BLT formalism (commonly used in Electromagnetic Topology) can describe high frequency EM coupling. Thus, the organization of the calculations may be based on an interaction diagram sequence, which follows the running of the power transferred into the cavities. Any network oriented computer code may be used to solve this EM problem with the PWB approach. However, with the idea of extending this approach with EM topology concepts, a code solving the BLT equation is more appropriate. This is the reason why the CRIPTE code, developed by ONERA and initially devoted to compute coupling mechanisms on multiconductor transmission lines networks, has been chosen.

Finally, the capability of the PWB approach to estimate high frequency coupling mechanisms has been shown on a simple object, a two-cavities cylindrical system. The EM environment in one of the cavity when the other is excited by a transmitting waveguide is estimated by the PWB and compared with measurements (Fig 1). The experimental configuration consists in measuring the S21 parameter between two waveguides for each position of a mechanical stirrer inserted in one cavity. Measurements are finally processed to extract the mean and the variance of S21 over a complete rotation of the stirrer.

It has been demonstrated how easy it is to implement this technique by using a network formulation. Its main interests are its rapidity of computation, the fact that it does not require an accurate description of the system geometry and, finally, the fact that it is only based on analytical formulas. The network formulation of the PWB approach is very promising since it should enable to process complex large systems at high frequency. However, the approach being based on statistics, its application depends on the type of objective aimed when solving the EM problem.

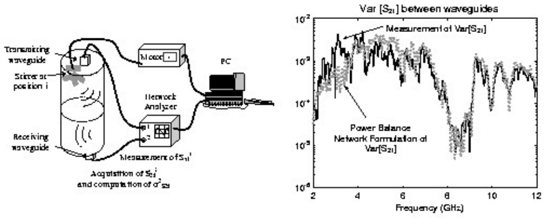

Figure 1: Application of the PWB approach to a cylindrical two-cavities structure

HPEM 5-9: Block Operations Within the MOM

N. Baganz, K.-H. Gonschorek
Dresden University of Technology, Chair of Electromagnetic Compartibility, 01062 Dresden, Germany

Within the current computation by the method of moments the coupling impedance matrix Z plays a very important role. The elements of Z-matrix are integrals which need a lot of FLOPs for their calculation. If more computations of similar systems are necessary it is possible to reduce the computing time by dividing the impedance matrix in blocks and recycle the elements.

This is only one part of the strategy for treading geometrical changes, the whole algorithm is outlined in the article "Reducing the efforts for computing the inverse of the coupling impedance matrix by block gauss algorithm in the method of moments (MOM)" ("Reduzierung des Rechenaufwandes zur Ermittlung der Inversen der Koppelimpedanzmatrix der Momentenmethode mittels Block-Gauß-Verfahren", EMV 2004 Düsseldorf)which will be referred later in this abstract as [1]. The mathematical background of the procedure, the consideration of the complexity and a numerical example are part of this publication, unfortunately the comparison of the numerical results with measurements have not been shown in this article. The aim of this presentation is to demonstrate the advantages by the help of two examples. The first explored application, see Fig. 1, consists of a loop (static part) and a short wire (dynamic part). The dynamic part is placed at the positions P1-P4 of the ground plane successively and, the currents are calculated for all five positions.

In Fig. 2 the linear system of equations (equation (1)), including the coupling impedance matrix, is shown which has to be solved for every position. A comparison of the coupling impedance matrices of every position shows that a division in four parts is possible. This block structure of the coupling matrix (see [1] for details) can be used for reduction of CPU-time. The self-coupling for the wires is the same in every step, so these parts of the coupling matrix can be recycled. Also the short wire which changes only it's position is always the same. Therefore only the coupling from the static (loop) to the dynamic is modified. The new algorithm needs a 0. step for the preparation of the calculation results, which will later on be reused. This step can be called initialisation step. For example the LU-decomposition of the matrix part which represents the self-coupling of the loop (static part) can be calculated in that step. The system of linear equations for the currents can than be transformed in a sparse linear equation system (see equation 2 of Fig. 2) and can thereby be solved with lower effort of time. This transformation has to be executed five times in the specified example. The recycled LU-decomposition is a main part of the coupling impedance matrix. A part of the results is shown in Fig. 3 and 4. The detailed discussion for all frequencies and positions will carried out with the presentation. A second example will be discussed in detail. Both examples will demonstrate the flexibility of the proposed procedure.

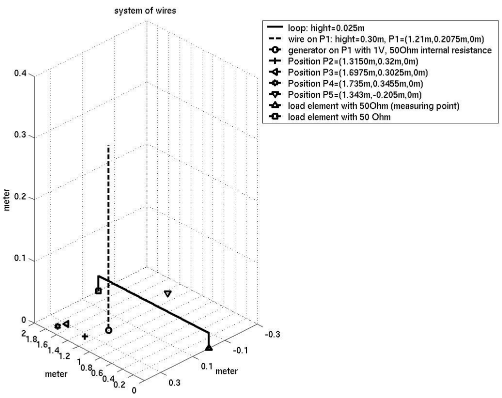

Figure 1: System of wires

U_l ... voltage sources of the loop

U_s ... voltage sources of the short wire

Z_0 ... coupling impedance matrix from loop with LU-decomposition ($PZ_0 = LU$)

$I_0 = Z_0^{-1} U_l$ ... currents without short wire

$$Z\begin{bmatrix} I_1 \\ I_2 \end{bmatrix} = \begin{bmatrix} Z_0 & Z_1 \\ Z_2 & Z_3 \end{bmatrix}\begin{bmatrix} I_1 \\ I_2 \end{bmatrix} = \begin{bmatrix} U_l \\ U_s \end{bmatrix} \quad (1)$$

Solution:

$$I_2 = (Z_3 - Z_2 Z_0^{-1} Z_1)^{-1}(U_s - Z_2 I_0)$$

$$I_1 = I_0 - Z_0^{-1} Z_1 I_2$$

Linear system of equations with spars matrix:

$$\begin{bmatrix} Z_2 & Z_3 \\ U & L^{-1}PZ_1 \end{bmatrix}\begin{bmatrix} I_2 \\ I_1 \end{bmatrix} = \begin{bmatrix} U_s \\ L^{-1}PU_l = UI_0 \end{bmatrix} \quad (2)$$

Figure 2: Background formulas

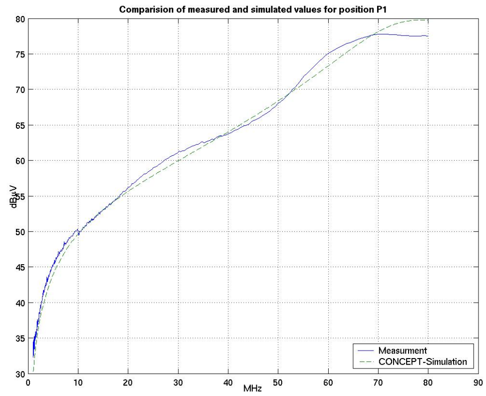

Figure 3: Voltage across a 50Ohm-load element calculated with CONCEPT compared with measured values for position 1

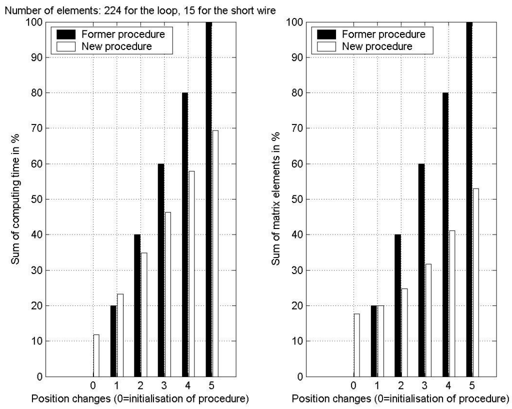

Figure 4: Comparison of CPU time (a) and number of elements with respect to the new and former algorithm as a function of position changes (0 = initialisation of the new procedure)

HPEM 5-10: Computational Radiated-Susceptibility Analysis on the Printed-Circuit-Board Level

M. Leone
Siemens AG, Corporate Technology, Erlangen-Germany

The radiated susceptibility of a printed circuit board (PCB) can essentially determine the vulnerability of an electronic system to an external electromagnetic field. Besides unintentional electromagnetic disturbances as given in an industrial environment or in the vicinity of a transmitting station, special importance is paid to the threat from an irradiation of a transient electromagnetic pulse like NEMP or high-power microwave (HPM).

The coupling of an external electromagnetic field into the circuitry on a PCB mainly occurs through the trace interconnections, which behave as receiving loop antennas. If the excitation frequency is sufficiently high, or equivalently, the trace sufficiently long, transmission-line resonances occur, incrasing the coupling efficiency to a maximum. At the ends of the traces the coupled energy is either directly delivered to the input of a component or proliferated within the circuit on the board. Consequently, partial functional failures or even irreversible damages can occur, depending on the signal shape and amplitude.

An experimental investigation under realistic conditions gives the possibility to definitely determine the degree of the radiated susceptibility of an electronic system. However, it is rarely possible to get a clear indication to what specific coupling phenomenon the susceptibility is due to. In order to prevent a pure trial-and-error approach, a more systematic strategy for identifying and eliminating the unknown coupling is to include complementary computational analysis and simulation in addition to measurements.

This paper presents a suitable numerical simulation method for the coupling of external electromagnetic fields to PCB traces. As an example, Fig.1 shows a trace net, which is exposed to a transient plane wave field (Ei) with NEMP characteristic. Computation was performed with the Method-of-Moment (Concept), using a numerically efficient equivalent thin-wire approach. The simulation allows to determine the coupled voltages and currents at any point on the structure, for arbitrary external electromagnetic field. The simulated terminal voltage response in Fig.2 is normalized to an excitation field strength of 1V/m (right y-axis). The oscillatory behavior is due to the multiple reflections between the trace ends. Scaling the negative peak value to a typical excitation amplitude of 50 kV/m yields a peak voltage-response magnitude of about 10V, which is high enough to damage the input of a semiconductor device.

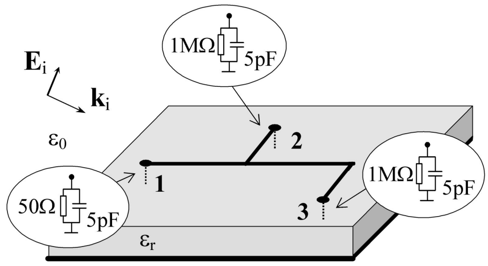

Figure 1: Simulation example of a trace net irradiated by an external NEMP field

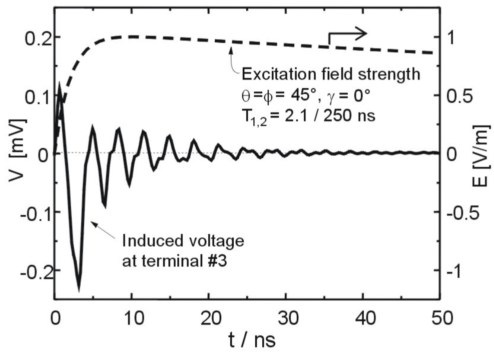

Figure 2: Simulated voltage response at terminal #3, normalized to a unit excitation amplitude (right axis)

HPEM 5-11: EM-ANN Usability and Efficiency on Connector Modeling

A. Arnaud[1], **M. Drissi**[2]
[1]*Thales*; [2]*IETR CNRS UMR 6164 Insa Rennes*

Abstract - This paper propose a new approach in modeling process by using electromagnetic – artificial neural network (EM-ANN) to model 3D complex structure like industrial connector (2mm- hard metric). These latter are configured for high speed signals and for differential pair signals with different ground return shields. Conducted and radiated phenomenon are tacken into account in the modeling process for a fully integration in electrical simulator. The propose solution use the artificial neural network capability to prevent and manage signal integrity problems.

Summary - Modeling for high speed interconnection is a challenge in signal integrity domain. Different methods are proposed to define an accurate model to use in electrical simulator. These methods can be derived from experimental measurements, from EM simulations or from combination of these two latter. In electrical simulator, the model representation can be adapted in function of desired accuracy, in function of computing time in

simulation. Modeling with discrete RLGC elements can be performed in Pi or T description. This method is not a wideband modeling but the computing time is really short. In an other way, behavioural modeling with polynomial description is an accurate method for a wide band approach but requires a large computation time (numerical inversion of Laplace transforms NILT), which is not acceptable when structure are complex. To find a compromise is necessary. Also, reduced order algorithms or a ladder network approach are actually in study to optimize electrical models.

An other approach makes use of artificial neural network in complex interconnection modeling process. Previous study has covered this subject with MLP (Multi Layer Perceptron) for CPW strip, via and multilayer coupled lines modeling. One observes the EM-ANN interest with a lower simulation time in comparison to models issued from EM simulations.

The proposed solution is to develop models based on ANN representation in which input parameters distinguish different 2mm hard metric connectors. For high speed applications, industrial connectors are defined with differential pair signals and shielding configurations. The physical connector (pin separation, contact design, housings materials) description is fixed and electrical characterisation is mainly determined (propagation delay, characteristic impedance, line loss).

Meanwhile for an accurate full electrical characterization tacken into account crosstalk, housing format, shielding structure and signal/ground ratio are necessary. ANN output is the scattering 4 by 4 S-parameters to cover the use of differential pair.

A previous work has been enabled to extract connector data (Scattering S-parameters) from experimental measurements and EM simulations using finite elements. This step is significant in an EM-ANN approach to feed neural network training with data samples.

An example is described on figure 1 with an elementary connector configuration with a full shielding structure around active differential pair lines. Electromagnetic simulation is performed with 3D field solver based on finite elements. The spectrum bandwidth is chosen in function of high speed signals rise/fall time fixed to an equivalent of 1Gbit/s. The study frequency bandwitdh is fixed to 1GHz – 10GHz.

EM-ANN usabilty and efficiency are discusting in this paper. ANN model will be developped arround MLP or radial basis networks. Other 2mm hard metric connector topologies are defined in function of input parameters defined previously. The sample data processing from EM simulation are validated by measurement results for several configurations. The ANN will be presented in the final paper.

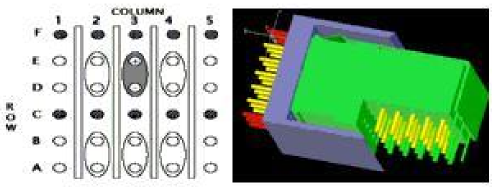

Figure 1: 2 mm hard metric connector (Right angle female and verticale male header) with differential pairs and shielding configurations.

HPEM 6 - Electromagnetic Topology

HPEM 6-1: Modes of Curved Waveguide Structures

C. Courtney, **D. Voss**
Voss Scientific

There is considerable interest in antenna and transmission line structures that are conformal to curved and cylindrical surfaces. In this paper we will describe two geometries that may be useful for a variety of conformal antenna and high power applications. The first geometry of interest is the double-baffled, coaxial transmission line (Encyclopedia of Physics, ed. S. Flugge, pg. 345, Springer-Verlag, Berlin, 1958), defined by inner and outer radii, and an arc length. The modes of such a structure have recently been derived (C. Courtney and D. Voss, "Modes of a Double Baffled, Cylindrical, Coaxial Waveguide," SSN 483, 2003) and conformal antenna concepts formulated. The second structure is known as the azimuthally propagating, truncated, coaxial transmission line, and is defined by inner and outer radii, and an axial length. This structure has transmission line and power distribution applications. In this paper we present the derivations of equations that describe the TE and TM, propagating modes of each structure. First, the characteristic equations that define the cut off frequencies of each mode are derived. Then the electric and magnetic fields of each mode are explicitly expressed. To show the use of the derived equations the lowest order TE and TM mode cutoff frequencies are computed and graphs of the normalized field components are presented for example geometries. Finally, we will close our presentation with examples of the use of these structures in power distribution and antenna systems.

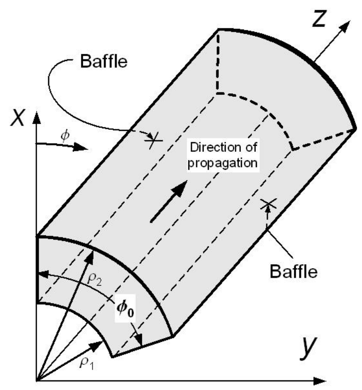

Figure 1: The double baffled, coaxial waveguide, is conformal to curved cylindrical surfaces.

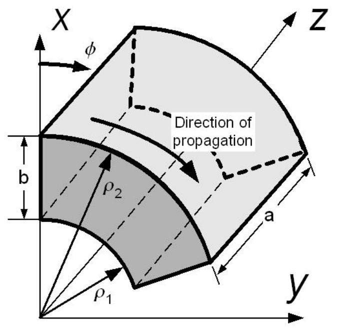

Figure 2: The azimuthally propagating, truncated, cylindrical, coaxial waveguide is defined by inner and outer radii, and a depth a.

HPEM 6-2: The Use of Distributed Ground Plane to Achieve EMC – A Practical Example

G. Undén[1], **S. Garmland**[2]
[1]*Defence Materiel Administration - FMV, Linköping, Sweden (goran.unden@fmv.se)*; [2]*Emicon AB, Lund, Sweden (sven@emicon.se)*

In the presentation we will give a practical example of how the electromagnetic environment in a complex facility can be improved by simple means. The basic idea is to use a distributed ground plane which is constructed by using existing metal parts in the facility. The presentation will mainly be focused on the practical realization and how to achieve a good EM topology in a complex system. The theories will be covered in an accompanying paper by T. Karlsson.

A good EMC practice is to make use of all present metallic parts in order to take advantage of their shielding properties. In this way a better electromagnetic environment can be achieved, practically without any extra cost. Examples of components in a

facility that can be used are ventilation drums, steel beams, reinforced concrete and rack-mountings. Such metallic parts should be bonded together to form a low-impedance grounding system. For low frequencies, this grounding system will reduce the potential difference between different parts in the installation. Even for higher frequencies such a grounding system is likely to give a cost effective shielding. To take advantage of the distributed ground plane it is also important that the installation of electronic equipment and cables as close as possible follow it.
When a distributed ground plane is to be created, parts in the installation that have no ground plane must first be identified. Such parts should be given a ground plane e.g. by attaching sheet metals in order to increase the shielding. Also cable trays should be used as a part in the distributed ground system. Even better is to provide the cable trays with vertical sides and best of all with lids as to create a totally surrounding shield.
A good basis for a distributed ground plane can often be found in existing facilities. Cables are normally placed on cable trays, equipment are mounted in metallic cabinets or at least rack mounted etc. Therefore, it is often possible to create, with rather simple complements, a distributed ground plane. In creating the ground plane it is important to make it continuous and make it cover the whole installation, i.e. cover all equipment and all interconnecting cables. The distributed ground plane will then be the metallic part of the boundary to a protected zone. As in all zone boundaries, it is necessary to take care of all cables entering or leaving the zone. All cable shields shall be connected to the ground plane and unshielded cables shall be supplied by transient protectors and/or filters bounded to the ground plane.
In the presentation a practical example of a small Swedish telecom facility with a zone boundary built by a distributed ground plane will be shown. Practical constructions will be illustrated by many pictures and the shielding effectiveness will be shown by measurement results.

HPEM 6-3: Ground Planes in a Controlled Electromagnetic Topology.

T. Karlsson
Emicon AB, Lund, Sweden

This presentation is about the use of ground planes in any kind of electromagnetic topology, may it be for protection against electromagnetic terror attacks or for achieving high reliability in critical electric systems or simply for decent EMC in any equipment. Countless number of contributions by Carl Baum has demonstrated the importance of a controlled electromagnetic topology. The role of the ground plane in this context was explained in (T Karlsson, "The topological concept of a generalized shield", AWFL Interaction note 461, 1988). In this talk it will be described how a shielding efficiency can be achieved for an installation close to a ground plane, and how the ground plane will be integrated into the system topology as part of a generalized shield.
The shielding effect of a ground plane is based on the well-known fact that the electric field vector parallel to the metallic surface and the perpendicular magnetic field vector both approach zero close to the surface. The currents induced by an external field into a circuit parallel to the ground plane will accordingly be negligible when the circuit is sufficiently close to the ground plane. Another positive effect of a proximate ground plane is that the field, which accompanies the circuit currents, is concentrated to a narrow volume between the circuit and the ground plane. This effect reduces the coupling between different circuits.
One can imagine a generalized shield at a certain distance from a circuit that is close to a ground plane. A ground plane that supports a cable bundle can be modelled as a two-dimensional case. From the geometry data the diameter of the generalized shield can be calculated for a given coupling requirement.
One ground plane may support more than one cable routing, in which case the coupling between two or more parallel circuits close to the ground plane must be considered. In such a case also the characteristics of the complete circuitry, with their end terminations, have to be included in the analysis.
The shielding efficiency can be improved by adding another ground plane on top of the circuitry. This will cause the external parallel electric field component between the two ground planes to decay exponentially from the edge toward the center of the ground plane. Still there will be a perpendicular electric field component that, due to the exponentially decreasing parallel component, rather soon will dominate the field coupling to the shielded circuitry. To mitigate this effect we can connect the two ground planes around the edges. This connection will function like a gasket, the requirement of which can be calculated from the geometry data.
It will always be useful for a system designer to understand the important properties of ground planes. Ground planes can be used as tubes between volume shields, which are boundaries to the same topological volume. In some cases sufficient shielding can be achieved by a ground plane, which may replace a volume shield in order to save cost and improve the logistics. This kind of distributed ground plane solution has been used with good results in Sweden. An accompanying paper (G Undén and S Garmland," The use of distributed ground plane to achieve EMC – A practical example.") gives more details about that.
We all know that ground planes have been used for a long time in almost all electronics design and allow for good functionality and immunity to disturbance. Electronic engineers construct a perfect electromagnetic topology in their systems – many without knowing anything about topology. They don't have to understand it; they know how it works anyway. But the topological view can give an extra possibility to get an overview of large systems and a possibility to find the right specifications for different subsystems.

HPEM 6-4: Stochastic Model of Electromagnetic Wave Propagation and Absorption in Turbulent Flow of Slightly Ionized Plasma

V. G. Spitsyn
Tomsk Polytechnic University, Department of Computer Engineering

The purpose of this paper is exploration of the process of electromagnetic wave multiple interactions with moving turbulent inhomogeneities in the absorbing flow of slightly ionized plasma. The method of solving this problem is based on the stochastic modeling of wave interaction with random discrete media [1, 2]. In paper [3] is considered the propagation of wave with arbitrary frequency spectrum in the turbulent flows with inhomogeneous profile of velocity turbulence. Here is investigated the transformation of frequency spectrum of electromagnetic signal propagating through turbulent flow with resonance absorption. This flow is characterized by inhomogeneous profile of velocity and concentration turbulences of slightly ionized plasma.
There is assumed that the wavelength of the wave is less than the sizes of the turbulent flow and incoherent scattering occurs on statistically independent discrete inhomogeneities. The oscillator of electromagnetic signal is presented as a source of photons with corresponding diagram of radiation. The initial coordinates of photons are assigned in the point of oscillator disposition. The type of wave interaction with discrete inhomogeneities is determined according to set cross sections of scattering and absorption. In case of fulfillment of a wave scattering condition the direction of photon propagation changes to in accordance with specified indicatrix of discrete inhomogeneities reradiation. If photon is emerged outside of flow there is occur the memorization of frequency and direction of photon moving.
Here is considered the source of electromagnetic signal, which disposed in the center of Cartesian coordinates system on the surface of a flow. There are presented the results of transformation frequency spectrum of incident wave with three Gaussian components in the flow with inhomogeneous profiles of velocity and concentration of turbulences. The frequency spectrum of incident wave, which consist of the three Gaussian components, is presented in the Fig. 1.
The computation results of angular and frequency spectrums of scattering signal are presented in the Fig. 2 - Fig. 4 for case of propagation wave across the axis of flow. The value of dimen-

sionless Doppler shift of frequency [1, 2] and the scattering angle, calculated from the direction of incident wave propagation, are presented in the horizontal plane in indicated figures. The energy of scattering signal, which is normalized on the maximum of energy for case of multiply scattering signal, is calculated by the vertical axis in this figures.

The results of computation are presented in the Fig. 2, Fig. 3 for the next meanings of parameters [1, 2]: parameter, describing a degree of inhomogeneous of the flow velocity μ =0,05; parameter, describing a degree of inhomogeneous of the flow concentration η =0,01; coefficient for define of middle track length of photon λ=0,005. In the Fig. 2 is presented the angular and frequency spectrum of scattering signal, which received for case of multiply signal interaction with turbulences. In the Fig. 3 is presented the results of signal propagation in the flow for case of single scattering signal on the turbulences. In Fig. 2 we can see more strong effect of resonance absorption on the frequency equal to 1,4 in comparison with Fig. 3. In addition to in Fig. 2 we have a filling of space between the maximums of three Gaussian components. This fact is explained by the large significant of effect of multiply signal interaction with moving turbulences.

The computation results of angular and frequency spectrums of multiply scattering signal are presented in the Fig. 4 for the next meanings of parameters: μ = 0,05; η = 0,01; λ = 0,01. We can do the conclusion about decreasing of filling the space between maximums of three Gaussian components in Fig. 4 in comparison with Fig. 2. In addition to in Fig. 4 (in comparison with Fig. 2 and 3) we can observe the appearance of positive energy of signal for angle of scattering $< \pi/2$.

In this paper has been considered the propagation of electromagnetic wave with frequency spectrum in a view of three Gaussian components through a plane-parallel turbulent flow with resonance absorption. On the base of receiving results analysis we can do the conclusion about large significant of effect of multiply photon interaction with moving turbulences, which lead to filling of space between the maximums of three Gaussian components of scattering signal frequency spectrum.

References

[1] V.G. Spitsyn, Development of a numerical model concerning electromagnetic wave propagation in turbulent flows, Journal of Applied Electromagnetism, Vol. 1, No. 2, 1997, pp. 67-78.

[2] V.G. Spitsyn, Modelling of radiowave scattering on the ionospheric plasma disturbances, created of space vehicle, Tomsk: Publishing House “STT”, 2002.

[3] V.G. Spitsyn, L.N. Kudryashova, A.A. Yakimchik, Modelling of electromagnetic wave propagation in the two turbulent flows of slightly ionized plasma, Scientific Computing in Electrical Engineering - Book of Reviewed Abstracts of 4th SCEE Conference, Eindhoven, The Netherlands, Publisher: Stichting SCEE, 2002, pp. 177-178.

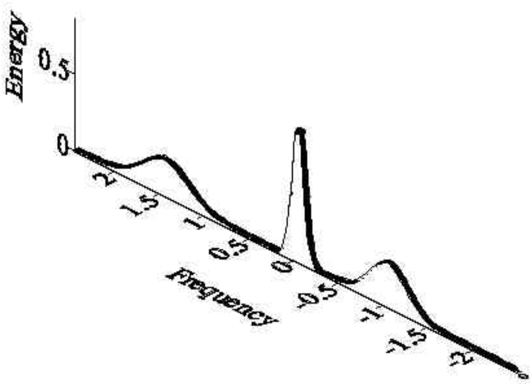

Figure 1: The frequency spectrum of incident wave

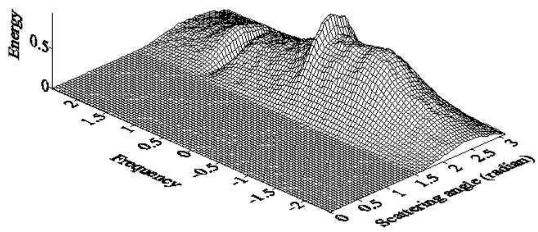

Figure 2: The angular and frequency spectrum of multiply scattering signal (μ = 0,05; η = 0,01; λ = 0,005)

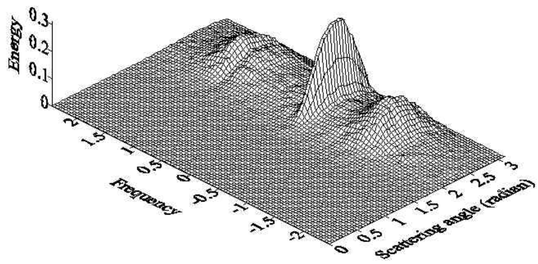

Figure 3: The angular and frequency spectrum of single scattering signal (μ = 0,05; η = 0,01; λ = 0,005)

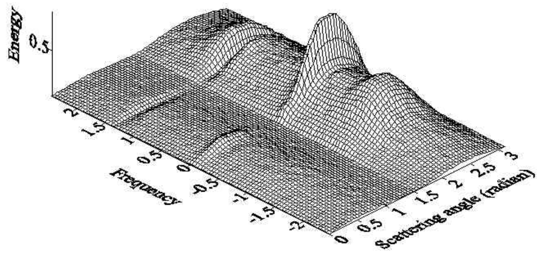

Figure 4: The angular and frequency spectrum of multiply scattering signal (μ = 0,05; η = 0,01; λ = 0,01)

HPEM 6-5: Path Loss Prediction in Urban Environment Using a Neural Network Approach

G. Cerri, **R. D. Leo**, **S. Pennesi**, **P. Russo**
Universita’ Politecnica delle Marche, Istituto di Elettromagnetismo

Propagation models used for planning wireless networks have to be able to produce good values for path loss in a very short time. These models are generally subdivided into two categories: empirical, where a formula is obtained from measurement data, or deterministic, where the expression of the field is calculated by the Geometrical Theory of Diffraction (GTD). Both these strategies suffer of inconveniences: while the first one is often not accurate enough, the second one has an excessive computational burden.

In order to have a fast and accurate method, this paper presents a new way to approximate this function, based on Artificial Neural Networks (ANN). The inputs for the ANN are characterised using a numerical technique based on ray-tracing. In this way the accuracy of the ray-tracing technique and the speed of a Neural Network approach are combined together. Moreover the use of a numerical technique, instead of a measurement campaign, for the training procedure assures the generalization of the network. The whole attenuation of the signal between two points can be written as the sum of the attenuation due to the space loss, and the antenna gains, (L0), and a term (La) that takes into account

the presence of the buildings, and their interference in the communication link. This term is a non-linear function whose input variables contain information about transmitter, receiver height and the database of the city under examination and whose output variable represents the predicted loss.
The ANN model, employed for the evaluation of the La term, is the well-known Feedforward Multilayer Perceptron (FLP), used as a universal approximator.
The input parameters are chosen considering a ray propagation, and supposing that the value of the field at the receiver is mainly determined by some dominant paths: the direct ray, the reflected ray from the ground, the two dominant reflected rays arriving to the receiver after reflections from vertical walls, and the ray diffracted by the last rooftop or by vertical edge depending on the relative position between transmitter and receiver. Taking into account the geometrical theory of diffraction, the Neural Network has been fed with 27 inputs: 4 inputs characterizing the direct ray, 3 inputs characterizing the reflection given by the ground, 12 inputs characterizing the two main rays reflected once by the vertical walls of the buildings, 5 inputs characterizing the ray arriving to the receiver after a diffraction, and 3 additional inputs related to the difference of phase between different paths. Example data for network training were collected by running many times an experimented 3D ray tracing software, "Armonica", provided by the University of Bologna and the fast fading effect was afterwards eliminated by averaging.
We trained an ANN composed by two hidden layers, the first of 10 and the second of 20 neurons.
As a validation of the network we applied it to a building configuration that was not included in the example set used for the network training. Considering several cases, we found that values calculated by ANN, considering areas approximately of 400x400m, averagely differ of less then 1 dB by the averaged values provided by "Armonica", which means that the ANN has reached a good level of generalization.
The results of the comparison between Armonica and the ANN for several cases will be presented at the conference.

HPEM 6-6: To Estimation of RI Appearance at the Receiver Input

V. B. Trigubovich, **V. A. Losich**
BelMAPO, Informatics dept., lecturer

One of the most important problems of modern radioelectronics is the problem of signal selection and separation in presence of radio interferences (RI). It is well-known, in the UHF range the distance is used to separate one RF communication system from others (direct visibility range). In cellular communication, more over, we can find elements of "distance separation" of signals. It enables us re-using of EM resource in frequent, temporal and spatial domains. The aim of the article to be presented is to estimate possibility of development of theory for "distance separation" .
Consider following situation. Let N RI sources are placed in some area of space with linear sizes limited by the range Rmax. The EM environment model is characterized as follows. Power of RIs has probability density function (PDF) w(P). The range from separate transmitters to "our" receiver is distributed with the law w(R). The amplitude range D=Pmax/P0 of interfering power as well as receiver's threshold level P0 are important parts of model to be discussed (A. F. Aporovich: Statistical theory of the radio system's EMC. – Mn.: Nauka publ., 1984, 215 p. (In Russian). One should estimate attenuation of RIs at propagating along trace transmitter-receiver, or the same, to find number Nin of RIs at the receiver input. If a general number N of RI sources is known, we can estimate average number RIs at the receiver input as Nin=NB, where B is the probability of excess by interfering signals of receiver threshold P0.
Similarly, the decision of the given problem as the statistical problem may be reduced to definition of PDF w(Pr) of interference power at the receiver input in view of PDF w(Pt) of transmitter power Pt and PDF of RI sources w(R).
We suppose that the attenuation of signals in view of distance separation is equivalent to out-of-band signal attenuation of second-order linear filter and attenuation ("range filtering") may be taken into account by a factor proportional to 1/(R*R).
In the complete research the problem of definition of probability B of RI incoming at the receiver input has been solved. The dependences of probability B on EM environment parameters have been obtained. New approach to estimation of signal separation by using distance has been discussed. The problem of optimization of limited EM resource is also discussed.

HPEM 7 - Biological Effects and Medical Application

HPEM 7-1: Immunomodulating Effect of Low Intensity Laser Irradiation

D. A. Cherenkov, **O. V. Glushkova**, **O. A. Sinotova**, **A. N. Sultanova**, **E. G. Novoselova**
Institute of Cell Biophysics of Russian Academy of Sciences

Low intensity laser irradiation is widely use in medicine, but mechanism of its effect on cell activity is not enough known. Among others, immune system is very sensitive to external factors, and in this regard the investigation of laser effect on the immune system is very important.
The aim of present work was to study low intensity laser radiation (λ=633 nm, 1 $\mu W/cm^2$) effects on interleukin 2 (IL-2), interleukin 3 (IL-3), tumor necrosis factor (TNF) production, and natural killer cell (NK) activity. The peritoneal macrophages, T-lymphocytes, and NK cells from mice spleen were exposed to laser light in vitro.
Male mice NMRI weighing about 25 g were used in experiments. Interleukin concentration was measured by immunoenzyme method. Macrophages TNF production was measured by cytotoxic activity assay using TNF-sensitive cell line L-929. NK cell activity using K-562 as target cells was measured by radioisotope method.
The increase of IL-2 and IL-3 production in splenic T-cells was observed after 1 min exposure to laser light. There were no significant changes in production of these cytokines after shorter (5 sec) or longer (3 min) exposure time. Exposure of both LPS-stimulated and untouched macrophages during 5 sec, 30 sec, 1 min and 2 min decreased TNF production. The amplitude of suppression of TNF production induced by laser radiation was in direct relation with the exposure time. Cytotoxic NK cell activity was significantly decreased only after 3 min exposure.
Thus, considerable immunosuppression followed by low intensity laser irradiation in vitro has been found. The significant changes in the cytokine production and NK cell activity had been observed, and what is more important, the direction as well as amplitude of laser effects was up to exposure time.

HPEM 7-2: The Effects of 910-MHz Electromagnetic Field on Rat Brain Collagen Fibril Architecture

M. Tzaphlidou[1], **E. Fotiou**[1], **N. V. Korovkin**[2]
[1]*Medical Physics Laboratory, Medical School, Ioannina University, Ioannina, Greece*; [2]*Institut for Fundamental Electrical Engineering and Electromagnetig Compatibility (IGET), Otto-von-Guericke-University, Magdeburg, Germany*

The aim of this study was to investigate possible effects of 910-MHz electromagnetic radiation on rat brain collagen fibril architecture. In the experiment, 32 Wistar rats were used. Sixteen animals were males 16 months of age and the rest females 5 months of age. Half males and females were exposed for 2 h per day for 30 consecutive days to radiation at 910-MHz. Half animals were sham-exposed and were used as controls. The irradiation set-up used, consisted of a CW electromagnetic generator with a maximum power output of 2.2 W and a dipole $\lambda/2$ antenna. Each time, four rats were exposed placed per two in two plexiglas cages. Rat cages were placed 5 mm away from the transmitting antenna from both sides, in order to ensure a near field and equal exposure of the animals. Dositometric analyses were performed through SAR. SAR was calculated by the FDTD method and the maximum value was found to be 0.42 W/kg averaged over 10g of tissue. Rats in groups of four were sacrificed 1 day and 2.5 months after the end of the experiment. Their brain was removed and arachnoid as well as dura mater were gently teased from the surface of the brain and the internal surface of the skull. The isolated menigiel material was prepared for further analyses as previously described (M. Tzaphlidou, J. Trace Elem. Exp. Med. 26:17-26, 2003). The axial periodicity of collagen fibrils was measured using an image processing method (M. Tzaphlidou, Micron 32:337-339, 2001) which was based on the periodic variations in intensity along the fibril. The mean value for control males is 54.4+2.8 nm and for females 56.2+2.9 nm. For the exposed animals 56.5+4.6 nm and 55.2+3.0 nm respectively. Statistical analysis shows that the values do not differ significantly (p>0.5) indicating that 910-MHz electromagnetic radiation has no effects on the axial periodicity of rat brain collagen. Thus we may conclude that in exposed material the triple helices themselves from which the collagen molecules are made up do not stretch and there is no sliding of the triples helices relative to each other. Staining patterns of control and exposed fibrils were further studied by fractal analysis. No statistically significant difference (p>0.5) between the treated and untreated patterns was found. As one of the main features represented by these patterns is the charge distribution along the fibril, the results from fractal analysis may indicate that no differences in charged amino acid composition occur between the control samples and those from rats exposed to 910-MHz electromagnetic radiation.

HPEM 7-3: The Effects of 910-MHz Electromagnetic Field on Rat Brain Collagen

M. Tzaphlidou, E. Fotiou
Medical Physics Laboratory, Medical School, Ioannina University, Ioannina, Greece

The aim of this study was to investigate possible effects of 910-MHz electromagnetic radiation on rat brain collagen. In the experiment, 48 Wistar rats were used. Thirty two animals were males half of them 5 months old and the rest 16 months of age. Sixteen experimental species were females 5 months of age. Half males and females were exposed for 2 h per day for 30 consecutive days to radiation at 910 MHz. Half animals were sham-exposed and were used as controls. The irradiation set-up used, consisted of a CW electromagnetic generator with a maximum power output of 2.2 W and a dipole λ/2 antenna. Each time, four rats were exposed placed per two in two plexiglas cages. Rat cages were placed 5 mm away from the transmitting antenna from both sides, in order to ensure a near field and equal exposure of the animals. Dositometric analyses were performed through SAR. SAR was calculated by the FDTD method and the maximum value was found to be 0.42 W/kg averaged over 10 g of tissue. Rats in groups of four were sacrificed 1 day and 2.5 months after the end of the experiment. Their brain was removed and arachnoid as well as dura mater were gently teased from the surface of the brain and the internal surface of the skull. The isolated menigiel material was prepared for further analyses as previously described (M. Tzaphlidou, J. Trace Elem. Exp. Med. 26:17-26, 2003). Considerable structural abnormalities in collagen fibrils were not detected with the exception of two cases, i.e. in males, at both ages when they were sacrificed 2.5 months after the end of the experiment. In these two cases irradiated collagen fibrils had a decrease in mean diameter compared to normal with a variability in width, with the former having a peak between 40 and 70 nm and the latter between 70 and 90 nm; in addition, disorganization in the packing of fibrils was observed. This effect was more pronounced in the older species.

HPEM 7-4: Inactivating and Activating Effects of High Pulse Electric Fields on Microorganisms

M. I. Boyko
RDI "Molniya" NTU "KhPI"

Effects of Combination of High Voltage Pulse Effects (CHVPE) on microorganisms in various liquid and fluid media has been investigated experimentally. Primary factor in Combination of High Voltage Pulse Effects is high pulse electric field.
Conception of rational action of pulse electric field in disinfecting treatment by Combination of High Voltage Pulse Effects was proposed. According to it, field pulses must have short front ($t_f \leq 20$ ns), so that field should penetrate into cell, and sufficient length to act effectively on cell membrane which results in its irreversible break down. In the process, too long pulses give increase of specific energy consumption at the same inactivating effect. Optimal pulse length is connected with cell size: the more the cell, the more the pulse length. Optimal pulse length for bacteria with characteristic size 1 μm is 0.1 μs$<t_i<$1.0 μs.
It was shown experimentally that inactivating action of CHVPE on microorganisms becomes irreversible after the temperature in treated liquid with microorganisms exceeds instantaneous critical temperature that is less than the temperature of heat pasteurization. Critical temperature T_c in itself is not able to carry out appreciable inactivation, between others and by reason of short duration of action. Under working intensities of pulse electric field $E \leq 100$ kV/cm in medium with microorganisms, T_c=(50$\cdots$60)$^\circ$C for most microorganisms. Experiments were conducted in different liquid and fluid media with different microorganisms. In particular, liquid food products, which we used as media with microorganisms, were juices, wines, milk with natural sowing with microorganisms. The results of experiments on representative microorganisms Anabaena flos aquae were published in (Boyko N.I., Bozhkov A.I.; Effect of Combination of High Voltage Pulse Effects and other physical factors on intensity of reproduction of Anabaena flos aquae; Biophizika; M-2002-V47, Issue 3-P531-538). Experimental plants, having voltage more than 100 kV and average power – tens of kilowatt, allow to achieve intensities of high pulse electric field more than 100 kV/cm and productivity more than 1 m^3/h and were described in (Boyko N.I., Tur A.N., Evdoshenko L.S., Zarochentsev A.I., Ivanov V.M.; High-voltage Generator of Pulses with average power to 50 kW for food product treatment; Pribory i technika eksperimenta; M-1998-N2-P120-126) and in (Boyko N.I., Tur A.N., Bozhkov A.I.; Plant for fluid product treatment with Combination of High Voltage Pulse Effects and research results; Tekhnichna electrodinamika; Kiev: Institute of Electrodynamics, NASU-2001-N4-P59-63). Working chambers were described in (Boyko N.I., Evdoshenko L.S., Tur A.N., Ivanov V.M., Zarochentsev A.I.; Working Chambers for food product treatment by Combination effect of high pulse electric fields; Pribory i tekhnika eksperimenta; M-2001-N6-P102-112).
Empirical mathematical model for description of result of microbial inactivation as function of a number of factors, of which the most significant are: pulse electric field intensity, temperature of medium with microorganisms treated, field pulse duration, was proposed. It was shown experimentally that, under CHVPE-treatment, biological and nutritional value of food products were preserved. For the first time it was experimentally shown that influence of CHVPE on microorganisms under high field intensities ≈100 kV/cm can be either inactivating or activating. The latter is possible if the condition of exceeding of instantaneous critical temperature is not fulfilled.
Method of treatment by Combination of High Voltage Pulse Effects was supported by patent on invention of Russian Federation N.2085508. The working chambers were supported by patents on invention of Russian Federation N.2157649, N.2193856. The patents were obtained with conventional priority of Ukraine.

HPEM 7-5: Electromagnetic Compatibility in the Medical Facility Environment with UWB Deployments

L. S. Cohen, L. E. Polisky
Comsearch, Network Solutions Division of Andrew Corporation

Description of Paper: Deployment of ultrawideband (UWB) systems will be occurring throughout society very soon. The UWB applications will include communications, detection, medical, and information-technology (IT). Many of these applications will occur in the hospital environment. This paper will describe the emission characteristics of representative UWB systems with respect to frequency, bandwidth, and power restrictions required by the United State's Federal Communication Commission (FCC). It will also show what frequency ranges the FCC has allocated for Wireless Medical Telemetry Systems (WMTS). The FCC limited theoretical UWB emissions will be overlaid on the measured electromagnetic environment within a typical American metropolitan hospital. An assessment of the potential electromagnetic interference from UWB systems to WMTS and resulting patient safety will be determined. In addition, levels of EMI caused by UWB systems will be correlated to the potential for the malfunction of critical patient monitoring and diagnostic equipment. This qualitative and quantitative assessment will show the combined electromagnetic interference effect of multiple UWB systems within a typical American metropolitan hospital.

HPEM 7-6: Stress Cellular Response Induced by Weak Microwave Irradiation

O. V. Glushkova, **E. G. Novoselova**, **O. A. Sinotova**
Institute of Cell Biophysics of Russian Academy of Sciences

It is known that low-density electromagnetic irradiation (EMR) could be delivered to stress factors. There are many studies that made an attempt to elucidate the mechanisms of EMR biological effects. The goal of the present study was in vitro investigation the effects of low-density centimeter microwaves (8-18 GHz, 1 mW/cm^2) on the production of some cytokines, nitric oxide (NO), and heat shock protein 72 (HSP72) expression in immune cells from healthy mice.

a) Tumor Necrosis Factor. The dose-effect curve for tumor necrosis factor (TNF) production in irradiated macrophages (exposure durations lasted from 30 min to 150 min) showed the increase cytokine production in these cells. The ability for EMR to stimulate the TNF production was in direct proportion to exposure duration. Interestingly, a stimulative potency of EMR was comparable with LPS effect (when LPS (5 mmol/ml) was added into cell culture). Similar results were got upon investigation of EMR effects on TNF production in splenic T-cells from healthy mice.

b) Interleukin 2 and Interleukin 3. Centimetric microwave irradiation in vitro during 1.5 hours did not cause a significant change in T-cell interleukin 2 (IL-2) production as compared with control. However, prolonged irradiation during 2.5 hours decreased IL-2 synthesis. In the course of our study we did not find remarkable changes in interleukin 3 (IL-3) production in exposed T-cells as compared with control.

c) NO. We had revealed that centimeter microwaves provoked the increase in NO production. The dose-effect curve was above control within the whole of exposure period. The peak of NO production (about 200% to control value) was detected upon 2 hours irradiation.

d) HSP 72. Low-density centimeter EMR caused the expression HSP 72, which was comparable with stress protein production in splenic mice cells after hyperthermia (42°C, 1 hour).

Conclussions: weak microwaves applied in vitro activated the signal pathways related to TNF, and conversely, suppress IL-2 synthesis. At the same time, pathways that regulate IL-3 synthesis did not participate in MW effects. The fact that low-density centimetric microwaves increase the production of stress markers, namely HSP72, TNF and NO, allows to consider immune cells as possible targets for weak electromagnetic radiation.

HPEM 7-7: Apparatus for Broadband Electromagnetic Pulse Therapy - Principle of Operation, Design and Results of Clinical Approbation

M. I. Boyko, **A. V. Bortsov**, **I. A. Safronov**
RDI "Molniya" NTU "KhPI"

Apparatus for broadband electromagnetic pulse therapy (ABEMPT) was created and tested experimentally. Frequency spectrum of each pulse is continuous and has frequencies from 0 to ≈10 GHz. Frequencies, exceeding 10 GHz, are represented by small (homoeopathic) power densities, which corresponds to approaches of information wave therapy. ABEMPT is protected by two twenty-year's patents on inventions: N.23040, Ukraine and N.2086271, Russia.

It was shown that the same apparatus ABEMPT can carry out therapeutic and prophylactic action by ordered electromagnetic pulses with help of various output devices (applicators, radiators, systems of field-forming) contactly, without contact, by means of plasma of low energy spark and corona discharges, pointwise, locally (on areas of body surface), globally (on the whole organism or group of patients). Creation of apparatus ABEMPT, which has not close analogue, and using it in practical medicine were supported and recommended by Committee on new medical equipment of Ukraine Health Ministry (Protocol N.13, 30.11.1994).

Principle of operation of apparatus consists in generation, forming, therapeutic and prophylactic application of electromagnetic pulses with front to 0.1 ns having broad frequency spectrum. Distinctive feature of effects of apparatus ABEMPT is high peak power in pulse P_p (to hundreds of kilowatt) at low average power P_a (less than 1 W). The most original is variant of action through low-energy spark or barrierless pulse corona discharges. Corona discharge in the form of great number of streamers arises when extremely thin, metallic plate (the thickness is several microns), of which sharp edge is placed at the distance ≈1 mm from body surface, is used as high-voltage electrode of applicator. In this case, main condition of corona discharge – presence of sharply non-uniform field – is completely satisfied. In the case when field is more uniformed at characteristic curvature radii of the point ≈0.05 mm and more, when high-voltage electrode of TEM-applicator is approaching surface of patient body at distance ≈1 mm, low-energy spark discharge arises (without corona stage).

Action through discharges can be carried out by means of galvanic contact of low-energy electrode with patient body or if capacitive connection exists between them. In the first case energetic effect is significantly stronger, which is manifested in intensification of patient sensation of "pinching".

All variants of contact action and action through discharges from ABEMPT are accompanied by sensation of "pinching" in patients. Intensity of the sensation depends on average power of action, i.e. of pulse repetition frequency and energy of single pulse. Remarkable property of spark variant of action is its exact addressing, because characteristic cross dimension of spark channel equals from several to hundred microns. This allows carrying out exact and sterile action on acupuncture points of body surface, which have cross diameter close to characteristic diameter of spark channel.

Big work on clinical approbation ABEMPT was conducted by Doctor of medical science, professor Tondiy L.D. Therapeutic methods on the base of apparatus ABEMPT were developed and successfully approbated. Clinical approbation showed that method of cure by ABEMPT has pronounced pain-killing effect, pronounced hypotensive action, improves regionary microcirculation, and has sedative action, increases adaptive abilities of organism.

HPEM 7-8: Cytokines and Nitric Oxide Production in Immune Cells

O. A. Sinotova, **E. G. Novoselova**, **O. V. Glushkova**
Institute of Cell Biophysics of Russian Academy of Sciences

Electromagnetic waves have significant interactions with biological systems, and the cells of immune system are increasingly being employed as a sensitive model. Numerous studies have determined the cytokines, produced by immune cells, showed many biological activities, including their therapeutic effects in a variety of diseases. In the present study tumor necrosis factor (TNF-alpha), interleukins (IL-2 and IL-3) and nitric oxide (NO) were chosen as markers of the cellular immune status. The mice with solid experimental tumors, which were originated by a subcutaneous transplantation of Ehrlich carcinoma cells, were used as animal cancer model.

Tumor growth during 30 days induced an extraordinarily in-

crease in macrophage NO production exceeding six times over the value in controls. Whole body microwave irradiation with extremely low intensity waves (42.2 GHz; 10 Hz amplitude modulation; 1 μW/cm^2, 1.5 h daily) increased NO production in healthy mice exposed during 10 days. After total body exposure of tumor-bearing mice for 30 days, a noticeably decrease in NO peak production compared to unexposed tumor-bearing mice was detected. As to TNF-alpha production, we observed an increase in macrophage TNF-alpha from tumor-bearing mice 10 days (up to 200%) and 20 days (up to 160%) after cancer cell transplantation, as compared to control mice. In addition, prolonged irradiation of healthy mice for 10 days increased TNF-alpha production to 150 percents as compared to untreated animals. In opposite, irradiation of healthy mice for 30 days did not change macrophage TNF-alpha production in macrophages. But subjection of tumor-bearing mice to microwaves for 30 days depressed TNF-alpha production (about to 70% as compared to controls). Stimulation of NO production in peritoneal macrophages in tumor-bearing mice could be considered as an adaptive response to tumor development. Remarkably, in the tumor-bearing mice, the highest level in NO production in peritoneal macrophages was demonstrated concurrently with depression in TNF-alpha production by these cells. We have demonstrated that weak microwave irradiation charges TNF-alpha and NO production but no charges IL-2 and IL-3 production in cells of tumor-bearing mice. Decreasing of IL-2 and IL-3 production in splenocytes we observed only in unexposed tumor-bearing group for 10 days after cancer cell transplantation. It seems that IL-2 and IL-3 are not a regulatory cytokines involved in cellular responses on weak microwave irradiation.
Based on the above results, microwave treatment did not protect an organism from immune system injury, which was induced by tumor growth.

HPEM 7-9: Medical Application of Noise Radiation of IMPATT Diode

Y. Savenko, **Y. Zinkovskiy**, **V. Pravda**, **N. Bogomolov**
"Kiev Polytechnic Institute", National Technical University of Ukraine

This paper presents results of investigations of positive biomedical effects on human organism by radiation of impact avalanche transit time (IMPATT) diode. In particularly, it considers questions of correction of a human immune system with noise mm-range radiation. It is also discussed a possibility of using this effects for various medical applications that had been used in clinical practise.
It is very important to understand the nature of low energy millimetre waves. In this range (λ=1...10 nm, f=30...300 GHz) waves have significant particularities. Quantum energy is less than heat energy kT. For example, heat energy is 2.53 eV at room temperature in comparison with quantum energy that is 10^{-3} eV at wavelength λ=1 mm. This energy is less than energy of electromagnetic transition, activation, oscillating energy of molecules and even the hydrogen coupling. It means that millimetre waves cannot influence even onto the weakest chemical couplings. It could be classified as non-ionising radiation.
Water adsorbs mm-range radiation too much. A human skin consists of 60% of water. Millimetre range radiation is practically entirely absorbed on depth in order of 0.7...1 mm. Millimetre waves do not reach to internal organs and have indirect influence on human organism. Human organism consists of about 10^{15} cells. Cells generate electromagnetic fields in mm-range. Amplitude-frequency responses of field radiation are different for normal and diseased organism. It means that any pathology is pathology of cells. External millimetre radiation of IMPATT diode stimulates self-organism radiation in this range that is operating as synchroniser for weak organism and forcing the organism for normal biorhythm. So therapeutic effects of noise radiation of IMPATT diode consist in mobilisation of human organism reserves. Essential advantage of noise mm-range therapy, it has no negative reactions onto health organism.
Real noise spectral power density is different for various IMPATT diodes. But differences are not essential and all of them have the same order of noise spectral power density in 10^{-19} W/Hz. Individuals have certain frequencies of self-radiation. These frequencies must be used for forcing of human organism reserves. It requires the procedure for selection of individual stimulating frequencies in case of using of fixed radiator in mm-range. Using of IMPATT diodes do not require this one, because an organism have selective possibilities. Thus it selects only same mm-waves as individual self-radiation. Another wavelengths do not participate in biostimulation of organism and its have not negative reaction onto normal or diseased human organism.
Medical researches have confirmed high efficiency of IMPATT diodes to treatment of disorder of the nervous system, disturbance of the immune system and exchange of substances etc. It would be consider the most perspective investigation as for treatment of drug addiction, alcoholism, nicotine addiction and rehabilitation as well.

HPEM 7-10: Correction of Immunopatology by Low-Intensity Electromagnetic Microwave

O. V. Glushkova, **E. G. Novoselova**
Institute of Cell Biophysics of Russian Academy of Sciences

The numerous biological effects of electromagnetic non-ionizing radiations arising from man-made sources can exist in all residential and occupational settings as the direct result of electric power generation, transmission, distribution, and utilization, thus affecting our lives everyday. Within last decade, there is substantial evidence that the biological effects of electromagnetic radiation depend on the physical parameters of the field, primarily on its intensity and frequency. Low-intensive centimeter and millimeter microwaves provide the different effects on biological systems. In addition, biological effects of microwaves depend on pathophysiology of exposed organisms. At present, the authors have elaborated on potential health effects of extremely low-intensity electromagnetic radiation focusing on it immunomodulative activity. In order to elucidate the new approach to noninvasive treatments that might result from exposure to microwaves, some animal models with modified immune status were developed.
The goal of present study was to reveal the effects of fractionated (1.5 h daily, for 30 days) exposure to low-density centimeter electromagnetic waves (8-18 GHz, 1 μW/cm^2) on immune system of animals with immunodepressive or immunostimulative animal model.
Materials and methods
Animals. The mice with the experimental tumors, which were originated by a transplantation of Ehrlich carcinoma cells, were used as model of an immunodepression. Eight to ten-week-old male NMRI mice weighing 24-26 grams were used for the experiments. Animal cancer model was formed by a hypodermic transplantation of 200000 or 2000000 Ehrlich ascite carcinoma cells per mouse in hind lymb. As other model that designs the changes in immune system activity, an antigenic stimulation of mice by foreign protein was provided. Mice were immunized intraperitoneally with affinity-purified carboanhydrase from bovine erythrocytes (Sigma), 50 μg/mouse. In the different experiments, the first and repeated injections of antigen were conducted either with, or without Freund's adjuvant (Sigma) supplement. When Freund's adjuvant was applied, the first immunization was performed with complete Freund's adjuvant. Each animal was injected 0.5 ml antigen/adjuvant mixture. For the second immunization a fortnight later, incomplete Freund's adjuvant was used.
WMW exposure. A sweep-type microwave generator (YA 2P-76/2, Russia) was used as the source of microwaves. Sweep frequency was 8.15-18.00 GHz of 1 s direct sweep time, and 16 ms of reversed time. The spectral width was better than 1 MHz and the frequency stability was better than 5%. Field distribution of the microwaves 20 cm from the center was registered to have a central maximum power density of 1.6 μW/cm^2 to 0.4 μW/cm^2. The average power density in the area of animal exposure was 1 μW/cm^2. MW irradiation was started on day 1. Sham-exposed mice were used as control.

TNF concentration assay. L929 cell line was used to measure the concentration of TNF by cytotoxicity test (Fesenko, E.E., Novoselova, E.G., Makar, V.R., and Sadovnikov, V.B. Bioelectrochemistry and Bioenergetics, V. 49, 1999). Tests were provided for each individual mouse in 12-15 wells/animal.
NO concentration assay. All of procedures concerned the NO determination were provided as earlier described (Novoselova EG, Ogai VB, Sinotova OA, Glushkova OV, Sorokina OV, Fesenko EE., Biophizika, 2002). Tests were provided for each individual mouse in 12-15 wells/animal.
Antibody concentration assay. Blood samples were collected by tail vein punctures on the 15th day after first or second immunization. Concentration of peripheral blood plasma antibodies was measured by enzyme linked immunosorbent assay (ELISA) with horseradish peroxidase-conjugated anti-mouse polyvalent immunoglobulins (IgG, IgA and IgM) (Sinotova, O.A., Novoselova, E.G., Ogay, V.B., Glushkova, O.V., Fesenko, E.E., Biophysics, 2002).
IL2 and 3 concentration assay. Concentration of IL2 and 3 was determination by ELISA.
Electrophoresis and immunoblotting. Expression of HSP 72 was determination by electrophoresis and immunoblotting (Glushkova OV, Novoselova EG, Sinotova OA, Fesenko EE., Biophizika, 2003).
Statistical analysis. Statistical significance was calculated by Student's t-test.
Results
Animal model of immunodepression. The mice with the experimental tumors were used as model of an immunodepression. In these conditions, a suitable cancer model lets to control of localization, growth rate, stage of development, metastasis, and also mouse life span. It was established that the prolonged exposure to microwaves increased the adaptive response of an organism to tumor growth, invoking an overproduction of the tumor necrosis factor (TNF), heat shock proteins (HSP 72), and nitric oxide (NO) and normalization of interleikine 2 and 3 (IL2 and IL3) concentration in cells from irradiated tumor-bearing mice. The direct relation was observed between the level of TNF production as well as TNF plasma concentration, and tumor growth inhibition, which was demonstrated by the tumor size lowering and the increase of tumor-bearing mice survival. The close reverse correlations were observed between HSP 72 expression and tumor sizes in irradiated tumor-bearing animals.
Animal model of immunostimulation. As other model that designs the changes in immune system activity, an antigenic stimulation of mice by foreign protein was provided. Prolonged exposure to centimeter waves increased plasma antibody concentration in immunized mice, and the degree of antibody productiveness enhancement was more substantial under the development of primary immune response. When immunization procedure was provided without adjuvant addition, a primary immune response was extremely low whereas prolonged irradiation of animals to centimeter waves increased antibody production to value, which had been reached only under the immunization with an adjuvant addition. Thus, the application of centimeter waves could completely compensate the omission of an adjuvant in antigen challenge procedure.
Conclusion
The interpretation of these data suggests that the exposure with centimeter low-level intensity electromagnetic radiation increases a resistance of an organism against tumor growth, and also gives a chance to be saved from the application of toxic adjuvants under immunotherapy.

HPEM 7-11: Microwave Effects on Gene Expression in Connection to Chromosome Conjugation

Y. G. Shckorbatov
Kharkov National University, Kharkov, Ukraine

The expression of some genes depends on the state of conjugation of homologous chromosomes in interphase nucleus. Such genes reveals the effect of transvection (Henikoff S. Nuclear organization and gene expression: homologous pairing and long-range interactions; Curr Opin Cell Biol. 1997. Vol. 9, p.388). Transvection effect may be expressed in two forms – transactivation and transinactivation. If a gene in one homologous chromosome inhibits expression of other gene in opposite chromosome one can observe the effect of transinactivation. In our experiments mutation brown Dominant (bwD) revealing transinactivation effect was used. This gene controls the eye pigmentation in flies (imago) of drosophila. The manifestation of this mutation depends on degree of chromosome conjugation in the nucleus. So investigating expression of this gene one can judge about changes in chromosome conjugation process in interphase nucleus. The gene white vco may be used in investigation of position variegation effect (PEV) after influence of electromagnetic fields. We influenced by low energy microwave radiation (0.1 and 0.2 mW/m^2) on drosophila eggs in synchronous laying. The effect of radiation was registered in flies developed from the irradiated eggs.
The studies were conducted in Drosophila melanogaster stocks number 6144, 4664, 245 (Bloomington Drosophila Stock Center), stock Canton-s, and hybrids of these stocks. The stock contained the gene bwD in heterozygous condition, the stock - gene brown in homozygous condition, stock - gene white vco in heterozygous condition, stock C-s - a wild type stock. Stocks 6144, 4664 and 245 were kindly supplied to us by A.O.Rudenko (Oxford University, Department of Zoology), stock Canton-s (C-s) was obtained from drosophila collection of the Department of Genetics and Cytology of the Kharkov National University.
We obtained the following results.
Microwave radiation of low intensity (0.2 mW/m^2) negatively influences upon reproductive ability and output of imago in stocks and hybrids of drosophila. The microwave radiation of millimeter range (the wavelength 3.8 mm) results in significant effects on eye pigmentation. The effect of the radiation depends on polarizations of the radiation. Linear polarized and left polarized radiations cause the reduction an amount pigment, right polarized radiation - an increase of pigment amount.
Since left polarized and Linear polarized radiation causes the reinforcement of the transinactivation effect we suppose that observed effect is a manifestation of the increase of degree of chromosome conjugation in interphase nucleus under the influence of the microwave radiation.
Under the influence of right polarized microwave radiation with wavelength 3.8 mm action increasing of eye pigmentation is observed. So we can see the reduction of the transinactivation effect connected as it is known with reduction of degree of chromosome conjugation in interphase nucleus.
The microwave radiation with wavelength 16 mm with linear polarization induces increase in amount of pigment in drosophila eyes connected with reduction of the transinactivation effect and , accordingly, reduction of the degree of chromosome conjugation.
The irradiation with wavelength 3.8 mm with linearr polarization induces increase of the PEV that is connected with hetrochromatinization of the area, adjoining to gene white vco.

HPEM 7-12: Changes in Mice Exploratory Activity Induced by Low-Level Microwave Exposure

C. Goiceanu[1], **G. Balaceanu**[1], **R. Danulescu**[1], **F. Gradinaru**[1], **D. D. Sandu**[2]
[1]*Institute of Public Health, Iasi, Romania*; [2]*"Al. I. Cuza" University of Iasi, Romania*

The aim of the present study is to investigate possible biological effects in mice due to chronic exposure to low-level microwaves. We tried to determine whether the low-level microwave fields, used in our experiment are able to influence the behaviour of exposed animals.
The microwave exposure experiment was carried out on Swiss male mice. A control sham exposed lot of ten male mice was kept in similar environmental conditions. All the animals were housed individually in separate glass jars. During exposure or sham exposure time intervals, the mice were placed in plexiglas cages. Inside a transverse electromagnetic (TEM) cell, mice were exposed to continuos travelling waves of $1mW/cm^2$

power density. To minimize the field perturbation in a location of a specific mouse due to the presence of other mice in its neighbourhood, each mouse was placed in its own cage. The cages were placed inside the TEM cell at the maximum possible distance one from each other. The frequency of the exposure field was 400 MHz. The exposure experiment lasted 13 weeks. Every week the mice were exposed 8 hours per day, five days per week. The behaviour of animals was assessed using three tests that investigate the exploring behaviour and motor activity: evasion test, perforated plate test and open field test. The test sessions were performed every two weeks.
The study emphasizes two kinds of changes in mice exploratory activity: a slight decrease in time and a phasic evolution of the exploratory ability consisting in two stages of activation and inhibition. The electromagnetic energy, interacting with nervous system, could act like as an exciting factor. After the activation period, a state of tiredness appears in the exposed mice and, consequently, their performances decrease. In our experiment, this phasic evolution appears to be repeatable, becoming a cyclic evolution. Thus, the microwave exposure acts as a repeated activation factor that, in time, induces tiredness as a result of repeated enhanced energy consumption in the periods of excitation of the central nervous activity of mice.

HPEM 7-13: Scientific Progress with the Effects of High-Power Millimeter Waves upon Tissue, Organs, and Behavior

D. M. Scholl
Air Force Research Laboratory, Directed Energy Bioeffects Division, Kirtland AFB, NM, USA

Millimeter wave energy beam illumination of laboratory animals and of humans at power levels above current occupational health and safety standards has produced informative results. Under approved animal research protocols, various energy levels of millimeter waves were explored in order to confirm the point at which injuries occur to skin and to the surface of the eye. Laboratory behavioral studies with humans have established the power levels at which self-protective responses occur such as eye blink, eye closure or facial aversion. Infrared thermographs also produced interesting findings of the quasi-optical effects of millimeter waves as they were reflected upon facial features. Millimeter wave energy beam research with humans, free to move about however they chose, also confirmed the self-protective nature of responses that prevent occurrence of any injury as a consequence of such illumination. Simply stated, senate creatures feel discomfort from the kinds of millimeter wave stimuli used in this research program. The beam hurts and because it hurts creatures act to protect themselves and they do so effectively to prevent any occurrence of injury. Details of research program findings will be presented.

HPEM 7-14: Effects of GSM and UMTS-like Basestation Fields on Human Cognitive Functions and Experienced Well-being

A. P. M. Zwamborn[1], **E. van Rongen**[2]
[1]*TNO Physics and Electronics Laboratory, Den Haag, Netherlands*; [2]*Health Council of the Netherlands*

A study was performed in a double-blind, crossover design, using two groups of 36 volunteers. Group A consisted of people with non-specific health complaints they attribute to electromagnetic fields emitted by GSM base station antennas. Group B were people without such complaints. Due to difficulties in recruitment, the composition of the groups was not balanced (differences in age and sex distribution). Each subject was exposed in an anechoic room in 3 sessions of approximately 25 minutes, with approximately 20 minutes washout periods in between sessions. One session always was sham exposure, the other two were either 900 MHz GSM, 1800 MHz GSM, or 2100 MHz UMTS-like signal. Peak exposure levels were 1 V/m (i.e. 1 V/m effective for UMTS and 0.7 V/m effective for GSM). During exposure, cognitive functions were tested using a TNO-developed Taskomat test battery with tests for reaction time, memory comparison, visual selective attention, dual tasking: general reaction and dual tasking: filtering irrelevant information. After each session a questionnaire was used to determine experienced well-being. The questionnaire consisted of a subset from a questionnaire developed for hypertension studies, leaving out the questions irrelevant for the present study. The 23 remaining questions were scored as Not at all (0), A little, slightly (1), A great deal, quite a bit (2) or Extremely, could not have been worse (3). The sum of all scores was used to determine any differences between sham exposure and exposure to each of the three modalities. A significant difference ($p<0.05$) was found in both groups between sham and UMTS-like exposure, but not for the GSM-exposures. Correction for multiple exposures did not change the significance. Comparison between groups A and B is not possible due to the unbalanced composition of the groups. A significant effect on cognitive functions was found in 7 out of the 30 possible combinations (5 tests x 3 exposure modalities x 2 groups). No clear pattern was observed, however. Correction for multiple exposures reduced the number of significant outcomes. The null-hypothesis – exposure has no effect – had to be rejected. The maximum SAR calculated per 10 g tissue in the head was 0.08 mW/kg, therefore the possibility of a thermal effect being the cause of the observed effects is considered unlikely.
This study is the first to demonstrate an effect on experienced well-being, which is to be considered as an health effect within the WHO definition of health. The study needs to be replicated and follow-up studies need to be performed.
The report of the study can be found at http://www.ez.nl/beleid/home_ond/gsm/docs/TNO-FEL_REPORT_03148_Definitief.pdf.

HPEM 7-15: Polyfrequency Signal Activity. Theoretical Approach.

V. O. Ponomarev, **A. V. Karnaukhov**, **V. V. Novikov**
Institute of Cell Biophysics, Pushchino, Russia

The effects of field low intensity (50 μT) and low frequencies ($<$ 100 Hz) magnetic are usually studied using monofrequency signal. The frequency of external field is selected to be equal to one of the harmonics or subharmonics of cyclotron frequency of biologically important ions. The theoretical explanation of the results obtaned is based on the assumption that the magnetic field changes the condition an ion-binding protein or the capacity of transmembran ion transport. Problems arising with this approach (the basic of these is the kT problem) have no satisfactory solution.
To avoid of these difficulties we used a more complex signal: $H = H_0 + H_1 \cdot \sin(t) \cdot \cos(2t)$, where H_0 is the intensity of the steady magnetic field, H_1 is the amplitude of the alternating component. The frequency was selected to be equal to the cyclotron frequency, and is a variable parameter. Our experiments showed that this signal is more effective than the monofrequency signal ($\omega_2 = 0$).
For the theoretical substantiation of the efficiency of a similar signal, we assume that the system being considered consists of two components. One of them we named the resonator, and the second, the effector. The influence of frequency ω_2 on the resonator results in an increase of the amplitude of an external signal above to the value exceeding the stochastic force of thermal fluctuations. The signal amplified by the resonator, influencing the effector, causes the biological response of the system. In the biological cell, the role of the resonator and effector can be plaied by various objects, for example, a protein and a charged amino acid or a protein and inorganic ions and other structures.
Here we present one of possible theoretical models realizing this approach. In our model, the effector is the Ca-binding protein proteinkinase-C, and the resonator is a cell membrane to which the protein is bound. The external field does influence on the protein, causes its fluctuations, which in turn generates elastic waves, which propagate along the membrane. If we assume that the frequency ω_2 is the resonance frequency of our system, the amplitude of protein fluctuations should appreciably increase.
However, the time necessary for the energy of membrane fluctu-

ations increases up to a value comparable with the thermal noise considerably exceeds that of experiment. To avoid this difficulty we invoked the concept of dissipative resonance investigated us in papers. The main point of this phenomenon is that the external field causes fluctuations of a large number of particles of the same type N. The interactions between these fluctuations give rise a self-organization process in the membrane - proteins system. This phenomenon results in an increase of the amplitude of fluctuations of each protein that is proportional to the number of proteins involved in the process. In this case, the time of energy increase is limited by the duration of the self-organization process, which is approximately equal to time of the experiment. A result of the phenomena described is a great increase in the amplitude of protein fluctuations. If we conceder our system in the frame connected with the protein, we obtain that the inertia force acts on an ion bound by the protein. The energy due to this force with a sufficiently large value of N and in the case that the is the resonance frequency of the membrane can exceed the energy of influences of the protein cavity walls. Thus have we solved the kT problem. Now, we choose the frequency ω_1 equal to the cyclotron frequency of the ion or its subharmonic. Our system can be further studied by the well known methods using the phenomenon of parametrical resonance, or interference of the connected ions. The results of these models are widely known and agree well with experimental data. Thus our approach makes possible the use of the models constructed earlier whose reliability was doubted because of failure to solve the kT problem.

HPEM 8 - Antennas

HPEM 8-1: Coupling Between Antennas in a Complex and Electrically Large Environment

J. P. Adam, **J. Geiswiller**, **Y. Béniguel**
IEEA Courbevoie, France

The coupling between two antennas in a complex environment still remains a problem when high frequencies are considered. The Uniform geometrical Theory of Diffraction (UTD) (P. H. Pathak, N. Wang, "Ray Analysis of Mutual Coupling Between Antennas on a Convex Surface", IEEE transactions on antennas and propagation, November 1981) is one of the most convenient technique to solve this problem. In addition to the direct wave traveling from the transmitter to the receiver, the interaction with the environment is simulated by scattered rays. This problem has been addressed at IEEA using software ULTRA developed over years and which combines the three calculation techniques : Method of Moments (MoM), Physical optics (PO) and UTD.

The environment is described by a set of NURBS surfaces and lines. NURBS are widely used to accurately describe an arbitrary shape. ULTRA is powered by openNURBS Toolkit. This library provides reliable NURBS capabilities to the asymptotic code. Generalized Fermat principle is implemented in the ray tracer. One of the major interests of the approach is that it allows combining in the same calculation different surface elements either meshed (directly obtained from the NURBS) or not and subsequently using the related calculation technique.

Once both emitter and receiver antennas are characterized, ULTRA searches the following rays transmitted by the first antenna, interacting with the environment and reaching the second antenna :

· Incident
· Reflection
· Wedge Diffraction
· Corner Diffraction
· Creeping
· Reflection - Reflection
· Reflection - Wedge Diffraction
· Reflection - Corner Diffraction
· Diffraction - Diffraction

For each ray, the electric field at the receiver is derived from the UTD scattering coefficients. The sum of all these contributions evaluates the effect of the transmitter on the receiver.

The code ULTRA is integrated in the CAD software GID. The result is a user-friendly interface. The geometry can be directly designed and GID's import features allow to use most of the common CAD formats (IGES, DXF, VDA,. . .). In addition, the user can easily select the parts of geometry to be taken into account in the computation. He can also choose the contributions ULTRA must calculate.

A typical calculation of coupling between antennas consists in defining the antennas vicinities by a mesh considered in the calculation by the MoM. The coupling via the structure is evaluated by UTD. A hybrid technique is consequently used. Another interesting possibility is to consider the antennas by means of their far field patterns and input impedances. This allows in particular looking for the best location, minimizing the coupling. In all cases the s matrix is provided by the calculation.

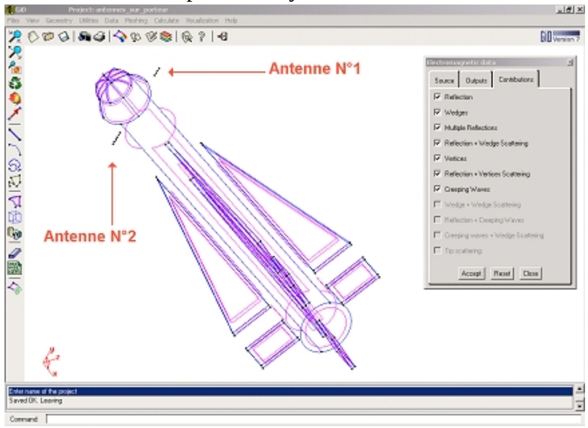

Figure 1: Missile described by NURBS to simulate coupling between two antennas mounted on that carrier.

HPEM 8-2: High Directivity Beam-Forming for Short-Pulse Arrays

S. Foo, **S. Kashyap**
Defence Research and Development Canada

This paper presents a beam forming technique that produces a highly directive radiation pattern for short-pulse systems. The technique is based on the cross-correlation algorithm developed for ultra-wideband (UWB) arrays (S. Foo, S. Kashyap. Time-domain array factor for UWB antenna array. IEE Electronics Letters, vol.39,no.18, 4th Sep., 2003, 1304-1305). With cross-correlation, the output of a short-pulse array is time-gated with respect to the reference element. By using a reference element located sufficiently far away from the array center, the cross-correlation eliminates the unwanted sidelobes, which are inherent in the conventional array-processing algorithm. The beamwidth of the resultant pattern is primarily determined by the pulse-width of the signal. For monocycle sinusoidal signals, the beamwidth can be further reduced by dual cross-correlation. In this case, the array outputs are cross-correlated to the in-phase and the out-of-phase components of the reference element. A sharp pencil beam can be obtained by processing sum and difference of the dual outputs. The beamwidth of the resultant pattern is determined solely by the location of the reference element and the pulse-width of the signal.

The concept is demonstrated using an array consisting of 11 elements with element spacing of 10cm. The UWB signal is a typical Gaussian modulated, monocycle, sinusoidal signal with an overall pulse duration of 700 nsec. Fig.1 shows the far-field pattern computed using the array center as the reference for the cross correlation. In this case, one gets a typical array pattern with a 3dB beamwidth of approximately 3.6 deg. Fig. 2 shows the cross-correlated far-field pattern with the reference element located at 10m away from the array center (along the array axis). The beamwidth is reduced to approximately 0.1 deg with two sidelobes at ± 0.3 deg. Fig. 3 shows the far-field pattern processed using the dual cross-correlation. With the reference channel located at 10m away from the array center, the beamwidth is 0.1 deg. The resultant far-field is a sharp brick-wall pattern without any sidelobes.

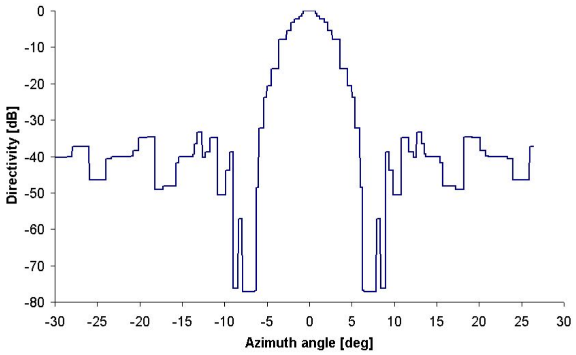

Figure 1: Cross-correlated array pattern with center element as correlation reference

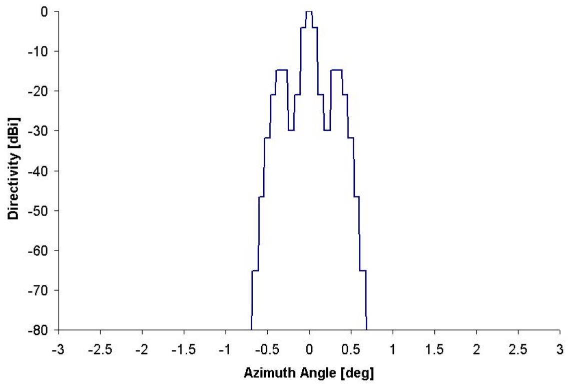

Figure 2: Cross-correlated array pattern with a remote element as correlation reference

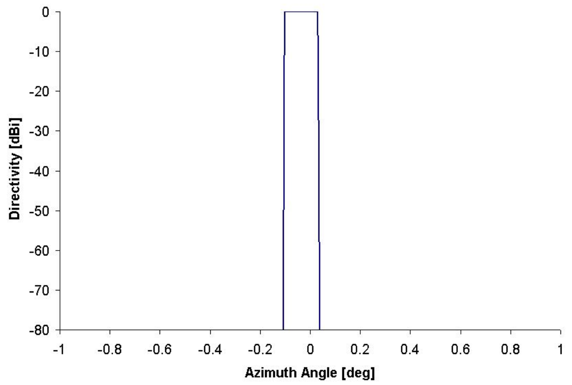

Figure 3: Dual cross-correlation array patern

HPEM 8-3: Optimization of Circularly Polarized Radiation of a Tilted Electric Dipole with Rectangular Screen

N. P. Yeliseyeva, **N. N. Gorobets**
V. Karazin National University of Kharkov

The calculated results (N. Yeliseyeva, 11th ICAP, Conference Publication No.480, IEE 2001) proved the possibility to increase sufficiently the directivity in the broadside direction of finite-size circularly polarized corner antenna by means of choosing suitable dimensions, dipole to corner spacing and the tilt angle of the dipole. Now the uniform geometrical theory of diffraction (UGTD) there has been used to analyse the conditions at which the circularly polarized (cp) radiation is formed by the finite - size metal screen with tilted halfwave electric dipole. There have been determined the highest possible power gain in definite direction in main observation planes, besides the normal to the screen, by means of choosing optimal dipole tilt angle at the one and the dipole dislocation concerning screen as a function of dipole to screen spacing at the fixed screen side dimensions.
A perfectly conducting infinitly thin rectangular screen was assumed to be the model for calculation. The screen side dimensions are W and L, and the screen is excited by an electrical halfwave dipole arbitrarily located at the height S above the screen. The location of the dipole is determined by its distances a and b from one of the screen apexes. Consider three cases of the screen excitation by the dipole: two ones with electric current I_1, I_2 of the dipoles horizontally oriented along the screen edges and with electric current I_3, of vertical dipole oriented along the screen normal. The asymptotic solution of the 3-D problem on the diffraction of the radiation of an arbitrarily oriented electric dipole by a perfectly conducting infinitely thin screen in the far field zone was obtained using the UGTD.
To analyse the polarization state of the screen- dipole field there have been calculated the module p of polarization ratio of the orthogonal components v and its phase $\psi = arg(v)$, the ellipticity factor σ of the polarization ellipse. In case of infinite screen, ψ (the curve 2, Fig.1) for the tilted dipole with electric current I_{13} ($I_{13} = I_1 \sin(\alpha) + I_3 \cos(\alpha)$) in the plane φ = 90° or I_{23} in the plane $\varphi = 0°$ are equal to 90° at any θ and S. So, from the condition that the module of polarization ratio must be equal to 1 (the curve 1, Fig.1), the circularly polarized radiation may be formed in any directions θ, besides θ = 0, by choosing the dipole tilt angle at the normal to the screen $\alpha_{cp} = \arctan[(\cos(\pi\cos(\theta/2))ctg(kS\cos(\theta)/\sin(\theta)]$ (the curve 6, Fig.1a) with field intensity $E^2 = E_\theta^2 + E_\varphi^2$ (the curve 4, Fig.1). However the computations of the polarization characteristics of the dipole-screen system with the account of the diffraction effects by finite - size screen had shown highly sensibility of ψ from θ (the curve , Fig.1).
The algorithms with account of the diffraction effects at fixed geometry of the dipole-screen system (W, L, S, a, b) and efficient computer codes have been worked out for calculating angle α for providing the condition p = 1 for any θ in the main observation planes. Then the angles θ have been selected, at which we have θ = 95° – 85° (the nearly to circular polarization), and corresponding to them the tilt angles α_{cp} and field intensity E_{cp}^2(on the curves 7, 5, Fig.1). The developed codes allow to choose θ, at which was formed the radiation with maximal σ and $E_{max}^2 >$ 1, when changing dislocation of the dipole a, b, and to find corresponding a_{max}, b_{max}. So for each S, L, W there have been made optimization of the circular polarization to determine σ_{max}, θ_{cp}, α_{cp}, E_{cp}^2, a_{max}, b_{max}.
On the base of worked out computer codes for the screen with the fixed side dimensions W, L the values of σ_{max}, θ_{cp}, α_{cp}, E_{cp}^2, a_{max}, b_{max} for different dipole to screen spacing S have been calculated. Fig.2 shows the calculated field intensity E_{max}^2 and σ_{max} in the plane φ =90°; as a function of S for the dipole being located at the infinite screen (the curves 1, 5), for the dipole located above the midpoint of the screen with W=L=3 wavelenghts (the curves 3, 4) and for dipole located above the same screen at optimal a_{max}, b_{max} (the curves 2, 4).

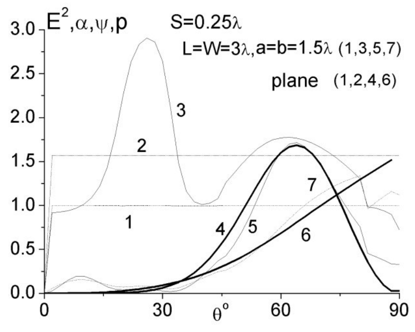

Figure 1: To the analyse of the field polarization state of the dipole screen system in the plane φ =90°;

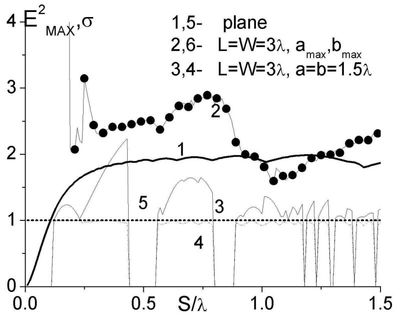

Figure 2: The calculated field intensity E^2_{max} and the ellipticity factor σ sub(max) in the plane φ =90°; as a function of S

HPEM 8-4: A Plasma Antenna for Magnetic Explosion Generators

V. A. Soshenko[1], **I. A. Vyazmitinov**[1], **O. O. Puzanov**[1], **V. V. Sinkov**[1], **V. E. Novikov**[2]
[1]*The Usykov Institute of Radiophysics and Electronics of NASU*; [2]*Science and Technology Center of Electrophysics, NASU*

A plasma jet is the explosion product of generators. Thus, plasma antennas show very good promises for using in portable sources. In such antennas, plasma serves as the radiating surface.
The development of a plasma antenna includes the following stages:
1. Achieving of the required particle density,
2. Achieving of the required plasma surface square,
3. Injection of the signal into the jet,
4. Excitation of a surface wave in the plasma.
The experiments have been started with the development of a plasma jet source. A plasma jet is shown in Fig.1. An exploder was used as a source. The jet power can be varied by changing the amount of the exploding substance and admixtures. In our experiments, the jet power ranged from 1.1 to 3 kJ. The plasma parameters were measured by a sounding probe. The probe consisted of two conductors having the diameter of 0.35 mm, with the distance of 6 mm between them. The probe currents for various distances from nozzle section are shown in Fig.2. These results enabled us to proceed to the signal injection into the plasma jet and excitation of the surface wave.
The block diagram of the device is shown in Fig.3. It was revealed that the radiated electromagnetic field increases when the plasma is excited by the internal coil current, with the gain of 20 dB.
Long jets were obtained while using a special source, allowing to shape a jet of 5 m and above. In these experiments, we used various signal injection tools. The experiments confirmed that a plasma jet generates a signal. The duration and the shape of the signal are determined by the plasma density, jet length and the type of signal injectors. We also have recorded signal harmonics arising due to the non-linearity of the antenna characteristics.

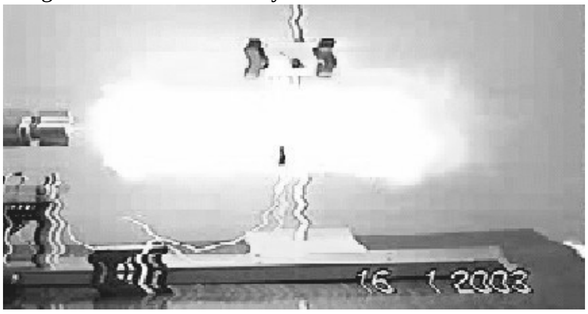

Figure 1: A plasma jet

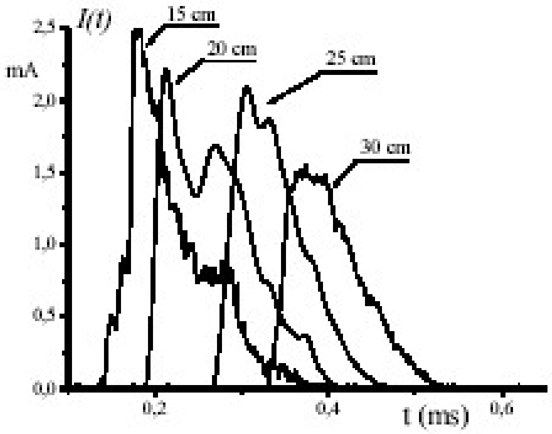

Figure 2: The probe currents for various distances from nozzle section

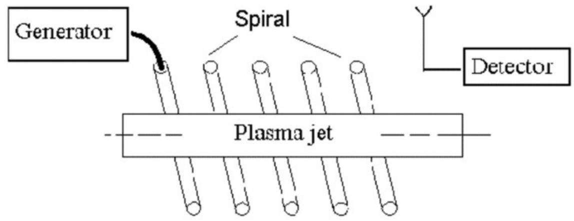

Figure 3: The block diagram of the device

HPEM 8-5: Introduction to IRAs

I. Kohlberg[1], **C. E. Baum**[2]
[1]*Institute for Defense Analyses*; [2]*Air Force Research Laboratory*

The reflector Impulse Radiating Antenna (IRA) (and other forms) was originally developed by Baum to produce a wideband, extremely large impulse electric field on bore-sight at distances of the order of kilometers. While this can cause upset and/or damage to electronic and communication systems, more important applications for IRAs have emerged, for example: impulse radars, mine countermeasures, etc. The expansion of applications has brought along the necessity to enable experts and non-experts in electromagnetic theory to better understand the unique electromagnetic fields generated by these antennas.
When the driving voltage source, and ideal step function, is applied, the IRA bore-sight field is the approximate delta function in the far field. When the source voltage has a finite but extremely short risetime, the bore-sight field is extremely large, being inversely proportional to the risetime. As we move off bore-sight the electric field begins to drop off dramatically. It is caused by time spreading of the pulse at the field point. Time spreading of a signal with finite energy reduces the magnitude of its electric field. IRA's have a very narrow beam-width. For situations where it is difficult to keep the bore-sight on target we need to examine quantitatively the consequences of electric field reductions off bore-sight. In addition, we need to be able to predict EMI consequences of the IRA-generated field in the induction and electrostatic regions.
We have developed a theoretical and analytical prediction of the electromagnetic field generated by a simplified model of an IRA; it does not include the pre-pulse and some other unique features attributable to IRAs. The model provides analytical expressions for the radiation, induction, and electrostatic contributions of the electromagnetic field in spherical geometry. The source is a uniform surface current on a square plane surface. Baum has shown that an IRA antenna could be represented by a planar source provided the following conditions are met: the frequencies of concern are high enough for many wavelengths across the aperture so that (1) the blockage of the feed arms is small, and (2)

the fields outside the aperture, but on the aperture plane, can be neglected. The assumption of a uniform current distribution produces uncertainties of about a factor of two because of the inhomogeneous TEM wave launched on the aperture by the TEM transmission (conical with reflector). Also, it does not account for the energy spillover around the reflector.

HPEM 8-6: Calibration of a Wideband Hybrid Antenna

M. Stecher, **B. Klos**
Rohde & Schwarz GmbH & Co. KG

To obtain free-space antenna factors (AFs) of hybrid antennas, two different calibration procedures have been used: one with ground reflection (ANSI method) and one without ground reflection (free-space arrangement). AFs of 38 antennas are compared in an overlapping frequency range. Also the standard deviation has been calculated over the frequency range to show the precision of the manufacturing process and effects of the calibration procedures. Finally some considerations are made regarding the application of hybrid antennas.

Key words: hybrid antennas, free-space antenna factor, antenna calibration, radiated emission measurement, radiated immunity test.

Introduction: The hybrid antenna under consideration is a combination of a V-type log-periodic antenna (LPA) and a biconical antenna as displayed in Fig. 1. V-type LPAs have several advantages over normal LPAs: They have (a) higher gain for obtaining lower noise levels below the emission limit near 1 GHz in terms of field strength, (b) almost equal E- and H-plane directivities for equal illumination of the EUT in both polarizations and (c) an excellent cross polar performance.

The calibration is done using the standard site method in three frequency subranges: 30 to 150 MHz, 100 to 1000 MHz and 1 to 3 GHz. Since in the lowest frequency subrange it is difficult to achieve free-space conditions, the reflecting ground plane is used in agreement with the method of ANSI C63.5. The test setup is depicted in Fig. 2.

In the upper frequency subranges, a free-space test setup is used for calibration as depicted in Fig. 3. This is possible due to the front-to-back ratio, the increased directivity and the height above groundplane relative to the small distance of approx. 3 m.

Design and calibration of a special type of hybrid antenna will be described. Depending on frequency range, free-space antenna factors are measured using two types of standard site methods: with and without a reflecting groundplane. In a transition frequency range, the results are in good agreement. The AF standard deviation will show the quality of the design and of the manufacturing process. It can also be used to find ambients which have been overlooked and to find further improvements of the calibration setup. The preferred application of hybrid antennas is for far-field radiated emission and immunity arrangements. For near-field applications, where standardized antennas are specified, hybrid antennas may be used for precompliance purposes.

Figure 1: Hybrid antenna combining a V-type LPA and a biconical antenna.

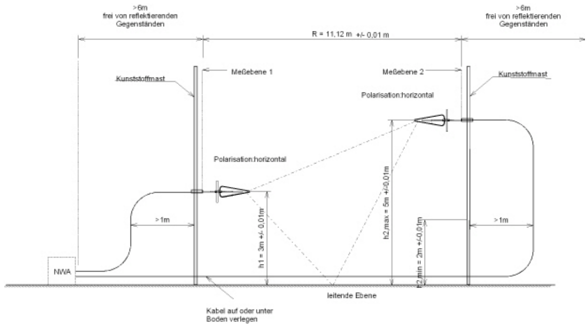

Figure 2: Test setup for the frequency range 30 to 150 MHz

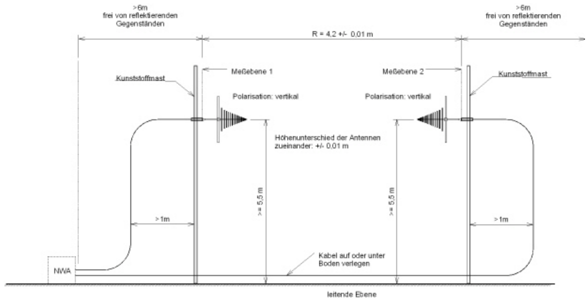

Figure 3: Free-space test setup for the frequency ranges of 100 to 1000 MHz and 1 to 3 GHz with approx. 3 m distance between the marked midpoints of the longitudinal axis of the LPA sections.

HPEM 8-7: Environmental Electromagnetic Fields Produced by Antennas

H. Singh[1], **I. Kohlberg**[2], **H. Moore**[1], **G. Boezer**[2], **J. Sarjeant**[3]
[1]*ARDEC, Picatinny Arsenal*; [2]*Institute for Defense Analyses*; [3]*University of Buffalo*

Electromagnetic interference devices are becoming more important as near term military weapons. Such devices might well be made from commercial components and become a popular weapon of choice. Over the last few years, variants of the Impulse Radiating Antenna (IRA) have demonstrated the capability to transmit potentially lethal or disruptive effects on electronic and communication systems within the kilometer range. In addition to IRAs, antenna designs based new wide-band sources and the use of artificial dielectric and magnetic materials could also produce lethal waveforms.

Until recently, the HPM susceptibility and survivability community has focused its attention on two separate issues: (1) source development, and (2) effects on selected targets produced by a variety of specific sources. As the sources mature and our understanding of effects improve, we need to deal with system issues. One of the major system issues is the susceptibility of the support systems for the source to transmit its waveform. Collateral damages and vulnerabilities of systems are stronger issues. What's the point of building a source if it causes its components to malfunction, causes damage or upset to nearby friendly assets, and causes possible adverse biological effects to humans? In order to answer these questions we need to examine the antenna's radiation, induction, and electrostatic fields in three dimensions. In some cases we may need to examine the fields within proximity of the antenna itself and possible causes of voltage breakdown in the antenna.

We examine the aforementioned EMI systems issues for several antennas used in the HPM area. We determine the frequency spectrum of the radiation, induction, and electrostatic components as a function of source voltages, generic targets, and biological effects. We also examine the time dependence of the waveforms. This collection of antennas includes the IRA antenna. For this antenna we use recently developed analytical results for the electromagnetic field.

HPEM 8-8: Pattern Reconfigurable Antenna Design by Using FDTA Method with Floquet's Boundary Condition

S. Xiao[1], **C. Yu**[2], **B.-Z. Wang**[1]
[1]*Institute of Applied Physics,University of Electronic Science and Technology of China,Chengdu 610054, P.R. China*; [2]*Institute of Applied Electronics,CAEP,MianYang 621900, P.R. China*

Periodic structures have been used as millimeter wave leaky-wave antennas, due to their advantages of light weigh, high directivity, and small size. Another intriguing property of the period structure leaky-wave antennas is that the main beam direction can readily be scanned. In these applications, there are some examples for frequency scanning antennas and pattern scanning antennas. The antennas proposed in [1](S. Xiao, "A novel reconfigurable CPW leaky-wave antenna for millimeter-wave application," International Journal of Infrared and Millimeter Waves, Vol. 23, No. 11, pp. 1637-1648, Nov. 2002.) [2] (L. Huang, "An electronically switchable leaky wave antenna," IEEE Trans. Antennas and Propagation, Vol. 48, No. 11, pp.1769 1772, Nov. 2000.) are pattern reconfigurable antennas, which can reconfigure the patterns at fixed frequencies by changing the period of the structures.
The finite-difference time-domain (FDTD) method plays an important role in the leaky wave antenna design [1][3](M. Chen, "FDTD analysis of a metal-strip-loaded dielectric leaky-wave antenna," IEEE Trans. Antennas and Propagation, Vol. 45, No. 8, pp.1294-1301, August 1997.) In literature [1], each state of the reconfigurable coplanar waveguide (CPW) leaky-wave antenna needs to be simulated to determine the maximal radiation direction. These performances will need a large amount of computational time. The structure of this pattern reconfigurable antenna is a periodic one, whose electromagnetic characteristics can be described by Floquet's theorem [4](R. E. Collin, Foundations for Microwave Engineering, New York: McGraw-Hill, 1995.) The FDTD method combined with Floquet's theorem can result in a reduction in the computational time and space [5](H. Lee , "Unit cell approach to full-wave analysis of meander delay line using FDTD periodic structure modeling method," IEEE Trans. Advanced Packaging, Vol. 25, No. 2, pp.215-222, May 2002.) because the simulation domain is restricted to a single unit cell of the periodic structure.
In this paper the pattern reconfigurable antenna introduced in literature [1] is re-designed by using the FDTD method combined with Floquet's theorem. The design results indicate that the presented novel method can predict the maximum radiation direction of each reconfigurable operation state accurately. The design time of the pattern reconfigurable periodic structure leaky-wave antenna can be reduced greatly because the simulation domain is limited to a single period unit cell for uniform period states.

HPEM 8-9: Analysis of 4 Element Array Antenna of Stacked Patches

V. K. Pandey, **B. R. Vishvakarma**
Department of Electronics Engineering, Institute of Technology, BHU, Varanasi-221005

Microstrip antennas are well suited for arrays, due to their low weight, low profile with conformability and low manufacturing cost. The major drawbacks of microstrip antennas are low gain and narrow bandwidth. A number of papers have appeared in the literature on bandwidth enhancement of microstrip antennas, such as electrically thick substrate, slot loaded microstrip antenna, stacked multipatch / multilayer antennas and impedance matching network. The bandwidth of the microstrip antenna can be enhanced by using parasitic elements.
In the present paper a linear four element stacked array antenna is analyzed and investigated. It is observed that single element stacked antenna as well as its array show marked improvement in the bandwidth, gain and directivity over the single element and single element array antenna respectively. It is further observed that both resonance frequency and gain are highly dependent on the thickness of the upper substrate and its permittivity. Typically the array antenna with stacked elements shows enhanced bandwidth of 13% as compared to 3.6% of single elements array.

HPEM 8-10: The Study of Slot Loaded Patch Antenna

Shivnarayan, **B. R. Vishvakarma**
Department of Electronics Engineering, Institute of Technology, BHU, Varanasi-221005

Narrow bandwidth is the major disadvantage of microstrip antenna in practical applications. For present day wireless communication system, global system for mobile communication system, digital communication system, and universal mobile telecommunication systems, increased bandwidths are needed for satisfactory and reliable communication. Several bandwidth enhancement or broadbanding techiniques are recently employed such as co-planar directly coupled and gap coupled parasitic patch, use of a thick air or foam substrate. It may be mentioned that bandwidth can be improved by loading the patch with suitable slots along the radiating edges of the patch. By embedding the suitable slots in the radiating patch, compact and dual-band microstrip antenna can be realized. Multiple slots are also used to control the impedance of the microstrip patch antenna.
In the present paper the analysis of a slot loaded rectangular microstrip patch antenna using equivalent circuit concept is presented. The slot is taken as a capacitive reactance on the patch. It is found that the resonance frequency decreases with increasing slot width for given slot length. It is further observed that the input VSWR remains almost invariant with the slot width and slot length, while the impedance increases almost linearly with the slot width but inversely with the slot length. The antenna shows the dual frequency behavior corresponding to TM100 and TM300 modes.

HPEM 9 - Nonlinear Dynamics and Chaos

HPEM 9-1: Interaction of Microwave with a Stochastic Jumping Phase (MSJP) with Overdense Plasmas or Gases and Electron Collisionless Heating by it

V. I. Karas'[1], **Y. B. Fainberg**[1], **A. M. Artamoshkin**[1], **R. Bingham**[2], **M. Lontano**[3], **V. D. Levchenko**[4], **I. F. Potapenko**[4], **A. N. Starostin**[5]
[1]*NSC "Kharkov Institute of Physics & Technology, Kharkov, Ukraine,* ; [2]*RUTHERFORD APPLETON LABORATORY, Oxford,United Kingdom*; [3]*Instituto di Fisica del Plasma "Piero Caldirola", EUROATOM-ENEA-CNR, Milano, Italy*; [4]*Keldysh Institute of Applied Mathematics of RAS, Moscow, Russia*; [5]*Troitsk Institute of Innovation and Thermonuclear Researches, Troitsk, Russia*

In NSC KIPT have been created newly developed plasma-beam microwave generators of intense stochastic radia-tion. These generators are based on electron beam interaction with a hybrid plasma waveguide. They have small weight and size at high output power. A 40 kW cw microwave radiation power in the 10 cm wavelength band, a 100 kW power in the shape of 4 ms long pulses, and an electron efficiency up to 50%, are ensured. The maximum power of 66 kW at the electron efficiency about 40% in the frequency range from 0.85 to 1.66 GHz was attained.
In present paper the results from a theoretical and experimental study as well as from numerical simulation of either direct or inclined incident to boundary vacuum-overcritical density plasma of the linearly polarized electromagnetic waves are discussed. The chief results of our studies are the following:
(i) at considered parameters the penetration coeffi-cient (PC) of the MSJP is about one order of magnitude higher than a PC of the wide-band regular electromagnetic wave (WREW);
(ii) in particular, at inclined incident of the MSJP an electron heating is most essential and besides the electron distribution function has high energy "tail";

(iii) there are indicated the necessary conditions for gas breakdown in stochastic fields. This anomalous behavior of a penetration coefficient, a breakdown conditions as well as the electron heating are connected with a jumping phase of MSJP.

HPEM 9-2: Intense Electromagnetic Field Interaction with Charged Particles

V. A. Buts
NNC "Kharkov Institute of Physics and Technology"

In the present report some results theoretical and experimental researches of interaction of the charged particles with electromagnetic fields of the large intensity are collected. Under field with large amplitude we shall understand the field, which satisfy to one of the following three conditions:
1. Fields for which the parameter of a wave force ( ) cannot be counted as a small parameter.
2. Intensity of fields are such, that width of nonlinear resonances at wave - particle type interactions and at a wave - wave type interaction are large than distances between these resonances.
3. Intensity of a wave field is such, that velocity of particles in it reaches phase velocity of one of virtual waves.
We shall note, that velocity of virtual waves may be small. Therefore this last case not necessarily corresponds to large intensity of fields.
According to these three cases the material of the report is allocated (see below).
1. Nonresonant Interaction of Electromagnetic Waves with Charged Particles
In this section the results of researches about interaction of particles with fields for a case when the parameter of wave force (parameter of nonlinearity) is any on size are collected.
The main achievement of modern electronics and electrodynamics are based on resonant interaction of electromagnetic waves with the charged particles. The necessity of resonances for an effective exchange of energy between particles and waves is determined by that fact, that parameter of a wave force ( ) in overwhelming majority of cases is small. Thus for a significant exchange of energy the maintenance of long synchronism is necessary. This synchronism represents resonant conditions. If parameter is not small, the charged particle gets velocity close to velocity of light during times about one period of a wave (on distances about length of a wave). In these conditions the resonances cease to play a determining role.
New nonresonant mechanisms of plasma bunch acceleration and short wave amplification are discussed in this section.
More detailed information on the contents of this section look in the separate report that has the same name as the name of this section.
2. Stochastic Heating
In this section the results of researches of interaction of particles with fields for a case when intensity of a wave is such, that width of nonlinear resonances is more than distance between these resonances are collected.
Some results of theoretical and experimental researches of stochastic heating of plasma by a field of regular waves executed in NNC "KhFTI" are stated in the report. The criteria of occurrence of dynamic chaos are formulated at interactions of a type a wave - particle and type a wave - wave.
The processes chaotization at a wave - particle type interaction allow to create conditions for more effective input of radiation energy in substance, than existing methods. Chaotization of the wave - wave type processes allows to form spectra of radiation with the given characteristics. In particular, they allow create generators of noise signals on the basis of regular generators (such as magnetron, klystron, etc.).
More detailed information on the contents of this section look in the separate report that has the same name as the name of this section.
3. Super-High Harmonic Exitation by Nonrelativistic Oscillators
In this section the results of researches of interaction of particles with fields for a case when intensity of a wave field is such, that velocity of electrons in a field of this wave are close to phase velocity of one of virtual waves are collected.
The some results of theoretic and experimental investigations about excitation high number harmonics by non-relativistic oscillators are represented in this section. Were shown that in media, which has even small periodic heterogeneity of dielectric permeability or potential, non-relativistic oscillators can radiate as relativistic particles. They can efficiency radiate high number harmonics. The theory as one particle radiation as selfconsistent nonlinear theory radiation of oscillator ensemble was created. The experimental results confirm the main results of theory. In particularly, there was exited ultraviolet radiation in experiment, when on a crystal intense ten-centimetric radiation was acting.

HPEM 9-3: Stochastic Heating

V. A. Buts
NNC "Kharkov Institute of Physics and Technology"

Some results of theoretical and experimental researches of stochastic heating of plasma by a field of regular waves executed in NNC "KhFTI" are stated in the report. The criteria of occurrence of dynamic chaos are formulated at interactions of a type a wave - particle and type a wave - wave.
For interactions of a type a wave - particle a condition of dynamic chaos occurrence are formulated for all known resonances: Cherenkov, cyclotron, cyclotron on abnormal and normal effects Doppler, parametrical, combinational. Is shown, that at performance of conditions of local instability development to the description of particles dynamics the methods of statistical physics can be used. At this condition the good qualitative consent of analytical results with numerical results is received.
Diffuse of particles in energy space was investigated by analytical and numerical methods. There was shown, that for simple, fast, qualitative estimations of efficiency of plasma heating by a regular electromagnetic wave field one can use following parameter , where - frequency of an electromagnetic wave, in which charged particles are traveling; - relation of nonlinear resonances width to distance between these resonances. This parameter represents effective collision frequency and characterizes speed of plasma heating. It is visible, that the effective collision frequency can be about frequency of an electromagnetic wave.
The comparison of stochastic heating efficiency by an external noise field and by field of a regular electromagnetic wave in conditions of development of dynamic chaos is carried out. Is shown that at an identical flow of capacity the efficiency of heating by regular waves considerably exceeds efficiency of heating by a noise field. Let's notice that in many real experimental conditions for the dynamic chaos does not develop. More often it is caused by unsufficient intensity of radiation. Is shown that practically always it is possible to alter conditions of experiment to achieve development of local instability.
The comparison of the known schemas of stochastic acceleration, which are used in plasma traps, with investigated by us, is carried out. Is shown that the time of heating in our schemas of acceleration in ratio is less, than in traditional schemas. Here - period of a high-frequency wave; - run time of the charged particle between stoppers of a plasma trap. The opportunity of heating of solid-state plasma up to thermonuclear temperatures is considered also at influence of several flows of laser radiation. Is shown, that at sufficient moderate intensities of laser radiation ( ) enough three beams of laser radiation for heating a solid-state target up to thermonuclear temperatures during the times smaller than dispersion time of a solid-state target.
The experimental researches of plasma heating in a plasma trap with using electron cyclotron resonances were carried out. The consent of theoretical results and experimental researches is received. If the conditions of local instability were not carried out, temperature of plasma did not exceed 100 eV. At creation of conditions for development of local instability temperature of plasma exceeded 1,5 MeV.
In conditions of experiment 50 % of high-frequency capacity that fall down on plasma, was transformed into a thermal energy of plasma particles. The time of plasma heating was short, and made up about hundred periods of a high-frequency field.
The conditions at which the interaction of a wave - wave type be-

comes chaotic, were formulated. All numerical researches confirmed this criterion (analytically received). Most important result of research of the wave - wave type interaction was the proof of fact, that the modified disintegration always is stochastic unstable. Use of this criterion has allowed to define frameworks of validity of the theory of regular dynamics weak-nonlinear interaction of waves. This condition also allows to define conditions, when for the description of wave - wave type interaction the methods of statistical physics can be used. As one of examples we shall consider the cascade of disintegrations arising at influence on plasma of intensive radiation on the beat-wave scheme. . The conditions of regular dynamics realization of such cascade and conditions for chaotic regimes of these disintegrations are found.

In the conclusion we shall note the most important possible applications of the investigated processes. The processes chaotization at a wave - particle type interaction allow to create conditions for more effective input of radiation energy in substance, than existing methods. Chaotization of the wave - wave type processes allows to form spectra of radiation with the given characteristics. In particular, they allow create generators of noise signals on the basis of regular generators (such as magnetron, klystron, etc.).

HPEM 9-4: Nonresonant Interaction of Electromagnetic Waves with Charged Particles

V. A. Buts
NNC "Kharkov Institute of Physics and Technology"

The main achievement of modern electronics and electrodynamics are based on resonant interaction of electromagnetic waves with the charged particles. The necessity of resonances for an effective exchange of energy between particles and waves is determined by that fact, that parameter of a wave force ( ) in overwhelming majority of cases is small. Thus for a significant exchange of energy the maintenance of long synchronism is necessary. This synchronism represents resonant conditions. If parameter is not small, the charged particle gets velocity close to velocity of light during times about one period of a wave (on distances about length of a wave). In these conditions the resonances cease to play a determining role.

New nonresonant mechanisms of plasma bunch acceleration and short wave amplification are discussed in this report. These mechanisms are based on the possibility of effective interaction of charged particle with a field of an intensive transverse electromagnetic wave. This interaction exists despite of both the absences of a resonant interaction of the particle and the wave and the absence of high frequency pressure forces. The possibility of the interaction results from the rigorous solution of the problem of a charged particle movement in electromagnetic field with an arbitrary strength. It is shown, that this interaction can be used both for effective acceleration of plasma bunches and for electromagnetic wave amplification. The strength of longitudinal electric field, that accelerates plasma ions can be more then the intensity of the transverse field of accelerating electromagnetic wave.

It is necessary to emphasize, that the dynamics of a particle in the field of intensive electromagnetic wave qualitatively differs from its dynamics in the field with small intensity. Leading role in the particle dynamics plays transversal motion, when the field strength parameter is small (, where are transversal and longitudinal momentum of particle respectively). When field strength parameter is large, longitudinal motion is more essential.

HPEM 9-5: Super-High Harmonic Exitation by Nonrelativistic Oscillators

V. A. Buts
NNC "Kharkov Institute of Physics and Technology"

The some results of theoretic and experimental investigations about excitation high number harmonics by non-relativistic oscillators are represented in this report. Were shown that in media, which has even small periodic heterogeneity of dielectric permeability or potential, non-relativistic oscillators can radiate as relativistic particles. They can efficiency radiate high number harmonics. The theory as one particle radiation as selfconsistent nonlinear theory radiation of oscillator ensemble was created. The experimental results confirm the main results of theory. In particularly, there was exited ultraviolet radiation in experiment, when on a crystal intense ten-centimetric radiation was acting.

HPEM 9-6: Stability of Stationary States and Nonlinear Chaotic Modes in Generators with Virtual Cathode and Feedback

V. E. Novikov[1], **I. I. Magda**[1], **A. V. Paschenko**[2], **S. S. Romanov**[2], **I. M. Shapoval**[2]
[1]*Science and Technology Center of Electrophysics, NASU*;
[2]*National Science Center "Kharkov Institute of Physics and Technology"*

Particle and electromagnetic feedbacks are used in real-life microwave devices with virtual cathode (VC) to increase the efficiency and output parameters control. An analytical theory of stability of oscillations in cathode-anode (C-A) and VC areas of vircators is considered. Conditions of feedback, nonlinear and chaotic oscillation modes in vircator systems with control circuits are analyzed.

In the considered approach it is supposed that feedback in the area of interest can be produced by means of particle flows and electromagnetic fields which are brought from other areas. It is also taken into account that a high-current diode dynamics is provided by particle flow instability in C-A area. The affect of feedback can be modeled with the help of the effective potential Ueff, introduced into definite area. A self-consistent model of the vircator with feedback which takes into account non-stationary processes in supercritical current diode and VC area is proposed. This model is based on the analysis of stationary states of the diode and their stability.

The study of system stability considers a two-beam (direct and reflected) and non-uniform problem. The closed analytical expressions for hydrodynamics, field and spectral characteristics of oscillations in the C-A and VC areas are obtained. The two-beam state instability in two coupled C-A and VC areas, as it is in typical VC system, depends on the voltage applied between C-A gap, the area dimensions, and the generalized beam parameter, which is connected with the effective potential q=q(Ueff). The feedback signal which is formed by reflected particles at initial stage is a "seeding" for instability in C-A area. The signal amplified by this instability is brought by direct beam into VC area, and provides additional modulation of VC oscillations. The conditions for optimum feedback correspond to unstable modes of VC.

The affect of control circuits (corresponding to particle and electromagnetic feedback) in vircator can be submitted by the dynamics of two coupled nonlinear oscillators. A qualitative analysis of these coupled oscillators and fields is carried out. Conditions for the system excitation and for transactions between chaotic and regular generation modes in regard to the effective potential Ueff are demonstrated.

HPEM 9-7: Nonlinear and Chaotic Modes of Oscillations Arising at Propagation of Short Pulses on Non-Uniform Transmission Lines

V. E. Novikov[1], **I. I. Magda**[2], **A. V. Paschenko**[2], **I. M. Shapoval**[2]
[1]*Science & Technology Center of Electrophysics, NASU*;
[2]*National Science Center "Kharkov Institute of Physics and Technology"*

Many effective methods for studying the signals propagation through the medium use its representation as a network of transmission lines. Usually these lines are considered ideal, but in real cases it is essential to take into account the interaction of short pulses while their multi-ray propagation, as well as the scattering and reflection at non-uniformities. The propagation of short pulses through medium with regard to scattering at non-

uniformities is considered, and the arising chaotic modes are analyzed. It is shown the occurrence not only variation in the pulse amplitude, but also essential changes in the spectrum.
For analytical decision of interaction problem for short pulses in the transmission line, a model of Riman waves interaction is used. The coefficient of reflection at non-homogeneities is assumed as frequency dependent on the frequency of the incident signal. The pulse envelope variations which arise at repeated reflections and complex signal formation are analyzed. This kind of evolution of the signal with wide frequency spectrum as a result of multiple reflections and interactions between pulses is equivalent to the existence of some effective nonlinearity in the line. A nonlinearity and dispersion which can exist in the line simultaneously, provide the possibility for occurrence a soliton-like decisions.

HPEM 9-8: Peculiarities of Particles Motion at Passing Through Stochastic Layer

V. A. Buts, **A. P. Tolstoluzhsky**
National Science Center "Kharkov Institute of Physics and Technology"

At development of dynamic chaos in a Hamiltonian system all phase space is divided into regions with random and regular behaviour. In particular, than Kolmogorov's entropy is greater, then the regions with regular motion are less. If the Kolmogorov's entropy is small, in regions with random behaviour the stochastic web can be formed and Arnold's diffusion can be arisen.
The investigation of regions' boundaries separating random behavior from regular, shows that these boundaries are fractal and have property "sticky". The result of such "sticky" can be the seeming breaking of the second law of thermodynamics [1].
For beam problems, i.e. for problems of electromagnetic waves generating and problems of charged particles acceleration by electromagnetic fields, the basic role is played the interaction of wave-particle type. Such interaction, more often, can be simulated by the equation of mathematical pendulum. At that the separatrix of mathematical pendulum, separates (flying) transit particles from trapped particles. In actual situations the separatrix is splitting (as a result of always available disturbances), forming a stochastic layer.
Dynamics practically all of beam instabilities contains the passing of beam particles through a stochastic layer as one of its elements.
In the present report, the peculiarities of charged particle passing through a stochastic layer are analytically and numerically investigated. As an example we considered the model of mathematical pendulum, which separatrix splitting by external high-frequency excitation, and which has a positive or negative dissipation. The most important and common peculiarity of such passing is the considerable increasing the time of particle passing through stochasticity region.
Besides that, we considered the case of excitation of a monochromatic wave by an electron beam at Cherenkov's effect. Also the peculiarities of beam particles dynamics are analyzed at such excitation.

1. George M. Zaslavsky, Physics Today, N8, 39 (1999).

HPEM 9-9: Un-Linear Processes in the System " Ferroelectric Working Body – Spiral MCG - Capacitive Load"

D. Tret'yakov, **A. H. Adzhiev**, **A. Soukatchev**
High Mountain Geophysical Institute

A ferroelectric working body under shock wave (Fig. 1) can be used for forming initial magnetic field in the spiral magnetic cumulative generator (MCG). If the shock wave is strong enough for transferring the working body material from ferroelectric to paraelectric state, depolarization current takes place in the working body.
Equivalent electric circuit of a ferroelectric working body can be represented as parallel connected source of current, capacitance and resistance. The depolarization current and the value of the resistance are un-linear functions of time, working body voltage and other parameters. The functions can be described by empirical formulae.
A point on the phase plane of non-dimensional parameters (Fig. 2) characterizes the energy state of the system. Non-dimensional parameters include I – current in the electric circuit of the spiral MCG, U – capacitive load voltage, L – initial inductance of the spiral MCG, C - capacitive load, P - change in polarization of the working body after the front of the shock wave, v – speed of the shock wave, b – linear dimension of working body.
Before the contact of the liner with solenoid the system has the phase path 1. After the contact the system changes phase path (2, 3 or 4). The new phase path depends on the time of the contact and on the un-linear process in MCG (D.V. Tret'yakov, "The Effect of the Insulation of the Wires of a Helical Magnetocumulative Generator on Its Operation" Electrical Technology Russia, # 2, 2001, p.124 -134). If the working body voltage exceeds the critical value an electrical breakdown takes place and the phase path of the system changes its form.
A cube ferroelectric working body with rib of 2 cm is able to change a capacitor of 1000 pF to 20 – 30 kV. Electric circuit of the ferroelectric working bodies is used for increasing of energy. Two ones are showed on Fig. 1. The accurate within 0,1 – 0,3 microsecond synchronization of process in other working bodies is not a difficult technology problem.

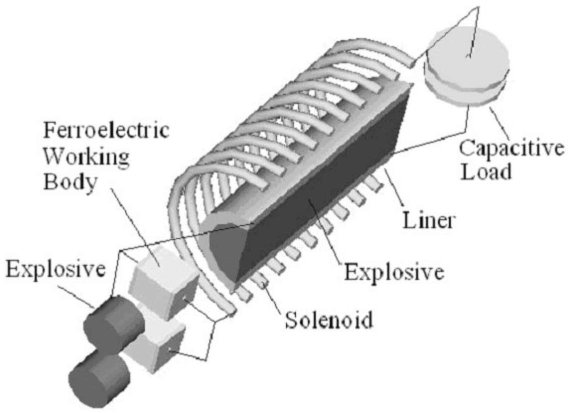

Figure 1: The system "ferroelectric working body – spiral MCG - capacitive load".

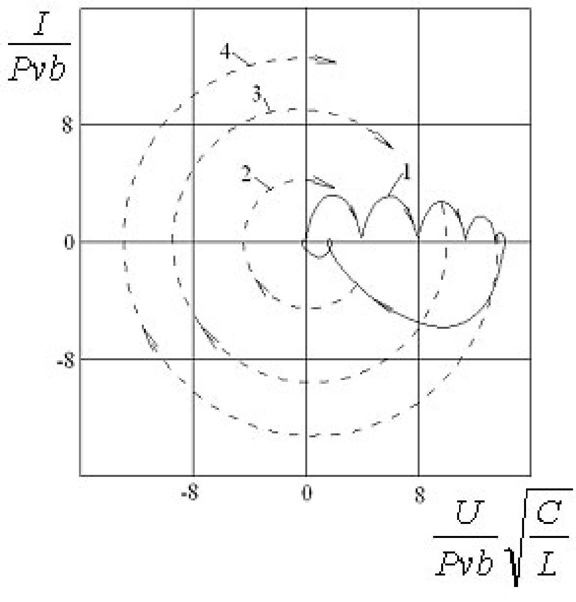

Figure 2: The phase plane of non-dimensional parameters.

HPEM 9-10: Self-Modulation and Chaos in a Free Electron Laser with Electromagnetic Pumping

T. Dmitrieva, **N. Ryskin**
Saratov State University

Free electron lasers (FELs) have the potential of providing very high-power, continuously tunable, coherent radiation over an extensive range of wavelengths [1], and are currently the subject of intensive research effort. In this paper, we discuss nonlinear dynamics of a model of a scattron FEL amplifier and oscillator based on the induced backscattering of two transversal electromagnetic waves on a relativistic electron beam [2]. We consider the system in the case of a moderately relativistic electron beam with accelerating voltage of 100-300 kV and pumping from a high-power millimeter wave source in order to produce radiation with frequencies in teraherz region.

In the first part of the work, we present the results of numerical simulations of the amplifier configuration. For the scattron FEL amplifier, self-modulation effect was observed for the first time in [2]. The physical origin of self-modulation in the FEL amplifier is the parasitic feedback that takes place due to counter propagation of the pump wave. Apart from [2] our approach correctly considers the frequency dependence of the FEL gain. Various periodic, quasi-periodic and chaotic self-modulation regimes are described in a wide range of the system parameters (input signal power and frequency, system length, etc.). Mainly, a quasi-periodic route to chaos takes place.

In the second part, we study the FEL oscillator with delayed feedback that can be realized by placing the system in a cavity. Two different mechanisms of self-modulation are described. With the increasing of either the beam current, or the cavity Q-factor, transition to chaos takes place. We compare the results with our previous studies of several microwave delayed feedback oscillators [3,4].

This work was supported by the CRDF (Award No. REC-006), Russian Foundation for Basic Research (Grant No. 03-02-16192), and by the Russian Ministry of Education program for graduate student support (Grant No. A03-2.9-810).

References

[1] T.C. Marshall. Free Electron Lasers. Macmillan, New York (1985).

[2] N.S. Ginzburg, A.S. Sergeev. Journ. Comm. Technol. Electron. Vol. 33, 580 (1988).

[3] T.V. Dmitrieva, N.M. Ryskin, Journ. Exp. Theor. Phys., Vol. 93, 1314 (2001).

[4] N.M. Ryskin, V.N. Titov, S.T. Han, et al., Phys. Plasmas, Vol. 11, No. 3, to be published (2004).

HPEM 9-11: Problems of Modeling Communication Channels Under Influence of Electromagnetic Fields with Chaotic Spectrum

S. J. Leonov, **V. D. Dmitrienko**, **A. A. Serkov**
National Technical University "Kharkov Politechnic Institute"

Wide introduction of computer networks, which frequently operate under conditions of serious electromagnetic interference, demands either improvement of known methods for their mathematical modeling or development of new ones. It especially concerns methods for modeling wire and the cable lines and terminal devices connected to them, which are the most vulnerable to electromagnetic interference,.

The most known mathematical apparatus for description of digital system is Boolean algebra. Being suitable for description of device structures and functional dependencies between their input and output, this classical mathematical apparatus doesn't allow adequate description of dynamics of system behavior evolving in time including transient processes and temporal characteristics of system elements, changes in amplitude and fronts of interference leading frequently to violation of preset function laws.

K-value logic (when signal front is represented as a sequence of segments – each with a certain time delay) allows taking into account the most of dynamic processes concerned with changes in signal amplitude and fronts. However this method fails to give natural account for differential and integral connections among system elements.

The method of continuous differential and integral equations allows detailed description of transient processes in digital and hybrid devices, but it requires too many computational resources for analysis of real-scale communication channels.

Thus, the analysis of known methods for mathematical modeling of communication channels shows that there are no such methods available combining adequate descriptive abilities with moderate requirements to computational resources in task of study of communication lines influenced by electromagnetic interference. So the most promising is to use K-value differential calculus (where K is a simple number). It provides a new class of mathematical models (K-value differential and integral models) for studies in finite and infinite spaces of digital and hybrid computer systems - analogous to the way it is done with Boolean differential calculus. K-value differential models allow more close estimation of communication channel serviceability than the one possible with Boolean rings and spaces. This is achieved due to K-valued – instead of binary – representation of physical signals. Usage of these models is also cheaper in comparison to modeling with continuous differential equations.

Testing this mathematical apparatus on simple model examples confirmed applicability of K-value differential models to either micro approach or macro approach – i.e. studying large-scale communication channels.

HPEM 9-12: Techniques for Maintaining Survivability of Electronic Systems Under Electromagnetic Interference of Chaotic Spectrum

A. A. Serkov, **V. I. Kravchenko**
NTU "Kharkov Polytechnic Institute"

In solving tasks of electromagnetic compatibility of radio-electronic systems, the frequency band of possible electromagnetic emissions is one of the most important parameters. In most cases, various co-placement topology of devices, emission directions, multiple reflection, interference, selective absorption of electromagnetic energy in certain frequency band, make it possible to talk of emergence of chaotic spectrum electromagnetic emission. This is most evident in impulse electromagnetic interactions characteristic for wide band electromagnetic emissions. When chaotic spectrum electromagnetic emissions reach certain power, its influence on radio-electronic system should be discussed in the aspect of survivability of those systems.

By system's survivability we mean its ability to adapt to new situation and continue to fulfill its main function resisting chaotic spectrum electromagnetic emissions due to corresponding internal reorganization of the system, alterations in functions of its parts and in general behavioral strategy. Concept of survivability is more general than concepts of adaptivity, stability and reliability, and should be more widely used in discussion of electromagnetic compatibility problems. It should be also noted that, due to their great extent, wire and cable communication lines of radio-electronic systems are the most vulnerable to influence of chaotic spectrum electromagnetic inference so do the devices directly connected to them. Traditional protection techniques use nonlinear protective devices, which usually don't solve all problems but introduce additional unpredictability to the character of electromagnetic spectrum that influences information signals transmitted in the system. To ensure electromagnetic compatibility it is desirable – starting on development stage – to provide abilities structural reorganization of the systems utilizing self-diagnosing structures. It especially concerns devices connected to long communication lines. As far as contemporary systems combine hardware and software components, it is necessary to use hardware and software protective means in complex.

In process of either developing new elements or testing elements of existing vital systems under chaotic spectrum electromagnetic interference, the proposed framework can be implemented as a set of techniques and rules, which can be used in an expert system for solving problems of electromagnetic compatibility and survivability of radio-electronic systems. The authors are currently developing such expert system.

HPEM 9-13: Analysis of Chaos in a Simple Resonant Circuit

W. Crevier
Jaycor/Titan

The Linsay circuit provides a convenient analytical and experimental method for investigating chaotic-like responses in circuits. The qualitative behavior of the response can be explained using simple circuit concepts. At resonance, period doubling for an un-modulated source results from the effective capacitance increasing a factor of four–resulting in a resonance at half the zero-voltage resonant frequency.
If a realistic model is used for the junction capacitance (one that eliminates the singularity at the built-in voltage), the nonlinear diffusion capacitance is found to be the source of period doubling and the more complex behaviors seen at higher source voltages. Even when the circuit response appears "chaotic", all circuit response parameters are limited in amplitude to well predicted values (Figure 1).
This work was sponsored by the Defense Treat Reduction Agency

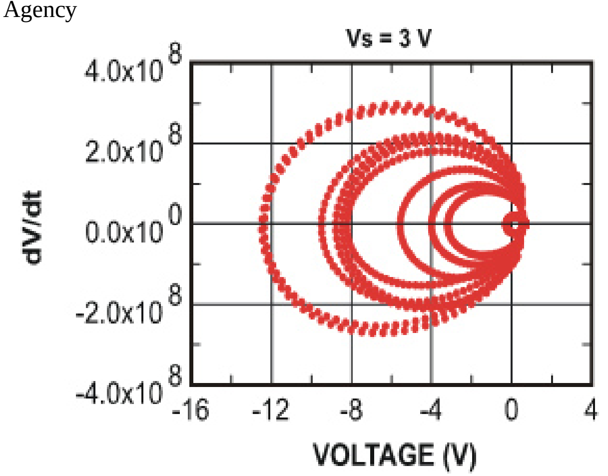

Figure 1: State space diagram of response at 3 V.

HPEM 9-14: Theoretical and Experimental Research of Chaotic Dynamics and Structure Formation in Electron Beams with Virtual Cathode

A. E. Hramov[1], **Y. A. Kalinin**[2], **A. A. Koronovskiy**[1], **D. I. Trubetskov**[1]
[1]*Saratov State University, Department of Nonlinear Processes* ;
[2]*Saratov State University, Scientific Reseach Institute "Open Systems"*

The analysis of oscillatory processes in extended intensive beams of charged particles in regimes of the virtual cathode formation is rather important and actual problem. It is well-known (N.N. Gadetskii, I.I. Magda et al, Plasma Phys.Rep. 1993; V.D. Selemir, B.V. Alekhin et al, Plasma Phys.Rep., 1994; V.G. Anfinogentov, A.E. Hramov. Radiophysics and Quantum Electronics, 1998; A.A. Koronovskii, A.E. Hramov, Plasma Phys. Rep., 2002) that such systems are characterized by complex dynamics and can show a wide spectrum of the nonlinear phenomena, including the dynamical chaos. Researches of complex chaotic oscillations in systems with the virtual cathode are very important both from the fundamental point of view to investigate of chaotic dynamics and pattern formation in the distributed active media and for the practical applications to create broadband noise-type microwave radiation sources.
The present report deals with theoretical and experimental research of oscillatory processes in an electron beam with an overcritical current (overcritical perveance). The purpose of this work is the investigation of physical mechanisms which lead to the broadband chaotic generation in the systems with the virtual cathode.
In our research we have used the numerical 2D simulation of processes in electron beam with a overcritical current. The method of large particles has been applied. It has been shown that strong dependence of virtual cathode oscillation characteristics on injected current and external focusing magnetic field takes place. If the value of focusing magnetic field is enough large, the movement of electrons in the beam is close to one-dimensional. In this case we have observed essential complication of microwave radiation spectrum with electron beam current (perveance) increasing. Thus, the transition from the regime of close to regular oscillations to a regime of the complex chaotic oscillations with a narrow-band power spectrum takes place. When the value of a magnetic field decreases the power spectrum of chaotic microwave generation becomes broadband. It has been shown, that such behaviour of system is determined by electron beam dynamics in a cross direction and formation of several virtual cathodes (electron structures) in electron-wave system with a overcritical current. This result is verified by means of Karhunen-Loeve decomposition of the space-time data. The interaction between these structures can be interpreted as the internal distributed feedback. It leads to the complication of the space-time dynamics of electron beam in vircator, and as consequence, to formation of the broadband noise-type chaotic microwave radiation.
The system with an intensive not relativistic electron beam with overcritical perveance has experimentally been investigated. This system is the diode space region with a braking electric field and intensive electron beam. It has been shown, that microwave signal generated by the electron beam with virtual cathode looks like noise-type oscillations in the wide range of frequencies (an octave and more). Experimental results of investigation of spectral and power characteristics of microwave generation of an intensive electron beam with virtual cathode agree qualitative with the results of the theoretical research well.
This work has been supported by Russian Foundation for Basic Research (project 02-02-16351), Program of Leading Scientific School Support (NSh-1250.2003.2) and U.S. Civilian Research & Development Foundation for the Independent States of the Former Soviet Union (CRDF), grant REC-006. A.H. also acknowledges "Dynasty" Foundation.

HPEM 9-15: Investigation of Chaotic Synchronization of Two Coupled Backward-Wave Oscillators

A. A. Koronovskiy, **A. E. Hramov**
Saratov State University, Department of Nonlinear Processes

This work deals with chaotic synchronization of two coupled simple models of backward-wave oscillator. The backward-wave oscillator is the simple (but important) microwave system demonstrating both periodic and complex chaotic behaviour (N.S. Ginzburg, S.P. Kuznetsov et al. Radyophysics and quantum electronics, 1979; D.I Trubetskov, A.E. Hramov. Lectures on microwave electronics for physicists. Vol. 1. (in Russian). Moscow, Fizmatlit, 2003). This system is widely used in different applications therefore the analysis of such systems is the most actual problem. The new approach of chaotic phase synchronization analysis has been proposed. This approach is based on the consideration of the instantaneous phase family introduced by means of continuous wavelet transform (A.A. Koronovskii, D.I. Trubetskov, A.E. Hramov. Doklady Physics, 2004). Using approach mentioned above it has been shown that the phase synchronization of two coupled chaotic systems takes place whereas the other traditional methods (see, e.g. A. Pikovsky, M. Rosenblum, J. Kurths. Synchronization: a universal concept in nonlinear sciences .Cambridge University Press, 2001) fail.
It has been shown that when the coupling parameter increases the phase synchronization arises. We have also proposed the new quantity characterizing the measure of the phase synchronization of two distributed chaotic system. This quantity is defined by means of the portion of the wavelet power spectrum energy being fallen on the synchronized time scales. It takes value between 0 (the phase synchronization does not appear) and 1 (the chaotic lag synchronization takes place). The dependence of the synchronization measure on the coordinate of the backward-

wave tube interaction space has been analyzed. The physical processes responsible for the transition from asynchronous oscillations to phase synchronization regime have also been considered.

This work has been supported by Scientific Program "Universities of Russia. Fundamental Research" and U.S. Civilian Research & Development Foundation for the Independent States of the Former Soviet Union (CRDF), grant REC-006. A.H. also acknowledges "Dynasty" Foundation.

HPEM 9-16: Reduction of the Three-Wave Decay Threshold Depending on the Multiplicity Passage of the Stochastic Layer

V. G. Lapin[1], **N. F. Yashina**[2]

[1]*State Architecture and Construction University, Iljinskaya st., 65, Nyzhny Novgorod, 603950, RUSSIA*; [2]*State Technical University, Minina st., 24, Nyzhny Novgorod, 603950, RUSSIA*

It is well known what in a dissipative media resonant three-wave decay process take place in the case the pump wave intensity exceeds the threshold value. We assume the pump wave has the biggest frequency and the preassigned field. If the threshold is exceeded, the generated waves intensities grows exponentially depending on the distance, passed by the resonant wave triplet in nonlinear medium. Otherwise there will be no generated waves at the exit of the sufficiently long layer.

In a stochastic dispersive medium the wave numbers varies depending on the position according to different laws. So, the space fluctuating wave number difference (or space nonsynchronism) $\Delta k(z)$ take place. The presence of $\Delta k(z)$ sufficiently modify the wave decay process. In the case $\langle \Delta k(z) \rangle = 0$ and delta – correlated, the threshold pump intensity rises in G/(2a) times in comparison to that of for uniform medium (G – fluctuation intensity, a – dissipation coefficient. We assume what $G >> a$, and in this case fluctuations are of importance). This result was obtained recently (C. Laval, R. Pellat, O. Pesume, A. Ramani, M.N. Rosenbluth, E.A. Williams. Phys. Fluids, 20, 2049,1977). We have analyzed the threshold value in the case the wave triplet passes medium, which is composed of large repeating identical stochastic layers i.e. multiple pass of the same layer. There is a long scale correlation of spatial fluctuations in this case. Hence substantial mathematical problems arises. So we have modified the method of diffusion – like stochastic process (V.I. Klyatskin, Stochastic equations and waves in nonuniform random media, Nauka, Moscow, 1980. in Russian) and examined the threshold intensity depending on the number of identical layer passes by the wave triplet. We have deduced, what at the exit of two identical layers the threshold is as much as G/(3a) times more then for uniform medium. In the case of three identical layers the same coefficient is approximately equal to G/(4a).

So we may draw a conclusion about the threshold diminishing while the random layers passes multiplicity rises. Threshold reduces with the multiplicity rise and tends to that of uniform medium.

It is strikingly what the addition of layer may lead to the appearance of the generated wave at the exit of the medium at the same time in the shorter medium averaged intensities of generated waves tends to zero.

HPEM 9-17: Analysis of the Adequacy of EMP Simulation

L. V. Vavriv, **A. E. Serebyrannikov**

National Technical University "KPI"

The present-day problem of an effective use of high-powerful EMP simulators for experimental estimations of radioelectronics stability is a correct choice of the testing pulses parameters. This choice must provide the highest authenticity of simulation to operation conditions. It is realized for the complete adequacy level. In this paper the possibilities of realization of the complete adequacy have been studied for an aircraft object modeled by a finite perfectly conducting cylinder.

For the correct choice of the parameters of testing pulses it is necessary to take into consideration a number of peculiarities of the fast transition EMP (FT EMP) interaction with the object both during the operation and tests in the simulators. To these peculiarities one can refer the resonant character of FT EMP interaction with an object, the superposition of the natural frequencies, defining the diffusion inside the object through the screen walls, is negligibly small and the principal penetration occurs through the irregularities in the walls of screen-casing. Therefore, we shall consider further only the latter interaction mechanism. Let us also suppose that the dimensions of irregularities are small in comparison with the dimensions of an object. In this case when some assumptions are met, it is sufficient to determine the distribution of current induced on the homogeneous screen and then to determine fields inside the screen that are mainly stipulated by the action of irregularities. For example, the resonant scattering of outer noise-carrying field on the object occurs during the interaction of nanosecond fields with the screen-casings of aircraft having the characteristic dimensions. As a result, the spectral density of a current induced on the envelope and defining the field levels of the high-frequency components inside the screen-casing has an explicit resonant character.

The spectrum of natural frequencies of electrodynamics system "test object - FSS" can be represented in the first approximation as a superposition of frequencies spectrums of the object located in the free space and of the FSS of simulator. The conditions when the complete adequacy could be realized have been defined using the analysis of the spectrum s of induced currents in cases of both operation conditions and simulation.

To solve this problem the advanced electrodynamics apparatus has been used. The problem is reduced for calculations of the currents induced on cylinder. It includes formulation of the problem using tensor Green functions, Pocklington integral equation for induced currents and its asymptotic solution on the basis of the method of sequential approximations.

The recommendations for further modifications of high-powerful EMP simulators have been formulated on the basis of obtained result. In addition, let us note, that the way for choice of the testing pulses parameters proposed in this paper at all is not limited by thin cylinder model. It has a common methodological importance.

HPEM 9-18: Effects of Production of Electrodynamic Fractal Structures and Extreme Fields in Beam-Plasma Systems under Pulsed Beam Action

A. V. Paschenko[1], **S. V. Adamenko**[2], **V. E. Novikov**[3], **I. M. Shapoval**[1]

[1]*National Science Center "Kharkov Institute of Physics and Technology"*; [2]*Electrodynamic Laboatory "Proton-21", Kyiv, Ukraine*; [3]*Science & Technology Center of Electrophysics, NASU*

The plasma-field structures arise under the action of pulsed energy sources onto the surface of condensed media. As pulsed sources, in the experiments carried out at "Proton-21" Electrodynamic Laboratory, we used relativistic electron beam with currents higher than 100kA. Those REB beams were generated in high-current diodes. As a result of the experiments, we have recorded regions in the anode with the extreme parameters. The densities in those regions exceeded by several orders of magnitude the densities in the metals, with their temperature being on the order of 35-38keV.

Under the action of high-current beams on the anode, a fast plasma creation takes place throughout the plasma volume, producing energy flows and those of matter from periphery to axis. While considering the macroscopic flows in these systems, the non-linear phenomena and peaking processes come into the foreground.

Our paper is aimed to study some novel possibilities of the production of extreme fields in plasmas that come into being in the conducting medium, resulting from the non-linear process maturity.

Among the non-linear processes that bring about the plasma extreme parameters, the major ones are those that involve the peak-

ing for the thermodynamic plasma parameters and emergence of the non-linear structures. In the course of structure creation in the plasmas, it is the electrodynamic processes that play the major role.
If the incoming energy and matter processes into the system occur faster than their dissipation, then, we witness the concentration of energy and matter. A non-linear wave of electron density comes along that steepens during its travel and falls back onto itself.
While fulfilling certain conditions on the electron and ion flows, in the sets of the Maxwell equations and characteristic equations with the cylindrical and spherical symmetries, there occur the quasi-stationary fractal plasma field structures with the spatial scale tapering from periphery to center (Fig.1.). Such fragmentation of the scales leads to a drastic enhancement (by 3 or 4 orders of magnitude) of the electric field and emergence of the extreme states of the matter that agree with the states, obtained in the experiments.

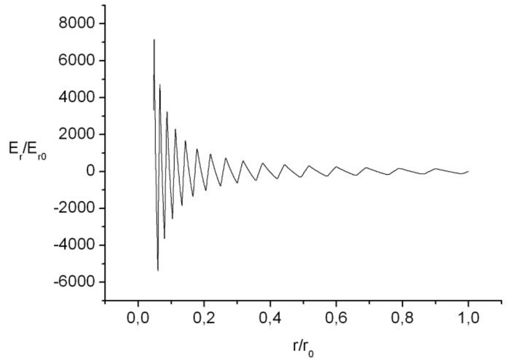

Figure 1: Fractal structure of the electric fields, expressed in the relative units in the plasma spherical region with virtual electrodes (radius measured in the units of the region dimensions)

HPEM 9-19: A Model of Non-Thermal Action of a Complex Sequence of Short Electric Pulses on Physical Properties of Oils on the Base of Non-Linear Dynamics of Molecules and Transmission Lines

V. E. Novikov[1], **V. A. Rozdestvenskiy**[2], **A. M. Naboka**[2], **I. I. Magda**[3], **A. V. Paschenko**[3], **V. F. Klepikov**[1], **V. I. Litvinenko**[1]
[1]*Science & Technology Center of Electrophysics, NASU*; [2]*Corporation "UkrGazNefteMash"* ; [3]*National Science Center "Kharkov Institute of Physics and Technology"*

This paper offers an approach for the solution of the problem of fast-growing asphalt-paraffin deposits (APD) in the oil wells and pipes on the base of the electrophysical methods of action on APD. As different from the common microwave techniques of combating the oil clog-ups that employ only their thermal action, we come forward with a sequence of short pulses, that cause rather the creation of quasi-stationary non-equilibrium states than a substantial heating of oil. In order to enhance the effectiveness of the technique, the sequence of pulses can be formed, as a complexly modulated one, retaining the shapes of the individual pulses.
The composition of the APD molecules includes the groups -CH- and C-C with the characteristic wavelengths of the oscillations that belong in the micron range. A physical model is considered for a long molecule, shaped as a string of interacting oscillators. In this model, one can consider the excitation of molecule owing to the impact action onto one of its extremities by e-m pulse and further perturbation propagation, starting from the pulse sequence in the molecule not unlike pulse propagation in the equivalent electric model, represented as a long transmission line with the non-linear interactions between the links (compounds included in the molecule composition). In the course of pulse propagation following that transmission line there appear microwave inclusions. In our approximation, we can roughly compute the action, composed of two fundamental frequencies, as corresponding to the one of individual pulse duration and that belonging to the characteristic pulse leading edge time. The analytic studies of the spectral composition of the oscillations following the long transmission line, for the two-frequency interactions, were made, obtaining the expressions for the higher-harmonic amplitudes as generalization of the Bessel-Foubini formula.
Amplitudes of the oscillations up to the one hundredth harmonic, concerning the line excitation on the two frequencies, have a rather large value.
To verify this concept, we carried out some experiments on bringing the action to bear on oil with the pulses that have the amplitude 60 keV, duration 5 ns, average rep rate 200 Hz during 5 seconds. The oil IR spectra were studied in the original state, after heating up to 80 degrees centigrade and treatment with the sequence of pulses of oil specimens with the mass 100 g during 5 s.
We demonstrate that the oil IR spectral variations, as a result of impact of the sequence of pulses, are equivalent to the IR spectral variations, resulting from the heating.
In this way, the effective oscillatory system excitation depends rather on pulse power input, a broad interaction spectrum and a high signal spectral power, in the frequency range characteristic of the molecules, than on the source energy, both owing to the duration of individual pulses and modulation of the sequence of those pulses.

HPEM 9-20: Universal Impedance Statistics of Metallic Enclosures

S. M. Anlage, **S. Hemmady**, **X. Zheng**, **E. Ott**, **T. M. Antonsen**
Physics Department, University of Maryland

Electromagnetic susceptibility of computer electronics to unintentional or deliberate high frequency microwave attack has been a topic of increased interest in recent times. Spurious signals may couple to PCB tracks and IC pins and lead to false triggering of computer components and memory, thereby threatening the operation of the system. One proposed method to address this issue is to understand the way electromagnetic energy couples to metallic enclosures through small openings (ports or channels). However, given the numerous possible internal configurations of such metallic enclosures, an analytic solution is impractical.
We have developed a statistical approach to this problem through the Random Coupling Model (RCM). The RCM is a stochastic model which assumes that the incoming rays ergodically fill phase space and bases its predictions upon the random plane wave approximation for the chaotic eigenfunctions. RCM makes explicit predictions for the universality of the complex impedance and scattering matrices of such multi-port systems. In this paper, we present our experimental tests of the RCM predictions for a one port system. The RCM predicts that the impedance is dependant upon the radiation impedance of the port- i.e. the impedance as seen with the port radiating into infinity, but retaining the same coupling geometry. In the absence of losses, RCM predicts that the one-port complex impedance is made up of two components- a mean part, which is equal to the imaginary part of the radiation impedance, and a universal fluctuating component that is Lorentzian distributed with a width equal to the radiation resistance. RCM introduces a normalization process that makes use of the radiation impedance of the port to bring out the universality in the probability distribution functions (PDF) of the real and imaginary parts of the normalized cavity impedance. These PDF's are smooth functions of loss and are experimentally testable.
Our experimental setup consists of a two-dimensional quarter bow-tie-shaped chaotic cavity, which allows only TM mode propagation under 18 GHz. The port consists of the center conductor of a coaxial cable that extends from the top lid of the cavity and makes contact with the bottom plate injecting cur-

rent into the bottom plate of the cavity. An ensemble of wave chaotic cavities is obtained by recording S_{11} as a function of frequency for 100 different positions and orientations of mobile perturbations within the cavity. The radiation impedance Z_{rad} is measured in a similar manner, but by placing microwave absorber along the inner walls of the cavity to simulate a radiation boundary condition.

The RCM has been tested under cases of varying loss (see Fig. 1) as well as antenna configurations and different cavity heights. We find that a single parameter simultaneous fit to two independent PDFs is remarkably robust and successful, and the fit parameter is physically reasonable. The normalized cavity impedance describes universal properties of the impedance matrix fluctuations that depend only on loss in the system. The RCM predicts new universal phenomena and accommodates non-universal system-specific features in its predictions.

We acknowledge support from the Department of Defense MURI Program under AFSOR Grant F496 200 110 374.

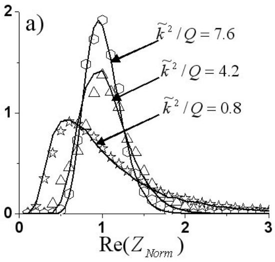

Figure 1: PDFs for the (a) real and (b) imaginary parts of the normalized cavity impedance Z_{Norm} for a wave chaotic microwave cavity between 7.2 and 8.4 GHz, for three values of loss in the cavity (open stars: 0, triangles: 2, hexagons: 4 strips of microwave absorber on wall). Also shown are single parameter simultaneous fits for both PDFs with fit parameters $k^2/Q = 0.8, 4.2, 7.6$, in order of increasing loss.

HPEM 9-21: Chaos in Driven Diode and Electrostatic Discharge Protection Circuits

S. M. Anlage[1], T. M. Firestone[2], J. Rodgers[2], E. Ott[1], T. M. Antonsen[1]
[1]*Physics Department, University of Maryland*; [2]*IREAP, University of Maryland*

There is interest in using HPM to induce chaos and upset in electronic circuits and systems. A key source of nonlinearity in modern electronics is the p/n diode junction. These diodes are particularly prevalent in electrostatic discharge protection circuits in advanced logic. The use of sinusoidal driving signals to create period-doubling and chaos in circuits containing a p/n junction has been studied extensively since the dawn of experimental nonlinear dynamics. We present a summary of our work in this area [http://www.ireap.umd.edu/MURI-2001/] in a format useful to others interested in this phenomenon. Emphasis is placed on the importance of time scales in this problem, with particular attention paid to the often-overlooked reverse recovery time and its role in the nonlinear dynamics [Renato Mariz de Moraes and Steven M. Anlage, "Unified Model, and Novel Reverse Recovery Nonlinearities, of the Driven Diode Resonator," Phys. Rev. E 68, 026201 (2003)]. This key time scale is found to be a nonlinear function of many parameters, including the sinusoidal driving frequency, amplitude, duty cycle, and dc bias. These nonlinearities, along with newly-identified interactions between rectification and nonlinear dynamics, can significantly enhance the volume of parameter space where period doubling and chaos can appear [Renato Mariz de Moraes and Steven M. Anlage, "Effects of RF Stimulus and Negative Feedback on Nonlinear Circuits," IEEE Trans. Circuits Systems I (in press, 2004). http://arxiv.org/abs/nlin.CD/0208039].

Because of the limitations created by the finite reverse recovery time, most conventionally doped p/n junctions will not show period doubling when directly driven by a sinusoidal signal at frequencies above roughly 1 GHz. We have investigated a new system that may extend the range of nonlinear behavior of long reverse-recovery-time diodes by integrating the diode into a transmission line structure. We will present theoretical and experimental results on this system and discuss its relevance to modern electronic systems.

We acknowledge support from the Department of Defense MURI Program under AFSOR Grant F496 200 110 374.

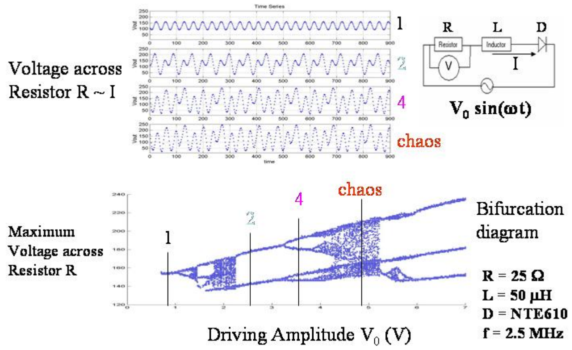

Figure 1: Illustration of chaos in the sinusoidal ac-driven series resistor-inductor-diode (RLD) circuit. The top panel illustrates the measured current through the diode as a function of time at various driving amplitudes. The lower panel shows a measured bifurcation diagram of the circuit illustrating the parameter ranges over which period 1, 2, 4, and chaotic oscillations of the circuit are observed.

HPEM 9-22: Numerical Model of Electromagnetic Wave Interaction with Longitudinal Oscillations of Plasma

V. G. Spitsyn
Department of Computer Engineering, Tomsk Polytechnic University

We consider the numerical model of electromagnetic wave interaction with longitudinal oscillations of plasma. The method of solving this problem is based on the stochastic modelling of electromagnetic wave interaction with random discrete media [1, 2]. The oscillator of electromagnetic signal is presented as a source of photons with corresponding diagram of radiation. The initial coordinates of photons are assigned in the point of oscillator disposition. The type of electromagnetic wave interaction with longitudinal oscillations of plasma is determined in according to set cross sections of scattering and absorption. In case of fulfillment of a wave scattering condition the direction of photon propagation changes to in accordance with the law of photon interaction with the quantum of plasma oscillations [3]. In the result of computation we received the frequency spectrums of electromagnetic signal after interaction with longitudinal oscillations of plasma.

There is supposed that the interaction of transverse electromagnetic wave with turbulent longitudinal oscillations of plasma take place in according to the isotropic scattering indicatrix. The frequency spectrum of incident wave, which consist of Gaussian component, is presented in the Fig. 1. The computation results are presented of angular and frequency spectrums of scattering signal in the Fig. 2 - Fig. 4. The value of dimensionless shift of frequency [2] and the scattering angle, calculated from the direction of incident wave propagation, are presented in the horizontal plane in indicated figures. The energy of scattering signal, which is normalized on the maximum of energy for case of multiply scattering signal, is calculated by the vertical axis in this figures.

In the Fig. 2 and Fig. 4 are presented the angular and frequency spectrum of scattering signal, which received for case of multiply signal interaction with turbulent longitudinal oscillations of plasma. In the Fig. 3 is presented the results of signal propagation in the media for case of single scattering of electromagnetic wave on the turbulent oscillations of plasma. In Fig. 2 and 3 we can see the appearing of the signal on the frequencies, which has shift relative the carrier frequency of electromagnetic wave aliquot to the frequency of longitudinal oscillations of plasma. In Fig. 4 is presented the computation results for case of half breadth frequency spectrum of incident wave and half frequency of longitudinal oscillations of plasma. We have appearing the second and next harmonics of scattering electromagnetic wave in Fig. 2 and Fig. 4. This fact is explained by the large significant of effect of multiply electromagnetic wave interaction with turbulent longitudinal oscillations of plasma.

Thus in this paper has been considered the propagation of electromagnetic wave with frequency spectrum in a view of Gaussian component through plasma with turbulent longitudinal oscillations. On the base of receiving results analysis we can do the conclusion about large significant of effect of multiply electromagnetic wave interaction with turbulent longitudinal oscillations of plasma, which lead to creation of multiple harmonics of scattering signal.

References

[1] V.G. Spitsyn, Method of computation of nonlinear electromagnetic wave interaction with stratified absorbing media, IEEE AP-S International Symposium Digest, Columbus, Ohio, USA, June 22-27, 2003, Vol. 4., pp. 398-401.

[2] V.G. Spitsyn, Modelling of radiowave scattering on the ionospheric plasma disturbances, created of space vehicle, Tomsk: Publishing House “STT”, 2002.

[3] V.N. Tsytovich, Nonlinear effects in plasma. Moscow: Publishing House “Science”, 1967.

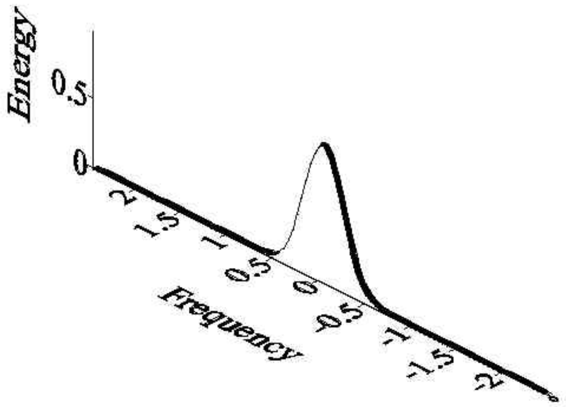

Figure 1: The frequency spectrum of incident wave

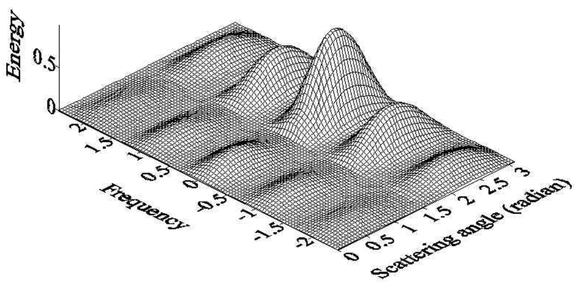

Figure 2: The angular and frequency spectrum of multiply scattering signal

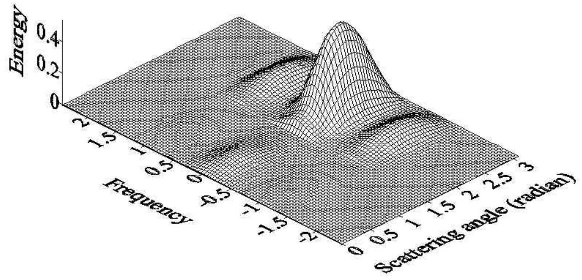

Figure 3: The angular and frequency spectrum of single scattering signal

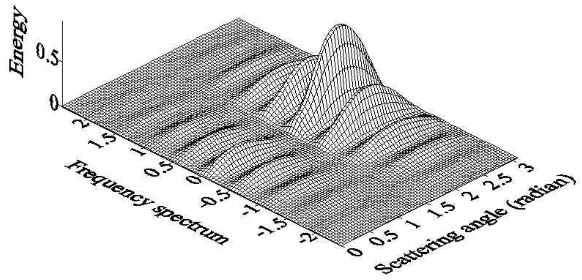

Figure 4: The angular and frequency spectrum of multiply scattering signal

HPEM 9-23: Modeling and Measurements of the Linsay Circuit and the Phase-Locked Loop

L. D. Bacon[1], **R. A. Salazar**[1], **L. L. Molina**[1], **G. M. Loubriel**[1], **P. E. Patterson**[2]

[1]*Sandia National Laboratories*; [2]*Ktech Corporation*

We are attempting to develop quantitative understanding of the nonlinear dynamics of electronic systems when driven by external stimuli. Our approach has been to model, measure, and refine our techniques iteratively on circuits of increasing complexity. This paper describes our progress for two reasonably simple electronic systems: the nonlinear diode resonator, or Linsay circuit, and the phase-locked loop.

The Linsay circuit, a simple series resistor-inductor-diode combination, is useful both for understanding nonlinear dynamics in an exceptionally simple electronic circuit and as a model of the response at the input pins of much more complicated integrated electronic systems. Input electrostatic discharge protection circuitry, for example, when combined with the inductance of the circuit trace, has the potential to turn the input pins of an integrated circuit into Linsay circuits. Many studies have used standard Spice diode models successfully to demonstrate chaotic effects qualitatively within predicted regions of operation. These models, however, do not predict quantitative measured results accurately. To explore the requirements for modeling chaotic behavior in electronic systems quantitatively, we measured the circuit parameters and responses of a Linsay circuit, including parasitics and specific diode parameters. We then applied numerical models of increasing complexity to the circuit and compared the results using time domain waveforms, frequency spectra, and standard measures of chaotic behavior, including phase-space trajectories and Lyapunov exponents. This study shows that conventional Spice diode models, although they exhibit the chaotic behavior of the Linsay circuit, do not properly reproduce actual circuit behavior unless the diode parameters are modified. We describe how a modified Spice diode model improves the simulation results.

The phase-locked loop is a more complex example of an electronic system that exhibits chaotic behavior. In the phase-locked loop, the nonlinear behavior is built into the topology of the cir-

cuit, rather than in the physics of the electronic devices as in the Linsay circuit. We present measurements, calculations, and measures of chaos of the behavior of the error voltage and frequency of a modern phase-locked loop for various classes of inputs.
Sandia is a multiprogram laboratory operated by Sandia Corporation, a Lockheed Martin Company, for the United States Department of Energy's National Nuclear Security Administration under contract DE-AC04-94AL85000.

HPEM 9-24: Basic Research in Nonlinear Circuit Response From Electromagnetic Interference*

J. A. Gaudet[1], **M. G. Harrison**[1], **S. M. Anlage**[2], **Y. C. Lai**[3]
[1]*Directed Energy Directorate, Air Force Research Laboratory, Kirtland AFB, NM 87117 USA*; [2]*CSR - Department of Physics, University of Maryland, College Park, MD 20742 USA*; [3]*Departments of Electrical Engineering and Physics, Arizona State University, Tempe, AZ 85287 USA*

Several years ago, the U.S. Department of Defense (DoD) became concerned about the potential threat posed by electromagnetic pulses on electronic systems. Consequently, they established in 2001 a Multidisciplinary University Research Initiative (MURI) on "The Effects of Radio-Frequency Electromagnetic Pulses on Electronic Circuits and Systems." One of the concentration areas of these university grants was nonlinear control and chaos in circuits. The University of Maryland, one of the MURI lead universities, has made significant progress in this area. In addition, the Air Force Office of Scientific Research (AFOSR) has been instrumental in researching the question of inducing chaos in electronic circuits, work that has been conducted at Arizona State University.
This paper will summarize the progress made in these two basic research efforts. We will show how nonlinear (including chaotic) behavior of the components of the majority of circuits that exist in both military and civilian systems can have a dramatic, and adverse impact from stray electromagnetic fields. We will discuss a variety of ways that the electromagnetic pulses can be tailored to cause effects through a chaotic response. Finally, significant progress in the theory of chaotic response in electronic circuits has been made. Areas of progress include p/n junction nonlinear behavior, the use of two frequencies to lower the threshold for chaos in a circuit, scaling laws for noise-induced chaos, noise-induced robust chaos, and the relevance of non-smooth dynamical systems to nonlinear circuit analysis. The status of these research efforts will be presented.
Finally, a discussion of how the results of these efforts may impact future research studies in the Air Force will be offered with suggestions given for areas of further study and possible validation experiments.
*S.M.A. is supported by STIC through the STEP Program and the Department of Defense MURI Program under AFOSR Grant F496200110374. Y.C.L. is supported by AFOSR Grant F496209810400 and NSF Grant No. PHY-9996454.

HPEM 9-25: Nonlinear Effects in Ionosphere in the Field

A. L. Gutman, **A. N. Manko**
Voronezh State Timber University

1. Introduction
In preceding works of the authors [A. Gutman. Grating and Exploiting Ionosphere Artifacts Using Specificity of Ultra Short Electromagnetic Impulses Propagation. Vega Press. 2003, CA, USA (in print); A.L. Gutman, A.N. Manko. Nonlinear phenomena at the distribution of video pulses to plasma (ionosphere). All-Russia scientific a conference - seminar. Ultra bandwidth signals in a radiolocation, communications and acoustics NDNA 2003, Murom, 2003] nonlinear effects in ionosphere without taking into account a possibility of changes of parameters of an impulse field were surveyed.
In the given work distribution of video pulses is considered in view of electron collisions with ions under variation of pulses duration concerning set time between collisions. Duration of collision is assumed to be infinitesimal that provides a continuity of a field under passage of a pulse through coordinate of a point of collisions between electron and a molecule.
Original correlations relating the changes of electron temperature and electric field are the equations from [V.L. Ginsburg. Distribution of electromagnetic waves. M.: Science, 1960]:
(1)
Field falling on plasma:
(2)
E0 - a pulse height of an electromagnetic field;
E(0, t) - a field of a pulse on the boundary [A.B. Shvartsburg. Video pulses and acyclic waves in dispersive media (precisely solved models), Uspekhi Fizicheskikh Nauk, v. 168, No. 1, 1998].
2. The equation of a field varying in plasma
In order to take into account the change of the pulse shape (in dimensionless coordinates) Eh(z,t) we shall represent it according to [L.A. Weinstein. Distribution of pulses. Uspekhi Fizicheskikh Nauk, v.168, No. 1, 1976]:
(3)
then the analytical expression for the pulse shape while its propagation in ionosphere can be presented as (see fig. 2):
(4)
In (4) t, z- dimensionless time and coordinate of electrons and field; z=wpz/c; t = wpt; t^3z/c and t^3z. One can see from fig. 2 that with an increase of a distance maximum of E2 is insignificantly increased while pulse duration at the reducing of its main part also increase due to the oscillating "tail". At a small depth of the E-layer and, respectively, short durations of staying of the pulse in E-layer [A.L. Gutman, A.N. Manko. Nonlinear appearances at distribution of a video of pulses to plasma (ionosphere). All-Russia scientific a conference - seminar. Ultra bandwidth signals in a radiolocation, connections and acoustics NDNA 2003, Murom, 2003] deformations of the pulse were not taken into account. For an estimation of a significance of the second term in (4) in fig.3 the plots are presented with and without the account the pulse shape.
Calculations of temperatures of plasma were carried out on the basis of the formula [A.L. Gutman, A.N. Manko. Nonlinear appearances at distribution of a video of pulses to plasma (ionosphere). All-Russia scientific a conference - seminar. Ultra bandwidth signals in a radiolocation, connections and acoustics NDNA 2003, Murom, 2003]:
(5)
where n - the number of collision.
3. The pulse duration is less than time between the next collisions
This case the most simple, but typical for the E-layer ionosphere since at present there are ultra-short pulse generators with t << 1/n0. It means that a pulse is finished on the average between impacts. In this case the general system of equations (1) becomes simpler:
(6)
Hence, from (1) we obtain
(7)
Kinetic energy of an electron in E-layer, accumulated in a field before the impact:
(8)
At K>>1,5kT an electron at one impact transfers energy [V.L. Ginsburg. Distribution of electromagnetic waves. M.: Science, 1960, s. 37]:
(9)
And per unit of time energy (in E-layer of ionosphere) energy will be equal [V.L. Ginsburg. Distribution of electromagnetic waves. M.: Science, 1960, s. 507]:
(10)
Temperature Te gained by an electron after escaping of a field per 1sek:
(11)
Estimation of the change of electron velocity allows to calculate its temperature Te after escaping of a field from E-layer of ionosphere
(13)

Where Δt - time of observation (for example, q=1/nî). Therefore, after escaping of the field the temperature of electron can be estimated as follows:
(14)
4. The pulse duration is more than time between the collisions t^{3}1/nî
Acceleration of an electron in a field of a pulse
(15)
Kinetic energy of an average statistical electron before collision is equal
(16)
At the first impact all this energy will pass into heat:
(17)
At q1^3 t >q, cq1^3 z>cq :
(18)
From here
(19)
5. Conclusion
1. Change of an electric field at passage of a short pulse through an ionosphere is noticeable already the time intervals between impacts an electron - a neutral molecule.
2. The accumulated kinetic energy of an electron between impacts as a result of impacts results in increase of temperature of in E-layer in ionosphere.
3. Along with increase of an electromagnetic energy of the falling field the probability of additional ionization of neutral molecules increases at collisions of electrons with molecules or ions.
4. In the work parameters of the field which correspond to a considerable increase of electron temperature are implemented and due to collisions – the temperatures of plasma due to the process of collisions.

$$m\frac{d\dot{y}}{dt} = eE_y(z,t) - \dot{y}m\nu_0\sqrt{\frac{T_e}{T}};\qquad \dot{T}_e = \frac{2}{3k}eE_y(z,t)\dot{y} - \delta\nu_0\sqrt{\frac{T_e}{T}}(T_e - T), \quad (1)$$

$$E_y(z,t) = E_0\Phi\left(\omega_p t - \frac{\omega_p z}{c}\right); \quad (2)$$

$$E_\eta(\zeta,\tau) = E_0\Phi\left(\omega_p t - \frac{\omega_p z}{c}\right), \quad (3)$$

$$E_\eta(\zeta,\tau) = E_0 exp\left(-\frac{\tau-\zeta}{2}\right)\left[2(\tau-\zeta) - \frac{(\tau-\zeta)^2}{2}\right] - E_0\zeta\int_0^{\tau-\zeta}\frac{J_1\left(\sqrt{(\tau-\overline{\tau})^2-\zeta^2}\right)}{\sqrt{(\tau-\overline{\tau})^2-\zeta^2}}exp\left(-\frac{\overline{\tau}}{2}\right)\left(2\overline{\tau} - \frac{\overline{\tau}^2}{2}\right)d\overline{\tau}. \quad (4)$$

$$T_{en} = \frac{e^2}{3km}\int_{(n-1)\theta_0}^{n\theta_0}E_y^2(z,t)dt - \delta\nu^*\sqrt{\frac{T_{e(n-1)}}{T}}(T_{e(n-1)} - T)\theta_o + T, \quad (5)$$

$$m\frac{d\dot{y}}{dt} = eE_y(z,t),\qquad \dot{T}_e = \frac{2}{3k}eE_y(z,t)\dot{y}. \quad (6)$$

$$\dot{y}(z,\theta) = \frac{e}{m}\int_0^\theta E_y(z,\tau)d\tau. \quad (7)$$

$$K = \frac{m\dot{y}^2}{2} = \frac{e^2}{2m}\int_0^\theta E_y^2(z,\tau)d\tau. \quad (8)$$

$$W = \delta\left(K - \frac{3}{2}kT\right), \quad (9)$$

$$\delta\nu_o\left(K - \frac{3}{2}kT\right) = \frac{3}{2}k\delta\nu_o(T_e - T). \quad (10)$$

$$T_e = \frac{2}{3k}\left(K - \frac{3}{2}kT\right) + T = \frac{2}{3k}K. \quad (11)$$

$$\left.\begin{aligned}\dot{y}(t) &= \dot{y}(0)exp(-\nu_o t)\\ T_e &= (T_e)_{\Delta t}exp(-\delta\nu_o t)\end{aligned}\right\}, \quad (13)$$

$$T_e(\theta,\tau,\zeta) = T + \frac{2m}{3k}exp(-\delta\nu_o\theta)\int_0^\theta E_y^2(t,\tau,\zeta)dt \quad (14)$$

$$\dot{y}(z,t) = \frac{e}{m}\int_0^t E_y(z,t)d\tau \quad (15)$$

$$\frac{m\dot{y}^2}{2} = \frac{e^2}{2m}\int_0^\theta E_y^2(z,t)dt, \quad c\theta \ge z > 0. \quad (16)$$

$$T_e(z,\theta) = \frac{2}{3k}\frac{m\dot{y}^2}{2} = \frac{e^2}{3km}\int_0^\theta E_y^2(z,t)dt + T. \quad (17)$$

$$\frac{d\dot{y}}{dt} = \frac{e}{m}E_y(z,t);\qquad \dot{T}_e(\theta_1) = \frac{e^2}{3km}\int_0^{\theta_1}E_y^2(z,\tau)d\tau + T_1 \quad (18)$$

$$T_e(\theta_2) = \frac{e^2}{3km}\int_0^{\theta_2}\dot{T}_e d\tau + T_2. \quad (19)$$

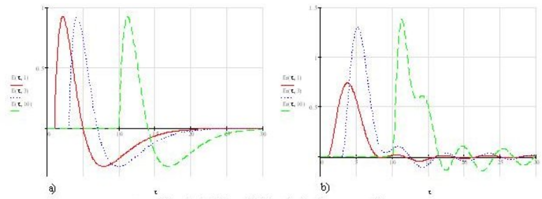

Fig. 1. A falling field - a) the first term (2);
b) the second term (2) on time for distance $\zeta = (1; 3; 10)$

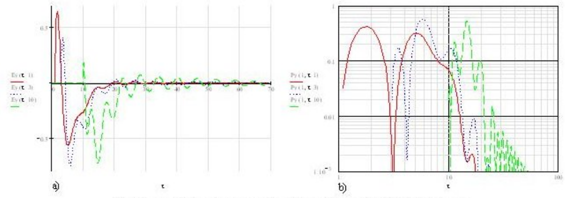

Fig. 2. A field in plasma as a function of time (2): a) E_y (for E_0=1);
b) $P_y = E^2_y$ at the distance $\zeta = (1; 3; 10)$

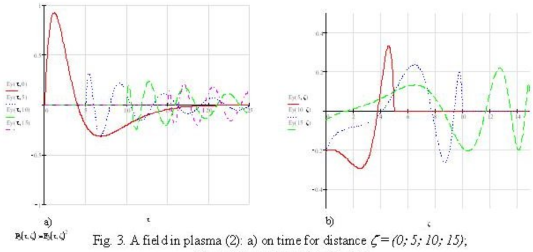

Fig. 3. A field in plasma (2): a) on time for distance $\zeta = (0; 5; 10; 15)$,
b) on distance for $\tau = (5; 10; 15)$

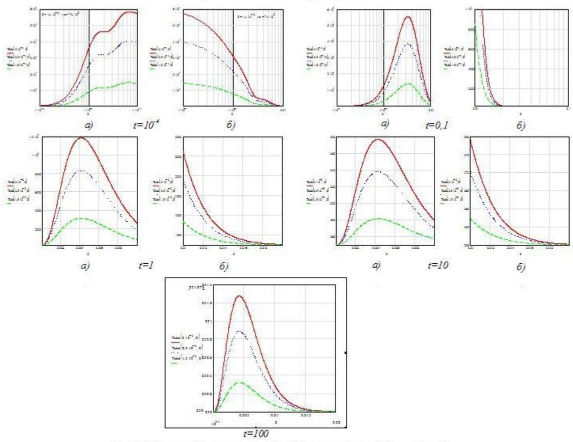

Fig. 4. Changes of temperature of the E-layer on time of observation θ
for the field strengths $E_0 = (3{\cdot}10^5;\ 2{,}5{\cdot}10^5;\ 1{,}5{\cdot}10^5)$V/m

HPEM 10 - Lightning - Measurement and Simulation

HPEM 10-1: A Study of Conventional Protector Stability to Direct Lightning Strikes

V. M. Kouprienko
Science Research Center of 26 CSRI

A wide application of automatic control systems and computer devices sensitive to lightning strikes and related electromagnetic radiations makes the problem of their protection quite acute. Available statistics indicates a considerable damage caused by direct strikes at buildings and constructions of electric power industries. It is found that low objects are primarily affected by descending positive and negative lightning discharges.
The available methods for the computation of strike probability and protector stability are based on experiments and long-term observations of the maintenance of constructions being protected. The data used for the computations and protector designs were obtained in laboratory experiments on discharge gaps of limited lengths 50 or 60 years ago. Recent studies have made on long sparks and aimed at increasing the efficiency of lightning protectors which were designed using the conventional methods for defining the protection zones. A higher efficiency is achieved by changing the protector tip geometry, i.e. by increasing the in-

duced charge.
The Research Center of 26 CSRI has undertaken a series of studies, using a wide range of object sizes, protection designs, and grounding conditions. A lightning discharge was simulated by a positive pulse discharge of 250-2250 μs duration occurring between a high voltage electrode and the ground. The discharge was ignited by a pulse generator at 6 MB and 0.96 MJ.
Extensive field studies of various protection designs have shown the inadequacy of defining the protection zone by conventional methods. It is found that the protection zone covered by multiple protectors does not exceed the total zone covered by single protectors. This disagrees with the generally accepted view that the multiple protector zone should be much larger than the total zone of the respective single protectors.
The field tests have shown that a reliable indicator of the rod and cable stability is the protection angle measured from the protector tip to the most remote and highest point of the object. In order to provide a high stability of these types of protector (at about PH $\approx$ 1), the protection angle should be smaller than or equal to 30°. Moreover, no evidence has been found for the effect of the induced charge value on the protection efficiency of tall buildings and constructions. The use of lightning receivers with tips of complex geometry, e.g. toroidal screens, does not increase the charge but changes the protection angle, increasing the protection reliability.
This paper reports the results on the effect of the long spark charge on the damage of objects with and without lightning protectors. We present data on the stability of protectors of various designs to positive pulses in long spark gaps. These results can contribute to a better understanding of problems associated with direct strike protection.

HPEM 10-2: A Simple Model of Repeating Lightning-Leader Pulses

C. E. Baum
Air Force Research Laboratory, DEHP; Directed Energy Directorate; Kirtland AFB, NM, USA

Leader pulses associated with lightning are a complex phenomenon. Experimental data in the fast-time regime (tens of nanoseconds) are limited. However, it is in this time regime that important things are occuring.
This paper investigates some implications of observed repeating fast lightning-leader pulses (steps), utilizing both optical and electromagnetic-pulse data. Estimates of learder-step length, current, charge, and pulse width are combined to give estimates of the resistance presented to the continuing current between the pulses which recharges the leader tip.
Another way to view the leader-step phenomenon is by a circuit analogy to a relaxation oscillator in which a capacitor is charged at some rate, and suddenly discharged when a critical voltage has been reached, the cycle then repeating.
The present calculations are truly of the back-of-the envelope form. However, one needs to start somewhere. Perhaps future data will lead to a refinement of this model.

HPEM 10-3: Shielding Characteristics of Transmission Lines: Analysis with a Leader Progression Model

K. Yamada[1], **Y. Ebinuma**[1], **T. Shindo**[2]
[1]*Shonan Institute of Technology*; [2]*Central Research Institute of Electric Power Industry*

For evaluation of shielding performance of transmission lines, an electro-geometric model proposed by Armstrong and Whitehead (A-W model) has been widely used for the analysis of lightning performance of transmission lines. Recent observations of lightning strokes to UHV transmission lines in Japan, however, show that almost horizontal lightning channel to a transmission line occurs which are unpredictable by the A-W model and number of shielding failures in UHV lines is larger than anticipated.
Recently new shielding models which take leader progression into account have been proposed and a review of these models has been made [1]. In this paper, aiming at precise analysis of shielding failures and transmission outage rates we have developed a leader progression model. The effects of several parameters (step length, equivalent charge of leader and so on) used in the model on the calculated shielding characteristics have been investigated. Effects of the characteristics of upward leaders from earthed objects on the shielding performance are also studied.
Using the leader development model with the appropriate parameters, we analyze shielding performance of transmission lines of different classes. The calculated ratio of number of shielding failure at each phase of a UHV transmission line is compared field observations conducted in Japan and fairly good agreement with observational results has been obtained. The effects of various parameters such as tower height of transmission lines, topographical conditions on shielding performance are also clarified. Furthermore, comparison between the results by the leader progression model and calculated shielding performance of the transmission lines by Lightning Outage Rate calculation Program (LORP), which is based on the A-W model and has been developed by CRIEPI, are also carried out. The difference between them is larger when the tower height of transmission lines becomes smaller.
[1] T.Shindo, Y.Aihara, "Review of lightning leader progression models", 5th International Workshop on Physics of Lightning (IWPL), Nagaya, No.3-4, 2001.

HPEM 10-4: On the Enhancement of Electric and Magnetic Fields from Lightning due to Close-by Metallic Structures

J.-L. Bermudez[1], **T. Gazizov**[2], **A. Negodyaev**[2], **D. Pavanello**[1], **F. Rachidi**[1], **A. Rubinstein**[1], **M. Rubinstein**[3]
[1]*Swiss Federal Institute of Technology, Lausanne, Switzerland*; [2]*Tomsk University of Control Systems and Radioelectronics, Tomsk, Russia*; [3]*Western University of Applied Sciences, Yverdon, Switzerland*

Sensors used for the measurement of lightning electric and magnetic fields are often placed close to or on top of buildings or other structures. Metallic beams and other conducting parts in those structures cause an enhancement effect on the measured fields. In this paper, we use spherical and parallelepipedal structures as models to study the enhancement of the electric and magnetic fields at different locations, both on the roof of a building and on the ground at different distances from it. We use analytical expressions when possible and numerical solutions using the method of moments otherwise. The results show that, although an "enhancement" is seen on both the electric and the magnetic fields, the degree of enhancement is actually different for each of them. The magnetic field can in fact be made smaller by the presence of the building. We further show that the enhancement can be a function of frequency and it can therefore distort the lightning fields.

HPEM 10-5: The Effect of the Measurement Time Constant of Analog Integrators on the Resulting Modeling and Simulation of Lightning

M. Rubinstein[1], **D. Pavanello**[2], **J.-L. Bermudez**[2], **F. Rachidi**[2], **W. Janischewskyj**[3], **A. M. Hussein**[3], **V. Shostak**[4]
[1]*Western University of Applied Sciences, Yverdon, Switzerland*; [2]*Swiss Federal Institute of Technology, Lausanne, Switzerland*; [3]*University of Toronto, Toronto, Canada*; [4]*University of Kiev, Kiev, Ukraine*

The study of the physics of lightning and proper simulation of its processes requires high quality data, free from distortions over the desired frequency range. Lightning return stroke currents, electric fields and magnetic fields are often obtained by measuring their derivatives and then integrating them either by way of operational amplifier-based analog integrators or numerically. When analog integrators are used, frequency distortion is purposely introduced to avoid saturation of the amplifiers due to offsets or to large ramps in the waveforms themselves, such as the well-known electrostatic ramp that is characteristic of return stroke fields from close lightning. In this paper, we discuss the distortion introduced both by properly and by improperly designed integrators. We further give methods to correct the distortion and we propose that data obtained from analog, integrator-based sensors be accompanied by the parameters that characterize the distortion and that can be used to equalize away the distortion.

HPEM 10-6: Electromagnetic Environment in the Immediate Vicinity of a Tower Struck by Lightning

D. Pavanello[1], **F. Rachidi**[1], **M. Rubinstein**[2], **N. Theethayi**[3], **R. Thottappillil**[3]
[1]*Swiss Federal Institute of Technology, Lausanne, Switzerland*;
[2]*Western University of Applied Sciences, Yverdon, Switzerland*;
[3]*University of Uppsala, Uppsala, Sweden*

The estimation of the electromagnetic field in the very-near area surrounding a communication tower struck by lightning is crucial for the correct design of the protection system against electromagnetic interference. The problem of lightning return strokes to tall towers was the subject of numerous recent studies (e.g. [1-3]). Compared with the electromagnetic field radiated by a lightning return stroke to ground, the field radiated by a lightning return stroke to tower presents levels that could be significantly different. Based on theoretical modeling and experimental observations, it is well established that the presence of a tower could result in a substantial increase (a factor of 3 or so) of the electric and magnetic field peaks and their derivatives (e.g. [1]) for observation points located at distances exceeding the height of the tower.
In this paper, we present simulation results to investigate the effect of the tower on the nearby electromagnetic field using two different approaches. In the first approach the tower is considered as an uniform transmission line characterized by constant reflection coefficients at its extremities. The current distribution along the tower and the channel is obtained as function of the 'undisturbed current', defined as the current that would be measured at the impact point under matched conditions. In the second approach the lightning channel and the tower inductance and capacitance are calculated using the charge simulation method. Using these inductances and capacitances as the transmission line parameters, the current distributions in both channel and tower are estimated using the finite difference time domain method. The current distribution obtained with each approach is then used for the field calculations. We show in particular that the effect of the tower at distances of about the height or the tower or less, could result in a significant decrease of the electric field.
The results obtained in this study have important implications in the estimation of the immunity level of sensitive electronics and, hence, in the design of lightning protection system.
[1] F. Rachidi, W. Janischewskyj, A.M. Hussein, C.A. Nucci, S. Guerrieri, B. Kordi, J.S. Chang, "Current and electromagnetic field associated with lightning return strokes to tall towers", IEEE Trans. on Electromagnetic Compatibility, Vol. 43, No. 3, August 2001.
[2] Rakov, V.A., "Transient response of a tall object to lightning", IEEE Transactions on Electromagnetic Compatibility, 43 (4), 654-61, 2001.
[3] F. Rachidi, C.A. Nucci, V. Rakov, J.L. Bermudez, "The effect of vertically-extended strike object on the distribution of current along the lightning channel", Journal of Geophysical Research, Vol. 107, No. D23, 2002.

HPEM 10-7: Lightning Currents Measured at the Peissenberg Telecommunication Tower between 1992 and 1999

F. Heidler
University of the Federal Armed Forces, Munich, Germany

In the year 1992 new current experiments were started at the Peissenberg telecommunication tower situated about 60 km from Munich, Germany. Between June 1992 and February 1999 more than 200 lightning to the Peissenberg tower occurred. Except of one event, all lightning discharges started with an initial continuing current. Due to this feature they are identified as upward lightning. The majority are negative upward lightning lowering negative charge to ground. Less than five percent are positive upward lightning and less than two percent lowered both positive and negative charge.
For the measurement of the current and its derivative a current monitor (frequency range from 0.15 Hz to 200 kHz) and a di/dt-loop probe (upper bandwidth limit $\approx$ 44 MHz) are located at the tower top. Additionally a current probe (bandwidth from a few 10 Hz to $\approx$ 20 MHz) and a di/dt-sensor (upper cutoff frequency $\approx$ 50 MHz) are placed close to the tower base in order to study the tower transient characteristics. Depending on the rise time the wave shapes of the impulse currents showed pronounced tower reflections. For short rise times up to some 100 ns the current peak values as well as the maximum current derivatives are about 30 % higher at the tower base compared to the tower top.
For the negative upward lightning two different types of impulse currents could be separated. It was found, that the impulse currents superimposed to the initial continuing current have about 2 times lower current peaks and about 4 times lower current derivatives compared to the subsequent impulse currents occurring after the cessation of the initial continuing current. Differing between these different types the statistics of important lightning parameters are given as the peak value, the maximum steepness and the full widths on half value of the current derivatives.
The given statistics also include the meteorological data as the temperature, the striking probability and the most important current parameters. Further, typical examples of current waveforms will be presented, e.g. concerning the different types of impulse currents and continuing currents.

HPEM 10-8: Lightning Peak Current Statistics Derived from Lightning Location System Data

G. Diendorfer
Austrian Lightning Detection and Information System (ALDIS), Vienna, Austria

Lightning Location Systems (LLS) infer the peak current of a lightning stroke from the remotely measured electromagnetic field. No information about the other typically given lightning parameters as charge transfer, action integral and maximum di/dt is available from LLS currently used in many countries all over the world. It is interesting to note, that the peak current distribution based on LLS data over the Austrian territory from 1992-2003 differs significantly from the peak current distribution that is specified in many lightning protection standards (e.g. IEC, CIGRE) as shown in Fig. 1. The peak current distribution specified by IEC is mainly based on data from direct measurements on instrumented towers.
Direct measurement of lightning currents to an instrumented tower (Gaisberg tower) started in Austria 1998. From 01/2000 to 07/2003 a total of 107 flashes with 448 strokes have been recorded at the tower experimental site. These directly measured data are a perfect reference for the validation of the LLS output. GPS time synchronization of both data sets allows direct correlation of measured peak current and LLS reported peak current for each individual stroke. Typical for elevated objects as the Gaisberg tower is a very high percentage of upward trigger discharges, where the upward leader bridges the gap between the grounded object and cloud and establishes an initial continuous current (ICC) with a duration of some hundreds of milliseconds

and an amplitude of some tens to some thousands of amperes. The upward leader and the ICC constitute the initial stage (IS) of natural upward lightning. In most cases the IS contains current so called α-pulses superimposed on the slowly varying continuous current. After the cessations of the ICC, one or more downward leader/upward return stroke sequences may occur and these pulses are referred to as β-pulses.

In Fig. 2 the correlation of directly measured peak currents and LLS reported peak currents are shown separately for α-pulses and β-pulses. A correlation of I_{ALDIS} = 1.09·I_{GB} (R^2 = 0.951) for α-pulses and I_{ALDIS} = 1.02·I_{GB} (R^2 = 0.973) for β-pulses. Obviously the LLS peak amplitudes are on average within the measuring error of the direct current measuring system and the significant discrepancies shown in Fig. 1 can not be explained by shortcomings in the peak current determination of the LLS. We therefore conclude that the LLS peak current distribution is a more realistic representation of the ground truth than the peak current distributions specified in different lightning protection standards.

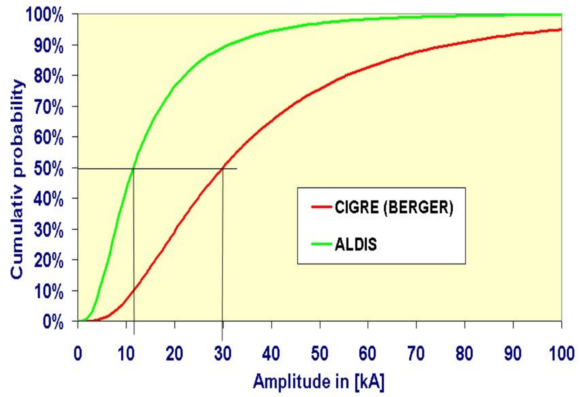

Figure 1: Cumulative Probability of Peak Currents - CIGRE versus ALDIS.

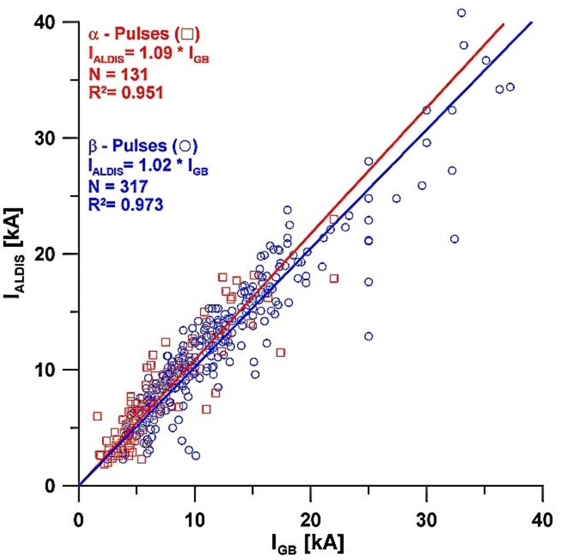

Figure 2: Peak Current Correlation for α-pulses and β-pulses.

HPEM 10-9: On Determining the Effective Height of Gaisberg Tower

N. Theethayi[1], **G. Diendorfer**[2], **R. Thottappillil**[1]

[1]*Division for Electricity and Lightning Research, Uppsala University, Sweden*; [2]*Austrian Lightning Detection and Information System (ALDIS), Vienna, Austria*

Tall structures, usually with heights more than 100 m on level ground, are frequently struck by lightning that is initiated by upward leaders from the tower, in addition to lightning initiated by downward leaders from the clouds. It has been observed that the total number of lightning strikes to the tower and also the percentage of lightning initiated by the tower, called upward flashes, increase with the height of the tower. Similar increase in the total number of lightning strikes to the tower and also in percentage of upward flashes is observed if the tower, even with heights less than 100 m, is on steep mountaintops. To account for these observations, towers on mountaintops are said to have an effective height that is often a few times larger than the physical height of the tower. Rakov and Uman [2003] and Rakov [2003] have reviewed the literature on lightning strikes to tall towers and have presented the effective heights of several towers on mountaintops.

In this paper we describe the methods that could be used to arrive at the effective heights of towers on mountaintops and apply it to the communication tower on top of mount Gaisberg in Austria [Diendorfer and Schultz, 1998]. Since 1998, this tower has been instrumented to measure lightning currents and therefore the actual number of lightning strikes is available. The four methods or definitions used to find the effective height of the tower are, 1) assigning the height of a tower on flat ground that would give the same percentage of upward flashes as the actual tower on mountain top as the effective height, 2) the height of a tower on flat ground that would attract the same number of yearly lightning strikes as the tower on mountain top, with same average flash density in the surroundings of both the towers, 3) assigning the height of a tower at level ground that would give the same critical field at tower top as that of the tower on the mountain top, and 4) the ambient ground field calculated at the instant of continuous leader inception at the tip of the tower on mountaintop and from this ambient ground field the height of a tower at level ground that would give the same leader inception criteria.

The first two methods are based on empirical extrapolation of experimental observation of lightning strikes to towers [Eriksson, 1987] and the last two methods are based on theoretical calculations. The Gaisberg tower is 100 m tall and is above a 750 m tall mountain. The mountain has a base radius of approximately 1.65 km. Application of the four methods results in quite different effective heights, from 300 m to 1000 m. The assumptions behind the methods of effective height calculations and the sensitivity of the estimated effective heights on the assumed parameters are discussed. [The first and last authors acknowledge support from Swedish Defense Material Administration – FMV (Göran Unden)].

HPEM 10-10: Airbus-A380 Rear Fuselage Induced Lightning Current Simulations

J. Ritter[1], **R. Lotz**[1], **D. Ristau**[2], **H.-W. Krüger**[2]

[1]*EADS-Military Aircraft*; [2]*Airbus Germany*

This contribution describes the numerical simulation of lightning induced currents at the rear section of the Airbus-A380 aircraft. Since major structural parts of this Aircraft-section are made from Carbon Fiber Reinforced Plastic (CFRP) Materials, the distribution of the ligthing induced currents differ significantly from the situation of aircraft having an all-metallic fuselage due to the reduced electric conductivity of the CFRP material compared to metal.

The simulations are performed using the Time Domain Finite Difference Technique incorporating formulations for wires, thin walls, and absorbing boundary conditions (PMLs). This technique is well established for the simulation of lightning induced currents and has been applied in the past by a large number of researchers.

Several facts increase the complexity of the simulations, if CFRP materials are involved. First of all, a considerable part of the interior geometry has also to be modeled with a sufficient level of fidelity, since some of the frames and spars below the aircrafts CFRP skin panels are metallic and therefore influence the current distribution. The thicknesses of the CFRP components must also be considered due to the skin depth. Care must be taken that the model

represents all significant current paths (including bonding

jumpers, structure joints, etc.) which contribute to the overall current distributions. In order to set up the geometric model of the aircraft, CAD models have been utilized. Due to the complexity of the existing models (about 1000 to some 10000 parts for the aircraft section under consideration) a special procedure has been established using Virtual Reality Modeling Language (VRML)-models extracted from the Digital Mock Up (DMU) model of the aircraft. Thus, the creation of special simulation-CAD models has been circumvented. As an example, the input geometry for a simulation case with current injection at the horizontal stabilizer is shown in Figure 1. The resulting Finite Difference meshes usually contained between 60 and 200 million cells. Figure 2 displays the FD mesh corresponding to the geometry from Figure 1.
The Simulations have been performed in a parallel PC environment using 18 CPUs. From the Finite Difference Simulations, currents and voltages at several test-points have been evaluated as response time signals of component A excitations. Besides other purposes, the simulations have been used for the validation of injected current levels for component tests.

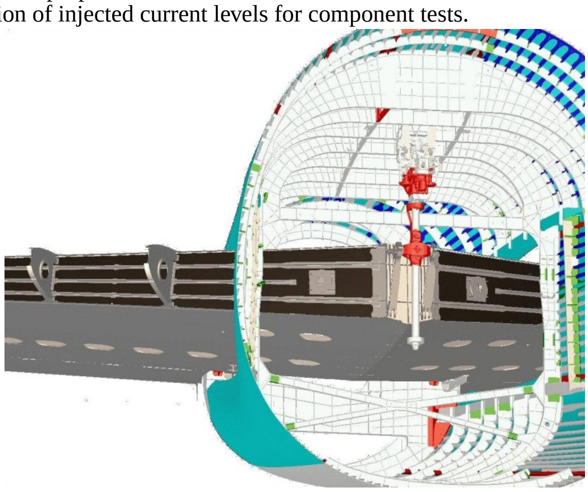

Fig. 1: Example of the geometric model used as input-data for the simulations.

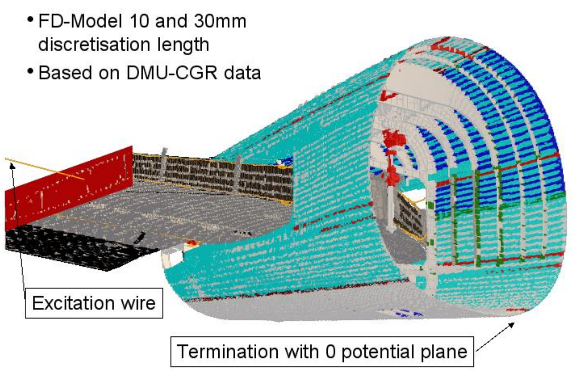

Fig. 2: Example of the FD-TD mesh for a simulation with current injection at the horizontal stabilizer of the aircraft.

HPEM 10-11: Lightning Test and Protection of Aircraft Radome

B. Nordström
Swedish Defence Material Administration

During the design of aircraft there are generally two areas of concern related to lightning, the prevention of physical damage that could result in aerodynamic instability, structural failure or excessive drag, and the protection of internal electronics from effects of harmful lightning-generated fields.
When an aircraft is exposed to lightning it will be struck at one or more points known as "attachment" points. The most probable attachment points are the nose and exhaust port. One of the primary attachments points is the radome. In the presentation protection and testing of the radome and pitot tube will be discussed starting in actual cases.
Figure 1 shows lightning attachment to a radome. If the radome wall is punctered earlier the lightning will pass through the radome wall, as shown at the lower figure, and the flight safety is threatened. How the radome wall could have been electrically punctered due to an insufficient antistatic layer besides an earlier lightning will be presented.
Every small puncture of the radome surface is necessary to repair as it introduces a severe risk for damages during a lightning. Also the test of the electric strength of the repaired wall will be presented.

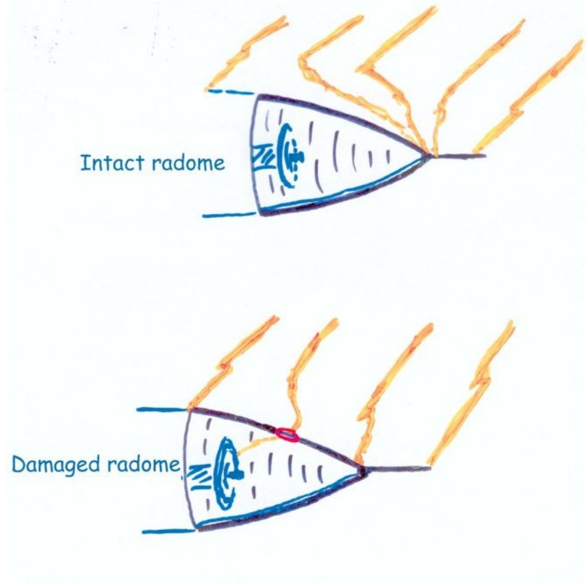

Figure 1: Lightning strike to radome.

HPEM 10-12: Modelling of the Lightning Swept Stroke During Strikes to Aircraft

A. Larsson
FOI, Swedish Defence Reseach Agency

In-flight statistics show that an aircraft can expect one lightning strike for somewhere between each 1000 and 10 000 hours of flight. For a commercial airliner, this is roughly equivalent to one lightning strike each year. This threat to aircraft safety is taken into account in the aircraft protection design and in the certification process through the concept of aircraft zoning. The objective of the zoning is to locate and classify surfaces on the aircraft where the lightning channel might have its attachment point and thus be a possible point of where the lightning current can be injected into the aircraft frame. Until now, these zones are defined on the basis of experimental and semi-experimental considerations. The purpose of this talk is to give the roadmap that has been followed to create a zoning tool based on a physical understanding and description of the lightning swept stroke along an aircraft in flight.
The understanding of the lightning strike to aircraft has been greatly enhanced during the last years thanks to a comprehensive analysis of available in-flight data. Based on this increased understanding, the detailed features of the lightning channel and its interactions with an aircraft in flight are now beginning to be revealed to us. For a detailed understanding of the interaction between the lightning channel and an aircraft in flight several subtopics must be considered. These include
· The lightning current.
· The properties of the lightning channel.
· The phenomena at lightning attachment points.
· The re-attachment process.
· The aerodynamic flow.
All these topics will be addressed, but most attention will be

paid to the properties of the lightning channel and the process of lightning channel attachment. Finally, some examples of lightning swept stroke simulations will be presented. Further details are given by Larsson (A Larsson, C. R. Physique, Vol 3, pp 1423-1444, 2000).

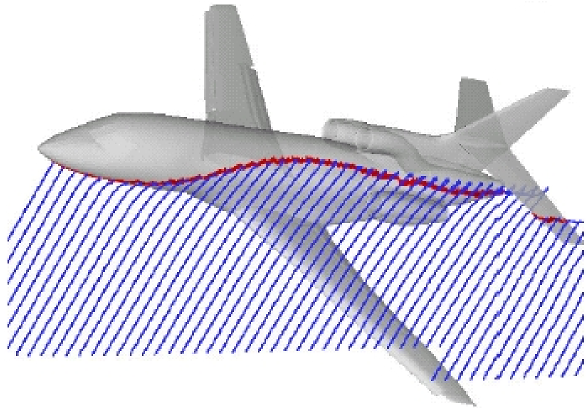

Figure 1: A lightning swept stroke simulation on a Falcon 2000 aircraft (E. Montreuil et al, "The lightning swept stroke model: a valuable tool to investigate the lightning strike to aircraft", Int. Conf. on Lightning and Static Electricity (ICOLSE), Blackpool, UK (2003)).

HPEM 10-13: Transient Voltages Induced in Signal Lines by Direct Lightning Strikes on the High Voltage Substations

A. Sowa, **J. Wiater**
Technical University of Bialystok, Poland

Direct lightning strike to the earthed components of high voltage HV substation can cause severe interference problems in electronic equipment and systems. In this case lightning current flows through the conductive-earthed structures over the ground and in earthing grids and induced transient voltages and currents in low-voltage cables. The problem with damages or misoperation caused by lightning transients has been observed in control buildings with electronic devices in measuring and controlling systems inside HV substation. Definition of existing lightning risk and develop the protection method required the study of lightning currents distributions in conductive elements of HV substation. The knowledge of these distributions allows compute the transient voltages in signal lines. The energetic system being modeled consists with 3 HV substation and overhead transmission HV lines between them. On each substation were the same arrangements of HV equipment and control cables. The 3D model of HV substation, the arrangements of control cables and same part of substation, which were used in calculation, are presented in Figures 1 and 2.

Mathematical model was employed for the prediction of induced voltages in signal cables over and under the ground (Fig. 2), during a direct lightning stroke to the area of substation. In analysis, the lightning current has the following mathematical expression:

$$i(t) = \frac{I}{\eta}\left(e^{-\alpha t} - e^{-\beta t}\right)$$

where: t - time, α - reciprocal of time constant, β - reciprocal of time constant, I - peak current and η - correcting factor

The parameters of the lightning current, for the first and subsequent lightning strokes, were taken according to the IEC 61312-1 for the III-IV protection level. In investigations the surge currents were injected to the different points of earthed structures in HV substation and this current is divided into:

- earthing system of this substation,
- grounding wires of HV lines,
- the earthing systems in substations, which were connected with substation in which the lightning danger was analyzed.

The transient voltages at equipment's interfaces in control building have been computed for cables, which have lengths 62m and distances between them 10 mm (Fig. 2). Some results of these calculations were presented in Figures 3 and 4, where (all cable numbers are according to real HV substation plans):

U861 – voltage of cable no. 861 (bounding bar) with reference to true earth
U1251-861 – voltage of cable no. 1251 (1st layer) with reference to the bounding bar (cable no. 861)
U1248-861 – voltage of cable no. 1248 (2nd layer) with reference to the bounding bar (cable no. 861)
U1245-861 – voltage of cable no. 1245 (3rd layer) with reference to the bounding bar (cable no. 861)
U1242-861 – voltage of cable no. 1242 (4th layer) with reference to the bounding bar (cable no. 861)
U1251-1229 – voltage difference between cabel no. 1251 (1st layer, 1st row) and cable no. 1229 (1st layer, 2nd row)
U1248-1229 – voltage difference between cabel no. 1248 (2nd layer, 1st row) and cable no. 1229 (1st layer, 2nd row)
U1245-1229 – voltage difference between cabel no. 1245 (3rd layer, 1st row) and cable no. 1229 (1st layer, 2nd row)
U1242-1229 – voltage difference between cabel no. 1242 (4th layer, 1st row) and cable no. 1229 (1st layer, 2nd row)

The mathematical method, which was used in calculations allows consider all possible configurations of conductive elements on the station, different points of lightning stoke to the station's area and different arrangements of signal lines.

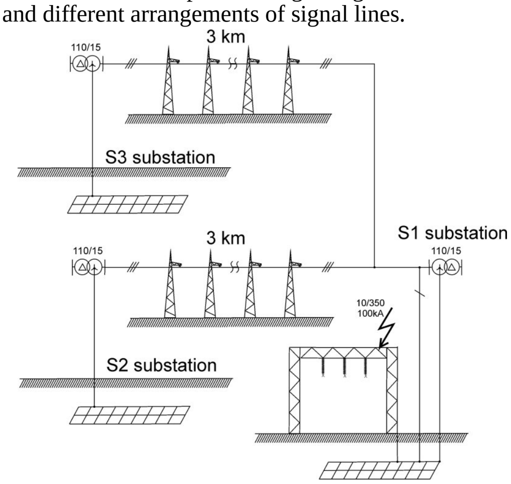

Figure 1: 3D substation model used in calculation.

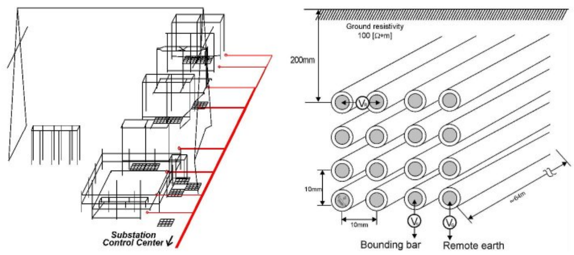

Figure 2: The part of substation model with control circuit wiring.

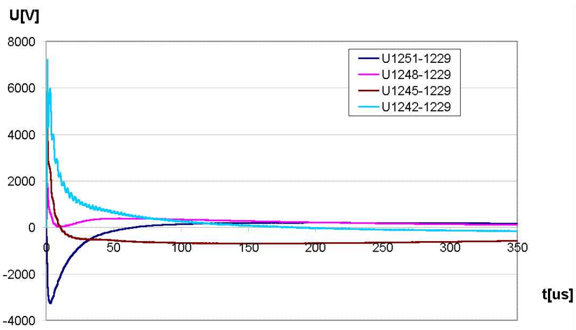

Figure 3: Voltage relationship between data transmission lines.

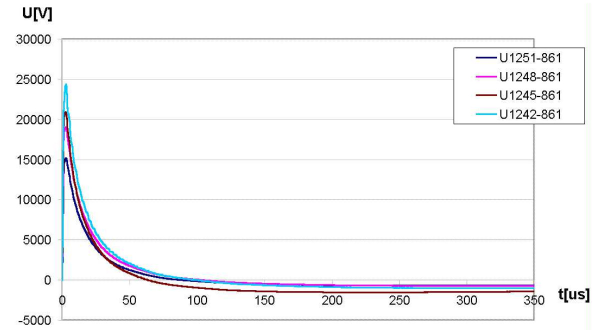

Figure 4: Transmission lines voltage depth relationship with reference to the bounding bar.

HPEM 11 - Measurement Techniques

HPEM 11-1: Low Invasiveness, High-Bandwidth Vectorial Pigtailed Electro-Optic Sensors for High Power Electromagnetics Measurements

G. Gaborit[1], L. Duvillaret[1], N. Breuil[2], B. Crabos[3], J.-L. Lasserre[3]

[1]*LAHC – Université de Savoie – 73376 Le Bourget du Lac Cedex – France*; [2]*THALES Systèmes Aéroportés – 2 av. Gay-Lussac – 78851 Elancourt Cedex – France*; [3]*DGA / DCE / Centre d'Études de Gramat – département DT/EX – 46500 Gramat – France*

Among the classical techniques used for the measurements of high power electromagnetics, most of them are either scalar (infrared tomography, calorimeters ...) or highly invasive (antennae). We present here vectorial pigtailed electro-optic (EO) probes that present the advantages of compactness, relative non-invasiveness, high-frequency bandwidth and very high spatial resolution. Based on Pockels' effect, theses probes are fully dielectric and perfectly adapted to very high electric field measurements (up to at least air breakdown electric field). This promising technique has emerged during the eighties, especially for on wafers electric field measurements. However, due to its relative difficulty of use, this technique stayed in laboratories and didn't spread into industry for two decades. Since the first development of pigtailed electro-optic probes at the beginning of this decade, thus solving the key problem of carrying the laser beam inside the EO crystal constituting the sensor, the situation may dramatically change very soon.

The principle of EO sensors consists in the use of EO crystals that present a birefringence induced by an applied electric field. Thus, by the measurement of phase retardation, either by using the EO crystal as amplitude, phase or polarization state modulator, one can obtain the value of the electric field applied to the crystal [1]. Moreover, as the phase retardation is induced by a unique electric field component in the case of anisotropic EO crystals, it is then possible to get a vectorial measurement of the electric field by measuring three electric fields components that are orthogonal each other. In case of isotropic crystals, we have shown that it is possible to get the amplitude of the projection of the electric field vector onto a plane [2].

We have built different EO sensors based on lithium tantalate crystals with bandwidth ranging from 100 MHz up to 5, 10 and 15 GHz. The experimental portable setup (A3 size) is based on a CW laser diode @ 1550 nm. As we have chosen to use the EO crystal as a polarization state modulator, the pigtailed sensors are based on polarization maintaining (PM) fibres. A schematic of the 15-GHz-bandwidth EO sensor and its picture are presented in Fig. 1. Its frequency response, between 0.1 and 10 GHz is shown in Fig. 2. As seen in Fig. 3, the sensor presents a good rejection of the electric field component that is perpendicular to the vector sensitivity [2], this latter one being collinear to the unique electric field component to which the EO sensor is sensitive. Finally, let us indicate that the dynamic range of the EO sensor spreads from 160 kV_{eff}/m up to 5 MV_{eff}/m (estimated value for 1 dB compression) for an analysis bandwidth covering the 0.1-10 GHz range, but the sensitivity is lower than 0.5 V_{eff}/m for a 1-Hz resolution analysis bandwidth. For these two analysis bandwidths the measurement dynamic of the whole system is respectively of the order of 30 dB and 140 dB with 1-Hz resolution analysis bandwidth.

We are presently developing new EO sensors based either on ZnTe or DAST (EO organic crystal) and we will present first characterizations and results during the conference. This work is supported by the DGA (Délégation Générale pour l'Armement, i.e. the French Military Programs Management and Procurement Agency).

References:

[1] "Electro-optic sensors for electric field measurements – part I: Theoretical comparison among different modulation techniques", L. Duvillaret, S. Rialland et J.-L. Coutaz, J. Opt. Soc. Am. B 19, pp. 2692-2703 (2002)

[2] "Electro-optic sensors for electric field measurements – part II: Choice of the crystals and complete optimization of their orientation", L. Duvillaret, S. Rialland et J.-L. Coutaz, J. Opt. Soc. Am. B 19, pp. 2704-2715 (2002)

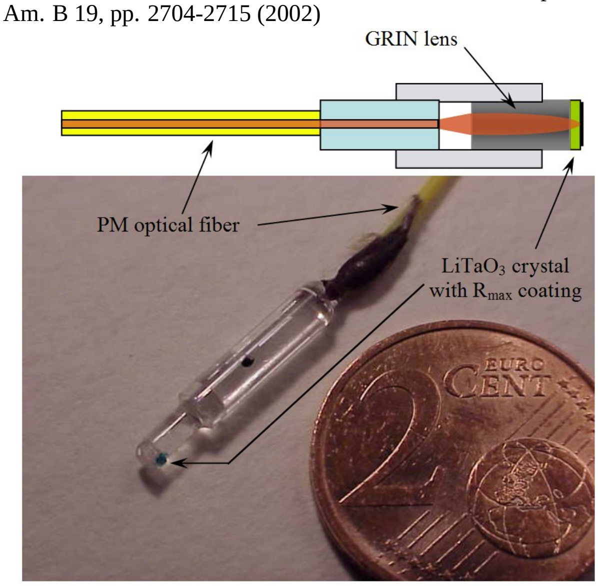

Figure 1: Schematic and picture of a $LiTaO_3$ EO sensor with a 15-GHz bandwidth

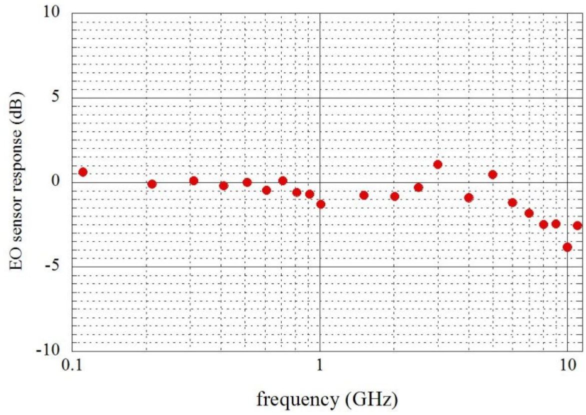

Figure 2: Frequency response of the EO sensor shown in Fig. 1

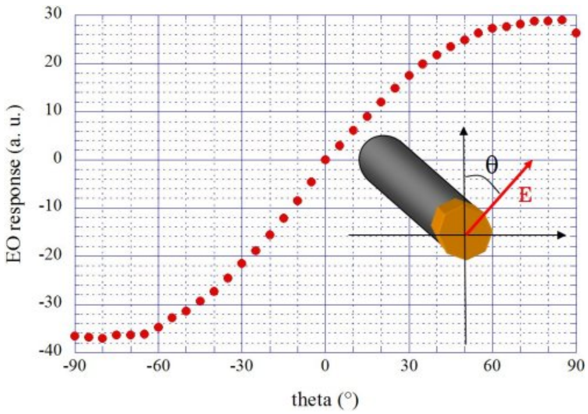

Figure 3: Angular response of the EO sensor

HPEM 11-2: High-Sensitivity Electro-Optic Sensors

D. H. Wu[1], **T. J. Wieting**[2], **A. Garzarella**[2], **S. B. Qadri**[1], **C. Kendziora**[1]
[1]*US Naval Research Laboratory*; [2]*SFA, Inc.*

The promise of electro-optic (EO) sensors as an alternative to conventional heterodyne detection of electromagnetic radiation is huge. These sensors have an extremely broad instantaneous bandwidth (ULF to several THz), they are predicted to be competitively sensitive (potentially < 1 μV/m-Hz1/2, NEI < 3 x 10^{-19} W/cm^2), they detect the true waveform of the electric field including the phase, and they have a large dynamic range (typically $\approx 10^7$, 1% error). Furthermore, they are small in size and interfere minimally with the fields they are measuring. The present challenge is to make these sensors more competitive by increasing the field-strength sensitivity by at least three orders of magnitude. We have previously achieved sensitivities of 2 mV/m with LiNbO3 (D. H. Wu, T. J. Wieting, and L. F. Libelo, Intermittent Bursting and an Intrinsic Feedback-Like Mechanism in a Nonlinear Electro-Optic Field Sensor, Proceedings of EMC Europe 2002, Sorrento, Italy, p. 631). In this paper we report the results of an investigation of a new class of mixed single crystals, SrxBa1-xNb2O6, where x = 0.75 and 0.60. SBN:75 and SBN:60 have much larger Pockels coefficients than LiNbO3. Our experiments on the EO response were carried out with the sensor in a polarization-rotation (rather than interferometric) configuration: stabilized lasers (near IR, red, green and blue) were used as the probe, the modulated electric field across the crystal was applied perpendicular to the direction of the beam, and a broadband integrated photodiode/amplifier was employed to detect the field. Since crystalline imperfections limit the accuracy in determining the rotation of the polarization vector, x-ray studies were made of crystals grown by the Czochralski, Stepanov, and floating-zone methods. Raman scattering studies were also employed in order to determine the useable bandwidth of the EO response, since the first strong infrared-active mode prevents propagation of the laser beam through the crystal. The present performance of these broadband sensors will be described, as well as prospects for further improvement.

HPEM 11-3: Wide-Band Coaxial-Type Resistive Sensor for HPM Pulse Measurement

M. Dagys[1], **Z. Kancleris**[1], **R. Simniikis**[1], **E. Schamiloglu**[2], **F. J. Agee**[3]
[1]*Semiconductor Physics Institute, A. Gostauto 11, Vilnius, 2600, Lithuania*; [2]*University of New Mexico, ECE Department, Albuquerque, NM 87131, USA*; [3]*AFOSR/NE, 801 N. Randolph St., Arlington, VA 22203, USA*

The electron heating effect in semiconductors leads to their resistance increase in a strong electric field. This effect is used as the basis for the performance of a resistive sensor (RS) that has found applications in high-power microwave (HPM) pulse registration. To-date waveguide-type RS's have been developed that demonstrate some advantages over semiconductor diodes that are also sometimes employed for the measurement of the HPM pulses. The RS can detect about 60 dB higher power level, is resistant to large power overloads and demonstrates very good long-term stability. It produces an output signal up to a few tens of Volts without any amplification circuit and is sufficiently fast to measure nanosecond duration HPM pulses. These features of the waveguide-type RS make them as one of most promising devices for HPM pulse monitoring and control.

Unfortunately, the waveguide-type RS is not free from some drawbacks. First, the frequency range where the particular device can be used is restricted by the bandwidth of the waveguide employed. Second, the sensitivity of the RS in the waveguide's band is frequency-dependent. It can vary by more than a factor of two over the frequency band. Therefore, in the last few years our activities concentrated on a coaxial-type RS that might be employed over a wider frequency range.

In this contribution, we present theoretical and experimental investigations that are the basis of a concept of a coaxial-type RS with flat frequency response. The coaxial-type RS is designed as a unit with an integrated 50 Ω termination and standard N-type coaxial connector used to connect the coaxial-type RS to the transmission line. A VSWR 1.6 was accepted as a limiting value for the device. It should be able to measure 1 kW pulsed microwave power in a frequency range 2-12 GHz. Prototypes of the coaxial RS have been manufactured and tested. A few types of low-pass filters preventing propagation of the microwave pulse to the measuring unit and providing matching of the RS with the transmission line have been examined. The sensitivity variation was found to be less than ± 15 % over the entire frequency range tested. The results presented in this paper strongly confirm that the resistive sensors are one of the most valuable devices for HPM pulse characterization.

* Work is supported by the European Office of Aerospace Research and Development under contract number F61775-02-WE030

HPEM 11-4: Characterization of High-Power Pulse Sources with the EMIR Method

P. Levesque[1], **J.-L. Lasserre**[2], **A. Paupert**[2]
[1]*ONERA, Département Structures et Dommages Mécaniques, BP 72, 92322 Châtillon cedex, France*; [2]*DGA/DCE/ Centre d'Etudes de Gramat, DT/EX, 46500 Gramat, France*

For more than ten years now, Onera has been developing a method for quantitative visualiza-tion of electromagnetic fields called the EMIR (ElectroMagnetic-InfraRed) method. In order to do a simple evaluation of EM fields, we developed a sensor consisting of a thin photothermal film (lower or equal than 25 micrometer), the electrical properties of which were chosen in order to transform a part of the incident field into heat. This heating is detected with an infrared camera. It is clear that this technique draws on knowledge of both electromagnetic and thermal phenomenas.

The field of applications of this method, civilian and military, is wide open. Practically speaking, we can distinguish two main types of applications. First, those in which we seek to characterize a radiating system (radar, telecommunications) or shielding (electromagnetic compatibility), and also those in which we use electromagnetic radiation to reveal structural flaws (non-destructive control, diagnostic) or to determine the dielectric constant (metrology) of raw materials or manufactured objects or to study the capacity of a unit to withstand electromagnetic disturbances (immunity).

Among these applications, we choose to present in this paper the reliability of the method for characterization of high-power pulse sources and also the capacity of the method to characterize electromagnetic fields induced in the structures by radiation.

In this abstract we will only discuss the first point of our paper:

- Characterization of high-power pulse sources.

A recent study demonstrated the feasibility of the method for characterizing high-power pulse sources. The energy measurements made up until now have been based on the use of calorimeters that have two drawbacks: their reflectivity is high, on the order of 25 %, and they do allow only for local energy measurement.

Figures 1 to 3 show an example of results obtained with the EMIR method. In Figure 1 we see the distribution of the maximal heating of the photothermal film subjected either to a microwave pulse (9 GHz) of a duration of several ns and with an intensity of several 10^8 W, or to a serie of 2 to 5 identical pulses at the repetition frequency of 100 Hz. As the heating of the film is proportional to the incident energy density, the EMIR method gives the distribution of this value in the plane of the photothermal film. Figure 2 shows the horizontal profile of the energy after 5 pulses.

We see in figure 3 the temporal variation of the heating of the film at the center of the spots shown in figure 1. With each pulse, the photothermal film absorbs part of the incident energy that is converted into heat. After each pulse, the temperature decreases according to a non-linear law that depends essentially on the radiation-convection losses. In case of several pulses and because of the time scale chosen, we do not see the decrease between each pulse in this figure.

A thermal model that takes into account these losses can be used to extrapolate these thermo-grams to any point of the film at the instant following the energy deposit, thus leading to the spatial distribution of the energy density sought. In return for a calibration preliminary of the photothermal film and the knowledge of the duration of the impulse, it is possible to evaluate the value of the electrical field. The measurement dynamic is in the order of 16 dB for an incident energy of 4 J/m2.

This method offers several advantages including the possibility of a 2D visualization of the energy with a large spatial resolution, low disturbance of the incident energy by the photothermal film (usual films have a reflectivity on the order of 3 %) and a wide pass-band (500 MHz to more than 20 GHz).

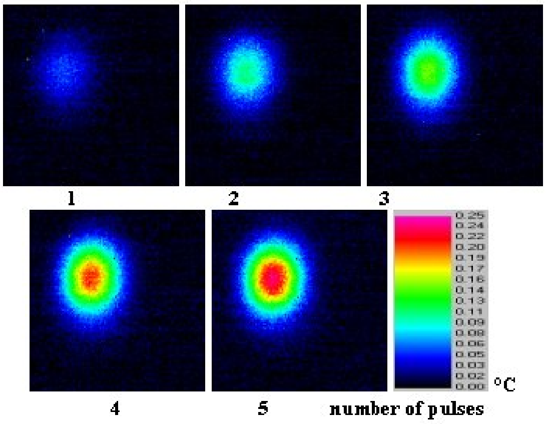

Figure 1: Images obtained with the EMIR method showing the maximal heating of the film subjected to a series of very high frequency pulses. These images represent the spatial distribution of the energy density of the source in the plane of the photothermal film.

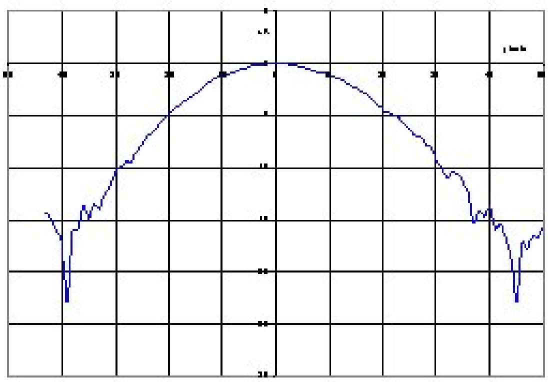

Figure 2: Horizontal profile of energy after 5 pulses

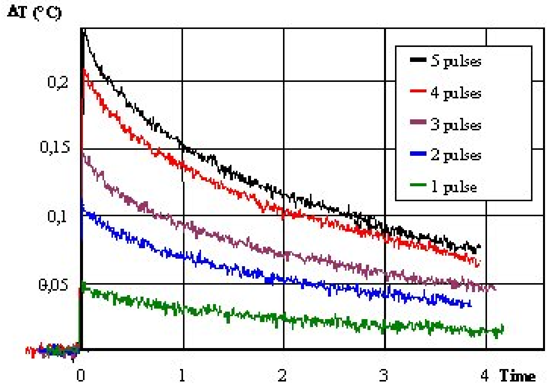

Figure 3: Temporal variation of the heating of the film subjected to a series of very high frequency pulses

HPEM 11-5: Infrared Imaging to Map Power on Target for a Millimeter Wave Source

M. W. Wilbanks, G. L. P. Patterson IV, H. Pohle, W. T. C. Clark III
AFRL/DEH

Infrared camera images are used to calculate the power deposited on a target by a high frequency system. Thin carbon impregnated sheets of Kapton are illuminated with RF energy, then infrared images in the 3-5 μm band provide temperature data that is used to numerically solve the heat equation and obtain power-absorbed values. Techniques to determine the electrical properties of Kapton above 84 GHz are developed.

HPEM 11-6: Questions of Metrological Maintenance of Measuring and the Check of Parameters of Electromagnetic Impulses of Major Energy

K. Danilenko, A. Mitrofanov, V. F. Molochkov, L. Siny
Research Institute of Pulse Technique

Metrological maintenance of measurement and control of amplitude-time parameters of electromagnetic high energy impulses includes the following basic scientific directions:

- making and metrological certification of the special standard of an unity of pulsing electromagnetic radiation (EMR) and the national testing plan for resorts of measuring instrument (MI) of parameters ER;
- development of methods and resorts of transmission(transfer) of the sizes of unities of intensity of pulsing electrical and magnetic fields from the standard of an unity to working MI, including, pulsing testing installations and standard measuring transformers which are applied at checking and a calibration of SI of parameters of electromagnetic impulses of major energy.;
- the analysis and an estimate(estimation) of the basic making errors of measurement of amplitude-time parameters of high energy electromagnetic impulses and, first of all, dynamic errors of measurings (DEM), and errors, the bound with nonlinearity of performances of transformation (PT) MI, which can have prevailing agency(effect) on the aggregate errors of electromagnetic impulses parameters measurement;
- development of hardware and programm methods of decrease of measurement errors;
- development of the working MI set up by new principles for measurings amplitude-time parameters of high energy electromagnetic impulses, a select of the rational nomenclature and expedients of a norming of their metrological performances (MP), trials, checking and a calibration of MI;
- an estimation of static and dynamic errors of a calibration of the working MI caused by agency(effect) of dynamic metrological performances of MSI and time parameters of pulsing testing installations, development of methods of their decrease.

In this paper discuss the basic aspects of Metrological maintenance (MM) of measuring and the control of amplitude-time parameters (ATP) of high energy electromagnetic impulses and

basic groups of MI for such measurings.
Now in Russia it designed and a lot of standard measuring instrument of unities of intensity pulsing electrical and magnetic fields in working MI which embrace various peak and time ranges of parameters ER and are applied to control and a calibration of working MI, and also working MI for measuring and the control of parameters electromagnetic high energy impulses.
It is necessary to allocate some basic groups of such MI:
1) Radiating installations EMR, which intended for a peak calibration of primary measuring transducers (PMT) of intensity electrical (EF) and magnetic (MF) fields of high energy (i.e. for the experimental definition of the performance of transformation (PT) or conversion coefficient (Kcc) PMT) or the experimental definition of pulsing performances PTM either transient responses PTM or measuring channels EMR as a whole.
2) Generators of electrical impulses which set modes of formation ER in and radiating installations of the first group, or intended for a peak calibration or for the experimental definition of the transition and pulsing performances of registrars of the electrical signals acting with IP (reference impulse generator).
3) Reference and working primary measuring transducers of intensity of pulsing electrical and magnetic fields, currents and voltages in electrical impulses with cable or optic communication links.
4) Registaring instruments of electrical impulses.
5) Attenuators and electric pulse amplifiers who intended for maintenance of measurings EMR in the given peak ranges.
6) Multichannel measuring systems (MMS), basic which measuring builders are working MI 3, 4 and 5 of set forth above groups.

HPEM 11-7: Simple Procedure for the Extraction of the Complex Cable Transfer Impedance of Coaxial Cables

A. Sawitzki, **K.-H. Gonschorek**
Dresden University of Technology, Chair of Electromagnetic Compatibility, 01062 Dresden, Germany

Coaxial cables are widely used for signal connection. But there is always an electromagnetic coupling from the outside of the cable to the inside, causing disturbed signals in the cable. This coupling effect can be described by use of the cable transfer impedance and the cable transfer admittance.
The cable transfer impedance is defined as the ratio of the current on the cable shield to the voltage across the load inside the cable. This coupling is depending on the length of the cable. It is described as impedance per length (Fig. 1).
A measurement system consists of a generator enforcing the current on the cable shield and a receiver to measure the voltage across the load. This coupled voltage across the load can easily be measured with a network analyser.
For feeding the current on the shield both unmatched and matched solutions exist.
In [1]: [Tiedemann, R., Schirmwirkung koaxialer Geflechtsstrukturen, PhD thesis, Technische Universität Dresden, 2001] an unmatched system is described. If the system is not matched, resonance effects occur in the current flowing on the shield. One way to reduce the influence of resonances is to select the length of the cable to be small compared to the wavelength. Therefore for higher frequencies the cable has to be very short. As one resulting effect the coupled voltage might be too small for measurements, depending on the shielding effect of the cable and the network analyser.
Other solutions use a matched connection between cable shield and current generator to enforce the current on the shield. IEC 96-1 uses a coaxial system with the shield of the cable to be measured as the inner part and a tube as the outer part. Although this system is very accurate, a suitable tube is not always available. A disadvantage is that the tube diameter has to be selected related to the diameter of the cable shield, in order to achieve the matching impedance.
This report introduces a new method to extract both magnitude and phase of the complex cable transfer impedance (Fig. 2). Because no tube is needed, it is more easy to use compared to the method described in IEC 96-1. It is similar to the system developed by Tiedemann [1], but resonant effects and the need for a short length of the coaxial cables are avoided by using a matched system to enforce the current on the shield.
The outer system is build locating the cable shield in a small distance above a finite conducting plate. According to transmission-line-theory (TLT) this system can be constructed to have an impedance of 50 Ohms and therefore it is matched to the forcing generator by simple connection. The distance between cable shield and an infinite metal plate together with the diameter of the cable shield predicts this characteristic impedance. The resulting impedance of the outer system (cable above a finite plane) can easily be controlled by S-parameter measurement.
The new measurement method is presented with some results for standard coaxial cable.

$$Z_T' = \frac{U_2}{I_{screen} \cdot l} \quad \text{, with } l \ll \lambda$$

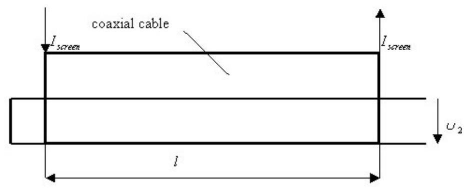

Figure 1: Definition of the cable transfer impedance

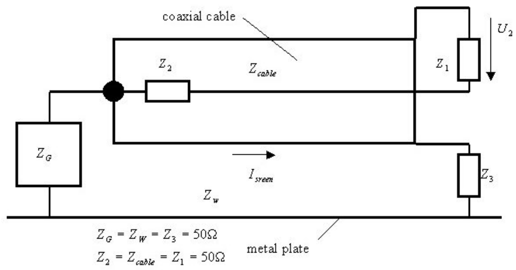

Figure 2: Measurement system

HPEM 11-8: Characterization of Antennas and Wireless Terminals in Loaded Reverberation Chambers

J. Carlsson[1], **P.-S. Kildal**[2]
[1]*SP Swedish National Testing and Research Institute, Borås, Sweden*; [2]*Chalmers University of Technology, Gothenburg, Sweden*

The paper will give a summary of the work on characterization of antennas for wireless and mobile terminals by using reverberation chambers, which has been done at Chalmers University of Technology the last years. We have developed procedures to measure radiation efficiencies (A. Wolfgang, J. Carlsson, C. Orlenius and P-S. Kildal, "Improved procedure for measuring efficiency of small antennas in reverberation chambers", IEEE AP-S International Symposium, Columbus, Ohio, June 2003) and "free space" impedances of small antennas (P-S. Kildal, C. Carlsson, J. Yang, "Measurement of free space impedances of small antennas in reverberation chambers", Microwave and Optical Technology Letters, Vol 32, No 2, pp. 112-115, January 2002), total radiated power of mobile phones, and diversity gain (P-S. Kildal, K. Rosengren, J. Byun, J. Lee, "Definition of effective diversity gain and how to measure it in a reverberation chamber", Microwave and Optical Technology Letters, Vol. 34, No 1, pp. 56-59, July 5, 2002.). We are able to measure with an extended uncertainty of less than 1 dB even if the chamber has a size of only 0.8m x 1.0m x 1.6m. The accuracy is much better than should be expected from what is known in the EMC area. The reasons are the new patent-applied stirring methods that we have developed; two efficient plate stirrers, platform stirring (K. Rosengren, P-S. Kildal, "Characterization of antennas for mobile and wireless terminals in reverberation chambers: Improved accuracy by platform stirring", Microwave and Optical Technology Letters, 20 September 2001), polarization stirring (P-S. Kildal, C. Carlsson, "Detection of a polarization imbalance in reverberation chambers and how to remove it by polarization stirring when measuring antenna efficiencies", Microwave and Optical Technology Letters, Vol. 32, No 2, pp. 145-149, July 20, 2002), and frequency stirring of the net transfer function. We have used a simple validation case (dipole near lossy cylinder) to validate measured radiation efficiencies against computed values (J. Carlsson, A. Wolfgang, P-S. Kildal, "Numerical Simulations of a Validation Case for Small Antenna Measurements in a Reverberation Chamber", IEEE AP-S International Symposium, San Antonio, Texas, USA, June, 2002). We have validated actual phone antenna measurements against measurements in anechoic chambers at Saab Ericsson Space and Sony Ericsson Mobile Communications. The agreement is in both cases very good. We have in cooperation with Samsung Electronics Co Lmt in South Korea developed a procedure to also measure diversity gain in the chamber. We have introduced the term effective diversity gain that is in much better agreement with fundamental theoretical limitations than any previously published results. We have developed a complete electromagnetic analysis model for two parallel dipoles used for diversity. The theoretical results are in very good agreement with measurements. Finally, in order to understand the performance of the chamber we have validated Hill's formulas for how lossy objects affects the Q-value (U. Carlberg, P-S. Kildal, A. Wolfgang, O. Sotoudeh, C. Orlenius, "Calculated and measured absorption cross sections of lossy objects in reverberation chamber", accepted for publication in IEEE Transactions on Electromagnetic Compatibility).

HPEM 11-9: Evaluation of Stirrer Efficiency in Reverberation Chambers

O. Lundén, N. Wellander, M. Bäckström
FOI Swedish Defence Research Agency, SE-581 11 Linköping, Sweden

Introduction: The efficiency of stirrers in reverberation chambers depends of a set of parameters. Traditionally it is often believed that it is the volume in relation to the chamber volume which is of primary importance. Based on this assumption many stirrers are designed with a relatively small diameter and large height. To get a better understanding about the stirrer performance in reverberation chambers a Factorial Designed Experiment was performed. This involved more than forty different stirrers and three chambers. For each configuration measurements were performed and the autocorrelation was calculated at each frequency to find the number of independent samples vs. frequency. The outcome was used to numerically model the response.
General Factorial Design: To perform a general factorial designed experiment, the investigator selects a fixed number of "levels" (or "versions") for each of a number of variables (factors) and then runs the experiments with all possible combinations. In the factorial experiment we have investigated three factors and their interactions. The factors were the diameter and the height of the stirrer and the chamber size.
Measurements were performed in the frequency range 100 MHz to 18 GHz in four bands. The chamber sizes were 27.1, 36.7 and 210 m^3. Stirrer diameters 0.72, 1.15, 1.55, 1.95 and 2.4 m. Stirrer heights 0.28, 0.40, 0.53, 0.8, 1.2, 1.6, 2.0 and 2.4 m.
Efficiency criterion: We have selected the lowest frequency at which we have at least 200 uncorrelated stirrer positions as the criterion for an efficient stirrer. Of course one can use a lower number of uncorrelated stirrer positions but that will give a higher uncertainty in the determination of the frequency. Data was sparsed to check the 200 to 50 stirrer steps performance relationship. The correlation coefficients is calculated using an autocorrelation function for all stirrer intervals at each frequency and compared with the 5% and 1% probability levels that are based on the number of samples. It is also compared with the correlation level of 1/e $\approx$ 0.37.
Modelling: The experiment has been carried as a full factor design at three levels. The results show that the diameter is the most important parameter for an efficient stirrer. An attempt was made with linear, quadratic and cubic polynomials to predict the stirrer response in different chambers. This however resulted in some physical unrealistic minima's why this approach was abandoned and some other models were introduced.
The measured data were fitted to the following model
(1)
where f_{200} is the lowest frequency in MHz at which we get 200 independent samples, A is a constant, V_{ch}, h, d, is the chamber volume, the height and the diameter of the stirrer. The powers γ, α and β are to be estimated
Taking the logarithm of (1) gives
(2)
which is well suited for least square fit of the coefficients. Based on the measured data we got the following result for the correlation level of 1/e $\approx$ 0.37.
$A = e^{6.2}$, γ = 0.31, α = 0.40 and β = 1.3. That is:
(3)
The root mean square logarithmic error is 0.09. This means that the error in the determination of the frequency is about 10 %.
Conclusions: It can be concluded that the introduced model will give a more realistic representation than the cubic, quadratic or linear polynomials. Validity of the model has been compared with measurements in a 1 m^{3}3 chamber as well as in a 1386 m^3 chamber with reasonable results.

$$f_{200} = A\frac{V_{ch}^{\gamma}}{h^{\alpha}d^{\beta}}$$

Eq. (1)

$$\log f_{200} = \log A + \gamma \log V_{ch} - \alpha \log h - \beta \log d$$

Eq. (2)

$$f_{200} = \exp(6.2)\frac{V_{ch}^{0.31}}{h^{0.40}d^{1.3}}$$

Eq. (3)

HPEM 11-10: Determination of the Number of Statistically Independent Boundary Conditions of Mode-Stirred Chambers

H. G. Krauthäuser[1], T. Winzerling[1], J. Nitsch[1], N. Eulig[2], A. Enders[2]
[1]*Otto-von-Guericke-Universität Magdeburg, IGET, Magdeburg, Germany*; [2]*TU Braunschweig, IEMV, Braunschweig, Germany*

The determination of statistically independent boundary conditions (stirrer positions) is very important when measurements are performed in mode-stirred chambers. One reason is that the number of independent boundary conditions is one important parameter for the lowest usable frequency (LUF) of the chamber. On the other side, the statistical theory of mode-stirred chambers is based on the assumption of statistically independent boundary conditions also. In the new standard IEC 61000-4-21, the determination of independent boundary conditions is discussed in the informative part only. There, an example is given with a fixed population size of 450 measured boundary conditions. In the literature, it is remarked by Lundén and Bäckström, that the population size has to be taken into account. Unfortunately, the proposed approach leads to results, that are not compatible with the well established measurement practice. Furthermore, the results seem to be unphysical since the number of independent boundary conditions can increase, when the number of measurements is decreased.
Our analysis of this approach leads to a modification that did not claim perfect statistical independents any more. In the contrary, the correlation should be smaller than a given limit, if boundary conditions are accepted to be sufficiently independent.
In the presented work, we give equations for that limit. This limit depends on the expected value for the correlation coefficient (that would be measured if an infinite number of boundary

conditions would be realized), on the error probability (1% or 5%, usually), and on the population size N (number of measured boundaries).
In that way, we will give limits that are compatible with IEC 61000-4-21, but can be used for arbitrary N with the same statistical significance. Since the expected value for the correlation coefficient has been given explicitly, now the determination coefficient is also a known parameter.
Measurements have been performed to demonstrate the differences between our approach and the approach of Lundén and Bäckström.

HPEM 11-11: Parametric Characterization of Reverberation Chambers: A Review

M. Piette
Royal Military Academy/Department Telecommunications/ Laboratory of Electro Magnetic Applications, 30 Renaissance Avenue, B-1000 Brussels Belgium

During the last two decades, reverberation chambers have received considerable attention from the EMC community (Bäckström & al "Reverberation Chambers for EMC Susceptibility and Emission Analyses", Revue of Radio Science 1999-2002) and from the aeronautical and car industry (RTCA/DO-160D, Sec 20, "Environmental Conditions and Test Procedures for Airborne Equipment", 1997) (Bronaugh & al., "Whole-vehicle EMC Testing in a Reverberation Chamber", EMC Zürich, 1997) thanks to their ability to generate high intensity fieldstrengths from a moderate electrical power and to physically produce statistically isotropic plane wave incidence. These two features make them particularly suited for immunity testing of systems encountering severe multipath effects like mobile or wireless communication systems used in urban areas (Y.Karasawa, "Multipath Propagation Theory and Modelling in Wideband Mobile Radio : the ETP Model Connecting Propagation and Systems", Radio Science Bulletin, N°302, Sep 2002) or indoor environments (Tobin & Richie, "Indoor Propagation : a statistical approach", EuroEM'94, Bordeaux). Other well known applications are shielding effectiveness measurements of radiofrequency gaskets, cables, enclosures, or material samples (Hatfield, "Background and Status of IEC Standard 61000-4-21 on Reverberating Chambers", EMC Zürich 2001), emission measurements (Corona & al, "Use of a reverberating enclosure for measurements of radiated power in the microwave range", IEEE Trans.EMC, vol.18, n°2 May 1976) or determination of the antenna radiation efficiency (Rosengren & al, "Measurement of Terminal Antennas Performance in Multimode Reverberation Chambers", Nordic Conf. Antenna 00, Kalmar, Sep 2000)(Piette, "Antenna Radiation Efficiency Measurements in a Reverberation Chamber", to be presented at ISAP'04, Sendaï).
This paper provides a critical review of all the parameters characterizing the quality of a reverberation chamber. After a short recall on the statistical modeling of the fields inside such a chamber and of some elements of the theory of the resonant cavity, a set of 13 parameters (N, SR, $\Delta\omega/\omega$, σ, ϱ, PDF, CDF, Q, Eav, CG, τ, Vt, LUF) characterizing the good operation and the performances of a reverberation chamber are reviewed and critically related by comparing measurement results extensively reported in the literature. The influence of the cavity shape and of the mode stirrer (location, shape, dimensions) are outlined. The loading effect of the equipment under test and the influence of the transmitting antenna are also addressed (Piette, "Champs électromagnétiques aléatoires en chambre de réverbération : théorie et applications", LEMA 2004/2 RS Report, Royal Military Academy). Measurements carried out in the LEMA reverberation chamber at the Royal Military Academy by means of a broadband triaxial E-field probe are presented, a.o. insertion loss, quality factor, relaxation time, resonance frequency shift, stirring ratio and spatial uniformity. About this last parameter, the use of the triaxial fieldprobe with flat frequency response enables to measure in real time and independently the three orthogonal components of the electric field (Fig.1). The optical signal from the laser diode integrated in the probe is transmitted by optical fibre to the opto-electric convertor and the spectrum analyser (Fig.2).

Figure 1: Triaxial E-field probe on non conductive tripod

Figure 2: Electro-optical receiver front panel & spectrum analyser

HPEM 11-12: Influence of Equipment Set-up and Directivity Radiating in Mode Stirred Reverberation Chamber

A. Maridet[1], **F. Paladian**[2], **F. Mangeant**[1]
[1]*EADS CCR, 12, rue Pasteur 92150 SURESNES, France*;
[2]*LASMEA, Université B. Pascal, 24, avenue des Landais 63177 AUBIERE, France*

INTRODUCTION
Since some years, the use of Mode Stirred Reverberation Chamber (RC) to make tests on electric equipment is more and more current. The physical phenomena and the methodology of the tests in immunity are nowadays well known, contrary to those of emission tests.
In comparison with Anechoic Chambers (AC), the saving of time is one of the most considerable advantages for the use of RC in susceptibility, quite as the necessity of having a sharply less powerful disruptive source. For emission, in AC, measuring the energy radiated in all the surrounding space, the number of

measurement to realize is relatively high.
Furthermore, the quality of these measurements notably depends on the distance taken between every point of measurement. Another factor to be considered to obtain a good quality of test is the reproducibility.
The aim of this paper, is to show some advantages of the using RC in certain cases.
GENERAL CONTEXT OF THE STUDY
Because of its physical working principles, RC creates a statistically homogeneous and isotropic internal electromagnetic field in the working volume. So, in susceptibility the test equipment has to be in this useful volume. Different topics arise naturally when considering emission: Is this criterion of location still obligatory ? Does the source directivity also affect on internal field distribution? Has the reception antenna position got influence ?
The study undertaken aims at showing that with RC, wherever the position is and whatever the spatial source orientation under the chamber, the internal power measured is similar.
EXPERIMENTATIONS
In the first experiment, we study the influence of the different position of the source and of the position of the reception antenna. The emitter is constituted of an emitting dipole which is located inside and outside the useful volume of a 8.4*6.7*3.5m reverberation chamber (see figure 1).We measured the total power emitted in the chamber. The fundamental frequency fo is 28 MHz and the turner angular step is 6°.
The total emitted power by the dipole Pt,EUT is given by equation (1) (D. A. Hill, "Electromagnetic Theory of Reverberation Chambers", NIST Technical Note 1506, National Institute of Standards and Technology, Boulder, Colorado 80303-3328, USA, 1998): where Q is the RC quality factor, V the chamber volume (m), l the wavelength (m), and <Pr> the mean of the power measured by the receiver.
By using the equation (1), the figure 2 shows the total emitted power at different locations of the dipole.
In the second experiment, we study the effect of the directivity of the source. We measured the total power emitted by equipments of different directivities. They were oriented in several directions. The test equipment is a monopole antenna placed under a box (800*505*365mm) which has various removable apertures, therefore various directivities.
The figure 3 shows the total emitted power depending on the equipment orientations.
CONCLUSION
The first experiment showed us that in emission, wherever the source location is (inside or outside the useful volume), for a stirred lap, we have ergodicity of the mean energy measured.
With the second test, we noticed that for equal directivity, as the apertures are oriented onto different directions (x, y, z), the total emitted power is comparable.
It would be interesting to compare the different equipment directivities between them. So, it is necessary to take into account the internal impedances. However, we face a problem because we do not know exactly these impedances. Different ways are now investigated to determine them.

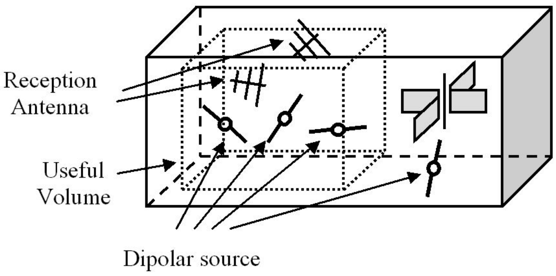

Figure 1: Description of the first experiment in RC

$$P_{t,EUT} = \frac{16\pi^2 V}{\lambda^3 Q}\langle P_r \rangle$$

Equation 1:

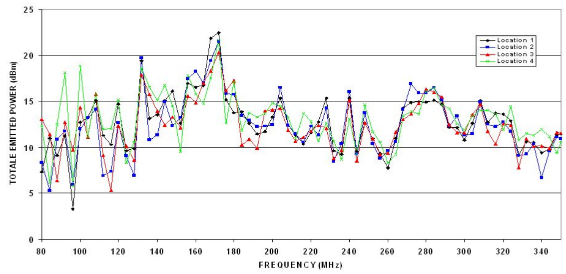

Figure 2: Total power emitted by a dipolar source placed in several locations

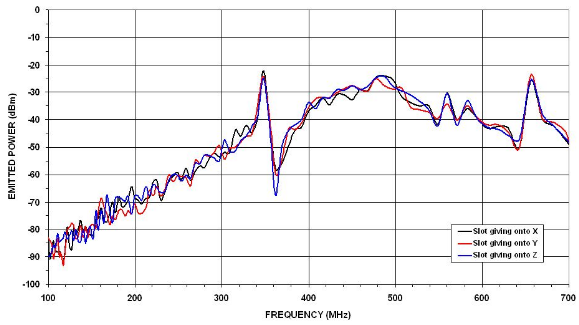

Figure 3: Totale power emitted by the equipment very directive oriented according the directions X, Y, and Z

HPEM 11-13: Comparison Between Experimental and Numerical Modelizations of a Mode-Stirred Reverberation Chamber

R. Vernet[1], **S. Girard**[1], **A. Maridet**[2], **P. Bonnet**[1], **F. Paladian**[1]
[1]*LASMEA UMR 6602 CNRS University Blaise Pascal Clermont II France*; [2]*EADS CCR, 12 rue Pasteur 92150 SURESNES France*

Introduction
One of the test facilities envisaged by EMC standards is the Mode-Stirred Reverberation Chamber (MSRC). The principle consists in using the properties of electromagnetic cavities to generate in a Faraday cage an electromagnetic field which will be statistically regarded as homogeneous and isotropic. In order to obtain such properties, a mode-stirrer is used to distribute uniformly energy inside the enclosure.
Simulation tools are useful to confirm some experimental results, to make the adjustments of experimentations easier and to improve the understanding of the physical phenomenon being at stake. Yet, any numerical simulation generates a discretization of space which is cubic for the "finite differences" approach
[K.S. Yee, 'Numerical solution of initial boundary value problems involving Maxwell's equations in isotropic media', IEEE Trans. Antennas Propagat., vol. AP-14, pp. 302-307, 1966]. That is why we have adapted the recent results of the geometry known as "digital" to model structures in an arithmetic way, and more precisely our mode-stirrer in a FDTD code. To make this approach valid, we propose to compare FDTD simulation and experimental behaviours of the electric field in a MSRC.
Modeling of the mode-stirrer with the digital geometry
Generally speaking, theorems of Euclidean geometry appear unsatisfactory when the used data are digital values in so far as those theorems are not adapted for discrete space. For example, the intersection of two planes is not necessarily a line in a discrete space.
The purpose of the digital geometry is to adapt the set of these "usual" geometrical transformations to discrete spaces while being based on rigorous arithmetical definitions [I. Debled-Renesson, 'Etude et reconnaissance des droites et plans discrets', Ph.D. thesis, University of Strasbourg, 1995].
Consequently, the concepts of this geometry have been applied to mesh the mode-stirrer of our MSRC, the dimensions of which are 6.7m*8.4m*3.5m. Figure (1) shows the real mode-stirrer and

figure (2) its representation in digital geometry.
Results and discussions
Measurements have been led in a step-by-step configuration of the stirrer as referred to the standard IEC-61000-4-21. According to the lowest start frequency of our MSRC, measurements are given for a frequency range from 80 to 120 MHz in order to obtain a significant comparison.
The FDTD simulation uses a lambda/10 discretization leading to a 10cm cell in each direction. The excitation is a gaussian point source located near a corner. In a first step, we consider walls and the stirrer as perfectly electrical conductors to perform the 45 computations corresponding to the 45 positions of the stirrer. The finite conductivity of our MSRC involves a quality factor which is taking into account in the numerical simulation with a specific filter [F. Petit, 'Modélisation et simulation d'une chambre réverbérante à brassage de modes à l'aide de la méthode des différences finies dans le domaine temporel', Ph.D. thesis, University of Marne La Vallée, 2002].
Figures (3) and (4) represent respectively the experimental and numerical behaviours of the total electric field versus the frequency. The comparison shows a good agreement between these two investigations. The slight frequency shift can be explained by the numerical dispersion of the FDTD-scheme. Moreover, differences between the two curves could be reduced by using a more-accurate mesh.
Conclusion
In this paper, we brought out a comparison between numerical and experimental results of a MSRC thanks to a temporal code and a digital geometry mesh of the stirrer.

Figure 1: Picture of the mode-stirrer.

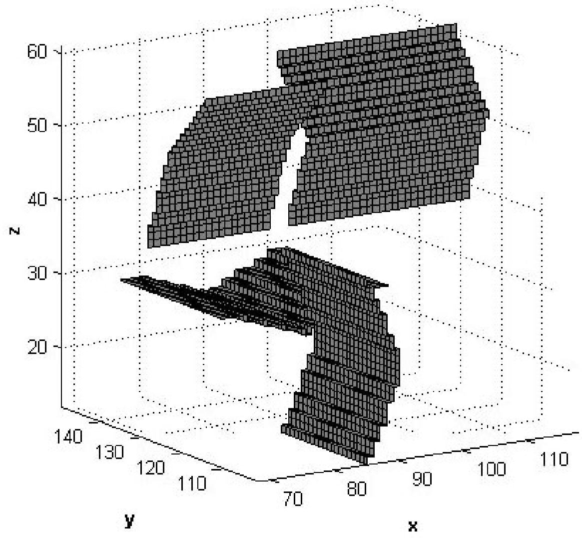

Figure 2: Digital-geometry discretization of the mode-stirrer.

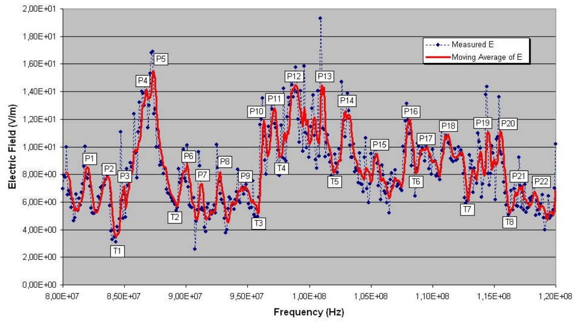

Figure 3: Experimental results of the electrical field in our MSRC.

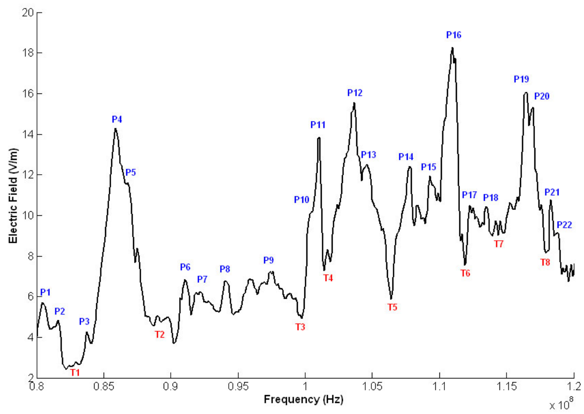

Figure 4: Numerical results of the electrical field in our MSRC.

HPEM 11-14: Shielded Closed HIRF/EMC Facility

I. Bertino, M. D'Urso
Alenia Aeronautica S.p.a.

The aim of the EMC/HIRF test on the aircraft is to reach a degree of confidence sufficient to allow aircraft flight in complex electromagnetic environments, taking into account the increased sophistication of electrical and electronic equipment installed on modern aircraft and the growing power densities of the powerful RF sources of internal and external transmitters.
In order to reach the desired degree of confidence in verifying the required aircraft flight clearances, according to military and civil international standards, Alenia Aeronautica have developed test facilities and EMC test areas which are suitable to perform con-

ducted and radiated tests on fighter and transport aircraft seen as a whole system. Up to now, all tests performed at Alenia's facilities are intended to be performed in open space; due to several constraints and limitations such as weather conditions effects, future higher EMC certification field level and testing of high sensible radio equipment, high intensity radiated field (HIRF) testing should be performed in a dedicated area. For this reason Alenia Aeronautica are studying and developing a shielded/anechoic chamber, suitable for HIRF/EMC testing on fighters without engines running.

Up to now tests performed at Alenia's facilities are intended to be performed in open space, on ground, with and without engines running and in a completely automatic mode in order to reduce test execution times.

The HIRF/EMC facility will have the dimensions of 30m(W) × 30m(L) × 20m(H) and it will be built in order to performe high intensity radiated field testing on medium size aerospace aircraft, in the frequency range 30 MHz - 18 GHz, according to the test procedures described in the documents MIL-STD-464 ("Electromagnetic Environmental Effects Requirements for Systems, 18 March 1997") and AC/AMJ 20.1317 ("Proposed Advisory Circular/Advisory Material Joint, November 1998"). An anechoic-shielded chamber represents the ideal solution to perform these tests, because it provides the electromagnetic shielding and protection against the internal (towards the external) and external (towards the internal) electromagnetic environments; the chamber also incorporates absorbing material on the inner walls and surfaces to suppress the effects of reflections within the structure. In addition an antenna measurement range will be developed and implemented, which will be used in order to test the antennas installed on the aircraft.

The anechoic shielded chamber (ASC) has been designed for two different typologies of testing: the major is HIRF/EMC testing in the frequency range 30 MHz - 18 GHz; the second one is the measurement of pattern of the antennas mounted on aircraft in the frequency range 500 MHz – 18 GHz. Therefore this project is a big challenge for the anechoic material industries and conceptions because the inner walls and surfaces of the ASC shall be covered by pyramid absorbers with low level reflectivity both in lower and higher frequencies.

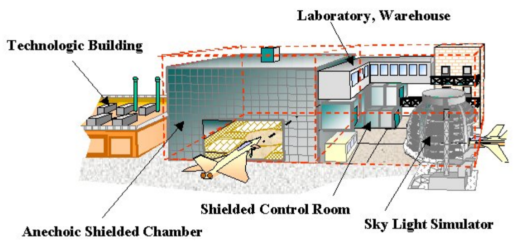

HPEM 11-15: Simple Measurement Techniques for the Shielding Effectiveness of Symmetric Enclosures

U. Paoletti[1], H. Garbe[2], W. John[3]

[1]*FhG IZM/University of Paderborn* - Berlin/Paderborn - Germany*; [2]*Institut für Grundlagen der Elektrotechnik und Messtechnik - Universität Hannover - Germany*; [3]*Fraunhofer Institute Reliability and Microintegration - Department ASE - Berlin - Germany*

The shielding effectiveness (SE) of enclosures is an important parameter for estimating radiation and susceptibility of electronic equipment at system level. It is well known that apertures negatively affect the shielding efficiency of conducting enclosures. It is also well known that for high frequencies the shielding efficiency is strongly dependent on the position where it is calculated and therefore it becomes less manageable. However it remains a subject of interest of many publications because it is a scalar quantity and it is easier to measure than field quantities. It is also often used for validating numerical techniques.

It is usually measured in a (semi)-anechoic room with an antenna at 3 meter distance, which corresponds to the position prescribed in international norms for the radiation from electronic equipment. At this distance it is possible for some antenna configurations to neglect their influence on the measurement. However for validating numerical techniques it can be useful to measure the shielding effectiveness with an antenna closer to the enclosure, where the influence of antenna and feeding cables can be significant.

For this reason a simple measurement technique based on the image theory has been proposed for measuring the shielding efficiency for the electric field of symmetric enclosures (U. Paoletti and H. Garbe and W. John, Measurement Technique for the Shielding Effectiveness of Symmetric Enclosures with the Use of the Image Theory, accepted for publication at the IEEE EMC Conference in Sendai, June 2004). It makes use of a well conducting surface in a (semi)-anechoic chamber. A half enclosure is laid on the surfaces and connected to it by means of copper foil. Monopoles are introduced through the plane and the shielding effectiveness can be calculated by comparison of measurement results with and without the enclosure. The results have been validated with literature and simulation results.

The same principle has been applied for measuring the shielding effectiveness in a GTEM cell, where far field radiation conditions are rebuild. A half enclosure has been laid on the bottom of the cell and connected to it with copper foil. A monopole has been introduced inside the enclosure underneath the GTEM cell. From measurements with and without the enclosure the shielding effectiveness can be derived.

Some results of these two techniques for the enclosure of figure 1 are shown in figure 2. For the measurement with the ground plane the external dipole was placed at 1.1m from the front face. The internal dipole was in the center of the enclosure for both measurements. As it can be seen there is a good agreement between the curves. The GTEM cell presents better results below 500 MHz, because the use of a second short monopole is avoided, whose dynamic is not sufficient in this frequency range.

Acknowledgement:
The reported R+D work in this paper was carried out in the frame of the Eureka project MEDEAplus MESDIE A 509 - Microelectronic EMC Design for High Density Interconnect and High Frequency Environment. This particular research was supported by the BMBF (Bundesministerium fuer Bildung und Forschung) of the Federal Republic of Germany under grant 01M 3061 J. The responsibility for this publication is held by the authors only.

* Competence Network Future EMC/RF Modeling and Simulation Methodologies (FhG IZM/University of Paderborn/University of Hanover)

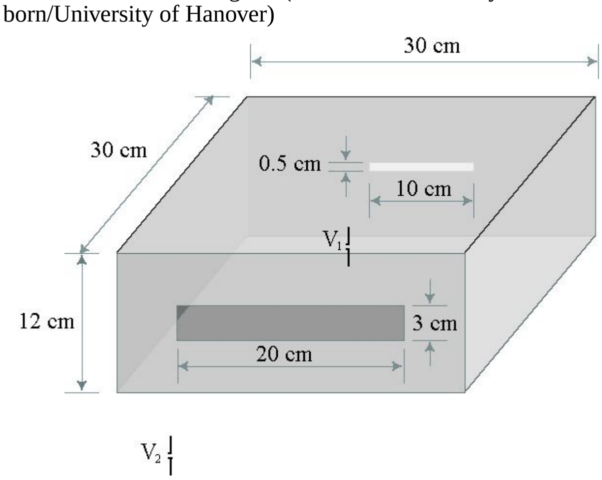

Figure 1: Geometry of the enclosure

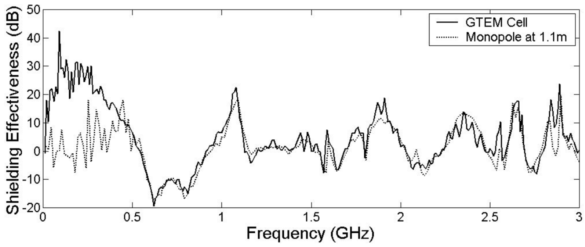

Figure 2: Measurement results in the GTEM cell and with the ground-plane

HPEM 11-16: Experimental Test of Signal Classes Identification

E. A. Ibatoulline, **A. M. Amro**
Kazan State University

Nowdays the problem of optimal identification of signal classes is essential. This problem consists of the determination of the parameter values of private probability densities specifying classes and of the association of signals to their classes.
Firstly, let us determine the concept of signal classes. By the class of signals we will understand the set of signals from one source with varying essential parameters, which varying from one signal to another randomly. By essential parameters we can define estimating (measuring) parameters. The possible origins of random changes in the signal parameter value are the equipment instabilities and measurement errors. A signal arrival time and its carrier frequency are examples of such random essential parameters. A procedure of the identification of signals precedes the identification of signal classes.
For the statistical description of signal classes, the concept of a mix of distributions is used, which is a sum of private probability densities with their weights in the mix (Patrick E.A. , The theory of images recognition).
When the kinds of probability densities of initial distributions and their number in the mix are known, it is possible to use the method of maximum likelihood. (Ibatoulline E.A. Decision making in connected information systems , 1986.)
Thus for the logarithm of likelihood function of a pack from n independent signals we shall have a sum of logarithm of mix of distributions.
Let's obtain a system of maximum likelihood equations for practically important case, when private densities of distributions of the moments of signal arrival submit to Gaussian's law. That obtained by doing differential on the logarithm of likelihood function to unknown parameters of distributions and equating result to zero.
We will consider that the weights of classes in the mix, and the variances are known, and the quantity of classes is three. It is required to define estimations for means which are proportional distances up to sources of emission.
Thus, we have system of nonlinear equations, to solve such system, only numerical methods can be used. One of such methods is the iterative method of Newton, by using which estimations for unknown parameters can be found.
To begin the iteration process we need to set initial values and then at every time step we compare the obtained values with the values at the previous iteration step. This process will be continued until the difference between values at neighbor steps will be less than the required accuracy of calculations. At this case we consider that the obtained estimations approached real means.
To check the algorithm of identification of signal classes, computing experiment has been done. Where samples of signal classes, with a various arrangement of mean relative to each other, were generated. At first, calculations were conducted, when classes were on enough big distance from each other then gradually they ware bringing close to each other until crossing. One of these cases is shown on Fig. 1.
Results are obtained at the following initial data: accuracy of calculations is (0,1-001), weights of distributions are P1 =0,3, P2 =0,3 P3 =0,4, variance is 0.09 identical to all classes, the size of samples is n=15-3000, initial value in the limits of (1-6) from the true value.
Experiment shows that, the correctness of the identification and the number of the iteration on which received estimations are approached to the played values of average, which depends on several factors namely, the size of sample, a degree of class crossing , initial values and as far as they are close to true values. Major of these factors is the last one; its influence becomes more significant in case of class crossing.
In a case when classes are not crossed the identification occurs even at initial values, taking place far enough from mean (at and more), and in case of crossing of classes, identification occurs only at initial values close to mean (one).

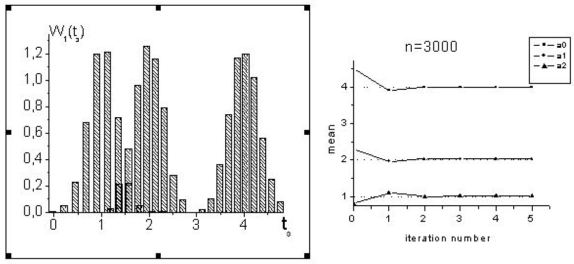

HPEM 12 - Simulators and Simulation Techniques

HPEM 12-1: Methods and Setups for Testing the Effects of High Power Electromagnetic Pulse Radiation

V. M. Kouprienko
Science Research Center of 26 CSRI

We discuss methods and equipment for testing the effects of the following electromagnetic radiation sources:
- RF electromagnetic fields;
- radar stations producing high power radiation;
- electromagnetic fields of 50 Hz frequency and short circuiting currents;
- lightning electromagnetic fields and currents;
- electromagnetic fields due to nuclear explosions.

A survey is made of the techniques and setups for testing the stability to electromagnetic effects and the possible compatibility of large size equipment and systems for various applications.

HPEM 12-2: Up Grade of an 350 kV NEMP HPD Pulser to 1.2 MV

M. Jung[1], **T. Weise**[1], **D. Nitsch**[2], **U. Braunsberger**[3]
[1]*Rheinmetall W&M GmbH, Heinrich Ehrhardt-Straße 2, 29345 Unterlüß, Germany, Phone: +49 5827 80 46 92, Fax: +49 5827 80 42 06, markus.jung@rheinmetall-wm.com*; [2]*German Armed Forces Institute for Protective Technologies, Humboldstrasse, 29633 Munster, Germany, Phone +49 5192 136 338, DanielNitsch@bwb.org*; [3]*Technische Universität Braunschweig, Institut für Hochspannungstechnik und Elektrische Energieanlagen, 38106 Braunschweig*

The paper will describe the upgrade of the 350 kV NEMP HPD pulse generator of the WIS in Munster, Germany to an output voltage of 1.2 MV by using a commercial available Marx generator.
The results of a PSpice investigation of the influence of the peaker capacitance and the line inductance on the pulse rise time, amplitude and width will be presented. The design, production and testing of the HV elements as feedthrough, pulse line and peaking capacitor under the restrictions of a short isolation distance and a high voltage will be discussed.
The paper will conclude with a presentation of the measured electrical field parameters as there are rise time, field strength, reproducibility etc. reached after the integration of the modified pulse-generator into the existing dipole hybrid antenna construc-

tion in Munster.

HPEM 12-3: CEG HPM Test Facilities

B. Chevalier, **J. Sallas**, **O. Ringuet**, **J. Tarayre**
Délégation Générale pour l'Armement - Direction des Centres d'Expertise et d'Essais - Centre d'Etudes de Gramat - 46500 GRAMAT FRANCE

In order to evaluate the vulnerability of targets against High Power Microwaves (HPM), different investigations are required : operational and functional analyses, low level coupling measurements, susceptibility and/or high level testing. To achieve such studies, the centre d'études de Gramat (CEG) has developed different facilities as well for coupling measurements (SOCRATE^2 and ETARCOS) as for high power illuminations (HYPERION). In 1992, a spherical near field range, named SOCRATE, has been developed for low level coupling measurements. The approach is based on the determination of the radiated pattern of the object under test, considered as a transmitting antenna, using near field measurements on a sphere. This device, designed for small objects ($d < 2m$), was operating between 100MHz and 6GHz. Last year, this facility has been upgraded to cover the frequency range 400MHz to 18GHz (SOCRATE^2). The total frequency range is divided in two sub-bands - 400MHz to 6GHz and 6GHz to 18GHz – using different measurements techniques. In the lower band, the field measurements are performed by means of a semicircular 63 dual polarised probes array, based on the modulated scattering technique. The higher band uses a more conventional technique : a wide band dual polarised horn moved mechanically on the meridian.
However, SOCRATE^2 can only deal with small systems. So a big facility, HYPERION, has been built. This facility includes a coupling measurement device (ETARCOS) for big targets and high power microwave sources for vulnerability testing.
As SOCRATE^2 uses an indirect method (the object is considered as a transmitting antenna), ETARCOS works in the direct way between 700MHz and 18GHz. Actually, the device under test is illuminated through dual polarised horns, fixed on a vertical mobile mast. For practical reasons, the measurements are done on a cylinder and not along a sphere. If between 700MHz and 4GHz, we do a near field to far field computation, for higher frequencies, we consider that we directly measure the far field.
SOCRATE^2 and ETARCOS give the transmitted EM power or field in the item under test ; at this step, the experiments are conducted on an unpowered system. In order to conclude in term of possible failures, some susceptibility / vulnerability tests on the operating system are required. So, relativistic magnetrons, covering the range 1.3GHz to 3.2GHz (3 sources), have been acquired. First of all, these tubes have been associated to a single shot 1MV marx generator. In this configuration, some 100's of MW can be generated with pulses of about 50 - 100ns length. Coupled with the compact range of HYPERION, up to 1kW/cm^2 can be generated on the target. In 2003, a repetitive 350kV Tesla generator has been developed to drive the magnetrons. The repetition rate is now continuously movable from single shot to 200Hz.

HPEM 12-4: Construction and Characterization of a Table-Top Mode-Stirred Chamber

S. Plate, **H. G. Krauthäuser**, **J. Nitsch**
Otto-von-Guericke-Universität Magdeburg, IGET, Magdeburg, Germany

We present the construction and characterization of a small mode-stirred chamber (MSC). Having a size of 0.9 m $\times$ 1.2 m $\times$ 1.5 m, the chamber is designed for frequencies above 1 GHz. A lot of devices under test, that have to be investigated in that frequency region, are small enough to fit into this volume. In MSCs, the field strength as a function of frequency increases up to a maximum and then decreases proportional to $\sqrt{f}$. For a laboratory room sized MSC, the maximum field strength is achieved at several 100MHz. Therefore, it is hard to achieve very high field strengths (>1000 V/m) in the GHz range. To fill this gap is one motivation for this work. On the other hand, it is easier to investigate, for instance, the influence of different stirrer-sizes and -geometries for a small setup.
We present results from the characterization of the chamber, e.g. normalized E-field and quality factor. Additionally, we compare different stirrer geometries by means of the autocorrelation of the fields.

HPEM 12-5: A Coaxial to Waveguide Adaptor Using a Tapered Post and a Disc-Ended Probe

B. Biglarbegian, **R. Fallahi**, **G. Dadashzadeh**, **M. Hakkak**
Iran Telecommunication Research Center, Tehran

One of the most important elements in a feed of reflector antennas and feeding different microwave waveguide systems, is coaxial to waveguide adaptors. Coaxial to waveguide adaptors is an indispensable component in microwave systems, providing a transition from coaxial to rectangular waveguides.
The important problem here is determining input impedance of this structure. Some methods such as MM (Moment Method), FDTD (Finite Difference Time Domain) and DGF (Dyadic Green's Functions) has been utilized for this purpose. In order to increase the operational bandwidth, the commercial adaptors resort to one of the following modifications:
1) A dielectric coated probe, 2) a conducting disc attached to the end of the probe. 3) A tuning post adjacent to the probe.
In this paper by mixing method 2 & 3 and modification in tuning post we have successed to increase the operational bandwidth of these adaptors. In this design, we have used a tapered post and a disc-ended probe(fig1) and by using finite element method and a conventional software for simulating with this method, HP HFSS, have optimized this adaptor for the frequency band 7 14 GHz with RL<10dB.
A schematic of this adaptor (fig2) and absolute of S11 of this adaptor is shown in figure attached (fig1).

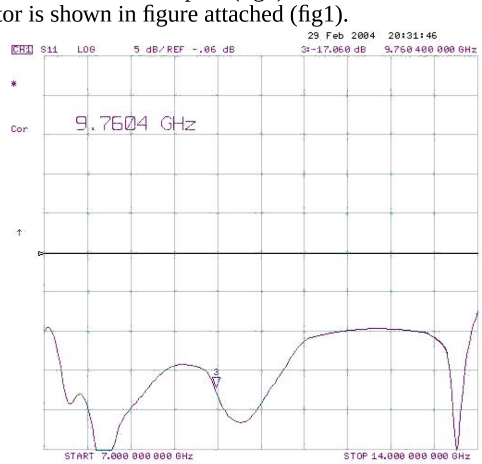

Figure 1: Absolute of S11 of the adaptor

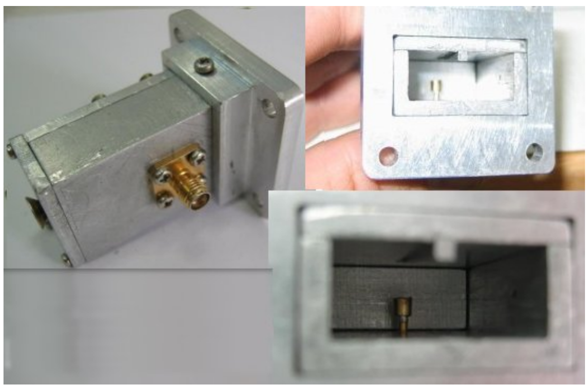

Figure 2: Schematic of this adaptor

HPEM 12-6: Instrumental Tool for System Design and Simulation

V. A. Losich[1], **V. B. Trigubovich**[2]
[1]*BSUIR, Comp. mach. dept.*; [2]*BelMAPO, Informatics dept.*

Continuous magnification of number of electronic devices to be used in economy, that is one of the distinguished features of modern society, causes the increasing of unintended radio interference (RI) level. So that one of the most important problems in modern electronics is how to provide electromagnetic compatibility (EMC) for different radio-electronic devices.
It is quite possible to suppose, that failure in electronic equipment can lead to increasing both inter-system and intra-system interferences. It also can cause creation of new channels of interfering interaction. It is obviously, that the above level of tools for both technical design and diagnostic of electronic devices, the faster both failures in electronic equipment as well as the reasons for RI creation are eliminated.
In the full-length paper the soft-ware part of "expert system for testing of electronic circuits" (V. Losich, V. Trigubovich, Technique for program.-apparatus testing of electronic circuits, EMD-2001 Proc.) has been described.
Main attention has been paid to investigation of such problems as construction of reference models of RI sources and typical ICs. Questions of ideology of soft-ware creation for such purposes are also examined.
The use of technology to be described enables us essentially to reduce time and cost for radio equipment design and testing.
As a prototype of technology to be discussed, the "family" of program-apparatus tools for diagnostic and testing of electronic devices "VECTOR" is used.

HPEM 13 - High Intensity Radiated Fields

HPEM 13-1: HIRF Testing of Military A/C in a Large MSC

S. Schultz[1], **M. Rothenhäusler**[2], **H. Werner**[2]
[1]*Philotech (in charge of EADS)*; [2]*EADS Germany*

Modern aircrafts like Eurofighter/Typhoon demand very high clearance levels which can hardly be achieved by the traditional methods like anechoic chamber or free field illumination. The costs for the required power amplifiers are almost unaffordable in these days. EADS Germany has got a free field HIRF test facility in Manching which is equipped with an 100 kW power amplifier and is able to generate these fieldstrengths in the frequency range from 5 to 30 MHz with far field conditions. But in the following frequency range from 30 to 1000 MHz the available power amplifiers (2 to 5 kW) have problems to produce the required fieldstrengths in far field conditions. The costs for more powerful amplifiers (20 to 40 kW), to illuminate an object like Eurofighter/Typhoon with far field conditions, would be uneconomic high. For this reason EADS Germany takes a large Reverberation (or Mode Stirred) Chamber into account. In principle this method would be able to solve this problem and has got the following advantages:
· the electromagnetic field remains enclosed in the test chamber and cannot pollute the outside public environment like the free field method does
· the electromagnetic field is (statistically) isotropic and needs no repositioning of the test object with respect to the illuminating antennas
· higher field strength levels are expected at the same RF power compared to free field illumination
· the testing time and the resulting costs can be reduced
Despite these promising advantages, up to now no facility is in use with a comparable size. The French military has built a chamber (EMILIE) with the same intention and almost the same size but this project is not free accessible. However, EADS Germany is strongly interested to introduce this method in the EMC clearance process of military aircraft, but the final decision needs certainty, about the following questions:
· can the required HIRF clearance levels be achieved?
· are the susceptibility thresholds, detected in an MSC, comparable with those detected with the traditional methods (may be a need to add a safety level of ?dB)?
· will the method will be accepted by the Customer?
· can the testing time be reduced by fulfilling the requirements of an A/C clearance?
For this reason, EADS Germany has started investigations in cooperation with different existing MSC-facilities (AIRBUS France, EADS CCR) and has a strong cooperation with the WTD 81 which builds a scaled 1 to 4 model of the planned EADS MSC. Main objectives of these investigations are:
· estimation of the chamber loading due to the carbon fiber structure of modern aircraft
· estimation on the effectiveness of highly conducting wall material under loading effects
· estimation of the necessary RF-amplifier power to achieve required field levels
· investigations on the design of the mechanical mode-tuner
· trade-off between smallest possible size of chamber (minimizes cost and RF-amplifier power) and large size chamber (30 MHz as lower test frequency desired, less influence on chamber calibration due to the test object).
Selected results of these investigations are presented.

HPEM 13-2: From Cubic Faraday Cage to HIRF Testing Reverberation Chamber

M. Piette
Royal Military Academy/Department Telecommunications/Laboratory of Electro Magnetic Applications (LEMA)

Converting a small cubic Faraday cage into a valid reverberation chamber for HIRF testing is a difficult issue. The cube is indeed far from being the best shape for reverberation purpose, because of its high degree of symmetry and the cavity mode degeneration (Piette, "Champs électromagnétiques aléatoires en chambre de réverbération : théorie et applications", LEMA 2004/2 RS Report, Royal Military Academy). The small dimensions of the RMA cage (2,5 x 2,5 x 2,5 m3) makes also unpractical the installation of more than one electrically large stirrer. Because the performances of a reverberation chamber depend mainly on the good differentiation between the resonance modes excited in the cavity on one side and on the stirring efficiency on the other side (Wu & Chang, "The Effect of an Electrically Large Stirrer in a Mode-Stirred Chamber", IEEE Trans.EMC, vol.31 N° 2, May 1989), the first logical step would be to expand the cage for tending to a 5-4-3 parallelepipede. This shape is indeed claimed to be the best compromise among practical shapes (Leferink & van Etten,"Optimal Utilization of a Reverberation Chamber", EMC Symp. 2000, Bruges, vol.1) for obtaining a good statistical field uniformity and the high Q factor needed for HIRF testing (High Intensity Radiated Fields) (EUROCAE/ED-14D, Section 20 "Environmental Conditions and Test Procedures for Airborne Equipment", 1997). Before doing this shape transformation, it is worthwhile to study to what extent the cubic shape constitutes actually a handicap and to investigate the efficiency of other means usable for improving the reverberation performance of the cubic chamber.
The key characteristics of the cavity available at RMA like mode number, mode density and Q factor are firstly determined. Then, with the stirrer in place, some relevant parameters of the cubic reverberation chamber are measured (stirring ratio, insertion loss, change of resonance frequencies, spatial field uniformity, composite quality factor, time constant and lowest usable frequency). The system used for field measurements consists of a small broadband triaxial E-field probe, an optical fiber cable, an electro-optical convertor and a spectrum analyser. Finally, the benefit from using irregular diffusors fixed at the chamber walls and metal plates breaking the right corners of the cubic chamber are assessed. The comparison of the results with those obtained after expansion of the cubic chamber to a rectangular one will get a better insight into the importance of the shape factor with regard to the reverberation performances of a chamber.

HPEM 13-3: Numerical Simulation of Real Antenna Scenario in HIRF Environment

M. Meier, **M. Rothenhäusler**
EADS Germany

The intention of this work was to replace electromagnetic human safety measurements of the HIRF test-site of EADS Manching by a numerical analysis. Until now the yearly evaluation of the human safety regulations take a big effort, because the whole area (about 500 m x 500 m) has to be measured by men with field probes. To reduce this work, a numerical model was created and evaluated. Main aspects of course was the modelling of the antennas, the ground and the buildings. The first question was which code should be used. The Method of Moments would provide big advantages for the antennas, but has also got disadvantages like:
- the scaling for the calculation time is N^2 or with modern methods $N \cdot \log(N)$, where N is the number of unknowns
- frequency domain method takes a lot of time for wide frequency ranges.
Our decision was the Time Domain method of the Finite Differences (FDTD) because of the following advantages:
- time domain method is faster for large frequency ranges
- the scaling for the calculation time is N, where N is the number of unknowns
- well known method with a high confidence level.
The first step was the modelling of the antennas. For the evaluation of the simulation, the scattering parameters of the antennas were used. Fig. 1 shows the antenna of the HIRF test-site of EADS Manching with a length of 40 m, width 40 m and a height of 25 m. The operating range is between the frequency 5 and 30 MHz. Fig. 2 represents the HIRF antenna in the frequency range from 30-100 MHz with a length of 6 m and a width of 5 m. This lecture shows the results of these simulations, the problem one had to deal with and an estimation of the replacement of the real measurements by the numerical simulation.

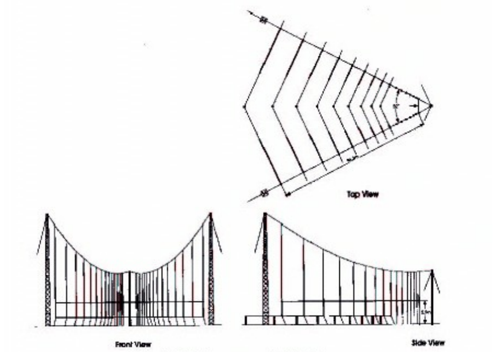

Fig. 1 HIRF antenna 5-30 MHz

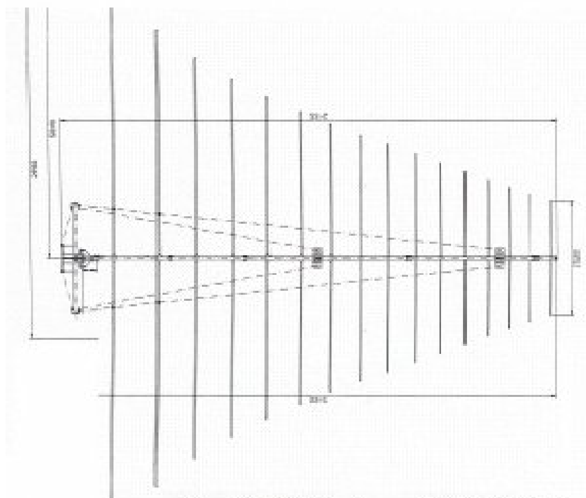

Fig. 2 HIRF antenna 30-100 MHz

HPEM 13-4: Laboratory Methods to Radiate High Power, Circularly Polarized Waveforms

T. McVeety, **C. Courtney**, **D. Voss**
Voss Scientific, Albuquerque, NM, USA

The effects produced by High Power Microwave (HPM) fields on target electronics are functions of many variables including frequency, incident power density, and angle of incidence. Effects can also be a function of the polarization of the incident HPM field. This paper describes two versatile methods to generate linearly and circularly polarized HPM fields in the laboratory for purposes of HPM susceptibility testing. The first method that will be described involves the use of a COBRA lens. The theory for the COBRA lens (C. Courtney, Design and Numerical Simulation of Coaxial Beam-Rotating Antenna Lens, Electronics Letters, vol. 38, no. 11, pp. 496 – 498, 2002) describes a method whereby an azimuthally symmetric aperture field (such as the TM_{01} circular waveguide mode typical of many types of laboratory HPM sources) can be made to radiate a boresight peak with linear or circular polarization. The second technique that will be described involves the use of two matched rectangular horn antennas, matched in the sense that the E-plane pattern of one is equivalent to the H-plane pattern of the other. By equivalently splitting the output signal from the HPM source into two paths with proper phase adjustment in one path, the two-antenna configuration will produce a circularly polarized radiated field on boresight. This second method is most compatible with HPM sources that produce their output in the fundamental mode of rectangular waveguide. The presentation will include a brief overview of the theory of the COBRA lens antenna, complete and detailed descriptions of both techniques, a discussion of high power considerations, and presentations of simulation results and measurements of the radiated fields of each antenna system concept.

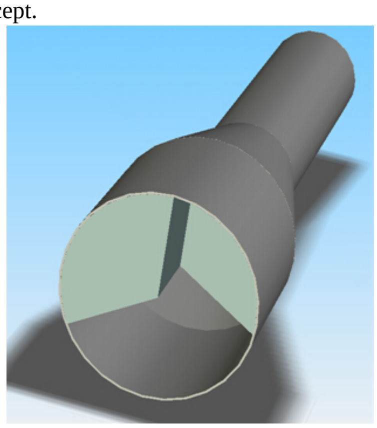

Figure 1: COBRA Lens antenna produces circular polarization on boresight.

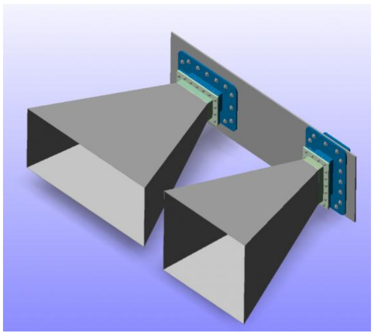

Figure 2: Two rectangular horn antennas radiating in unison produce circular polarization on boresight.

HPEM 13-5: Low Level Swept Techniques and Convolution with Time Domain Environments

A. Wraight[1], **R. Hoad**[1], **I. Morrow**[2]
[1]*QinetiQ, Spectrum Solutions, Cody Technology Park, Farnborough, United Kingdom* ; [2]*Laboratory of Electromagnetic Research, Cranfield University, United Kingdom*

Low Level Swept (LLS) techniques (N J Carter, Revision of EMC Specifications for Military Aircraft Equipment, 1985),(NATO Air Electrical Working Group (AEWG), Verification Methodology for the Electromagnetic Hardness of Aircraft Study 7116AE, 1999),(Eurocae, ED107 - Guide for the Certification of Aircraft in a High Intensity Radiated Field (HIRF) Environment, 2001),(ARP5583 - Guide for the Certification of Aircraft in a High Intensity Radiated Field (HIRF) Environment, 2003) are currently used for the clearance of both civil and military aircraft to electromagnetic environments known as High Intensity Radiated Fields (HIRF).

Specifically, Low Level Swept Current (LLSC) is used over a frequency range of 500kHz to 400MHz and measures the transfer functions of cable looms of interest, this information is used to predict the level of Bulk Current Injection (BCI) required for susceptibility testing. Low Level Swept Field (LLSF) is used between 200MHz and 18GHz and provides the attenuation characteristics of aircraft bays of interest with a view to setting the levels to be used for localised HIRF testing. There has been considerable interest in this area over recent years and the techniques are under constant review (N J Carter, The past present and future of aircraft EMC, 2003),(G Fuller, Are we doing HIRF testing sensibly?, 1991),(G Fuller and A J Poggio, A Fresh Look: A More Economic Approach to HIRF Certification, 1995),(G Fuller and W E Larsen, Avionics HIRF Certification for the 21st Century, 1996).

This paper reviews the LLS techniques and focusses on the use of LLSC data when predicting induced currents as a result of an incident time domain waveform. The process used will be discussed and examples given with particular focus on the response to Nuclear Electromagnetic Pulse (NEMP) waveforms. The validation of this technique will also be presented.

This work was supported by MoD CRP SEW funding.

HPEM 13-6: Functional Susceptibility Evaluation of Warfare System to HIRF by Global Illumination (10kHz-18GHz)

A. Saïdani, **M. Cantaloube**
DGA/DCE/CEAT, Balma, France

1. *HIRF environmental analysis*

Increasing power levels of civil and military radio-radar emitters useful spectrum make HIRF environment become more and more severe. Standards and normalisation dedicated to these external threat are recent and defined by very simple average and peak electric field values. It is noticed that average and peak value are not correlated and often correspond to different emitters. For both, the values are RMS values (root mean square value). Actually, the HIRF threat levels presented in existing standards (STANAG 4234, MIL STD 464, FAA/JAA AC/AMJ20) are expressed on the whole frequency band 10kHz-18GHz, with average E field levels or average power density levels and peak E field levels or peak power density levels. H field environment is not indicated but sometimes plane wave notions or high Impedance wave are mentioned for very low frequencies. With the actual definition of HIRF envelop environment, some hypothesis have been made by US and European normalisation committees as maximum gain and maximum power considerations, wave reflection, near field correction factor... Nevertheless, this definition suffers from uncertainties and silences that make the use of standards difficult. The purpose of this document is to present an actual approach of the evaluation (or qualification) methodology for aircraft and other military systems against this envelop threat with a description of available test facilities. This philosophy is actually more exhaustive than representative.

2. *Demonstration methodologies*

The demonstration methodologies often include numerical calculations, equipment and systems tests and theoretical analysis. Because of the widespread frequency spectrum, there is as many approach as sub frequency band. But in each of them, the both following methodologies are necessary and complementary: low level tests with E field and current transfer functions and threat level system tests with real time functional check of the system. In fact the threat level system test is essential for militaries and more applicable than functional NEMP or lightning system test because of pulse aspect of these time-dependant threats.

2.1 *Current injection (10 kHz – 1st structural resonant frequency or 30 MHz)*

Because of the difficulty to radiated homogeneous and high E field level of 200 V/m at low frequency on large surface, the following test method is proposed: Injection of conducted current with a level linked to the surface current density J_S, up to and above the first resonant frequency of the system (about 10 MHz for fighter aircraft). It is demonstrated that for the worst case incident polarisation (E field parallel to aircraft axis), the surface current density is driven by the only magnetic transverse H_y component (essentially for systems with 2D symmetry). The Figure 1 presents this methodology of the injected current into coaxial return controlled by the skin magnetic field H_y referred to the transfer function H_y/E_{inc}. This transfer function is evaluated by 3D numerical simulations or experimental magnetic skin measurements with 1 V/m incident E field.

2.2 *Global illumination with power amplifiers and antennas in anechoic chamber (between 1st resonant frequency to 100 MHz)*

Large sized Log-periodic antennas (5-6 meters) with 10 kW amplifiers are sufficient and can be used to reach the desired 200 V/m on overall system with large surface (Figure 2).

2.3 *Global illumination inside Reverberation Chamber (100 MHz – 18GHz)*

2.3.1 *Near-field or far-field?*

With very high levels, standards usually describe situations of the system's life where the system is inside near field region of the emitter's aerials. The community use the Alexander Gross approach that suggests to take into account correction factor in the classical formula $P_d = P_t \cdot G \cdot c/(4\pi r^2)$. But the calculated power density value has different characteristic than E field used in actual free space tests. That introduces the problem of incident threat representativeness and the indeed test results. As an alternative of free space global system illumination, the use of a mode tuned reverberation chamber is interesting. It is demonstrated that avionic bays environment is similar to reverberation chamber environment, and equipment test in such facility is justified and acceptable. But the methodology and the demonstration of compliance by the use of reverberation chamber for global system test is still a challenge. The interest for the use of aircraft sized reverberation chamber is increasing (Australia, France,...). In fact, this facility allows to verify the correct operation of complete powered systems continuously on the whole frequency band.

2.3.2 *EMILIE project objectives: 1) Radiated emissions measurements, 2) System radiated susceptibility*

Faraday chamber with strong performances (attenuation: 120 dB) with specific reverberation chamber equipment. 2500 m^3 test volume (24m x 15m x 7 m) able to test from small missile to fighter aircraft. Pulsed and CW radiated field sources with achievable 600 V/m average field and 6000 V/m peak field, because of spatial energy density addition concept from TWT amplifiers and klystron sources. Different test volumes by the use of removable walls inside the Reverberation Chamber. Questions to solve: the use of reverberation chamber for system test is an undeniable progress in regards to current demonstrations, essentially for security aspect and flight clearance before 1st flight. This type of facility is completed by a research program with the following axes:

- Correlation and transformations between standing wave environment inside reverberation chambers and the external normalised environment or the test environment or combination of test and real environment.
- Reverberation concept extension for the test of very large sys-

tem as transport aircraft (use of poor metallic integration or assembly or maintenance hall).

3. *Conclusion*

This document presents the current test methodology used by CEAT to make a functional evaluation of a warfare system to the radio-radar environment. The presented methodologies and facilities (coaxial return + anechoic chamber + reverberation chamber) could offer a solution to cover continuously the 10 kHz-18GHz frequency band. Some questions are not solved, but first solutions are reachable and will be exposed in the next few years. This evaluation philosophy is actually more exhaustive than representative.

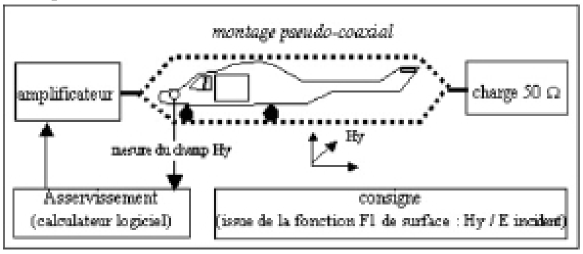

Figure 1

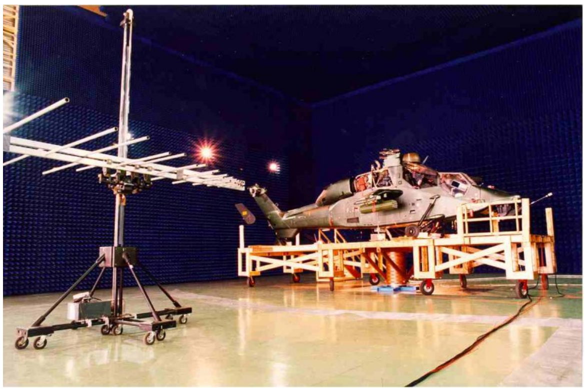

HPEM 14 - IEMI Protection Methods

HPEM 14-1: Protection Approach for Commercial Buildings against Intentional Electromagnetic Interference (IEMI)

W. A. Radasky
Metatech Corporation, Goleta, CA, USA

The problem of intentional electromagnetic interference (IEMI) is not new, and it is time to move beyond the investigations of sources, antennas and waveforms. In particular this threat can be produced today by hackers, criminals and terrorists, and it is important to begin to deal with the protection aspects for commercial equipment and the businesses that use this equipment.

It is important to recognize that IEMI has several similarities to the high-altitude electromagnetic pulse (HEMP) produced by nuclear explosions. These similarities include the production of intense EM field pulses that have important content at frequencies above 1 MHz. There are of course important differences. The HEMP is produced at altitudes above 30 km, and therefore the incident fields appear locally as plane waves. This means that the HEMP fields do not vary over the dimensions of a large building. On the other hand, the IEMI is produced from a mobile source, which produces fields that typically decrease a factor of 10 for range variations from 10 to 100 meters.

This paper describes the significant similarities and differences between HEMP and IEMI in order to understand which of the well-known HEMP protection methods may be applied to protecting commercial buildings. These will include the effectiveness of HEMP-qualified EM shields, gaskets, filters and surge arresters to the IEMI problem.

Given the range variation of IEMI environments, it is clear that distance should be used as part of a protection scheme for a building. This also suggests that monitors may be effective in revealing the presence of an IEMI attack. Of course the types of monitors and their frequency capability are important to their effectiveness. This paper summarizes the distances of interest for current IEMI threats and also suggests the types of monitors to be applied, both for radiated and conducted IEMI threats.

HPEM 14-2: Technical Means to Study an Immunity of Infrastructure Objects to Intentional Electromagnetic Interference

L. L. Siniy, **V. Efanov**, **V. Fortov**, **Y. V. Parfenov**, **L. Zdoukhov**
Research Institute of Pulse Technique, Institute for High Energy Densities, Moscow & FID Technology Corporation, St. Petersburg, Russia

Powerful electromagnetic interference is a threat to electronic systems, which ensure normal operation of infrastructure objects. In particular, UWB electromagnetic pulses and high voltage pulses are among these interference's. A safety of an infrastructure of states will be under a threat if terrorists will get sources of such interference in their own hands [M. Wik, R. Gardner, W. Radasky, "Electromagnetic terrorism and adverse effects of HPEM environments", 13th International Zurich Symposium on Electromagnetic compatibility, 1999; R. Gardner, "Importance of standards for intentional electromagnetic interference", International Symposium on EMC, Magdeburg, 1999; V. Fortov, V. Loborev, Yu. Parfenov, L. Siniy, "About potential possibility of commitment of large-scale terrorist acts by using electrotechnical devices", International Symposium on High Power Microwave", Euroem-2000, Edinburgh, Scotland, 2000].

An important preventive measure is a development of the means that will permit us to estimate an immunity of infrastructure objects to intentional electromagnetic interference and to test efficiency of protection. With this purpose we designed the small-sized UWB source with controlled frequency spectrum and also the experimental model of a building power network.

The UWB source with controlled frequency spectrum consists of the solid-state generator of high-voltage pulses and the TEM horn array antenna. The generator forms periodically repeated bursts of voltage pulses. A spectrum of an emitted field may be controlled in a frequency range from 0.5 GHz up to 5 GHz by variation of polarity and time delay of generator voltage pulses. The developed UWB source with controlled frequency spectrum permits to test objects against intentional irradiation of all existing conventional UWB emitters. The experiments executed on real objects have shown that intentional injection of high voltage pulses into power and earthing circuits represents serious danger. The development of the theoretical model was a first stage of our research. The Conducted Threats computer code has been developed on the basis of this model. This code allows analyzing susceptibility of infrastructure objects to electromagnetic terrorism acts, which are carried out by intention injection of powerful electromagnetic pulses into power and earthing circuits. However to develop reliable means of protection it is impossible to be limited only to calculations. Experimental researches that would confirm correctness of the conclusions made on the basis of calculations are necessary also. So the special experimental model of a building power and earthing network was developed that is intended to study effects of high-voltage disturbance injected into power and earthing circuits. This model is a part of an actual three-phase power network. This network is located on two floors of the building. A lot of experiments have been executed by using this model. These experiments were performed when 0.4 kV working voltage was absent, i.e. the three-phase feeding was switched off. A definition of a transfer factor of an injected pulse into adjacent phases was the first problem of experimental researches. Waveforms of voltages penetrating into various circuits approximately correspond to the injected voltage waveform. The peaks of voltage pulses penetrating into adjacent phases are about 60% of the peak of injected voltage pulse.

A justifying of the conclusion made on the basis of calculations with using Conducted Threats computer code was the second problem of experimental researches. This conclusion was the following. The installation of a single pole single-throw is in

one phase of power net does not protect against penetrating of high voltage pulses into this phase and into other phases.
The estimation of an opportunity of standard protection devices application to prevent of adverse consequences of an intentional injection into a power net was the third problem of experimental researches. Varistors were used in these experiments. These protection devices were installed in different points of power network experimental model. These experiments have shown, that basically standard protection devices are capable to provide protection against intentional injection of high voltage pulses. However efficiency of these means strongly depends on a point of an installation, a way of injection and parameters of injected pulses.
Problem of the subsequent experimental researches will be a choice of the most effective ways of protection, and also a performance of experiments at the included power voltage. Thus, two means to estimate an efficiency of protection of an infrastructure against acts of electromagnetic terrorism are offered:
- a compact UWB pulses source with a control spectrum;
- an experimental model of a building power and earthing network.

Using these means in a combination with calculations allows operatively and enough cheaply to define weak spots of critical infrastructures and to choose adequate ways of protection.

HPEM 14-3: Research Concerning the Influence of Ultrawideband (UWB) Electromagnetic Fields on Electronic Cash Machines

Y. V. Parfenov[1], **L. Zdoukhov**[1], **W. A. Radasky**[2]
[1]*Institute of High Energy Density, Moscow, Russia*; [2]*Metatech Corporation, Goleta, CA, USA*

Electronic cash machines (ECMs) incorporate computer devices to perform their functions. ECM failures caused by unexpected electromagnetic influences (intentional or unintentional) can paralyze the work of a large department store or a supermarket. Therefore research into the influence of ultra wide band (UWB) electromagnetic fields on ECMs has been performed. The objects of investigation were two different electronic cash machines.
An UWB emitter was used for performing this study. This emitter consists of a semi-conductor generator of subnanosecond voltage pulses and a UWB antenna. The antenna consists of a system of four TEM horns. The basic characteristics of the UWB emitter are indicated below.
Basic characteristics of the UWB emitter:

Parameters	Values
Amplitude at 20m distance:	2 kV/m
Pulse duration:	0.2 ns
Pulse repetition rate:	up to 1000 Hz
Antenna aperture:	0.35 x 0.35 m^2

The investigations performed have shown that UWB fields can distort the data memory (RAM) of electronic cash machines. The critical UWB field level is equal to $2\cdots 2.5$ kV/m. If such an exposure on electronic cash machines lasts for several seconds, then RAM failures occurs. The further functioning of the electronic cash machine becomes impossible. At UWB field levels above 5 kV/m, an irreversible lockup of the keyboard controller occurs.
The immunity of ECMs to UWB fields can be increased by EM shielding. If the ECM is placed in a simple common screen, a distortion of the memory takes place at a peak level of external fields of 5.2 kV/m. If only the processor block is shielded, the critical UWB field level is 3.5 kV/m. Thus, partial shielding results in some increase of immunity of an electronic cash machine, but to a lesser degree, than its full shielding. Apparently in the latter case, lack of operation of the ECM is caused by the influence of UWB fields directly on the keyboard and its connecting wires.

HPEM 14-4: Electromagnetic Interference Related Susceptibility of COTS Network Components

R. Hoad, **D. Herke**, **S. P. Watkins**
QinetiQ, Cody Technology Park, Farnborough, Hants, UK

Information Technology (IT) equipment and specifically Personal Computers (PCs) are an essential and integral part of business processes and our every day lives. Whilst existing EMC specifications, such as ISO/IEC EN55022, provide a test regime that prescribes emission and immunity limits, the actual level of susceptibility for equipment is not readily ascertained. A measure of equipment susceptibility is useful for those seeking to understand upset mechanisms and protect equipment from intentional and unintentional Electromagnetic Interference (EMI). Networks of computers are perhaps more at risk from upset or disruption from intentional or unintentional EMI, than stand alone systems due to coupling routes via interconnecting cables. If the IT equipment is used in a security or safety critical application then upset or disruption is extremely undesirable.
The radiated susceptibility level of a Commercial Of The Shelf (COTS) IT network and network components has been assessed using the mode stirred (reverberation) chamber technique at QinetiQ, Farnborough, UK. The reverberation chamber technique was used to provide a highly stressing, uniform, isotropic field, with every illumination angle and polarisation covered equally. An advantage to this technique is that the cable layout is far less critical to the measured overall susceptibility level. To this end a series of susceptibility tests were performed using an iterative approach. In this way networking components were gradually added to a standalone PC to form a fully functional network.
Results are provided which demonstrate the good repeatability of the method used and critical failure nodes of the network. A large range of failure modes was observed, from network failure, i.e. Denial of Service, (DoS) through to permanent component damage.
It was found that in many cases DoS preceded severe failure of the PC by a significant margin. This means that less radiated field stress was required to deny network service, than to severely disrupt a PC. In some instances the level of stress required for denial of service was an order of magnitude lower than that required to cause severe failure to the PC.
Once service was denied it was not possible to restart the network connection with the EM stress present. Once the EM stress was removed, it was possible to re-initiate network traffic, but only from the control PC.
The cause of the DoS failures was most likely due to coupling to the peripheral network components, Hub and Router, via the power supply cable, the network cable and the enclosure.

HPEM 14-5: The Impact of HIPDI as Related to 100BaseTx Ethernet

I. Jeffrey, **C. Gilmore**, **J. LoVetri**
University of Manitoba, Winnipeg, MB, Canada

In recent work we have formally defined the concept of Hardware Invariant Protocol Disruptive Interference (HIPDI) as any electromagnetic interference, capable of severely degrading or stopping communications using a particular protocol, independent of the hardware implementation or the network geometry involved (Hardware Invariant Protocol Disruptive Interference for 100BaseTx Ethernet Communications, submitted to IEEE Transactions on EMC, special issue on Intentional EMI, 2004). Specifically, HIPDI has been defined as being a covert threat to network communications designed such that the interference contains minimal power and does not effect hardware functionality.
The existence of HIPDI for a given protocol is made theoretically possible by considering interference signals indistinguishable from data. Herein, in an attempt to exploit this theoretical HIPDI, we review the concept of Protocol Aperture used in determining the parameters required for interference to contain the significant features of communication data. The concept of Protocol Aperture uses the given parameters of a protocol to formu-

late the desired interference and relates to the idea of Point-of-Entry in EMC testing. Time-domain, frequency-domain as well as time-frequency-domain information obtained by the Continuous Wavelet Transform, are capable of extracting Protocol Aperture information from a given protocol.
To exemplify the validity of the concepts of HIPDI and Protocol Aperture, results are presented for 100BaseTx Ethernet communications under interference designed by our Protocol Aperture method. Tests were performed under various network configurations using different hardware interpreters in which network throughput measurements were taken as a function of the radiated interference. Numerous interference signals, some that we postulated to be HIPDI and some that we did not, were considered. Using interference defined by the Protocol Aperture of 100BaseTx Ethernet we were able to achieve 100% throughput reduction for every network configuration considered using simple CW and AM interference. Moreover, reduction occurred without adversely affecting hardware functionality. The results suggest that using the concept of Protocol Aperture for defining HIPDI could be a serious threat to current communication networks.

HPEM 14-6: Electromagnetic Protection – Shielding Specification Techniques and Measurement Methods

W. D. Prather
Air Force Research Laboratory, Kirtland AFB, NM, USA

If properly implemented, electromagnetic shielding can protect vulnerable electronic systems from harmful interference. The first step in the proper implementation and maintenance of a shielding system is to define the shielding topology and to create a properly written set of specifications in units. If the shielding topology is properly conceived, and the specifications for the shielding components are written in physically realizable units, the shielding system can be analyzed and measured in an unambiguous manner. Then, verification, and maintenance will follow in a straightforward manner.
Using aircraft as an example, this paper discusses basic shielding topology, electromagnetic shielding penetrations that are specified in engineering units. Various methods of measuring shielding transfer functions are described, and some illustrative examples are presented.

HPEM 14-7: Response of Surge Protective Devices to Very Fast Transient Conducted Pulses

R. Thottappillil, R. Montano, D. Månsson
Division for Electricity and Lightning Research, Uppsala University, Sweden

The objective of this work was to investigate how standard low voltage surge protective devices used in electronic equipments and low voltage networks respond to fast transient pulses with rise times in the order of nanoseconds. The standard devices investigated here were originally designed for handling transients caused by lightning with rise-times in the order of microseconds. Two kinds of devices, a metal oxide varistor (MOV) and a sparkgap (gas discharge tube), have been subjected to fast transient pulses with waveshapes 5/100 ns, 10/300 ns, 25/1000 ns and 35/3000 ns, and peak voltages up to 2.5 kV. For comparison, standard lightning impulse from a combination generator, 1.2/50 – 8/20 μs, was also applied. The components responded very fast to applied pulses, but the initial voltage peaks when the devices operated were significantly larger than the voltage peaks with slower pulses. This initial voltage peak was higher for spark gap than for varistor. For example, when a 5/100 ns pulse with peak voltage of 2.5 kV was applied to a spark gap with a nominal dc firing voltage of 90 V and with axial leads, the minimum time it has taken to operate was about 7 ns, but the initial voltage peak was in excess of 1 kV. The influence of the packaging of the surge protective devices on its response to fast transients and the characteristics of the residual surge passed on to the next stage will be discussed at the conference.
The existing models of the low voltage MOV's and spark gaps, developed for lightning surges, do not always work very well with fast transient pulses. Modifications to the models to make it suitable for fast transients are suggested.
[This research is in part supported by FMV (Barbro Nordström) and FOI (Mats Bäckström). Contributions of Lars Noresten, Yaqing Liu, and Boris Zitnik in the initial stages of this work are acknowledged.]

HPEM 14-8: UG Filtering - An Effective Technology Against IEMI and HPM

E. Recht[1], T. Naxon[2], A. Cohen[2]
[1]*ELOP LTD. & SigNext LTD.*; [2]*SigNext LTD.*

Developing and verification of new technology for filtering of ultra high frequencies range (above 1 GHz), called “UG series”, will be presented in this paper. UG technology is implemented in protection systems against High Power Microwave (HPM) electro-magnetic field, and in filtered connectors that must be able to filter those frequencies. This technology is the best answer yet high cost effective for all types of signals, including power lines, video & audio lines, communication, balanced and un-balanced. These lines require significant attenuation at very high frequencies.
The UG filtering technology had been developed and evaluated in the EMC lab. The technology is mature and implement in some military projects. It is also well suited for other rush environment (like MIL-STD-464-Navy). The combination of standard filtering and UG technology provide wide frequency interference attenuation. Integrated these filters into the connector make it very attractive for upgrading IEMI programs.

HPEM 15 - Space Weather and Geomagnetic Storms

HPEM 15-1: Space Weather Risk

R. Pirjola, K. Kauristie, H. Lappalainen, A. Viljanen, A. Pulkkinen
Finnish Meteorological Institute

The term ”Space Weather” refers to electromagnetic and particle conditions in our space environment that may disturb the technological infrastructure of the society, such as satellites, telecommunication, navigation, aviation, electric power transmission, etc., and even endanger human health or life. Space weather is an interdisciplinary area, in which expertise both in scientific research and in technological applications is needed. The origin of space weather is in explosions on the Sun, from where the effect is carried by the solar wind to the Earth. The interaction between the solar wind and the geomagnetic field results in the formation of the Earth's magnetosphere which is coupled to the ionosphere. Space weather thus constitutes a complicated chain of phenomena from the Sun to the Earth's surface. Understanding the different physical processes involved in space weather, which is necessary to be able to develop forecasting tools and means to avoid or minimise the space weather risk, requires knowledge of space plasma physics, electromagnetics, etc.
Space weather is a new subject, and its importance continuously increases with the dependence of the society on reliable space-borne and ground-based technology, interruptions of which may lead to huge economical and other losses. Today, space weather is considered one of natural hazards. However, observed space weather phenomena date back to the mid-1800s when the first telegraph systems were disturbed: at times the systems were inoperational while at other times the equipment even worked without a battery. On the ground, space weather manifests itself as geomagnetic storms and ”geomagnetically induced currents” (GIC), e.g., in electric power transmission grids and oil and gas pipelines. GIC constitute a risk to the systems. The most famous GIC catastrophe occurred in Québec, Canada, in March 1989 when the whole province suffered from a long black-out due to GIC. Although GIC problems are most probable at high latitudes, Finland has not had GIC troubles but active research

on the phenomenon has been carried out for more than twenty-five years.
Research efforts of space weather aim at forecasting techniques of the risk and at the development of services for users who may be impacted. In Europe, space weather research and applications are coordinated by the European Space Agency (ESA), and the issue is also being introduced to the Sixth Framework Programme of the European Union (EU).

HPEM 15-2: Discovering Temporal Patterns from Events and other Multivariate Data

M. Nuñez, **R. Fidalgo**, **R. Morales**
University of Malaga

One of the most important aspects of space weather is related to avoiding the consequences of space weather events either by system design or by efficient warning and prediction systems (Koskinen, et al. Space Weather effects Catalogue, 2001). Some of the users of these predictions are telecommunications operators and the electric power industry.
In the case of power systems, for instance, it is important to predict changes (events) of solar wind. Changes in solar wind affect the geoelectric field (Weaver, J. Mathematical Methods for Geo-Electromagnetic Induction, 1994), which may produce different voltages between the grounding points of two transformers, and therefore may produce a current in the power transmission line connection between the transformers. This geomagnetically induced current (GIC) is a source of disturbances and permanent damages, and for this reason it is important to be able to forecast geomagnetic storms and GIC magnitudes at different sites of power systems. Exact GIC predictions are not available in practice yet, but research work on the topic is intensive (Viljanen A. et al. Modeling Geomagnetically Induced Currents During Different Ionospheric Situations, 1999).
Several methods may be applied to forecast geomagnetic activity, as for any other time series problem, using neural networks or auto-regressive moving average methods (Mugellesi-Dow et al. SOLMAG: An operational system for prediction of solar and geomagnetic indices, 1993), among other approaches. However, these prediction methods are suitable for problems with a single time scale of temporal dependences: the output at any time step can be determined from the input values for a small number of time steps in the recent past. Unfortunately, the temporal scales in complex problems, like space weather, vary over many orders of magnitude from years (solar cycles effects on ionospheric propagation) to hours (Koskinen, et al. Space Weather effects Catalogue, 2001).
The presented method, BPL (Núñez, M., et al. Automatic Discovery of Rules for Predicting Network Management, 2002), automatically analyzes different time scales in a single multivariate problem. That is, it discovers temporal windows of different orders of magnitude. The purpose is to discover temporal patterns for predicting events. This method discovers temporal patterns by taking into account observed events, static attributes of the observed systems and their environments. BPL uses a novel technique to detect chaotic behaviors. When chaos is present only short-term predictions are possible.
The main strategy of BPL is: 1) building training examples as events arrive and 2) constructing regression trees from the training examples. In the first process, the training examples include values of static, dynamic attributes and new attributes like repetition of events, which is the frequency of past events during a latency window, and oldness of past events, which is the distance from past events. In the second process, BPL takes these training examples and uses them to construct a regression tree for each target event to be predicted. Regression trees may be seen as a set of rules. Rules have confidence associated to them. Figure 2 shows real prediction rules.
We empirically validated BPL prediction accuracy with two non-linear systems: the Double Well Oscillator and the Lorenz system. In the first system, there is a mass that vibrates on a filament. An electromagnetic force (see Figure 1a) is exerted on the mass. The differential equation (see figure 1b) describes the system, where x(t) is the displacement of the mass. The objective of these experiments is to observe the behavior of the system during a period of time and, then, predict the occurrence of frequent values of x (short-term predictions) and non-frequent values of x of the object (mid-term predictions) in non-chaotic and chaotic configurations of the differential equation. We also performed similar experiments with the Lorenz system, which describes the interrelations of temperature variation and convective motion using a set of differential equations.
We compared results with an ARIMA model in both experiments. Results showed that BPL notably outperforms ARIMA models in the case of less frequent events and is similar in the case of frequent events. A limitation of ARIMA models is that they cannot predict categorical (non-numeric) events. While statistical ARIMA methods forecast trends and curves, BPL may predict better the first occurrence of important numeric and categorical events.
Another experiment with BPL is the prediction of events in a real application. Figure 2 shows two of the 52 rules created by BPL for predicting events in a computer network:
Figure 2.
The first prediction rule says: "If the WntEventLog component generated an errorCode6005 alarm [50 to 65] seconds ago, AND the Netlogon component generated an errorCode5721 alarm in the last 720 seconds, then the W3svc component will probably generate an errorCode14 alarm in [90; 129] seconds; The confidence of the prediction 82%.". The second rule has a special antecedent and consequent: "If the WntEventLog component does not generate the errorCode6005 alarm during the last 1200 seconds, then the component W3svc will probably not generate the errorCode14 alarm during the next 600 seconds".
Note that these rules describe temporal patterns with time scales of different orders of magnitude: 50 ... 65 seconds, 90 ... 129 seconds, 600 seconds, 720 seconds and 1200 seconds. These time scales are calculated automatically. On the other hand, BPL rules are understandable by the user. This is important for users that want to learn something new about the application domain.
RF components generate alarms when they detect abnormal behavior. These alarms are received and managed in Telecommunication Network Management Centers. We propose to use BPL in these centers to predict RF alarms directly from space weather and RF multivariate data and events. Thus, telecommunication users could apply preventive actions to avoid potential problems. The space weather multivariate data would be received from Space Weather Centers.

$$F(t) = F_o \cos(wt) \qquad \text{(a)}$$
$$x'' + x' - x + x^3 = F_o \cos(t) \qquad \text{(b)}$$

Figure 1: (a) Force exerted to the mass (b) Differential equation that describes the system

IF Oldness("WntEventLog= *ErrorCode6005*")= [50; 65] seconds, AND
Repetition ("NetLogon= *ErrorCoder5721*")= [1; 1] in 720 seconds
THEN "W3svc= *ErrorCode14*" in [90; 129] seconds]. Confidence 82%

IF Oldness("WntEventLog=*ErrorCode6005*")=Never in the last 1200 seconds
THEN "W3svc= *ErrorCode14*" will probably not happen in 600 secs. Confidence 68%

Figure 2: Two rules generated by BPL for predicting computer network events

HPEM 15-3: Further Studies in the Enhancement of Electric Fields Near Oceanic Boundaries

J. Gilbert
Metatech Corporation, 358 S. Fairview, Suite E, Goleta, CA 93117

This presentation is a continuation of "The Enhancement Near Oceanic Boundaries of Electric Fields from Geomagnetic Disturbances," which was presented at the EUROEM 2000 conference in Edinburgh. In that presentation, we showed that the horizontal electric field perpendicular to shorelines is enhanced on the shore side by the presence of the highly conducting seawater. This enhancement extended out to approximately a skin depth on the landward side (where the skin depth is calculated in the ground), and the total enhanced voltage could be calculated numerically by the solution of an integral equation. We noted then

that the integral of the enhanced electric field appeared to have a simple value when the ratio of the ocean conductivity to the land conductivity was very large.
Since that presentation, we have found an analytical solution to the limiting form of the integral equation in terms of error functions. This solution, which was obtained using the Wiener-Hopf technique, validates the numerical solutions, gives us an improved form for the limits and provides insight into the behavior. We have also calculated the decrease in the horizontal electric field parallel to the shoreline on the landward side. Combining the two solutions allows us to calculate the integral of the horizontal electric fields on an arbitrary path so we can determine the applied voltage along cables. Due to the behavior of the field parallel to the shoreline, the integral is dependent on the path of the conductor of interest between the shore facility and an inland facility, and does not depend merely on the location of the two ends. Figure 1 shows the spatial behavior of the fields on the landward side, calculated for exponentially rising fields. The distance is measured in skin depths.
These enhancement effects are of interest for both power generation facilities (often located on the shoreline for cooling purposes) and seafloor fiber optic cable facilities (the cables have a central conductor to supply power to repeaters located periodically along the length of the cable). The presentation will present both numerical studies and "rules of thumb" for engineering purposes.

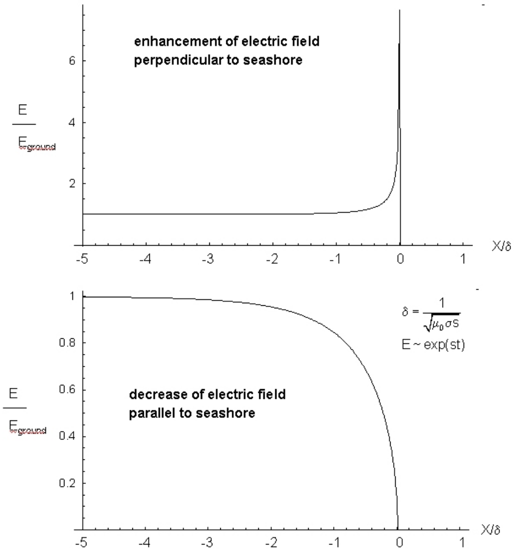

HPEM 15-4: Real-Time Forecast Service for Geomagnetically Induced Currents

H. Lundstedt, P. Wintoft, M. Wik, L. Eliasson
Swedish Institute of Space Physics

The goal of the project is to develop a forecast service to be used by electric power companies in southern Sweden. The service will be able to mitigate the effects of geomagnetically induced currents (GIC) caused by space weather.
When a coronal mass ejection (CME), a huge plasma cloud, is ejected from the Sun towards Earth we can expect increased geomagnetic activity within 1-2 days. If the solar wind speed is high and the magnetic field BZ is negative energy from the solar wind will be fed to the magnetosphere. Strong current systems of the order of several million amps will then be created in the ionosphere. The magnetic field from these ionospheric currents will induce currents in power systems on ground. This can cause overheating of transformers, damage to transformer windings and in worst case a system blackout.
GIC have been recorded by the power industry for many years and in some cases caused disturbances. In March 1989 there was a total collapse of the Hydro-Quebec power system leaving 6 million residents without power for about 9 hours. On Oktober 30, 2003, there was a power failure in Malmö in southern Sweden and 50000 residents where without power. Both events where caused by GIC.
The service shall include a neural network model that is able to forecast dB/dt from solar wind data. Data from ACE and the IMAGE magnetometer network will be used for training. Earth´s conductivity and a DC-model of the power system will then be used to calculate GIC in all transformers and transmission lines. Data analysis will also be used to study the characteristics of a GIC event. Direct forecasting of GIC using neural network is also a possibility.
The service developer is the Swedish Institute of Space Physics (IRF) in collaboration with the Finnish Meteorological Institute (FMI). Elforsk AB is contributor and user. The project shall result in a software package implementing a prototype service, and a cost-benefit analysis of the service. The service shall also be coordinated with the Space Weather European Network (SWENET) and Regional Warning Center Sweden.

HPEM 15-5: Electromagnetic Research as Input to Space Weather Monitoring

V. Korepanov
Lviv Centre of Institute of Space Research

The Space Weather (SW) is directly dependent on solar events, that is why the main source of information about SW development is Sun observations. The Sun eruptions of different nature produce severe geomagnetic storms at the Earth which may strongly disturb functions of human and technological systems mainly through electromagnetic effects. So, the study of electromagnetic phenomena connected with SW both in space and on ground is of critical importance. It is necessary to underline that the man-made and natural hazards at the Earth's surface also can give considerable input in SW state.
The organization of efficiently operating monitoring system needs the development of coordinated research in this branch and establishment of new kind of partnership in R&D between scientists in Europe in order to coordinate the activities that traditionally fall within separate domains.
The SW R&D recently is intensely developed in Ukraine and is the main topic of international collaboration for Ukraine, which, having considerable scientific and technological potential in space research, also is ready to participate in this program with the following contribution.
It is known that in order to have efficiently operating SW monitoring system it is necessary to have the corresponding data both from the space and from the ground stations. All these stages of the SW monitoring are under the development in Ukraine. First, the ground based support is realized already at several scientific institutions of Ukraine. The leading role plays Main Astronomic Observatory of National Academy of Sciences of Ukraine (NASU) in Kyiv with its departments in Crimea and Caucasus mountains. Other site is modern electromagnetic observatory operating at Ukrainian Antarctic station "Akademik Vernadsky". Due to exclusively clean electromagnetic environment there it became possible to carry out the observations at the lowest possible electromagnetic sensors sensitivity threshold. Next stage – continuous ionosphere observations – will be realized in the year 2004 when the Ukrainian remote sensing satellite "SICH-1M" will be launched into polar sun-synchronous orbit (altitude 650 km) with the specialized scientific electromagnetic equipment "VARIANT" onboard. Other ionospheric experiments dedicated to SW program are also under realization. This is Russian-Ukrainian "ENVIRONMENT" mission with international participation aimed at the continuous monitoring of electromagnetic state of the ionosphere onboard Russian segment of International Space Station. The feasibility study is over and the foreseen launch date is 2006.
It is known that ISS is rather noisy space object and there is a little hope to get the reliable results of the measurements of low level signals produced by ionospheric disturbances related to SW. That is why a new Russian-Ukrainian experiment aimed at SW effects observations in ionosphere is accepted. The experiment will be realized onboard microsatellite CHIBIS which is under development now at Space Research Institute of Rus-

sian Academy of Sciences. It will be launched in 2005 at the independent orbit about 500 km high using ISS infrastructure.
The ground based observation sites together with LEO satellites have to help also in the understanding of the impact of Earth generated processes upon the ionosphere. This influence cannot be ignored in conceptual space weather model and its study can help us in the solution of very important modern problem: monitoring of human activity (e.g., intense power consuming and CO2 producing enterprises) and natural hazards (e.g., thunderstorm activity, earthquake preparation processes) from LEO satellites. The key questions here are the mechanism of the transport of energy released into Earth's lithosphere and in neutral atmosphere to the terrestrial plasma and the methodology of separation in the ionosphere of the effects "from top" and "from bottom".
The detailed information about the existing and planned study of electromagnetic signatures related to SW, as well as expected deliverables of this activity in Ukraine to European Community are given in the report.

HPEM 15-6: Coordinated Approach to Investigation of Space Weather Effects on Human Health and on Biological Systems on Earth.

M. Cermack[1], **O. Atkov**[2], **R. Favre**[3], **F. Jansen**[4], **S. Palmer**[5], **R. Pirjola**[6], **M. Rycroft**[7]
[1]*International Space University, Strasbourg, France*; [2]*Cardiology Research Center, Moscow, Russia and International Space University, Strasbourg, F*; [3]*Swiss Re-Insurance, Zurich, Switzerland*; [4]*Greifswald University, Greifswald, Germany*; [5]*Cranfield University, Cranfield, U.K.*; [6]*Finish Meteorological Institute, Helsinki, Finland*; [7]*Cranfield University, Cranfield, U,K., and International Space University, Strasbourg, France*

International activities related to the investigation of space weather phenomena have increased significantly in recent years. Most of these address effects of solar-terrestrial interactions on space-borne and terrestrial technical systems and are thus associated with space plasma physics. The available data about the influence on biological systems and on human health are rather limited although radiation hazards to spacecraft and aircraft crew and passengers are well understood. The information, in particular about effects of electromagnetic fields induced by geomagnetic disturbances, is scattered across various national journals in various specialities; they are difficult both to access and to interpret. The results of similar studies are sometimes contradictory because of inconsistent methodologies and insufficient explanations of possible interaction mechanisms.
In January 2004, an international working group has been established at the International Space University in Strasbourg, France. Its purpose is to outline a coherent strategy for the investigation of space weather effects on biological systems on the Earth, to create an international, multidisciplinary information exchange platform, to conduct and co-ordinate research on possible interaction pathways between geomagnetic disturbances and physiological systems, to increase the level of understanding of space weather effects within the medical community, and to examine the feasibility of both the prediction and the mitigation of space weather effects on human health.
We outline the steps and structure necessary to achieve these goals, and present some results of earlier studies, which demonstrate a significant influence of geomagnetic disturbances on human physiology.

HPEM 15-7: Spherical Model of Generation of Geomagnetic Perturbations on the Earth's Surface from High Energy Sources

A. Y. Matronchik
Moscow State Engineering Physics Institute (MEPHI)

The geomagnetic perturbations are low-frequency oscillations of electromagnetic field in the range from 10-3 to 10 Hz. These perturbations are recorded on the Earth's surface. Various atmospheric and ionospheric processes (lightning discharges, earthquake precursors, earthquakes, underground, contact and atmospheric explosions, absorption of gamma- and x-rays from solar flares and cosmic bursts) result in generation of ionospheric currents with formation of an electric and magnetic fields.
A determining role in the formation of geomagnetic perturbations plays the E-layer of the ionosphere. In this layer, for example, the energy of acoustic and magnetohydrodynamic waves from high energy sources change to the energy of electric conduction currents. These currents propagate by oscillating diffusion along and cross the E-layer and generate quasistationary magnetic fields on the Earth's surface. In recent years, this mechanism for the generation of geomagnetic perturbations has been the subject of considerable discussions (L. P. Gorbachev and A. Yu. Matronchik, Radiations mechanism of generation of geomagnetic signals from underground and contact explosions, Journal of Applied Mechanics and Technical Physics, vol.39, No6, 1998; V. V. Surkov, Electromagnetic effects from earthquakes and explosions, Moscow Engineering Physics Institute, 2000; L. P. Gorbachev and an., Generation of geomagnetic perturbations from nonstationary sources of high energy, Moscow Engineering Physics Institute, 2001), based on the plane model of ionosphere.
The goal of the present work is to consider the spherical three-dimensionally inhomogeneous model of ionosphere. The calculation of geomagnetic fluctuations at long epicentral distances (over 1000 km) based on the Maxwell equations in a quasistationary approximation with the conductivity tensor of the ionosphere, conductivity of the Earth, dipole geomagnetic field and the extrinsic electric currents. After simple transformations, we obtain equations for electric field components in the spherical coordinate system with boundary conditions. In the limiting case, where the force lines of the geomagnetic field are vertical and epicentral distances less 1000 km, system of equations becomes the well-known equation for ring current in plane model. To calculate the electric fields we use the two-layer spherical model of ionosphere: first layer is the Earth and atmosphere below 80 km, second layer is E-layer of ionosphere. These fields excite electric conduction currents in second layer and in first layer. The obtained currents form horizontal components of the magnetic field on the Earth's surface. The amplitude-frequency parameters of geomagnetic signal are estimated. A determining role of the spherical model at long epicentral distances is shown.

HPEM 15-8: Geophysical Plasma Generation Inside Energy Active Zones

E. Protasevich
Tomsk Polytechnic University

It is known the destruction of rocks and minerals is accompanied by the generation of wide range frequency radio emission. The destruction can be caused both under mechanical and thermal or radiation action. Breakdown and luminescence of the atmosphere near the Earth can be explained if one consider the energy active zones as open resonator by nature origin. Such approach allows one to treat the physical nature of the formation in the atmosphere of long-lived plasma bunches.
It was experimentally found the phenomenon of decreasing of gas discharge recombination velocity due to the cooling of charged and neutral particles when relative air humidity is from 95 to 97.5%. The processes of particles cooling and plasma decay velocity decreasing were simulated. It was elaborated the model of metastable plasma being formed as a result of ionization of humid air by nature emission inside energy active zones. It was developed the theory explaining the water vapour action on the formation of metastable, excited states due to 200 plasma chemical reactions.
It is experimentally found the shape of localized cold nonequilibrium plasma bunches depends on wavelength and structure of nature emission electromagnetic field. The shape of the bunches can be spherical, cylinder, ring and so on. The type of the discharge luminescence and its size are changed when the wave length or oscillations type are varied. The air composition

and chemical pollution including water vapour ejection affect on the colour and luminescence shape of geophysical plasma. It is determined using the statistical processing the correlation between atmosphere luminescence, solar activity and earthquakes energy.

References

1. Protasevich E.T. Cold non-equilibrium plasma. Generation, Properties, Application. Cambridge Inter. Science Publishing, 1999.
2. Protasevich E.T. Electromagnetic waves. Tomsk Polytechnic University Publishing.
3. Protasevich E.T., Skavinsky V.P. Geophysical background objects and phenomena. Tomsk Polytechnic University Publishing, 1996.

HPEM 15-9: The Ionospheric-Magnetospheric Alfven Resonator (IMAR) in the Case of a Dipole Geomagnetic Field

A. Ovchinnikov

In the present paper we continue the investigation of the ionospheric-magnetospheric Alfven resonator (IMAR) (A.O.Ovchinnikov "The joined theory of the ionospheric and the magnetospheric Alfven resonators" XXV th GA URSI. Abstracts, p. 647, 1996, Lille, France; A.O.Ovchinnikov "An Ionospheric Alfven Resonator for the Spherical Model of the Earth's Surface" Geomagnetism and Aeronomy, Vol. 39, No. 1, 1999, pp. 64-68.).This object of new type located in the near-earth space. This object is generalization of two other earlier separately considered objects - ionospheric Alfven resonator (IAR), and magnetospheric Alfven resonator (MAR). Therefore the IMAR possesses a number of new properties escaping of the account of interaction between IAR and MAR. In the present article the problem of eigenfrequencies of IMAR in a case of a dipole geomagnetic field are executed.

Range of considered frequencies f = (0,01 - 10) Hz. The solution of a problem is executed in spherical system of coordinates (r, θ, ϕ) which center is placed in the center of the Earth. The angle θ is counted from a direction connecting northern and southern magnetic poles. We will consider that properties of medium do not depend on an angle ϕ, and propagation occurs in a plane of a geomagnetic meridian. A surface of the Earth in given frequency range is considered indefinitely conductive.

If in earlier published papers (A.O.Ovchinnikov "The joined theory of the ionospheric and the magnetospheric Alfven resonators" XXV th GA URSI. Abstracts, p. 647, 1996, Lille, France; A.O.Ovchinnikov "An Ionospheric Alfven Resonator for the Spherical Model of the Earth's Surface" Geomagnetism and Aeronomy, Vol. 39, No. 1, 1999, pp. 64-68.) we believed, that the angle between a field-line of a geomagnetic field and a vertical α (θ) is equal to a polar angle θ in the present paper this restriction is removed. The case, when tan($\alpha(\theta)$) = 1/2 (tan θ), corresponding to a field of a magnetic dipole is in detail examined. The solution of a problem thus essentially becomes complicated, as in the equations there are new parameters.

Earlier considered case when α (θ) = θ corresponds to linear dependence of coordinate h along a field-line of geomagnetic field from θ. The solution of a problem for this special case is in detail investigated in publications (A.O.Ovchinnikov "The joined theory of the ionospheric and the magnetospheric Alfven resonators" XXV th GA URSI. Abstracts, p. 647, 1996, Lille, France; A.O.Ovchinnikov "An Ionospheric Alfven Resonator for the Spherical Model of the Earth's Surface" Geomagnetism and Aeronomy, Vol. 39, No. 1, 1999, pp. 64-68; A.O.Ovchinnikov Ionospheric-magnetospheric Alfven resonator (IMAR.) AMEREM 2002. International symposium. Abstracts. Annapolis. Maryland. USA. 2002. P. 46.) further we shall make comparison with this case. The second case corresponds to a field of a dipole, we shall name further this problem modified. Dependence between h and θ in this case appears more difficult and the analytical solution does not manage to be constructed even for the elementary cases spherical layered medium. The length of the modified field-line (hm) is more than in the first case (hm$>$ h). The IMAR in this case has lower eigenfrequencies which number on a unit frequency interval will be essentially more for high latitudes, and it is less for low latitudes.

It is shown that the solution of the modified problem can be executed by a method sequential approach, basing on the solution of an initial problem. Resonant frequencies and good qualities of modes of IMAR are numerically found in case of the modified field for conditions night and the maximal solar activity in a frequency range [0.01 – 1.0] Hz.

As a result of the done analysis it is received:

For latitude of 60 degrees - 27 resonant frequencies from 0,045 Hz - the first frequency up to 0,962 Hz - 27-th frequency (initial model - 15 resonant frequencies),

For latitude of 30 degrees - 11 resonant frequencies from 0,125 Hz - the first frequency up to 0,996 Hz - 11-th frequency (initial model - 15 resonant frequencies).

The quality factors of modes changes from 3 up to 700.

HPEM 16 - High Power RF Source Technology

HPEM 16-1: DIEHL High-Power RF Source Development

D. G. Staines, **D. J. Urban**
DIEHL Munitionssysteme GmbH

Compact, reliable high-power radio frequency (RF) sources are under development by DIEHL, Germany for potential RF weapon (RFW) applications. Typical development projects include the DS350 high-power laboratory source for electromagnetic effects testing, the DS110 range of compact sources, and ultra high repetition rate UWB communications jammers. The DS110A array systems intended for longer range applications where single-antenna RF sources are limited by atmospheric breakdown over the exterior of the antenna will also be discussed.

The DS350 laboratory system has been shown to produce field strengths of more than 300 kV/m at 1 m range, and operating at frequencies of 50-100 MHz. A radiated pulse energy of 30 J has been obtained at 50 MHz. The system was not optimised for compact volume, but rather as a reliable, modular laboratory testing system. One useful feature of this system is the convenience with which different antennas can be connected, allowing maximum flexibility during either effects testing or antenna development. A brief description of the system, together with simulated and measured radiated field results will be presented.

The DS110 range of compact autonomous sources are available either integrated into small suitcases or in cylindrical geometry. Radiated field measurements will be presented to show that field strengths of approximately 100-160 kV/m at 1 m range are obtainable with a 350 MHz damped sinusoidal pulse approximately 6 ns long. A peak radiated field strength of over 300 kV/m normalised to 1 m range has been achieved with a simple add-on reflector. Of particular interest for testing applications is the DS110B tuneable source, with a tuneable centre frequency range of 100-300 MHz. A new long-pulse version of the DS110B known as the DS110B-LP has been tested which is specifically intended for test applications. The antenna is DC-charged to up to 100 kV, and can produce pulse lengths in excess of 10 cycles with excellent pulse repeatability. Both the frequency and duration of this pulse can be varied. A lower frequency (150 MHz) version of the DS110 antenna will also be discussed to show that both the frequency and bandwidth of the DS110 sources can be selected according to specific requirements, so that there is the possibility to optimise these sources to optimise coupling to targets.

The HRR-8G high repetition rate jammer is the latest in a series of sources which can effectively jam communications signals over a 20-500 MHz frequency range using UWB pulses with a repetition rate of more than 1 MHz. A brief description of this source will be provided, together with measurements of the radiated power spectrum.

The DS110A3 3-antenna high-power array has been show to produce stable pulses of over 600 kV/m normalised to 1 m range.

The advantages of this system are not only higher field on target, but also enhanced directivity which prevents radiation in undesired directions. The development of larger array systems with 6 antennas or more is underway to achieve even higher radiated fields. The DS110A3 has been integrated into a small trailer to allow the evaluation of mobile RFW scenarios.
Research is continuing to develop the full potential of these unique high-power sources and to transition this technology into commercially viable prototype systems.

HPEM 16-2: HPM Resonators for Indirect Deployment

J. Urban, G. Staines, R. H. Stark, J. Bohl
Diehl Munitionssysteme GmbH & Co. KG, Fischbachstr. 16, D-90552 Röthenbach a.d. Pegnitz

High power microwave systems (HPM) represent a new and additional capability for tactical operations enabling the user to deactivate command posts and information infrastructures. The superior objective is to acquire the guidance superiority by enforced disturbance of relevant systems up to the destruction of electronic components within such systems. Due to the non lethality of HPM pulses the collateral damages at such operation can be reduced to a minimum.
Besides direct deployable systems there are also compact and for the indirect deployment optimized systems under development. The presented contribution focuses on the latter ones. The critical requirement for indirect deployable systems is the limited time frame for interaction with localized targets. Due to these limitations systems which operate repetitive within the time regime of seconds or single shot systems could be realized. According to this at Diehl in cooperation with Rheinmetall W&M different resonator concepts are under development.
For the repetitive operation damped sinusoidal resonators which radiate either a pulse with damped sinusoidal shape or bursts of such pulses are presented. For the burst operation mode units were tested which radiate up to six pulses within a period in the 100 ns range. By operating also the feeding high voltage pulse generator such bursts can itself be repeated with 100 Hz or higher. Despite the short interaction time a designated target system is irradiated with a multitude of pulses containing different frequency regimes.
For single shot systems the requirements of the HPM resonator are different. The high voltage units used for those applications are usually designed to generate only a single high voltage pulse, however, having mostly very high pulse energy in the kilo joule range. The resonator development is aimed to use this high feeding pulse energy as effectively as possible and to convert in radiated HPM pulse energy. We differ therefore between mid energy (ME, $<=$ 100 J) and high energy (HE, $>$ 100 J) resonators. Correspondingly for both energy ranges exist concepts which can be integrated together with the required HV generator in different carrier platforms as i.e. a MLRS.

HPEM 16-3: Vircator: Status and Perspective.

A. N. Didenko
Institute of Thermophysics of Extremal State Russian Academy of Sciences

Among various high-power microwave sources, vircator is of special interest because of its simplicity, high-power capability and wide-range tuning of generation frequency. Vircator do not require the external magnetic field and it allows to decrease its size, weight and cost. The most actual question for vircator is increasing of the beam energy transformation to microwave radiation energy.
Vircator with a special additional feedback, named virtod, allows to increase the efficiency of generator, but it is connected with using very complicated additional system what significantly decrease the advantages of vircator (I. Magda, S. Korovin). In this report it is shown that vircator, especially reflex triod, has self- consistent feedback and at definite sizes of cavity it is possible to receive the optimal feedback system that allows to increase the efficiency of generator. The increasing of efficiency is more great in the case of the small energetic spread of electron.
Very interesting system with using of virtual cathode was proposed by W. Jiang, M. Sato and K. Yatsui. In this configuration two electron beams are injected into the cavity through the cavity wall with very high transparency. In this case it is not possible to change the frequency of generation but it is possible to preserve another advantages of generator with virtual cathode and to increase the efficiency of such systems.
In report the comparison the vircator of various types will be done.

HPEM 16-4: Measurement of Reflection and Transmission Properties of Fresh Cement-Based Materials by Using Free-Space Method

S. N. Kharkovsky, C. D. Atis, U. C. Hasar, S. Dover
University of Cukurova, Department of Electrical and Electronics Engineering, 01330, Adana, Turkey

The results of measurement of reflection and transmission properties of cement-based materials (mortar, concrete) during the first hours after their preparing at microwave frequencies (X-band) are presented. A simple and inexpensive measurement system that utilizes the non-destructive and contact-less free space method is used-Fig.1. The measured material is located in a special container-Fig.2. A five-layered model of measurement cell (the container with material) in air is analyzed. Dependencies of the amplitudes of reflection and transmission coefficients on water-to-cement (w/c) ratio, thickness of the container walls and specimens are demonstrated. It is shown that the transmission coefficient (in dB) gradually decreases with time and depends on w/c ratio for given operating frequency, dielectric permittivity and cell dimensions(Fig.3) while the reflection coefficient changes unpredictably and depends on physical phenomena at the near surface regions of the sample. (Fig.4)

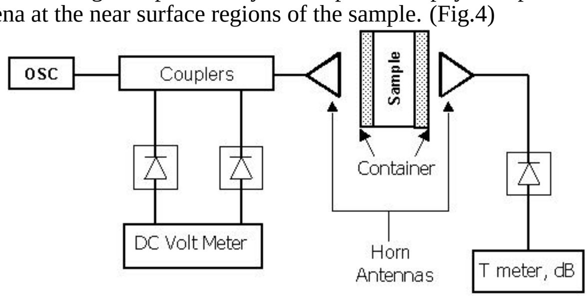

Figure 1: Schematic diagram of the measurement set-up.

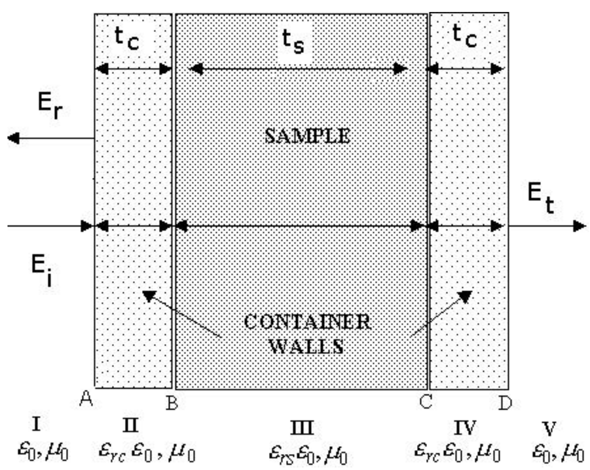

Figure 2: The configuration for reflection and transmission measurements.

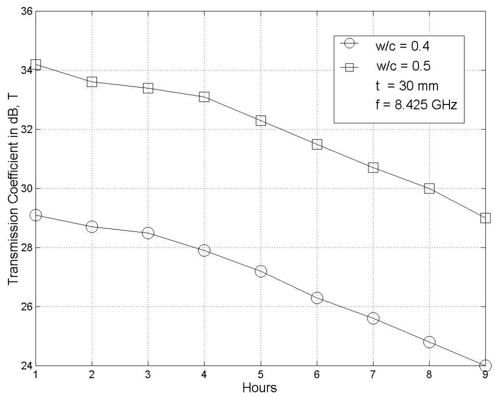

Figure 3: The transmission coefficient, T (dB) of mortar with two w/c ratios(w/c = 0.4; 0.5) over time at operating frequency f = 8.425 GHz.

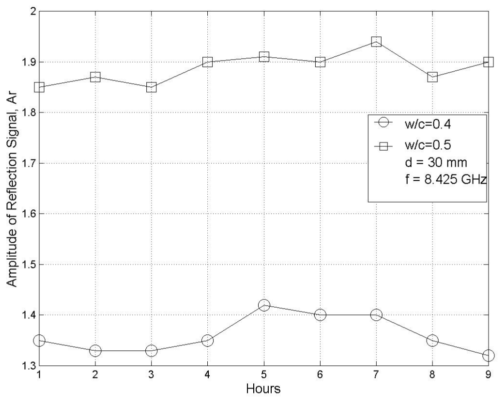

Figure 4: Amplitude of reflection signal, Ar (Arb.units), of mortar with two w/c ratios(w/c = 0.4; 0.5) over time at operating frequency f = 8.425 GHz.

HPEM 16-5: About the Physical Effects VHF Radiation on Semiconductor Diodes

A. N. Didenko, **V. V. Shurenkov**
Moscow Physical Engineering Institute (State University)

There are many publications on research of a microwave radiation effect on various semiconductor devices in a wide frequency range and interval of powers. But still now there is a problem of definition of the physical mechanism of microwave radiation effect on semiconductor devices.
We modeled some effects a microwave radiation on semiconductor diode earlier [A.N. Didenko, V.V. Shurenkov, " Modeling of interaction of the VHF - radiations with diode structures ", Engineering physics N4, 2001, pages 16-19]. It was supposed, that main physical effect defining positive bias diode behavior under microwave radiation is the growth of a recombination current in the p-n depletion region of under electrical microwave field. We considered, that the excess carriers recombination was determined by Shockley-Hall-Read (SHR) statistics, i.e. the recombination - generation was carried out through deep energy centers. And that the dependence of capture section of carriers by deep centers was determined by Poole-Frenkel effect, i.e. by lowering of the Coulomb barrier of recombination center if there is a strong external electrical field of a microwave source (owing to Poole-Frenkel the speed of emission and capture of carriers by impurity centers in the depletion region and in p- and n- bulk regions depends on an electric field strength). According this model the direct current through the diode is growing when microwave radiation power is growing too even at zero bias of the diode. These calculated results qualitatively completely corresponded to experimental results obtained in [Abljazimova N.A. et al., Electric of property of silicon p-n junctions in strong VHF fields.-FTS , 1988, v.22, N11, pp 2001-2007].
But some experimental results, for example, appearance of sites with a negative differential resistance (NDR) on a direct branch current - voltage characteristic (CVC) of the diode require clarification of offered model. It is possible to explain the indicated problem outgoing from the considered above model and outputs of [J. Furlan, Z. Gorup, F. Smole, M. Topic "Modelling Tunneling-Assisted Generation-Recombination Rate in Space-Charge Region of PN A-Si:H Junction", J. Of Modeling and Simulation of Microsystems, Vol.1, No.2, Pages 109-114, 1999]
According [J. Furlan et. all] an additional component of a recombination current at direct bias in the diodes with high density of deep recombination - generation centers on boundary of p- and n-regions arises at a high electric field strength in depletion region. This current defined both Poole-Frenkel effect and tunneling of majority carriers in depletion region to deep centers with the subsequent recombination of majority carriers.
It is known, that diode current has four components - drift, diffusion, recombination and generation currents. The total current through the diode is equal to zero when zero bias or zero external radiation. When any voltage are applied or there are any radiation (electromagnetic, charge particles, phonons and so on) a dynamic equilibrium between these currents are changed.
So, the effects of a high power microwave radiation on the diodes looks like this. At zero bias or small direct voltage in diodes with high concentration of recombination centers near the boundary of p- and n- regions a main current is the recombination current. This current created by the majority carriers recombination on the deep centers in a forbidden zone. These carriers overcome a triangular barrier predominantly by tunnel and then are captured by recombination centers in depletion region, creating thereby recombination current. The tunneling of the carriers, not having sufficient energy to reach recombination centers in the depletion region, is more possible because a microwave radiation creates high electric field strength E in any diode region and in the depletion region too. The probability of tunneling increases proportionally $e^{-c/E}$. The field strength E is proportional to a microwave of power P as $\sqrt{P}$.
At further increase of a complete current the recombination component share is reduced. It is possible originating of a NDR in a direct branch CVC at high injection levels when the depletion region voltage drop becomes compared to the diode base voltage drop. As a microwave radiation induces recombination, the electrons from a conductivity zone captured by traps, promote capture of holes from valence zone by these traps. The increasing number of traps is filled by holes and holes lifetime increases and the conductivity of base increases too in result at further growth of a direct current. It results, in spite of current growth and depletion region voltage growth too the voltage drop on the diode base. And the whole voltage falls and current-voltage characteristic became S- figurative. The similar - mechanism of NDR in a direct branch CVC observed by us earlier in irradiated diodes, in which the deep centers were the radiation defects [I.F. Nikolaevsky and V.V. Shurenkov "Some properties of electron-irradiated silicon diodes" Soviet Physics Semiconductors, 7, June 1974 pp 1509-1511].
The attitude of a microwave field concerning a depletion region field attitude according to offered model does not influence recombination processes at all. The electric field strength is relevant only. Experimental confirmation of this effect of independence of recombination processes from a field direction is a direct current at zero voltage and originating of NDR sites in a direct branch of CVC under microwave radiation, when microwave field was parallel planes p-n junction [Abljazimova N.A. et all].
The dependence of effect of a microwave - induced recombination from a microwave signal frequency should be determined by relation between the carriers lifetime and dielectric relaxation time on the one hand, and microwave signal frequency with other. The effect of a microwave - induced recombination can be observed up to frequencies, while the period of microwave oscillations exceeds relaxation time.

HPEM 16-6: Application of High Power Microwaves Generated by a Coaxial 2D Bragg Free Electron Maser Driven by an Annular Electron Beam

B. A. Kerr[1], **S. N. Spark**[1], **A. W. Cross**[2], **I. V. Konoplev**[2], **A. D. Phelps**[2], **P. McGrane**[2]
[1]*QinetiQ, St. Andrews Road, Malvern, Worcestershire, WR14 3PS, UK*; [2]*Department of Physics, University of Strathclyde, Glasgow, G4 0NG, UK*

The use of two-dimensional (2D) Bragg structures has been suggested for application in microwave electronics to synchronise radiation from different parts of an oversized active medium and to improve mode selection inside the interaction space. Computational modelling and experimental measurements of the field evolution inside co-axial 2D Bragg structures as well as recent progress in the use of these structures to define the cavity of a high power Free Electron Maser will be presented. The 2D Bragg cavity has been designed and constructed. Microwave measurements have been performed using a Vector Network Analyser. Good agreement between the measured transmission properties of the 2D Bragg structures and PiC code (MAGIC) simulations was obtained.
The high current accelerator to drive the FEM consists of a Marx bank power supply which resonantly charges a transmission line which subsequently discharges through a high pressure (16Bar) nitrogen-filled spark gap providing a 200ns duration flat-top high voltage pulse to an explosive emission electron (EEE) gun diode immersed in a 0.6T guide field provided by a 30cm diameter 2.25m long solenoid. The guide magnetic field insulates and confines an annular relativistic electron beam of energy 500keV. The oversized (7 cm diameter) annular electron beam was passed through an azimuthally symmetric wiggler with the interaction space defined by two-dimensional (2D) Bragg structures. The maximum possible beam current transportable through the diode region and interaction space was calculated using the 2.5D PiC code KARAT. An electron beam of power 750MW has been measured in the experiment. An FEM output efficiency of up to 15% has been predicted by the calculations. This paper will present the progress made towards the generation of 100MW of power from the co-axial 2D Bragg FEM operating at a frequency of 37.5GHz.

HPEM 16-7: Novel Crossed-Field Tubes for Compact HPM Systems

J. W. Eastwood, **M. P. Hook**
Culham Electromagnetics and Lightning Ltd

This paper presents results from our investigations of variants of MILO-like crossed-field devices. It will be shown these make possible substantially higher efficiency and operating frequency than have so far been reported.
The motivation for the work is practical applications of the technology that need reliable, compact and portable high power systems. These in turn drive the need for high power tubes that operate at higher frequency, higher impedance, higher efficiency, lower current density, and lower operating voltage.
The Tapered MILO (Eastwood, Hawkins and Hook, IEEE Trans Plasma Sci 26 698–712, 1998; Barker and Schmaligoglu, eds, High power microwave sources and technologies, chap. 3, IEEE 2001) has been shown to deliver approximately 15% power efficiency at 1GHz, 2GW rf power and 250J per pulse with a 500kV power supply. Constraints on peak current density and mode stability limit the upper frequency at which such powers can be obtained. The power consumed to maintain the insulating magnetic field limits maximum efficiency to approximately 25%.
The causes of the performance limitations of the Tapered MILO will be discussed. Our understanding of these limitations has allowed us to devise novel crossed-field designs that have better mode stability at higher frequency and lower current density for power output levels demonstrated by the Tapered MILO. Studies of variants of these designs have shown that higher impedance operation, increased maximum efficiency and more compact power extraction schemes are possible. The result of these changes is that substantial reduction in system mass and volume may be realised without sacrificing microwave output power.

HPEM 17 UWB 10 - Susceptibility of Components and Electrical Circuits

organized by the IEEE German EMC Chapter

HPEM 17-1 UWB 10-1: Influence of the Repetition Rate of a Recurrent HPM Perturbing Signal on the Behaviour of a Duffing Oscillator

J. Rabaste, **M. Demko**
EADS Nuclétudes, Courtaboeuf, France

In the studies of vulnerability of electronic systems (circuits or components) to HPM electromagnetic disturbances, it is in practice extremely difficult to make a precise analysis in a deterministic way, as well as the theoretical or practical point of view. The smallest variation of some parameters can lead to an important modification of the E and H field distribution within the enclosures including the electronic devices, and thus of the perturbation applied on the components of the system: cables and wires position, relative orientation of target and polarisation of the disturbing field, closing defects of the enclosures (a defect of a few tenths of mm only can decrease the shielding efficiency by several dB for high frequencies) etc.
Extrapolating conclusions from one test configuration to another, even looking similar, is thus extremely difficult when the electronic system shows a great sensitivity to external parameters. This is particularly highlighted in dynamic systems showing a chaotic behaviour, which have as a particular property to be able to rock in very different states even for a weak variation of one significant parameter (bifurcation parameter). Recent studies have shown that circuits with negative feedback attacked periodically by a pulsed RF signal could show a chaotic behaviour, even for low amplitudes of the electromagnetic aggression.
In this experimental work, we studied a circuit with a feedback loop derived from a Duffing oscillator, having every properties necessary to show a chaotic mode. The oscillator excitation frequency was selected so that the circuit moves in a different way, rocking alternatively between two symmetric equilibrium points. This circuit was stressed by a conducted recurring HPM signal applied to the input of an operational amplifier. We particularly studied the influence of the repetition rate and the RF frequency of the HPM perturbing signal on the behaviour of the oscillating circuit. We highlighted experimentally that the evolution of the system either towards a chaotic mode, or towards a stable mode that can be qualified forced, depends on the repetition frequency of the aggression, while all the other parameters remained invariant.
In the phase plane, the representation of the operation of the circuit is as follows (Fig. 1). In this presentation, we will describe more precisely the experimental conditions and we will discuss the influence of the HPM perturbation parameters, and specifically its repetition rate, on the behaviour of the circuit.

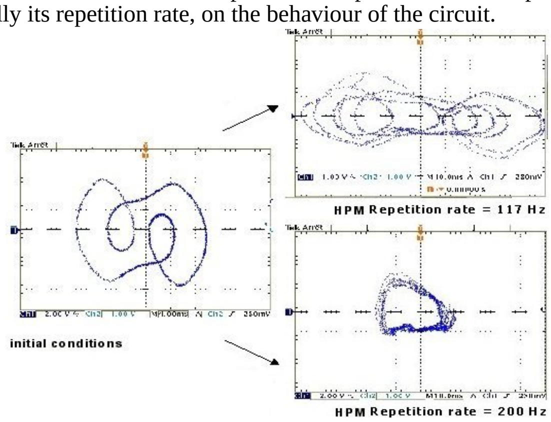

Figure 1: Experimental results: evolution either towards chaos or forced stability.

HPEM 17-2 UWB 10-2: The Effects and Diagnostic Uses of the Interaction of Radio Frequency Electromagnetic Radiation with Digital Electronic Systems

A. C. Marvin, **I. D. Flintoft**, **M. P. Robinson**, **K. Fischer**
University of York, UK

When radio frequency electromagnetic radiation impinges on a digital electronic system the possibility of unwanted interactions arises and the digital system may be subject to interference effects. Modern digital systems' immunity to such interference is provided by the inherent physical immunity of the system provided by the combined effects of shielding, circuit layout and the electronic device technology used along with the added immunity provided by error detection and correction software. Observation of the presence and effect of interference is obscured by this combination of immunity mechanisms and indeed the presence of the interference may not be apparent. A reduction in processing rate or locking of the system may be the first symptom to emerge. Neither of these symptoms is uniquely associated with external interference.
In this paper we report on a technique that enables the physical immunity of the system in the presence of interference to be observed. The technique utilises the radiated emissions from the victim system, the spectrum of which is modified by the presence of the interference. The modification mechanism is linear and, at higher interference levels, non-linear modulated scattering of the interference by the system's internal signals. The effects on the systems circuits is observed when the scattering changes from the linear to the non-linear regime and manifests itself as dynamic (jitter) and static (false switching) device failure depending on the severity of the interference.
This paper will present measurements of these phenomena from both simple test circuits and from more complex digital hardware. The correlation of the characteristics of the emission spectra with the device interference symptoms will be shown for CW interference signals and the potential uses of the phenomena for diagnostic immunity measurements will be discussed.

HPEM 17-3 UWB 10-3: HPM Susceptibility of Electronic Circuit Boards

B. Chevalier[1], **M. Martin**[2], **R. Brette**[2]
[1]*Délégation Générale pour l'Armement, Centre d'Etudes de Gramat, Gramat, France*; [2]*Délégation Générale pour l'Armement, Etablissement Technique de Bourges, Bourges, France*

It has been demonstrated a long time ago that electromagnetic radiation have some effects on electronics behaviour. Nevertheless, the threshold level can be in some cases strongly dependent on the waveform shape (ie carrier frequency, kind of modulation,...). The aim of this study was to analyse the electronics behaviour for different microwave environments in order to optimise the threat which is necessary to disrupt circuit boards.
Three families of electromagnetic threats have been studied: continuous waves, pulse waves and amplitude modulation (modulating frequencies: 100 kHz, 1 MHz and 10 MHz). The experiments conducted in a mode stirring chamber show as expected that CW is the most stressful waveform; the addition of an amplitude modulation on the CW signal has no real effect on the threshold level. However, a CW threat is not really convenient in terms of energy if you want to design a weapon.
If we look at pulsed radiation, two parameters are mainly available to optimise the threshold level of electronics: pulse repetition rate and pulse duration. For example, if we increase the repetition rate from 1 kHz to 10 kHz, the field strength required to upset the circuit can be reduced by 25 dB and the mean power by 15 dB. Concerning the pulse duration, the study points out two different behaviours with a boundary set at around 3 μs length. For duration beyond 3 μs, the field level for upset is almost the same when increasing the pulse length; only a 2 dB benefit between 3 μs and 100 μs corresponding to a raise of 12 dB for the mean power. When we reduce the pulse duration below 3 μs, the field strength for upset begins to raise: 5 dB between 3 and 2 μs, corresponding to an increase of 3 dB of the mean power.
To conclude, if you want to design an electromagnetic weapon, you have to find some compromise between pulse duration and pulse repetition rate in order to optimise the energy required.

HPEM 17-4 UWB 10-4: Study of HPM Effect on Electronics: Parasitic Reset

B. Chevalier[1], **P. Hoffmann**[1], **F. Sonnemann**[2]
[1]*Délégation Générale pour l'Armement, Direction des Centres d'Expertise et d'Essais, Centre d'Etudes de Gramat, Gramat, France*; [2]*Diehl Munitionssysteme GmbH & Co. KG, Röthenbach a.d. Pegnitz, Germany*

Theoretical and experimental studies have pointed out that electronic equipment could be strongly disturbed by HPM threat. But before defining a generic model of HPM equipment susceptibility, it's useful to focus on a particular effect and try to understand the whole phenomena from metallic enclosure coupling to component susceptibility.
In this paper, we will study the effect of HPM on the reset function of a logic components card constituted by memory, microcontroller and EPLD devices. This card is inserted inside a metallic generic missile (GENEC) which is part of a French/German cooperation. This study is based on different experimental, numerical and theoretical results. We focused on reset effect because it involves main troubles in real-time electronic applications with a quite weak threshold level.
So, we will start with a theoretical and experimental explanation of the HPM coupling outside and inside the missile body. Generally, the wings and their associated slots constitute the first backdoor coupling path according to frequency. In the GENEC case, the first cut-off frequency is near 1.6 GHz which is also very closed to the resonance frequency of the first electromagnetic mode excited inside the missile cavity. Thus, for frequencies around 1.6 GHz, the field strength inside the missile and in the vicinity of the circuit board is high enough to induce a significant parasitic signal on the PCB traces. Then after analysing the routing of the reset line, we can see that this line is a good candidate to strong coupling. The results of different susceptibility tests validate this fact. To well understand the nature of failure, we simulated with SPICE numerical tool the behaviour of the reset input port and made a functional analysis of the reset failure to define a predicted model of such a susceptibility. Finally, we will conclude this paper with some general reflections concerning this kind of HPM effects.

HPEM 17-5 UWB 10-5: Measuring the Upset of CMOS and TTL due to HPM-Signals

N. Esser, **B. Smailus**
ABB AG Corporate Research Center, Ladenburg, Germany

To measure the performance of electronic components when stressed by High Power Microwave signals a setup was designed and tested which allows a well-defined voltage signal to enter the component during normal operation, and to discriminate its effect on the component.
The microwave signal is fed to the outside conductor of a coaxial cable and couples into the inner signal line connected to the device under test (DUT). The disturbing HF-signal is transferred almost independent from frequency to maintain the pulse shape in the time domain. The configuration designed to perform a TEM-coupling within a 50 Ohm system prevents the secondary system from feeding back to the primary system and, due to the geometrical parameters chosen, the coupling efficiency is as high as 50-90%. Linear dimensions and terminations applied allow for pulses up to a width of 12 ns and up to a voltage level of 4-5 kV on the outside conductor. These pulse parameters proved to be sufficient to upset the DUTs tested so far.
In more than 500 measurements a rectangular pulse of increasing voltage level was applied to different types of CMOS and TTL until the individual DUT was damaged. As well the pulse width (3, 6 or 12 ns) and its polarity were varied in single-shot or repetitive-shot experiments (500 shots per voltage at different

a repetition rates). The state of the DUT was continuously monitored by measuring both the current of the DUT circuit and that of the oscillator providing the operating signal for the DUT.
The results show a very good reproducibility within a set of identical samples, remarkable differences between manufacturers and lower thresholds for repetitive testing, which indicates a memory effect of the DUT to exist for voltage levels significantly below the single-shot threshold. For the interpretation of the results an "aging model" was applied to describe the influence of the parameters on the individual thresholds.

HPEM 17-6 UWB 10-6: Electromagnetic Susceptibility

S. Bazzoli[1], **B. Demoulin**[1], **P. Hoffmann**[2], **M. Cauterman**[3]
[1]*Université des Sciences et Technologies de Lille (Laboratory TELICE), Lille, France*; [2]*Délégation Générale pour l'Armement (DGA), Gramat, France*; [3]*Ecole Supérieure d'Electronique (SUPÉLEC), Gif-sur-Yvette, France*

Aim of this paper will be to characterize the electromagnetic susceptibility of usual digital circuit under high power microwave coupling. Normally this may be performed by means of HPM sources incoming electromagnetic beam on PCB's. Tracks of the board behave as small antenna inducing a voltage at the input (or output) ports of the components connected at both ends. Although this method is a realistic way, the reproducibility of these experiments is not sure; furthermore these require expensive testing facilities. So, we propose perform this test in using a target coupling given by crosstalk phenomena occurring either throughout a multiwire shielded cable or a track assemblies on PCB's. This method allows to inducing disturbance on a line without any electrical contact with high frequencies. These measurements will be focused toward the susceptibility of the component under high frequencies disturbances, especially, at wave quarter resonance appearing on standard PCB's tracks at frequencies above 1 GHz. We can imagine, that between two components, a trace bounded by short-circuit and high impedance load. When the frequency of the disturbance is just with quarter wave, the voltage at the input port of the component increase dramatically and non-linear effects occur. Consequently, behavior of the line changes and the component output voltage drops or rises. However, packaging's inductance and capacitance may seriously influence these phenomena. The IBIS model (I/O Buffer Information Specification) provide some data on these, we will point out this at high frequency range. So, in order to understand these phenomena we propose to test the component through a crosstalk involving bench test of various lengths. Experiment will start with a coupling trough a cable of three meters long in order to have a wave quarter resonance at frequency close to 15 MHz. Decreasing the length with a couple of two tracks of few centimeters long, the wave quarter resonance will grow to 1.5 GHz. We will propose some experimental data showing the effect of the frequency on the electromagnetic susceptibility, we start on simple diode and transistor and extend these to usual IC's digital circuits. Aim of these measurements will be to select the main parameters, which influences the component susceptibility.
From the preliminary experiments we can conclude that the nonlinear effects depend mainly of the ESD clamping diodes. These, produce a distortion of the induced voltage, which involve high frequencies harmonics, which may be tuned on the wave quarter resonance of the PCB's track. Some data showing the disturbing effect of these diodes and the filtering effect due to packaging inductance and capacitance will be presented. To conclude these will be extended to usual digital IC's found in computer equipment.

HPEM 17-7 UWB 10-7: Analysis of Opamp Operation under High Power EMI

F. Fiori, **P. S. Crovetti**
Eln. Dept. Politecnico di Torino, Turin, Italy

The wider and wider diffusion of wireless communication systems has dramatically raised the level of electromagnetic environmental pollution over the last years. As a consequence, the amplitude of radio-frequency interference (RFI) which is superimposed onto the nominal voltages and currents in almost any electronic system is very often comparable with the amplitude of nominal signals or even larger. For this reason, the prediction of the effects of RFI on the operation of analog integrated circuits (ICs) has become a critical EMC issue.
Operational amplifiers (opamps), which are surely among the most common analog building blocks, are extremely susceptible to RFI. In particular, it was observed that continuous wave (CW) RFI, which is superimposed onto the input voltages of a negative feedback opamp circuit, induces an offset in the opamp output voltage. This phenomenon was previously investigated through computer simulations and Volterra series analysis. Unfortunately, computer simulations provide accurate predictions of the RFI-induced offset voltage, but they do not give an explicit relationship between offset voltage and opamp design parameters whereas Volterra series provide a closed-form expression for the RFI induced offset voltage which is accurate only if the amplitude of RFI which is superimposed onto the opamp input terminals is small enough.
In this paper, a new model which provides a simple and very accurate analytical expression of the RFI induced offset voltage in CMOS opamps is presented. Such a closed-form expression, which is valid even under large-signal RFI excitation, is derived employing the technique presented in thanks to the adoption of a new nonlinear model for the MOS transistor. The predictions which are provided by the new model are in very good agreement with experimental results and they can be directly employed to derive design criteria.

HPEM 17-8 UWB 10-8: UWB, HPM and EMP Susceptibility of Complex PC Systems

A. Bausen, **J. Maack**, **D. Nitsch**
WIS Munster

The Electromagnetic Effects Branch of the WIS Munster is working among other topics in the area of electromagnetic interferences. Here the focus is on the examination of the influence of electromagnetic fields on military systems. Especially modern military systems are often equipped with PC systems (C3I). Therefore the examination of the susceptibility levels of those systems and a follow on hardening based of this data is of large importance.
The decreasing structure size in integrated circuits and the decrease of the logic levels in computer systems to achieve higher clock rates are causing lower disruption and destruction levels. Beside the susceptibility of the implemented integrated circuits the coupling to and disruption and destruction behaviour of the peripheral components like keyboard, printer, mouse and monitor are of interest.
In this paper the susceptibility of nine different PC systems to several threats like UWB, HPM and EMP will be presented. With this approach the different disruption and destruction effects and mechanisms of those threats will be observed and discussed.
Firstly the technical data like rise time, pulse shape and repetition rate of the different pulse generators will be shortly introduced. Secondly the measurement set-up will be presented. Hereby much effort was put into the reproducibility of the set-up. All cables, the positioning of the peripheral components and the PC systems were fixed in a wooden structure (see Fig. 1). Thirdly the measurement results of the susceptibility examinations will be presented and discussed with respect to the different effective parameters of the three threat types.

Figure 1: Measurement set-up for the PC susceptibility investigations

HPEM 17-9 UWB 10-9: Classification of the Destruction Effects in CMOS-Devices after Impact of Fast Transient Electromagnetic Pulses

M. Camp, **S. Korte**, **H. Garbe**
Institut für Grundlagen der Elektrotechnik und Messtechnik, Universität Hannover, Germany

Risks as a result of upset effects of electronic circuits are ranging from artless breakdown effects of household appliances to perilous failure effects of medical equipment, culminating in a total collapse of traffic-, communication- and defense-systems of modern developed nations, with fatal consequences for the affected areas. New developed pulse generating devices can be built in a very small volume due to the low energy content of the pulse. In combination with broadband antennas it is possible to damage arbitrary electronic equipment in a great distance. Therefore the investigation of the susceptibility of electronic devices is of great interest.
In this investigation the destruction effects in CMOS-devices after impact of fast transient electromagnetic pulses have been classified. In contrary to TTL-devices, identical CMOS-devices are much more complex concerning the layout. Anyway, the destruction effects are similar to the destruction effects observed at TTL-devices in previous investigations [M. Camp, H. Garbe, D. Nitsch, Influence of the Technology on the Destruction Effects of Semiconductors by Impact of EMP and UWB Pulses, 2002 IEEE International Symposium on Electromagnetic Compatibility, USA, Minneapolis 2002, August 19-23, ISBN: 0-7803-7265-6, pp. 87-92]. The destruction effects can be separated into component-, onchipwire- and bondwire-destructions. First, at lower field amplitudes, component destructions, mostly as a result of flashover effects, occur. If the amplitude increases also onchipwire destructions appear. Further increase of the amplitude is leading to additional bondwire destructions and multiple component- and onchipwire-destructions.
In addition a classification concerning the location areas have been performed. It will be shown that first, at lower field amplitudes, the input protection circuits of the tested CMOS-devices are damaged. If the ampliude increases additional destructions of the output circuits appear. Further increase leads to destructions directly inside the electronic circuit (between input and output circuits).
This investigation is part of the study Susceptibility of Electronics to EMP and UWB, Phase II, commissioned by the Armed Forces Scientific Institute for Protection Technologies - ABC-Protection (Munster, Germany).

HPEM 17-10 UWB 10-10: Coupling and Effects of UWB Pulses on Complex Systems

D. Nitsch
WIS Munster

Due to the high dependency of our communication, economy, safety, traffic and medical equipment on modern electronic devices, it is very important to ensure their undisturbed functioning. Beside other sources of interference, transient electromagnetic pulses are becoming more and more important. On the other side the susceptibility of electronic equipment to interferences is rising due to the decrease of typical structure sizes and logic levels in integrated circuits.
Transient electromagnetic pulses with rise times in the picosecond regime have got an ultra wideband spectrum. Besides natural sources (lightning, electrostatic discharge) those pulses can be generated by technical sources. Here civil applications (switching pulses, ultra wide band communication and radar) as well as intentional interferences in civil and military areas are playing an important role.
In this paper a method to calculate the coupling and the impact of those pulses on complex electronic systems is presented. This method is based on the description of the huge number of coupling paths into complex electronic systems with one overall transfer function which can be simplified to a complex function by calculating its shape. A descriptive system vector of a complex system can be calculated by using an estimation of the shape. The spectra of the ultra wide band pulses can be assessed with respect to this system vector to calculate the coupling and impact of those pulses to the system. This assessment is done with help of limited Hoelder norms in the frequency domain, which compress the complex spectra of the ultra wide band pulses to important scalar quantities like energy efficiency or effective amplitude.
The applicability and the limits of this method are tested with coupling measurements to generic structures and susceptibility investigations of microprocessor boards and computer systems.

HPEM 18 - Coupling to Structures & Cables

HPEM 18-1: Current Distribution in Parallel Wire-Shields Observing the Skin and Proximity Effect

Y. Varlamov[1], **J. Nitsch**[2], **V. Chechurin**[1], **N. V. Korovkin**[2]
[1]*State Polytechnical University, St. Petersburg, Russia*;
[2]*Otto-von-Guericke-University, Magdeburg, Germany*

The problems of electromagnetic energy penetration through braided metal shields are of great interest. The current distribution in the wires changes significantly when the field frequency increases, due to the skin and proximity effect. Accordingly, the screening properties of the shield are changed as well. Therefore, it is important to calculate these effects.
The problems of electromagnetic field computation are considered, when the sources of the electromagnetic field are the currents which flow along the cylindrical shield consisting of a set of thin wires. Solutions have been obtained for single and double layers of cylindrical shields, flat shields (with infinite extension), and for a single layer shield placed above perfectly conducting ground observing the skin and proximity effect.
It does not seem to be adequate to solve the problems using a numerical method like FEM for the computation of the electromagnetic field. This is because of a tremendous difference (three to five orders of magnitude) between the dimensions of cables and the skin depth in the wires at frequencies of the field between 0.1-10 GHz. Therefore, the integral equation method is applied.

The boundary conditions couple the tangential components of the electric and magnetic fields at the surfaces. This allows the computation of the electromagnetic field when the number of the wires exceeds several hundreds.
It is proven that the real current distribution over the cross section of a single layer of cylindrical or plane wire-shields may be replaced by electric surface currents. Simple relations between the geometrical parameters of the shields, the frequency of the electromagnetic field and the current distribution on the wires are found. The derived expressions permit the calculation of the transfer impedance.

HPEM 18-2: Analytical Solution for the Transfer Impedance of Cylindrical and Plane Parallel-Wire Shields

V. Chechurin[1], **J. Nitsch**[2], **N. V. Korovkin**[1], **Y. Varlamov**[2]
[1]*State Polytechnical University, St. Petersburg, Russia*;
[2]*Otto-von-Guericke-University, Magdeburg, Germany*

The transfer impedance of cylindrical wire shields like the shields of cables strongly depends on the frequency of the exciting electromagnetic field. The analysis of this dependency is of great interest for engineers. Measurements in the frequency range between 0.3-0.5 GHz are complicated and sometimes lead to contradictory conclusions. This may be one reason that the theoretical considerations of the dependency of the transfer impedance on the field frequency and on the geometric configuration of the cables are actual.
In the paper we derive new analytical formulae for the transfer impedance of cylindrical and flat shields which are constituted of a set of parallel wires. We assume that the penetration depth of the electromagnetic field into the wires is much less than the wavelength. Therefore the assumption of a surface current distribution is justified. This distribution can be calculated using the impedance boundary condition or considering a wire as a perfect conductor. We assume the surface current distribution to be known as a function of the angle, $j = j(\alpha)$, around the perimeter of the wire.
Using the trigonometric Fourier series expansion of the surface current around the perimeter of the wire, the vector potential and the e.m.f., induced in the central conductor are found. The analytical expressions are derived taking into account the skin and proximity effect. In fact, in the analyzed conducting system the proximity effect as well as the skin effect contribute to the redistribution of the surface current on the wire. The obtained formulae show the dependency of the transfer impedance on the geometric configuration of the shield (number of wires, distance between the wires, radii, etc.), and on the frequency of the electromagnetic field.
One can use the obtained expressions to explain the experimental data for braided wire shields. Due to the inhomogeneous current distribution on the surface of the wire-shield the values of the transfer impedance are modified, compared to usual considerations. We also study the influence of a conducting ground on the transfer impedance.

HPEM 18-3: EMP Coupling on Large Structures.

J.-P. Percaille, **E. Kerhervé**, **I. Pouget**
DGA/DCE/CEG Centre d'Études de Gramat, Gramat, France

Deployed forces are made up of large military or civilian structures, networked shelters or buildings. The vulnerability of the systems located inside (command and control units, or communication or information systems)facing electromagnetic threats is highly dependent on the coupling effects with those structures. Moreover, the experimental measurement of coupling effects on large structures is very difficult..
The ARTEMIS facility has been designed to study the nuclear electromagnetic pulse coupling with large structures.
The frequency response of the system under must be linear. Working in continuous wave at low level, the emitting part of ARTEMIS radiates an electromagnetic plane wave between 300 kHz and 1 GHz. The receiving part of ARTEMIS is a multi-channels network analyzer and is linked to sensors by optical fibers. The incident radiated field and the conducted/radiated stresses induced outside and inside structures are measured in magnitude and phase. Time domain responses of systems under test are computed using a signal processing routine on the experimental data.
ARTEMIS is easy movable and has been used to study coupling effect of EMP with several large structures (aircraft carrier, fixed communication systems). The results presented here are related to experiments carried out for two kinds of structures. The first one is a deployed air base, the second one is a civilian building. The radiated and conducted stresses have been measured on various points characteristic of critical functions (energy, telephony, computer network). To conclude, by taking into account some hypothesis on the equipment susceptibility threshold levels, a statistical assessment of the systems vulnerability is provided.

HPEM 18-4: Field Coupling to Printed-Circuit-Board Traces Measured in Reverberation Chamber

S. Silfverskiöld[1], **M. Bäckström**[2], **J. Lorén**[2]
[1]*Swedish Armed Forces Headquarter*; [2]*Swedish Defence Research Agency FOI*

We have previously reported an experimental study of microwave, 0.5 to 18 GHz, field-to-wire coupling for some basic wire geometries above a ground plane. Coupling measurements were performed in Anechoic (AC) and Reverberation Chambers (RC). Receiving parameters and comparisons between measurements in the two chambers were presented. We found that the ratio between the maximum and average values of the realized Gain G_R may exceed 15 dB in the AC, the average being equal to G_R measured in the RC. Furthermore the antenna receiving cross section S_w of wires and G_R measured in the RC was found to follow a χ^2-distribution with two degrees of freedom, with respect to different stirrer positions at a given frequency. The measurements of G_R in the AC did not follow the same distribution, with respect to different angles of incidence and polarizations (at a given frequency).
In this study we are interested in knowing the receiving parameters for traces on Printed-Circuit-Boards (PCBs) in order to make analyses of system susceptibilities based on component susceptibility data. The approach is to regard the traces on the PCBs as receiving antennas, where the antenna receiving cross section, CS_w, is defined by (1) where P_{load} is the power received by the load and S_{inc} is the power density of the incident field.
For an antenna, CS_w is given by (2) and (3) where G is the gain, p the polarization mismatch factor, q is the impedance mismatch factor and S_{11} is the reflection factor, measured with a Network Analyzer (NA). D is the directivity and η the antenna efficiency, representing the ohmic losses (η = 1 for the lossless case). In the statistically isotropic environment of the RC the following relations hold: (4).
In this study we report field-to-printed-circuit-board (PCB) coupling for some single-sided, double-sided and multi-layer PCBs performed in RC. We present receiving parameters such as the realized gain G_R, the impedance mismatch factor q, the input resistance R_{in}, the receiving cross section CS_w and the effective antenna length h_e. The effective antenna length h_e normalized to the wavelength was plotted for the different PCBs. For each PCB the maximum value of h_e/l in the frequency interval 0.5 to 18 GHz was selected. These maxima come in a range of 0.34 to 0.74, thus h_e for PCBs is bounded by l. This result agrees with our previous field-to-wire coupling measurements. The impedance matched receiving cross section is bounded by l2/8p, as was expected.
Finally, we show that sw of traces on PCBs, measured at different stirrer positions in the RC, follows, except at the low frequency end, a χ^2-distribution with two degrees of freedom. The statistical distribution of the power received by an antenna in the RC is known to be a χ^2-distribution. We therefore conclude that the statistical properties of traces on PCBs are the same as those of an antenna.

$$CS_w = \frac{P_{load}}{S_{inc}} \tag{1}$$

$$CS_w = \frac{\lambda^2}{4\pi} \cdot G(\theta, \phi) \cdot p(\xi) \cdot q = \frac{\lambda^2}{4\pi} \cdot D(\theta, \phi) \cdot eta \cdot p(\xi) \cdot q = \frac{\lambda^2}{4\pi} \cdot G_R(\theta, \phi, \xi) \tag{2}$$

$$q = 1 - |S_{11}|^2 \tag{3}$$

$$\langle D \rangle = 1 \text{ and } \langle p \rangle = ½ \tag{4}$$

HPEM 18-5: Scattering-Current Based Procedure for the Transient Analysis of EM Field to Cable Bundles Coupling

M. D'Amore, **M. S. Sarto**, **A. Scarlatti**
Dept. of Electrical Engineering, University of Rome "La Sapienza", Italy

The increasing complexity of wiring systems aboard of aircraft, as well as in automotive systems or telecommunication apparatus, combined with the wide-spreading use of electronics and automation, has pushed to the foreground safety problems originated by electromagnetic interference produced by transient electromagnetic fields.

The transmission line (TL) approach is one of the most commonly used method for the analysis of the radiated susceptibility of complex cable bundle networks. One of the critical aspects of the developed TL procedure consists in the definition of the most suitable field-to-line coupling model to use for the evaluation of the induced effects. In fact, depending on the characteristics of the exciting EM field, the TL model can be formulated either in terms of both the electric and magnetic field components of the incident field, or of the incident electric field components only, or of the incident magnetic field ones. Correspondingly, the three different field-to-line coupling models of Taylor, Agrawal, and Rachidi are available in the literature [1]-[3].

A new field-to-line coupling procedure based on the scattering current formulation has been developed in [4] for the transient analysis of complex cable bundles. The method is suitable for the analysis of multiconductor transmission lines excited by low-impedance transient field, and in particular for the prediction of the induced effects in cable harness networks without simplifying hypotheses. The proposed formulation allows the calculation of the induced effects in wiring systems onboard lightning struck aircraft by using the magnetic field components only [5].

This paper discusses the features of the different field-to-line coupling simulation models to be used for the transient analysis of the EM induced effects of the direct lightning interaction with aircraft, based on the total voltages and total currents, on the scattered voltages and total currents, on the total voltages and scattered currents. The choice of the scattered-currents model is suggested by the quasi-magnetostatic nature of the lightning interaction problems: numerical inaccuracy are generated in the calculation of the electric field solution inside the computational domain. It is demonstrated that the use of the field-to-line coupling model based on the use of the magnetic field components allows to avoid numerical inaccuracy.

References

[1] C.D. Taylor, J.P. Castillo, "On Electromagnetic-Field excitation of unshielded multiconductor cables", IEEE Trans. on EMC, vol. 20, pp. 495-500, 1978.

[2] A.K. Agrawal, H.J. Price ans S.H. Gurbaxani, "Transient response of a multiconductor transmission line excited by a nonuniform electromagnetic field", IEEE Trans. on EMC, vol. 22, no. 2, pp.119-129, 1980.

[3] F. Rachidi, "Formulation of the field-to-transmission line coupling equations in terms of magnetic excitation field", IEEE Trans. on EMC, vol. 35, no.3, pp.404-407, Aug. 1993.

[4] M. D'Amore, M.S. Sarto, A. Scarlatti, "Modeling of EM field coupling with cable bundle harnesses", IEEE Trans. on EMC, August 2003.

[5] M. Aprà, M. D'Amore, M.S.Sarto, A. Scarlatti, V. Volpi, "VAM-LIFE: Virtual Aircraft ElectroMagnetic Lightning indirect eFfect Evaluation", International Conference on Lightning and Static Electricity - ICOLSE'01, Seattle (WA), Sept. 11-13, 2001.

HPEM 18-6: The Effects of Contents and Apertures on the Structure of Electromagnetic Fields in Enclosed Spaces

A. C. Marvin[1], **J. F. Dawson**[1], **R. Kebel**[2], **M. P. Robinson**[1]
[1]*University of York, UK*; [2]*Airbus*

Aircraft cabins represent complex environments for the propagation of electromagnetic waves with multiple reflections and losses due to cabin furniture, passengers and apertures. In addition, the presence of cables provides other guided wave paths for the transport of electromagnetic energy within the cabin.

The use of passenger borne portable radio systems inside aircraft cabins is generally prohibited as is the use of digital electronic devices. The reason for this prohibition is to reduce the possibility interference to aircraft electronic systems. Comparable electronic devices directly associated with the cabin are allowed as their effects can be characterised during aircraft qualification. Electromagnetic waves are also able to enter and exit the cabin through the cabin windows and other apertures raising the possibility of interaction between internal and external electronic systems.

Future aircraft cabins are likely to be equipped with a wider variety of radio based electronic devices including those using UWB technology. The general prohibition of passenger borne devices is likely to become less acceptable to the passenger as the variety and use of such devices increases. Thus the management of the electromagnetic environment in future aircraft cabins is crucial to their design. This management requires that the electromagnetic environment be properly understood and characterised. In this paper we will describe in detail the issues associated with this management task and present some results of initial studies of the computation of the electromagnetic field structure in such a cabin in the presence of absorptive contents, apertures and cables. The statistics of the field structure in the UHF frequency range will be described and compared with those found in mode-stirred chambers as used for assessment of interference and in those found in other multi-path propagation scenarios.

HPEM 18-7: Interchanging Frequency and Directional Dependencies in Susceptibility Testing

M. Höijer
Swedish Defence Research Agency FOI

It is known that the susceptibility of electronic equipment toward electromagnetic microwave irradiation varies with from which direction the equipment is irradiated as well as the polarisation in use. The polarisation dependence can easily be taken into account (M. Höijer et al., A Heuristic Statistical Method to tackle that No Information of the Partial Directivity Properties of the Equipment Under Test is given from Testing in the Reverberation Chamber, 2004), but it is harder to take the directional properties into account.

The polarisation non dependent part of the susceptibility does also vary with the frequency in use. There are six different contributions to this frequency dependence. First, as a general trend, the susceptibility of any equipment decreases with the square of the frequency. Secondly, the mismatch factor of the critical part of the equipment varies with the frequency. Thirdly, the radiation efficiency of the equipment varies with the frequency. The second and third effects are part of the shielding effectiveness of our equipment. Fourthly, the maximum directivity of the susceptibility varies with the frequency. Fifthly, the susceptibility lobes turn with the frequency (P.G. Landgren, Some Directivity Properties of Test Objects in the Microwave Region, 2001). There is also an important frequency-dependence in the inherent susceptibility of the actual electronic components, but that effect is not taken into account in this work.

It would be practically beneficial if one could substitute the directional dependence with the frequency dependence or vice versa. Intuitively one could think of turning the susceptibility lobes, by varying the frequency, as being equivalent to turning the electronic equipment, but in practice all the frequency effects described above have to be taken into account.

We have tested to substitute an irradiation from many (thousands) different directions with an irradiation from only three different directions, but with many (typically hundreds) different discrete frequencies within a bandwidth around the centre frequency. Typical bandwidths have been from 10 % to 100 % of the centre frequency in use. Our results show that the frequency substitution method seems to work, except at the strong resonance frequencies of our electronic equipment. That is due to, that the radiation efficiency is so much larger at the strong resonance frequencies than at the surrounding frequencies, that the other frequency dependent contributions are negligible at these strong resonance frequencies.

HPEM 18-8: Coupling of Indirect Lightning to Coaxial Cables at Naval Ships

R. Vick
EMC-Experts, Dresden, Germany

A large number of system cables are installed outside of the hull of naval ships. If direct or indirect lightening strokes the ship, large transient voltages may be coupled into cables. Therefore, the function of electronic equipment which is connected via these cables could be degraded of destroyed due to the resulting transient voltages. Information about the waveform and the amplitude of the resulting transients at the connection terminal of the equipment could help to optimize the design of protective measures at the equipment or along the cable. This paper describes a method to determine the resulting transient voltages at the beginning and the end of coaxial cables.
To calculate the transient voltages, the current distribution on the cable screen has to be determined in a first step. For the shown examples, this was done for stroke of standardized surges of the type 10/350 μs and 0.25/100 μs. In a second step, the cable transfer impedance of the coaxial cable and the current distribution on the screen are used to calculate the voltage, which is coupled into the coaxial cable.
The first simulations are shown for simple structures. These simple cases make it possible to show the influence of the quality of the screen, i.e. cable transfer impedances, on the transient voltage coupled into the cable. Measured values of the cable transfer impedances of different coaxial cables were used for the analysis.
An example of a more complicated installation on a naval ship is shown, when a lightening stroke hits a middle mast of a ship and coaxial cables are mounted on the mast. The program CONCEPT was used for simulation, which is based on the methods of moments. The influence of different connection and bonding techniques of the influenced cable on the resulting transient voltage were analysed. The described method can be applied on different structures an can be used to optimize the cable routing or the design of protection devices.

HPEM 18-9: Incident Field Excitation of a Random Two-Wire Transmission Line above a Lossy Ground Plane

J. C. Pincenti, **P. L. E. Uslenghi**
University of Illinois, Chicago, IL, USA

The problem of finding the terminal response of a random two-wire transmission line above a lossy ground plane excited by an external field is considered. Often in practice, the exact orientation of a transmission line is not known and therefore the electromagnetic field excitation of the line is probabilistic and has to be studied as such. This problem will be analyzed in the frequency domain using multiconductor transmission line (MTL) theory. In particular the line will be modeled as a 3-wire non-uniform MTL excited by an external field where the lossy ground acts as the reference conductor. The solutions will be found with use of the chain parameter matrix, which relates the currents and voltages on the line. The use of the chain parameter matrix has the advantage of allowing for the solution of a non-uniform MTL. The non-uniformity will be modeled by dividing the line into smaller discrete uniform sections, finding the chain parameter for each section and then cascading the segments together to approximate the overall line. Both the per-unit-length (PUL) parameters and orientation of each segment with respect to the incident field will be varied randomly thus creating an overall random cable. A number of such random cables will be generated producing a statistical solution. The random nature will take two forms. First, the spacing between the wires and height above the ground plane is not maintained and will vary randomly along the length of the line. This will cause the PUL parameters of inductance and capacitance to vary accordingly. Second, the orientation of the wires with respect to the incident field will vary randomly along the length of the line. This is due to the various twists and bends of the wires and variations in the ground plane and will affect the amount of coupling of the external field to the line. In addition, such variables as partial illumination of the line, angle of incidence of the external field and resistive losses of the wires will be considered. From this model, a distribution of the response will be determined thus showing the expected variation due to the random nature of the line.

HPEM 18-10: Penetration into Nested Cavities through Apertures

D. Negri, **D. Erricolo**, **P. L. E. Uslenghi**
University of Illinois, Chicago, IL, USA

Under consideration in this research is the penetration of the electromagnetic field into nested cavities through apertures. The investigated geometry consists of N perfect electric conducting nested cavities, each of which presents an aperture. The cavities divide the entire space in $N+1$ regions: the most external region, $N-1$ intermediate regions (regions between two cavities), and the most internal region. Since each cavity has an aperture, the electromagnetic field penetrates into the innermost cavity.
The solution of this problem is based on the equivalence theorem. By applying the theorem, the N apertures are closed by a PEC and N unknown equivalent surface magnetic currents are introduced on the apertures. In order to find the equivalent currents, the boundary conditions forcing the continuity of the tangential component of the magnetic field on the apertures are then imposed. The boundary conditions lead to N coupled integral equations, which can be solved by means of the method of moments. This procedure transforms the integral equations into N linear systems, or, equivalently, into one single comprehensive system of linear equations. Then, by inverting the system matrix the problem is formally solved, i.e. the equivalent currents become known. Once the equivalent currents are known, also the electromagnetic field in the $N+1$ regions and the induced surface electric currents on the N cavities are known, because they can be expressed as functions of the equivalent currents.
In order to provide an explicit form for all the terms that appear in the system, some "auxiliary problems" are introduced. This procedure follows the "generalized impedance matrix" approach, which was developed by R. F. Harrington, J. R. Mautz and T. Wang ("Electromagnetic scattering from and transmission through arbitrary apertures in conducting bodies"; IEEE Trans. Antennas Propagat., vol. 38, no. 11, pp. 1805-1814, Nov. 1990) and applied to the case of one cavity only.
The innovative element of the present research is the solution of the problem of the penetration into nested cavities through apertures. Furthermore, the problem is solved taking into account the contribution of the external scattering of each cavity. Future developments of this research may include the analysis of the penetration into a system of cavities with more than one aperture on each cavity and where the most external cavity contains other cavities not necessarily nested.

HPEM 18-11: The Mutual Impedance between Dipole Antennas within Cavities as Derived from the Reciprocity Theorem

F. Gronwald, **E. Blume**
IGET, Otto-von-Guericke-University, Magdeburg, Germany

The influence of an electromagnetic interference (EMI) source on an EMI victim can often be modeled by the electromagnetic coupling between two antennas. To determine, in turn, the antenna coupling requires the knowledge of the mutual impedance between both antennas. In free space a convenient formula for the mutual impedance can be derived from the reciprocity theorem (R.S. Elliott, Antenna Theory and Design, 1981). The derivation relies on the asymptotic behavior of the generated electromagnetic field at infinity.

We show that an analogous formula is valid if the antennas are placed within a finitely extended cavity of either perfect or finite conductivity. By this method the computation of the mutual impedance essentially reduces to the computation of the current distribution on a single antenna within a cavity if excited by a specific source. As an example we obtain the current distribution on a single dipole antenna by the solution of both Hallen's and Pocklington's equation within a rectangular cavity. The calculations rely on the method of moments and make use of a quickly converging representation of the cavity's Green's function. From this the mutual impedance between two parallel dipole antennas within a rectangular cavity is obtained by the derived formula in a straightforward way.

The results indicate the strong influence of cavity resonances on the antenna coupling, in particular in case of high quality factors. It is obvious that this effect needs to be taken into account during the design phase of systems which require to put electronic equipment in resonating environments that might be exposed to EMI sources.

HPEM 18-12: On the Theory of the Propagation of Current Waves along Smoothly Curved Wires

S. Tkachenko, **J. Nitsch**
Otto-von-Guericke-University, Magdeburg, Germany

Nowadays, we need more than ever before an analytical theory which describes the penetration of currents and voltages into multi-conductor wire systems, due to the permanent increase of frequencies, both for operating signals and for external interferences. At very high frequencies, where the transverse dimensions of the line are no longer small compared to the wavelength, the usual transmission-line theory (TL) fails.

Recently, in a number of papers different approaches to TL (generalized for high frequencies) have been proposed. Haase and Nitsch, e.g., (H. Haase, J. Nitsch, "Full-wave transmission line theory (FWTLT) for the analysis of three-dimensional wire-like structures", Zurich Symposium on EMC, Feb.2001, pp. 235-240, and Interaction Note 561) have shown that currents and potentials in a multiconductor wiring system, which has two specific points (a terminal source and a terminal load, two terminal sources, etc.), can be described by a system of first-order differential equations containing (so-called) global parameters which depend on the frequency, on the coordinate along the wire, and they are defined by the geometry of the system. (The inclusion of an additional external field which excites the wiring system in this approach is carried out by some iteration procedure).

Different from their approach, Nitsch and Tkachenko ("Complex-Valued Transmission Line Parameters and their Relation to the Radiation-Resistance, Interaction Notes, Note 573, Sept. 2002; "The Circular Loop above Conducting Ground - A Transmission Line Description", Electromagnetics in Advanced Applications (ICEAA 03), September, 2003-Torino, Italy, pp. 401-404; "Eine Transmission-Line Beschreibung für eine vertikale Halbschleife auf leitender Ebene", 11. Internationale Fachmesse und Kongress für Elektromagnetische Verträglichkeit, Düsseldorf, 2004, pp. 291-300) have dealt with high symmetry wiring configurations: an infinite, uniform transmission line above a perfectly conducting ground, a horizontal circular loop and a vertical semi-circular loop above a perfectly conducting ground. It has been shown that the Maxwell equations for these wiring structures can be cast into the form of a telegrapher equation for each mode, which is connected to the parameter of representation of a symmetry group corresponding to the considered wiring structure (translation group or axial rotation group). Corresponding distributed modal parameters - capacitance and inductance, which are constant along the line, are complex-valued, frequency and mode-dependent and contain the radiation resistance. Also it can be shown that other types of high-symmetry wires (like a helix wire) can be treated in the same manner. A connection of the introduced modal parameters with earlier investigated global ones is established.

For all the considered high-symmetry wiring systems the geometrical parameters of the curve of the wire axis (curvature and torsion) are constant. We assume that if the curvature and torsion do change slowly along the wire (the relative changing over a wavelength is small), the same modal parameter approach can be approximately used for a wire of arbitrary geometric form.

A smoothly curved wire of arbitrary geometric form excited by an external electromagnetic field is considered. It has been shown that the exact Maxwell equations for the induced current and potential can be approximately reduced to the system of the telegrapher equations for each mode. The modes now are characterized by the parameters in their expansion into Fourier integrals (for infinite curves) or into Fourier series (for finite curves). For constant values of curvature and torsion of the curve the obtained system is exact. Corresponding frequency dependent modal transmission line parameters-inductance and capacitance-are now slowly dependent on the length of the curve. We have found approximate expressions for these parameters in terms of a universal function depending on the frequency and the geometry of the wire.

The obtained equations give the possibility to investigate current waves´ propagation along the curved wire without external excitation. In this case the approximate solution can be found by a WKB approach. Moreover, by using the obtained modal parameters, the global parameters can be found. As an example of application of the developed theory we consider the coupling of an external electromagnetic field into the vertical semi-elliptical loop above a perfectly conducting ground. The result of our calculations is in agreement with results of a NEC calculation.

HPEM 18-13: Electromagnetic Field Coupling to a Circular Loop inside a Rectangular Cavity

S. Tkachenko, **J. Nitsch**
Otto-von-Guericke University, Magdeburg, Germany

Nowadays, the description of currents and voltages penetrating into multiconductor wire systems is a major issue in electromagnetic compatibility. In the engineering practice wirings are placed in packages, into enclosures, etc., and into resonator-like structures. Typically, such a cavity is characterized by specific resonant modes. These may interact with the line modes and critically change the usual coupling behaviour.

A general analytical approach to evaluate electromagnetic field coupling into thin wire structures inside cavities has been proposed in the paper of S. Tkachenko, F. Gronwald, J. Nitsch, and T. Steinmetz ("Electromagnetic field coupling to transmission lines inside of resonators", V Int. Symp. on EMC, St. Petersburg, 16-19 September, 2003, pp. 68-74). An exciting electromagnetic field in the cavity can be thought of as being created by penetration through an aperture or by other sources inside the cavity (another radiating antenna inside the cavity, a lumped voltage source in the considered wire, etc). Then the induced current on the transmission line is defined by an electric field integral equation (EFIE), having the Green's function of the cavity as kernel. To solve this equation a hybrid representation of the resonator's Green's function (D. I. Wu, D. C. Chang, "A hybrid representation of the Green's function in an overmoded rectangular cavity", IEEE Trans. on Microwave Theory and Techniques, vol. 36, No. 9, Sept. 1988) is used, which decomposes the Green's function into two parts: a singular part, which looks like a quasi-Green's function of free space, and a resonant part, which can be represented as a sum of eigenmodes of the resonator, located in the frequency domain in the narrow band. It was shown that if the resolving operator for the singular part of the resonator's Green's function is known, the EFIE (which defines an induced current) can be reduced to a system of linear algebraic equations, which order is given by a relative small number in the above mentioned narrow band. Earlier, a finite straight wire parallel to the resonator floor was considered, for which it is convenient to use an approximately resolving opera-

tor in the transmission line approximation.
In the present paper we consider another practically important case-a circular loop inside a rectangular cavity. Since the singular part of the resonator Green's function essentially depends on the difference of space arguments, the resolving operator in this case, as for a circular loop antenna in free space (T. T. Wu, Theory of the Thin Circular Loop Antenna, J. Math. Phys., V.3, N 6, Nov.-Dec. 1962, pp. 1301-1304) can be obtained exactly by a Fourier transform, however, with different modal impedances. Thus it is possible to obtain an exact (within the accuracy of the Green's function decomposition) analytical solution for the considered problem. For an electrically small loop the obtained result merges the earlier investigated result for a magnetic dipole antenna inside a resonator. The results of our calculations for some examples are in agreement with results of numerical calculations.
Using the obtained results it is possible to show that the currents and potentials induced in a wiring inside cavities, as in free space (H. Haase, J. Nitsch, "Full-wave transmission line theory (FWTLT) for the analysis of three-dimensional wire-like structures", Zurich Symposium on EMC, Feb.2001, pp. 235-240, and Interaction Note 561) can be described by a system of first-order differential equations containing (so-called) global parameters which depend on the frequency, on the coordinate along the wire, and they are defined by the geometry of the system. To find these parameters, we have to know the current and potentials induced by a lump voltage source placed at the end of the line (J. Nitsch, S. Tkachenko, "Eine Transmission-Line Beschreibung für eine vertikale Halbschleife auf leitender Ebene", 11. Internationale Fachmesse und Kongress für Elektromagnetische Verträglichkeit, Düsseldorf, 2004, pp. 291-300).
We note that for further investigations the obtained results could be used a basis for the development of a statistical theory (for example, by averaging the obtained results over the azimuth rotation angle of the loop antenna).

HPEM 18-14: Coupling Measurement Technique for Symmetrical Structures Applied to a Generic Missile Mock-up, Called GENEC

F. Sonnemann[1], **G. Staines**[1], **C. Braun**[2], **A. Tänzer**[2]
[1]*Diehl Munitionssysteme GmbH & Co. KG, Röthenbach a.d. Pegnitz, Germany*; [2]*Fraunhofer Gesellschaft FhG-INT, Euskirchen, Germany*

The paper presents measurement results of coupling and propagation of EM-fields in cylindrical systems applied to the GENEC missile mock-up. The measurement technique uses a $\frac{1}{2}$-GENEC configuration over groundplane by taking the advantage of the symmetrical structure of the GENEC. This allows a complete field mapping in the center plane without any disturbing influence of sensors or measurement cables inside the GENEC body. In total 100 sensor positions are available, geometrically fixed by a perforated center plate.
The coupling measurement itself was performed within a GTEM cell at the Fraunhofer Institut FhG-INT in Euskirchen. Coupling data was recorded by using a VNWA at various sensor positions in the GENEC center line for different configurations. The results clearly show the influence of the individual coupling paths (e.g. wing, wing slot, seeker front end) and the influence of integrated PCB and wires.
Coupling data was further processed to achieve the time response for typical UWB and HPM fields. Furthermore, the optimum incident pulse for maximising the field amplitude at a given position inside the GENEC with minimum energy can be determined by using matched filter theory. For a specified maximum incident pulse energy this allows the calculation of the maximum field amplitude for the coupled pulse at critical positions in the body interior (e.g. position of detectors, sensors, electronics). This value can be used to define a certain minimum safe distance for disruption in order to guarantee immunity to standardized EM-fieldstrength levels for any kind of pulse shape.

HPEM 18-15: Measurement Validation of an ILCM Model of a Generic Missile System

S. P. Watkins, **R. Hoad**
QinetiQ, Cody Technology Park, Farnborough, Hants, UK

The Intermediate Level Circuit Models (ILCM) developed by York and Nottingham Universities (University of York and University of Nottingham, "Intermediate Level Modelling Tools for EMC Design - Final Report", EPSRC projects GR/L-89723 & GR/L-89716, 2000) exploit the modal structure of fields within enclosures by representing each mode by an equivalent transmission line. The total solution is determined by summing the solutions for each mode. The accuracy of the total solution is determined by the number of modes included in the summation process. Often, accuracy comparable with that of a full wave solver can be obtained by summation of a few dominant modes in a fraction of the time needed for the full wave solver approach.
A combined work programme is currently being undertaken to develop and validate suitable modelling tools to enable the prediction of interference upset to systems. This is a collaboration between York University (development of ILCM modelling techniques), and QinetiQ (model validation).
The modelling effort and validation exercise centres on a system known as GENEC. GENEC is a simplified modular representation of a generic missile system. The shell of GENEC comprises a hollow cylindrical enclosure, but its modular construction allows additional features such as internal circuitry and winglets to be added so that modelling and measurements can be undertaken for varying levels of complexity. GENEC was designed using CAD techniques so its geometry and physical dimensions are precisely specified to optimise modelling accuracy.
This paper will focus on the RF measurement techniques that were undertaken to validate the ILCM frequency domain models for coupling of internal currents to short monopoles. The measurement techniques that were used to validate these modelled scenarios will be the main topic of this paper.

HPEM 19 - Electromagnetic Compatibility

HPEM 19-1: Mitigation of Power Line Interference on Railroad Wayside Signal Systems

R. Perala[1], **R. Macmillan**[1]
[1]*EMA, Inc*; [2]*CSX Transportation*

High voltage transmission lines and low voltage distribution lines often share a corridor with railroads. The load currents in these lines radiate an electric field that induces voltages and currents in the rails, which are connected by cables to the signal system electronics. These voltages and currents can exceed 100V and 100A at the power line frequency and can have several effects:
- Interference with signal sytem function
- Damage to signal system equipment
- Creation of a human shock hazard

It is therefore important to mitigate this interference to acceptable levels. One approach is to use impedance bonds across the track circuit insulated joints. This has the effect of providing a short circuit across the insulated joints for the interfering currents and thereby reducing the voltage.
The objective of this paper is to describe the induction process and the application of this mitigatiion technique with both analytical and experimental results. In particular, there are significant issues related to the creation and connection of earth groundsto the impedance bond system, especially in double track signal territory.

HPEM 19-2: Filter Design Using the Parametric Resonance Phenomenon

A. S. Adalev[1], **N. V. Korovkin**[2], **M. Hayakawa**[1]
[1]*The University of Electro-Communications, Tokyo, Japan*;
[2]*Otto-von-Guericke-University Magdeburg, Magdeburg, Germany*

At present one of the most important EMC problems is a problem of wide-band passive noise suppression for protecting devices from high-frequency electromagnetic impact. Therefore a large number of works are devoted to the design of a stop-band filter based on a non-uniform transmission line (NTL) that offers a certain advantage compared to ferrite and lumped-circuit filters due to the upper frequency limit absence.
The present work is dedicated to the problems of synthesis of stop-band structures based on NTL with parameters periodically or quasi-periodically distributed along the line. The parameters variation is achieved by changing of the structure geometry (Fig.1a) or medium properties (Fig.1b). It is well known that the resonant phenomena with multiple growth in the impedance are observed in periodical systems with certain relationship of parameter values, exciting force frequency, and spatial period of parameter variation.
The structures considered in the paper under the condition of absolute periodicity (1) are known as photonic crystals and used widely in optics as dielectric mirrors, filters, etc. Lately a keen interest in using photonic crystals in the radio-frequency range is observed. Here in the main they are 2-D PCB structures. The parametric optimization of PCB photonic crystals is predominantly based on enumeration of possibilities and repeated electromagnetic field calculations.
In the paper a TEM model of 1-D structures is suggested. By the model NTL is presented as the plurality of uniform lines connected in cascade. Each line is characterized by the matrix of chain parameters. We examine the voltage transmission coefficient (2) frequency response as an objective characteristic of NTL. Presetting the sufficient value of noise suppression (threshold) in the given frequency range [F1, F2], it is possible to determine a width of the maximum stop-band and to formulate the optimization problem mathematically in the form of (3).
The periodical structures investigation have shown the following.
1. The central frequency of the first stop-band depends on the parameters of the structure according to the expression (4). In addition the widest and deepest first stop-band is observed under the condition (5) that is similar to Bragg's law in optics.
2. There exists a certain optimum NTL length (in our cases 5-10 periods), such that the increase in the line length over this value for the given threshold does not result in the substantial stop-band widening. Under this length the considered stop-band turns into the complete band-gap with a permanent width that is directly proportional to the central frequency and relative variation of the line parameters.
The proposed NTL model based on the TEM approach allows us to carry out the optimization of nonuniformity distribution along the line i.e. to solve the problem (3). In a number of cases there is a possibility of sufficient widening of the stop-band due to changeover from the periodical structure to a quasi-periodical one (Fig.2).
The genetic algorithm is used to get the solution of the problem (3) since such properties of the problem as unevenness and so non-differentiability of the functional, a large number of local extremes and a fairly large number of variables do not allow us to use any gradient method. It is necessary to note that the realization of the genetic algorithm with reference to the problem (3) needs not only a traditional proce-dure of "twins" exclusion but also normalization of variable vectors and smoothing of the objective characteristic by some median filter at the beginning of the optimization.

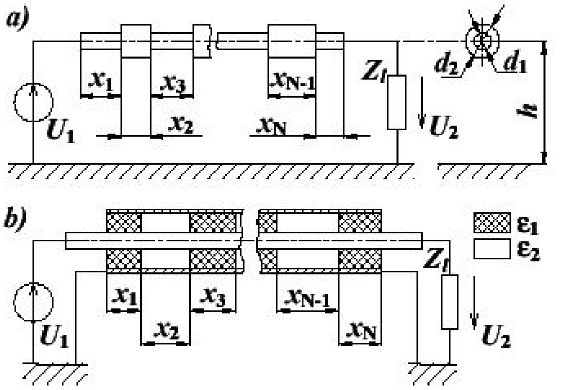

Figure 1: Structures

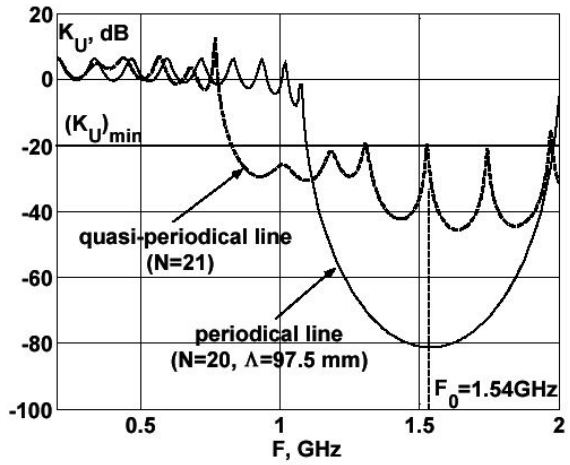

Figure 2: Results

$$x_{2k} = \delta,\ x_{2k-1} = \Lambda - \delta,\ k = 1..N/2 \quad (1)$$

$$K_U = 20\log_{10}\left|\frac{U_2}{U_1}\right| \quad (2)$$

$$\left(\max_{F\in[F1,F2]} \Delta F\right)_{K_U=(K_U)_{\min}} \xrightarrow[\mathbf{X}=\{x_i\}]{} \max \quad (3)$$

$$F_0 = \frac{c}{2\Lambda n_1\left[1+\left(n_2/n_1-1\right)\delta/\Lambda\right]},\quad c = \frac{1}{\sqrt{\varepsilon_0\mu_0}},\quad n_i = c\sqrt{\varepsilon_i\mu_i},\quad i = 1,2. \quad (4)$$

$$\delta/\Lambda = \frac{1}{1+n_2/n_1} = \frac{\lambda_2}{\lambda_1+\lambda_2} \Leftrightarrow \Lambda = \frac{\lambda_1}{4}+\frac{\lambda_2}{4} = \frac{\lambda_{average}}{2} \quad (5)$$

Figure 3: Formulas

HPEM 19-3: Optimisation of an EMP Test Facility for Large Systems

T. Lange[1], **G. Löhning**[1], **M. Koch**[2], **H. Schwarz**[1]
[1]*Brandenburg University of Technology, Cottbus, Germany*;
[2]*University Stuttgart, Germany*

Electromagnetic susceptibility testing of large systems gains more and more importance due to an increasing use of electronics and computer systems. This article deals with a new pulse-based test method for large systems, e.g. railway vehicles, which enables susceptibility testing of the whole system under operating conditions. First EMC tests of an industrial locomotive were already carried out in a prototype facility.
Numerical simulations of the test facility were made in order to optimise generation, propagation and absorption of the electromagnetic test pulses. A circuit model (PSpice) was used to simulate the discharge in the pulse-generating spark gaps. The very high capacitance of the spark gaps was identified as the main cause for oscillations of the generated test pulses. This capacitance forms a resonant circuit with the inductivities of spark channel and electrodes and the spark resistance. By re-designing

the electrode arrangement of the spark gaps these oscillations were strongly reduced (figures 1 and 2). At the same time the amplitude of the field pulses increased by around 50 % and the pulse width decreased from 5 nanoseconds to 3.5 nanoseconds, resulting in a broader usable test frequency range.
A three-dimensional field model of the entire test generator was created with CST Microwave Studio. This simulation model was used for calculation and visualization of the field propagation. We were able to identify points of reflection in the waveguides and to investigate the influence of the equipment under test.

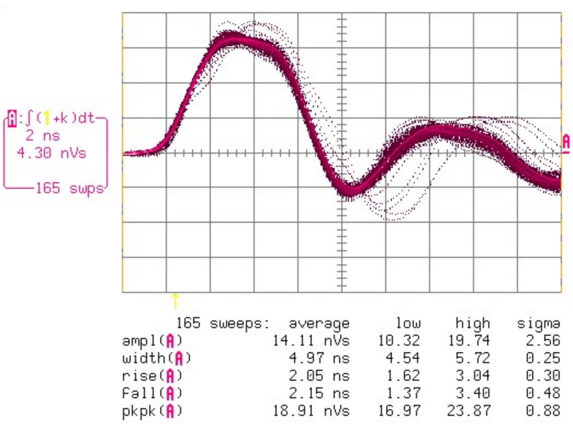

Figure 1: Test pulses before optimisation of the spark gap

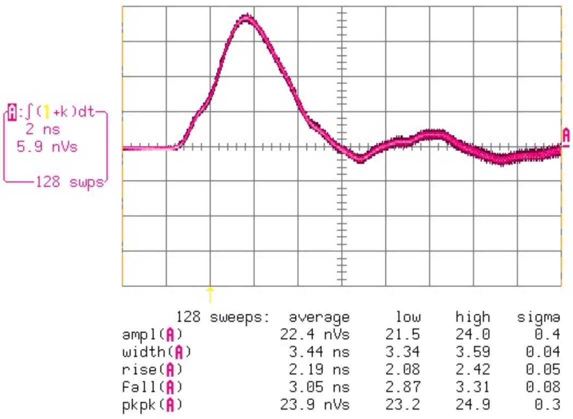

Figure 2: Test pulses with re-designed electrode arrangement

HPEM 19-4: Recursive Modeling of Coupling in TEM-Cells Using Fractional Derivative

A. El Abbazi[1], **B. Haussy**[1], **M. Ramdani**[1], **M. Drissi**[2], **J. L. Levant**[3]
[1]*ESEO Angers,4 rue Merlet de la Boulaye, BP30926,49009 Angers cedex1, France*; [2]*CNRS IETR UMR 6164,INSA de Rennes 20 Av des Buttes de Coesmes, France*; [3]*ATMEL, Nantes*

Summary :
This paper proposes a new theoretical approach using fracional derivative to model electromagnetic coupling. Measurements were performed in order to determine the S-parameter of the coupling between a transmission line and the TEM-cell. The authors compare S parameter measurements with simulations using the proposed model and demonstrate the validity of this approach.
Key words : Electromagnetic Coupling, EMC, Susceptibility, TEM-Cell, fractional derivative.
1.Introduction :
Nowadays, micro-electronic technology implies ever smaller sizes/dimensions (nanometric dimensions). The rise in frequencies, the quick changeovers of internal currents in integrated circuits (IC), the complexity of the manufacturing process are parameters which make the IC ever more sensitive to internal and external aggressions of the component[1]. The noise margin, which is getting slighter, and the ever growing number of aggression sources (Base station RF BTS , Radar, wireless telephony . . .) make proper IC operation more and more difficult to achieve.
In order to predict the susceptibility of integrated circuits to electromagnetic aggressions, our objective is to develop a complete electromagnetic model of the IC.
2. susceptibility of integrated circuits:
Several methods are used for measuring the influence of electromagnetic perturbations in the micro-electronic field. This article deals with measurements using the TEM cell method.
The TEM cell is mainly a rectangular wave guide, which works in TEM mode in a free space where a conductor (Septum), is inserted in the middle of the cell, with a 50Ω adaptation via coaxial connectors (see figure.1)
In our study, we chose a 105-mm long, 3-mm wide transmission line and a 1.6-mm high substrate with 4.7 relative permittivity. This line is placed above the septum, excited by two ports, furthermore two other ports excite the cell in order to estimate the different parameters of the line-cell setup. These measurements are performed up to 3 GHz (figure.2).
3.Fractional derivative method
The use of fractional derivative is nowadays intensive in different domains of physical modeling. For example, in order to model the propagation of damage in viscoelastic materials, a progressive degradation of the mechanical properties of the material is introduced in a recursive manner[4]. Our purpose is to apply the same modeling methodology to the case of electrical losses in a TEM cell.
First of all, an identification of the electrical parameters of its response is performed, then recursive factors are identified in order to match the slope of the S12 S-parameter, and an equivalent model based on the repetition of a simple pattern with degraded parameters is built and simulated. The number of patterns is discussed in order to improve the precision of the model; simulation results are in accordance with experimental data and with results obtained from 3D electromagnetic solvers.
We are interested in this study in the 50Mhz -1.9 GHz frequency band in order to validate our model using fractional derivative.
4.Results :
see figure(3,4)
5.Conclusion :
The establishment of susceptibility models for integrated circuits is a major preoccupation in IC EMC research. Various simulations were performed in order to validate a recursive model using fractional derivative, the results of which proved to be successful.

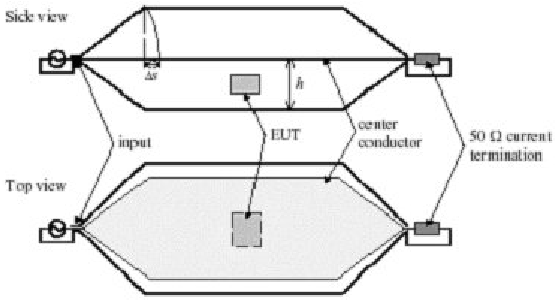

Figure 1: Functional schematic of the TEM-Cell

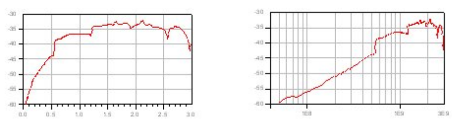

Figure 2: S12 Parameter of the coupling between the cell and the line (measurement) : linear(left) and logarithmic(right)

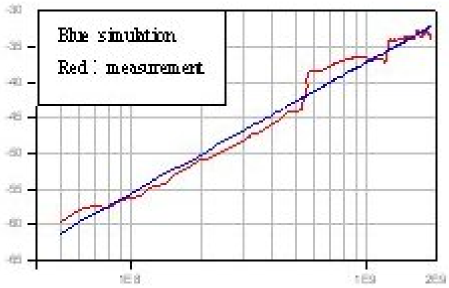

Figure 3: S12 Parameter of the coupling between the cell and the line (measurement and simulation)

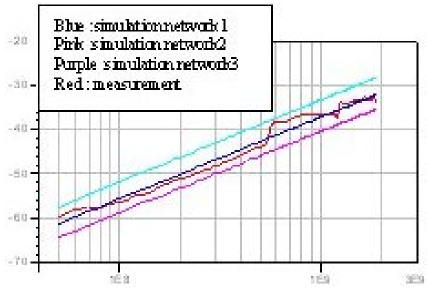

Figure 4: S12 Parameter of the coupling for different networks

HPEM 19-5: Storing Independent Passive Loggers of a Pulse Magnetic Field

V. P. Goncharov, **V. A. Ksenofontov**, **V. F. Molochkov**, **M. M. Filatov**
Research Institute of Pulse Technique

The independent passive loggers are intended for diagnostics of pulse magnetic fields with duration from 0,1 ms and more, at absolute value of a magnetic induction from 0,1 T up to 1 T. The pulse signal can be both unipolar, and two-polar, by the way of two half-waves, with amplitude of the second half-wave it is no more 0,7 from amplitude of the first half-wave. Dimensions of loggers are no more than 7 $\times$ 5 mm. Storage time of the information is not less than 24 hours.

The loggers make induction maximum monitoring of a pulse magnetic field. They can be utilized at trials of different radio-electronic and electrotechnical instrumentation on resistance to pulse electromagnetic effect, in experiments on lightning simulation. The loggers do not include power supplies, measuring lines and electronic components. The small dimensions and construction of loggers enable to use them in hard-to-reach places, hermetic volumes, and also in requirements, where the effect of plurality of the unfavorable factors does not admit presence of staff. The usage of loggers allows to easy the procedure of an information accumulation at multipoint measurements of pulse magnetic fields, that it is important especially for cost intensive single-pass experiments.

Basis of loggers is small-sized solid-state magnetic elements having a remanence. At measuring these elements made in cases, are disposed in the. After transiting an impulse magnetic field the loggers are extracted from the tested area and then performed sequential measurements of their remanence by a contactless way with the help of a fluxgate type reader of the information. The usage of this high-sensitive reader allows to register a weak dispersion field that enables to reduce dimensions of loggers up to several millimeters. The preparation of loggers for performing the following cycle of measurements is made by a compact pulser of a strong magnetic field.

The productivity of loggers was confirmed at multipoint measurements of a pulse current with amplitude about 100 kA, shaped at high voltage discharge experiment on simulation of lightning effect on the open area. The measuring of the current was carried out on its magnetic field, in conditions, extremely unfavorable for operation of usual recording devices (pulse electric field up to 1 Mv/m, poor weather conditions). The parallel measurements that have been carried out with the help of fibre-optical channels, have yielded results conterminous to limit of measurement errors.

HPEM 19-6: On the Measurement of the Transfer Impedance for Shielded Cables

S. Tkachenko, **N. V. Korovkin**, **J. Nitsch**, **H.-J. Scheibe**
Otto-von-Guericke-University, Magdeburg, Germany

The necessity to define the cable transfer impedance arises in many EMC problems which are connected with the operating system itself and with its susceptibility to external disturbances. Nowadays, operating and disturbance frequencies increase continuously. As a consequence, the transfer impedance also increases with frequency, in particular for cables with braided shields. Therefore, the development of new and the improvement of available methods of experimental studies of the cable transfer impedance are essential.

The usually used method for the experimental estimation of the transfer impedance Zt, the so-called current line method, yields stable results for the frequency range up to hundred MHz. As the frequency goes up, the measurement error increases noticeably. This phenomenon is caused by the resonances of the used experimental set up. A characteristic dimension of the measurement unit is about 1 m; therefore first resonances appear for frequencies about 75 MHz. The technique of Gonschorek et. al.(Gonschorek, K-H., Tiedemann, R., "Messung der komplexen Kabeltransferimpedanz bis 2 GHz", In: Schwab, A. (Hrsg): EMV 2000. Duesseldorf, VDE Verlag, 2000) is able to compensate this measurement error by specific calculations up to several GHz. The extraction of reliable values for the transfer impedance for higher frequencies is difficult. Therefore the development of high – frequency measurement techniques for the transfer impedance is a subject of interest.

In the present paper we propose a new technique for the transfer impedance measurement by the experimental set up shown in the Fig. 1. The cable under test is placed into a GTEM cell. A current in the cable shield is excited by an incident plane electromagnetic wave, with the propagation direction which is shown in Fig.1. The voltage across the internal load induced by the shield current is measured. The internal conductor is terminated with the characteristic impedance at the other end. For the considered geometry the shield current is obtained by an exact electrodynamical solution which can be calculated by a Fourier transform (J. Nitsch, S.Tkachenko, "Eine Transmission – Line Beschreibung für eine vertikale Halbschleife auf leitender Ebene",11 Int. EMC Congress Düsseldorf, 2004.). With this solution and the obtained experimental data it is possible to define a transfer impedance of the investigated cable. The proposed method was applied (using the GTEM cell of the Otto-von-Guericke University) in the frequency range from 5 MHz up to 1.8 GHz. The observed results in the low-frequency region are in agreement with the results obtained by the current line method. However, the proposed method does not have the problems of the current line method in the high-frequency region beyond 500 MHz. Thus, in the authors' opinion, the proposed method is promising for experimental investigations of the transfer impedance of shielded cables.

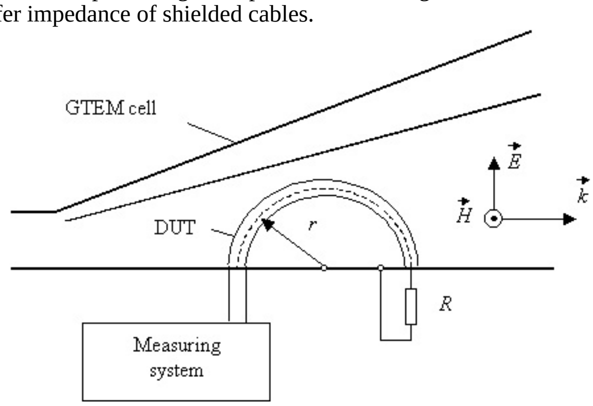

HPEM 19-7: Time-Domain Modeling of Skin Effect for Improved SI Analysis of Interconnect Systems and Packages

A. E. Engin[1], **W. Mathis**[2], **W. John**[3], **G. Sommer**[3]
[1]*FhG-IZM / University of Paderborn*; [2]*University of Hannover*; [3]*FhG-IZM*

Chip packages and printed circuit boards provide the interconnection between integrated circuits in digital systems. Due to the increasing bit rates and faster rise times in high-speed digital systems, the parasitics associated with the package leads and PCB interconnects need growing attention regarding the electromagnetic compatibility (EMC) and signal integrity (SI) (Ege Engin, Mart Coenen, Heiko Koehne, Grit Sommer, and Werner John. "Three-Pole Analysis Model to Predict SI and EMC Effects". EMC Compo, 3rd International Workshop on Electromagnetic Compatibility of Integrated Circuits, p. 105–8, November 2002). A bottleneck of interconnect simulation is the accurate modeling of skin effect resistance, since a lumped model representation for the frequency-dependent skin effect resistance and internal inductance cannot be obtained in a straightforward manner.

The external inductance, which is due to the magnetic flux external to the conductors, can be assumed to be constant. The internal impedance is defined as the sum of the resistance and the reactance due to the internal inductance; therefore it forms the basis for modeling of skin effect. Equation (1) shows a commonly used approximation for the internal impedance (C.R. Paul. Analysis of Multiconductor Transmission Lines. John Wiley and Sons, 1994), where "s" is the Laplace variable. Implementation of equation (1) in skin effect simulations has been limited to the frequency-domain, since it represents a non-rational impedance. Various realizations of the immittance "sqrt(s)" have been extensively discussed in (Suhash C. Dutta Roy. "On the Realization of a Constant-Argument Immittance or Fractional Operator". IEEE Transactions on Circuit Theory, Vol. 14, p. 264–274, September 1967). We use the rational function approximation of "sqrt(s)", which is RL impedance realizable. A general overview and some interesting results for the realization of nonrational functions can be found in (V. Belevitch. "On the Realizability of Non-Rational Positive Real Functions". International Journal of Circuit Theory and its Applications Vol. 1, p. 17-30, 1973).

We rewrite the internal impedance as in equation (2), such that "B=B1*sqrt(B2)", and substitute the square root term with its rational polynomial approximation. The parameters in equation (2) can be obtained by ensuring that three important variables are modeled correctly: dc resistance "Rdc", dc internal inductance "Ldc", and the skin effect resistance "R(f1)" at frequency "f1". If we substitute "s=jw", the rational polynomial tends to the impedance given in equation (3) at dc as a first order approximation. The parameters "B1" and "B2" can be obtained simultaneously from equations (4,5), which provide the correct skin effect resistance and dc internal inductance. Finally, the correct dc resistance can be obtained by setting the parameter "A" as in equation (6), which merely implies that the first resistance term in the synthesis of the rational polynomial should be set as Rdc. The internal impedance of a round wire can be computed analytically using modified Bessel functions of the first kind as in equation (7), where "r" represents the radius. The proposed model has been applied on the example of a round wire using "n=8", which is RL impedance realizable with "N=n+1=9" number of elements. A very good correlation between the proposed model and the exact results computed using the analytical expression can be seen in Figure 1, both in real and imaginary parts. Figures 2 and 3 show the resistance and partial inductance of a 1m long conductor with a square cross-section (4.62mm x 4.62mm), which were computed with the freely available tool FastHenry. Since the external inductance, which is included in the figure, dominates the behavior at high frequencies, the total inductance can be modeled very accurately at all frequencies using a small number of elements. It can be seen how the bandwidth of the model regarding the skin effect resistance can be extended by including more elements in the rational polynomial approximation, if it is required.

Acknowledgements:
The reported R+D work in this abstract was carried out in the frame of the Eureka project MEDEAplus MESDIE A 509 - Microelectronic EMC Design for High Density Interconnect and High Frequency Environment. The MESDIE project deals with the analysis and optimization of electromagnetic compatibility aspects on high speed and high density silicon and package design applications, respectively. In this frame the reported particular results are part of a task which aims at the modeling of transmission lines and power/ground planes. This particular research was supported by the BMBF (Bundesministerium fuer Bildung und Forschung) of the Federal Republic of Germany under grant 01M 3061 J. The responsibility for this publication is held by the authors only.

$$(1)\quad Z(s) = A + B\sqrt{s}$$

$$(2)\quad Z(s) = A + B_1\sqrt{B_2 s} \approx A + B_1 \frac{\sum_{r=0}^{p}\binom{n+1}{2r}(B_2 s)^r}{\sum_{r=0}^{q}\binom{n+1}{2r+1}(B_2 s)^r} = Z'(s),$$

$$\text{where } p = q = n/2 \text{ for } n \text{ even and}$$

$$p = (n+1)/2,\ q = (n-1)/2 \text{ for } n \text{ odd}$$

$$(3)\quad \lim_{\omega\to 0} Z'(j\omega) \approx \frac{B_1}{n+1} + j\omega B_1 B_2 \frac{n^2+2n}{3n+3}$$

$$(4)\quad R(f_1) = B_1\sqrt{B_2 \pi f_1}$$

$$(5)\quad L_{dc} = B_1 B_2 \frac{n^2+2n}{3n+3}$$

$$(6)\quad R_{dc} = A + \frac{B_1}{n+1}$$

$$(7)\quad Z_{coax}(j\omega) = \frac{\sqrt{j\omega\mu/\sigma}}{2\pi r}\frac{I_0(r\sqrt{j\omega\mu\sigma})}{I_1(r\sqrt{j\omega\mu\sigma})} \quad \text{Ohm/m}$$

Figure 1 : Internal impedance of a round wire

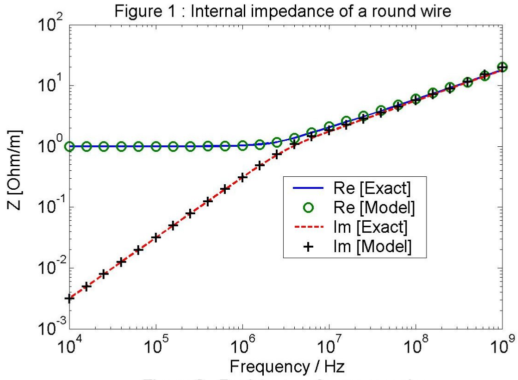

Figure 2 : Resistance of a square wire

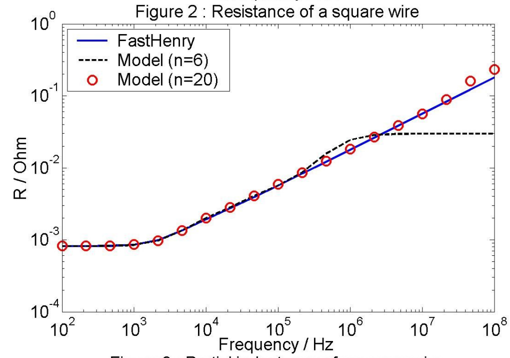

Figure 3 : Partial inductance of a square wire

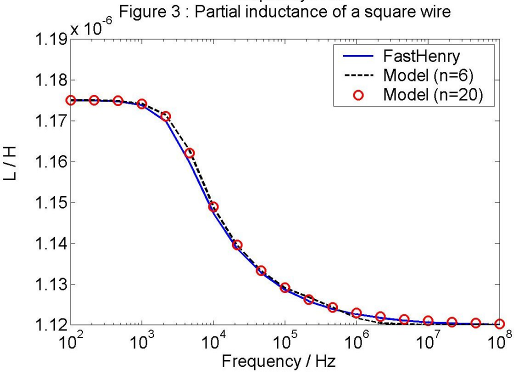

HPEM 19-8: A Recording Technique to Enhance the Dynamic Range of a Time-Domain EMI Measurement System

S. Braun, **P. Russer**
Technische Universität München, Germany

0. Abstract
In this paper a dynamic-enhanced ultra-fast, broadband time-domain EMI (TDEMI) measurement system is presented. Measurements were performed in the 30 - 1000 MHz range. Using digital signal processing for spectral estimation and detection, the measurement time is reduced by a factor 10 in comparison to a conventional EMI Receiver. Dynamic performance is improved by using 2 analog-to-digital-converters (ADCs) in different amplitude resolutions. Thus the dynamic range is enhanced by up to 18 dB. In this paper an algorithm to set up the optimal amplitude resolution for each ADC in order to maximize the signal-to-noise Ratio (SNR) is described. By measurements of the emission of a hand held mixer, an improvement of the dynamic range by 14 dB is shown.

1. Introduction
EMC and EMI measurement equipment which allows to extract comprehensive and accurate information within short measurement times will allow to reduce the costs as well as the time to market of electronic systems. The drawback of todays EMI receivers is the long measurement time. Spectral estimation via Fast Fourier Transformation (FFT) allows to reduce the measurement time by a factor of more than 10. The drawback of such a system is the limited dynamic range given by the resolution of the ADC. Subdividing the amplitude range in two or more intervals and performing the AD conversion in these intervals with different amplitude resolution allows to enhance the dynamic range.

2. TDEMI measurement system
A TDEMI measurement system has been presented in (F. Krug and P. Russer, The Time-Domain Electromagnetic Interference Measurement System," in IEEE Transactions on Electromagnetic Compatibility, May 2003). It consists of a low noise amplifier, an anti-aliasing lowpass filter, an oscilloscope for data acquisition and a PC for digital signal processing. In Fig. 1 the dynamic enhanced TDEMI measurement system is depicted. By a power splitter the analog signal is provided both ADCs. The amplitude resolutions of both ADCs are chosen different from each other. ADC1 is set to cover the complete amplitude range whereas ADC2 is set to a higher sensitivity. ADC2 is clipping the amplitude peaks of the input signal but yields a higher resolution at lower signal amplitudes.

3. Signal-to-noise Ratio
In order to obtain a time-dependent spectrum, which is used to evaluate the spectrum under the different detector modes (F. Krug, S. Braun, Y. Kishida, and P. Russer, A novel Digital Quasi-Peak Detector for Time-Domain Measurements," in 33th European Microwave Conference, Munich, Germany,2003), the STFFT (L. Cohen, Time-Frequency Distributions - A Review," in Proceeding of the IEEE, 1989) is used. By the window function the IF-Filter is modelled. For the SNR we consider the SNR of each calculated spectrum during the STFFT. Thus we obtain also time-dependent SNR. An example of a signal in time-domain of a hand held drill machine, and the corresponding SNR and spurious free dynamic range (SFDR) for one ADC is shown in Fig 2.

4. Optimum Amplitude Resolution
For a single signal acquisition the amplitude resolutions of the ADCs are set to provide a maximum SNR for the whole acquisition. By the first ADC the signal is recorded without any clipping. In order to set up the second ADC we consider the relative frequency of the sampled discrete values of the first ADC. Certain values show a relative frequency that is several orders of magnitudes higher than the rest of the values.
The quantization noise level P_N is given by (1) where d_i is the quantization step of the ADC i, and $H[k]$ is the relative frequency of the quantization value k. In order to minimize the noise level during acquisition the second ADC is set up to sample the range of values where the the relative frequency is very high. We divide the amplitude range into three intevals. The interval $I_1 =]a_{21}, a_{22}[$ is digitized by the second ADC and the amplitude interval $I_2 = [a_{11}, a_{21}]$ and $I_3 = [a_{22}, a_{12}]$ that are digitized by the first ADC. a_{21} and a_{22} are calculated to have minimum noise level.
The optimized values for a_{21} and a_{22} are taken to simulate the SNR and SFDR of the system with 2 ADCs. The result is shown in Fig. 2. The SNR is enhanced by about 18 dB. Further simulations show that the used amplitude resolutions also enhance the dynamic range of the TDEMI measurement system for all other occurring transients, that are emitted by the hand held mixer. Though the amplitude resolution does not perfectly fit, the dynamic range is in this case enhanced about 13 dB.

5. Measurement Results
In Fig. 3 the measurement of a hand held mixer is shown. The measurement was performed in the frequency range 30 - 1000 MHz. A low pass filter with a stop-band attenuation of 60 dB at 800 MHz was used to evaluate only the noise originating from the measurement system. In the measurement an improvement of the dynamic range up to 14 dB is shown.

6. Conclusion
The presented TDEMI measurement system allows spectral estimation with a higher dynamic range by using two ADCs in different amplitude resolutions. It was shown that for a transient signal
the Dynamic Range is improved about 14 dB. Though the recording was performed with two ADCs, the measurement time is reduced by a factor of 10 in comparison to a conventional EMI-Receiver.

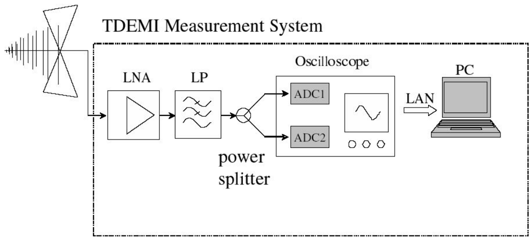

Figure 1: TDEMI Measurement System

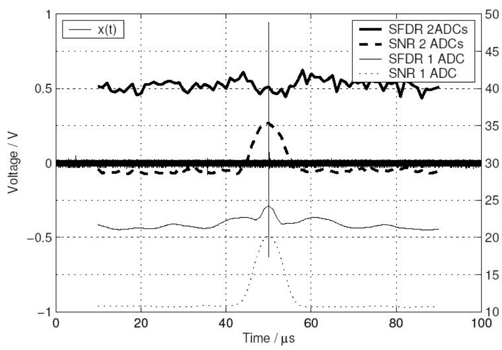

Figure 2: SNR and SFDR of a system with 1 ADC and with 2 ADCs

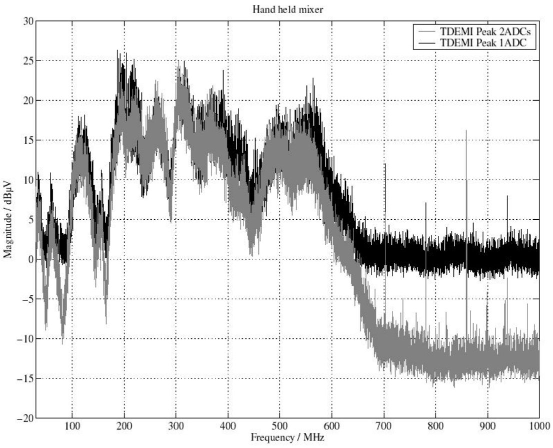

Figure 3: Spectrum of a hand held mixer

$$P_N = \frac{1}{12N}(d_1^2 \sum_{k=a_{21}}^{a_{22}} H[k] + d_2^2(\sum_{k=a_{11}}^{a_{21}} H[k] + \sum_{k=a_{22}}^{a_{12}} H[k]))$$

Equation 1

HPEM 19-9: Analysis of Effect of External Wave on a Lossless Microstrip Bended Line

B. Biglarbegian
Iran University of Science and Technology

In this paper analysis of effect of radiation of an external magnetic field on a lossless bended microstrip line is discussed. In recent years utilization of integrated planar circuits, because of their low cost, low weight and ability of integration with other important elements of circuit, has been developed in different electronic and communication systems. In these circuits, microstrip lines has interface role. Calculating induced voltage and current, caused of external waves for immunizing against such distortions is necessary. In many papers effect of external wave on the microstrip line has been studied. In this paper based on method of (Bernardi, P.; Cicchetti, R.; Response of a planar microstrip line excited by an external electromagnetic field, Electromagnetic Compatibility, IEEE Transactions on, Volume: 32, Issue: 2, May 1990) and developing this method for bended microstrip lines, distributed voltage and currents for this microstrip bend is calculated. In the problem solved by (Bernardi, P.; Cicchetti, R.; Response of a planar microstrip line excited by an external electromagnetic field) after calculating induced voltage and current sources in the line caused of external wave, by using Green's function of this structure, distributed voltage and current can be calculated. But in this structure (fig1) calculating Green's function is not a simple task. So we will solve the differential equation of this structure directly. And by applying the circuit equivalent of the bend and having 4 equations showing relation between currents and voltages in the load places and the bend, one can find the voltage and current at the load or bend place. Then finding the other voltage and currents is a simple task. In this paper we have outlined this voltage and currents and as a result we have assumed a 2 line with equal length and (fig2) shows the induced voltage and current one branch of line.

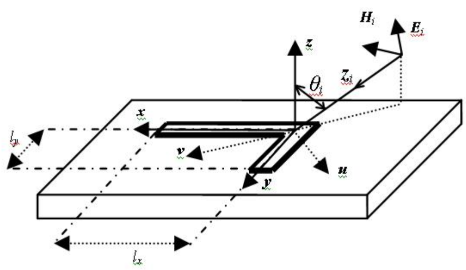

Figure 1: a microstrip bend and an external wave is radiating on it

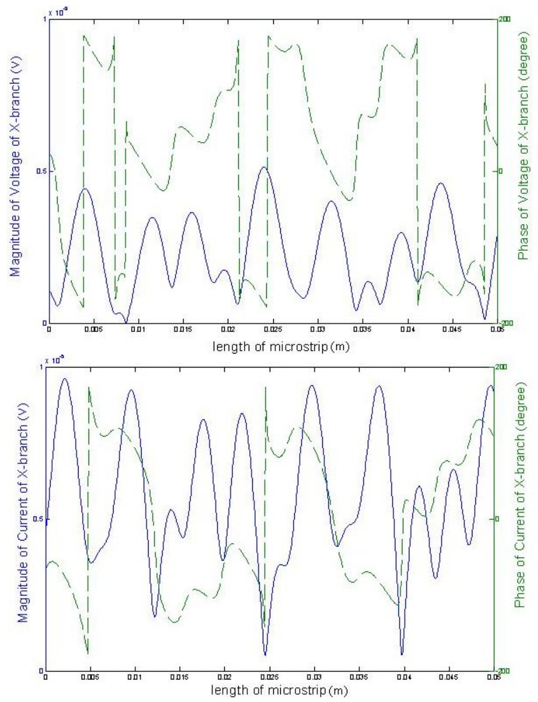

Figure 2: magnitude and phase of voltage and current of x-branch

HPEM 19-10: The Right Pinning to Reduce the Electromagnetic Emission of Integrated Circuits

B. Deutschmann[1], **G. Winkler**[2], **T. Ostermann**[3], **A. Tanda**[3]
[1]*austriamicrosystems AG*; [2]*Technical University of Graz*; [3]*University of Linz*

As more and more complex functions are required in modern IC designs, there is also an increasing need to integrate these functions in the right package. For modern IC products, packaging is an integral part of the chip design and production process because IC packages have to meet the performance requirements of today's high-speed applications. Not only the package, also the right location of the pins (especially the location of the GND and VDD pin) plays an important role in the generation of unwanted electromagnetic emissions of integrated circuits. This presentation will show the improvements that can be reached in the electromagnetic emission when the right pinning is chosen for the power supply.

IC package types have evolved from the early DIP (Dual Inline Packages) to a variety of packages ranging from ultra-thin SOPs (Small-Outline Packages) and CSPs (Chip-Scale Packages) for low-pin-count applications to BGAs (Ball Grid Arrays) and MCPs (Multi-Chip Packages) with over 1,500 solder ball connections. Modern ASICs (Application Specific Integrated Circuits) with their advanced functionality need high-lead-count packages to successfully interface with the rest of the system. As additionally the number of I/O pins increases, the number of power supply pins must be increased, too in order to keep the ground noise and the electromagnetic emission to a minimum. This leads to an annual growth rate of 10-11 percent of the number of pins or balls per package. In 2005 the expected number of pins/balls on an advanced ASIC will be more than 3,000.

The impact of the parasitic inductances on ground bounce seems to be obvious. Ground lead inductance is a strong function of the package type. Additionally the electromagnetic emission of an integrated circuit depends on lead lengths as well as the location of GND/VDD pins in the package. It was found that a die assembled with a center pinout of the GND and VDD pins has approximately 10-15% less ground bounce than a die assembled with the standard pinouts (corner pinout). In our presentation we will show the effect of corner vs. center pinning of the power supply pins on the electromagnetic emission of an IC. The elec-

tromagnetic emission of an EMC-test chip is measured using the so-called TEM-cell method, which is described in the new standard for the characterization of the electromagnetic emission of ICs (IEC 61967-2). Furthermore, the use of multiple GND and VDD pins offers, by adding more parallel GND and VDD inductances on a chip, advanced products with lower ground noise compared to other products with only one GND and one VDD corner pin. Multiple ground/power pins improve the electromagnetic emission of an IC by reducing the total ground/power lead inductance.
Figure 1 shows a first measurement result of the radiated emissions in a frequency range from 150kHz – 1GHz of an EMC test chip using corner pinning. According to the IEC 61967 standard the maximum electromagnetic emission of an IC can be characterized by two letters and one number. As can be seen, in this case the maximum emission can be figured out as “Cb”. In the second measurement center pinning is used instead of corner pinning. The measurement result of figure 2 clearly indicates that the electromagnetic emission of the EMC test chip has been reduced. The reduction is about 10dB in some frequency ranges. Additional to the experimental results we will show in our presentation the modeling and simulation of the influence of the “right” pinning on the EME of ICs.

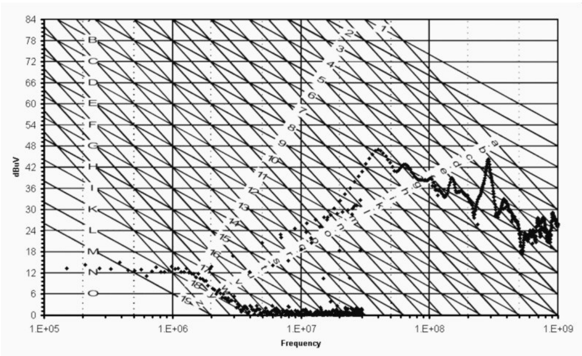

Figure 1: Maximum electromagnetic emission corner pinning

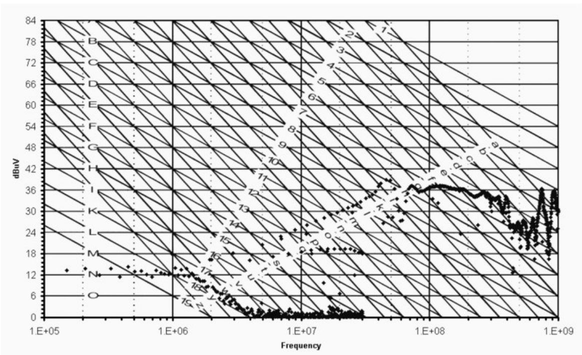

Figure 2: Maximum electromagnetic emission center pinning

HPEM 19-11: Synthesis of Nonlinear Compensators as Truncated Volterra-Picard Series

N. V. Korovkin[1], **J. Nitsch**[1], **E. Solovyeva**[2]
[1]*Otto-von-Guericke-University, Magdeburg, Germany*; [2]*State Electrotechnical University St.-Petersburg, Russia*

One of the important current problems to compensate nonlinear distortion-signals is the prevention of low-frequency noises that arise from the intermodulation of two-tone (high-frequency) input signals due to nonlinearities in the input blocks of electronic devices. It is possible to show that low-frequency oscillations occur even in the case when high-frequency protection filters are used. The presented method simplifies the synthesis of the nonlinear compensator which is considered in our work “Suppression of Two-Tone Disturbances in Nonlinear Circuits”.
The method of the compensation of nonlinearities is based on the representation of operators of the initial nonlinear device and on the compensator synthesized by a truncated Volterra-Picard functional series (VP-series). The problem of the nonlinear compensation consists in the removal of nonlinear components in the truncated VP-series of the initial nonlinear device. This problem is solved with the aid of the special formation of parameters (Volterra kernels) in the finite VP-series of the compensator. The method of the nonlinear compensator synthesis consists in the following:
- The output signal of the initial nonlinear device is represented as finite VP-series with the help of Picard’s iterative procedure.
- Volterra’s kernels of the initial nonlinear device are extracted from the obtained VP-series.
- Volterra’s kernels of the compensator obtained from the linearisation conditions are formed on the basis of the above-mentioned kernels of the initial nonlinear device.
- The VP-series operator of the nonlinear compensator is constructed and the obtained mathematical model of the compensator is realized as a nonlinear circuit.

Advantages of the presented method consist in the following:
- There is no problem with the ambiguity of the parameters for the compensating circuit (this problem is of principal nature for the compensator synthesis by the method of suppression of two-tone disturbances).
- The truncation of Picard’s iterations simplifies the synthesis procedure since Volterra’s kernels of the compensator are formed separately.
- The mathematical description of the compensator can easily transformed from the pre-compensator to the post-compensator and vice-versa.
- The finite VP-series of the compensating circuit has a simple form, convenient for the synthesis and practical realization of the compensator.

In our work examples of the synthesis of nonlinear compensating circuits are presented and the degree of low-frequency noises compensation is evaluated.

HPEM 19-12: Experience of the General Estimation of a Power Transformers Technical Condition on the Basis of Own Electromagnetic Radiation Spectrum Analysis

N. Silin[1], **A. Popovich**[2], **M. Belushkin**[3], **V. Katanaev**[3]
[1]*Far-eastern state technical university*; [2]*Institute of automatic and control processes* ; [3]*Maritime State University*

Last years both in Russia and abroad the researches on perfection existing and to creation of a new quality monitoring in operation of a transformers condition as a whole and separate units are actively realized. For the continuous control of working transformers are widely used: the analysis of the gases dissolved of oil, measurement and localization of partial discharges, methods and means of temperature definition of the most heated points. Particularly, the analysis of the gases dissolved of oil is an indirect method of definition of various defects development on presence of the gases dissolved of oil, as a rule, hydrogen, methane, ethane, ethylene, acetylene, oxide and dioxide of carbon. Up to 60 % of transformers defects are connected to rise and development of partial discharges which intensity is associated with total gas content in isolation. Quantity G characterizes a dielectric destructiveness under influence of partial discharges, overheating and its oxidations from contact with air oxygen. The processes connected with gassing, cannot be accompanied by rise in temperature, however communication of these processes with partial discharges the most direct.
Researches on measurement and the analysis of own electromagnetic radiation of the high-voltage electro power equipment in a wide frequency band with the purpose of its current technical condition estimation have been started in 90th years of the last century. It is supposed, that own electromagnetic radiation, particularly, the power transformer alive is the electro physical process describing an object condition and its separate units, and also dynamics of isolation quality change on stream. The sources of electromagnetic radiation are various kinds of dis-

charges: corona discharge, superficial partial discharge in internal isolation. The spectrum upper bound from corona discharges makes 100-150 MHz. These signals almost are not observed higher then 100-150 MHz. Time of the partial discharge in entrapped gas makes 10E-8 – 10E-9 second. Hence, the top part of a frequency band from discharges in the gases contained in oil, can stretch up to 10 GHz. The condition of high-voltage isolation, and also process of its ageing (degradation) vastly depend from the presence of gas inclusions, process of gases allocation, and consequently also partial discharges intensity. Measurement of a gases concentration degree entails change of the own electromagnetic radiation general capacity of the equipment, and this information broadcasts continuously.

In the majority of Russian power supply systems the values of gases boundary concentration witch are resulted in normative documents “Management directive 34.46.302-89” and completely transferred in new “Management directive” (values SO; and SO2 are changed only) are used. Recently the tendency to revision of maximum legitimate values G was designed, having provided their definition for each power supply system separately. It is required to reconsider also boundary concentration of gases through the certain term of operation (5-7 years) for each class of a voltage. Thus, uncertainty of this parameter, which values strongly depend on objective (various age structure and design features of transformers, distinctions of used technologies, methods and means of measurements) and biased (a different level of the organization and qualification of personnel) reasons compel to searching for new criterions, and also the integral quantity which reflecting a degree of a gas content isolation [Dividenko I.V., Komarov V.I. Use of mathematical statistics methods for reception of criterions of an estimation of a power transformers condition by results of chromatographic analysis of the gases dissolved of oil. Electro, No1, 2003]. Such parameter can become energy of a spectrum of the electromagnetic measurement accompanying work of each high-voltage equipment unit.

On fig. 1 signals power spectral densities of own electromagnetic radiation near the power autotransformers 500 KV in a range from 40 up to 460 MHz are submitted.

All diagrams resulted on fig. 1 are characterized by intensive radiation in a range from 45 up to 150 MHz and less powerful signals on higher frequencies, the saturation of a spectrum very non-uniform.

The comparative analysis of spectral density for such same equipment as transformers, allows revealing background spectrum of electromagnetic radiation, characteristic for the given substation and by that to exclude it from the further analysis.

Let’s allocate a site of autotransformers spectrum of phases A and B in ranges of 210-250 MHz and 390-430 MHz. In these ranges steady excess of signals spectral density level of a phase B above a phase A (fig. 2) is observed. The technical condition of researched transformers was known and was characterized by the following data:

· the condition of isolation of high-voltage inputs 500 and 220 KV phases A was in norm (one of inputs recently has been replaced on new), chromatographic analysis of oil did not specify excess of a critical mark total concentration of gases (G = 1,242 %), separate components on gases (Ginputs = 0,011%; Gtank+ruv = 1,231%);

· the condition of phase B inputs isolation was in norm, however parameter G = 0,04372 % exceeded a corresponding parameter of a phase A (G=0,02619 %) in 1,9 times.

Spectrum energy in a range of frequencies from f1 up to f2 calculate by formula: (fig. 3)

For a range 210 – 250 MHz the quantity of spectrum energy in relative units has made: phase A - 107043.75, phase B - 190743.82. Excess of spectrum energy for a phase B above a phase A makes 1.78 times.

The comparative spectrum energy analysis for a range of 400-440 MHz has gave the following results: a phase A - 74870.45, a phase B - 82711.13; energy ratio EB/EA=82711.13/74870.45=1.1.

Thus, dividing a range into sub-bands and calculating spectrum energy in them, it is possible to reveal a maximal excess size of the spectrum energy value. In our case the comparison of spectrum energies values in sub-band 210-250 MHz has shown the maximal excess of phase B radiation above phase A.

Let’s consider other autotransformer. It’s technical condition was characterized by normal parameters on phase A. Gas content of a phase A on inputs makes GA=0.00755 %, and the phase B is characterized by value GB=0.03981 %. The ratio of concentration of gases makes GB/GA=5.27.

The ratios of spectrum energies in a frequencies range 210-250 MHz make: EV/EA=258044.23/92321.08=2.8. Excess of phase B values above phase A is obvious. However the general gas content of phases has more smaller difference: GA=0.73855 % and GB=0.75421 %, - that makes GB/GA=1.021.

Correlation between gas content, a technical condition, and size of spectrum energy of electromagnetic radiation at other autotransformer also confirms, that once again indicates to expediency of application of such comparison method.

Resume:

1. The results indicating communication, between concentration of gases in isolation of the high-voltage equipment and intensity it’s own electromagnetic radiation are received;

2. The further researches should be aimed at the received statistical data on correlation a spectrum energy with the parameters determining gas content in isolation;

3. Final sum of spent researches can become manufacture of the new criterions reflecting a degree of an isolation gas content, and also development of principles of the continuous control of an isolation condition.

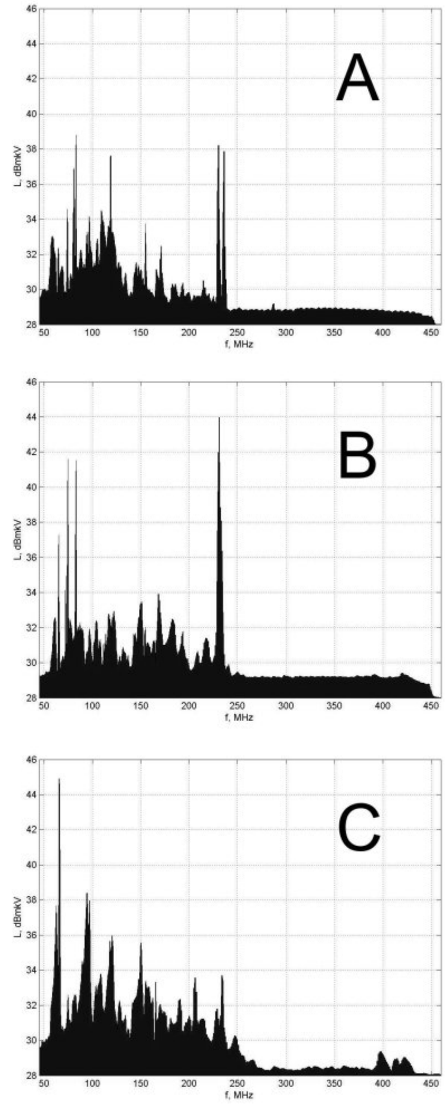

Figure 1: Spectrums of electromagnetic radiation, in time 20 seconds, near the power autotransformers, phases: A, B, C from top to down accordingly.

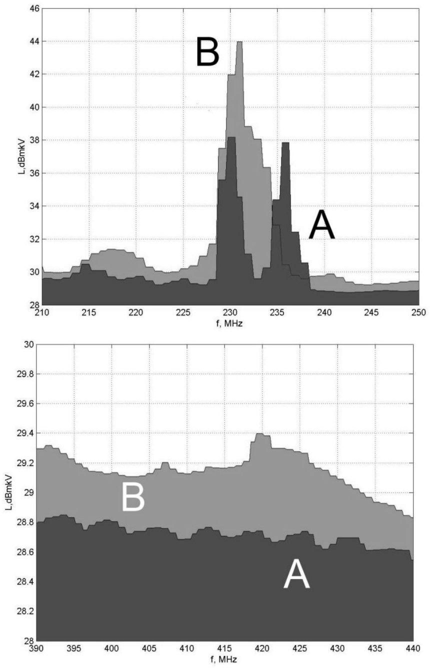

Figure 2: Spectrums of electromagnetic radiation, in time 20 seconds, near the power autotransformers, phases A and B in frequency band: a) 210-250 MHz; b) 390-440 MHz.

$$E(f) = \int_{f_1}^{f_2} S_U^2(f)df$$

Figure 3: Formula for spectrum energy calculation in a range of frequencies from f1 up to f2

HPEM 19-13: External Magnetic Field Analysis of Electric Machines

M. Roytgarts
OJSC "Power Machines" Brunch "Electrosila", Turbogenerator Department

The modern electric machines are powerful concentrators of magnetic field energy. For example, in turbogenerators power of 110 MW, the magnetic flux amounts to 4.4 Wbs, and by the further power increasing, it rises proportionally on the average to power. The part of a magnetic flux is closed through the ambient space outside of an electric machine, influences operation of electronic equipment, and also effects on an environment and servicing staff.
The basic sources of external magnetic fields of electric machines, feature of their distribution, dependence of fields on geometrical and electromagnetic machine parameters, degrees of saturation, efficiencies of shielding of a magnetic field by structural elements are examined in this paper. On external magnetic field analyzing, the conditional separation of ambient space into near-field and far-field zones is used.
The method of an approximated estimate of an external magnetic field of a series of the geometrically similar electric machines by the results of the calculation or the field measuring of the base machine of a series is given.
The influence of machine external surface configuration, housing and end shields on the value and spatial distribution of an external magnetic field is studied.
The results of experimental investigations of an external magnetic field in the near-field zone of a powerful turbogenerator and household electromotor are applied. The measurings were carried out under the no-load testing condition at rated voltage on the stator terminals and under the sustained short-circuit condition at the stator rated current. The internal field in stator and turbogenerator end zone was simultaneously inspected.
It is shown, that at the magnetic field action determination, it is necessary to take into account both induction local values, and integrated characteristics, for example absorbed power or magnetic field energy.
REFERENCES
[1] GOST R 50010-92 Electromagnetic compatibility of technical means. Force electrical equipment. Limits for the low-frequency periodical electromagnetic field, Moscow, p.4, 1993.
[2] A.Henneton, D.Roger, E.Napieralska, "Study of electromagnetic phenomena contributing to external radiation of machines," ICEM 2000 Proceedings, Helsinki, Finland, vol.II, pp.1125-1129,. August 2000.
[3] F. Ollendorf, Potentialfelder der Elektrotechnik, Berlin: Springer 395s,. 1932.
[4] M.Roytgarts, "External magnetic field and shielding factor of frame and end shields of induction motors," in Calculation and design of electrical machines, Leningrad, pp.3-9, 1975.
[5] Erma Victor A. "Perturbation Approach to the Electrostatic Problem for Irregularly Shaped Conductors," J. Math. Phys., vol.4, 12, pp.1517-1526, 1963.
[6] M.Roytgarts, "External magnetic field of electrical machine", Proceedings of the Academy of Sciences of USSR. Power Engineering and Transport, 2, pp.60-69, 1980.
[7] M.Roytgarts, " External magnetic field calculation of geometrically similar electrical machines", Electrotechnica ,8, pp.8-11, 1980.
[8] M.Roytgarts, "Electromagnetic compatibility and vibration activity of electrical machines", Digests 1 International) conference on electromechanotronics EMT-97, St.Petersburg, pp 62-63, 1997.
[9] M.Roytgarts, "External noise-carrying magnetic field of electric machines", ICEMS 2001 Proceedings, Shenyang, China, August 18-20, 2001.

HPEM 19-14: System Power Budget Analysis of Microwave Radio Links

M. Can, A. H. Serbest

Microwave Radio Links are widely used in cellular communication networks in order to develop the transmission infrastructure between BTS, BSC and MSCs. In this work, numerical analysis of system power budget is performed for radio link network design and transmission planning purposes; measured and calculated results are compared in order to analyse microwave radio link performance in Adana Region under different conditions. The behaviour of three different frequencies; 10,5 GHz, 23 GHz and 38 GHz are examined under the influence of such parameters like transmitter power output level, rain rate, fog density, distance, polarisation type, antenna radius, temperature, foliage depth and etc. Received power levels are measured, calculated and reported for different radio link types and environmental conditions. A new program is developed in order to make system power budget analysis and design better microwave radio links. Measured and calculated values are compared, and the reasons of possible differences between them are investigated and interrogated.
It is well known that, in microwave communication systems, transmission loss is accounted for principally by the free space loss. Gaseous losses occur when molecules of Oxygen (O2), water vapor (H2O) and other gaseous atmospheric constituents absorb waves traveling through the atmosphere. These losses are greater at certain frequencies coinciding with the mechanical resonant frequencies of the gas molecules. Microwave propagation is also affected by rain. Raindrops are roughly the same size as the signal wavelengths, and cause attenuation of the radio signal. In order to make an estimation of attenuation due to fog, the formulas given by ITU-R P.840-2 are used. Foliage loss is calculated by the empirical relationship that has been developed for the case where the foliage depth is less than 400 meters. In our digital radio link analysis program, cable loss is assumed to be 3 dB for 100 meters. Feeder, connector and any other loss factors are considered as the additional losses and are assumed to be any value considered by the transmission planner.
When analysing the system power budget, we have measured the receiver power and then compared it with the values taken from

the program developed. In order to measure the received power level, two methods are used. First one is to connect a wattmeter to the outdoor unit mounted to the back of parabolic antenna. The power measured here is in watts, which can be converted into dB form. But here, the influence of cable loss cannot be determined since the measurement is made at the outdoor unit. The second method is to connect locally to the indoor unit of the radio link through LMP port available.
Some numerical results are taken from the program in order to show the influence of such parameters to the behaviour of the links. In order to compare the numerical data taken from the program with the measured values, eight different radio link hops were examined for three different conditions; 33°C without rain, 17°C with 22,4 mm/h of rain rate and 21°C with 78,5 mm/h of rain rate, all with vertical polarization and the maximum transmitter powers available (16 dBm for 38 GHz, 18 dBm for 23 GHz and 25 dBm for 10,5 GHz).

HPEM 20 - EM Standards & Specifications

HPEM 20-1: Status of EU Standardization for Human Exposition Control and its Implications

A. Enders
Institute for EMC, TU Braunschweig

Basic exposure levels for human exposition control in electromagnetic fields are mostly referenced to ICNIRP guidelines. This has also been done in the European Council Recommendation 1999/519/EC. Due to this recommendation a standardization mandate was given to CEN, CENELEC and ETSI to develop standards with which the basic exposure levels can be controlled. At first glance this seems to be superfluous but the basic exposure levels can´t be measured directly in most cases. Therefore alternative measures like reference field strengths, total emittable power etc. and corresponding measurement methods have to be developed.
This contribution will discuss the present situation of the standardization process as well as efforts to improve it.

HPEM 20-2: Stress Transfer Functions

B. Roemer

Necessary Functions for Achieving Unified Electromagnetic Environmental Effects (UE3)
General:
The complexity of the electromagnetic environment E2 is increasing. One consequence of this is, that the amount of standards, qualification tests and the associated controlling and managing business is also increasing. The intention of this abstract is, to present a basic idea of a method, which is likely capable to reduce the costs of the development of electromagnetic protection, even if the complexity of E2 is increasing.
The method is called UE3 – protection, which is based on a barrier concept which provides well defined interaction zones when established correctly. The analysis of the barriers leads to new functions which is called stress transfer functions (STF) and which are based on wave form norms. These functions can be linked to the susceptibility levels of electronic devices and they offer the opportunity for UE3 – protection. The STF is a new function which can describe the E3-coupling phenomena even if Non-Linear Effects (NLE) occur. NLE e.g. can be caused by sparking, diodes, dispersion, melting etc..
The advantages of the use of STF in the area of electromagnetic protection will be presented.

HPEM 20-3: The New Standard IEC 61000-4-20 for Testing with TEM Waveguides

M. Heidemann
Universität Hannover

Fail-save electronic equipment is nowadays often necessary in order to ensure the safety of men and to enable modern electronic business. Therefore, emission testing, immunity testing, and HEMP transient immunity testing of electronic equipment are of increasing importance. Reliable and economic test procedures are needed to proof the desired properties of equipment.
TEM waveguides are widely used for radiated emission and immunity testing of small EUTs [1], and for HEMP transient immunity testing as well [4]. Several standards use product specific test set-ups with TEM waveguides. For example, presently TEM waveguides are used for immunity and disturbance tests on broadcast receivers (CISPR 20), telephones (EIA/TIA-631), equipment on board vehicles (CISPR 25, ISO 11452), and also emission tests of mobile devices (IEC 60489-1+3), low-voltage electrical equipment (ANSI C63.4), as well as for calibration of field sensors (IEEE Std. 1309).
To support TEM waveguide applications IEC has now published the international basic standard IEC 61000-4-20 on EMC testing and measurement techniques using TEM waveguides [3]. This new standard includes a general section for TEM waveguide verification, and three chapters about radiated emission, immunity, and HEMP transient testing. It covers all types of TEM waveguides, like TEM cell, GTEM cell, and strip-line [2].
This presentation summarises the standard, describes the validation procedure of a TEM waveguide, and shows the general application of testing small EUTs.
The intention of IEC 61000-4-20 is to enable manufacturers to qualify EUTs by using many of the same laboratory equipment. The same TEM waveguide can be used for radiated emission and immunity testing. Many of the radiated immunity test equipment can also be used for radiated HEMP transient testing.
For these purposes a TEM waveguide needs to fulfil several requirements. The requirements are defined for a test volume, since later on the EUT is placed in this test volume. The TEM waveguide shall propagate a plane wave and provide a dominant transversal electromagnetic (TEM) field in the test volume, like the far field of an antenna in free space. Additionally, in the test volume the magnitude of the TEM field shall be within a defined small range (cw), or the peak electric field shall be uniform (HEMP), respectively. For HEMP testing also the double exponential pulse shape in time history (HEMP waveform) and the bandwidth are verified. Different types of TEM waveguides may meet certain requirements more or less easily. In general, a small test volume can fulfil the specifications with smaller tolerances in parameter variations than large ones. Its size is chosen by the user, but limited by the allowed maximum size of the test volume, which depends on the size of the waveguide. Beside others, the size of the test volume limits the allowed size of the EUT.
One advantage of a closed TEM waveguide (cell) compared to an OATS is the closed outer conductor. Due to this shield, emission measurements are not disturbed by ambient signals, and in case of immunity testing the environment is not disturbed by the test field. Therefore, it can also be used inside usual laboratories.
References:
[1] Groh, C.; Kaerst, J.P.; Koch, M.; and Garbe, H., “TEM waveguides for EMC measurements”, IEEE Transactions on EMC, vol. 41, no. 4, pp. 440-445, Nov. 1999.
[2] Heidemann, M.; Garbe, H.: “Using TEM waveguides according to the new IEC 61000-4-20“ 2003 IEEE International Symposium on EMC, Istanbul, Turkey, May 12-16 2003, session TU-A-R3-5, paper #272, ISBN 0-7803-7780-X..
[3] IEC 61000-4-20 - Ed. 1.0, Electromagnetic Compatibility (EMC) - Part 4: Testing and measurement techniques - Section 20: Emission and immunity testing in transverse electromagnetic (TEM) waveguides, International Electrotechnical Commission (IEC), Switzerland, Jan. 2003.
[4] Mojert, C.; Nitsch, D.; Friedhoff, H.; Maack, J.; Sabath, F.; Camp, M.; Garbe, H.: “UWB and EMP Susceptibility of Microprocessors and Networks”, 14th International Zurich Symposium & Technical Exhibition on Electromagnetic Compatibility, Switzerland, Zurich, Feb. 2001, ISBN 3952119954.

HPEM 20-4: EMC of High Voltage Gas Insulated Substations Under Service Conditions and Tests

E. Kynast, **A. Groiss**
Siemens AG, PTD H TTH

High voltage switchgear up to the highest rated voltages of 550 kV and 800 kV are subjected to EMC questions in various ways. For GIS and also for AIS (Air Insulated Substations) the gas SF6 is used for insulating and switching purposes due to its excellent properties in these respects. With SF6 under pressure the insulating requirements up to the range of 2 MV and switching requirement of short-circuit switching up to 100 kA can be fulfilled.

Due to the physical properties of SF6 voltage breakdowns lead to VFT (very fast transients) which have to be considered in respect of EMC. During switching operation of capacitive loads voltage collapse occurs within less than 5 ns during strikes across the contact gap. Especially during opening and closing of disconnectors a very large number of repetitive strikes occur with amplitudes of up to 2 p.u. which means voltage steps in the range of 1 MV within 3 ns. By these voltage steps traveling waves are generated in GIS with frequencies up to 100 MHz, classified as Very Fast Transients (VFT). For the high voltage insulation in the primary circuit special attention has to be paid to VFT.

Although the primary circuit is enclosed by the grounded metallic pressure vessels these VFT have to be considered for the secondary technique like control, auxiliary and measurement circuits. Service conditions can be simulated by special switching tests with the whole GIS-system in the high voltage laboratory to check the reliability of the GIS concerning the primary as well as the secondary circuits.

Standardized tests for the secondary circuits have to be carried out as type tests in respect of the electromagnetic compatibility. Emission tests as well as immunity tests are prescribed for secondary equipment with electronic components. The immunity of the complete secondary system or of subassemblies, such as central control cubicles, has to be verified with burst tests and oscillatory waves, simulating switching in the secondary system respectively switching in the main circuit.

HPEM 20-5: Coaxial Impulse Current Generator for Investigation of Surge Protective Devices

S. Kempen[1], **D. Peier**[1], **M. Wetter**[2]
[1]*University of Dortmund, Institute of High Voltage Engineering, D 44222 Dortmund* ; [2]*Phoenix Contact GmbH & Co. KG, D 32825 Blomberg*

Surge protective devices (SPD's) are tested with standardized impulse currents of high amplitude to guarantee their duly function. They represent the typical load types which occur in real power lines. The curve progression of the 8/20μs- test impulse is defined in [1] and it simulates the load type due to switching operations in power lines [2]. Furthermore this pulse represents disturbances caused by an ohmic-inductive coupling of residual disturbances from an outer into an inner lightning protection zone [3]. The standardized lightning current test impulse with the wave form 10/350μs is directly derived from the statistical analysis of measured positive lightning currents [4,5]. For both test impulses an oscillation and under-shoot free current-time-characteristic is demanded. At the example of a compact coaxial 100 kA- 8/20μs generator (Fig. 1) it is demonstrated, that it is possible by a more or less complete coaxial design to generate an ideal type of such an impulse without higher frequent superposition and without undershooting (Fig. 2). Circular arranged, low-inductive impulse-capacitors represent the energy-storage devices, which are discharged via a coaxial weir-system with a vacuum circuit breaker, placed in series to the device under test in the center of the construction. Due to fact that the high-current generator is also optimized for high-frequency applications, the mode of operation can be simulated on the base of the equivalent circuit diagram of the construction. At the end, it is shown, that the advantageous construction can also be expanded to an 10/350 μs generator with crowbar-technology. On the basis of simulations, the possibilities of the generation of an ideal 10/350 μs test-impulse are illustrated.

References
[1] IEC 60060-1: 1989-11-00: High-voltage test techniques; Part 1: General definitions and test requirements
[2] Schimanski, J.: Überspannungsschutz- Theorie und Praxis, 2. Auflage, Hüthig Verlag Heidelberg 2002
[3] Hasse, P., Wiesinger, J.: EMV Blitz- Schutzzonen- Konzept, VDE Verlag, Pflaum Verlag München 1994
[4] DIN V VDE V 0185-1: 2002-11: Blitzschutz, Teil 1: Allgemeine Grundsätze
[5] IEC 61024-1:1990-03-00: Protection of structures against lightning; Part 1: General principles

Figure 1: Coaxial 100 kA - impulse current generator with capacitive energy storage and without charging unit

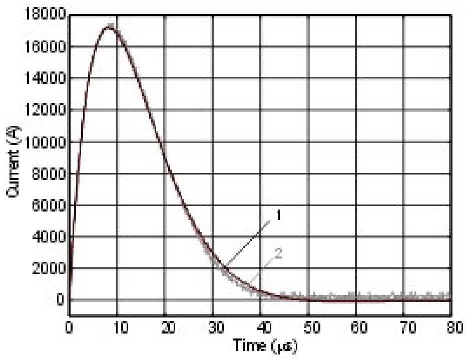

Figure 2: Simulation (curve 1) and measurement (curve 2) of the 8/20μs impulse current output generated by the impulse current source

HPEM 21 - High-Power Microwaves

HPEM 21-1: An Undergraduate High Power Electromagnetic Effects Research

G. Baker, **J. Rudmin**, **N. Olive**, **J. Darragh**
James Madison University

James Madison University has established a new Integrated Science and Technology curriculum that combines applied science, social context, and business curricula to produce graduates with broad interdisciplinary problem solving skills. Degree requirements include performing a formal research project. This year, two junior undergraduate students are investigating high power electromagnetic effects produced by readily available commercial sources including radar systems and microwave ovens. The project has involved analytical-range-to-effect calculations, designing and fabricating a simple microwave sensor, measuring the shielding effectiveness of a Faraday cage test chamber, modifying a microwave oven to serve as a high power EM source, and testing HPEM effects on personal computers. The project has been a successful learning experience on many aspects of HPEM and general research procedures including: familiarity with EM analysis techniques, experiment design, data gathering procedures and HPEM safety practices.

HPEM 21-2: Microwave Breakdown in Slots

U. Jordan[1], **D. Anderson**[1], **A. Kim**[3], **M. Lisak**[1], **M. Bäckström**[2], **O. Lundén**[2]
[1]*Department of Electromagnetics, Chalmers University of Technology, Göteborg, Sweden*; [2]*Swedish Defence Research Agency, FOI, Linköping, Sweden*; [3]*Institute of Applied Physics, Russian Academy of Sciences, Nizhny Novgorod, Russia*

The development of high power microwave (HPM) technology has been one of the fastest growing fields of applied physics during the past decades. The nonlinear phenomenon of microwave induced gas breakdown through electron impact ionisation is a common feature in many situations involving HPM radiation. In most situations microwave breakdown is a harmful effect to be avoided, however, in some situations it may provide an inherent protection against HPM radiation penetrating into an electrodynamic structure.

In the present work, transmission of microwave radiation through narrow slots is studied both theoretically and experimentally; for a more extensive presentation see (U. Jordan et al., Microwave Breakdown in Slots, ISRN CTH-EMT-R–6–SE, Chalmers University of Technology, 2004). The emphasis is on determining the threshold and the associated "switching" time for microwave induced breakdown of the gas in the slot, including their dependence on parameters pertaining to the slot itself, the gas surrounding the slot, and the microwave pulse. Furthermore, the protective effect due to the breakdown process has been studied in terms of the peak leakage power, the stationary leakage power, and the total transmitted energy, in relation to the aperture transmission cross section of the slot and the pulse characteristics.

The theoretical study includes estimates of the linear electric field enhancement and a simplified model for the breakdown plasma based on the electron density continuity equation. Pulsed breakdown theory has been extended to give results for microwave pulses taking into account the finite rise time of the pulse. In particular, linearly and exponentially shaped rising pulse flanks have been considered. The main result is a much slower scaling of breakdown time versus incident field strength, as compared to what is obtained from the classical rectangular pulse approximation, evidently due to the ionisation being less efficient during most of the slowly rising flank.

In the experimental study, resonant slots in a metal plate backed by a large cavity were irradiated from varying distances by microwave pulses with a duration of 1 μs and rise time of 80 ns generated by a 700 kW S-band magnetron. The experiments were carried out at atmospheric air pressure. Consequently, the shape of the incident pulses was kept constant, while the intensity varied. The transmitted field incident upon the slot, and the field received after propagation through the slot was recorded, as well as other parameters related to the experimental environment. From the recorded data breakdown time, leakage power and the energy transmitted through the slot have been extracted. Typical breakdown levels of 13 kV/m incident field strength and energy damping up to 25 dB were observed. The results from the experimental and theoretical studies are found to be in good quantitative agreement.

HPEM 21-3: Using Output Reflections for Spectrum Control in the High-Power Microwave Devices

R. M. Rozental, **N. S. Ginzburg**, **A. S. Sergeev**
Insitute of Applied Physics, Russian Academy of Sciences

The generation of high-power microwave signals with variable radiation spectrum is important problem for different practical applications, such a radioacoustic sounding, microwave processing, plasma heating and others. In this work a method of the radiation spectrum control for powerful relativistic gyrotrons and backward-wave oscillators (BWO) is discussed. This method based on introducing additional reflector in the output waveguide and forming special mode spectrum in the hybrid microwave system which includes interaction region and section of the output waveguide limited by a such reflector. It is well known that the complex multifrequency signal can be generated in the self-modulation regimes under sufficiently large exceeding operating current over threshold. It is found that under proper conditions in the self-modulation regime frequency spectrum could be close to the set of eigenfrequencies of the hybrid cavity. In this situation excitation of the several axial eigenmodes takes place and distance between spectrum frequencies could be controlled by varying the position of the output reflector.

Based on a 2.5-D version of the PIC-code KARAT we carried out simulation of spectrum control for the experimental models of X-band relativistic BWO (Ginzburg N.S., Zaitsev N.I., et al., Phys.Rev.Lett., 2002, 89 (10), no.108304) and gyrotron (Zaitsev N.I., Ginzburg N.S., et al., IEEE Trans. Plasma Sci., 2002, 30 (3), 840). It is shown that for gyrotron the region of parameters where Q-factors of first and second axial eigenmodes close to each other is the most favourable for self-modulation regime. Depending on reflector position this regions are alternated with the region of stationary oscillations. As a result the self-modulation frequency could be varied stepwise from 120 to 80 MHz. Contrary to gyrotrons in BWO the continuos change of self-modulation frequency from 100 to 60 MHz vs. the reflector position is obtained.

HPEM 21-4: High-Efficiency Operation of the Relativistic X-Band Gyrotron with Strong Output Reflections

R. M. Rozental, **E. V. Ilyakov**, **I. S. Kulagin**, **N. I. Zaitsev**, **N. S. Ginzburg**
Institute of Applied Physics Russian Academy of Sciences

High-efficiency operation of the relativistic X-band gyrotron (Zaitsev N.I., et al., IEEE Trans. on Plasma Sci., 2002, 30 (3), 840) with 50% reflections in the output waveguide is presented. For the electron beam energy of 230 keV and the injection current of 12 A the maximum efficiency exceeding 50% was achieved in the steady-state regime with output power of about 1.5 MW. As the injection current growth up to 32A the output power increased up to 2.8 MW with efficiency more than 30%. At a current of 55 A, the regime changed to a periodic self-modulation with a period of about 15 ns with average output power and efficiency up to 1.9 MW and 15% correspondingly. This values was two times greater that were reported earlier for 80% reflector. At the same time the maximal modulation depth reduced from 100 to 35%. The further possibilities of increasing output power in the steady-state regime in the gyrotron with end reflections was demonstrated by using 2.5-D version of the PIC-code KARAT. For the 280 kV, 60A electron beam in the gyrotron with resonator of reduced length output power could achieved 7 MW with efficiency >40%.

To achieve chaotic self-modulation regime in the experiment the distance between output reflector and gyrotron resonator opening was increased from 9 to 54 cm. It should be noted, that under general theoretical consideration (R.Vallee and C.Narriott., Phys. Rev. A, 1989, 39 (1), 197; T.M. Antonsen, et al., Phys. Fluids B, 1992, 4 (12), 4131.) the increasing of the delayed time (in the given case the distance between resonator and reflector) decreases the bifurcation parameters for the periodic and chaotic self-modulation regimes. The output power increased up to 2.8 MW with 15% efficiency for periodic self-modulation regimes in this configuration. As a injection current growth the period doubling route from the periodic to chaotic self-modulation regimes was observed . The maximum output power of 2.5 MW with 17% efficiency was obtained in the chaotic oscillation regime.

The work was supported by the Russian Foundation for Basic

Research (Grants No. 03-02-17560 and No. 03-02-16650).

HPEM 21-5: Design of a 4-Cell Load-Limited Compact MILO

R. Cousin[1], **J. Larour**[1], **P. Raymond**[2], **A. J. Durand**[3], **P. Gouard**[4]
[1]*LPTP/Ecole Polytechnique, Palaiseau, France*; [2]*Institut Polytechnique Saint-Louis (ISL), Cergy-Pontoise, France*; [3]*Thales Electron Devices (TED), Velizy, France*; [4]*CEA/DAM/IDF/DPTA, Bruyeres-le-Chatel, France*

The Magnetically Insulated Line Oscillator (MILO) is a high power microwave (HPM) pulsed device, potentially of gigawatt power, that combines the technologies of magnetically insulated electron flow with a slow wave structure, terminated by an adjustable load. This combination makes the tube a device capable of operating over a wide voltage range. A very high level of HPM generation has been already achieved at the Air Force Research Laboratory (AFRL): 400 ns microwave pulse duration at 1.2 GHz, leading to 1.5 GW output power (M. D. Haworth et al, IEEE Trans Plasma Sci 30, 992-997, 2002). So far, the pulsed power generators driving these tubes are relatively large. Our concern is to design a cost effective experimental setup of small footprint, combining a compact ISL-Marx generator and a small size MILO tube.
Electrons are emitted in vacuum from a cylindrical velvet cathode and drift over the cathode surface due to crossed electric and magnetic fields inside the tube. The cylindrical external electron layer thus created interacts predominantly with the transverse magnetic (TM) modes of the slow wave structure. Instabilities occur and slow electromagnetic waves are amplified by transfer of potential energy from this layer.
This process is described and explained using the electromagnetic-PIC software MAGIC, in order to optimize the energy conversion efficiency. 2-D and 3-D simulations are performed and benchmarked by comparison with the experimental data. Attention is paid to the different phases of the evolution of the electron discharge (parapotential electron flow, magnetic insulation and bunching). Optimization of the design of the resonator yields a simulated output power of 1.6 GW at 2.44 GHz. An experimental bench is currently under construction at ISL for experimentation at Ecole Polytechnique, and the first aim is to characterize the relativistic electron beam.

HPEM 21-6: Threat and Potential Value of RF Weapons

J. Bohl, **R. H. Stark**, **D. J. Urban**, **D. G. Staines**
Diehl Munitionssysteme GmbH & Co. KG, Röthenbach a.d. Pegnitz, Germany

Radio frequency (RF) weapons are noval weapon systems which are designed to generate high power electromagnetic radiation which is deployed in a single pulse or radiated over a short and limited period of time. The high power electomagnetic radiation targets the control and computer electronics of modern weapon systems and infra structures. Due to the small feature size and low supply voltage modern electronics are susceptible to intense electromagnetic fields. After coupling to the target system, the electromagnetic radiation is converted into current and voltage in signal and power lines. Dependend on the amplitude of the signals induced, the electronics and electronic components may be disrupted or even distroyed. In both cases the system loses the functionality it was designed for. RF weapons therefore offer a noval and unique capability to eleminate command posts, survailance and information infrastructures and to achieve superiority at minimum collateral damage. Short-pulse RF weapons are not anticipated to cause undesirable biological effects on personnel in the target area. A range of high power microwave (HPM) and ultra wide band (UWB) sources were developed which are possible candidates for future RF weapon applications. These sources range from small, autonomous, man-portable systems to larger high power devices and multi-antenna arrays. Field strengths exceeding 500 kV/m normalised to 1 m range have been realised by those systems, with pulse duration in the range of 1-50 ns. An overview on various source technologies including typical scenarios and target effects will be presented. Threat and potential value of RF weapons for soldiers in combat and peacekeeping missions are emphasised.

HPEM 21-7: Characterization of Modes in Coaxial Vircator

S. Hao, **Y. Zhanfeng**, **L. Guozhi**
Northwest Institute of Nuclear Technology

Previously researches on the generation of HPM pulse by coaxial vircator are mainly focused on the electron beam interaction with TM_{01} mode. The role of TE_{11} mode in coaxial vircator has not been given enough emphasis. The analysis of modes character stimulated by the E-beam in coaxial is given in this paper. Theoretical analysis proves that TE_{11} mode has almost the same coupling coefficient as that of the TM_{01} mode. 3-D simulation of modes character with code KARAT also had been carried out to give the modes difference between axisymmetric geometry and unaxisymmetric geometry. The results indicate that TE_{11} mode is the dominant mode under axisymmetric geometry and even enhanced in the unaxisymmetric geometry. Meanwhile, experimental results support that TE_{11} mode dominates the whole pulse duration. The farfield pattern of HPM radiation was also obtained respectively by microwave discharge tube and microwave detector in the experiment.
With TE_{11} mode output, coaxial vircator can be easily used in HPM radiation without mode converter, meanwhile its comparatively high efficiency also indicates the promising applications.

HPEM 21-8: Relativistic Magnetron with Injected Electron Beam

M. Fuks, **E. Schamiloglu**
University of New Mexico

We consider a relativistic magnetron whose cathode is outside the interaction space. The role of a negative electrode in a relativistic magnetron with an injected high current electron beam is carried out by its own space charge. Synchronous interaction of electrons with the operating wave is provided by an azimuthal drift of external electrons in cross fields: the radial electric field of the space charge of the inner electrons and the applied axial magnetic field. The anode current is formed by electrons whose radii are greater than the synchronous radius, part of which is captured in electron spokes by the azimuthal electric field of the operating wave. The electron beam is formed by a radially magnetically insulated diode outside the interaction space. This configuration provides the possibility of choosing a channel for electron beam propagation for an initial stationary state of the beam with electron potential energy in the interaction space which can be transferred to radiation, substantially exceeding the electron kinetic energy (G.P. Chernogalova, G.P. Fomenko, M.I. Fuks, et al., "Experimental investigations of the magnetically insulated diodes and microwave generation in relativistic magnetrons," Proceedings Beams-86, Kobe, Japan, 1986, pp. 573-576). This can be a state with beam current close to the space-charge-limited current, or a state with a virtual cathode and negligible kinetic energy. The merits of a magnetron with an injected electron beam include:
1. long cathode lifetime because the cathode is external to the interaction space and does suffer from electron impact;
2. increased pulse duration of radiation because the interaction space does not fill with the cathode plasma;
3. adaptability to variations in applied voltage and magnetic field because of a weak dependence of the azimuthal field of the operating wave, which is responsible for capturing electrons into spokes and forming anode current, on the thickness of the electron beam. In magnetrons with traditional design even the consistent increase of applied voltage and magnetic field to maintain synchronous interaction leads to unstable generation and a decrease in radiated power and efficiency because of the rapidly decreasing azimuthal electric field of the operating wave in the

electron flow over the cathode whose thickness decreases as the square of the magnetic field.
However, there is problem in providing a regime of stable generation, the necessary condition for which is a constant potential of the electron beam when there is a balance between outgoing electrons moving towards the anode and incoming electrons moving into the interaction space. Results of computer simulations (using the MAGIC particle-in-cell code) of the A6 magnetron with different initial stationary states of the injected electron beam demonstrate that stable regimes of generation are possible.
This work was supported by an AFOSR/DoD MURI grant on compact pulsed power.

HPEM 21-9: HPM – A Serious Threat to Vital Parts of the Net Centric Warfare Concept

S. Silfverskiöld[1], **T. Johannesson**[2], **M. Bäckström**[3], **S. E. Nyholm**[3], **K.-G. Lövstrand**[4]
[1]*Swedish Armed Forces Headquarter*; [2]*Swedish Armed Forces*; [3]*Swedish Defence Research Agency FOI*; [4]*Swedish Defence Materiel Administration FMV*

The authors have participated in a recent study performed by the Swedish Armed Forces Headquarter entitled “HPM – a Threat to the Concept of Net Centric Warfare and an Opportunity to be Used”. The C4I concept Net Centric Warfare (NCW) is currently developed in Sweden and other nations. NCW is heavily dependent on all kinds of sensors, military and civilian distributed telecommunication networks. These include nodes, routers, links etc. In order to ensure electromagnetic immunity of these systems it is important that proper EMC protection measures are undertaken. Sweden and USA among others have defined Electronic Warfare (EW) as Electronic Attack (EA), Electronic Protection (EP) and Electronic Support (ES). EMC measures belong to EP.
High Power Microwave (HPM) weapons are, like Lightning Electromagnetic Pulses (LEMP) and Nuclear Electromagnetic Pulse (NEMP), a serious threat to all unprotected military and civilian electronic equipment. HPM-weapons have been of interest for several years as potential weapons for a variety of combat, sabotage, and terrorist applications. Military systems have high demands concerning reliability and availability. Modern aircraft and warships, for instance have within a confined volume a considerable large number of advanced electronic systems. In order to achieve tactical and operational deployment in a hostile electromagnetic environment, EMC protection measures have become more and more important.
In this study we have listed possible situations in peace time and in war where an adversary might get an advantage by using different kinds of HPM-weapons. Different reactions to each situation were suggested. The presumed purpose of the attack as well as possible platforms, i.e. airborn, seaborn, mounted on a larger truck, wan, car or portable were discussed.
In conclusions it is very important that the Swedish Armed Forces can state requirements on civilian communication network operators that might be used for part of the communication needs of the future NCW concept. The civilian network operators must, just as the military network operator does, undertake electronic protection measures against peace and wartime HPM-threats. This would be possible using a boundaryless approach, with cooperation between the Armed Forces and civilian authorities such as the Swedish Emergency Management Agency KBM and the National Post and Telecom Agency PTS.
HPM weapons gives the user a possibility to perform operations with high accuracy, with small collateral damage and with a presumably low political cost.

HPEM 21-10: Wide Band Power Circularly Rectenna

J. Zbitou[1], **M. Latrach**[1], **S. Toutain**[2]
[1]*Electronic Departement, Ecole Supérieure d’Electronique de l’Ouest, France*; [2]*IRCCyN- SETRA, Ecole polytechnique de l’université de Nantes, France*

In this paper, a new circularly polarized wide band power configuration rectenna “Rectifier+Antenna” was developed and designed at 2.45 GHz, for wireless band applications. The technique used in this study, to achieve circular polarization, from a single feed patch, is to feed the patch on one of the sides and truncate the corners of a square patch (W.L. Stutzman. Antenna Theory and Design. John Wiley & Sons, Inc. , second edition, 1998. R. A. Sainati. CAD of Microstrip Antennas for Wireless Applications. Artech House, Inc., 1996. N. Andersson, S. Sandberg. Aerosonde Tracking using a smart antenna system. Master’s thesis, Lulea University of technology, 2002. J. R. James. Handbook of Microstrip Antennas. Peter Peregrinus Ltd., 1989).Then, the antenna element achieved ,for the rectenna system, is a four element truncated patch array with circularly polarization as shown in Figure 1(a). This array was simulated and tested, as shown in Figure 1(b), the simulation and measurements results of the return loss are in agreement. The radiation pattern is shown in Figure 2, we obtain approximately the same gain input results for Phi=0° and Phi=90° .
Two identical types of this antenna were associated to two RF-DC rectifiers (Figure 3). In order to design a wide band power rectenna. The first RF-DC rectifier is based on the use of an HSMS 2850 Schottky diode (Data Sheet of Schottky diode HSMS28xx, Agilent technologies) suitable for low power levels associated with a RF Monolithic limiter(J.Zbitou, M. Latrach, S. Toutain “ Limiteur de fortes puissances à large bande de fréquence” Télécom 2003 & 3ème JEMMA, 15-17 Octobre, 2003 Marrakech, Morocco.); and the second one use an HSMS2820 (Data Sheet of Schottky diode HSMS28xx, Agilent technologies) for high power applications.
The final rectenna, achieved, presented in figure3, proves good performances for rectifying operation, with high detection sensitivity, and an important RF-DC conversion efficiency as shown in Figure 4(a) and Figure 4(b).

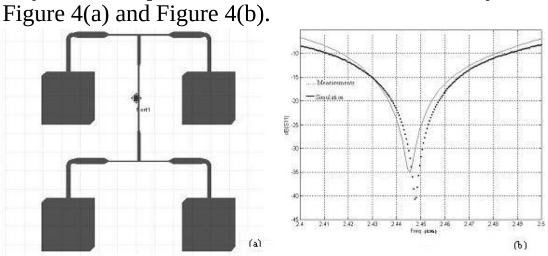

Figure 1: (a) The circularly polarized layout patch array, (b) The return loss versus frequency.

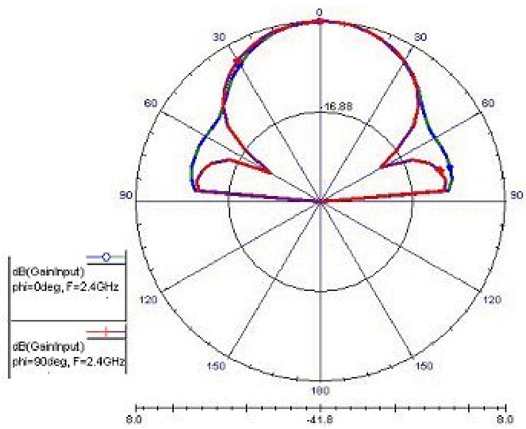

Figure 2: Radiation pattern circularly patch array.

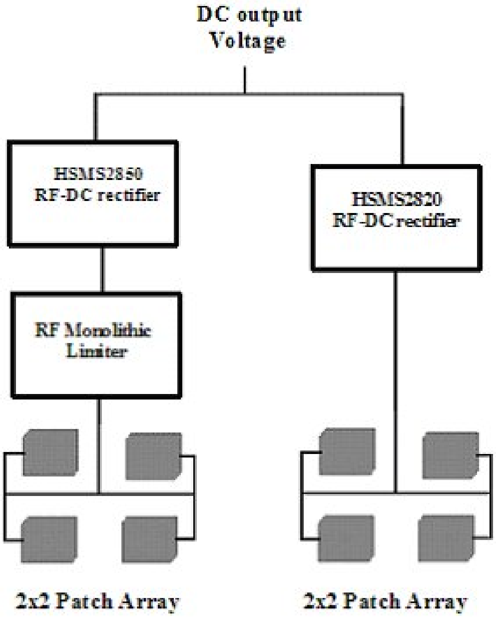

Figure 3: Wide power band circularly polarized rectenna configuration.

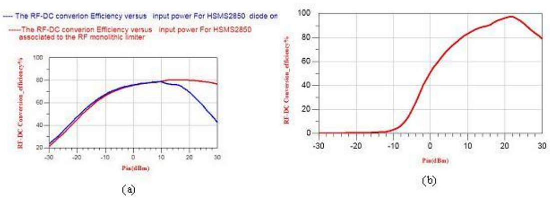

Figure 4: (a) The RF-DC Conversion efficiency versus input power for HSMS2850 diode only and associated to a RF Limiter, (b) The RF-DC Conversion efficiency versus input power for HSMS2820 diode.

HPEM 21-11: Periodic Waveguide as a Frequency Selective Microwave Power Switch

V. A. Pogrebnyak[1], **U. C. Hasar**[2], **M. Güler**[1], **Ö. E. Inan**[1], **T. Eraslan**[1], **A. N. Küçükaltun**[1]

[1]*Department of Electrical and Electronics Engineering, Faculty of Engineering and Architecture, Çukurova University, Adana, Turkey* ; [2]*Department of Electronics and Communication, Faculty of Engineering, Atatürk University, Erzurum, Turkey*

We have designed and investigated experimentally a planar periodically corrugated waveguide that allows to control the transmitted microwave power for a selected frequency. The switching is controlled by shifting of one periodic plate with respect to another on a haft period of corrugation. In the "off" state the waveguide is transparent for microwave radiation of other frequencies.

Theory

Wave phenomena in the periodic corrugated waveguide are investigated in detail. It is shown that the corrugation causes resonant interaction between the transverse modes (standing waves). The interaction results in the non-Bragg nature resonances and gaps (stop bands). The width of the non-Bragg gap as well as the Bragg gap depend on the relative position of two periodic plates. It varies from zero to a maximum value upon shifting of one periodic plate with respect to another on the half period of the corrugation. When a frequency of the electromagnetic wave coincides with one of the gaps, the wave does not propagate through the waveguide, and it is a state "off" (V.A.Pogrebnyak, J. Appl. Phys.94 (2003) 6979; Optics Communications 232 (2004) 201.

Experiment

A standard microwave setup with three horn antennas was used for measuring of the transmission characteristics of the periodic waveguide at a frequency range 8-12 GHz. The waveguide was made of two metal plates having the identical sinusoidal profiles. The upper plate could slide with respect to the lower making the phase shift θ between the plates. We investigated propagation of the TE wave having the polarization vector parallel to grooves of the corrugation. Location and a width of the forbidden gap could be tuned by changing a waveguide thickness and a period of the corrugation. The observation of the switching phenomena at the Bragg frequency f = 9.1 GHz is shown in Fig. 1. If $\theta = 0$, the stop band has a maximum value and the transmitted power equals zero (the state "off"). At $\theta = \pi$, the gap closes and the transmitted power reaches maximum the value (the state "on").

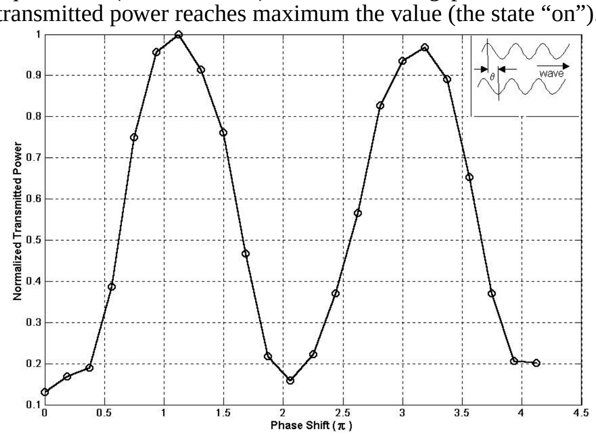

Figure 1: Transmitted power vs a phase shift θ. The inset shows the phase shift θ between the plates

HPEM 21-12: A New High-Power Crossed Field Tube

G. I. Churyumov, **T. I. Frolova**, **A. V. Gritsunov**

Kharkov National University of Radio Electronics, Kharkov, Ukraine

One line of attack on the problem of increasing of output power in the crossed field tubes there is a one connected with creating the non-traditional crossed field tubes (Churyumov G.I., Sergeev G.I., The new concepts of development of crossed-field microwave devices with azimuthal symmetry. Proceedings 8-th International Symposium on Non-Linear Electromagnetic Systems. 12-14 May, Brounschweig, 1997, p. 295-296). Among the non-traditional constructions of the crossed field tubes are the one's of the two-stage magnetron. It is necessary to stress that the preliminary results of computer modeling in the two-stage magnetron have been described in paper (T. I. Frolova, G.I. Churyumov and G.I. Sergeev. The computer modeling of the electron-wave interaction in combined magnetron. Proc. First IEEE International Vacuum Electronics Conference (IVEC'2000), Monterey, California, 2000, pp. 542-543).

In this paper the full 3D computer modeling of the electron-wave interaction in the two-stage magnetron is presented. All investigations are carried out by using a new 3D code SICM 3D 3.01. The main geometrical and electrical parameters of the two-stage magnetron are in Table 1.

Fig. 1 shows the phase bunching along azimuth direction and longitudinal (axial) distribution of electrons in the interaction space of the two-stage magnetron on condition that only internal stage is operated. These data are obtained for one operating point on the V – I characteristics, when 23 kV and 16 A. Giving anode voltage pulse to the external stage of the two-stage magnetron we change its operation. In this case the results of computer modeling are presented in Fig. 2. The operating points on the V – I characteristics of the two-stage magnetron were the following: 23,5 kV and 19,7 A (for internal stage), 28 kV and 6,2 A (for external stage).

The quantitative analysis showed that output power of the tube is increased by 40 - 60 percents after turning on the external stage and the efficiency of the two-stage magnetron is deteriorated no more than 5 -7 percents.

The obtained result allows considering the two-stage magnetron as new tube in which can be used the switching mode of the output power in operation. Besides, the carrying out an optimization both the construction of the two-stage magnetron and electron-wave interaction mechanism permits to improve the attained result.

Table 1

Magnetron parameters	Internal stage	External stage
1. Number of resonators	12	12
2. Radius of cathodes, mm	5.65	15
3. Radius of anodes, mm	10	11
4. Height of cathodes, mm	24	24
5. Magnetic field, G	2500	2000
6. Anode voltage, kV	23.5	28.0

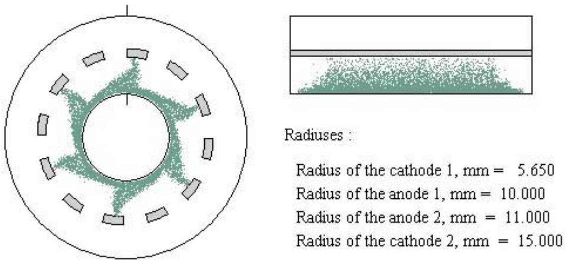

Figure 1: Results of computer modeling of the internal stage

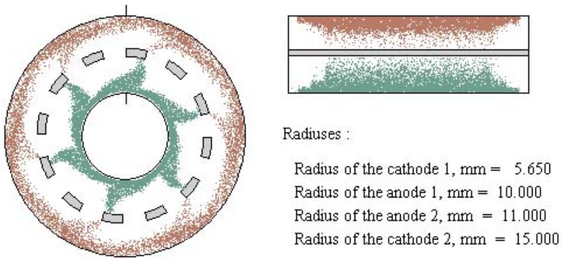

Figure 2: Results of computer modeling of the two stage magnetron

HPEM 22 - Numerical Methods

HPEM 22-1: Application of Fast Integral Equation Techniques to the Numerical Solution of High Frequency Electromagnetic Scattering Problems

U. Jakobus, **J. J. van Tonder**
EM Software & Systems - S.A. (Pty) Ltd, Stellenbosch, South Africa

Many different techniques exist for the numerical solution of electromagnetic scattering problems, the most popular include FDTD (Finite Difference Time Domain), FEM (Finite Element Method), or MoM (Method of Moments). However, these days there is a particular interest in high frequencies, and when the typical dimensions of the objects exceed several wavelengths, these traditional techniques become too expensive with respect to memory requirement and run-time, even on modern fast and parallel computer systems. To this end special high frequency techniques were developed, like PO (Physical Optics) or UTD (Uniform Theory of Diffraction). These are high-frequency approximations, and for instance when applying PO the consideration of certain effects like multiple reflections for arbitrarily shaped objects is again a time-consuming exercise.

In this contribution, we would like to focus on a fast extension of the MoM, which - though still being a numerical technique with discretisation errors etc. - can be considered an exact solution method, it is not based on approximations as PO or UTD are. We apply an MLFMM (Multilevel Fast Multipole Method) solution scheme, which differs from the formulations typically found in literature in a sense that we focus in particular on the EFIE (electric field integral equation). The reason for this is not only the ability to model wire structures, but more the feasibility of this approach to also model objects which are not closed (i.e. open structures like in the simplest case a plate, but more generally objects with apertures and holes).

Within our MLFMM approach, an arbitrary number of levels is supported, the actual number of levels is determined automatically by a sophisticated algorithm, taking not only the wavelength and the dimensions of the object into account, but also for instance any separations of multiple objects in the scenario under consideration. Due to the highly ill-conditioned nature of the EFIE, a robust pre-conditioning technique is a must. Here in our approach a sparse ILU (incomplete LU-decomposition) is used in conjunction with an adaptive renumbering scheme to reduce the level of fill-in. As an iterative solution technique for the resulting system of linear equations, we have several choices like BiCGStab (biconjugate gradient stabilised) or CGS (conjugate gradient squared) or also TFQMR (transpose free quasi minimal residuum).

A number of application examples (which will be shown during the conference presentation) have confirmed the theoretically expected scaling of memory with $N \log N$ and for the run-time of $N \log^2 N$ with N being the number of unknowns. As compared to the values of N^2 and N^3, respectively, for the MoM this is a drastic improvement. For instance, just for one example of N = 226 000 unknowns, the MLFMM memory requirement (including all the overhead for pre-conditioning etc.) is 3.2 GByte, the run-time is 3.1 hours (sequential run). For the MoM the memory requirement is already 765 GByte, and the run-time on the same platform can be estimated to be about 2 months.

HPEM 22-2: Capability of a DFDT Code to Analyze the EM Coupling into a System at Microwave Frequencies

J.-C. Joly, **B. Pecqueux**
Centre d'Etudes de Gramat 46500, Gramat, France

This work presents a methodology to study, to assess and to understand the EM coupling to generic missile (called Genec) with a FDTD code (called Gorf). This methodology is statistical in nature because of the complexity of the system, the size of the studied volumes, and the frequency range. Moreover, this presentation focuses on the numerical results which can be helpful for experimental choices.

Generally, the electronic devices are located in faradized zones, like in the hold of the Genec. Due to their sizes and the frequency range, these volumes can be considered as resonant cavities. The numerical simulations can provide us with characteristics of the EM ambiance in terms of homogeneity, isotropy and distribution functions.

This information helps us for choices before a second experimental step in terms. It concerns :

- the number of sensors and the number of EM zones
- the location and the direction of the sensors
- the adjustment of the same field in a mode stirring reverberation chamber in order to test subsystems (PCBs) without the constraint of the system itself

Moreover, in a vulnerability approach, the same meshing provides us with other numerical results. The presented results concern :

- the most coupling frequencies corresponding to the resonance of the slots and the wings
- the most coupling incidences with the radiating pattern
- the predominant paths of penetration and their relative contributions according to the frequency

Numerical tools are not ready to replace experiments entirely, and this presentation insists on their complementary aspects. Of course, the methodology has been applied here to a generic system which is specially designed for easy measures and calculations. Actually, a more realistic system would involve difficulties, particularly to identify and simulate faradization and conduction defaults. However, this methodology would be still valuable and helpful.

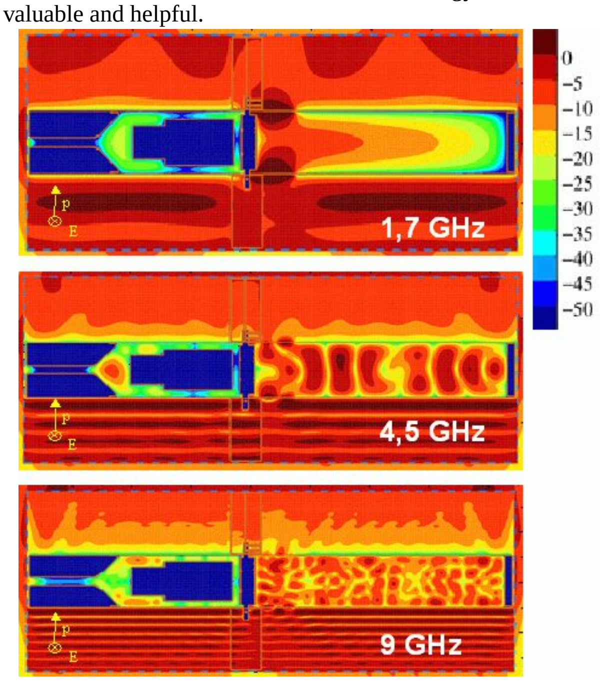

Figure 1: The GENEC at 1.7, at 4.5 and 9 GHz (Einc=1V/m=0dB)

HPEM 22-3: Eliminating Signal Processing Artifacts due to FFT in the Analysis of Broadband Signal Using the Matrix Pencil Method

S. Burintramart, **T. K. Sarkar**
Department of Electrical Engineering & Computer Science, Syracuse University

In this paper, we introduce the Matrix Pencil (MP) method for the purpose of frequency domain analysis. Based on Harmonic modeling, any signal can be expressed in the form of sum of complex exponentials. It has been shown that the MP method can estimate both amplitudes and frequencies of the signal in noise (Y. Hua and T. K. Sarkar, Matrix pencil method for estimating parameters for exponentially damped/undamped sinusoids in noise, 1990). When the signal is corrupted by noise, signal and noise spaces can be separated via the Singular Value Decomposition (SVD). By setting enough number of dominant frequencies, i.e. number of largest singular values, we can get similar result as when using the Fast Fourier Transform (FFT). One aspect of the MP method is that there is no limitation of spectral sampling interval which is limited by the length of the sampled signal in the FFT. Therefore, close frequency components can be estimated with less number of samples.

We analyzed sample signals using the MP method with window size of 400 samples, and compared the results with the FFT with 1921 samples using measured data. The results were similar for both cases except that the MP method gave the more accurate frequency information than the FFT. However, since the number of estimated frequencies in the MP method is proportional to the window length, the results from the MP method showed less number of data than the other. We also applied the small length window to the data, and observed only some important frequency of the signal. It turns out that resonant frequencies could be estimated although the window length is smaller than the signal waveforms. Therefore, it is possible to reveal some information about the signal with a limited number of samples.

The Matrix Pencil method is an alternative tool for high accuracy spectrum analysis and it can also be used to estimate the resonant frequencies of targets of interest using very few samples of the signal.

HPEM 22-4: FDTD Simulation and Spark Voltage Dependence of Electromagnetic Fields Due to Electrostatic Discharge

O. Fujiwara[1], **H. Seko**[1], **Y. Yamanaka**[2]
[1]*Nagoya Institute of Technology*; [2]*Communications Research Laboratory*

The electrostatic discharge (ESD) due to charged metal objects produces electromagnetic (EM) fields having broad-band frequency spectra over the microwave region, which cause serious EM interference (EMI) to electronic equipment. For the EMI of this kind, it has widely been accepted that the lower spark voltage ESD causes the stronger EMI to high-tech information equipment, whereas its mechanism still remains unknown. With the aim of elucidating this mechanism, in order to analyze the ESD fields caused by charged metal spheres as a canonical problem, we previously developed two kinds of the finite-time difference-domain (FDTD) computation techniques, which were based on gap excitation by the source of a spark current / spark voltage being analytically obtained in a closed form from the Rompe-Weizel formula for the time-variant spark-resistance.

For the ESD event due to charged metals except the spheres, however, the spark current and spark voltage cannot be derived in closed forms so that the above-mentioned methods are not applicable to analyzing the EM fields in that case. We therefore proposed a new FDTD algorithm based on gap excitation with the time-variant conductivity and electric field of a spark channel using a specific relationship between the time-variant conductivity and internal electric field of the spark channel, which was derived from a hypothesis of the Rompe-Weizel formula where the conductivity of the spark channel be proportional to the internal energy injected into the channel. This algorithm enables one to predict the ESD fields due to charged metals having arbitrary shapes, which was validated by a spark experiment.

In the present study, with the above-mentioned FDTD algorithm we simulated a spark discharge between cylindrical metal bars, which effectively behave as a dipole antenna, in order to analyze the resultant magnetic field in conjunction with the gap length, and examined its spark voltage dependence. As a result, we found that the lower spark voltage produces the higher magnetic field level, while a certain spark voltage causes the highest magnetic field. This result supports that the lower spark voltage may cause the stronger EMI to high-tech equipment, and it also implies the presence of an ESD specific condition due to charged metals that gives the highest EM fields. The finding obtained here was confirmed by spark experiments using the same metal cylinders as those used for the FDTD computation.

HPEM 22-5: French/German Simulations of EM Coupling into the GENEC Testobject

J. Ritter[1], **J.-C. Joly**[2]
[1]*EADS-Military Aircraft, Germany*; [2]*Delegation Generale Pour l' Armement, CEG, France*

This contribution documents some results of numerical simulations of the GENEC test-object. The "GENEC" object (see Fig. 1, cut-away view) is a generic test object intended to be used as a reference object for high intensity microwave test facilities and computer simulation codes. The GENEC has about the dimensions of a shoulder-launched surface-to-air missile but is designed completely generic, so that the object can be handled without any restriction.

The simulations have been carried out by the French military test-center (Centre des Etudes de Gramat, CEG) of the DGA and by the Signature Technology dept. of EADS Military Aircraft located in Bremen, Germany.

The simulations have been performed during a cooperative effort between CEG and EADS-MA within a French-German initiative on numerical modeling. For Frequencies up to 10GHz, the GENEC geometry has been simulated using different Methods, namely the Finite Difference Time Domain Method, implemented in the GORF-Code from the CEG and the Multilevel Fast Multipole Method implemented in the Protheus-Code from

EADS-Military Aircraft .
Besides the computation of the EM-field at several test-points within and on the structure, the transfer function for the E-field has been computed at several points, where also measurement results were available. As a result, good agreement between the different simulation-techniques as well as the measurements can be stated (see fig. 2, comparison of transfer functions for the E-field at a specific test-point inside the GENEC). In fig. 3, the resonant fields inside the GENEC is shown for three different frequencies, as computed by the FD-TD code of the CEG. It can be seen, that for 0.5GHz, the field cannot propagate into the cavity (below cutoff), while at 4.5GHz the standing wave pattern of a single mode can be observed. At 9GHz, many modes can propagate inside the cavity, so that a nearly homogenous field exists inside the GENEC. Fig. 4 shows the surface current densities at 10GHz for three different incident fields as computed by the Protheus/MLFMA-code of EADS-Military Aircraft.

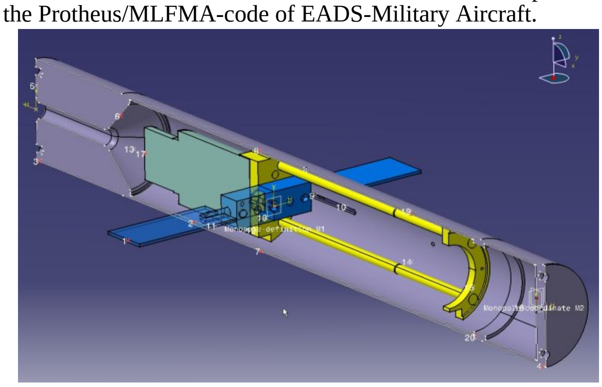

Figure 1: Cut-away view of the GENEC object used in the simulations

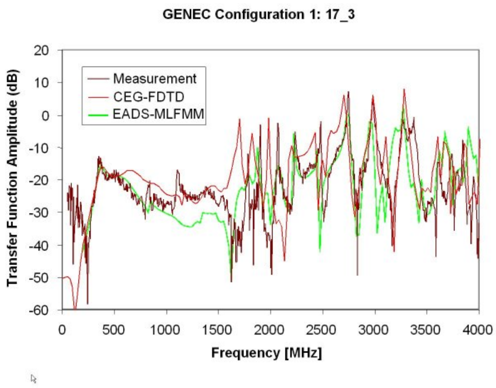

Figure 2: A representative result for the transfer function of the electric field from the free-space wave to a test point inside the GENEC. Comparison of the CEG results with results from the Protheus/MLFMA code and with measurements

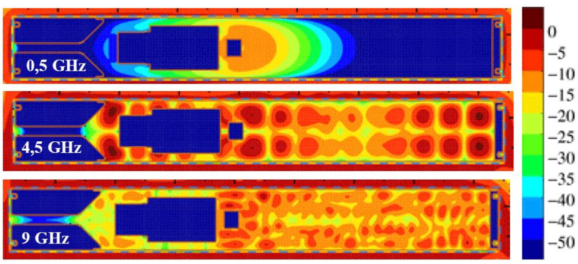

Figure 3: Field distributions inside the GENEC (on the symmetry plane) for three different frequencies as computed by the FD-TD code from CEG.

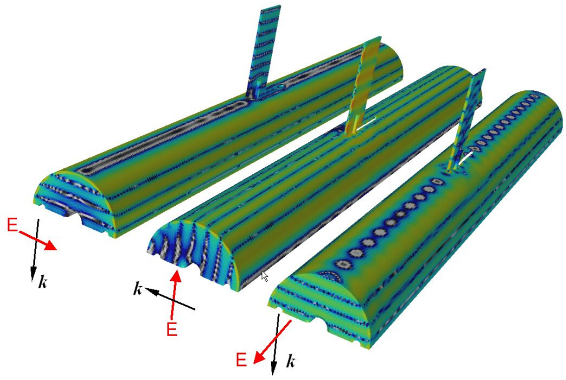

Figure 4: Surface current densities at 10GHz for three different incident fields as obtained by the EADS-Code Protheus/MLFMA

HPEM 22-6: Histogram Solution of the Maxwell Equations Inside Rectangular Enclosure which is not Electrically Large

J. S. Hämäläinen[1], **P. S. Järviö**[1], **T. Martin**[2], **M. Bäckström**[2]
[1]*Finnish Defence Forces Technical Research Centre, PvTT*;
[2]*Swedish Defence Research Agency, FOI*

One of classical topics in EMC modelling is shielding effectiveness of rectangular enclosures with apertures, i.e., the attenuation of the external electromagnetic field due to an enclosure. The external field is characterized by the frequency, polarization and direction of propagation, which determines together with the geometry of the enclosure the level of penetration. If the frequency is high enough, the field inside the enclosure becomes overmoded and the field distribution inside the enclosure is known to follow χ^2 statistics (T. H. Lehmann, The Statistics of Electromagnetic Fields in cavities with Complex Shapes, Phillips Laboratory, Albuquerque, New Mexico, Interaction Note 494, 1993). For lower frequencies, the field is more or less "deterministic".
Let us now concentrate on these lower frequencies and look at large number of field values inside enclosure for estimating the field distribution. To carry on, let us consider to nonparametric density estimates of the field. In particular, we consider histograms of the field inside the enclosure, which correspond to a certain frequency of the field. We note, that Charles Bunting has studied histograms over a given frequency interval, see e.g. (C. F. Bunting, Shielding Effectiveness in a Two-Dimensional Reverberation Chamber Using Finite-Element Techniques, IEEE Transactions On Electromagnetic Compatibility, Vol. 45, No. 3, 2003, pp .548-552.). Our motivation is due to the fact that shielding effectiveness of the enclosure varies along its determination point inside the enclosure. Thus, we think that by considering a large sample of field values, better understanding of the overall shielding properties of the enclosure should be achieved.
Let us introduce a histogram solution of the Maxwell equations by the histogram of the field amplitude or field component values over the observed (calculated) field values. Let us split the range [min(X), max(X)] of the field X values into K equal-length subintervals, call them bins, and denote by Ik be the indicator function of kth interval. The indicator function is Ik(x)=1 if x is on kth interval and 0 otherwise. With these notations, histogram is a double summation over indicator functions and observed field values.
Histograms provide a good picture of how probable some field strength inside the enclosure is and they are easy to construct from the observations. But, if the histogram will be used to estimate probability density function of the field, a lot of attention should be paid into the selection of number of bins in order to minimise errors between histogram and pdf. For instance, in (D. W. Scott, On optimal and data-based histograms, Biometrika, Vol. 66, No. 3, 1979, pp. 605-610.) an optimal bin width for Gaussian samples was proposed to be $3.49sn^{(-1/3)}$, where n

is the number elements in sample and s is the sample standard deviation. Unfortunately, we cannot assume that the field is distributed like a Gaussian sample, and the variances of the 'samples' differ very much as frequency of the field differ, so that we have to use 'well-educated' guesses for the choice of numbers of bins.
As examples, we consider field histograms inside three shielded enclosures with slightly different inner structure. The goal is to find out whether and/or how much the histograms change, when the inner structure changes. Furthermore, we test the change of the histogram as the frequency was slightly changed. The size of the enclosure is 29 cm × 29 cm × 20 cm. The first case is that a piece of absorbing material is included inside, in the second case we populate the enclosure with seven thin wire antennas and finally we divide it by a wall. The external field is modelled by a propagating plane wave towards the top side, where small apertures were placed, of the enclosure. The selected frequencies of the field are between 500 MHz and 4 GHz. As conclusive notation, we like to say that histograms provide a good insight into the overall behaviour of field inside the enclosure. The negative side is that the computed results are hard to verify experimentally.

HPEM 22-7: Investigation of Parallel Cluster for the Numerical Simulation of EMC Problems

U. Schenk, **D. Nitsch**, **A. Bausen**
WIS Munster

Due to the fact that modern electric systems rely on more and more electronics it is very important to use numerical simulation in order to get a better understanding of electromagnetic coupling and shielding. A cheap and fast solution is the use of parallel computer codes.
The "Wehrwissenschaftliches Institut für Schutztechnologien" (WIS) also known as the Research Institute for Protective Technologies which focuses on protecting against Nuclear, Biological and Chemical Weapons performs experiments and simulations in the field of electromagnetic field coupling. We are using the program CONCEPT (Code for the Numerical Computation of Electromagnetic Processes for Thin Wire and Thin Shell Structures).
Developed by the Department of Theoretical Electrical Engineering of the Technical University of Hamburg-Harburg, CONCEPT is a program system for the numerical computation of electromagnetic radiation and scattering problems. CONCEPT is based on the method of moments (MOM) for the numerical solution of integral equations for the electric field (EFIE) and the magnetic field (MFIE).
In order to improve the performance of our calculations we make use of multiple CPU's. The WIS has used a system of 16 PC's (P II 400 MHz) that was upgraded to 28 PC's (P IV 2400 MHz). We examine the influence of the number of PC's and show the importance of different processor types on the time needed for our simulations.
The time to solve a system of linear equations by LU decomposition on a distributed memory system is: (see Equation 1)
a = Latency in s
b = 1/ Transfer rate of the net work in byte/s
g = 1/FLOPS for a Matrix-Matrix-Multiplication
We will show that the use of faster processors has a huge influence on the time needed to solve a matrix equation (Eq 1). We will investigate the communication need of more CPU's (up to 28) to investigate the behavior shown in Fig. 1 for a greater number of processors.

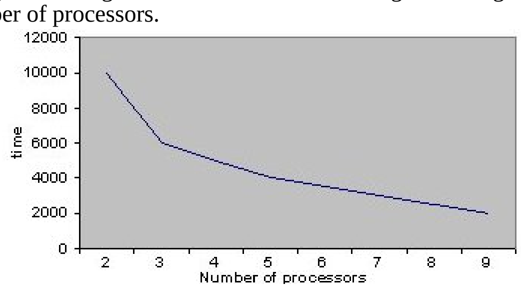

$$T_{LU} = 2\left(n \cdot \log_2(P) \cdot \alpha + \frac{n^2}{G}(2 \cdot Q + P \cdot \log_2(P)) \cdot \beta + \frac{2 \cdot n^3}{G} \cdot \gamma\right)$$

Equation 1

HPEM 22-8: Modelling of Electromagnetic Wave Propagation in Periodic Absorbing Media inclusive a Semitransparent Object

V. G. Spitsyn
Tomsk Polytechnic University, Department of Computer Engineering

We consider the stochastic model of electromagnetic signal multiple interactions with discrete inhomogeneities chaotically disposed in the stratified media with periodic structure. The media is contained a semitransparent spherical object. The method of solving this problem is based on the stochastic modelling of wave interaction with random discrete media [1 – 3].
Here is assumed that the wavelength of the wave is less than the sizes of the layers or period of inhomogeneous structure and scattering occurs incoherently by an image on statistically independent discrete inhomogeneities. The oscillator of electromagnetic signal is presented as a source of photons with corresponding diagram of radiation. The initial coordinates of photons are assigned in the point of oscillator disposition. The type of wave interaction with discrete inhomogeneities is determined according to set cross sections of scattering and absorption. In case of fulfillment of a wave scattering condition the direction of photon propagation changes to in accordance with specified indicatrix of discrete inhomogeneities reradiation. In the result of computation we receive the energy of scattering signal and energy of absorption signal in space of coordinates.
There is supposed that the interaction of wave with random discrete inhomogeneous take place in according to the isotropic scattering indicatrix. In the Fig. 1 and Fig. 2 are presented the input data of the middle free wave propagation distance and the coefficient of wave absorption in the media. The stratified media are characterized of presence the periodic structure and one object in a view of sphere with radius r = 1 and the coordinates of the centre x = 2,5; y = – 3,0; z = 3,5. This data is showed in the cross-section in the plane yz for the meanings of x = 2,5. In this paper is supposed that all distances measured in the relative units. In the Fig. 3 and Fig. 4 are presented the results of computation the distributions of scattering and absorption signal energy into media. The value of energy is normalized on the maximum of energy in the every frame. Here is considered the source of electromagnetic signal with isotropic indicatrix of radiation, which disposed in the centre of Cartesian coordinates system on the surface of media.
It is necessary to observe the contrast image of layers and spherical object in Fig. 3 in comparison with Fig. 4. This fact is explained of small free path of photons in indicated areas. The increasing of photons subsistence time in the cells of coordinate space is leaded to growth the energy of scattering signal in according to equation (1) from [2].
Thus in this paper has been solved the task about propagation electromagnetic wave in stratified media with periodic structure, which included the semitransparent spherical object. There is explored the distribution of scattering and absorption signal energy from the parameters, describing the nonuniform of random discrete media structure. On the base of receiving results analysis we can do the conclusion about more stronger contrast image of spherical object and layers for the case of scattering signal energy image in comparison with absorption signal energy image.
References
[1] V.G. Spitsyn, Development of a numerical method of electromagnetic wave propagation analysis in the three - dimensional random discrete media, IEEE AP-S International Symposium Digest, San Antonio, Texas, USA, June 16-21, 2002, Vol. 4, pp. 288-291.
[2] V.G. Spitsyn, Method of computation of nonlinear electromagnetic wave interaction with stratified absorbing media, IEEE AP-S International Symposium Digest, Columbus, Ohio, USA, June 22-27, 2003, Vol. 4., pp. 398-401.

[3] V.G. Spitsyn, Modeling of radiowave scattering on the ionospheric plasma disturbances, created of space vehicle, Tomsk: Publishing House "STT", 2002.

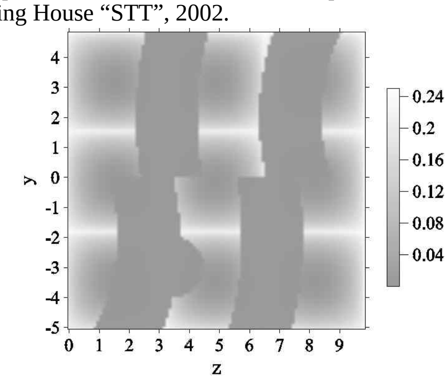

Figure 1: The middle free wave propagation distance in the media

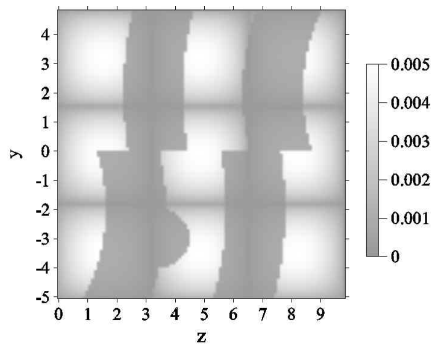

Figure 2: The coefficient of wave absorption in the media

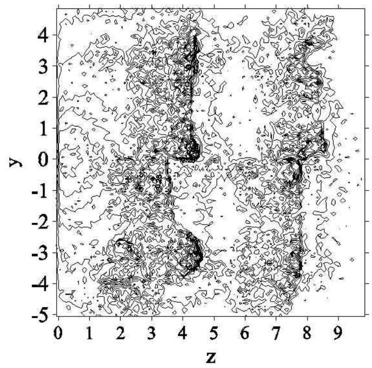

Figure 3: The distribution of scattering signal energy

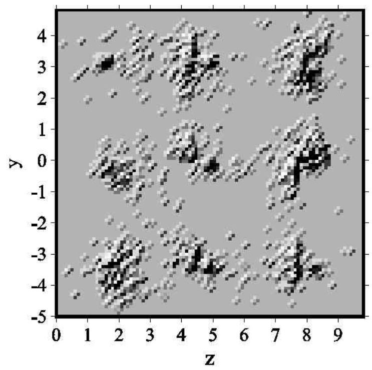

Figure 4: The distribution of absorption signal energy

HPEM 22-9: Numerical Assessment of Coupling in the 500MHz-10GHz Band Using an Inverse Approach with FDTD- Application to GENEC

N. Rouvrais[1], **F. Therond**[1], **J.-C. Joly**[2], **B. Pecqueux**[2], **Y. Beniguel**[2]

[1]*GERAC, 105 Avenue du Général EISENHOWER, 31037 Toulouse, France*; [2]*Centre d'Etudes de Gramat, DGA/DCE/CEG, 46500 Gramat, France*; [3]*IEEA, Courbevoie, France*

This study is backed by the Centre d'Etudes de Gramat.

Finite Difference Time Domain (FDTD) techniques have been widely used over years to tackle electromagnetic (EM) interference issues for lightning and Nuclear EM Pulse (NEMP). However, there are no intrinsic characteristics of FDTD that would limit its application to 'low frequency' concerns.

For NEMP or lightning, the EM threat has a known waveform and use of FDTD is straightforward, either through global plane wave illumination or direct injection. For so-called HPM, or UWB, problems arise in a different manner, since a wider spectrum is possibly available, with no well-established or standardised waveforms. Moreover, on a given structure, the angle of incidence impacts more and more the coupling as the frequency increases.

The purpose of this presentation is to show the FDTD capabilities, in an HPM context, to assess EM coupling on complex structures and, in particular, dependence versus frequency and angle of incidence.

Using the reciprocity theorem, a radiating element is placed inside the simulated structure, at selected key locations, and the far-field patterns are obtained through a built-in specific time domain near-field to far-field transformation module. Calculations are carried out on a whole sphere centred on the simulated structure, with adequate angular sampling, to get a full overview of angle of incidence influence. Fourier transforms, associated to a first basic processing, yield either raw data, or gains, or coupling cross-sections in the frequency domain. The primary outcomes of the simulations are thus coupling results over 4π st, and on a wide frequency range. Complementary data processing, some of which statistical, is required to point out and display the most important features of coupling. To this end, specific combinations of 1D/2D/3D visualisations are implemented in order to provide an adequate overview of the coupling phenomena.

These 'inverse' approach calculations are indeed time consuming, but are much faster and practical than the equivalent of numerous 'direct' plane wave illuminations.

Samples of results and data processing will be given on a mock-up of generic missile (GENEC), on which actually two FDTD meshes were used, associated to two wide-band waveforms. Results will be discussed in terms of computation time, accuracy, pros and cons with respect to frequency domain numerical techniques, and potential application to larger structures. Comparisons with results provided by a Method Of Moments technique with respect both to the resources required (sampling, computation time) and the result accuracy will be presented.

The method and calculations presented here are meant to provide a modelling equivalent to the so-called 'SOCRATE' spherical near-field facility at CEG. The main features and capabilities of those experimental and numerical tools will be assessed in the HPM context.

HPEM 22-10: The Method of Auxiliary Sources for Solving Some Electrodynamic Problems

R. S. Zaridze, **G. N. Ghvedashvili**, **K. N. Tavzarashvili**, **D. G. Kakulia**

Georgia

1. The Method of Auxiliary Sources (MAS) has been intensively used in last three decades for solving the boundary problems of mathematical physics, particularly EM scattering problems upon Complex, Electrical Large Bodies with an Open Cavity and Distributed Systems. The key idea of the MAS is to represent the unknown scattered field by a sum of fundamental solutions of

appropriate wave equation – Auxiliary Sources (AS), whose radiating centres are located on some auxiliary surface, shifted outside the area where the field is to be found. Unknown coefficients are determined from boundary conditions satisfaction. This shifting sharply reduces necessary number of unknowns, gives high accuracy and fast convergence of the solution. Besides, the MAS has capability of representing the scattered field by several AS, placing them to the Scattered Field Singularities (SFS), which are located on caustic surface of the Scattered Field (SF). This idea allows to AS represent SF from big part of the surface as mirror image method. During presentation it will be demonstrate general methodology of SFS localisation (R. Zaridze, G. Bit-Babik, K. Tavzarashvili, N. Uzunoglu, D. Economou. "Wave Field Singularity Aspects Large-Size Scatterers and Inverse Problems." IEEE Transactions on Antennas and Propagation, vol. 50, No. 1, January 2002, p. 50-58.). As the basic functions satisfy the wave equation by itself, the margin of error of the simulation is determine by, how accurately one satisfies the boundary conditions, which can be controlled easily during calculations. On average, the margins of errors in below discussed results of calculation are nearly 0.1-1% and in extreme cases not more then 10%. All calculations were performed on the regular PC – Pentium III or IV.

2. A numerical study of EMC/EMI problems related to the resonance enhancement of the EM field inside vehicles, its influence on the passengers and on the inner sensitive electronic devices is given. Car could be considered as a hollow metallic structure with partitions, enclosing dielectric objects that simulates the human bodies and other dielectric inclusions. This system behaves as a resonator on some frequencies of incident EM waves. It was shown, that entire vehicle structure strongly influences on the performance of the vicinity antenna, especially when wavelength is comparable with vehicle's dimensions. Some simplified model of the automobile with partition and enclosed lossy dielectric body is considered to investigate its resonance characteristics. The geometric dimensions of considered car model are: 5m$\times$2.5m$\times$1.5m. The calculated resonance characteristics – integrated radar cross-section (IRCS) – of the objects under investigation - were obtained in a wide frequency band (20MHz-800MHz). Density and values of re-radiated and standing wave fields on such resonances sharply increase at high frequencies. Investigations of some particular cases have been performed allowing tracking the process of eigen-field forming inside the cavity. The formation and creation of new directional lobs in the pattern at the point of resonance frequency of the cavity – appearance of new spectral component in a far field is given. So, the MAS methodology allows determining and analyzes the basic characteristics of the 3D cavity – eigen-field, eigen-mode and eigne-values at the same time. Some analyses done how could create an undesirable influence on the passengers' health as well as on the sensitive electronic systems inside the vehicle.

3. The Electromagnetic Compatibility (EMC) and estimation of Specific Absorption Rate (SAR) problems are discussed together with interaction of the cellular telephone antenna field with the user considering the shape of the telephone housing. The radiation characteristics of cellular handset antennas strongly depend on the objects in vicinity of the phone. When the wavelength of the radiated field is comparable with the dimensions of the objects located near the handset those objects disturb performance and change electrodynamic properties of the antenna. Solution of this complex EMC problem we started with the investigation of the different types of antennas together with the feeding modeling in order to obtain high radiation efficiency and an antenna structures well-matched with open space. The next step was to redirect the radiated field to one the hemisphere out form the user's head in order to minimize interaction with objects in the vicinity, and then to consider IEEE Standard Anthropomorphic Head model. Here we consider mutual interactions of all previously described elements of the structure including the handset itself and the user's hand, brain, hard models. To this end the physical model was created and appropriate package of the program was developed to simulate and perform numerical experiments. Parametric change of geometry helps to achieve the best matching and radiation characteristics of the system. Some results of investigations will be done in report.

HPEM 23 - Hardness Assurance & Maintenance

HPEM 23-1: Transfer Function Measurements on a Composite Helicopter between 300 kHz up to 18 GHz

D. Dupouy[1], **Y. Daudy**[1], **W. Tauber**[2]
[1]*DGA/DCE/CEG, Centre d'Etudes de Gramat, Gramat, France*; [2]*OTEE/O, Eurocopter Deutschland GmbH, Munich, Germany*

In the frame of the European civilian program called "EMHAZ", studies have been started in order to improve aircraft protection against electromagnetic hazards, taking into consideration new configurations, including equipment, system and airframe, as well as new materials. In order to assess the behavior of a real aircraft (i.e. helicopter with composite fuselage) to external radiated EM fields in a wide frequency band, transfer function measurements have been implemented between 300 kHz up to 18 GHz using specific CEG test center experimental tools dedicated to test large sized systems. The ARTEMIS facility, which is a transportable low level transmitting system composed by two radiating parts, providing vertically polarized low level electric field ($\approx$0.1 V/m) at several hundred meters between 300 kHz and 1 GHz. The receiving system is in particular constituted by a 12 independent measurement channels network analyzer.

The ETARCOS facility, cylindrical measuring base constituted by various bi-polarized horn antennas moving on a vertical pylon, in order to realize complementary transfer functions between 0.5 GHz and 18 GHz.

Measurements are performed on a BK 117 C2 EUROCOPTER composite helicopter, under various configurations (threat polarizations and incidences, helicopter configurations,...). They consist of internal EM fields, currents on real cable looms (anticollision light wires, NAV and VOR coaxial cables, windshield flexballs,...) and currents and voltages on defined simple cable looms configurations, in order to do further close comparisons with theoretical works.

The results are presented in terms of transfer functions; the values are normalized to a 1 V/m incident electric field. Due to the bandwidth limitation of the sensors, the currents measurements are limited to 250 MHz. All the results, as well as the one's coming from additional lightning tests which have been implemented at the CEAT test center on the same helicopter, must be used later to verify the theoretical models developed by the other partners of the EMHAZ program (CRIPTE code from ONERA for example) and also to extend the experimental data base suitable to validate the theoretical modeling applicable to this kind of problem.

HPEM 23-2: Feasibility of Reflectometry Techniques for Cable Bundles Diagnostics aboard Aircraft

M. D'Amore, **M. S. Sarto**, **A. Tamburrano**
Dept. of Electrical Engineering, University of Rome "La Sapienza", Italy

The development of efficient tools for the fault prognostics and diagnostics of cable bundles onboard aircraft is a key-issue in order to guarantee maximum flight safety and to reduce the time required for maintenance. The early detection of defects in the cable shields and in the bonding connections of the onboard wiring system is also needed to assure EMI protection of the avionics apparatus.

Reflectometry techniques are widely used for the identification of faults in electrical and telecommunication networks [1]-[4]. They allow to verify the presence of defects, the damage level and the position of defects along the cable. However, their application to the wiring system onboard aircraft is critical, due to the complexity of the system, the non-uniform configuration of the cable bundle, the branches of the network, the presence of numerous electrical components and the reduced geometrical dimensions of the harnesses sections. Attempts of applying reflectometry diagnostics to simple aeronautical cable configurations are reported in [5], [6].

A two-year research project has been coordinated by the EMC Group of the University of Rome “La Sapienza” and carried out in collaboration with the University of Ancona, and the University of L’Aquila. The scope of the project was to exploit reflectometry techniques for the fault diagnostics of the wiring system onboard aircraft. The results of the experimental diagnostics tests performed by applying the frequency-domain reflectometry technique on different cable typologies are presented in [7]. The tests are performed on aeronautical cables supplied by Alenia Aeronautica in the Electromagnetic Compatibility Laboratory of the University of Rome “La Sapienza”, and aboard the Airbus 321 aircraft of Alitalia.

The scope of this paper is to discuss the feasibility of cable fault diagnostics and prognostics onboard aircraft, by considering the following critical aspects: the definition of reliable test procedure for single-core unshielded cables; the definition of the relation between the frequency span used in the reflectometry test and the characteristics of the cable bundle under investigation; the assessment of the influence of the cable bundle configuration on the reflectometry analysis of faulty cables.

References

[1] C. Weber, L. Jung, J.L. ter Haseborg, “Characterization of inhomogenities in shielded multiconductor cables by evaluation of the coupling parameters and frequency domain reflectometry”, 14th International Symposium on EMC, February 20-22, Zurich, 2001.

[2] E. Martinod, P. Nadeau, N. Feix, M. Lalande-Guionie, A. Reineix, B. Jecko, “Transmission link radiation and localized defect contribution”, IEEE Transactions on EMC, Vol.43, No.2, May 2001.

[3] L. Jung, J.L. ter Haseborg, ”Measurements of complex transfer impedances of shielded multiconductor cables with inhomogeneities inside cable bundles”, International Symposium EMC Europe 2000, Brugge, September 11-15, 2000.

[4] F.M. Tesche, T.K. Liu, “Techniques for the automatic surveillance of the electromagnetic hardness of electrical systems”, NATO TLG-3 Meeting, Brussels, July 17, 1987.

[5] C. Furse, Y.C. Chung, R. Dangol, M. Nielsen, G. Mabey, R. Woodward, “Frequency domain reflectometery for on board testing of aging aircraft wiring”, IEEE Transactions on EMC, Vol.45, No.2, May 2003.

[6] S. Field, P. Arnason, C. Furse, “Smart wire technology for aircraft applications”, Fifth Joint NASA/FAA/Do/ Conference on Aging Aircraft, Orlando, FL, September 2001.

[7] M. D’Amore, M.S. Sarto, A. Tamburrano, “Experimental diagnostics of aeronautical cables using frequency domain reflectometry”, submitted to EMC EUROPE 2004, Int. Symp. On EMC, Eindhoven, The Netherlands, Sept. 2004.

HPEM 23-3: Electromagnetic Susceptibility of a Structure Composed of Several Shelters Networked in a Complex Manner and Constituting a Command Control Unit

J. Geiswiller[1], D. Asfaux[1], Y. Béniguel[1], E. Kerhervé[2], B. Pecqueux[2], J.-C. Joly[2], W. Tabbara[3], M. Hélier[3], D. Lecointe[3]

[1]*IEEA, Gramat, France*; [2]*CEG, Gramat, France*; [3]*SUPÉLEC, Gif-sur-Yvette, France*

The object of this paper is the study of the susceptibility of a very large structure composed of different kinds of elements: antennas (in the HF band and above), shelters of different shapes and sizes, power supply equipments, ... all of them being networked in a complex and arbitrary manner. This may correspond to the deployment of a command control unit. The threat we consider, is an electromagnetic threat, typically for this study a plane wave illumination. For this kind of structure one exhaustive analysis including all parameters of the problem, both electromagnetic (direction of arrival, field polarisation, levels,...) and geometrical, including the environment: ground electrical characteristics, terrain profile,..., is impossible and meaningless.

The analysis technique that we have developed for this study is a statistical technique based on the Kriging approach. It includes mainly two stages:

- Find what is called the “observables” which can be seen as the basis parameters. Once defined and known any other variable of the system can be subsequently determined.
- Define a model to characterize the susceptibility of these observables to the threat.

The definition of observables is partly based on a restricted analysis. If we consider for instance one typical shelter, the electromagnetic environment inside this shelter can be obtained by rigorous calculation and a representative “worst case” defined. A typical result for the field density in dB is presented on figure 1.

The equipments inside the shelter and their connecting cables are considered. Variables of interest are of two kinds: fields inside the shelter and currents on cables. Observables are of these two kinds and correspond to points locations inside the most critical areas. In this first case the shelter is considered as a standalone element and its susceptibility is related to the impinging field. Connecting this shelter to a second one still leads to a tractable problem. A second kind of intrusive signals is exhibited induced by coupling currents between the two shelters. Again the worst case is retained for subsequent analysis. This first stage of the study allows to build a phenomenologic model and define the “observables”. The second part of the study is the statistical study, more precisely the implementation of the Kriging technique. This is essentially one interpolation technique in which a regression model is related to the realization of a stochastic process.

The different steps of the statistical study are:

- To build a database, varying the input parameters (of any kind) on a broadband range
- To build histograms of the “observables”
- To find the best “fitted” related probability distribution
- To find the covariance function and the best suited estimator

This being done, the accuracy of the model can be checked. The process can be iterated regarding in particular the choice of the probability distribution function (law and parameters).

One of the major interest of this Kriging technique is the fact that the model can be enhanced by the knowledge of any subsequent data set originating either from a calculation or a measure. This directly interacts, in particular, with the definition of a measurement campaign and on the choice of relevant sample cases. The results obtained will be presented for a typical arrangement of the different elements constituting the deployment.

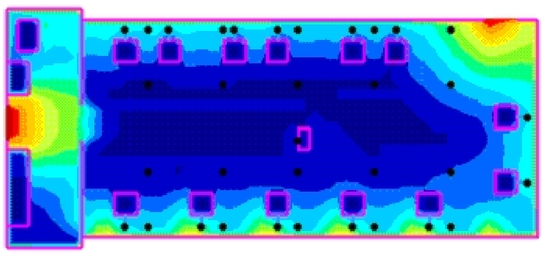

Figure 1: Field density in dB in a shelter.

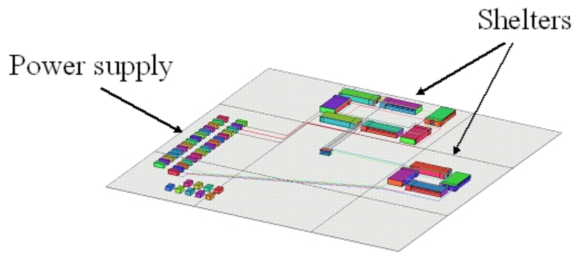

Figure 2: Typical arrangement of the different elements constituting the deployment.

HPEM 23-4: Successful Certification of WLAN Systems in Commercial Passenger Aircrafts

I. Schmidt[1], **A. Junge**[1], **M. Schwark**[1], **S. Pötsch**[2], **A. Enders**[1], **R. Kebel**[2]
[1] *Institute for Electromagnetic Compatibility, Technical University at Brunswick*; [2] *Airbus Germany*

Airlines and manufacturers work eagerly to make secure use of portable electronic devices (PED) on aircrafts possible. In addition, today's costumers desire internet access, E-Mail and other services directly at their seats. Ideally these services are available via Wireless LAN (WLAN) for use with passenger owned devices (Laptop, PDA). Airline companies also take advantage from wireless applications for their own demands (crew communication, maintenance monitoring and security surveillance).
Currently on-board WLAN technology is developed by airlines and manufacturers to satisfy these needs. Given that WLAN systems are intentional transmitters of electromagnetic radiations, these systems need a certification from aviation authorities. Main part of the certification process is the verification of non-interference of installed equipment with any other aircraft system.
We present a thorough test procedure, designed to simulate the regular operation of WLAN standards (IEEE 802.11a, IEEE 802.11b) in different types of aircrafts. All tests are performed on ground in cooperation with qualified technicians and engineers, who operate and observe all aircraft instruments.
The test configuration consists of a λ/4 monopole antenna emitting either a real WLAN signal taken from an on-board access point or an artificial WLAN signal generated by a digital signal generator. The artificial signal is a modulated carrier conforming to the standard with or without data packages included. Worst case conditions are examined by amplifying the selected signal to a multiple of the original signal level (up to 45 dBm) in both cases. The output level is controlled by a power meter and waveforms of all signals are monitored by an EMI test receiver.
An entire test takes several hours to complete, because a large number of aircraft systems has to be checked at all relevant transmission frequencies in 2.4 GHz (802.11b) and in 5 GHz bands (802.11a). Additionally, the procedure has to be repeated at several test positions of the antenna. The required number and locations of test positions vary between different aircraft models. Special attention is paid to flight critical aircraft systems (navigation, communication) mainly located in cockpit and electronic equipment compartment.
The test procedure is capable to detect unintentional interaction between aircraft systems and an installed WLAN system and yields reliable results. By presenting corresponding non-interference results to the aviation authorities, airlines and manufacturers are able to obtain the required certifications.

HPEM 23-5: Lightning- and Radiation Induced Voltages and Currents on Internal Wires Inside a Wing Fuel Tank.

G. Eriksson
AerotechTelub AB

Motivated by a small number of accidents, all commercial aircraft manufacturers have been instructed to thoroughly review the protection against any threat that can lead to an explosion inside the fuel tanks. As part of the work to review the safety of the Saab 340/2000 aircraft, numerical and analytical tools have been used to estimate the level of lightning- and HIRF (High Intensity Radiated Field) induced voltages and currents on wires running inside the wing fuel tanks. Doing this in a systematic manner, general physical understanding is gained and resource-consuming tests can be avoided. By comparing the computed voltage, current, and energy levels with those known to be able to cause explosions due to sparks or filament heating of short-circuiting metal fragments, it is possible to demonstrate that the risk for such events is acceptably low.

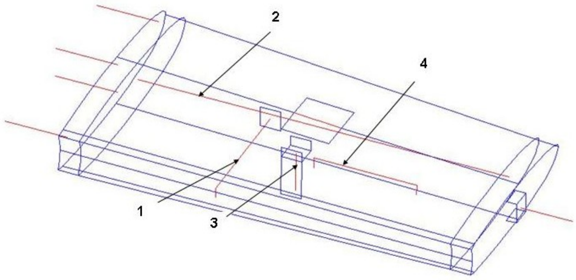

Figure 1: The interior of the wing section, including the four probe wires (numbered).

HPEM 24 - New Frontiers in Effects Analysis for Electromagnetic Interference

HPEM 24-1: On the Derivation of Physical Relations From Effects Data

R. L. Gardner

When we take a series of measurements to better understand electromagnetic effects or coupling, our end goal is to develop a physical relationship or formula connecting the observables of interest. Maxwell's equations were developed using a similar process, in which the supporting research spanned over two hundred years. For example, Henry Cavendish began with a series of measurements of the forces between spheres carrying electric charge. The initial work estimated the $1/r^2$ decay in the forces to about 10% [Maxwell, JC, ed., The Electrical Researches of Henry Cavendish, Frank Cass & Co, Ltd, London, 1967]. Since then, the errors in the $1/r^2$ fall off have been tightened to less than 10-15.
Extending the mechanics of the combined physical and empirical relationships to the effects part of electromagnetic compatibility research is somewhat more difficult because of the categorical nature of the results of the effects experiments. To derive the physical trends directly from the data, we typically use various forms of regression analysis. If the data follow a threshold-like form, we can fit the regression equations to a logistic distribution. This distribution maps the -∞ to ∞ range of the regression analysis to the required [0,1] range required for statements of probability. With the regression approach, we can look at the variation with several variables and the potential interactions between the parameters. The result is limited to locally linear behavior in the regression variable. The regression variable is often a more complex function of one or more physical variables. Each of these functional forms of the regression variables must be chosen by the analyst. The regression tests the chosen form but does not directly make it appear.
In this paper, we will take data on effects experiments and work through the development of physical inference. For example, effects sensitive to peak electric field, like some forms of upset, will often scale with peak electric field. On the other hand, effects like the opening of a fuse respond to combinations of received power and energy. Whatever the result of such an analysis process the empirical and physical relationships developed from the data or first principles must agree or one of them is wrong. Deriving such a relationship is what took the various researchers so long the development of Maxwell's equations. They could see the measured behavior of the important parameters, but it took some time before the physical relationships became apparent.

HPEM 24-2: Bayesian Data Analysis and Optimal Experimental Design for RF Effects

T. J. Clarke
Air Force Resarch Laboratory

Probability of Effect (Pe) models are a fundamental building block for analyzing RF effects data and for predicting effects. Two seemingly unrelated questions are how to analyze effects data, which are discrete binary observations, to build continuous Pe models, and how to plan effects tests to generate useful data most efficiently. We will show how these questions can be addressed together within a Bayesian framework. We will first describe how to derive Bayesian confidence bounds for a Pe model by generating a posterior distribution of Pe models from a given data set and specified prior. Next, we will discuss how to make use of a Bayesian method to design an effects experiment, using an approach that optimizes some measure of the information expected from the test. The particular information measure we adopt depends on the specific objectives of the experiment. Finally, we will discuss an adaptive approach to test design that combines Bayesian data analysis with optimal design, allowing us to maximize the information collected given a fixed total number of effects observations.

HPEM 24-3: EMI Effects Analysis Techniques that Yield Exportable (Test Bed Independent) Results

C. Ropiak[1], **P. Hayes**[2]
[1]*Envisioneering, Inc.*; [2]*CEMTACH*

Central to the success of a susceptibility program is the analysis and subsequent application of results from electromagnetic interference (EMI) experiments. To this end, devising a model that accurately captures the results of an EMI experiment is a primary goal. A secondary and arguably more important objective is for the model to be exportable, reasonably independent of the test house so that one may use the model to predict the outcome of new EMI experiments, or to simply draw general conclusions about the response of the test objects used in the experiment.
The model itself should provide a functional connection between experimental parameters and the resulting EMI effects on the test objects. The more general the parameters, the better the chance of result exportation. For example, parameter classes that include things such as source location and orientation will be intricately connected to the source, whereas parameters classes that include things such as peak electric field on target or peak power on target are less dependent on that particular source and may be generalized to be association with a source type making the results broader in applicability. Hence, the closer the parameter class choices are to electromagnetic (EM) environment descriptions and less contingent on source specifics the better.
To this end, a fabricated EMI data set is created. The statistical technique known as multivariate logistic regression (MLR) is used to provide a model for the data set. Different parameter class choices ranging from the most restrictive, source parameters, through electromagnetic environment parameters, and ending with induced current parameters are investigated. The strengths and weaknesses of each type of parameter class are investigated as they pertain to the accuracy of the fitted model as well as its exportability.

HPEM 24-4: Footprints - A Tool for Visualizing Electromagnetic Radiation Patterns

P. J. Vail
AFRL/DEH

HPEM 24-5: Communications-Theoretic Techniques: Keys to Pulsed IEMI Problems? - Conceptual Foundations

R. Boling, **I. Kohlberg**
Institute for Defense Analyses

This paper will present the foundations for addressing pulsed intentional electromagnetic interference (IEMI) mitigation through the application of some communication theoretic methods. Probably the most vulnerable targets of IEMI attacks are probably local area networks (LANs), because they are usually designed to operate in relative secure, very "quiet" environments, with high signal-to-noise (S/N) levels. In such settings, very little (if anything) is usually done to deal with any interfering signal, such as IEMI. We will address the basic characteristics of typical LANs, and similar unprotected communication channels, as well as some basic timing characteristics of typical current IEMI waveforms. The resultant bit-level interference will be described and examples presented.
Because the actual interfering signal rarely takes the form of an ideal pulse, we will explore techniques to further characterize the interfering waveform by considering the "distortion" of incident fields in realistic target environments (e.g., those that contain multiple scattering surfaces within a single enclosure). Each scattering event stretches and reshapes the incident pulse waveform. In a recent paper (URSI, Boulder, 2004), the authors presented a generalized scattering model to illustrate how multiple scattering events could shape IEMI to enhance their potential impact on bit errors in a communications system. Normalized analytic techniques will be presented to characterize pulse stretching and reshaping actions due to surface scattering interactions. Included within this context are contributions from diffraction effects at scattering surface edges.

HPEM 24-6: Communications-Theoretic Techniques: Keys to Pulsed IEMI Problems?

R. Boling, **I. Kohlberg**
Institute for Defense Analyses

This paper proposes various schemes for encoding information such that bit errors due to pulsed interference in data communications could be completely eliminated for a wide class of waveforms. The development proceeds from techniques that compensate for single bit errors to a more general class of coding and bit manipulation schemes capable of eliminating multiple bit errors over a data communications channel. It is shown that the greatest gain from message coding occurs for systems in which the interfering pulse repetition rate is significantly slower than the signaling bit rate, or where the pulse width of the interfering pulse is less than or comparable to the signaling bit pulse width. The price paid for error-free communications is a lower data rate and an increase in transceiver complexity. However, in typical local area networks (LANs) or control links configured for a low-noise environment, there is usually a surplus of unused bandwidth, and these typical "target" systems may easily accommodate the higher bit rate required to maintain the same (unencoded) information rate.
The paper addresses both sides of the resulting competition (information disruption techniques versus mitigation of interfering signals). If the coding and transmission rates are known for the encoded system, we present ways to optimize the waveform of the IEMI. On the other hand, building upon the basic communications-theoretic notions of signal coding and message packaging, we explore a generalized, adaptive approach that optimizes the code selection based upon measurable parameters of the interfering pulse

HPEM 24-7: An Overview of the Mission Degradation Analysis (MIDAS) Program

M. Sward[1], **A. Costantine**[2], **M. Mcgovern**[2], **P. Spraggs**[2]
[1]*Defense Threat Reduction Agency*; [2]*SAIC*

National resolve to mitigate the effects of a variety of attacks (including EMP and RF) on infrastructure elements has resulted in the use of a multiplicity of independent assessment methods to determine and fix vulnerabilities. These independent approaches are not adequate given the complexity of the interdependencies of the various infrastructure sectors. The purpose of the Defense Threat Reduction Agency Mission Degradation Analysis (MIDAS) Program is to conduct research and development efforts to fill the shortfall in critical infrastructure protection assessment and mitigation strategies.
Critical infrastructure protection is defined as the identification, assessment, protection and assurance of physical infrastructures and cyber elements essential to the continued operation of the system-of-systems complex upon which our society depends. This includes infrastructures essential to sustain the U.S. com-

mercial/private sector, foreign commercial/private sector upon which we rely, and the means to sustain military operations for DoD.

There is broad recognition that nation's infrastructures are becoming increasingly complex and interdependent and face a broad spectrum of threats and that the ability to formulate an effective national protection strategy requires access to sophisticated assessment capability that does not presently exist.

The MIDAS technical approach is to deal directly with the issue of sector interdependencies (e.g., electrical grid and telecommunication) so that the goal of providing an integrated assessment and mitigation toolset is met. The program is structured to:

- Perform research and develop tools to assess the degradation of Critical Infrastructures and the impact on missions and functions following manmade or natural disasters

n Provide the tools and methodologies that will enable integrated vulnerability assessments in support of critical missions

- Provide tools and techniques for database mining, infrastructure interdependency analysis, integration of vulnerability assessments, and mitigation/remediation planning
- Provide information and results using advanced visualization techniques for support to analysts, assessment teams, mission planners, and risk managers
- Validate outputs of MIDAS predictive tools and models by use of actual hardware and operating software such as the use of the SAIC/Telecordia Technologies "Next Generation Network" (NGN) testbed.

Figure 1 summarizes the research and development areas of the MIDAS program.

This paper will provide an overview of the MIDAS R&D program, accomplishments to date, and planned activities.

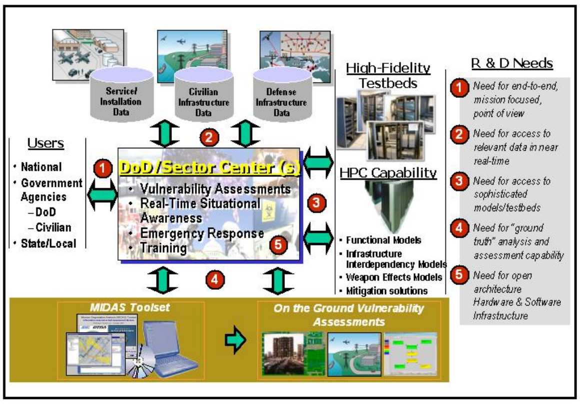

Figure 1: Research and Development Areas for the MIDAS Program

HPEM 24-8: Use of a "Hardware Testbed" to Determine System of Systems Vulnerabilities

M. Sward[1], **P. Spraggs**[2], **A. Costantine**[2], **F. Varcolik**[2], **D. Ambrose**[3], **M. G. Linnel**[4]
[1]*Defense Threat Redcution Agency*; [2]*SAIC*; [3]*Power Systems Consulting*; [4]*Telcordia*

The purpose of the Defense Threat Reduction Agency Mission Degradation Analysis (MIDAS) Program is to conduct research and development efforts to fill the shortfall in critical infrastructure protection assessment and mitigation strategies. A primary research area of the MIDAS program involves the use of actual hardware and operating software such as the SAIC/Telecordia Technologies "Next Generation Network" (NGN) testbed.to validate the outputs of MIDAS predictive tools and models. This paper will describe the software and hardware testbed simulations used to assess the effects of communication network losses for a supervisory control and data acquisition (SCADA) system patterned after a network proposed to provide connectivity within the western United States for monitoring and controlling the power grid.

There is a clear pattern of movement from private control of the information and control signals within a power system to use of public data/information networks for this purpose. Presently most power networks obtain information (e.g. line frequency, voltage, generator settings) and send control signals (e.g. breaker closure, change generator settings) to the network as part of their SCADA system using privately owned networks such as microwave and landlines owned by the power system. The use of the public information networks (e.g. Internet) represents a potential vulnerability to the power system that has already been exploited in other infrastructures, such as by the Slammer worm attack in January 2003.

The purpose of this research and development effort was to establish a testbed combining a simulated, but highly realistic, power system including SCADA control and RTUs (Remote Terminal Unit) with an actual operating Next Generation Network (NGN) as the communications link in the SCADA system. The particular test sequence described in this paper was designed to act as a proof of principle that this could be done and to provide initial results related to failures in the communications network.

The Next Generation Network (NGN) Laboratory at Telcordia in Red Bank, NJ was used in this methodology development. This work expands on previous activities performed for DTRA under the EM/INFRA 2010 and MIDAS programs in which SAIC and Telcordia Technologies developed test plans and conducted tests to examine the possible performance of a telecom infrastructure under a specific set of network failure modes.

This SCADA/Telecom testbed experiment aimed specifically at examining interdependencies between the telecommunications network and the power network with respect to communications losses incurred by a variety of potential threat to include RF weapons and electromagnetic effects.

In the presentation we will identify scenario(s) that produced outages based on both a software and "hardware in the loop" testbed simulation of an eastern Colorado utility grid disruption and communication delays that might result in collapse of the powergrid.

HPEM 24-9: HPM Effects on Central Processor Units

R. F. Gray, **W. M. Bollen**
Mission Research Corporation

Mission Research Corporation (MRC) performed an electromagnetic (EM) susceptibility test on a single-board computer. The purpose of this work was to develop a better understanding of the high power microwave (HPM) induced upset process for digital circuits in general and processors and computers in particular. The outcome of this test effort is an understanding of what determines the probability of upset (at a circuit level) of the microprocessor at a given power density level and microprocessor state. The methodology used for this susceptibility testing was developed by MRC on a previous program.

A single-board computer was selected as the test object. The computer used is a Crystal CS5OO with an AMD 386-SX microprocessor. Electrical specifications for the computer are provided in Figure 1. The test computer was connected to a control computer via a serial port cable. The control computer was used to initiate the test and receive messages from the test object during and after RF exposure.

To obtain the susceptibility information of interest, the RF pulse was made to occur while the test object was in a known state. This was accomplished by forcing the test object to repeatedly execute the same instruction while the RF pulse was applied. However, there was no control over the relative time of the RF pulse and a specific command execution. The test set-up is shown in Figure 2.

Upset data were collected across a range of environment parameters including pulse width (100 ns to 10,000 ns), repetition rate (10 kHz to 1.5 MHz), and number of pulses (1 to 100). For a specific environment setting (pulse width, repetition rate and number of pulses), the output power level was adjusted across a range that included no effect to at least a 50% probability of effect. Each test condition was repeated to obtain valid estimates of the probability of effect. The number of tests at each output

level varied between 25 and 50 to assure a reasonable confidence bounding of the data point. All of the data were collected for a set of simple CPU instructions to allow ease of analysis.
The paper will document the testing performed, the development of a statistical model, and comparisons of the model with the actual test results. We have shown that a relatively simple statistical model can be used to explain the upset behavior of a complex piece of electronics exposed to an HPM. The data presented was taken for a very basic instruction set to allow repeatable results with small sample sizes. The importance of this work relates to the fact that processors are critical elements in the control electronics presently in-use for complex electronics systems. Further, these control processors appear to be the critical elements that dominate upset.
An example of the upset data obtained and correlation with a simple model is shown in Figure 3. The data presented are the probability of no effect when the microprocessor was exposed to a single HPM pulse. The probability of no effect, Pne, is related to the probability of effect , Pe, by noting that Pne = 1- Pe.
This preliminary investigation demonstrates the potential for developing a methodology for the prediction of upset due to HPM. Such a methodology could provide a means to analytically predict system failure from a limited number of system level tests.

Manufacturer	Crystal Group
CPU	AMD 386-SX
CPU Clock Speed	40 MHz
Hard Drive Capacity	520 MB
RAM	4MB
Floppy Drive	1.44MB
Video Card	None (Modified BIOS)
Operating System	DOS 5.0
Terminal Program	CTTY (Part of DOS)
Communications Ports	2 Serial Communications Ports
Keyboard Port	Keyboard Port available, but not used.

Figure 1: Test Object Specifications.

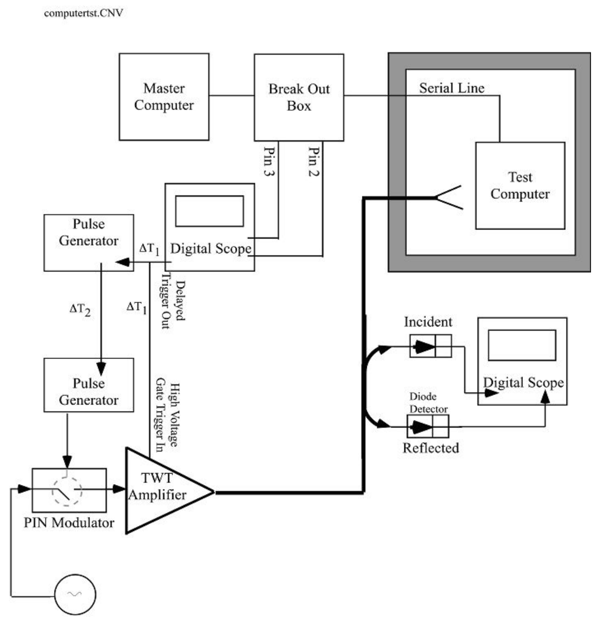

Figure 2: Test setup to measure probability of kill. Pin 2 initiates the start of events.

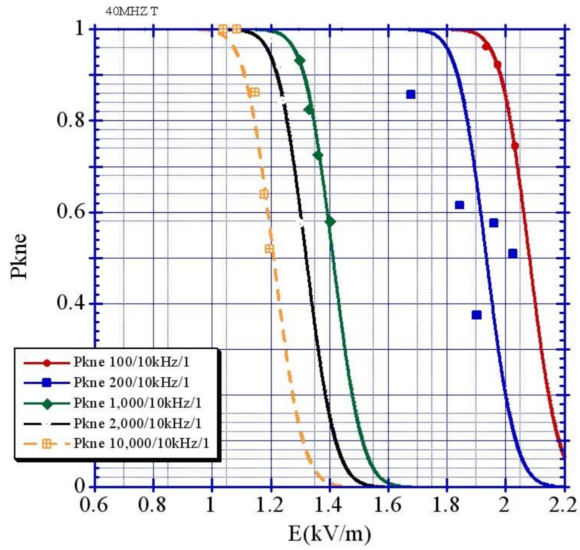

Figure 3: Comparison of test data and model.

HPEM 24-10: Investigation of Radio Frequency Modeling Techniques for Cavities

T. D. Andreadis[1], M. Starosta[1], J. Shue[1], P. W. Grounds[1], P. G. Girardi[2]
[1]*Naval Research Laboratory, Washington, DC*;
[2]*Envisioneering Inc, King George, VA*

This effort describes the investigation of a modeling approach to predict the coupling of microwaves into a resonant cavity enclosure, with the intention of using this information to determine the effects of the coupled RF on electronic circuitry inside the enclosure. The approach was to use the finite-difference time-domain (FDTD) method to calculate the electromagnetic fields inside the cavity enclosure, and then to compare this with experimental data. The probe to measure the RF was incorporated into the simulation geometry so that it is identical in both the experiment and the simulation. The FDTD method was used in combination with the fast Fourier transform (FFT) technique to calculate the frequency response of the cavity across the frequency range of interest. To accommodate the fill time of the cavity enclosures, a simulation time of over two hundred nanoseconds was required before the coupled signal would reach steady state. After each computer simulation, the results were compared with experimental data and refinements to the model geometry were made. This information was used to determine the portions of the geometry that had the greatest effect on the accuracy of the simulation. Several experimental test setups were used to determine the repeatability of the experiments and to determine the sensitivity that a small change in the test setup would have on the final results. Different experimental and simulation setups were compared. The final simulation and experimental results are in good agreement with each other.

HPEM 24-11: Statistical Approach of Efficiency of HPM Weapons and Systems Vulnerability.

J.-P. Percaille
DGA/DCE/CEG Centre d'études de Gramat 46500 Gramat France

Many parameters are necessary to define a HPM threat : power, frequencies, repetition rate , duration.
The coupling effect on a system is also highly dependent on angles of incidence, polarization, and azimuth.
For front door coupling, a determinist approach can be used.
On the other hand, back-door effects are highly dependent on threat and system characteristics. So, back door results can be differently appreciated depending on whether they are analyzed as the target point of view (vulnerability) or as the weapon point

of view (efficiency).
This study shows that a statistical approach, applied to back-door effects, permits to point out that the range for the weapon and the safety distance for the target are two different concepts.
In this statistical approach the disruption probability is obtained as a function of the weapon -target distances. The stresses induced on the system electronics, as well as the threshold levels, are assimilated to random variables of known distributions. The disruption probability is obtained by calculations on these two distributions.
It is shown that the weapon efficiency is quite different if some target weaknesses (in terms of frequency or angles configuration) are supposed to be known.
As well, the method permits to quantify the increase of the target vulnerability by taking into account some weapons capabilities.
All steps of the method are illustrated by numerical and experimental results issued from targets studies. Especially, the one carried out on a generic missile is used to assess the advantage obtained by a repetitive, tunable frequency weapon.
Various assumptions made on targets or weapons can strongly influence the final results.
The statistical method, presented here, provides definitions of weapon efficiency and target vulnerability. They are expressed in terms of probability function of the range.
This method is also able to quantify the main parameters of most weapons efficiency and targets vulnerability.

UWB - Ultra Wide Band

UWB 1 - Special Session to Honor Carl Baum

UWB 1-1: Dr. Carl Baum: One Remarkable Career

W. D. Prather
Air Force Research Laboratory

In a career that has spanned more than 40 years, Dr. Carl Baum has made a remarkable number of advances in electromagnetics and has for most of that time been one of the world's leaders in the development of new theory and concepts for antennas, transmission lines, sensors, EMP simulators, and pulsed power systems.
He has authored, co-authored, and edited literally hundreds of leading technical notes and papers, creating a library of information that is used throughout the world today.
He established the Nuclear Electromagnetics Meeting (NEM) that has grown and endured to become what we observe here today as EUROEM 04. He has given workshops and short courses in the United States and around the globe.
In this paper, we will give a brief overview of Carl's history and career from the 1960's to the present day.

UWB 1-2: Reminiscences about working with Carl Baum for over 3 decades

D. V. Giri
Pro-Tech

UWB 1-3: Carl E. Baum: 40 Years of Leadership in Developing Sensors for Electromagnetic Pulse (EMP) Measurements both Inside and Away from Nuclear Source Regions

J. C. Giles
Los Alamos National Laboratory, Los Alamos, NM, USA

Dr. Carl Baum began developing accurate ("'calibrateable' by a ruler"), fast (sub-nanosecond rise times in several cases) EMP sensors in the mid-1960s at the U.S. Air Force Weapons Laboratory in Albuquerque, NM (now part of the Air Force Research Laboratory). Baum's leadership led to broad lines of electric field, magnetic field, and current sensors as well as ancillary instrumentation by the time he and coauthors published a summary paper in a Joint Special Issue on Nuclear Electromagnetic Pulse in February 1978. Accurate broadband sensors with simple transfer functions are needed to measure transient electromagnetic fields and related quantities. Various sensor designs have been developed and iterated over the years to achieve this in an optimal manner. Such sensors are designed for use in a "free-space" environment (such as an EMP simulator or on a system under test in such a simulator) or in a nuclear-source region that includes local source current and perhaps conductivity.

UWB 1-4: Exploting Noisy Transient Response using the Fractional Fourier Transform

S. Jang, **T. K. Sarkar**
Department of Electrical Engineering & Computer Science, Syracuse University

The goal of this paper is to obtain the electrical properties of the target from the received transient noisy time domain waveforms. Because of their aspect independence, complex resonant frequencies of a conducting object are used as a signature of the object to discriminate it from others for the purpose of target identification. The singularity expansion method (SEM) proposed by Baum has been applied to express electromagnetic response in an expansion of complex resonances of the system. It has been shown that the dominant complex natural resonances of a system are a minimal set of parameters that define the overall physical properties of the system. So, a transient scattering

response is analyzed in terms of the damped oscillations corresponding to the complex resonant frequency of the scatterer or target. Since the resonances describe global wave fields that encompass the scattering object as a whole, the SEM series representation encounters convergence difficulties at early times when portions of the objects are not yet excited. Early time response is strongly dependent on the nature of the source, the location of the source, and the location of the observer. Usually the early time response shows impulse-like characteristics. Because of this difficulty, most previous techniques such as Matrix pencil method (MPM) used just late time signals only. It is necessary to include 'entire function' to represent early time impulse-like components. The 'entire function' is subset of the analytic function but it doesn't have any singularities.
In this paper, the transient noisy electromagnetic response is considered in the time domain and in the fractional Fourier transform (FrFT) domain. The whole time domain data set is used to test. Fractional Fourier transform (FrFT) is a generalized Fourier transform. Using the FrFT it is possible to discriminate an impulse-like component from the other components of the signals. Because of this property, impulse-like early time components can be separated from the damped exponentials. To describe the early time response a Gaussian pulse is selected. Gaussian pulse is an entire function and is quite adequate to describe pulse-like components in early time. Complex exponentials are used to describe the late time signals. The concept of a 'Turn-on time' is utilized to consider a time when the fully excited resonance can be used, formally. The results for wire scattering element and finite closed cylinder with various SNR show that if SNR is greater than 30dB it is possible to get meaningful parameters using proposed techniques.

UWB 1-5: E.M. Topology: From Theory to Application

J.-P. Parmantier
ONERA

The first mentions of EM Topology (EMT) go back to the late 1970s [1] but Carl Baum is the one who really put all the pieces together to build up the formalism of this theory [2]. From a qualitative point of view, this theory emphasizes the decomposition of a system in volumes in order to manage EM coupling analysis. From a quantitative point of view, it offers the BLT equation as a network tool to estimate EM coupling in the system. Within my PhD at Dassault Aviation and ONERA, I got the chance to work on that theory in the late 1980s discovering Carl's massive written production (and very personal notations!). At this time, no application of the theory was available in the open literature and our idea was to take advantage of the modularity offered by EMT in order to improve calculation performance. Starting from general volume decomposition concepts, and even if many specific bricks already existed [3], we quickly discovered that the system level modeling background was not mature enough to apply the full theory on a complete system. Therefore, we restricted the application scope on EM coupling on electrical cable networks running in multiple-volume structures. All this work led to the development of the CRIPTE code in the early 1990s and to joint experiment validations carried out with Centre d'Etudes de Gramat (CEG). One of our most memorable success was obtained during the EMPTAC experiments held at the birthplace of EMT, in Albuquerque, from 1993 to 1996. We demonstrated that applying the BLT equation on a very large wiring system [4] was feasible and could provide predictive results [5].
Nowadays, many computer codes addressing the problem of EM coupling on multiconductor cable networks have spread out among the world and are available at industry level. The field-to-transmission line theory appears as an effective method to link cable problems and scattering problems based on full wave computer code resolutions. However, to our knowledge, CRIPTE is the only code to be based on the BLT equation, enlarging thereby the scope of future EMT-related applications. As an example, the equation is now fully optimized by using the description of the topology in order to map the sparse structure of the matrices [6].
All the work on cable networks required an adaptation of the theory, mostly used as a guidance for organizing EM calculation on a large system [7]. Nevertheless, the recent developments carried out on the Power Balance method seem to provide a new domain of application of EMT for the determination of EM coupling on large systems at high frequencies and seem to be perfectly matched to the original formalization of the theory [8].
Today several challenges related to EMT are already identified:
- the development of multi-domain techniques offering the capability to assemble with a network formulation any type of numerical solver. Some results are already available at demonstration stage but the challenge is to make automated the exchange of data,
- the development of techniques inspired from the Non Uniform Transmission Lines (NUTL) theory aiming at a generalization of Transmission Line equations to any type of geometry. This work is still at a theoretical stage but is very promising for possible EMT generalizations.

References

[1] F. M.Tesche, "Topological Concepts for Internal EMP Interaction," IEEE Trans. AP, Vol. AP-26, No. 1, January 1978, pp. 60-63.
[2] C. E. Baum. The Theory of the Electromagnetic Interference Control. Interaction Notes. Note 478, December 1989 and, Modern Radio Science 1990, pp. 87-101, Oxford University Press.
[3] K.S.H Lee : A complete concatenation of technology for EMP Principles, Techniques and Reference Data Interaction Notes. December 1980.
[4] C. E. Baum, T. K. Liù, F. M. Tesche. On the Analysis of General Multiconductor Transmission-Line Networks, Interaction Notes, Note 350, November 1978.
[5] J-P. Parmantier, V. Gobin, F. Issac, I. Junqua, Y. Daudy, J.M. Lagarde, L. Paletta, ETE III : Application of Electromagnetic Topology on EMPTAC, Interaction Notes, Note 527, May 1997.
[6] J-P. Parmantier, X. Ferrières, S. Bertuol, C. E. Baum : Various Ways to Think of the Resolution of the BLT Equation with an LU Technique. Interaction Notes, Note 535, January 1998.
[7] J-P. Parmantier, P. Degauque : Topology Based Modeling of Very Large Systems. Modern radio Science 1996. Edited by J. Hamelin. Oxford University Press. pp. 151-177.
[8] I. Junqua, J-P. Parmantier, F. Issac : A network formulation of the Power Balance Method For High Frequency Electromagnetic Coupling Applications. Interaction Notes, Note 551, November 2002.

UWB 1-6: Newest Developments in Transmission-Line Theory and Applications

J. Nitsch, S. Tkachenko
IGET, Otto-von-Guericke-University Magdeburg, Germany

Linear structures constitute an essential part in electrical and electronic circuits, switch-boards, devices, systems, and buildings. Therefore, it is unavoidable to treat the electromagnetic interaction of electromagnetic fields with these structures, and in recent days this interaction has to take into account higher and higher frequencies, currently reaching up to several GHz. Thus the usual, regular transmission-line theory is no longer sufficient to cover all the modern requirements for complex systems, and the need for greater accuracy has led to a need for better models. Such models have to be capable of modeling very complex geometries, like finite lines, bends, nonuniform line conduction with curvature and torsion, including periodic structures, they have to include radiation losses and non-TEM coupling at higher frequencies. Even for thick cables or cable-bundles at high frequencies azimuthal current distributions will become of remarkable amplitude and have therefore also to be treated in an extended new transmission-line theory.
In the presented paper we describe a new model which is based on a full-wave theory, however, which can be cast in the form of telegrapher equations, and therefore most of the existing techniques for solving such equations and for applying the solutions can be used. In general, in applications the new theory is compu-

tationally more efficient than other full-wave methods. Other advantages are the possibilities to derive a physical interpretation of the new line parameters and to establish a relation between thick wires and multiconductor lines. The new line parameters become complex-valued, gauge-dependent, and they depend on the local coordinate and on frequency. In the modal representation of these parameters their imaginary part is related with the modal radiation resistances. They can be transformed into their global (physical) representation with the aid of lengthy (mathematical) expressions.
New results are also presented for a thick transmission line above perfectly conducting ground. In this case the telegrapher equations are completed by an additional (third) equation for the angle-component of the current. The inductance per unit length and the capacitance per unit length for a thick wire become matrices of (in general) infinite dimension. Besides the longitudinal inductance matrix we also obtain an azimuthal one. The three coupled telegrapher equations for the longitudinal component of the current, the azimuthal component of the current, and the scalar potential can be reduced to the usual two equations. In these equations, however, the line matrices become modified again. Another interesting result deals with the proximity effect. Evaluating this effect we can show that a thick wire may be described by a multiconductor wire-system of thin wires of (in general) finite number. We conclude our paper with some useful application examples of wire configurations including thick wires. A short comparison with the results of Sommerfeld will be performed. Eventually, we conclude our paper with an outview also comparing our results to those obtained with other methods.

UWB 1-7: The Evolution of Impulse Radiating Antennas

E. G. Farr
Farr Research, Inc.

The original paper in 1989 by Carl Baum on Impulse Radiating Antennas touched off a long odyssey of development and innovation. Along the way, Carl has been at the center of that development. The research continues today, because IRAs are one of the few known antenna design that can radiate two (or more) decades of bandwidth in a non-dispersive pulse.
Originally, the IRA was conceived as a paraboloidal reflector fed by two feed arms in the so-called facing plate configuration. Resistors at the end of the feed arms would damp out late-time ringing. This design had a number of problems associated with it, including too high an impedance, and excessive feed blockage. Carl had the idea of placing feed plates edge-on to the aperture, and using a second pair of feed arms to reduce the impedance. Each pair of feed arms was placed in the plane of symmetry of the other pair, so one pair would not affect the other. This configuration is referred to as the $\pm 45^\circ$ configuration, because each of the feed arms were positioned at 45° to the vertical, for vertical polarization. Using two pairs of feed arms reduced the impedance to 200 ohms, but a balun was still needed to bring the impedance down to 50 ohms. For that, Carl conceived of the splitter balun, consisting of two 100-ohm cables connected in parallel at one end and in series at the focus. Carl also contributed to the fundamental mathematics of complex number theory during his analysis of IRAs. When calculating the radiated field, one encounters an aperture field that normally would have to be integrated numerically. Carl found a way to convert the surface integral to a contour integral, which was then converted to a closed-form expression. This expression allows one to easily optimize the impedance of an IRA.
At high voltages, Carl realized that the splitter balun would not work, so he developed two strategies for dealing with the high fields at the apex. First, he placed the final switch directly at the apex, so there would be no need for a balun. This resulted in the so-called "big IRA", built by David Giri, which holds the record for field radiated at a distance. He also suggested building a half IRA with a feed-point lens, which solves the problem of converting the unbalanced coax to the balanced mode of the IRA.
Later innovations included placing the feed arms at $\pm 30^\circ$ to vertical in order to reduce the crosspol, adding a ground plane for ruggedness, and a number of schemes to add structural support to the apex. A collapsible IRA, or CIRA, was developed to allow portability. Dual polarization has also been investigated. And lens-based IRAs have been shown to have a reduced sidelobe level. Continuing research includes the development of IRAs on parachutes, or the Para-IRA. A spaced-based IRA is being developed that will be automatically deployable, and will be fabricated from space-qualified materials. IRAs are currently being used in a wide variety of laboratories to carry out broadband measurements. Applications that are being investigated include broadband communications and UWB radar to detect a variety of objects.

UWB 1-8: Aperture Engineering for Impulse Radiating Antennas

J. S. Tyo
ECE Department, University of New Mexico, Albuquerque, NM, USA

At the 1999 URSI General Assembly at the University of Toronto, I took a moment outside the Commission E oral session to chat with Carl Baum about the open problems in impulse radiating antennas (IRAs). For high power applications, making the source more powerful is often not an option. If we could devise techniques to improve the radiated field from the antenna for a given input voltage, they could have an important impact on performance fo future generations of IRAs.
That day Carl mentioned to me the idea of altering the feed arm angles of 200-Ohm, 4-arm IRAs. He told me that we could use a good understanding of how the IRAs perform as the feed arm angle changes. That conversation led to several studies by Carl, myself, and others, on how we could use aperture engineering to improve the prompt response from IRAs.
I use the term aperture engineering to describe a broad range of techniques that are designed to improve the performance of focused aperture antennas by paying close attention to the effect of the antenna geometry on the distribution of the TEM mode in the aperture of the IRA. In an earlier paper, we had introduced a concept of prompt aperture efficiency for IRAs (C. J. Buchenauer, et al., IEEE Trans. Antennas. Propagat. v. 49 p. 1155, 2001). In that paper, we described the important factors affecting prompt aperture efficiency as being spillover – the energy contained in the portions of the TEM mode that miss the aperture – and vector field nonuniformity. Because of the non-dispersive nature of the IRA, the feed must be TEM, and the TEM mode is by its very nature non uniform. It turns out that while certain types of IRA feeds – namely those used in lens IRAs – are inherently aperture efficient, reflector IRAs suffered greatly. The class of reflector IRAs that is represented by the "big IRA" (D. V. Giri, et al., IEEE Trans. Plasma Sci., v. 25, p. 318, 1997) were only 25% aperture efficient.
Over the past several years, we have developed a number of techniques to improve the radiated field performance from reflector IRAs. The first was a study to find out where to best place the arms of the IRA feed to maximize field uniformity for a given input impedance (J. S. Tyo, IEEE Trans. Antennas. Propagat., v. 49, p. 607, 2001). We found that aperture efficiencies in excess of 35% could be achieved with this technique alone.
Next, we turned turned to other techniques such as aperture trimming and resizing the aperture to maximize performance. These studies demontrated that the radiated field from IRAs could be even further improved beyond what we could do with the original IRAs. Finally, these studies have led to the development of theory for the performance of IRAs in off-boresight directions. At every step, the experimental and numerical analyses relied upon the simple and accurate theory developed by Carl for predicting prompt response from IRAs. And at every step, Carl provided insight to help interpret the emerging results.

UWB 1-9: A Differential Geometric Approach to EM Lens Design

A. Stone

University of New Mexico, Albuquerque, NM, USA

A differential-geometric approach to EM lens design was originally developed by Baum in the late 1960's. This design technique for transitioning TEM waves between cylindrical and conical transmission lines used differential geometry with Maxwell's equations and the constitutive parameters in an orthogonal curvilinear coordinate system. Isotropic but inhomogeneous media were considered. It was also shown that rotational coordinate systems obtained from complex analytic transformations in the plane could be utilized in the design process and that a class of solutions to the design problem existed. Later work led to many examples, which included two-dimensional lenses and various anisotropic lenses for launching TEM waves on conducting circular conical systems.

More recent work involved the study of unipolarized inhomogeneous TEM plane waves in lens synthesis. Since the formal fields were assumed to have only one component, some restrictions on the coordinate surfaces were removed. These considerations led to a study of generalized TEM, E, and H modes. The presence of longitudinal components brings in additional constraints on the allowable coordinate systems with the result that transient lenses supporting E and H modes are limited to a subset of those supporting TEM modes.

UWB 1-10: New Equation of Motion for Classical Charged Particles Meaning and Implications

C. T. C. Mo
Northrop Grumman IT DES

After postulating the existence of electric charges, Classical Electrodynamics (CED) consists of two parts: the Maxwell's field equations that governs the electromagnetic (EM) field generation from given charges' motion and the equation of motion that governs the charges' motion in given external fields. The latter part was incomplete and inconsistent until the New Equation of Motion we proposed [Mo and Papas, Phy Rev D 4, p3566 (1971)]: $m\dot{u}^\mu + Ru^\mu = eF^{\mu\nu}u_\nu + e_1F^{\mu\nu}\dot{u}_\mu$ where m is the particle's mass, e its electric charge, u^μ its 4-velocity, R its radiation, $e_1 = (2/3)e^3/m$ its acceleration charge, $F^{\mu\nu}$ the external EM field tensor, and $\dot{} = d/ds$ the proper time derivative. The new equation rigorously accounts for the particle's radiation reaction. Without invoking the Maxwell's equations, the new equation alone implies $R = -2e^2\dot{u}^\mu\dot{u}_\mu/3$, identical to the radiation obtained separately from the Maxwell's equations by integrating the charge's far zone Poynting vector over retarded sphere. Thus, the CED integrates EM fields and charge dynamics and is a complete and self-consistent theory.

Follow up work of the classical radiation reaction was sparse mainly because the "well-known" notion that it is almost always negligibly small in practical cases and that when it is not negligible Quantum Electrodynamics (QED) takes over. I will show that this is not the case. Even fully constrained by today's accepted QED, there is a wide parameter space of relativistic motion and high EM fields that CED applies and the radiation reaction force dominate over the usual Lorentz force [see Fig 1]. Even in daily engineering encounters, radiation reaction explicitly manifests itself, e.g. the antenna radiation resistance aggregated from the many charges' motion. To delineate the theoretical relation and implications of the various CED parameters and variables, we will present their logic flow, quantify their domain of applicability, and show the particle's mass m originating as the ratio of two coupling coefficients between the charge and the EM field. Then, we present the new solution that explicitly expresses the charge's radiation R in terms of its 4-velocity and external EM field, $R = (\frac{3m^2}{2e^2})\sum_{k=1}^{\infty}(\frac{e_1}{m})^{2k}u \cdot F^{(2k)} \cdot u/\sum_{k=0}^{\infty}(\frac{e_1}{m})^{2k}u \cdot F^{(2k)} \cdot u$ where the 2-tensor $F^{(2k)}$ is scalar product of $2k$ of $F^{\mu\nu}$.

We will conclude with thoughts on new research areas of radiation reaction implied by the new equation of motion. One potentially productive area is its high non-linearity and consequences, such as solution regions of sensitive-discrete chaotic stability and attraction orbits in small impact-parameter charge scattering dynamics when full radiation reaction and time retardation are accounted for.

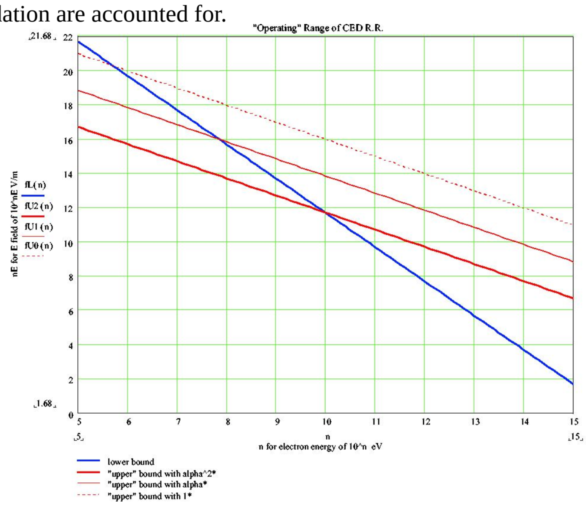

Figure 1: Operating Range of CED R.R.

UWB 1-11: Lightning Model Development: The Contribution to High Power Electromagnetics

R. L. Gardner

In lightning model development, we are attempting to establish the relationship between two observables, such as current and electric field, in such a way that we can extend data sets and extend our models to explain more of the complete observed lightning process. Baum and his colleagues [EMP Note Series and Lightning Electromagnetics, RL Gardner, ed., Taylor & Francis, New York, 1990] have established the most complete set, so far, of these types of models. Their work begins with a set of experiments that were conducted with better electromagnetic fidelity than available before and extend to relatively complete models relating geometry, fields, brightness, and current. This group has concentrated on the cloud-to-ground lightning return stroke because of the high energy density in this process and the consequent potential damage to electronic systems.

The cloud-to-ground lightning return stroke begins with a conducting charge filled channel that has been formed by earlier lightning leader processes. Upward and downward traveling leaders join within a few meters of the ground and begin the return stroke. The channel that forms consists of a current carrying channel and a surrounding corona. Baum has described the fundamental physical features of that configuration to form a basis for later propagation models of the channel. The current waveforms are observed to travel up the channel at around 1/3 of the speed of light. First principles arguments made by Baum support that observation. Later work based on these physical models present numerical and analytic descriptions of the phenomena Baum describes. These include, but are not limited to, models that predict the fields emitted from the lightning currents. These models differ from models shown elsewhere in the literature in that they include the effects of finite propagation (less than c), channel resistivity, and the corona environment. Data from the Kiva experiments that were designed and led by Baum provide unique linkage among explicit and simultaneous measurements of the brightness, current and fields caused by the lightning discharge.

In this paper we will survey the evolution of these models and the impact on the high power electromagnetics community. Each of the models examines quantitatively, with clear vision, the behavior of particular parts of the lightning discharge process. These models can then be used, with data, to bound the discharge parameters for system specifications.

UWB 2 - Propagation

UWB 2-1: Propagation of HV Short Pulses Through Wire Transmission Lines

J. Ashkenazy, **A. Pokryvailo**, **Y. Yankelevich**
Propulsion Physics Laboratory, Soreq NRC, Yavne 81800, Israel

As is well known, wire transmission lines, e.g. twin-line, four-line or multi-wire arrangements, can support TEM dispersionless propagation modes. Thus, ideally a short pulse could propagate along such a guiding structure unattenuated and undistorted. In reality however, Ohmic and radiation effects, depending on the geometry, wire conductivity and pulse width (frequency), could result in both attenuation and distortion. When high voltage pulses are considered, the very large electric fields near the wires may result in the creation of a corona which could propagate alongside the high voltage pulse and affect its properties. The propagation of high voltage pulses through wire transmission lines and the associated effects are the subject of an experimental research, results of which will be presented.

UWB 2-2: Penetration of Ultra Wide Band (UWB) Communication Signals Through Walls

M. Feliziani, **C. Buccella**, **G. Manzi**
Dept. of Electrical Engineering, University of L'Aquila, Poggio Roio, 67040 L'Aquila, Italy

UWB communication system is an emerging technique which is very attractive for low cost consumer applications. The UWB communications systems are relativity immune to multipath cancellation effects and produce low interference to existing narrowband systems due to low power spectral density [1]-[3]. UWB systems can be used for short- and medium-range communications in many areas. An important aspect to deep is the performance of UWB communication systems in presence of walls for indoor application. A series of measurements in time domain have been performed in the EMC lab of the University of L'Aquila to evaluate the attenuation of UWB signals produced by walls of common materials as glass, wood, plaster and plastics. The measurements have been performed using a commercial UWB pulse generator, the PulseOn EVK200 by Time Domain Co.. A numerical procedure based on equivalent transmission line method has been also developed to study this kind of problems [4]. A comparison between computed and measured values is finally presented.
A series of measurements to evaluate the propagation through walls of commonly used materials as glass, wood and plaster have been performed. The measurement set-up is given by the wall under examination placed between the transmitter (TX) and the receiver (RX) [5]-[8]. Walls constituted by different materials are considered and the measured values are compared with those obtained without the wall. The measurements are quite critical, due to the complex multipath propagation scenario and to the limitations of available instrumentation. In fact, the EVK P200 acquires the synchronization autonomously and does not use a trigger reference signal. As consequence, it is impossible to guarantee in all experiments that the first received pulse is not a multipath component. In order to mitigate this problem, the separation distance d between the transmitter (Tx) and the receiver (Rx), is taken twice lower than the distance h from ground, $d<2h$. This choice guarantees that the propagation travelling time td of the electromagnetic wave from the Tx to the Rx is always lower than that of the reflected signal from the ground. This approach avoids erroneous interpretation since the first path received by the RX is the transmitted one. Other problems concerning this kind of measurements depend on the size of the wall and on the distances between the wall and the Tx and Rx, since finite size walls could imply some diffraction phenomena. These problems are negligible because only wide size walls have been considered and the transmitter and the receiver have been placed both close to the wall under test. Measurement and simulation results are presented considering a single wall between the Tx and the Rx. The experimental setup is shown in Fig. 1. According to this figure, the geometrical quantities are for the glass: t = 0.005m, dtx=0.25m, h=1m. Figs. 2, show the transmitted signal. The simulation result is carried out defining the circuital network shown in Fig. 3, considering a wall. The transfer matrix Twall is defined in frequency domain as: Twall = [T11 T12; T21 T22] where T11=cosh(gt); T21=Zc sinh(gt); T21=(1/Zc)sinh(gt); T22 = cosh(gt); where g is the wall propagation constant, Zc the wall characteristic impedance and t is the thickness of the wall. g and Zc are depending on the frequency. The equivalent circuit is shown in Fig.3. It is valid in frequency domain. The signal Sin is the FFT transform of the measured template shown in Fig. 2. The IFFT of the computed Sout is compared in Fig. 4 with the measured results.
In the final paper measurement and computed results for different wall configurations will be presented.

References

[1] FCC Notice of Proposed Rule Making, "Revision of Part 15 of the Commission's Rules Regarding Ultrawideband Transmission Systems", ET-Docket 98- 153.
[2] M. Z. Win, R. A. Scholtz, "Characterization of Ultra-Wide Bandwidth Wireless Indoor Channels: A Communication-Theoretic ViewÊ", IEEE Jour. on Selected Areas in Communications, Vol. 20, No. 9, Dec. 2002.
[3] D. Cassioli, M. Win, A. Molish, "A Statistical Model for the UWB Indoor Channel", VTC 2001.
[4] M. Feliziani, F. Maradei, G. Tribellini, "Field penetrable conductive shields by the finite-difference time-domain method with impedante network boundary conditions (INBC's)", IEEE Trans. on Electromagnetic Compat., Vol. 41, No. 4, November 1999.
[5] J. Foerster and Q. Li, "UWB Channel Modeling Contribution from Intel", IEEE P802.15-02/279-SG3a.
[6] A. Molisch, M. Win, and D. Cassioli, "The Ultra-Wide Bandwidth Indoor Channel: from Statistical Model to Simulations", IEEE P802.15-02/284SG3a and IEEE P802.15-02/285-SG3a.
[7] J-M Cramer, R. Scholtz, M. Win, "Evaluation of an Indoor Ultra-Wideband Propagation Channel", IEEE P802.15-02/286-SG3a and IEEE P802.15-02/325-SG3a.
[8] S. Ghassemzadeh and V. Tarokh, "The Ultra-wideband Indoor Multipath Loss Model", IEEE P802.15-02/282-SG3a and IEEE P802.15-02/283-SG3a.

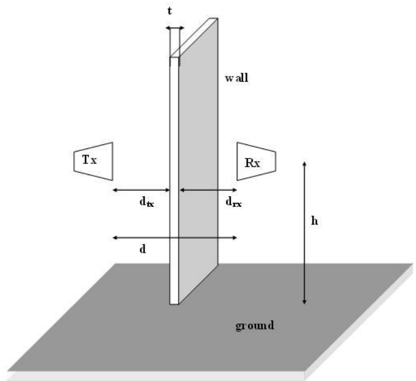

Figure 1: Measurement set-up.

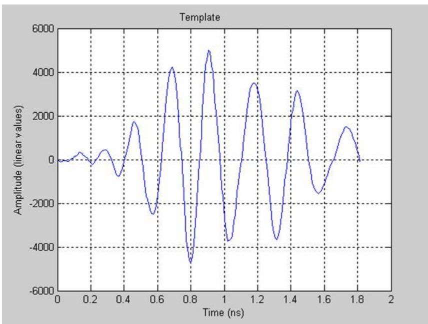

Figure 2: Transmitted signal.

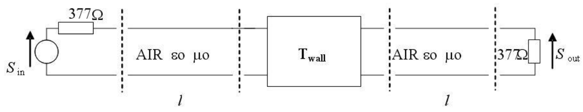

Figure 3: Equivalent circuit of a glass wall.

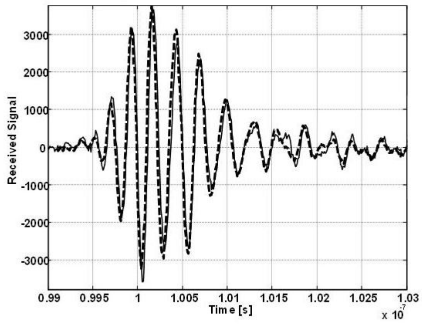

Figure 4: Measured (continuous line) and computed (dashed line) signal in presence of a glass wall.

UWB 2-3: Phase-Space Spectral Analysis of Transient Field Propagation in Anisotropic Medium

T. Melamed
Ben-Gurion University of the Negev

A phase-space spectral representation of transient fields propagating in an anisotropic medium is presented, in which the transient field is modeled by pulsed-beam propagators, emenating from all space-time points, and in all directions from a planar surface. The anisotropic medium is described by a generic wavenumber profile. The beam propagators are formulated by a transient plane-wave distribution and the propagation is obtained by saddle point asymptotics directly in the time domain to extract the pulsed beam phenomenology in the anisotropic environment under UWB/short-pulsed excitation. The resulting field is parameterized in terms of the spatial evolution of beam curvature, beam width, etc., which are mapped to local geometrical properties of the generic wavenumber profile. Emphasis is placed on formulating and analyzing the spectral integral directly in the time-domain.

UWB 2-4: Measurements for UWB MIMO Channel

J. Keignart, **C. A. Rjeily**, **C. Delaveaud**, **N. Daniele**
CEA-LETI (CEA/Direction de la Recherche Technologique)
F-38054 Grenoble Cedex 9 FRANCE

UWB channel has been extensively measured during last years in both frequency and time domains, but always in SISO configuration. Most of worldwide measurement databases have been used to contribute to IEEE normalization (J. Foerster, Channel Modeling Sub-committee Report Final, IEEE P802.15-02/490r1-SG3a, February 2003). Nevertheless, it is well known that multiple-input multiple-output (MIMO) systems with multi-antenna at the transmitter and at the receiver increase capacity especially in wide band purpose. A next step to MIMO propagation study is to evaluate the spatial correlation of a channel by moving for example receive antenna with a short separation between antenna positions. Obviously, in this “virtual array” the channel is assumed totally static (Cliff Prettie, David Cheung, Leslie Rusch, Minnie Ho, Spatial Correlation Of UWB Signals In A Home Environment, IEEE Conference on Ultra Wideband Systems and Technologies, Baltimore, USA, May 2002), (Ada S Y Poon and Minnie Ho, Indoor Multiple-Antenna Channel Characterization from 2 to 8 GHz, Proc. IEEE International Conference on Communications, vol. 5, pp. 3519-3523, May 2003). Although, a main drawback of this kind of approach is to neglect the possible electromagnetic coupling between antennas and array effect (T.N. Ogurstsova, G.P. Pochanin, P.V. Kholod, Multi-element UWB receiving Antenna, International Conference on Antenna Theory and Techniques, Sevastopol, Ukraine, pp. 549-552, September 2003).
Some interesting works have been published concerning the capacity of MIMO systems with closely spaced antennas but in a bandwidth lower than 500MHz (Volker Jungnickel, Member, IEEE, Volker Pohl, and Clemens von Helmolt, Capacity of MIMO Systems With Closely Spaced Antennas, IEEE Communications Letters, vol. 7, no.8, August 2003). The main difficulties limiting UWB MIMO measurements are: instrumentation devices and antennas. Now, we will focus our investigation on the 3-5GHz bandwidth. Concerning instrumentation, to perform frequency domain measurement it is necessary to have a multi-port Vector Network Analyzer (a 4-ports allows to measure for example 1 input to 3 output channels). For time domain, a pulse pattern generator with derivative filter, power amplifier and some more filters are used to generate the desired waveform (matching with the frequency spectrum) on each emitting antenna (Fig 1). On the receiver side, the different channel (up to 4) of a 20GS/s sampling oscilloscope (or real-time oscilloscope in sampling mode) are used. Finally concerning the antennas, UWB dedicated ones have been designed and miniaturized for integrated application. Moreover a special attention has been paid to antenna design in order to keep a stable temporal behaviour (pulse shape) of the radiation for any angle. Different configurations of multi-antenna structures have been tested in order to highlight its role in UWB MIMO system. Results from 3 to 5 GHz in both LOS and NLOS scenarios are presented with a comparison between frequency and time domain measurements for SISO configurations. Moreover, data processing methods are briefly outlined and some statistical characterization of the MIMO channel are extracted as well.

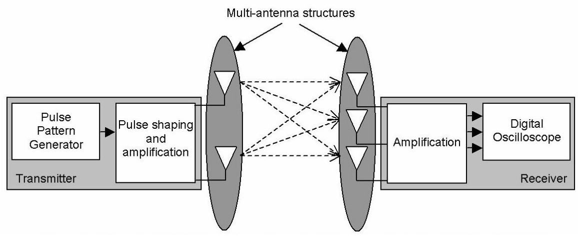

Figure 1: Example of MIMO configuration using 2 inputs and 3 outputs in Line Of Sight environment

UWB 2-5: A Deterministic Indoor UWB Space-Variant Multipath Radio Channel Modelling

Y. Lostanlen, **G. Gougeon**, **Y. Corre**
SIRADEL

Many studies have been initiated worldwide on indoor communication systems based on ultra wide band signals. The interest has been even greater since the 2002 FCC ruling decision.
European projects (Ultrawave, Pulser), French projects (Erable, Aubade) have been labellised in the past three years. Each project contains at least a sub-workpackage dealing with the “indoor UWB channel characterisation” showing first the importance of the topic and second the fact that this channel has not been fully understood yet. Many channel sounders have been deployed. A few statistical models have appeared. These preliminary results have indicated how complex the topic is.
In USA research works have been published for a decade now giving many reference papers in the field.
A standard IEEE 802.15.3a is currently in discussion. We believe our work is complementary for some aspects to the IEEE 802.15.3a channel model, which was useful for the selection process of the new standard for UWB high-data rate communications [A. Molisch, “Channel models for ultrawideband personal area networks”, IEEE Wireless Communications, December 2003, Vol. 10, n°6].
The work we present here consists in a study of a deterministic solution to model the indoor UWB channel.
The method has been adapted (in the frame of national research studies) to communication systems from successful algorithms applied to UWB radar domain (see [Y. Lostanlen, ”Modelling

and Processing of the ultra wideband radar signal. Targets modelling with FDTD, radar clutter modelling in the time domain, signal processing with parametric method.", 250 p, PhD Thesis, INSA Rennes, Dec 2000] – [Y.Lostanlen, B. Uguen, G. Chassay, H.D. Griffiths, "Modelling of the Air-Ground Interface for Ultrawideband Radar Applications.", UWB Polarimetry Chapter, UWB-SP Electromagnetics, vol. 5 ed. S.R. Cloude & P.D. Smith, September 2002]).

A first draft of the method was explained and presented in [B. Uguen, Y. Lostanlen et al. " A Deterministic Ultra Wideband Channel Modelling.", UWBST 2002 Conference, Baltimore, Maryland, 2002].

These developments process the signals over a wide range of frequencies taking into account the different behaviour of interactions at each frequency.

Many refinements of the method have been performed. Then we have coupled this approach with optimised ray-tracing tools (Y. Lostanlen et al. "A solution to predict the 3d indoor propagation for future wireless mobile communication systems." PIERS 2003, Singapore, Y. Lostanlen et al. " Studies on indoor propagation at various frequencies for radio local networks.", COST 273 Workshop, "Opportunities of the Multidimensional Propagation Channel", Finland, May 2002).

Among the attractive features we have now included in our more realistic 3D tool, we could mention the multi-floor aspect and the handling of the frequency dependence of material. Illustrations of these capabilities will be given in the proposed paper.

This work mainly intends to provide a tool helping understanding the physics underlying the propagation of a signal from the transmitter to the receiver by illustrating the multipath components. Starting from the antennas, that have to be modelled over this wide range of frequencies, the signals interacts with many scatterers leading to various behaviours depending on the electromagnetic material composition, frequency, nature (transmission, reflection, diffraction ,...). The strength of the solution is to easily provide the resulting pulse after a simple phenomenon (e.g. a diffraction and a reflection) as well as a complex bidirectional spatio-temporal channel for a chosen configuration. The attached figure illustrates a very simple example showing an incident Ricker pulse and its shape after interactions with a metallic edge. Obviously far more complex impulse responses have been generated and compared with real measurements. But we want also to show simple phenomena as they may help understanding the complex channel by discriminating the interactions. Indeed communication system designers and antenna specialists need to clearly understand how the signal behaves to provide the optimal system. We hope this tool could be helpful for them.

This method may be used as an elementary module for any kind of UWB techniques (pulse, frequency domain, OFDM, PPM, ...).

The proposed paper will show the novelty and the maturity of the approach by clearly explaining the process. Comparisons between Impulse Response simulations obtained thanks to this modelling solution and real signals (channel sounder) will be described and analysed. The geometry of the analysed scene, the configuration of the experimentations and the equipment will be also described.

UWB 2-6: On the Fading Properties of a UWB Link in a Dynamic Environment

P. Pagani, **P. Pajusco**
France Telecom R&D/DMR/OIP

1. INTRODUCTION

In order to design adapted UWB receivers for the mitigation of multipath phenomena, the fading properties of the UWB propagation channel are of particular interest. Most of the available analyses are based on experiments involving a measurement grid, resulting in series of channel realisations ([R. J. M. Cramer, R. A. Scholtz, M. Z. Win, "Evaluation of an Ultra-Wide-Band Propagation Channel", IEEE Trans. on Antennas and Propag., Vol. 50, No. 5, pp. 561-570, 2002], [J. Kunisch, J. Pamp, "Measurement results and modelling aspects for the UWB radio channel", IEEE Conf. on Ultra Wide Band Systems and Tech., pp. 19-23, 2002]). This technique allows one to consider the spatial fluctuations of the signal, which would be experimented by a user with a mobile terminal. However, a number of applications of the UWB technology will involve fixed access points and terminals, and the signal temporal fluctuations will mainly result from the movements of people in the close vicinity of the system [D. Porcino, W. Hirt, "Ultra-wideband radio technology: potential and challenges ahead", IEEE Communications Magazine, Vol. 41, No 7, July 2003]. This paper reports on an experiment designed to conjointly study both spatial and temporal fluctuations of the UWB signal in a typical indoor office environment. The proposed analysis of the small-scale amplitude distribution shows significant differences between the two concepts, and provides original results complementing the available studies.

2. THE UWB PROPAGATION EXPERIMENT

The experiment took place in fully furnished conference room (Fig. 1). The Tx antenna mounted on the measurement grid was situated on a central table, while the Rx antenna was successively situated inside and outside the room for LOS and NLOS measurements. The measurement apparatus consisted of a Vector Network Analyser HP8510C sampling the channel response between 3.1 and 11 GHz. In order to evaluate the spatial fluctuations of the signal, up to 1841 measurements were performed over a 1 m^2 grid in the empty room. To assess the temporal fluctuations of the signal, about 200 successive measurements were performed with a number of persons in the room varying between 1 and 10. Due to the measurement duration, real-time sounding of the radio channel is not technically feasible over a frequency band of 8 GHz. Instead, a pseudo-dynamic measurement technique was applied, where all persons in the room were keeping still for the measurement duration, and modified their position between measurements. As a result, a set of realistic realisations of the channel in an occupied conference room were obtained.

3. STATISTICAL ANALYSIS

A. Total received power

As a first analysis, Fig. 2 presents the CDF curves of the total received power for each configuration in the LOS case. A normalising factor has been applied to result in a mean received power equal to unity. The static curve (a) gives an idea of the power fluctuations inherent to the measurement process. One can note that an increasing number of moving persons in the conference room results in an increasing dispersion of the received power. The statistics observed for the measurement grid (i.e. for a moving terminal) seem to be an upper bound to the power fluctuations due to the people motion. The log-normal distribution is well-suited to represent the small-scale statistics of the total received power in both situations with 10 moving persons and with a measurement grid. Nevertheless, this latter case should be taken as a worst case scenario, as the resulting standard deviation represents twice the one recorded with 10 moving persons.

B. Evolution of the amplitude distribution

A further analysis consists in deriving the multipath fading statistics experienced in each configuration at a given excess delay. We computed the CDF of the received signal envelope at each delay τ of the impulse response h(τ). Correspondingly, Fig. 3 and 4 represents the empirical CDF curves of the signal envelope, for the measurement sets obtained with 1, 4 or 10 mobile persons in the vicinity of the radio system, and with a measurement grid of 225 emitter locations. Fig. 3 corresponds to an excess delay representing the 2nd main echo in the Power Delay Profile, while Fig. 4 corresponds to a cluster of dense multipath (τ = 68.1). The signal envelope has been normalised to result in an instantaneous power equal to unity. For the sake of comparison, the theoretical CDF corresponding to a Rayleigh distribution have been represented (dashed lines). On Fig. 3, the data set related to the measurement grid is highly dispersed. This result linked to the measurement grid technique in conjunction with the high temporal resolution of UWB signals, suggests that the use of a grid of measurement is not a suitable approximation to evaluate the fading experienced in a fixed communication system in a dynamic environment. On the contrary, data sets corresponding to situations with moving persons present a quite different distribution, and a regular evolution of the dispersion is noticeable. However, in regions of dense multipath (Fig. 4) both temporal and spatial fluctuations of the UWB signal seem to be well represented using a Rayleigh distribution.

C. Distribution fit

In order to properly model the fading properties of the channel in both situations, we propose to fit the experimental statistics to a general distribution. The Weibull distribution is selected as characteristic of most of the data sets collected during the experiment. The parameters of this distribution are then studied in the cases of a moving terminal and a dynamic environment, and their evolution with the number of persons in the vicinity of the communication system is presented.

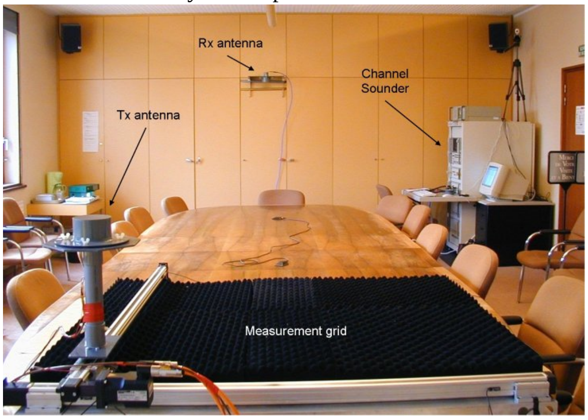

Figure 1: Experimental setup

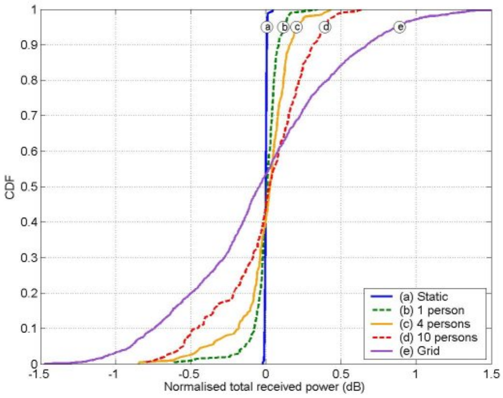

Figure 2: Empirical CDF of the normalised total received power (LOS case)

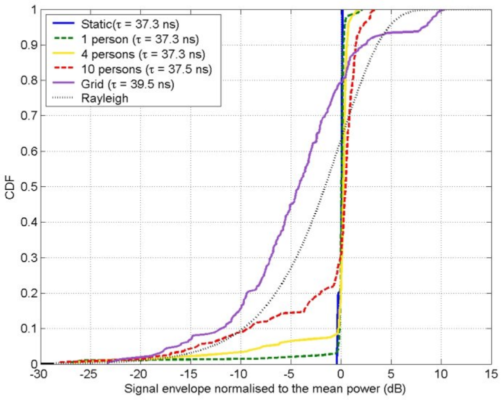

Figure 3: Empirical CDF of the signal envelope: PDP 2nd main echo (LOS case)

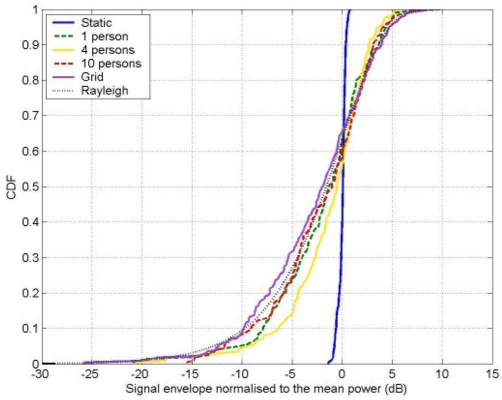

Figure 4: Empirical CDF of the signal envelope: cluster of dense multipath at τ = 68.1 ns (LOS case)

UWB 2-7: Dynamical Evolution of the Brillouin Precursor in Rocard-Powles-Debye Model Dielectrics

K. E. Oughstun
University of Vermont

When an ultrawideband electromagnetic pulse penetrates into a causally dispersive dielectric, the interrelated effects of phase dispersion and frequency dependent attenuation alter the pulse in a fundamental way that results in the appearance of precursor fields (L. Brillouin, Wave Propagation and Group Velocity, Academic Press, 1960; K. E. Oughstun and G. C. Sherman, Electromagnetic Pulse Propagation in Causal Dielectrics, Springer-Verlag, 1994) . For a dielectric described by the Rocard-Powles extension of the Debye model, the dynamical field evolution is dominated by the Brillouin precursor as the propagation depth typically exceeds a single penetration depth evaluated at the carrier frequency of the input pulse. This is because the peak amplitude in the Brillouin precursor decays only as the square root of the inverse of the propagation distance. Because of its unique nonexponential peak decay, the Brillouin precursor has direct application to foliage and ground penetrating radar, medical imaging, remote sensing and wireless communications in adverse environments; however, this also means that current safety standards for exposure to electromagnetic radiation may need to be carefully examined for such ultrawideband pulses. Of equal importance is the frequency structure of the Brillouin precursor which exhibits a complicated dependence on both the material dispersion and the input pulse characteristics. A Brillouin pulse is then defined and shown to possess near optimal (if not indeed optimal) penetration into a given Rocard-Powles-Debye model dielectric.

UWB 3 - UWB- Interference with Aircraft Systems

UWB 3-1: General Analysis of Leaky Section Cables for Multi-Band Aircraft Cabin Communications with Different Measurement Techniques

S. Fisahn[1], **M. Camp**[1], **N. R. Díaz**[2], **R. Kebel**[3], **H. Garbe**[1]
[1]*Institut für Grundlagen der Elektrotechnik und Messtechnik, Universität Hannover, Germany*; [2]*Deutsches Zentrum für Luft- und Raumfahrt (DLR), Oberpfaffenhofen, Germany*; [3]*Airbus Deutschland GmbH, Hamburg, Germany*

Next generation of aircraft will provide more convenience for passengers, including personal communications facilities. Thus it will be possible to use Portable Electronic Devices (PEDs) in the cabin, such as laptops, mobile phones, etc. (A. Jahn, M. Holzbock, J. Müller, R. Kebel, M. De Sanctis, A. Rogoyski, E. Trachtman, O. Franzrahe, M. Werner, and F. Hu, Evolution of aeronautical communications for personal and multimedia services, IEEE Communications Magazine, vol. 41, pp. 36-43, July 2003). In order to enable wireless communication for these PEDs, an onboard system like a Wireless Local Area Networks (WLAN) has to be built up. For this purpose the cabin may be equipped with a so called leaky section cable (LSC) which can be used as an antenna for WLAN and other applications like GSM, UMTS, DECT (N. Riera, Narrowband measurements in an Airbus A319 for in-cabin wireless personal communications via satellite, Proceedings of the 1st International Conference on Advanced Satellite Mobile Systems (ASMS 2003, Frascati, Italy). The system integration process requires detailed information about the radiation and transmission behaviour as well as the interference potential of the leaky cable in the frequency range from 450 MHz up to 6 GHz.

In this investigation different measurement techniques have been used to determine the leaky cable parameters. In a first stage radiation measurements in the near and far field have been carried out with continuous wave (CW) signals. The radiation patterns have been obtained for different frequencies by Gigahertz Transverse Elegromagnetic Mode (GTEM) cell measurements as well as open area test side (OATS) measurements. In addition the near scanning technique has been used to analyze the distribution of the electric field strength along the cable. Furthermore the transmission behaviour of the cable has been measured. In the second stage transient measurements have been performed. Fast transient pulses with double exponential character have been used to determine the radiation and transmission behaviour in time and frequency domain. It will be shown that it is possible to obtain the complete system behaviour of the cable accurately and with small effort, if pulses with very short rise times (UWB) are applied.

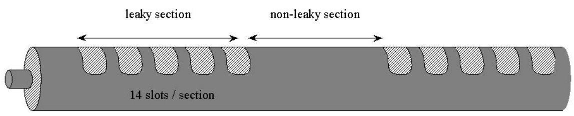

Figure 1: Principle buildup of a leaky section cable

UWB 3-2: Measurement of the Mutual Interference between Bluetooth Devices

A. Schoof, J. L. ter Haseborg
Department of Measurement Engineering/EMC, University of Technology Hamburg-Harburg, Germany

The wireless communication standard Bluetooth, working within the worldwide-license free 2.4 GHz ISM-Band, has found its way into most parts of consumer electronics. Due to the high distribution of Bluetooth-equipped devices, it is estimated that in the future many of them will be taken with into aircraft cabins or within similar, emission-sensitive, areas. From the airlines point of view, the security aspect of using radio transmitters within partially highly sensitive airplane electronics stands against the economical aspect of allowing or even providing these kinds of services. Not only the use of wireless transmitters can lead to a reduction of wirings within the passenger cabin and thus permits an easier reconfiguration of the seat allocation as well as a serious weight reduction and hence a higher capacity. Due to the growing economical pressure, toleration or even provision of formerly not allowed services like Bluetooth or WLAN linked communication- or entertainment solutions also seems to become inevitable.

Studies have been made, determining the effects of Bluetooth and/or WLAN under mutual interferences or the influence of these sources on conductive structures (A. Schoof, T. Stadtler, J. L. ter Haseborg, Two dimensional simulation and coupling of Bluetooth signals into conductive structures, 2003 IEEE Symposium on Electromagnetic Compatibility, Boston). Still, the question remains how the cumulative influence for an EMC point of view, also referred as multiple equipment factor, of several or many of these transmitters on their environment can be estimated.

In this paper mutual interference between commercial Bluetooth transmitters is examined. The field superposition is measured for miscellaneous filter bandwidths, transmitter combinations and data throughputs. The commonness of the collisions is compared with the statistical expected collision probability. Also the spatial field distributions of stand-alone and Bluetooth equipped devices are measured and will be presented and discussed.

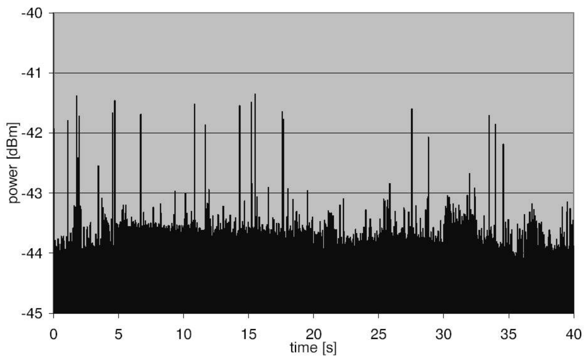

Figure 1: Field superposition due to mutual interference between two Bluetooth-modules, each -44 dBm

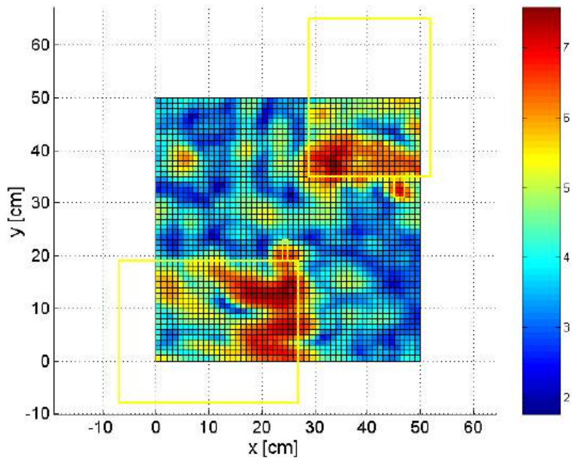

Figure 2: Electric field strength [V/m] underneath two laptops with paired Bluetooth-modules

UWB 3-3: Simulating the Response of Semi-Shielded Systems: Electromagnetic Topology Technique

P. Kirawanich[1], R. Gunda[1], N. Kranthi[1], N. Islam[1], J.-P. Parmantier[2], S. Bertuol[2]
[1]*Department of Electrical and Computer Engineering, University of Missouri, Columbia, MO, USA*; [2]*ONERA, Meudon, France*

The effects of lightning and high power electromagnetic pulses (EMP) on electronic systems can result in coupling and the generation of undesired voltages and currents that could propagate to sensitive elements of the system. In both commercial and military aircrafts, for example, interactions with lightning and man-made electromagnetic pulses are a possibility that cannot be overlooked. Previous studies of such interactions include experimental measurements [J. E. Nanevicz, E. F. Vance, W. Radasky, M. A. Uman, G. K. Soper, and J. M. Pierre, EMP susceptibility insights from aircraft exposure to lightning, 1988] as well as simulations using measured values for transfer functions for the interaction [J. P. Parmantier and J. P. Aparicio, EM Topology: Coupling of two wires through an aperture, 1991].

For simulation studies, it is generally possible to separate the response mechanism into independent processes such as external interaction, energy penetration and the excitation of the electrical system [C. D. Taylor, External interaction of the nuclear EMP with aircraft and missiles, 1978.]. Using conventional codes for such studies would not only require a huge mesh and large computation time but the vast data generated would also be

difficult to analyze. An alternate approach is an electromagnetic topology (EMT) based code which allows for the volume decomposition of the electrical system into manageable volumes, each interacting with the other through preferred paths [C. E. Baum, Electromagnetic Topology: A formal approach to the analysis and design of complex electronic systems, 1982.].
External-internal interactions with EMT based code require the determination of the transfer functions from the external volume to the interior [F. M. Tesche, Topological concepts for internal EMP interaction, 1978.]. Once the parameter is known, wave propagation around cables and junctions can then be evaluated.
In this paper we use an electromagnetic topology based simulation code and apply a concept [F. C. Yang and C. E. Baum, Use of matrix norms of interaction super-matrix blocks for specifying electromagnetic performance of sub-shields, Interaction Notes 427, 1983] to determine the transfer function for external-internal interactions (Fig. 1). The methodology described is first validated on a simple system consisting of a single transmission line connecting two electronic systems and is then applied to the general case of a multi-conductor transmission line, such as an aircraft wiring system under external electromagnetic pulse threats.
We have compared our simulation results (Fig. 2) with previous experimental measurements and the results are in good agreement. We have also shown that the response of the system depends on a number of factors including the distance of the semi-shielded system from the aperture, the terminating impedances of the internal circuitry, and the frequency of external pulses.

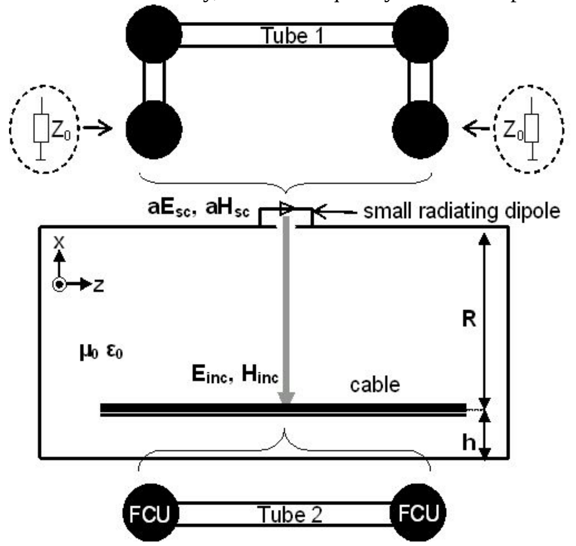

Figure 1: Representation of the entire system processes for external-internal interactions and transfer function in EMT based code

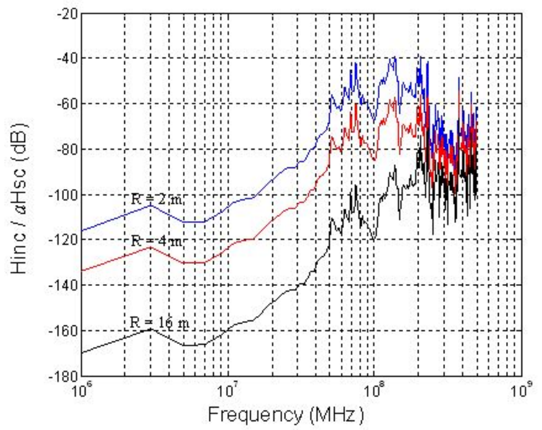

Figure 2: Aperture to cable H-field ratio as functions of cable distance and frequency

UWB 3-4: Simulation of a Cabin Wireless Lan Antenna Inside an Airbus A340-600 Wide-Body Transport Aircraft

J. Ritter[1], **R. Kebel**[2]
[1] *EADS-Military Aircraft*; [2] *Airbus*

The integration of Wireless Lan (WLAN) services in an aircraft cabin environment requires the WLAN equipment to be compatible to the electronic aircraft installations. This contribution documents the simulation of a cabin WLAN antenna within an Airbus 340-600 cabin segment. This work is motivated by the electromagnetic compliance requirements for radiating equipment inside the aircrafts passenger cabin. The most significant effect of the antennas radiated emission is the excitation of common mode currents on four characteristic cable bundles, where one bundle is located in close proximity to the antenna while the remaining three bundles run in a larger distance from the antenna. In the intended installation, the main beam of the antenna is oriented parallel to the cabin axis. For the common mode analysis, each cable bundle is treated as one cable, so that four separate cables are considered. A cabin section having a length of six meters is considered in the simulations.
The simulations have been performed using the Time Domain Finite Difference technique, allowing a wideband analysis within one simulation run. Within the simulations, the antenna was fed by a wideband signal within 2GHz...3GHz bandwidth. Since only the farfield radiation pattern of the antenna was known, a special excitation technique (spherical wave source) has been developed. Using this technique, the field radiated by the antenna in their close proximity is described based on the given radiation pattern. For this purpose,the spherical wave representation of the antennas radiation pattern has been generated; based in this representation, a far- to near field transform has been performed allowing the near fields to be used as sources on a Huygens-Contour (separating total field zone outside from the scattered field zone inside the contour).
The common mode currents on the cables under consideration were evaluated by current probes, performing an integration of the magnetic field around the cables. These current probes are placed along the four cables under consideration throughout the cabin section. Furthermore, the electric field distribution in a longitudinal cut of the cabin has been transformed into the frequency domain between 2.4GHz and 2.5GHz, where measurements are available for reference. The enclosed image fig. 1 shows the simulation model (FD-Mesh) of the cabin, while fig. 2 displays field distributions from different timesteps. Figure 3 shows the resulting common mode currents, averaged over the frequency range from 2 to 3 GHz along the cabin axis.

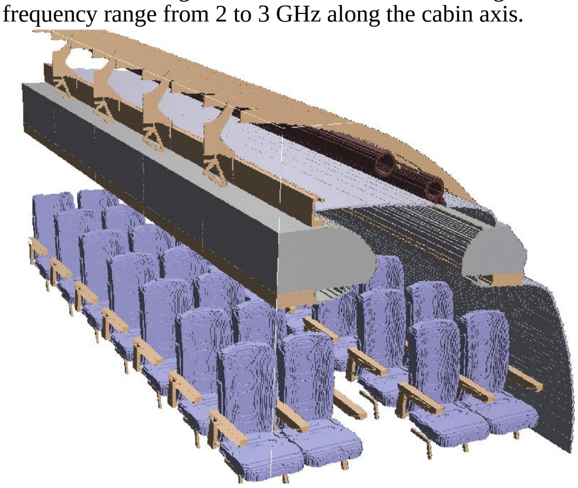

Figure 1: A view of the FD-TD meth utilized in the simulations. The meshsize has been about 32.000.000cells.

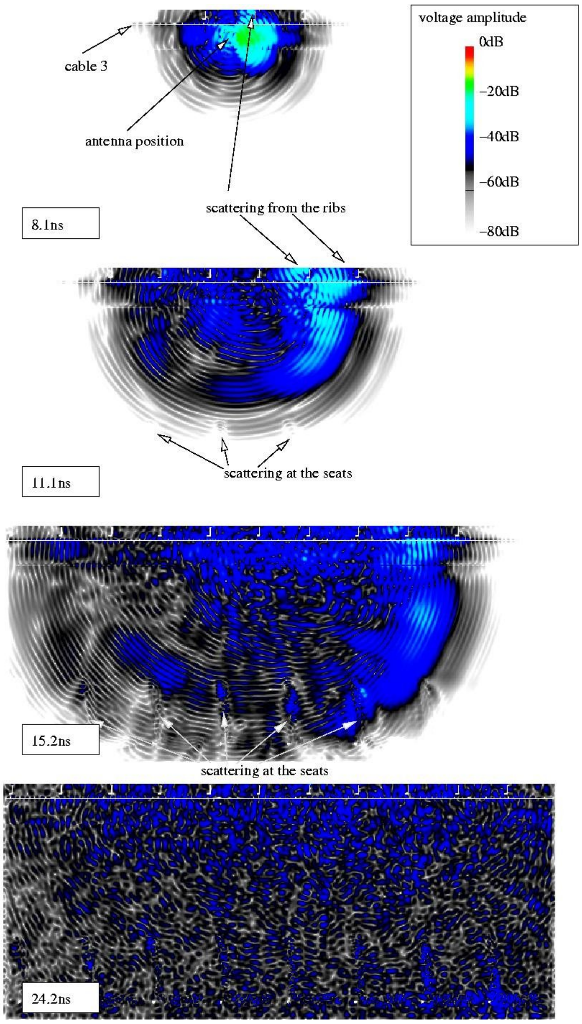

Figure 2: Time-domain field distributions inside the analyzed cabin segment for different times.

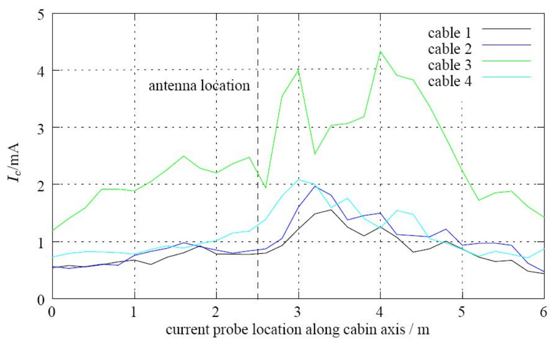

Figure 3: Common mode currents, averaged over 2 to 3GHz along the cabin axis.

UWB 4 - Time-Domain Computation Techniques

UWB 4-1: FDTD Simulation of Electromagnetic Radiation from Vertical Dipoles in Inhomogeneous Air-lossy Medium Space

K. Paran, **M. Kamyab**
K. N. Toosi University of Technology, Tehran, Iran

Since the presentation of FDTD method in 1966, this method has found applications in different fields of electromagnetics. However FDTD method is rarely used in analysis of propagation problems. In the few works which have been carried out in this field, radiators were considered in the form of vertical or horizontal line sources (not actual antennas) and in most cases the earth's surface was assumed to be a PEC. In the present research, radiation from vertical dipoles in inhomogeneous air-lossy medium space is simulated using FDTD method in cylindrical coordinates taking rotational symmetry into consideration. In this work lossy medium is considered to be dry soil (relative permittivity = 4, conductivity = 0.005 S/m). Excitation source is considered to be a delta-gap-generator in the middle of the dipole.

FDTD method enables us to solve this problem comprehensively and accurately, taking the effects of all participant electromagnetic phenomena into account. However the inhomogeneity of space and presence of a propagating mode in the form of surface-wave make the near-field to far-field or even far-field to far-field transformation a very difficult task (if not impossible). Therefore the only way to find field values at long distances with an acceptable accuracy (especially at points near the air-lossy medium interface) is to obtain these values directly by FDTD method. This increases the required memory and CPU time severely. In this simulation an efficient non-uniform meshing scheme is used, so it is possible to use fine cells wherever in mesh which are necessary (in models of dipole and lossy medium) and use coarse cells in other parts, without facing any sudden change in cell width throughout the mesh. In this manner the required memory and CPU time can be considerably reduced. The presence of a lossy medium at some parts of mesh boundaries creates a need for a special mesh truncation technique capable of truncating inhomogeneous-lossy media. Therefore a novel generalized PML with a simple formulation was introduced which has this capability. In this simulation the excitation signal is considered in the form of sine carrier modulated by Gaussian pulse (SCMGP). SCMGP unlike ordinary Gaussian pulse (GP) has very small low-frequency content. Also by using SCMGP, it is possible to concentrate or spread the spectrum density around the main frequency arbitrarily. Therefore we can raise the spectrum density at frequencies of interest and reduce it at other frequencies and consequently increase the accuracy of calculations for considered frequencies. In each time step, computations are limited to that part of mesh where radiated wave are passing (computational window). The other parts (region that radiated pulse hasn't reached there yet and region which radiated pulse and all reflections and refractions of it have passed there) are excluded from computations. This could reduce the CPU time to less than one-tenth. By using discrete Fourier transform, the spatial distribution of radiated field can be obtained at each specific frequency (50MHz in this work). Fig. 1a shows the spatial variations in amplitude of radiated field in the case which radiator is a half-wave dipole antenna located 18m above the ground. Variations are shown up to a distance of 100m, from 9m below to 55m above the ground. This figure clearly displays the formation of interferential lobes above the ground surface and the wave attenuation below it. Fig. 1b and Fig. 1c are continuations of Fig. 1a which show the variations in field amplitude from a distance of 100m to 1000m and from 1000m to 3000m (500 wavelengths) respectively. Field values, which were used for drawing these figures, had been obtained directly by FDTD method.

The performed simulations show the unique capabilities of FDTD method to solve propagation problems in the case of inhomogeneous-lossy media. Also these simulations show that the values of radiated field at long distances (up to 500 wavelengths in this work) can be obtained directly by FDTD method.

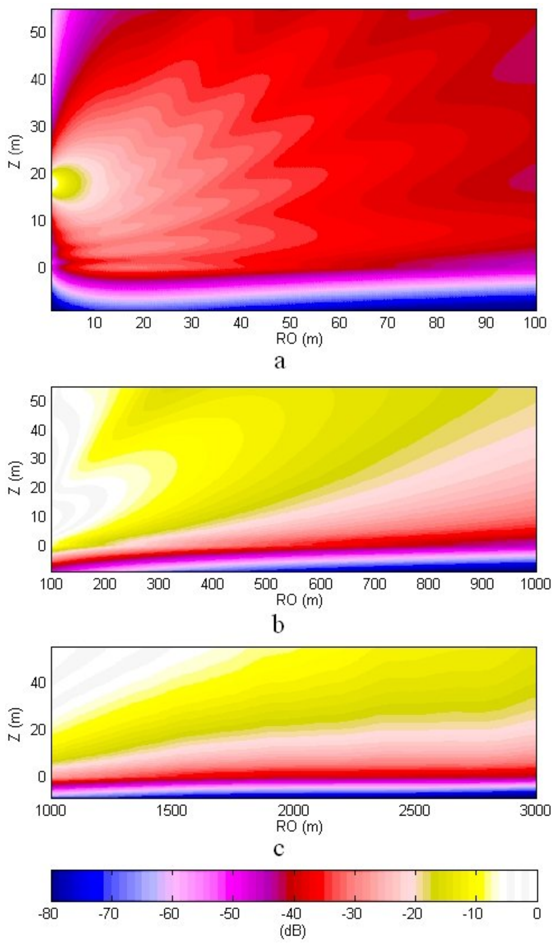

Figure 1: Spatial variations in amplitude of radiated field at f=50MHz. (a) Up to 100m (from radiator). (b) Between 100 and 1000m. (c) Between 1000 and 3000m. Radiator is a half-wave dipole antenna located 18m above the ground (dry soil).

UWB 4-2: Enhanced Electromagnetic Field Analysis with the Finite Integration Technique

M. Balk, **T. Weiland**
Technische Universität Darmstadt, Institut für Theorie Elektromagnetischer Felder (TEMF)

Time domain simulation methods can be regarded as the method of choice for many electromagnetic applications, which is particularly true, if broadband results are desired. This trend can be noticed by the great popularity of the Finite Difference Time Domain algorithm (FDTD, K.S. Yee, 1966) and the exceeding number of publications in this area.
In this paper we discuss some recent developments concerning the Finite Integration Technique (FIT, T.Weiland, 1977). The FIT is computationally equivalent with FDTD, if it is applied to standard Cartesian grids and combined in time domain with the leapfrog time integration scheme. Thus, FIT shares all of FDTD's advantageous properties like the small memory needs and the efficient explicit time stepping algorithm. In most applications, the standard FIT discretization method is 2nd order accurate, and the Courant stability limit for the time step width defines an area of operation, where the approximation errors of the time and space grid are well balanced. Beyond the leapfrog algorithm, FIT can also be applied to static or time-harmonic problems, or be combined with alternative time integration schemes, e.g. for low-frequency problems.
However, there are several weaknesses of the standard FIT formulation, including:
1) The resolution of geometric details is realised by globally refining the spatial discretization. Thus, in case of a small detail compared to the computation domain, this results to an unnecessary large amount of unknowns and to an unnecessary long simulation time as well.
2) The simulation of electrically large structures is limited by the error due to numerical dispersion.
3) In the field of particle accelerators there is the need to simulate moving charged particles with appropriate boundary conditions. In particular, the particles should move with an arbitrary velocity.
This paper gives an introduction into FIT and its main properties. Moreover, some recent developments facing the problems above are presented. For instance:
1) Techniques to increase the modeling accuracy:
- A locally refining subgridding scheme, which preserves the properties of FIT as stability, charge conservation and energy conservation. (F.Mayer, R. Schuhmann, T. Weiland, Flexible Subgrids in FDTD Calculations, Digest of the IEEE AP-S/URSI 2002)
2) Techniques to reduce the dispersion error:
- A higher order leapfrog scheme for explicit time stepping, which shows good performance regarding the stability, convergence and dispersion. (H. Spachmann, R. Schuhmann, T. Weiland, Higher Order Explicit Time Integration Schemes for Maxwell's Equations, Int. Journal of Numerical Modelling, 2002)
3) Techniques to handle accelerator structures:
- First, a line current represents the moving charges within the calculation domain and second, an equivalent current on the boundaries of the calculation domain is needed. (M. Balk, R. Schuhmann, T. Weiland, Modelling of Open Boundaries for FIT/FDTD Simulations of Particle Beams, Proceedings of the IEEE AP-S/URSI 2003)
Finally we will present some applications, including the simulation of a scattering problem and the simulation of a typical accelerator structure.

UWB 4-3: Solving Time Domain Electric Field Integral Equation for Thin-wire Antennas using the Laguerre Polynomials

Z. Ji[1], **T. K. Sarkar**[1], **B. H. Jung**[2], **M. Salazar-Palma**[3]
[1]*Department of Electrical Engineering and Computer Science, Syracuse University, NY, USA 13244*; [2]*Department of Information and Communication Engineering, Hoseo University, Asan, Chungnam 336-795, Korea*; [3]*4Depto. Senales Sistemas y Radiocomunicaciones, Politechnic University of Madrid, Spain*

Transient response of thin-wire structures have been of interest for many years. Recently, this area has received considerable attention because of problems involving the investigation electromagnetic pulse (EMP) effects on thin wire structures. These developments can be applied to some important areas such as target identification through short-pulse radar, electromagnetic compatibility (EMC) and interference (EMI) problems, and wideband radio communication. Several techniques have been developed over the years to determine the transient responses of these structures In this paper, a numerical method to obtain an unconditionally stable solution of the time domain electric field integral equation for arbitrary conducting thin wires is presented. The time-domain electric field integral equation (TD-EFIE) technique has been employed to analyze many electromagnetic scattering and radiation problems. However, the most popular method to solve TD-EFIE is typically the marching-on in time (MOT) method, which sometimes may suffer from its late-time instability. Instead, we solve the integral equation by expressing the transient behaviors in terms of weighted Laguerre polynomials. By using these orthonormal basis functions for the temporal variation, the time derivatives can be handled analytically and stable results can be obtained even for late-time. Furthermore, the excitation source used in scattering and radiation analysis of electromagnetic systems typically is done using a Gaussian type pulse. In this paper, both a Gaussian pulse and other signals like a rectangular pulse or a ramp like function have been used as excitations for the scattering and radiation of thin-wire antenna with and without junction. The results are compared with the inverse discrete Fourier transform (IDFT) of a frequency domain analysis.

UWB 4-4: Fast Time Domain Integral Equation Solver for Dispersive Media

E. Bleszynski, **M. Bleszynski**, **T. Jaroszewicz**
Monopole Research, Thousand Oaks, CA 91360

We describe elements and representative applications of a new fast time domain integral equation algorithm, applicable to a broad variety of problems involving interaction of wide-band pulses with dispersive media. Although there has been recently significant interest in developing fast solution methods for time domain integral formulations of Maxwell equations, relatively little attention has been given to the development of such tools for dispersive media, a problem which poses a challenge from both analytic and numerical points of view.

In this paper we report our new analytical formulation of integral equations specially tailored to general problems involving dispersive media. The formulation is both general and significantly simpler than the conventional approaches: instead of using the customary integral equation operators involving the Green function and its derivatives, we construct effective integral equation operators equal (i) to the Fourier transform of the dispersive medium Green function, (ii) to the Fourier transform of the product of the dispersive medium Green function with the frequency dependent dielectric permittivity, and (iii) to the Fourier transform of the product of the dispersive medium Green function with the inverse of the dielectric permittivity. An important benefit of such a formulation is that the resulting integrals involve only single (and not double) time convolutions. Our integral formulation for the dispersive media is implemented in the context of a fast solution algorithm based on the FFT space-time matrix compression scheme, which we introduced earlier and reported on at the AMEREM 2002 conference. The algorithm relies only on the translational invariance of the Green function. Its computational cost is independent of the degree of dispersion of the medium and scales as

$$O(N_t N_s \log N_t \log N_s)$$

and

$$O(N_t N_s^{4/3} \log N_t \log N_s)$$

for volume and surface problems, respectively, where N_t and N_s denote the number of temporal and spatial samples.

We will present results of complete analytical calculations and the corresponding numerical procedures for the evaluation of matrix elements of the integral operators, executed in the framework of the full Galerkin scheme in space and time, for the “conductive Debye medium” (i.e., for a medium with the electric permittivity given by the Debye formula supplemented with a term responsible for the medium conductivity), as well as for the limiting cases of the conductive Debye medium, including the lossy, the Debye, and the non-dispersive media.

Applications of our approach for problems involving a conductive Debye medium will also be discussed. Particular areas of applications of our method may be found in such contexts as the detection of concealed objects in biological media, foliage penetration, or transient effects in antenna arrays.

UWB 4-5: A Novel Technique for Accurate Simulation of Pulse Wave Scattering

L. Velychko, **Y. Sirenko**
Institute of Radiophysics and Electronics, UAS, Kharkov

The paper is devoted to simulating the transient processes in various electrodynamic structures that scatter and radiate pulse waves. The basic result of the work is exact ‘absorbing’ conditions (EAC) for initial boundary-value problems describing these processes. EAC allow one, for arbitrary time intervals, to carry out the analysis in bounded spatial regions that enclose all sources and scatterers. Actually, the only well-known exact radiation condition for outgoing waves at the points that are not reached by the excitation in a finite time interval is transferred onto closed artificial boundaries, i.e. into the region with an arbitrary intensity of the spatial-temporal field transformations. For the integro-differential operator entering into EAC, the explicit analytical representations have been obtained. The artificial boundaries divide the infinite analysis domain of the original problems into two regions: the bounded and unbounded ones. In the former, the standard computational methods are used for calculating the scattered field, whereas in the latter, the field is determined from its values on the artificial boundary.

The original ‘open’ problems are equivalent to the modified ‘closed’ ones. This is supported by the following facts: the original problems are uniquely solvable; the solution to the original problem is, at the same time, the solution to the modified problem (according construction); the solution of the modified problem is unique. The last-mentioned fact can be proved in the framework of the standard procedures based on the ‘energy’ estimates for the scalar or vector function describing the scattered field.

The obtained results remain valid with almost arbitrary variations both in geometry of the bounded region and geometry and electrical parameters of scattering objects. However, these variations must not violate the existence of the regular unbounded domain, where the outgoing pulse waves are propagating freely. The standard finite-difference schemes are rather flexible. The use of EAC essentially increases their reliability thus widening the range of rigorously solvable ‘open’ problems of nonsinusoidal wave electrodynamics.

We have also considered the problem how to prevent the unpractical extension of the computational domain when using the long initial signals or in the cases where the sizable sources are far removed from the scatterers and where a series of ‘elementary’ inhomogeneities are connected by long regular waveguides. The approaches suggested are simple enough and universal. The principal steps and peculiarities in their implementation are demonstrated by a number of practical examples.

UWB 4-6: On the Efficient Time Domain Processing of Aperture Antennas

G. Marrocco, **M. Ciattaglia**
DISP - Università di Roma ”Tor Vergata”

Ultra-wide band (UWB) technology is recently producing lots of new applications in communications, electronic warfare, measurements and radar identification and imaging [R.J. Fontana, in Ultra-wideband short-pulse electromagnetics 5, pp.225-234, Kluwer Academic/Plenum Publisher 2000]. Design of UWB antennas requires to exploit true time domain (TD) electromagnetic models, not only to quickly achieve a broadband antenna response but also to investigate on wavefront propagation and distortion directly in the time domain. To this purpose, time-dependent effective height, defined in terms of the Radon transform of the (electric or magnetic) current impulse response is commonly used for the complete characterization of the antenna properties [A. Shlivinski, E. Heyman, R. Kastner, IEEE AP-45, pp. 1140-1149, 1997], [E. G. Farr, C. E. Baum, Sensor and Simulation Notes, Note 350, Nov. 1992.]. Since in most the cases the analytic modeling is forbidden by the antenna geometrical and electrical complexity, local numerical tools, and first of all the Finite–Difference Time-Domain (FDTD) method, have to be used to calculate and store antenna surface current in time domain. Calculation and application of TD effective height is therefore a time-consuming process. Recently, the authors have proposed a combined application of FDTD method, data-fitting models and TD Radiation Integral [G. Marrocco, M. Ciattaglia, to appear on IEEE AP-52 2004] for the transient analysis of aperture antennas such as slots, open-ended waveguides and ridged horns. Starting from this approach, this contribution presents a numerical formulation for the efficient calculation of effective height avoiding time consuming processing and allowing to compress the whole space-time antenna phenomenology into a small set of parameters, which are simple to store and able to regenerate the antenna space-time response to any kind of input signal.

For an aperture antenna S_a, the TD effective height can be written as in Fig. 1 where ρ is a coordinate vector on the aperture, the time variant vector inside the integral is the aperture field impulse response and the Dirac function with (1) superscript denotes derivative. The FDTD model, sourced by a test gaussian-like pulse, provides the transient aperture field which is fitted, at run-time, onto space-variant vector basis functions according to time-dependent coefficients $v_p(t)$. In turn, coefficients are expanded onto time-variant basis functions consisting of complex exponentials and early time entire-function. Starting from [A. Poggio, M. VanBlaricum, E. Miller, R. Mittra, IEEE AP- 26, pp. 165-173, 1978], [G. Marrocco, F. Bardati, IEEE MTT- 49, pp.1321-1328, 2001], customized signal deconvolution algorithms have been developed to obtain scalar impulse responses from coefficients $v_p(t)$ according to a proper time domain model. In particular, two alternative time-domain representations are discussed, the first requires a smaller amount of data to represent the field phenomenology, and has been denoted Complete Fitting (CF) model (Fig. 2) the second, referred to as Incomplete Fitting (FI) model does not include the entire function and involves a simpler deconvolution procedure. Finally, the effective height of the aperture antenna system is retrieved by means of the TD radiation integral formalism which, taking advantage from the space and time fitting models, can be calculated in closed form, at least along the antenna boresight (Fig. 3) and along the principal planes. Comparisons about efficiency and accuracy of the two impulse response models will be discussed by means of examples concerning a rectangular slot on an infinite ground plane (Fig. 4) as well as a rectangular ridged horn antenna.

$$\boldsymbol{h}\ (\hat{\boldsymbol r},\tau) = 2\left[-\frac{1}{\eta_0}\hat{\boldsymbol r}\times\iint_{S_a}\boldsymbol E_a^\delta(\boldsymbol\rho,\tau+\frac{\hat{\boldsymbol r}\cdot\boldsymbol\rho}{c})d\boldsymbol\rho\times\hat{\boldsymbol z}\right]*\delta^{(1)}(\tau)$$

Figure 1: Definition of time-domain effective height for transmitting aperture antennas.

$$g_p^C(\tau)\approx g_{p,\infty}\delta(\tau-t_p)+\sum_{k=-K_p}^{K_p} g_{pk}e^{s_{pk}\tau}U(\tau-t_p)$$

Figure 2: Scalar Complete Fitting (CF) model for the calculation of aperture impulse response.

$$\underline{h}(\hat r,\tau)=2\sum_{p=1}^{N}\underline{i}_p g_p(\tau)*\delta^{(1)}(\tau)$$

Figure 3: TD effective height on the antenna boresight. $\underline{i}_p$ **denotes a constant vector.**

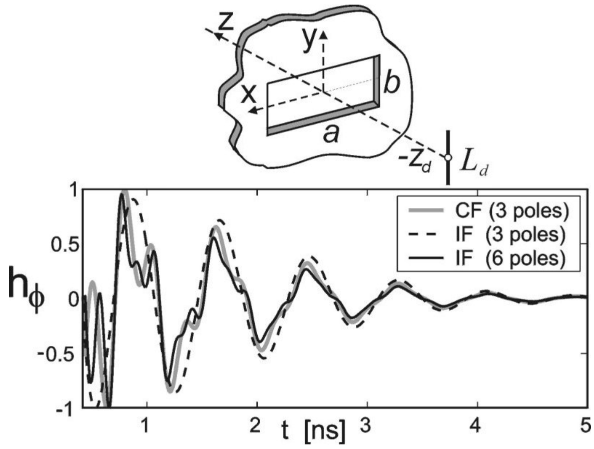

Figure 4: up) Dipole-sourced rectangular slot on an infinite ground plane (sizes in [cm]: a**=10,** b**=5,** L_d**=11.5,** Z_d**=9). down) Effective height on antenna boresight obtained by means of two different fitting models of aperture field and different number of poles.**

UWB 4-7: The Influence of Multitone Disturbances on Nonlinear Systems

Y. Bychkov[1], **J. Nitsch**[2], **N. V. Korovkin**[2], **S. Scherbakov**[3], **S. Diomkin**[1], **A. Himeen**[1]

[1]*St. Petersburg Electrotechnical University "LETI"*; [2]*Otto-von-Guericke-University*; [3]*Pskov State Polytechnical Institute*

In this paper we numerically and analytically analyze nonlinear systems which are excited by a two-tone disturbance. The nonlinear system is perturbed by an input signal of the form: $u(t) = U_0[\sin(\omega_1 t) + \sin(\omega_2 t)]$; $\omega_1 \approx \omega_2$. It is well known, that the impact of the demodulation on the nonlinear part of a system leads to the occurrence of currents and voltages with frequencies $n\omega_1 \pm m\omega_2$; $n, m = 1, 2, \ldots$. Amplitudes of these oscillations can reach up to $0.5U_0$, and thereby may interfere with working quantities of the system [1]. For this reason two-tone disturbances represent a more substantial hazard for complex electronic objects than single-tone interferences.

The design of a protection measure against two-tone interferences needs the use of a reliable software. In [2] it is shown, that the PSPICE standard package yields essentially incorrect results when it is used for beat. This is due to the solvers of the differential or finite-difference equations used in standard packages. The highly reliable new method of integration offered in [3] and used in this paper gives accurate and effective solutions for beat problems.

We solve our problem using an analytical-numerical method of variable order. This method is intended for the analysis and synthesis of nonlinear non-stationary, nonautonomous systems with arbitrary sources described by ordinary integro-differential equations. It is based on the description of solutions by means of generalized functions with regular components applying Taylor's series and the generalized Laplace transformation. It consists of analytical and numerical parts. In the analytical part the nonlinear integro-differential equations are identically transformed to algebraic equations which are linear with regard to Laplace images. In the numerical part the maximum possible step of calculation and minimal possible order of the method are specified at their optimum combination to ensure numerical stability of the solution. The basic advantages of this approach are reduced to the determination of areas containing unknown values of exact solutions, with the opportunity of the investigation of the singular components in these solutions.

For disturbing frequencies equal to $\omega_1 = 2\pi \cdot 1.71$GHz, $\omega_2 = 2\pi \cdot 1.89$GHz the calculation step was at a level of $(1 \cdots 1.2)\cdot 10^{-11}$. The used procedure of setting and controlling the length of the integration step provides the opportunity to the following analyses: the existence and uniqueness of the solution, coordination of step length and speed of change of the solution, as well as the control of limiting levels of local and global errors. In correspondence with the specified conditions the procedure of step setting is fully adaptive. At the level of the absolute local error of calculation $e = 10^{-14}$, the order (the order of Taylor's polynomial) is equal to 18. This order is a function of e and of the dynamic properties of the system considered. The level of the global error of calculation of one period of the process is 10^{-12}, and after ten periods - 10^{-11}. Detailed research has shown, that the required solution has a stable character.

1. J.Nitsch, N.Korovkin, E.Solovyeva "Examination of the Demodulation Effect of Two-Tone Disturbances on Nonlinear Elements", Review of Radio Science, 2004

2. K.Y.Huang, Y.Li, C.-P.Lee "A Time-Domain Approach to Simulation and Characterization of RF HBT Two-Tone Intermodulation Distortion", IEEE Trans. Microware Theory Tech., vol. 51, pp.2055-2062, Oct. 2003.

3. J.A.Bychkov., S.V.Scherbakov: "Analytical-numerical calculation method of dynamic systems", St.-Petersburg, Energoatomizdat, 2001.

UWB 4-8: Suppression of Two-tone Disturbances in Nonlinear Circuits

E. Solvyeva[1], **J. Nitsch**[2], **N. V. Korovkin**[2]
[1]*State Electrotechnical University*;
[2]*Otto-von-Guericke-University*

Nowadays, there is a marked trend for the increase in frequency and shifting of the amplitude maximum of noise fields into the high-frequency region. The shielding factor of non-ideal shields is reduced with increasing frequency (for example, the increase in the transfer impedance of cables with braided shields). Therefore, problems of protecting electronic devices, as a whole, become complicated with increasing frequency, and this trend will prevail in future.
In this paper the mechanism for the occurrence of low-frequency noise due to the demodulation of the external two-tone high-frequency electromagnetic field is examined. The two-tone high-frequency electromagnetic field penetrates into the internal (protected) volume of the electronic device and generates a low-frequency noise that propagates further into electronic circuits. These low-frequency oscillations represent a significant threat to the electronic equipment, since standard filters do not suppress low-frequency harmonics. The low-frequency disturbances can produce a number of problems for the electronic equipment, among which we will note the following:
1) The frequencies in the (1-103) kHz range are considered here as low-frequency noise, and can be close to operational frequencies of analog electronic devices. In this case, the low-frequency noise directly distorts a useful signal of the electronic device.
2) The low-frequency noise can shift the operating points of transistor cascades of electronic circuits substantially and thereby changing their operating conditions.
3) The low-frequency noise can be a source of dynamic instabilities in complex electronic systems.
In this paper we demonstrate the universal way to suppress the demodulation effect of the external two-tone high-frequency electromagnetic field on the basis of Picard's iterations including nonlinear protection elements against low-frequency oscillations.

UWB 5 - Target Detection & Discrimination

UWB 5-1: A Group Theoretical Symmetry Filter for Discrimination of Landmines in the Subsurface

M. Phelan, **C. Gilmore**, **I. Jeffrey**, **H. Su**, **J. LoVetri**
University of Manitoba

An application of Group Theory in the development of a spatial symmetry filter for the purpose of discriminating AP landmines in the subsurface is presented. The filter is designed to detect bodies possessing even-ordered axial symmetry such that the symmetry axis is perpendicular to the ground surface. The concept is appropriate for discriminating landmines from subsurface clutter since many landmines inherently posses even ordered axial symmetry while in general, clutter does not.
Scattered electromagnetic fields from the subsurface can be separated into symmetric and antisymmetric components (C. E. Baum, "Symmetry in Electromagnetic Scattering as a Target Discriminant", Interaction Note 523, Phillips Laboratory, October 1996), (C. E. Baum, "Interaction of Electromagnetic Fields with an Object which has an Electromagnetic Symmetry Plane", Interaction Note 63, Air Force Research Laboratory). Information regarding the physical symmetry in the subsurface can be extracted from these components. It has been shown that the symmetry of a subsurface target at a known location can be quantified by defining a symmetry metric (J. M. Stiles et. al., "A group Theoretic Analysis of Symmetric Target Scattering With Application to Landmine Detection", IEEE Trans on Geosci. and Rem. Sens., Vol. 40, No. 8, August 2002). It will be shown that if the location of subsurface targets are unknown in a 2D plane perpendicular to the ground surface, the symmetric and antisymmetric fields extracted along successive parallel SAR measurements on either side of this plane can be used first to "filter" out field components with little symmetry and then to discriminate regions of interest by assigning a threshold to the symmetry metric. The sensitivity of the detection scheme can be manipulated by varying the threshold value of the symmetry metric. The method is applicable for both monostatic and bistatic radar topologies as long as the antenna system possesses two-fold rotation/reflection symmetry (C2a symmetry) and that targets of interest are limited to even ordered axial symmetry.
The theory of the method is introduced and experimental results taken in a controlled environment are presented to demonstrate validity and practicality.

UWB 5-2: Detection and Classification of Targets Behind Walls

W. A. Chamma, **S. S. Gauthier**, **S. Kashyap**
Defence R&D Canada / Dept. of National Defence

In recent years ultra wideband (UWB) radar systems have been proposed for many civilian and military applications such as ground penetration, terrain profiling, foliage penetration, synthetic aperture radar imaging and the detection of objects behind walls and barriers. UWB short pulse radars with pulse widths less than 1.0 ns can be used to effectively detect various targets. The short-pulse characteristic gives these radars many desirable properties that conventional radars do not have. The advantages include high-accuracy range determination, improved target classification, and reduced clutter and multipath interference in the received signal.
In an earlier work, (W. Chamma and S. Kashyap, Detection of targets behind walls, AMEREM 2002) the authors investigated, through numerical simulation, the capabilities and limitations in the use of a UWB radar system to detect targets inside a room with concrete floor and wooden walls. The signals in a one-dimensional transmit/receive array were used in the construction of the detected images. In this paper that work is extended to include more real-life structures and situations using the full-wave finite-difference time-domain (FDTD) method (K.S. Yee, IEEE APS, 1966), which allows the modelling of complex inhomogeneous structures efficiently. A 4.5mx3.0mx3.0m concrete room with 15 cm thick walls is used as the basis of our model. Objects are placed inside the room at different locations. These objects include conducting cubic boxes and a human model phantom with and without a rifle (Fig. 1). The human model used is based upon scans from magnetic resonance imaging (MRI) and consists of twenty-three tissue groups. The physical parameters (permittivity and conductivity) of these tissue groups are specified at the transmitter's centre frequency. The concrete room is illuminated by a dipole antenna located outside the room, transmitting a UWB short pulse with a centre frequency of 2 GHz. The scattered field due to the objects inside the room is calculated and recorded at several receiver points outside the room. Using the back-projection technique, images of the objects inside the room are constructed. The quality of these images depends on the UWB radar system's transmit/receive parameters. These include the size of the antenna array and the spatial resolution of its transmit/receive points. In our numerical experiments, a two-dimensional receiver array is used to record the EM field outside the concrete room. This paper will describe the effect of various parameters, such as the number of the transmit/receive points and the target material composition, on the performance of the detection setup. Additional simulation and measured data for a UWB short pulse detection system operating at 10 GHz will also be discussed and presented.

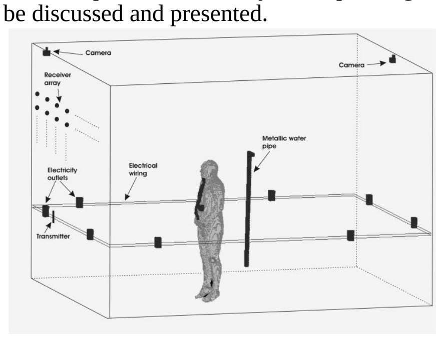

Figure 1: Modeled objects inside the concrete room

UWB 5-3: Application of UWB Near-field Polarimetry to Classification of GPR Targets

A. Yarovoy, **V. Kovalenko**, **F. Roth**, **L. P. Ligthart**
Delft University of Technology

Recently considerable efforts are put in development of GPR sensors to be included into multi-sensor system for landmine detection. The principal mission of such GPR sensor is reduction of false alarms produced by a metal detector. In the contrary to a metal detector (which signal does not contain much information over the target) GPR signals contain much larger amount of information about detected targets, from which numerous features of targets can be extracted. Several of such features, which might be very useful for discrimination between mines and friendly objects, can be extracted from polarimetric processing of scattered signals. To verify usefulness of polarimetric information for classification of detected objects, we have performed a detailed analysis of the data acquired at the test facilities for landmine detection systems located at TNO-FEL by a multi-waveform full-polarimetric system developed at the International Research Centre for Telecommunications-transmission and Radar (IRCTR) in the Delft University of Technology.

In a typical landmine detection scenario a target is situated in the antenna near field. If the target situated in the broadside direction of the antenna system, the elongation factor and the orientation of elongated targets can be determined from the eigen values of polarimetric scattering matrix. However if the target is not situated in E- or H- plane of the antenna system, a substantial depolarization of EM waves scattered occurs even by a rotationally symmetric target. As a result majority of previously developed UWB polarimetric approaches for classification of targets and improvement of signal-to-clutter ratio do not work. To this end we have suggested two new approaches to the data processing.

Within the first approach the co- and the cross-polar (with respect to the antenna system) images of the subsurface are computed using traditional migration techniques. We have demonstrated that for rotationally symmetrical targets the co- and cross-polar images have specific azimuthal dependence, which can be used as a template for detection. Influence of surface and subsurface clutter on such a template is not critical.

Within the second approach we have developed a full-polarimetric tomography algorithm, which produces single subsurface image based on a full-polarimetric data set. It is shown that the point-spread function of such an algorithm is narrower than that of conventional migration algorithm.

UWB 5-4: Ultra Wideband Radar for the Search of Avalanche Victims

W. A. Chamma, **H. Mende**, **R. Robinson**
Defence R&D Canada / Dept. of National Defence

Recently ultra wideband (UWB) radar systems have been proposed for many civilian and military applications such as ground penetration, terrain profiling, foliage penetration, synthetic aperture radar imaging and the detection of objects behind walls and barriers. The advantages of a short-pulse UWB include high-accuracy range determination, improved target classification, and reduced clutter and multipath interference in the received signal.

Search and rescue (SAR) operations of snow avalanche victims would be one civilian application that could benefit from the use of the UWB technology. Conventional SAR is done by using tracker dogs and probing poles to find victims in accessible areas or by the use of helicopters to carry rescue personnel with probing poles to designated areas. The use of ground penetrating radar (GPR) has been tested at 500 MHz (Jurgen Niessen, et al., The use of GPR to search for persons buried by avalanches, GPR'94) and a vertical range profile image was obtained for a depth of 8 meters. In this test, the presence of a volunteer (inside a buried shaft at 2 meters deep) was indicated by a "hyperbola" trace in the generated image. In general, SAR operations will start as soon as a snow avalanche occurs, hence, a radar setup that would provide an image of a potential buried victim will make the operations more efficient. Using short pulse UWB radars with pulse width less than 1.0 ns will provide fine range resolution and the synthetic aperture radar processing technique will provide high cross-range resolution. This work, sponsored by the Canadian National Search & Rescue Secretariat (NSS), investigates through numerical simulation and measurements, the feasibility of using short-pulse UWB for SAR operations. In our numerical simulation the finite-difference time-domain (FDTD) method (A. Taflove et. al., Computational Electrodynamics, the finite-difference time-domain method, Artech House, 2000) is used to study the capabilities and limitations of the UWB radar system to detect objects buried in snow. This method allows the modelling of complex inhomogeneous structures efficiently. A planar radar system consisting of nine transmitters and n receiver points is set at a distance d from the snow surface. In modelling a buried human body, a human model phantom is located below the snow surface at different depths. To make our simulation close to real-life situations, the human model used is based upon scans of magnetic resonance imaging (MRI) and consists of twenty-three body tissue groups. The physical parameters (permittivity and conductivity) of these tissue groups are specified at the transmitter's center frequency. The snow surface is illuminated by a 0.5 ns UWB pulse with a centre frequency of 2 GHz. The scattered field due to the buried objects is calculated and recorded at several receiver points in the transmitter/receiver plane. Using the back-projection technique, images of the buried objects at different depths can be constructed. Figure 1 shows a three-dimensional sketch of the modelled space including a buried human phantom. Figure 2 shows the image generated from the received signals on a horizontal plane cut using numerical simulation. A UWB radar measurement setup is also being examined to test its capability to detect and classify buried objects in snow. Initially, classical targets (e.g. metallic sphere) are used and will be followed later with realistic objects. This paper will describe the effect of various parameters such as the transmit/receive points' location, target material composition, and various snow conditions on the performance of the detection setup.

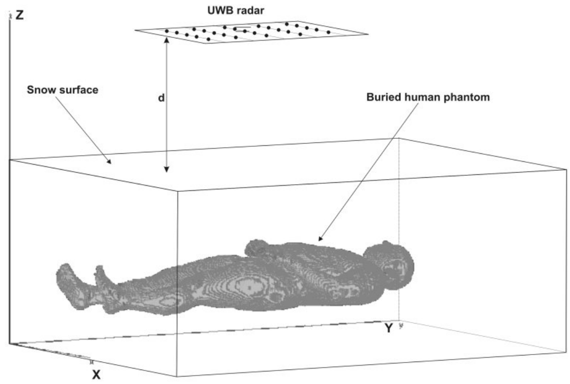

Figure 1: Computer model of a UWB setup illuminating a buried human phantom in snow

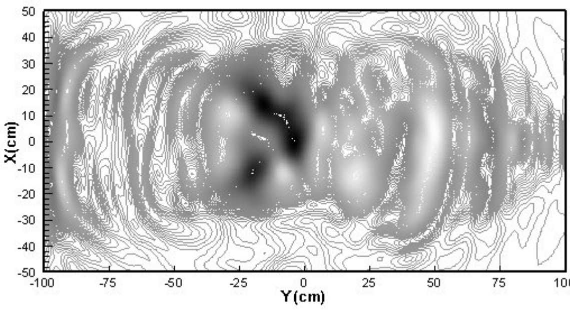

Figure 2: Image of a human phantom at a 50 cm below the surface of a freshly fallen snow

UWB 5-5: Radar Target Detection at Noise and Clutter Background

V. I. Koshelev, **V. T. Sarychev**, **S. E. Shipilov**
Institute of High Current Electronics, RAS

A new approach for ultrawideband (UWB) radar signal detection at noise and clutter background is suggested. The basis of the aproach is successive application of matched filtering (MF) and inter-period correletation processing (ICP). It is demonstrated that in comparison with ICP, this approach allows increasing the efficiency of UWB radar signal detection under conditions of joint action of noises and broadband continuous clutter as well as selecting the signal reflected from the target at noise and UWB pulse clutter background. Two modifications of the suggested approach have been considered. Their application domain depends on radial velocity of a sounding target. Probabilities of correct detection at different noise/signal and clutter/signal ratios have been calculated for them. It is demonstrated that preliminary averaging of received signals is efficient at low target velocities. Thus, at the fixed probability of false alarm of 1.4.10-3 and possibility of averaing by 100 realizations of a signal, the probability of correct target detection exceeds the value of 0.9 at the noise/signal ratios in the range from 0 to 5 and clutter/signal ratio equal to 2. At the higher velocities it is suggested to make averaging by calculated covariations of signals received at the neighbouring periods of time. Thus, in case of averaging by 100 covariations, probability of correct detection decreases in comparison with averaging by realization of received signals. Probability of correct target detection exceeded the value of 0.9 at the noise/signal ratios in the range from 0 to 1.5 and the clutter/signal ratio equal to 2. However, in this approach the averaging number has no influence on the maximum allowable target velocity.
According to simulation, at the joint application of MF and ICP, the radar signal covariation exceeds the UWB clutter covariation. At application of only one ICP method the level of covariation clutters can exceed the level of radar signal covariation that makes impossible target detection at applicaion of a threshold detection.

UWB 5-6: Comparison of Seismic Migration and Stripmap SAR Imaging Methods for GPR Landmine Detection

C. Gilmore, **H. Su**, **I. Jeffrey**, **M. Phelan**, **J. LoVetri**
University of Manitoba

Traditionally, migration methods have been used in seismic signal processing, while SAR processing has been used for radar applications. Today, migration imaging is used for a wide range of radar applications yielding improved results over the traditional SAR approach(C.Cofforio et al, SAR Data Focusing Using Seismic Migration Techniques, 1991), (B. Scheers, UWB GPR With Application to the Detection of AP Land Mines, Ph.D. Thesis, 2001), (M. Soumekh, Synthetic Aperture Radar Signal Processing With Matlab Algorithms, 1999). This paper explores and compares the theoretical and practical aspects of seismic migration methods and stripmap SAR methods as applied to Ground Penetrating Radar (GPR) for the use of land mine detection. Theoretical aspects of seismic migration and stripmap SAR techniques are reviewed. Typically, seismic migration methods make fewer assumptions than conventional SAR, and are theoretically superior, although sometimes are more computationally expensive. We compare the different methods using a Stepped-Frequency Continuous Wave (SFCW) Ultra Wide Band (UWB) radar with sub-bands selected in the 1-12 GHz range. Imaging methods are applied to numerically generated and experimental data. Both metallic and dielectric targets are considered because common Anti-Personnel (AP) landmines and UXO have such physical properties. Various test environments such as a sand box filled with dry and wet sand are investigated.
All the methods considered form range vs. cross range images of the sub-surface containing known targets. Several quantitative metrics are employed to compare the performance of the different imaging methods. Performance is defined as target detection and accurate localization, multiple-target resolution and suppression of radar artefacts. Computational cost is compared for the different techniques. The comparisons are useful for determining which techniques will be most effective for AP and UXO imaging.

UWB 5-7: Target Detection and Imaging Using Time-Domain Measurements of Ultra-Wideband Signals

B. Chen[1], **H.-L. Cui**[1], **X. Huang**[1], **R. Pastore**[2]
[1]*Department of Physics and Engineering Physics, Stevens Institute of Technology, Hoboken, New Jersey 07030, USA*;
[2]*U.S. Army CECOM-RDEC, Fort Monmouth, New Jersey 07703, USA*

In this study we carry out forward modeling of target detection and imaging using ultra-wideband (UWB) pulses, and then develop an algorithm for image reconstruction based on time-domain measurements of reflected UWB pulses.
UWB signals have been used for radar applications for several decades. Recent studies have been carried out for applying UWB technology to military and commercial communications, such as high-speed mobile local area networks, surveillance systems, military communications, ground penetration radars (S. Vitebskiy et al., Ultra-wideband, short-pulse ground-penetrating radar: Simulations and measurement, 1997), automotive sensors, medical imaging instrument, and wireless personal area networks. UWB through-wall imaging systems detect the location or movement of persons or objects that are located on the other side of a structure such as a wall. Obviously, the propagation of UWB signals in indoor-outdoor environments is the most important issue with significant impacts on the success of the UWB technology (R. J.-M. Cramer et al., Evaluation of an ultra-wide-band propagation channel, 2002). It has been noted that the geometry of the situation and the building/wall architecture can have a significant effect on the received signals (Q. Spencer et al., Modeling the statistical time and angle of arrival characteristics of an indoor multipath channel, 2000).
UWB is an RF wireless technology, and as such is still subject to the same laws of physics as every other RF technology. For narrow band radio wave propagation, the signal propagates from the transmitter to the receiver via many different paths. At the receiver, these different echoes overlap - either constructively or destructively, depending on the exact location of transmitter, receiver, and scatterers. In UWB systems, different echoes can be distinguished based on their run time between transmitter and receiver. The resolution capability is the inverse of the system bandwidth. Thus, a UWB system with 10 GHz bandwidth can distinguish signal echoes that differ by 100 ps in their run time, and thus 3 cm path length can be resolved.
The reflection, scattering, and diffraction of the incident wave by the target will result in multipath UWB propagation channel and UWB signal distortion. In this study, the combined method of ray tracing and diffraction (CMRTD) is used to compute the reflected and back-scattered field by target (B. Chen and J. J. Stamnes, Scattering by simple and nonsimple shapes by the combined method of ray tracing and diffraction: application to circular cylinders, 1998). In the CMRTD the target will be replaced by multiple equivalent phase objects (EPOs). The physical parameters of each EPO, such as the position, amplitude and phase are determined using ray tracing. The Kirchhoff diffraction theory is then employed to compute the scattered and back-scattered fields from the EPO.
For image reconstruction, we basically employ the reflection tomography theory (e.g., A. C. Kak and M. Slaney, Principles of Computerized Tomographic Imaging, 1988). Moreover, our image reconstruction algorithm will be based on limited data sets of reflected and back-scattered UWB signals (B. Chen et al., Image reconstruction in diffraction tomography from limited transmitted field data sets, 2000), which is useful in practice.
Applications of the technique described in this paper may include through-wall imaging, ground penetration radars and surveillance systems.

UWB 5-8: Ultra Wideband Impulse Radar Data Exploitation

G. Barrie
Defence R&D Canada / Dept. of National Defence

Defence R&D Canada (DRDC) has an active research program in many aspects of ultra wideband (UWB) radar systems, including simulation, data analysis and hardware prototyping. UWB radars are capable of producing high-resolution images by combining the benefits of sub-nanosecond impulse technology and synthetic arrays. One particular application of this is in the area of through-wall sensing, where relatively low center frequencies enable good radio frequency (RF) penetration of typical building materials. A second project involves the use of UWB radar systems for search and rescue of avalanche victims. This is a Canadian multi-department venture including Parks Canada, the National Search and Rescue Secretariat, and the Department of National Defence.

A challenging but nonetheless necessary requirement for military, and civilian application of UWB radar is the ability to detect and characterize possible targets through relatively dense, inhomogeneous materials. This paper outlines some of the progress that has been achieved in target discrimination capability, achieving enhanced signal to noise ratios (SNR), and verification of target velocity thresholds using experimentally obtained data. Sets of measurements were carried out examining the motion of a target rotating about a radius of 0.5m. Using a sphere as an idealized target ensured a relatively uniform RCS, independent of the point of its orbit.

As is typical of impulse radar returns that lack the filtering commonplace in narrowband systems, individual returns are severely impaired by the presence of thermal noise, clutter and external interference. Data must be processed efficiently to yield an acceptable SNR, and to enhance structural details of the return pulse. This is achieved by a combination of ensemble averaging to reduce thermal fluctuations and the newly developed Background Noise Conditioning (BNC) method, used to remove isolated spectral interferers. BNC was developed here at DRDC to periodically examine spectral noise properties, and automatically configure an appropriate notch filter. For the radar data presented in Figure 1, averaging over a relatively small number of pulses is insufficient to raise the desired returns appreciably above the noise floor. Typical SNR values at N = 1 are around 18 - 19 dB. Beyond ten pulses, SNR improves approximately linearly. Integration of about 80 pulses results in a SNR maximum of about 35 dB, with an associated improvement of 15 dB over the untreated data (that is, BNC not applied). For values $N > 80$, the averaging takes place over a long enough time period that returns become blurred due to target motion. This effectively defines the upper limit of N that can be achieved without additional processing to focus the returns.

Using the space-time backprojection technique, reconstructed data clearly shows the oscillatory motion (Figure 2) of the target, but the signal vanishes as the radial velocity approaches zero at the two extremes of motion. Using the data, we were able to verify the minimum detectable velocity for the system as indicated in Figure 3. This information can be employed to construct a non-doppler MTI filter for target velocity discrimination (G.S. Gill, Waveform Generation and Signal Processing in Ultra Wideband Radar, SPIE Proc. Vol. 2235, 1994). In turn, this will be used to further enhance SNR by time-aligning the integrated return pulses.

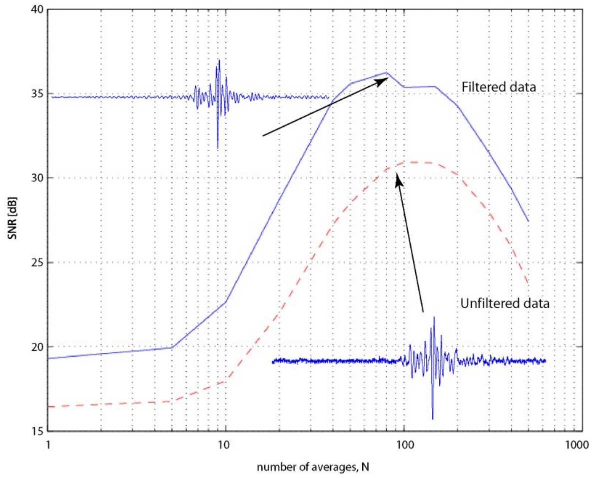

Figure 1: SNR vs. number of integrated pulses, with and without BNC applied

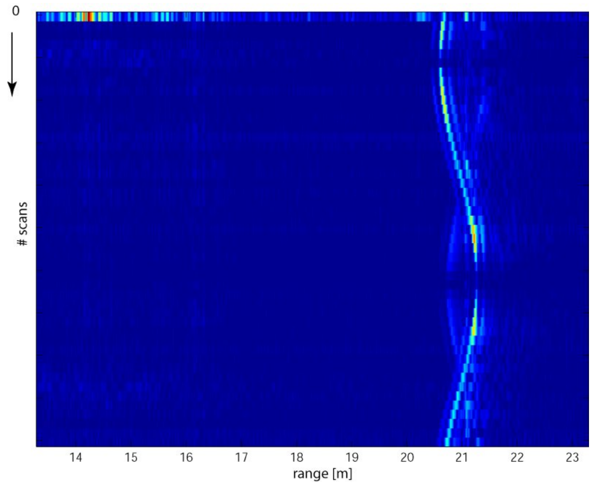

Figure 2: Reconstructed data from backprojection technique. Target is centered at 21m, rotating about a radius of one-half meter.

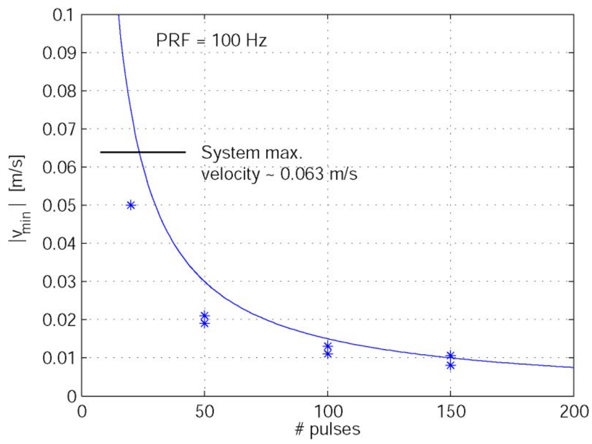

Figure 3: Comparison of theory (solid line) with experiment showing minimum detectable target velocity.

UWB 5-9: Reduction of Clutter in GPR Data by CROW-Search Technique

V. Kovalenko, A. Yarovoy, L. P. Ligthart
IRCTR, TU Delft

The humanitarian demining is one of the most challenging problems confronting mankind. Significant efforts have been made worldwide to develop high-tech tools, which could help to solve the problem of the detection of antipersonnel mines (APM). The ground penetrating radar (GPR) is considered one of the several most promising technologies in this context. The APM normally are small electrically low-contrast objects and thus their detection in the natural ground is inherently difficult problem. It called for development of the principally new generation of GPR devices specifically dedicated to this task. The GPR of this type normally operate in higher frequency band and meet higher demands in terms of the internal stability than their conventional counterparts.

The IRCTR at TU Delft has developed such a device and successfully tested it in the special facilities for landmine detection systems testing located at TNO-FEL, The Hague The Netherlands. During this measurement campaign we have collected GPR data from 3 different test sites, which mimic the minefields in the dry sand, wet sand and grass. It has been found during the dry sand data analysis (V.Kovalenko, A.Yarovoy, Analysis Of Target Responses And Clutter Based On Measurements At Test Facility For Landmine Detection Systems Located At TNO-FEL, 2003) that the electromagnetic responses of all the mines share the same shape of their wavelets when the quasi-monostatic mode of antenna configuration is used. In this case the wavelets of main responses of all mines differ primarily in amplitude but not in the shape, regardless of the APM type and its depth.

We use this circumstance to define the canonical response of object wavelet (CROW) construct the filter, which gives high output where the wavelet is present in the data and has fast roll-off elsewhere. This filter improves signal to clutter ratio in the processed data and thus mines detectability. The filter consists of two stages, with first one locating the minima of distance in L2 between the CROW and the second one shaping the filter output in the desired way.

The filter is placed in the data processing chain: Moving Window Background Removal → CROW Filter → SAR Migration → Windowed Energy Projection → Receiver Operator Curve (ROC). In the paper we discuss the optimal parameters of the filter and its influence on the ROC of the radar, calculated by the device performance on the minefield simulator spot with known groundtruth.

UWB 5-10: Echo Cancellation using the Homomorphic Deconvolution

W. Choi, **T. K. Sarkar**
Department of Engineering and Computer Science, Syracuse University

Deconvolution is an important preprocessing procedure often needed in the spectral analysis of transient exponentially decaying signals. Homomorphic deconvolution techniques is studied and applied to the problem of canceling the echo in the signal. Signal processing applications use the collection of nonlinear techniques known as cepstral analysis. These are based around the core concept of the complex cepstrum. One of the more important properties of the cepstrum is that it is a homomorphic transformation. Under a cepstral transformation, the convolution of two signals becomes equivalent to the sum of the cepstra of the signals. Multiplication and convolution are also common means of mixing signals together. If signals are combined in a nonlinear way (i.e., anything other than addition), they cannot be separated by linear filtering. Homomorphic techniques attempt to separate signals combined in a nonlinear way by making the problem become linear. That is, the problem is converted to the same structure as a linear system. The logarithm of the power spectrum of a signal containing an echo has an additive periodic component due to the echo, and thus the Fourier transform of the logarithm of the power spectrum should exhibit a peak at the echo delay.

In this paper we simulated electromagnetic waves scattered from a conducting sphere, along with its echo components to demonstrate the applicability of this procedure.

UWB 5-11: Combining Polarimetry with SEM in Radar Backscattering for Target Identification

C. E. Baum
Air Force Research Laboratory, DEHP; Directed Energy Directorate; Kirtland AFB; NM; USA

In identifying radar targets based on the poles (resonances) in the singularity expansion method (SEM), there is additional information to be gained from the residues. The polarizations of the substructure resonances can also be used as a target signature. In addition, the relative times of arrival of the various resonances at the radar can also be used as another way to construct a target image.

A fundamental concept concerning the properties of the residues is target symmetry. The geometrical symmetries of the target evidence themselves in the symmetries of the scattering dyadic. A simple example is a symmetry plane (say y=0). In such a case with incidence parallel to the xz plane the residue vectors are polarized parallel to or perpendicular to this plane, this being observable by a receiver on or near this plane.

Bodies of revolution with axial symmetry planes extend the above, since at least one of these symmetry planes extends through the observer. In this case there are two $\vec{c}_\alpha$ to consider (with the same s_α, i.e., degeneracy) which are aligned parallel and perpendicular to this symmetry plane. This is particularly convenient if the symmetry plane is vertical, thereby fitting into the h, v radar coordinates with no crosspol in backscatter.

While previous considerations have concentrated on the symmetries of the total target, one can consider the properties of substructure resonances to the extent that they can be separated from the overall target scattering. This can be accomplised in part by temporal isolation of the scattered singal from that of other “clutter” such as earth or water surface or other nearby large structures. (Such symmetries can be termed “partial symmetries”.)

With substructures small compared to the overall target dimensions the substructure resonances have various signature properties. With, say, vertical incidence and scattering, one may observe the polarizations of more htan one substructure. The relative angles between these polarizations are themselves target signatures. Based on the time of return of the substructure resonances one can estimate the relative heights (and height from the ground) of these substructures. If we combine the relative delays from various susburcturces is backscatter as measured from different anles of incidence we can make a three-dimensional image of the target based on the substructures. We might call this a resonance image.

UWB 5-12: Substructure SEM

C. E. Baum
Air Force Research Laboratory, DEHP; Directed Energy Directorate; Kirtland AFB; NM, USA

In recognizing (identifying) and object (target) from a scattered electromagnetic wave, various problems present themselves. Among these are low-frequency limitations on radars due to antenna size and associated beam width in transmission and reception. As a result many scatterers have their major linear dimensions large compared to the sensing wavelengths.

From the singularity expansion method (SEM) we have a target signature consisting of the aspect-independent natural frequencies (pole locations in the $s = \Omega + j\omega$ plane). For large scatterers the lower-frequency poles may then not be sufficiently excited to be useful for identification purposes. However, there are higher-order poles which may be in the frequency range of our radar.

The higher-order poles sα of interest have the smaller damping constants (-Ω_α), i.e., are more resonant. These can be associated with substructures on the larger scatterer. By substructures let us think of these as local perturbations on a surface (perfectly conducting or otherwise) with larger characteristic dimensions. It is then of interest to have some perturbation techniques to develop the SEM represetation of such substructures. This applies not only to the scattering theory, but also to the data-processing techniques to be used to identify the presence of such substrcture

resonances.
This is just a beginning on the subject of substructure SEM. It would be helpful to have calculations for various canonical substructures. Equally important are the data processing algorithms for experimental impementation.

UWB 6 - Applications of Hyperband Systems and Antennas

UWB 6-1: Measurement of the Pulse Radiation of an IRA in Time Domain

T. Stadtler[1], **J. L. ter Haseborg**[1], **F. Sabath**[2]
[1]*Technische Universität Hamburg-Harburg, Department of Measurement Engineering / EMC, Hamburg, Germany*;
[2]*Armed Forces Scientific Institute for Protection Technologies, Munster, Germany*

Summary
For radiation of UWB pulses special impulse radiating antennas (IRA) have been designed and are continuously improved. In this paper a novel test set up to determine the transient near field of this antenna type is described. The double probe near field scanner is able to measure the two dimensional field distribution in time domain.

Introduction
Often the effects of fast transient fields on modern electronic systems are investigated using a test setup consisting of a high power pulse source and a reflector type Impulse Radiating Antenna (IRA). In order to optimize the far field response a number of investigations and improvements to the basic design of the IRA were made during the last years. Particularly susceptibility investigations in anechoic chambers or small tests sites require a detailed characterization of the near field of the antenna. In this paper a novel test set up to measure the transient near field response in two dimensions is described.

Set up
A drawing of the described near field scanner can be seen in figure 1. In front of the IRA a field probe is located. It is mounted on an actuation unit which is able to move in two dimensions. A second field probe is placed on a fixed position in the field, it can be replaced by a voltage probe or a picoTEM probe (T. Weber, J. L. ter Haseborg, “A new broad-band probe for the measurement of ultra-fast transients“, EMC EUROPE 2002, Sorrento, Italy, Sept. 9-13) in the feed wire of the antenna. Both sensors are connected to a 2 channel digital oscilloscope with a sufficient sampling frequency. The antenna is connected to an UWB pulse source.
To acquire a field mapping the movable probe is moved to different coordinates. On each coordinate the pulse source is triggered and the signal of both probes are sampled. Of course this procedure requires a relatively high repeat accuracy of the pulse source.

Synchronization of the measured data
The field points are measured successively. The signals of the fixed probe are used to synchronize all data. All signals of the fixed probe ideally should be identical except for a time shift and noise. Neglecting the noise, the time shift of each measurement can be calculated and corrected, which makes the synchronization. This can be done in time or in frequency domain. Each method has advantages and disadvantages. For transients synchronization in time domain generally is preferable.

Results
The results of near field scanner measurements can be evaluated in different ways. For transients a reasonable evaluation is the display of the field strength of the measurement plane at a given point in time as a color chart. Showing these diagrams one after another this visualization results in a movie clip of the transient field in time domain. The field distribution is shown in a kind of extremely slow motion. In the measurement of the reflector type IRA the propagation of the pre-pulse with negative phase can be clearly seen first and after that the more directed main pulse is observed. Other theoretical known and simulated behaviors of the IRA can be easily recognized in this type of visualization.
Further on other kinds of diagrams and movie clips can be calculated from the measured data. Examples are a minimum and a maximum chart. The minimum chart (figure 2) displays the pre-pulse because of its negative phase (based on the direction of the probe of course). The maximum chart (figure 3) displays the main pulse.

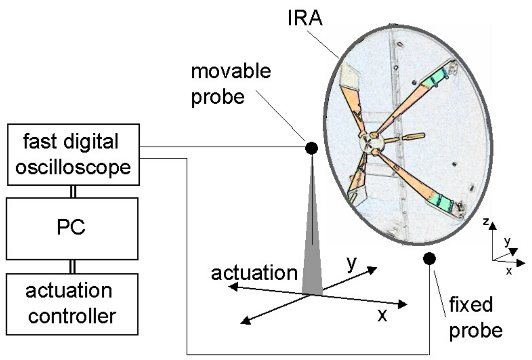

Figure 1: Set up for the measurement of transient field distribution

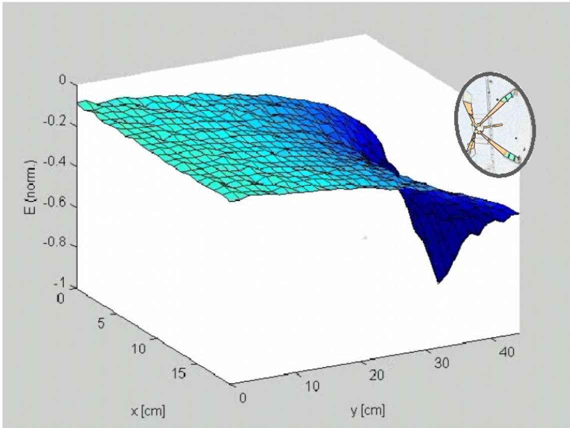

Figure 2: The temporal minimum (negative maximum) of the field distribution shows the pre pulse

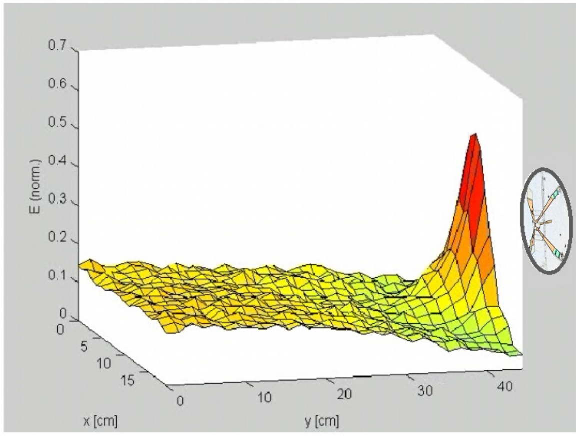

Figure 3: The temporal maximum of the field distribution shows the characteristics of the main pulse

UWB 6-2: Antenna Development for Impulse Radar Applications in Civil Engineering

C. Maierhofer, **T. Kind**, **J. Wöstmann**, **H. Wiggenhauser**
Bundesanstalt für Materialsforschung und -prüfung (BAM), Berlin, Germany

The field of application of impulse radar (GPR, ground penetrating radar) for non-destructive testing in civil engineering has increased considerably during the last ten years (Ch. Maierhofer,

Non-destructive evaluation of concrete infrastructure ground penetration radar, 2003). This is due to the fast and reliable use of this technique but also to the development of high frequency impulse generators and antennas and of reconstruction software enabling the visualisation of structural requests with high resolution (K. Mayer et al: Non-destructive evaluation of embedded structures in concrete: modelling and imaging, 2003). Typical structures in civil engineering to be investigated with radar are:
· reinforced concrete infrastructure buildings likes bridges, dams, fixed railway track beds, tunnels (quality assurance and early damage assessment)
· brick and stone masonry structures and in particular historic buildings (supporting building research and damage assessment)
· subsoil areas (detection of buried elements)
Testing problems are the detection of metallic reinforcement and tendon ducts and of other metallic inclusions like anchors, the localisation of voids and honeycombing, the determination of layer thickness of concrete cover, concrete slabs, repair mortar and plaster, the localisation of service pipes in walls and subsoil and the localisation of enhanced moisture content.
The application of impulse radar to this large variance of testing problems related to isolating materials having different dielectric properties requires the application of optimised antennas. Frequency and antenna impedance have to be adjusted to obtain high penetration depth and good spatial resolution.
The development of two different antennas had been performed at BAM in the frame of two European Research Projects together with further European Partners.
For the investigation of concrete structures and in particular for the detection of tendon ducts behind dense reinforcement in concrete bridges, a high frequency radar antenna had been developed with optimised material and geometry having a centre frequency of 2 GHz. For realising only a minimum of reflection at the antenna/concrete interface and thus a high efficiency of penetration of electromagnetic radiation, the flat metallic bow-tie antennas was glued directly onto a small concrete plate. The backside of the concrete plate was protected with a metallic sheet, therefore the thickness of the concrete plate has to be adapted to obtain constructive superposition of the backward reflected signal. The radiation characteristic was determined with the help of a concrete half sphere. An opening angle of only 20°was determined in the plane of the electric field which is lower than that of commercial antennas and which enables high lateral resolution.
For the localisation of service pipes in the subsoil, a second antenna was developed based on the same geometry but operating at lower frequency (300 to 500 MHz). For minimizing the distortion of the transmitting and receiving impulses, additional composite foam absorbers with a layered structure were integrated in a shielded enclosure assembled by tin plated metal sheet. Different sequences of absorber layers with changing conductivity were tested and qualified regarding maximum penetration depth and bandwidth limitation of the antenna.
In this presentation, examples of the successful applications of these new and other antennas will be demonstrated and results of different case studies (concrete bridges, historic masonry buildings, test field with service pipes) will be displayed.

UWB 6-3: Broad-Band Antenna Characterization for Landmine detection

M. Sato[1], **T. Savelyev**[1], **T. Kobayashi**[2]
[1]*Tohoku University*; [2]*JST/Tohoku University*

We are developing a GPR system for landmine detection. In a broad-band GPR system, antenna chrematistics are quite important. This is a array type GPR system which operates in the frequency range of 40kHz to 4GHz (M. Sato et al., GPR using an array antenna for landmine detection, Near Surface Geophysics, 2004). We are planning to use this GPR system in landmine detection in Afghanistan. So we designed the system which is suitable for relatively dry soil. Therefore, the system can use broader frequency range compared to conventional GPR systems for landmine detection. We have developed a Vivaldi type antenna for the GPR system and evaluated its performance in laboratory experiment and FDTD simulation. We characterized antenna transfer function and applied the results to signal pulse compression. Also, we checked the response to some theoretical results and found a good agreement.
The designed system is tested in laboratory condition and showed very good performance. With the array antenna configuration and synthetic aperture signal processing, the GPR system could detect buried landmine models under very high ground surface rough ness conditions.
In this paper, we will introduce the GPR hardware and show broad-band antenna response to buried objects. It will include time-frequency analysis and identification of targets using this information. A GPR system normally uses separated transmitting and receiving antennas. The mutual coupling of the antennas is also important in designing the GPR system. We evaluated the antenna mutual coupling experimentally and FDF simulation. These approaches will give a good example of designing and optimizing a broad-band radar system.

UWB 6-4: Through-the-Wall Imaging using Impulse SAR

J. Tatoian[1], **G. Franceschetti**[1], **D. Giri**[2], **G. Gibbs**[3]
[1]*Eureka Aerospace, Pasadena, California*; [2]*Pro-Tech, Alamo, California*; [3]*MARCORSYSCOM, Quantico, Virginia*

The paper presents the results of analysis associated with timed antenna arrays, both real and synthetic in order to understand inter-parametric dependence and the performance of an Impulse SAR operating in a transient (impulse regime) as applied to "Through-the-Wall" imaging. The key array parameters including the effective length and area, radiation diagram, effective antenna beamwidth, directivity are gain are examined and assessed. It is shown that many expressions for the transient array antennas can be obtained directly from the corresponding expressions associated with conventional narrowband systems, if the wavelength is substituted by the spatial extent of the radiated pulse. A procedure, necessary for radiating narrow pulses is discussed along with its impact on antenna efficiency in terms of gain and directivity. Synthetic aperture beamwidth for a transient array is computed explicitly and subsequently, the azimuthal (cross-range) resolution of an Impulse SAR is evaluated, which turns out to be identical to its steady state counterpart (narrowband SAR case). Preliminary considerations regarding an impulse SAR processing are presented. Finally, one-dimensional "Through-the-Wall" measured radar signatures of man, M16 rifle, and file cabinet using an impulse radar system, exhibit unique features to be exploited by an operational Impulse SAR system for target detection and identification. A prototype impulse SAR system, designed for "Through-the-Wall" imaging is currently under development; full-scale field tests are expected to commence at the later part of 2004.

UWB 6-5: High-Power Microwave System for Stopping Vehicles

J. Tatoian[1], **D. Giri**[2], **G. Franceschetti**[1], **G. Gibbs**[3]
[1]*Eureka Aerospace, Pasadena, California*; [2]*Pro-Tech, Alamo, California*; [3]*MARCORSYSCOM, Quantico, Virginia*

A compact High-power Electromagnetic System (HPEMS) is being developed for immobilization of the vehicles. The system consists of a portable tunable high-power source and a directive antenna capable of delivering appreciably large microwave energy to disable/damage vehicle's control module/microprocessor (MP). The approach consist of three major tasks: (1) developments of system concepts for a non-lethal area denial to vehicles, (2) identification of MP's "vulnerable frequencies", (3) building a compact power source/high-gain antenna subsystem and (4) execution of a full-scale field tests involving multiple vehicles made by various manufacturers. The developed concepts include 5-km perimeter denial to vehicles, where high-value targets are protected against an incoming hostile vehicle, and also concepts for bringing a vehicle to a halt on a multilane highway, urban and suburban areas. The search for "vulnerable frequencies" consists of a systematic study of MP responses in a wide range of frequencies, spanning 300-2000 MHz range where two different test regimes were utilized: CW and transient measurement using 46-cm Impulse Radiating Antenna (IRA). A prototype HPEMS is expected to be ready for full-scale field tests by December 2004.

UWB 6-6: UWB Antenna for Artillery Applications

H. Herlemann[1], **M. Koch**[1], **F. Sabath**[2]
[1]*University of Hannover, Hannover, Germany*; [2]*Armed Forces Scientific Institute for Protection Technologies, Munster, Germany*

Electronic components and subsystems (e.g. microprocessor boards) are essential parts of modern civilian and military systems. A setup or failure in these systems could cause a major accident. Due to the impact of electromagnetic fields on the functionality of electronic components, microwave applications are of large interest for the development of non lethal weapons. The capabilities of High Power Microwaves (HPM) and Ultra Wide Band (UWB) weapons are the reason for intensive research activities in the area of microwave sources, components and antennas. UWB-sources with an output voltage of several MV are published in open literature.

For military applications it is of interest to affect distant targets with HPM or UWB type fields. In contrast to the output voltage however, the maximum amplitude of the electrical field strength at the target is limited by the wave propagation and the dielectric strength of air. Due to these limitations the distance between the microwave weapon and the chosen target my not exceed a few km depending on the susceptibility of the target systems. Therefore the necessary range for several military applications can only be achieved by using carrier systems (e.g. artillery shells). Nowadays UWB-sources which can be integrated in artillery shells are available. In contrast to the source systems the integration of UWB-antennas is an unsolved problem.

The standard Impulse Radiating Antenna (IRA) is a reflector type antenna with the ability to radiate broad band pulses with a high directivity. A recently solved problem is the integration of an antenna with a diameter of approximately 2 m into an artillery shell with a diameter below 150 mm. A textile IRA integrated in a standard parachute was developed at WIS, Germany in 2000. The design and first measurements were presented in 2001. From these tests emerged three major questions demanding further research:

1) What is the best type of parachute for the application in question?

2) The construction of a feeding section capable of handling very high voltage.

3) The development of textile resistors which are needed to match the feedarms to the reflector.

These questions were subject of subsequent studies in 2002 and 2003. The existing parachute IRA was modified and tests were conducted. In addition a second IRA exhibiting different aerodynamic properties was developed and tested. In this contribution test results and the properties of different parachute designs will be discussed.

Figure 1: Test Setup for the Parachute IRA

Figure 2: Test Setup for the Parachute IRA

UWB 6-7: The Application of Wire-Loop Antennas in High-speed UWB Links

S. Krishnan[1], **L.-W. Li**[2], **M.-S. Leong**[2]
[1]*Institute for Infocomm Research, Singapore*; [2]*Department of Electrical and Computer Engineering, National University of Singapore*

In addition to the traditionally studied parameters such as radiation pattern and impedance bandwidth, the suitability of a UWB antenna has to be determined from the way in which it affects system parameters such as data rate, Bit-Error-Rate (BER) and range. This approach to determining the suitability of loop antennas for UWB applications is the focus of this paper. The ways in which the conventional circular loop can be modified to improve both the antenna performance as well as the system performance is discussed. The experimental and simulated results of modified loop structures and their radiation and impedance characteristics in comparison with conventional loop antennas is also presented.

A probe-fed half-loop antenna which had a length of half-a-wavelength at 1 GHz was selected for evaluation of its performance in the 3 to 10 GHz band. Both simulation and experimental results indicated that the antenna generally exhibited greater directivity at higher frequencies. This is not a disadvantage as, contrary to common assumptions, the UWB antenna does not necessarily have to be omni-directional. In fact, for point-to-point UWB links, directional antennas provide a better performance. The more important point of concern was that the bandwidth of the antenna was rather narrow, with points of resonance repeating at approximately 1 GHz intervals. Nevertheless, to conclusively verify the performance in UWB applications, it was deployed in an experimental point-to-point 500 Mbps high-speed wireless link (Fig.1). The average transmitted power density was less than –41.25 dBm/MHz as designated by FCC for indoor transmission. Despite the narrow impedance bandwidth of the antennas, they were still found to be sufficient for a BER of less that 10E-4 at a range of 1 meter. Encouraged by these results, ways of improving the performance of the antenna was investigated. Attention was particularly focused on improving the impedance bandwidth. It was found that commonly used techniques such as resistive loading of the antenna, while improving the impedance bandwidth, did not significantly improve the performance of the system. So other methods of improving the performance of the antenna such as using parasitic elements, multiple radiating elements and collocated elements were investigated. It was found that by using multiple collocated radiating loops, a -10 dB fractional bandwidth of greater than 50% could be achieved and also a corresponding improvement in the system performance could be observed. The system BER was now less than 10E-5 at a range of more than 2 meters. This showed that with suitable modifications, loop antennas could actually be a low-cost option for practical high-speed UWB systems.

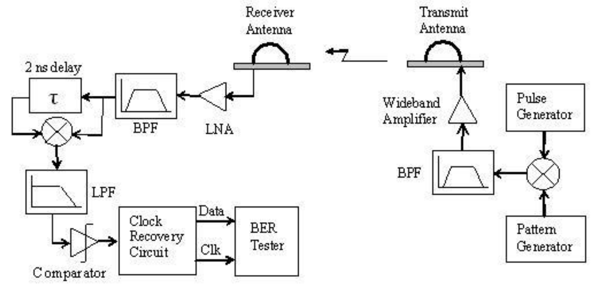

Figure 1: Schematic of setup for testing effect of antenna on system bit-error-rate

UWB 6-8: Coupled Transmission Lines as a Time-Domain Directional Coupler

C. E. Baum
Air Force Research Laboratory, DEHP; Directed Energy Directorate; Kirtland AFB; NM; USA

Directional couplers are a well-established microwave subject, various bibliographies and texts being available. Here our attention is limited to TEM transmission-line couplers for their potential time-domain application. This is further restricted to uniform two-conductor plus reference transmission lines of finite length because, as we shall see, the coupler samples the waveform of interest over a time window of twice the transit time in the coupler without distorting the waveform. This can be compared to another type of directional couplers which senses the time derivative of the waveform. These kinds of directional couplers have application to various measurement situations, including measuring the returning transient signal in a radar antenna which is also used for transmission of the radar pulse.

The reader may consult some relevant references for related previous results. Our general derivation covers these with some extensions. In particular the principal result is reinterpreted in time domain. Note that some authors refer to this type of device as a contra-directional coupler.

A traditional type of transmission-line directional coupler can also be made to operate for temporal waveforms. There is a time-window of width $2t_l$ (t_l = transit time through the coupler) during which the coupled waveform is the same as the incident waveform times a constant. This requires that, in the simplest operation, $2t_l$ be longer than the time duration of the pulse of interest. One can extend this to longer times by appropriate data processing, noting the more complete description of the coupler scattering-matrix elements.

Our general approach to the theory has revealed various cases of potential interest. The fully symmetric case (symmetry between wires 1 and 2 as well as source and load impedences) with identical resistive impedances (cable characteristic impedances) on all four ports gives rather simple final answers. There are, however, more general cases that still lead to zero transmission from port 1 to 4 (the directional-coupler criterion) as discussed in Section 4. These may deserve further consideration.

Noting that a transmission-line model is used for the coupler, there are some errors in modelling a real such device. In particular, at frequencies high enough that radian wavelengths are not large compared to the cross-section dimensions, a full wave analysis may be required. Near the ports the abrupt changes in the cross-section geometry may make evanescent modes significant there. (Details, details!)

UWB 7 - Time-Domain Techniques for the Transient Analysis of Complex Problems

UWB 7-1: Unified Framework for Numerical Methods to Solve the Maxwell Equations

H. de Raedt, **K. Michielsen**, **M. T. Figge**
Dept. of Applied Physics, University of Groningen

We present a comparitive study of numerical algorithms to solve the time-dependent Maxwell equations for systems with spatially varying permittivity and permeability. We show that the Lie-Trotter-Suzuki product-formula approach can be used to construct a family of unconditionally stable algorithms, the conventional Yee algorithm, and two new variants of the Yee algorithm that do not require the use of the staggered-in-time grid. We also consider a one-step algorithm, based on the Chebyshev polynomial expansion, and compare the computational efficiency of the one-step, the Yee-type, the alternating-direction-implicit, and the unconditionally stable algorithms. For applications where the long-time behavior is of main interest, we find that the one-step algorithm may be orders of magnitude more efficient than present multiple time-step, finite-difference time-domain algorithms.

UWB 7-2: A Hybrid Time-Domain Technique that Combines ADI-FDTD and MoMTD to Solve Complex Electromagnetic Problems

S. G. Garcia, **A. R. Bretones**, **R. G. Rubio**, **M. F. Pantoja**, **R. G. Martin**
University of Granada

This communication describes a hybrid technique directly operating in the time domain that combines the Alternating Implicit Finite Difference Time Domain (ADI-FDTD) [1-2] and the integral-equation-based Method of Moments in the Time Domain (MoMTD) [3] techniques to analyze complex electromagnetic problems involving thin-wire antennas radiating in the presence of inhomogeneous dielectric bodies whose shape can be arbitrary. The ADI-FDTD/MoMTD method combines the ability of the FDTD to deal with arbitrary material properties and that of the MoMTD to analyze arbitrarily oriented thin-wire structures [4]-[5]. Working in the time domain provides wideband information from a single execution of the marching-on-in-time procedure.

The ADI-FDTD formulation has been included so that the time step is only constrained by the maximum significant spectral component of the transient excitation and not by the Courant condition, with the consequent saving in computational resources when a fine mesh is needed to model part of the computational domain but a high temporal resolution is not needed. Moreover, the new hybrid method does not exhibit the late time instabilities observed in some cases in the hybrid explicit-FDTD/MoMTD method and therefore its use may be preferable even for problems where the computational burden is comparable for the two hybrid techniques.

The hybridization technique, which is based upon the use of Huygens' principle will be described and application examples showing its capabilities will be given. In particular the hybrid ADI-FDTD/MoMTD method has been applied to model a ground penetrating radar system consisting of a V thin-wire antenna located near an inhomogeneous media. The V antenna is optimized for pulse radiation using genetic algorithms (GA) [6] in order to reduce unwanted reflections at the ends of the antenna while retaining high fidelity and efficiency. As application example, the possibilities of the system to detect cracks in a marble block are investigated.

References

[1] Namiki, T., ”A new FDTD algorithm based on alternating-direction implicit method,” IEEE Trans on Microwaves Theory and Techniques, vol. 47, no. 10, pp 2003-2007, 1999

[2] Zheng, F., Chen, Z. and Zhang, J., “A finite-difference time-domain method without the Courant stability conditions”, IEEE Microwave Guided Wave Letters. vol. 9, no. 11, pp. 441-443. 1999

[3] A. Rubio Bretones, R. Gómez Martín and A. Salinas, ”DOTIG1, a time-domain numerical code for the study of the interaction of electromagnetic pulses with thin-wire structures”, COMPEL, vol.8, n.1, p. 39-61, 1989

[4] González García, S., Rubio Bretones, A., López, M.A.H. and Gómez Martín, R., “A new hybrid method combining the ADI-FDTD and the MoMTD techniques” Electromagnetics, vol. 23, no. 4, pp 103-118, 2003

[5] Gómez Martín, R., Rubio Bretones A., Monorchio A., Fernández Pantoja M. and González García S., ‘Time domain

hybrid methods' in Time Domain Techniques in Computational Electromagnetics, D. Poljak Ed, WIT Press, London, 2003.
[6] Fernández Pantoja, M., Monorchio, A., Rubio Bretones, A. and Gómez-Martín., R., "Direct GA-based optimization of resistively loaded wire antennas in the time domain" Electronic Letters, vol. 36, no. 24, pp. 1988-1990, 2000.
This work has been partially supported by projects TIC2001-3236-C02-01 and TIC2001- TIC-2001-2364-C03-03.

UWB 7-3: Unconditionally Stable ADI Finite-Difference Time-Domain Method for Bioelectromagnetic Problems

S. Schmidt, **G. Lazzi**
Dept. of Electrical and Computer Engineering, North Carolina State University, Raleigh, NC, USA

As more applications of wireless devices in the personal space are emerging, the interaction between electromagnetic energy and biological objects has become increasingly important to researchers and the public. Due to the fear and awareness that health damage may be caused by the use of wireless equipment, it is important to minimize the electromagnetic interaction between wireless designs and the human body. Repetitive prototyping and measurements for the minimization of the specific absorption rate (SAR) often are too expensive and time consuming; hence, efficient and fast numerical methods are a very attractive alternative. Electromagnetic problems involving inhomogeneous dispersive media are easily solved using the finite-difference time-domain (FDTD) method.
In a large number of bioelectromagnetic problems, the spatial discretization is dominated by very fine geometric details rather than the smallest wavelength of interest. When an explicit FDTD scheme is used, these fine details dictate a small time-step due to the Courant-Friedrichs-Lewy (CFL) stability bound, which in turn leads to a large number of computational steps. The alternating direction implicit (ADI) method has been suggested for the time-domain analysis of electromagnetic problems in order to eliminate the CFL stability bound inherent in the explicit FDTD method. The ADI method appears to be of particular interest for large bioelectromagnetic problems and problems in which the larger dispersion and phase error is tolerable. Further, in this class of bioelectromagnetic problems, it is often necessary to truncate the model and therefore extend a dielectric material into the absorbing boundary conditions (ABC). Using the D-H-formulation allows easy implementation of perfectly-matched-layer (PML) ABC with unsplit field components, independent of the materials modeled in the FDTD space.
An unconditionally stable FDTD method based on a D-H-formulation and the ADI marching scheme with a material-independent formulation of the PML ABC was previously proposed for the simulation of bioelectromagnetic problems and the computation of SAR. For spherical geometries, the method showed good agreement with experimental results and the explicit FDTD method. However, the ADI FDTD method, as previously proposed, does not converge as quickly as the explicit FDTD methods with resistive source implementation.
We developed a new resistive source condition for the unconditionally stable ADI method to achieve convergence rates that are similar to those of the explicit FDTD method. We present numerical results of the reflection errors of our PML ABC implementation. We also computed SAR in spherical geometries and models of the human head using the D?H ADI FDTD method with a resistive source condition. The results obtained using this method were compared to the explicit FDTD method as well as previously published experimental results.

UWB 7-4: Modeling Propagation of Time-domain Pulses in Cole-Cole Dielectrics

P. G. Petropoulos
New Jersey Institute of Technology, USA

The Cole-Cole dielectric model exhibits fractional time derivatives and is thus cumbersome to implement in standard time-domain CEM codes. I will present a procedure for computing an alternative exact representation of the time-domain Cole-Cole susceptibility function which is singular at time $t = 0$ and decays algebraically for large time. The method will be accompanied by an error bound. Also, I will derive short- and long-time asymptotic results for electromagnetic pulses propagating in Cole-Cole media. Comparisons with numerical experiments will be shown.

UWB 7-5: Accuracy and Application of a Stable FDTD-TDFEM Hybrid

T. Rylander, **A. Bondeson**, **Y. Liu**
Department of Electromagnetics, Chalmers University of Technology

In applications where different regions of space have different characteristics, hybrid numerical algorithms can be very advantageous. In [1-3], we have combined the FDTD, which is very efficient in free space, with a a more time-consuming TDFEM scheme, that can however accurately model fine and complex geometrical details. If the TDFEM is used only in thin regions near material boundaries, the hybrid method combines the advantages of the two basic schemes.
Other attempts to formulate such hybrids have encountered instabilities. Our hybrid achieves stability by using FEM-based methods for joining the two schemes. One basic observation is that the FDTD time-stepping (viewed as a scheme for the second order equation for E) can be derived from a FEM formualtion with edge elements for E and "lumping" of both the "epsilon" term and the curl-curl operator. Such lumping can be achieved by applying trapezoidal integration when computing the matrix elements in the FEM formulation. The hybrid grids consist of FDTD regions with cubes and FEM regions with unstructured tetrahedral grids, joined by a single layer of pyramids. The pyramids allow us to find an edge element representation of E, where the tangential components are everywhere continuous [4]. For the spatial operators, our hybrid method uses trapezoidal integration on the FDTD cubes and exact integration on the tetrahedrons. On the pyramids, a mixed scheme is used. This procedure makes all the operators symmetric. Hence all the eigenfrequencies of the corresponding frequency domain formulation for a closed PEC cavity are real. This is the basic reason why the hybrid is stable.
In a first version [1], the above procedure was applied only to the spatial operators, and the choice of implicit or explicit time-stepping was made on the basis of the edges (E-components). In a second, improved version [3], the degree of implicitness was associated with the elements (cubes explicit, tetrahedra and pyramids implicit). For this algorithm, it is possible to prove stability of the time-stepping by a von Neumann stability analysis. The result [3] is that the scheme is stable if (a) the implicitness parameter on the FEM grid is large enough and (b) the time-step does not exceed the CFL limit for the FDTD, $h/(c \cdot \sqrt{3})$. This is a very advantageous property of the hybrid for cases where the geometry contains details much smaller than a wavelength. These can then be resolved by FEM without reduction of the timestep. In [3], we used scattering on a PEC sphere as a test case, and studied the accuracy as a function of resolution both for the hybrid and for the FDTD with several different strategies on stair-casing. The results showed that, with equal resolution, the errors with the hybrid are 6 times smaller than the FDTD with the best choice of stair-casing. Since the convergence is quadratic with mesh size, this means that the hybrid achieves the same accuracy with a 2.5 times larger step-size. In 3D this gives a factor 15 reduction in memory and 40 of execution time. In practice, the extra memory and operation count for the FEM region reduce these gains slightly. Another gain of the hybrid is that it maintains quadratic convergence very accurately, which means that one can use extrapolation to improve on accuracy and efficiency. This is not possible for the FDTD where the convergence is too oscillatory.
In [2], the hybrid was applied to compute the RCS of the NASA almond very accurately. Also for the almond, the errors behaved as powers of the step size (although the power for horizontal

polarization was about 1.2, because of a singularity at the tip). Thus, extrapolation to zero grid size could be used and the RCS of the almond was computed with an error of at most 0.1 dBm^2, which is far better than previous calculations. Of the true application problems to which we have applied the hybrid, we mention a calculation of GHz fields radiated from a small patch antenna mounted on the rear-view mirror inside a car. Here, it is necessary to resolve the small details of the patch accurately (done with FEM), while the large interior of the car is modeled by the FDTD. The calculations used 8 million FDTD unknowns and 13000 FEM unknowns. About 8000 time steps were needed for the antenna diagram to converge, and this took about 8 hours on a 2 GHz processor. The calculations show that the car body acts as a resonator for the GHz fields and has a very strong influence on the antenna diagram.

[1] T. Rylander, A. Bondeson, "Stable FEM-FDTD method for Maxwell's equations", Computer Phys. Comm., vol 125, pp 75-82, 2000.
[2] T. Rylander, A. Bondeson, "Application of stable FEM-FDTD hybrid to scattering problems", IEEE Trans. Antennas Propagat. vol 50, no 2, pp 141-144, Febr.2002.
[3] T. Rylander, A. Bondeson, "Stability of explicit-implicit hybrid time-stepping schemes for Maxwell's equations", J. Comput. Phys. vol 179, no 2, pp 426-438, July 2002.
[4] J.L. Coulomb, F.X. Zgainski, Y. Marechal, "A pyramidal element to link hexahedral, prismatic and tetrahedral edge finite elements", IEEE Trans. Magn. vol 33, pp. 1362-1365, March 1997.

UWB 7-6: Efficient FDTD Parallel Processing on Modern PC CPUs

W. Simon, **A. Lauer**, **D. Manteuffel**, **A. Wien**, **I. Wolff**
IMST GmbH

This paper describes special algorithms for FDTD based field solvers, which increase the simulation speed. The new processor generations like Pentium III/Pentium IV and Athlon have extensions that allow multiple floating point operations within one processor cycle. These extensions can be used to speed up Finite Difference Time Domain simulations. To exploit these extensions efficiently it is necessary to create automatically a processor and structure dependent assembler code for each simulation. As soon as the structure pre-processing is finished the CPU of the current PC is detected and a special CPU dependant assembler code is created for the simulation. Even structure dependant code is created where is taken into account if e.g. lossy media or non lossy media is considered so that in all cases the easiest Maxwell equations can be solved. Fig. 1 shows an example assembler code using Pentium (TM) (IV) SIMD commands in the inner FDTD kernel. The simulation time can be reduced by more than a factor of four if these extensions are used. A side effect of using these extensions which can perform four floating point operations at one processor cycle is that the memory bandwidth of the PC becomes very important. Even the fastest memory configurations (DDR Ram / Rambus memory) are fast not enough not to cause the CPU to wait for data from the memory.

These algorithms have been applied to a simulation of a antipodal vivaldi antenna (Fig. 2). Here we investigated the simulation time for calculating the scattering parameters and the farfield pattern. The return loss of this UWB antenna is better than 10 dB for the frequency range from 3 GHz up to 20 GHz. Based on the frequency dependent farfield characteristics the spatio-temporal transfer function of the antenna is calculated. This allows the determination of all relevant quality measures of UWB antennas such as effective gain or ringing.

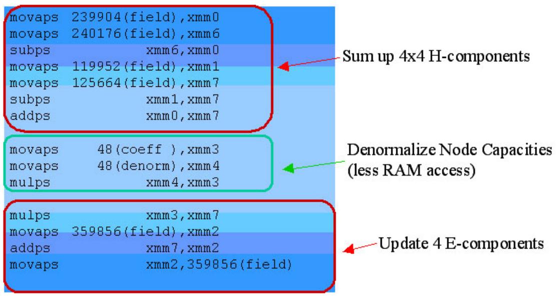

Figure 1: Example assembler code with Pentium (TM) (IV) SIMD commands using 4 float numbers/register

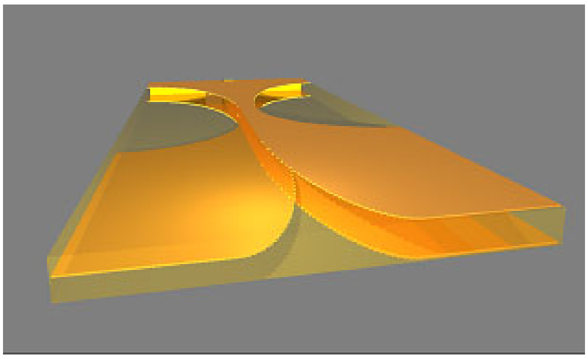

Figure 2: 3D view of antipodal vivaldi antenna (simulation model)

UWB 7-7: UWB Radio Link Modeling in Indoor Environment

B. Uguen, **F. T. Talom**
IETR (Institut d'Electronique et de Télécommunications de Rennes), France

UWB technology is an emerging field for radio-communications applications either for high or low data rate. Both IEEE.802.15.3 and IEEE.802.15.4 future standards are considering UWB technology as the appropriate physical layer. UWB systems are expected to provide in a near future high data rate and location awareness in difficult propagation channel, firstly for WPAN and probably next for WLAN applications. In that perspective, system designers need to have accurate channel modeling both statistical and deterministic. In order to help in designing high level and added value fonctionnalities of future systems, this paper presents the general problem of site-specific UWB channel prediction and present our recent work on the topic. There is a great complementarity between ray-tracing techniques and UWB. As the bandwith increases some ray paths becomes resolvable by the system and can conversely be discovered by a ray tracing tool. The proposed paper presents an enhanced ray-tracing techniques well suited to UWB channel characterization, and present signal processing procedure used to generate the received time domain response. An important part of the paper will focus on the inclusion of the antenna into the modeling. The antenna is included either from simulation software or measurements obtained over a wide band of frequency in a near-field chamber.
Following files illustrate elements which will be presented in the final paper.

Figure 1 is an example of a ray-tracing in a given indoor environment.
Figure 2 is the corresponding infinite bandwith impulse response.
Figure 3 illustrates CIR for a given transmitted UWB impulse for the same Tx-Rx configuration.
Figure 4 illustrates CIR for a narrower transmitted UWB impulse for the same Tx-Rx configuration.

By comparison of figure 3 and figure 4, it can be noticed that such an approach allows to compare the behaviour of a given channel versus a large set of parameters. This is expected to be useful for UWB location algorithm evaluation.

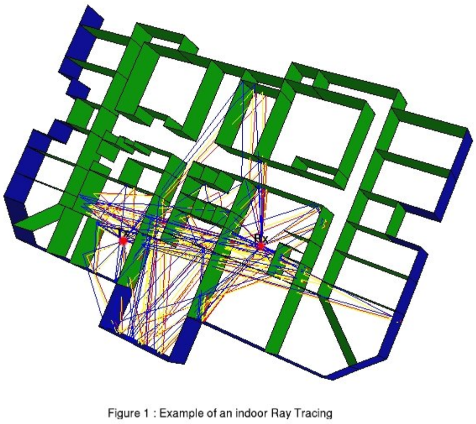

Figure 1: Example of an NLOS indoor ray-tracing.

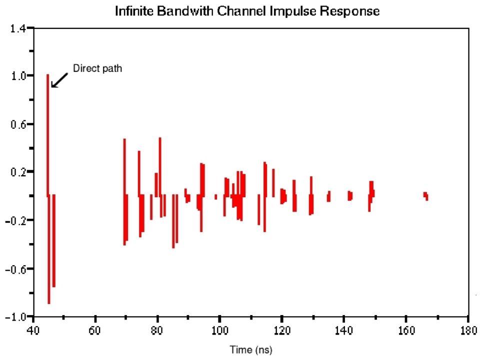

Figure 2: The corresponding infinite bandwith channel impulse response.

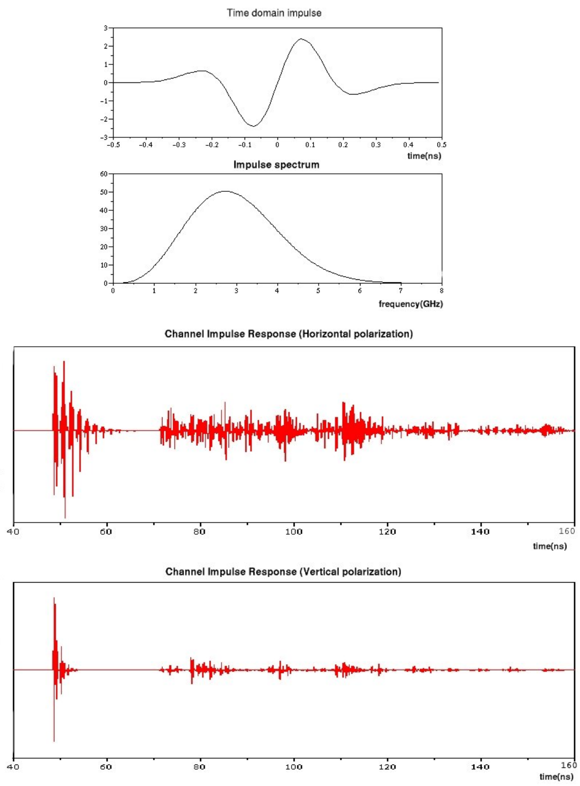

Figure 3: Example of an obtained CIR (case 1).

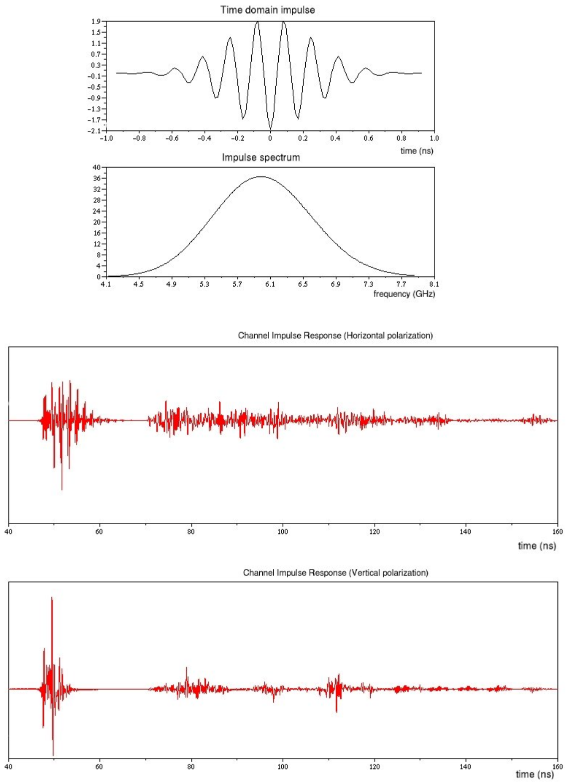

Figure 4: Example of an obtained CIR (case 2).

UWB 7-8: Phase-Space Beam Summation Formulations for Ultra Wideband Radiation

A. Shlivinski[1], **E. Heyman**[2], **A. Boag**[2]
[1]*Department of Electrical Engineering, University of Kassel, Germany*; [2]*School of Electrical Engineering, Department of Physical Electronics, University of Tel Aviv, Israel*

Beam summation representations are an important tool for tracking high-frequency wave-fields, since they provide a framework for ray-based, spectrally uniform, solutions in complex configurations. They are intimately related to phase space formulations since they express the field in terms of localized wave objects in a configuration-spectrum domain, that are tagged by the beams locations and directions. It is well known that such continuous phase space distributions are highly overcomplete, and hence may be a priori discretized. A well known example is provided by the Gabor series, that samples the field on a sparse phase-space lattice whose unit-cell area in the configuration-wavenumber phase-space is 2π. This describes the field in terms of a phase-space lattice of beams that emerge from a discrete set of points and a discrete set of direction such that the unit-cell area in the location-direction space is c/f, where c and f are the wavespeed and frequency. Consequently, Gabor-based beam formulations are inappropriate for UWB applications where it is desired to have the same beam lattice for all the frequencies in the excitation band.

Following previous publications, we present here an UWB beam-summation formulation for the radiation from extended UWB aperture source distributions that circumvent the difficulty noted above. The formulation is expressed in the frequency domain and utilizes Gaussian beams (GB) propagators organized on a frequency-independent lattice, such that their propagation trajectories need to be traced only once. The mathematical framework of this formulation is provided by the theory of overcomplete frame expansions, where we introduce a novel relation between the overcompleteness and the frequency, such the location-direction phase space is sampled on a frequency-independent lattice. It is further shown that using properly chosen iso-diffracting Gaussian beams (ID-GB) not only provides the snuggest frame expansion for all frequencies, and thereby stable and local expansion coefficients, but the evolution of the beam parameters along the propagation trajectories is non dispersive and needs to be calculated only once for all frequencies. The ”basic” concepts in the preceding paragraph can be applied to signals with arbitrary large bandwidth. Yet, for signals with bandwidth much greater than one octave, a greater numerical efficiency is achieved by dividing the signal spectrum into a hierarchy of one-octave sub-bands. With this division, the ”basic” algorithm above can be applied self-consistently within the sub-bands so that the beam-lattices at the lower sub-bands are decimated sub-sets of the lattice at the highest band. This leads to a greater numerical efficiency at the lower bands without having to trace new sets of beams there. The concepts above will be demonstrated in the calculation of uniform field solutions due to UWB focused sours distributions. In a companion paper we present an alternative formulation, where all the data processing tools and propagators are expressed directly in the time domain.

UWB 7-9: Pulsed Beam Summation Formulation for Short-Pulse Radiation Based on Windowed Radon Transform Frames

A. Shlivinski[1], **E. Heyman**[2]
[1]*Department of Electrical Engineering, University of Kassel, Germany*; [2]*School of Electrical Engineering, Department of Physical Electronics, University of Tel Aviv, Israel*

In a companion paper we presented a phase-space beam summation formulation for the radiation of ultra wideband (UWB) fields from extended aperture-source distributions. The formulation there has addressed the problem from a frequency domain (FD) point of view and is useful mainly if the data (fields or sources) or the system parameters are given/required as a function of the frequency. In this paper we present an alternative formulation where the data processing tools and the propagators are expressed directly in the time domain (TD). Here, the radiated field is expanded into a discrete lattice of shifted, tilted and delayed pulsed beams (PB). The PB excitation amplitudes are extracted from the space-time data via a windowed Radon transform (WRT). This processing tool can be regarded as a windowed version of the slant stack transform (SST) which is widely used to extract the time-dependent plane-wave spectra of source or field distributions. The TD formulation is based on a new class of frame sets, termed WRT frames, whose properties are discussed. It is further shown that using properly chosen isodiffracting PB (ID-PB) window functions provides:
(a) the snuggest WRT frame expansion, and thereby local and stable coefficients;
(b) simple window functions for processing the space-time data; and
(c) analytically tractable PB propagators.
The new WRT frames can, in fact, be applied in other disciplines and applications. We therefore start the presentation by discussing the mathematical properties of the WRT frames in a general R^3 domain, and then apply this new expansion/transformation to the present problem of time-dependent aperture-source radiating into a 3D space domain, where the data is identified by two space and one temporal coordinates. Special emphasis will be given to demonstrating the phase space localization and resolution properties of the WRT frames.

UWB 8 - UWB Antennas

UWB 8-1: Transmission and Reception by UWB Antennas in Time Domain

D. Ghosh, **T. K. Sarkar**
Syracuse University

The transmission and reception properties of several UWB antennas, including the biconical antenna and the TEM horn antenna, are presented. In the time-domain, the transmitting transient property for a UWB antenna is proportional to the derivative of the receiving transient property (Dr. Motohisa Kanda, Time-Domain Measurement in Electromagnetics, 1986). The radiated wave from a biconical transmitting antenna is exactly identical to the driving point voltage waveform. Following the general property of UWB antennas as stated before the current induced in a biconical receiving antenna is the integral of the input waveform. On the other hand, in the case of a receiving TEM horn antenna, the induced current is a replica of the incident field. If the TEM antenna is used for transmission then the radiated E-field is the first derivative of the input pulse.
All of these properties have been verified by simulating the antennas by using the WIPL-D software (B. M. Kolundzija, J. S. Ognjanovic, T. K. Sarkar, R. F. Harrington, WIPL Software for Electromagnetic Modeling of Composite Wire and Plate Structures, 1995) which can simulate the antenna response for a wide band of frequencies. The time-domain response is obtained by inverse Fourier transform of this data. The input is the derivative of a very short duration Gaussian pulse. It is seen that several reflections occur due to the finite length of the antennas. So during simulation these reflections can be reduced by rounding off of the edges by placing additional structures at the edges or by decreasing the discontinuities of the structures. It is seen that during transmission from a biconical antenna to a TEM horn antenna, the wave-shape of the input pulse is identical to the output pulse. So by this process we can obtain direct measurement of the input by observing the output. Further analysis using a dipole antenna has shown that in the wide band the dipole behaves in a manner similar to a biconical antenna when the duration of the transient input pulse is very small compared to the electrical length of the dipole. But in the case of a dipole it is hardly possible to avoid the reflections from the edges of the dipole.

UWB 8-2: Analysis of Transient Radiation from a Dielectric Wedge Antenna

A. Yarovoy
Int. Research Centre for Telecom and Radar, Delft University of Technology

The demand in new types of impulse radiating antennas grows rapidly with the development of new ultra wideband radars and communication systems. Together with a requirement of an ultra wide bandwidth such antennas should possess a linear phase characteristic and a constant polarization. One of the best-known antennas for radiation of short pulses is the TEM-horn. However strong and long lasting coupling between two such antennas within a transmit/receive system makes it is difficult to use the TEM-horn in a short-range radar (because the coupling masks the reflection from a target). Besides the basic TEM horn antenna has large physical dimensions. To overcome these disadvantages a Dielectric Wedge Antenna has been developed.
The Dielectric Wedge Antenna is based on a TEM horn filled with a dielectric material. The electromagnetic field in this structure is concentrated mainly in the dielectric wedge between metal flairs. Such design may reduce the coupling between Tx and Rx antennas and reduce the antenna's physical dimensions. Besides with such design it is easier to reduce the reflection from the antenna aperture, which is responsible for the antenna ringing. Several antenna prototypes have been developed to work with a 0.8ns monocycle generator. Different dielectric materials with relative permittivity from 4 to 6 have been used in the prototypes.
Antenna analysis has been done theoretically by means of the FDTD method and experimentally by means of time-domain measurements. Numerical simulations have been used to determine the optimal geometry and size of the dielectric wedge. It was found that the electromagnetic wave, which propagates within the wedge, is not a TEM wave. Also it was found that the dielectric wedge itself supports surface waves, which contribute to the radiated field. The amplitude distributions and the waveforms of these waves have been investigated.
Theoretical results have been verified by the experiment. The antenna prototypes have been fed by a 0.8ns monocycle generator. The antenna reflection, the radiated waveform in the near-field and the far-field have been measured in time domain. Good agreement has been observed between theoretical and experi-

mental results.
Based on the antenna analysis a modification of the antenna has been suggested. The antenna has been covered by dielectric slabs in order to reduce the antenna pre-pulse and the surface wave radiation. The suggested modification has been verified experimentally. It has been found that as the result of the modification the antenna gain has been increased by 2dB and the antenna footprint size has been decreased.

UWB 8-3: A Lens TEM Horn with an Artificial Dielectric

W. S. Bigelow[1], **E. G. Farr**[1], **L. H. Bowen**[1], **D. E. Ellibee**[1], **D. I. Lawry**[2]
[1]*Farr Research, Inc., Albuquerque, New Mexico, USA*; [2]*Air Force Research Laboratory, Directed Energy Directorate, Kirtland AFB, New Mexico, USA*

Ultra-wideband radar systems could contribute significantly to the detection and identification of unknown objects in environments where conventional radars fail, such as looking through foliage or soil. However, UWB radars lack an antenna with low sidelobes, which can also radiate a clean impulse. Currently available UWB antennas, such as the reflector impulse radiating antenna (IRA), suffer from sidelobes that are difficult to treat.
Using both theory and data, we advance the argument that a lens TEM horn with collimated output should have lower sidelobes than a reflector IRA. To demonstrate this, we built a prototype UWB lens TEM horn and measured its antenna pattern to characterize its sidelobes. The planar-spherical lens design employed the assumptions of paraxial geometric optics. To reduce the weight penalty imposed by a conventional dielectric lens, we machined the collimating lens from a commercially available artificial dielectric material. Measurements of the prototype lens TEM horn demonstrated that it is capable of radiating a clean impulse with sidelobes smaller than those of a highly optimized reflector IRA. Moreover, the gain of the 30-cm aperture lens horn was found to be comparable to that of the larger 46-cm IRA. Design enhancements will reduce the return loss and transform the prototype lens TEM horn into a rugged device suitable for field use.

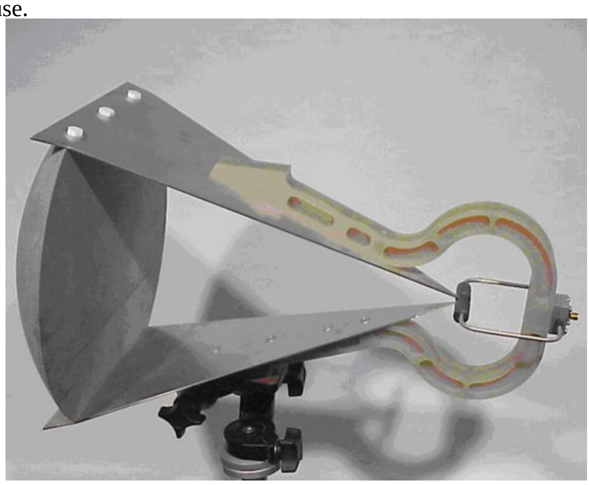

Figure 1: Prototype UWB lens TEM horn.

UWB 8-4: Partial Dielectric Loaded TEM Horn Design for Ultra Wide Band Ground Penetrating Impulse Radar Systems

A. S. Turk, **D. S. A. Sahinkaya**
The Scientific and Technical Research Council of Turkey (TUBITAK)

The Ground Penetrating Radar (GPR) techniques are increasingly being used for detection and identification of buried artifacts and structures within the upper regions of the earth's surface. The choice of the central frequency and the bandwidth of the GPR pulse are the key factors for the detection performance of the subsurface features. The higher frequencies are needed for better range resolution and detailed echo to determine small size objects, nevertheless the lower frequencies are preferred to detect something buried too deep because of the dramatically increased attenuation of the soil with increasing frequency. Thus, the GPR system that transmits Ultra Wide Band (UWB) impulse signal is used in order to benefit from both low and high frequencies. The impulse waveform is generally Gaussian shaped in time and its frequency band may vary from 100 MHz to 5 GHz (up to 8 GHz for stepped-frequency GPR) depending on the application. Here, the main problem is to design UWB T/R antennas to radiate GPR impulse signal uniformly shaped into the ground and receive pulses scattered from subsurface objects with high efficiency. The antennas must have flat and high directivity gain, narrow beam, low side lobe and input reflection levels over the operational frequency band to reach the largest dynamic range, best focused illumination area, lowest T/R antenna coupling, reduced ringing and uniformly shaped impulse radiation, respectively [D. J. Daniels, Surface Penetrating Radar, 1996].
Although some planar antennas such as dipole, bow-tie and spiral are mostly designed especially for hand-held compact GPR systems, TEM horn is one of the appropriate antenna type because of its relatively broadband radiation characteristics.
In this paper, UWB TEM horn antennas are investigated for ground penetrating impulse radar systems. The Partial Dielectric-loaded TEM horn (PDTEM) structure is described that maintains ultra-wide band antenna characteristics over a bandwidth ratio greater than 25:1 to improve the impulse radiation characteristics for GPR systems. The Partially Loaded Transmission Line antenna Method (PLTLM) is introduced to analyze narrow plate-angle PDTEM horns, efficiently. It is shown that high gain and low input reflection levels over the operational band are attainable for TEM horns with proper dielectric, absorber and resistive loadings. The performances of planar antennas and TEM horns are compared with calculated and measured data. Moreover, some adaptive antenna designs for the multi-sensor operations of GPR with EMI detector are presented.

UWB 8-5: A Dual-Polarity Impulse Radiating Antenna

L. H. Bowen[1], **E. G. Farr**[1], **D. I. Lawry**[2]
[1]*Farr Research, Inc., 614 Paseo Del Mar NE, Albuquerque, NM, 87123*; [2]*Air Force Research Laboratory / Directed Energy Directorate, 3550 Aberdeen Ave. SE, Kirtland AFB, NM 87117-5776*

Dual polarity Impulse Radiating Antennas may be useful in a variety of applications, such as UWB radar, target identification, and surveillance. Adding a second polarization to a single antenna essentially provides twice the information with the same aperture area. Until now, no design has been built and tested, so we report here the results of the first dual-polarity IRA.
Until now, we have not tried to construct an IRA with dual polarity, due to the difficulty of maintaining a good impedance match throughout the antenna. However, we recently built a poorly matched IRA with a single unbalanced 50-Ohm feed, with surprisingly good results. These results inspired us to try a dual-polarity IRA, in hopes that any mismatch at the feed point might be tolerable for those applications where reflections within the system are not of great importance.
The dual-polarity IRA described here, designated IRA-1D, is very similar to the IRA-1 developed by Farr Research, Inc. For the IRA-1D we used the same feed arm configuration as used on the IRA-1, which had four feed arms spaced uniformly around the aperture, with the electrical center of the feed arms intersecting the edge of the reflector. The only difference in the IRA-1D is that each pair of opposite feed arms is connected to a separate 50-to-200-Ohm balun. This produces a mismatch from 200 to 400 Ohms at the focus of the reflector on each channel. In spite of this 2:1 impedance mismatch, the antenna characteristics of the IRA-1D are quite good up to at least 10 GHz. We provide here the antenna characteristics for both polarizations of

the IRA-1D, and we compare these results to those of the standard IRA-1. We also compare the IRA-1D to other versions of the 18-inch IRA.
The dual-polarity design of the IRA-1D is currently being integrated into the design of an Ultra-Compact IRA (UCIRA) for UWB surveillance applications from space. The UCIRA is a 1.22 m (48 inch) diameter antenna that can be deployed from a very compact package.

UWB 8-6: Effect of Reflector Defocus on the Radiation Patterns of Impulse Radiating Antennas

J. S. Tyo[1], **E. G. Farr**[2], **D. I. Lawry**[3]
[1]*ECE Department, University of New Mexico, USA*; [2]*Farr Research, Inc., Albuquerque, NM, USA*; [3]*Air Force Research Lab, Directed Energy Directorate, USA*

The reflector on an impulse radiating antennas (IRAs) is normally designed to be paraboloidal in shape, and are oriented so that the electrical feed point of the TEM feed line coincides with the focal point of the paraboloid. In many practical cases, the feed point and focal points are not exactly aligned, producing some defocus of the reflector. There are two types of defocus that can be analyzed exactly in the geometric optics approximation: converting the paraboloid into either a hyperboloid or a prolate spheroidal (elliptical cross-section) reflector. The paraboloidal reflector converts the spherical wave emanating from the feed point into a plane wave (i.e. a spherical wave focused at infinity. The hyperboloid converts the expanding spherical wave into a second expanding wave which appears to emanate from the second focal point of the hyperboloid (which is behind the reflector); the prolate spheroid converts the expanding spherical wave into a second spherical wave that converges on the second focal point of the spheroid (which is in front of the reflector). The two cases are roughly equivalent to moving the electrical feed closer to the reflector (hyperboloid) or further from the reflector (prolate spheroid). Previously, we derived the E- and H-plane responses from an in-focus IRA, and demonstrated that these responses are symmetric with respect to the center of the response (J. S. Tyo, et al., Sensor and Simluations Notes #472, C. E. Baum, Ed., Air Force Research Lab, Kirtland AFB, NM, 87117, 2002). However, when compared with expermental data, the theory of focused IRAs could not predict the exact nature of the transient radiation patterns. Specifically, the theory predicted that the transient radiated signal should be symmetric with respect to the temporal center of the response. In this paper, we examine the effect of hyperboloidal defocus and we find that allowing defocus causes the transient responses to be asymmetric. Results are computed in both the E-plane and H-plane with excellent agreement with measured data. We extrapolate these results to the frequency domain as well and demonstrate the effect on gain when the IRA is to be used as a broadband frequency domain radiator. We find that the effect of defocus is to broaden the radiation pattern to an angle that can be determined from the geometry of the hyperbola. The theory presented in this paper can be used to experimentally determine the amount of defocus in an IRA after it has been assembled.

UWB 8-7: Characterization of the Radiation Pattern of Reflector IRAs by Time Domain Measurement Techniques

S. Schulze, **H. G. Krauthäuser**, **J. Nitsch**
Otto-von-Guericke-University Magdeburg, IGET, Germany

The radiated electromagnetic field of reflector impulse-radiating antennas has been sufficiently described by equations which can be solved for the field analytically and numerically for the principal beam direction. But it is few known about the amount of radiation in other directions. Many measurements have to be performed to tackle this problem and to get an acceptable resolution. One component of the radiated electric field strength of a 36”-antenna was measured in the university’s semi-anechoic chamber at a distance of 12m with 1 degree steps in the horizontal plane. Additionally a vertical scan was taken at each angular step. From the analysis of the measured signal some characteristic features of the pulse have been extracted and presented in appropriate figures. Those features concern, e.g., the pulse width, the maximum field strength, and the rise time or the energy content of the signal. Some interesting effects have been recognized. Another objective was to find out whether these effects could be derived from the well known antenna theory.

UWB 8-8: Directivity of Parachute Antennas for Microwave Weapons

U. Schenk
WIS Munster

Microprocessors and other electronic components are essential parts of modern technical military equipment and weapon systems. An upset or malfunction in one of these components can cause severe damage to expensive equipment. On the other hand modern electronic digital systems use lower logic level. For this reasons it is very easy to disrupt those systems with electromagnetic (EM) weapons including microwave weapons that use frequencies in the GHz region.
Microwave technology is of great interest because it can be used to develop EM weapons which simply disable enemy attack without causing any human death. One of the key components of a microwave weapon is the antenna. In order to have as much electric field strength near the target as possible different types of microwave weapons are possible; direct weapons, that emit the electromagnetic radiation through the atmosphere and indirect weapons where the EM source is shot towards a target and radiation is emitted in the near vicinity of the target. The latter system offers the advantage that the electromagnetic radiation is not absorbed in the atmosphere so radiation levels can be maximized near the target.
One interesting system under development is a parachute made of conductive material that acts as a reflector type antenna in combination with an EM source for emitting short pulses. These parachutes system could be dropped over a target area and affect all systems within their ranges.
The effective need of parachute antennas is being investigated and compared to systems using other antennas such as dipole antennas or horn antennas. I will show that with the use of a reflector type antenna field strength and hence the effectiveness of the EM weapon can be significantly increased. Antenna diagrams and the striking distance for all three systems (parachute, dipole, horn) will be compared.

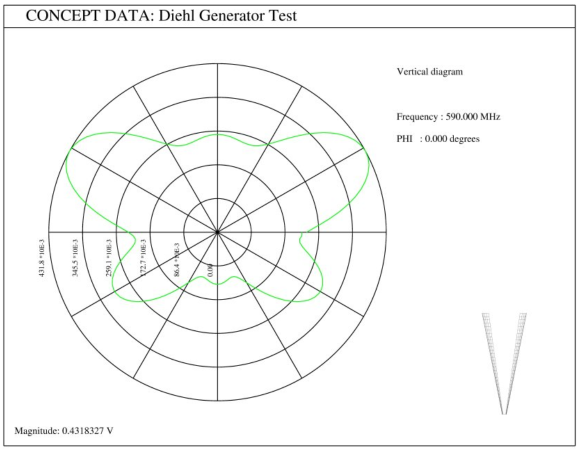

Figure 1: Radiation pattern

UWB 8-9: Resistively Loaded Discones for UWB Communications

L. H. Bowen, **E. G. Farr**
Farr Research, Inc.

Ultra-Wideband (UWB) antennas are a critical component of UWB communications systems, such as the Joint Tactical Radio System (JTRS). For this system, the antenna must cover a

bandwidth of 20 MHz to 4 GHz, be omnidirectional, be convenient to transport, and be able to handle 200 Watts of power. A leading candidate for such a system is a discone, due to its very wide bandwidth.
We describe here a series of modifications to a commercially available discone antenna which greatly improved the low frequency response of the antenna. The antenna selected was a Diamond D-130J as shown in Figure 1. The D-130J is about 1.71 m (67.2 inches) high, including the vertical element, and is rated at 200 Watts. The bandwidth given in the Diamond catalog for this antenna is 25 to 1300 MHz receive, 80 to 1300 MHz transmit. The vertical element with the loading coil can be removed if 25-50 MHz reception is not required.
The low frequency response of the antenna was greatly improved by resistive loading of the antenna elements based on work by T. T. Wu and R. W. P. King (The Cylindrical Antenna with Nonreflecting Resistive Loading, IEEE Trans. Antennas and Propagation, May 1965, pp. 369-373). From this work we derived Equation 1 (Fig. 2) which gives the resistor values for loading the antenna elements. The equation has a singularity for the Nth resistor so for this last resistor we rather arbitrarily used twice the value of the previous resistor.
The D-130J has eight elements at 28.5° from the vertical which gives N_r = 8 and θ_0 = 28.5°. Z_0 is 377 Ohms. We divided each element into 6 segments which gives N = 6. A resistor with a standard value closest to the calculated value was centered in each segment.
In addition to the resistive loading, we also modified the ground plane. In all, we made measurements on five versions of the D-130J discone antenna as follows:

(a) Commercial Off-The-Shelf (COTS) discone.
(b) Same as (a) but with resistive loading in the conical section.
(c) Same as (a) but with the ground plane enlarged to match the diameter at the base of the antenna.
(d) Same as (c) but with tapered resistors in the conical section (loaded like (b)).
(e) Same as (c) but with resistors in both the conical section and the ground plane.

We studied each of the above configurations both with and without the vertical element attached. By progressing through these five modifications step by step we are able to see the effect of each modification and evaluate its effect on the performance of the discone antenna. The experimental data as well as the numerical analysis performed using NEC-Win Plus, a Method-of-Moments (MoM) wire antenna analysis code, showed a definite improvement with each modification. The overall effect of the modifications was a dramatic improvement in the VSWR of the antenna at low frequencies as shown in Figure 3 where we show the VSWRs of the original antenna, case (a), and the final version, case (e). We are confident that additional improvements are possible and that we can improve the response at the high end by refining the feed connection and using a solid cone and ground plane near the feed point.

$$R_i \;=\; N_r \frac{Z_0}{\pi} \ln\left(\cot\left(\theta_0/2\right)\right) \ln\left(\frac{N-i+1}{N-i}\right)$$

Equation 1.

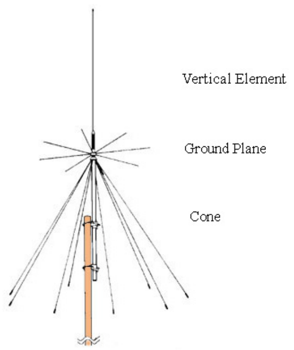

Figure 1: The Diamond D-130J discone antenna

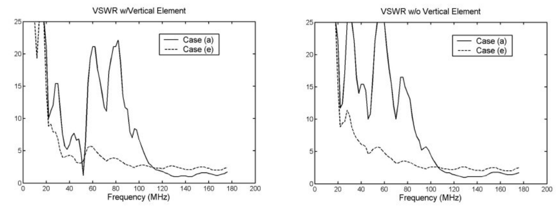

Figure 2: Comparison of case (a) and case (e).

UWB 8-10: Small and Broadband Planar Antennas for UWB Radio Applications

Z. N. Chen
Department of Radio Systems, Institute for Infocomm Research, Singapore

The available ultra-wideband spectrum has lead to much effort to develop low-cost systems for a variety of emerging radio and radar applications. For example, the frequency range covering 3.1-10.6 GHz can be used for short-range, high-data-rate wireless communications. For possible applications, the requirements for antennas are very critical due to small size and extremely broad bandwidths as well as low cost. In design considerations for antennas, should not only impedance or gain but also phase or group delay bandwidths be considered (Chen Z. N. et al., Considerations for source pulses and antennas in UWB radio systems, IEEE Trans. Antenna Propagation, 2004). Therefore, the planar antennas (dipoles or monopoles) become the attractive candidates for UWB radio, especially portable UWB impulse radio devices.
In this Summary, we first examine the characteristics of existing planar antennas based on the special considerations for UWB impulse radio systems, and then present roll antennas for the enhancement of the performance of conventional planar antennas. A conventional planar monopole usually consists of a perfectly electrically conducting sheet. The radiating sheet can be shaped for good impedance matching across a broad bandwidth. Usually, it may meet the requirements for the impedance and gain bandwidths over the frequency range of interest. However, they also suffer two shortcomings. One is that its radiation will not be azimuthally omni-directional due to its asymmetrical structure if the omni-directional radiation is required by systems. Another is that large lateral size may result in the distortion in waveforms of radiated impulses. So, we propose roll structures to mitigate these drawbacks (Chen Z. N. et al., Optimization and comparison of broadband monopoles, IEE Proceedings: Microw. Antennas and Propagat., 2003). The simulation and experiments have demonstrated that the roll structures feature the broadband characteristics as a planar antenna and omni-directional radiation performance as a thick cylindrical monopole.
Furthermore, the characteristics of planar antennas etched on a finite-size PCB are examined numerically and experimentally. This will be conducive to the antenna design in the context of portable devices.

UWB 8-11: Antipodal Vivaldi Antenna for UWB Applications

X. Qing, **Z. N. Chen**
Institute for Infocomm Research, Singapore

Introduction
In general the electrical properties of antenna are characterized by input impedance, efficiency, gain, radiation patterns and polarization. This is suitable for the antennas that are used for multiple narrowband services or channels. However, these classical antenna parameters are not sufficient for the characterization of the transient radiation behavior [E. G. Farr, C. E. Baum, Extending the definitions of antenna gain and radiation pattern into the time domain, 'Sensor and simulation note #350', 1992]. Instead, the transfer function of the antenna is of more importance. It is well known that the response of a linear system to any excitation can be completely determined when either the "transfer func-

tion" (in frequency domain) or the "impulse response" (in time domain) of the system is known. For a system comprising linear subsystems connected in cascade, the overall system response can be expressed in terms of the transfer functions of the individual cascaded subsystems. For an UWB antenna, the transmitting transfer function is not the same as receiving one. According to Rayleigh-Carson reciprocity theorem [R. W. P. King, The Theory of Linear Antenna, 1956], the transmitting transfer function is the time derivative of the receiving transfer function. In other words, the ratio of the transmitting transfer function of an antenna to the receiving transfer function of the same antenna is proportional to frequency. If two antennas are separated by a distance R as shown in Fig. 1, for an UWB excitation, the system output $V_{out}(\omega)$, will be the product of the transfer functions and $V_{in}(\omega)$.

Antipodal Vivaldi antenna

The Vivaldi antenna is an aperiodic, continuously scaled, gradually curved, slow leaky end-fire traveling wave antenna [P. J. Gibson, The Vivaldi aerial, Proc. 9th EuMC, 1979]; theoretically, it has unlimited operating frequency range. Vivaldi antenna has been used in arrays for radar and communications for years. Its broadband characteristics offer great promise for UWB radar and communications applications. An antipodal Vivaldi antenna was designed for UWB applications as shown in Fig. 2. The antenna is composed of a microstrip feed line, a tapered transition from the microstrip line to parallel strip line, and a tapered slot line. Two quarter-ellipses with different major and minor axes are used to form the plate; two semi-circles are added to the end to eliminate diffraction. Two metallic plates on either side of the PCB form the tapered slot.

Results

The proposed antenna was designed and fabricated on a 32mils RO4003 substrate. The measured gain and return loss are shown in Fig. 3. The frequency range for –10dB return loss is from 2.3GHz to 28.1GHz. The gain is relative flat over 3GHz to 22GHz ranging from 4.0dBi to 9.6dBi. The transfer functions of the proposed antenna were also measured based on S-parameters, the impulse response can be obtained by using inverse Fourier transform. For a defined input signal $V(t)$ or $V(\omega)$, the radiation field is the product of transmitting transfer function and $V(\omega)$, or the convolution of transmitting impulse response and $V(t)$. The output response of the antenna is the product of receiving transfer function and $V(\omega)$, or the convolution of receiving impulse response and $V(t)$. Fig. 4a shows the waveform of the radiation field with a Gaussian monocycle input, which is the second-order derivative of Gaussian monocycle. The input signal was double differentiated when the proposed antenna was used for transmitting. Fig. 4b shows the output response when the proposed antenna receives a Gaussian monocycle; the response is a Gaussian doublet. When the signal goes through the receiving antenna to the receiver, it will be differentiated.

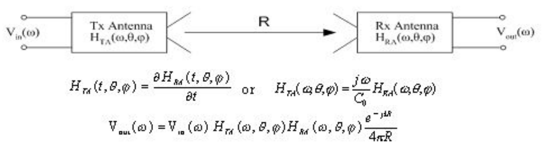

Figure 1: A block diagram of system transfer function

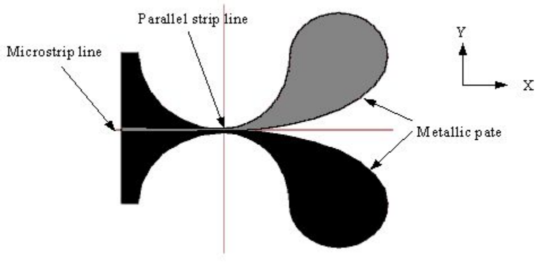

Figure 2: Configuration of the antipodal Vivaldi antenna

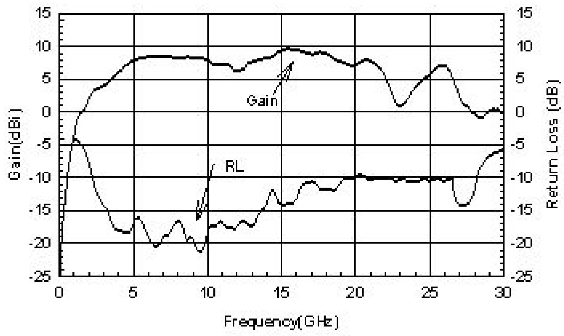

Figure 3: Measured gain and return loss

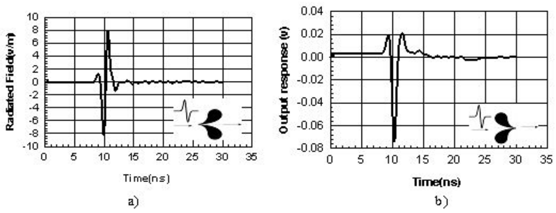

Figure 4: a) Radiated field with Gaussian monocycle input, b) Output signal with Gaussian monocycle received

UWB 8-12: Extending the Bandwidth of Printed Monopole Antennas

T. Dissanayake, **K. Esselle**
Macquarie University, Sydney, Australia

A printed monopole antenna consists of a radiating element printed on a microwave substrate, usually fed by a microstrip or co-planar waveguide feedline. The ground plane of the structure is limited to the feedline section, and it is truncated where the feedline meets the radiating element. The lack of a ground plane under the radiating element allows the antenna to radiate freely in many directions - a useful feature in some applications. Other advantages of these antennas are the simplicity, small size, ease of fabrication and ease of integration with printed circuits. Recent research on printed monopole antennas resulted in successful configurations of multi-band printed monopole antennas for wireless communication applications (e.g. Kin-Lu Wong, Printed Double-T Monopole Antenna for 2.4/5.2GHz Dual-Band WLAN operations, IEEE trans on Ant. And Prop., Vol.59. No.9. Sept 2003). In this paper we explore the potential of printed monopole antennas as a broadband antenna with at least an octave bandwidth.

We considered several configurations of printed monopole antennas for broadband applications. The theoretical analysis and design was done with Ansoft HFSS commercial software package. We have also fabricated a few antenna prototypes on low-cost FR4 substrates (dielectric constant = 4.4) and tested their input return loss and radiation patterns. The preliminary results of our research are very promising. They clearly indicate the potential of this type of antennas in broadband applications. One of our prototype antennas has shown a measured 10dB return-loss bandwidth from 4.2 GHz to 9.8 GHz. The radiating element of this antenna is relatively small, only about 10 mm long and 14mm wide. Another interesting feature of this antenna is that its radiation pattern does not change much throughout the operating frequency range. Our theoretical results further suggest that, by appropriately choosing the design parameters of the antenna, it is possible to make the antenna to operate over one continuos frequency band or two separated bands (dual-band).

UWB 8-13: A Coplanar Strip Antenna with Improved Matching

A. Y. Butrym[1], **S. Pivnenko**[2]
[1]*Radiophysics Department, Kharkov National University, 4, Svobody sq., 61077 Kharkov, Ukraine*; [2]*Oersted-DTU, Technical University of Denmark, Oersteds Plads, bldg. 348, DK-2800, Kgs. Lyngby, Denmark*

Since its introduction in 1979 by Gibson, tapered slot antennas (TSAs) on dielectric substrate attract attention due to their potentially wideband properties, low cost, low weight, and other advantages. A lot of work has been done on optimisation of these antennas for different applications, especially for wideband phased arrays (e.g. J. Shin, D.H. Schaubert,"Parameter study of stripline-fed Vivaldi notch antenna arrays", IEEE Trans. Ant. Prop. May 1999). There were reported also results of short pulse radiation and time-domain application of such antennas (C.R. Lutz, A.P. DeFonzo,"Far-field characteristics of optically pulsed millimeter wave antennas", Appl. Phys. Lett. May 1989). Main disadvantages of the "classical" TSAs are the high level of the side lobes and high cross-polarization.

In this paper, a new design of the TSA is presented, which is based on a V-shaped linearly tapered slot antenna described in (R.N. Simons, et.al. "Integrated uniplanar transition for linearly tapered slot antenna" IEEE Trans. Ant. Prop. Sep. 1995). In contrast to the slot-line made in infinite metal film, the coplanar strip-line (CPS) provides additional flexibility because its characteristic impedance depends on both the slot width and the strip width. In the proposed antenna design, the slot width was chosen to vary according to the exponential law, while the strip width was calculated according to the requirement that the impedance should vary exponentially along the antenna. The characteristic impedance of the tapered line in the region close to the feed point, where the tapering is small, was calculated using formulas for the CPS. The region close to the aperture, where the tapering becomes essential, was approximated by a flat biconical line. The main efforts of the study were put into widening the matched bandwidth of the antenna while keeping the overall dimensions unchanged.

Special attention was paid to reducing reflection from the ends of the antenna arms and thus providing low level and smooth behaviour of the reflection coefficient versus frequency. The last feature is essential when the antenna is used for radiation/reception of short pulse signals since it provides a "clean" single radiated pulse without late-time subsequent pulses. The undesirable reflection from the ends of the antenna arms is suppressed by loading these with resistive films of special form.

Wide use of the TSAs is also hampered by difficulties of their efficient wideband excitation. Numerous microstrip-to-slotline and other baluns are typically based on resonant open/short-circuited stubs and thus provide limited bandwidth. There are, however, few baluns with direct transition from coplanar waveguide (CPW) to CPS, which are inherently wideband (S. Kim, et.al. "Ultra-wideband CPW to CPS transition", Electron. Lett. June 2002). The balun mentioned above was scaled up to work at the frequencies from 0 to 10 GHz that allowed to use a standard SMA connector. The resulted balun was optimised to ensure low insertion loss and linear phase characteristics in the whole frequency range of interest.

Several prototypes of the antennas with different layout of the antenna arms were manufactured. The measured return loss and the radiation patterns have good agreement with those simulated with HFSS software. The measured return loss of the antenna with approximate size 200mm x 300mm does not exceed –10dB in the range from 0.3-10GHz.

UWB 8-14: A Portable Automated Time-Domain Antenna Range - The PATAR(TM) System: Functions and Operation

W. S. Bigelow[1], **L. H. Bowen**[1], **E. G. Farr**[1], **L. M. Atchley**[1], **T. C. Tran**[2]
[1]*Farr Research, Inc., Albuquerque, New Mexico, USA*; [2]*Air Force Research Laboratory, Directed Energy Directorate, Kirtland AFB, New Mexico, USA*

Time-domain antenna ranges offer several advantages over their frequency-domain counterparts. A single time-domain measurement provides over two decades of frequency bandwidth, reducing the time required to characterize an antenna. Also, the data acquisition equipment (a fast pulser and sampling oscilloscope) is less expensive and far less sensitive to temperature variations than a vector network analyzer (VNA). Finally, the PATAR(TM) system is simple to set up for temporary field use, eliminating the need for a dedicated facility.

PATAR(TM) system hardware includes a pulse generator, calibrated TEM horn transmitting antenna/support, digital sampling oscilloscope, and a high-precision two-axis positioner/mast assembly for support of the antenna under test (AUT). A laptop computer communicates with the oscilloscope over an Ethernet LAN connection and with the positioner over a RS232 cable.

PATAR(TM) system software provides for a choice of oscilloscopes and alternate positioners. In support of antenna characterization, the software provides for acquisition and analysis of pulser, TDR, and transmitter calibration waveforms. These are required in processing raw AUT impulse response and TDR data to obtain return loss and gain as functions of frequency. A "wizard" is available to set up a sequence of the necessary acquisition and processing operations.

The PATAR(TM) system provides computer controlled fully automated scanning of antenna orientations in azimuth and elevation. At each orientation, the software commands the oscilloscope to acquire a waveform and to return the resulting data for display, storage, and processing. Processing of acquired data to determine and display antenna gain occurs in near real time, as the orientation scan continues. Post-scan processing of the data generates displays of gain as a function of orientation and frequency.

In addition to impulse radiating antennas, the PATAR(TM) system has been used to measure a variety of standard antenna types, including the double-ridged waveguide horn, log-periodic, Yagi, and folded dipole. These measurements are discussed in a companion presentation.

UWB 8-15: Practical Implementation of PxM Antennas for High-Power Applications

J. S. McLean, **R. Sutton**
TDK Corporation

PxM antennas, antennas derived from a combination of electric and magnetic dipoles, have received attention because they possess several desirable characteristics including, but not limited to, a useful radiation pattern and broad impedance bandwidth for a given electrical size ("Some Characteristics of Electric and Magnetic Dipole Antennas for Radiating Transient Pulses", C. E. Baum, AWFL Sensor and Simulation Notes, Note 125, Jan. 1971; "The PxM Antenna and Applications to Radiated Field Testing of Electrical Systems", F. M. Tesche, AWFL Sensor and Simulation Notes, Note 407, July 1997). One form of the PxM antenna exhibits the radiation pattern of the hypothetical Huygens source ("Some New Forms of Huygen's Principle," V. H. Rumsey, IRE Trans. Antennas and Propagation, December 1959). The radiation pattern is also referred to as the Ludwig 3 ("The Definition of Cross Polarization", IEEE Trans. On Antennas Prop., Vol. AP-21, No.1, Jan. 1973) pattern and is a unidirectional pattern comprised of a cardioid of revolution about the axis of maximum radiation intensity. The radiation Q of such an antenna is approximately half that of an isolated electric or magnetic dipole. In principle, this should facilitate broadband impedance matching. However, practical implementations of such antennas are problematic and have not been thoroughly investigated. In the area of spherical near field metrology, the Huygen's source has been identified as desirable as a near field probe (J. E. Hansen, Ed., Spherical Near-field Antenna Measurements, 1988) but because such a probe is not very easy to implement in practice, very few are used in commercial near field measurement systems. Fundamental to the operation of a PxM antenna is the relationship between the electric and magnetic dipole moments. That is, the quasi-static dipole moments must be orthogonal in spatial orientation and in phase electrically. For the combination of an electrically-small linear dipole and loop, this amounts to the currents in the antenna elements being in phase quadrature ("Electric Lines of Force of an Electrically-Small Dipole-Loop Antenna Array", P.L. Overfelt, IEEE Trans. Antennas Prop., Vol. 46, No. 3, March 1998). In a numerical or analytical model, it is not difficult to specify the relationship between the magnitude and phase of two independent sources. However, in practice, such an antenna is usually driven from a single source with finite output impedance. It is therefore necessary to implement a network capable of maintaining the proper magnitude and phase of the dipole moments over some bandwidth. For many applications a low-loss passive network is most desirable. Such a network is subject to the limitations on realizable passive networks. Moreover, despite the desirable reduced radiation Q of the antenna, the driving point impedances at the bases of the two dipole elements vary widely. In principle, it should be possible to utilize an electric and a magnetic radiator with complementary input impedances. One such proven approach is the monopole-slot combination ("The Monopole Slot: A Small Broad-Band Unidirectional Antenna", P. E. Mayes, W. T. Warren, and F. M. Wiesenmeyer, IEEE Trans. Antennas and Propagation, Vol. AP-20, pp. 489-493, July 1972). This configuration is, in the ideal case, a PxM radiator. While the monopole-slot antenna has been shown to work well in terms of pattern behavior, such a design is burdened by low radiation efficiency as well as the requirement of a sufficiently large ground plane. For a compact, isolated design, it is more desirable to employ a combination of a magnetic loop and electric dipole. Unfortunately, the loop is problematic in that the simple single-turn loop does not exhibit the complementary impedance to that of the short dipole. The loop has a stronger frequency dependence of radiation resistance and higher radiation Q than its counterpart, the linear dipole, and much higher Q than the end-loaded dipole. Moreover, the frequency dependence of the far-field electric field transfer function of the loop is different than that of the dipole. Thus, two problems must be overcome: first, appropriate practical electric and magnetic radiators must be found or designed, and second, a low-loss passive network to combine the two must be implemented in such a way that PxM operation is maintained over some reasonable bandwidth. Additionally, if losses are to be kept to a minimum, the circulation of reactive power within the matching network must be minimized. For a simple electric or magnetic dipole this reduces to the requirement that the matching network store energy of the opposite form as the antenna does; that is, if efficiency is to be maximized and both capacitive and inductive elements are available with the same Q, a short electric dipole should be matched with an all-inductive matching network ("Radiation Efficiency of Electrically-small Antennas Combined with Matching Networks," G. S. Smith, IEEE Trans. Antennas and Propagation, Vol. AP-25, pp. 369-373, May 1977). Here the situation is more complex in that the antenna stores both electric and magnetic energy.

We discuss in detail a practical implementation of the PxM antenna utilizing low-loss components and providing PxM operation over more than one octave. The antennas presented here are based on a broadband loop/dipole combination. Several experimental prototypes have been constructed that operate from 25-100 MHz, although true PxM performance is maintained over a smaller bandwidth. The prototypes utilize broadband type II equal-delay transformers in conjunction with delay lines to scale the impedance functions while maintaining proper phase relationships. A numerical model and predicted performance are presented. Measured input impedance, complex field transfer functions, and pattern characteristics for the prototypes are presented.

UWB 8-16: Optical and Acoustic Pulse Radiation Antennas

A. Vyazmitinova[1], **I. I. Magda**[2], **V. Pazynin**[1]
[1]*Institute of Radiophysics and Electronics, National Academy of Sciences of Ukraine*; [2]*Kharkov Institute of Physics Technology*

One of the most difficult problems of the modern theoretical and applied electrodynamics and, in particular, in the antenna theory and engineering is the development and practical realization of high-performance UWB radiating and receiving antennas. The operational requirements for the radiating and receiving pulse antennas and, consequently, conditions of their work, differ too much. As a rule, the receiving antennas operate with the fields of relatively low power and their principal purpose is an effective reception of UWB signals from the specified direction and transmission of them into input circuit of a receiver with minor distortions. Unlike, the demands that are imposed on impulse radiating antennas (IRA) are the formation in the given spatial region of ultra-short pulsed intense electromagnetic fields (USP IEM). For the UWB IRA some distinctions between the spectral composition of the radiated field and the spectral composition of source's field can be allowed. These distinctions have to be exactly specified and not only predictable. For many practical applications such as, for example, testing of large-sized objects under conditions of powerful pulse electromagnetic fields of ultra short duration or operation as radiators of USP IEM radars it is important to make the most use both of the pulse power of the primary source and the possibility to control the directional properties of the radiating system.

In this work we consider some aspects of designing the UWB IRA of both optical and acoustical types and their various compositions. The main IRA electrodynamic characteristics have been investigated by theoretical FDTD method with the proper truncation of the computation domain through using the exact "absorbing" conditions on virtual boundaries. These IRA involve the laminated Luneberg lenses, reflectors of parabolic and elliptical profiles, horn radiators with axially symmetric and radial lenses comprised of metal plates. The investigated structures have been optimized for the given parameters. Special attention has been given to the practical realization of the structures when operating with the excitatory pulses having the amplitude of $\approx$ 109 V and the steepness of pulse edge of $\approx$ 1015 V/s.

UWB 8-17: A Portable Automated Time-Domain Antenna Range: The PATAR(TM) System – Performance

E. G. Farr[1], **L. M. Atchley**[1], **L. H. Bowen**[1], **W. S. Bigelow**[1], **T. C. Tran**[1]
[1]*Farr Research, Inc.*; [2]*U.S. Air Force Research Laboratory / DE*

The Portable Automatic Time-domain Antenna Range, or PATAR(TM) system, provides a convenient and inexpensive method of testing both narrowband and wideband antennas. The system includes a fast step generator, a fast digital sampling oscilloscope, a calibrated sensor, an elevation/azimuth positioner, and a laptop computer. In a companion paper we describe the functions and operations of the system. In this paper we describe its performance, by making comparisons of its measurements to a variety of other sources.

We have found that the accuracy of each measurement is dependent upon a variety of factors. These include the bandwidth of the antenna under test (AUT), the resonance properties of the AUT, and the properties of the ground upon which the system is place. By comparing our results to a number of results from other antenna ranges, we are able to get a very good idea of how the system performs. We compare our results to those obtained by other laboratories taken in the frequency domain, and to manufacturer's specifications for a given antenna. We begin by measuring a number of non-resonant antennas, including two Farr Research Impulse Radiating Antennas and a tapered ridge waveguide. For these non-resonant antennas, we obtain good agreement across the entire frequency band from 200 MHz to 20 GHz. Next, we measured a log-periodic dipole array that operates from 200 MHz to 5 GHz. These results were not satisfactory, because of the long ringing time of the impulse response. We next attempted to measure a variety of narrowband antennas operating below 1 GHz, in order to quantify how low in frequency our measurements of narrowband antennas would be reasonable. First, we measured a folded dipole operating at 900-930 MHz, and we found the results to be consistent with the manufacturer's specifications. Next, we measured two Yagis operating near 450 MHz and 230 MHz. Because of late-time ringing, these two results were unsatisfactory. This series of experiments allowed us to set the low end of the frequency range for all antennas, including resonant ones, to around 900 MHz. Finally, we characterized an X-band horn, intended to operate between 8.2 and 12.4 GHz. We considered this to be a particularly interesting test of our antenna range, because this antenna would normally never be driven by an impulse. Nevertheless, our measurements were consistent with the manufacturer's specifications to a surprising level of accuracy.

The high end of the system is determined primarily by the bandwidth of the sampling head of the digital sampling oscilloscope. While we are currently using a 20 GHz sampling head, others are available that reach 50 GHz. The low end of the system is limited by late-time ringing of resonant antennas. There is a possibility that the low end could be extended either by increasing the time window of the measurements, or by fitting a sum of poles to the signal within the same time window. This will be an area of future research.

We conclude that the PATAR(TM) system operates well for all antennas above 900 MHz, and for non-dispersive antennas above 200 MHz. The high end of frequency range is currently 20 GHz, but that could be extended with modest improvements.

UWB 8-18: Antenna-Aperture Synthesis for Hyperband SAR Antennas

C. E. Baum
Air Force Research Laboratory, DEHP; Directed Energy Directorate; Kirtland AFB; NM; USA

This paper introduces an aperture-synthesis procedure for producing a desired pulse shape, including the desired frequency spectrum of the pulse. This is accomplished by controlling the time-of-arrival of fields on the aperture plane, thereby synthesizing a delay as a function of radius for the arrival of a step-function TEM-like wave on the aperture plane. Amplitude taper as a function of radius can also be included. The procedure is illustrated with gate and sawtooth waveforms radiated on boresight.

A previous paper addresses this problem by illuminating the aperture with a spherical TEM wave. There it is observed that with a circular aperture centered on the direction to the observer (the z-axis) and the spherical-wave center also on this axis, the radiated field on boresight has notches in the frequency spectrum. In terms of step-function temporal excitation this is due to a second step associated with the truncation of the aperture at a particular radius, a. In the previous paper one method for eliminating the second step and replacing it with a constant-times-time decay to zero was investigated. This involved a resistive sheet with a special profile (function of radius, Ψ) on the aperture.

The present paper delves further into this problem. In particular we consider altering the spherical wave illuminating the aperture by increasing the delay near the aperture edge. As we shall see, this also can be designed to eliminate the second step, in a more efficient manner.

UWB 8-19: Analysis and Optimization of New Ultra Wide Band Antenna to be used in Wireless Communication

A. A. L. Neyestanak, **F. H. Kashani**, **M. Khosroshahy**
Iran University of Science & Technology

In this paper, a variety of simulated annealing method is proposed to increase the bandwidth as well as to access ultra wideband antennas. Antennas of Bowtie and Inverse Bowtie and their combinations are simulated using MoM and their bandwidths are increased using the optimization method of the simulated annealing algorithm.

Simulated annealing results from the physical process of annealing metals, in which a metal is heated and then little by little cooled in order to form strong crystalline bonds within the structure (Moldover.R. and Coddington.P., Simulated Annealing, http://www.npac.syr.edu/REU/reu94/ramoldov/proposal/section3_2.html, Aug. 2001). Choices of simulated annealing proposed in this paper are:

1) Original Simulated Annealing: The original simulated annealing uses a random number generator with a uniform distribution to produce the new configurations (within the step size).
2) Boltzmann Annealing: Boltzmann annealing uses a random number generator with a gaussian distribution.
3) Fast Annealing: In fast annealing the temperature decreases at a quicker rate than the other annealing methods described beyond.
4) Very Fast Re-Annealing.

Antennas geometry is presented in figures 1 and 2 (Aaron Kerkhoff, Robert Rogers, Hao Ling, "The use of the genetic algorithm approach in the design of ultra-wideband antennas", Apr. 2001).

Figure 3 gives the VSWR of a wide-band Bowtie (optimized by simulated annealing) and shows that the optimized bowtie antenna has about 38% fractional bandwidth. Results obtained show that the optimized combination antenna has led to a wide BW compared with others about 75% fractional BW at 1.5GHz-3GHz frequency band. The measured results of the optimized antenna validate a high compatibility between the simulation and the real experience.

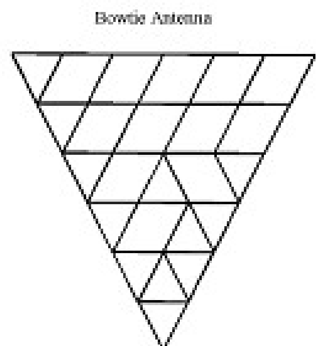

Figure 1: Geometry of wide-band Bowtie and their combinations antennas

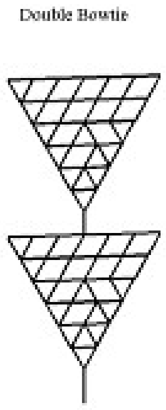

Figure 2: Geometry of wide-band Bowtie and their combinations antennas

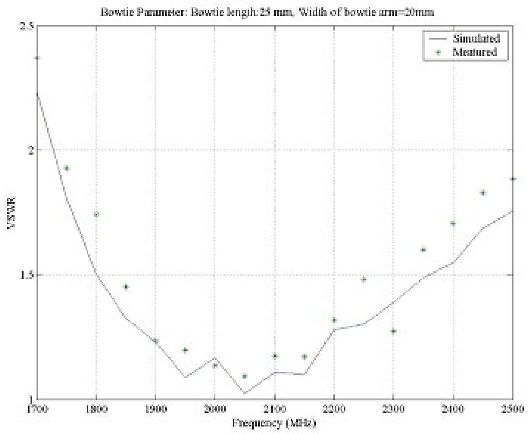

Figure 3: VSWR vs. Frequency

UWB 9 - UWB Radar Systems

UWB 9-1: Through-Wall Imaging by means of UWB Radar

R. Zetik[1], **J. Sachs**[1], **P. Peyerl**[2]
[1]*TU Ilmenau*; [2]*Meodat GmbH*

Ultra wideband (UWB) radar is of great interest for a vast number of applications such as surface penetrating radar, surveillance and emergency radar, medical instrumentation, non-destructive testing in civil engineering and the food industry, industrial sensors and microwave imaging and many others.
In the article, the possibility to use UWB radar for through-wall imaging will be presented. There are a number of situations where the entering of a room or a building is considered hazardous and it is desired to inspect the interior from outside through the walls, an example includes the tracking of people in dangerous environments (for policemen, firemen etc) and so on. One solution for such a applications is to use UWB radar. The fractional bandwidth of UWB radar sounding waves for such types of applications should be as close as possible to 200 % or higher which results in a high spatial resolution and good penetration of the sounding waves through the wall. UWB radars are able to detect hidden objects and a high bandwidth results not only in good spatial resolution but also in improved capabilities for object recognition. It means that it is not only possible to detect and track some objects or persons situated behind the wall but it is also possible to distinguish between different objects or persons.
The goal of this article is to illustrate the ability of multi-channel (3Tx, 4Rx) UWB radar to detect, position and track a person behind walls. A UWB radar module developed within the European project IST –2000-25351 (DEMAND) by Meodat GmbH and TU Ilmenau was used for the experiments. It covers the band from near DC to 5 GHz and it transmits continuous low crest factor signals (spreading sequences) instead of ultra short pulses. The circuit schematics are laid out in a completely symmetrical manner providing the opportunity to feed all types of antennas. Signal capturing, averaging and impulse compression were managed by commercially available components mounted on a 150 x 90 mm PCB.
Firstly, the article describes the UWB radar used for the measurements in more detail and then experimental results of the real-time measurements are illustrated.

UWB 9-2: Analyzing the Target Recognition Capability of an Ultra-Wideband Radar System Using Time Frequency Algorithms

G. Oßberger[1], **T. Buchegger**[1], **E. Schimbäck**[2], **A. Stelzer**[2], **R. Weigel**[3]
[1]*Linz Center of Mechatronics GmbH*; [2]*Johannes Kepler University of Linz*; [3]*Friedrich Alexander University Erlangen-Nuremberg*

In this paper a pulse-based Ultra-Wideband radar system for precise target detection is presented. The radar set-up was used to get real radar reflection data to analyze and evaluate various linear and quadratic time-frequency algorithms in terms of target resolution capability and denoising properties. Figure 1 shows the implemented test set-up containing the pulse generator, a pair of wideband antennas, a set of moveable targets,a LNA and a sampling oscilloscope for data acquisition. We used two different pulse generators, one self developed pulse generator using two step recovery diodes (SRD's) for decreasing the rise and fall time of the pulse (Upp=2.8 V; pulse width=330 ps). Figure 2 shows the prototyped pulse generator which generates a pulse train with a pulse repetition frequency (PRF) of 4 MHz by using an internal clock oscillator, furthermore, other PRFs can also be provided by using an external clock source. The second pulse generator from Picosecond Pulse Labs (Upp=2.7 V; pulse width=100 ps) was used to compare the achievable resolution depending on the transmitted pulse width.
The first investigation part concerning signal processing was to analyze the performance of different algorithms in terms of their denoising capability for UWB pulse radar signals. That means that we used real noisy reflection data at different target distances and simulated reflection data to compare the algorithm performances. To the artificial signal we can add arbitrary Gaussian white noise to achieve a defined peak signal to noise ratio (peak SNR). The algorithms which were compared range from classical linear time-frequency algorithms (STFT, Wavelet transform) to more advanced quadratic time-frequency representations (Spectogram, Scalogram, a set of Wigner distributions). The results show that the Wavelet transform can achieve the best performance if a mother wavelet similar to the receiving pulse, like Daubechies 4 or Mexican hat, is used. The performance which can be obtained is a pulse detection capability up to –5 dB peak SNR. In comparison, other time-frequency representations, where the received signal is decompose into a set of sinusoids, can also detect the searched pulse up to –4 dB peak SNR. The main disadvantage for these representations is that a huge amount of cross terms appear, which makes the interpretation of the results very difficult. Figure 3 shows the determined pulse position using the scalogram algorithm (squared wavelet coefficients) with a Mexican hat mother wavelet for a simulated signal with –2 dB peak SNR.

The next part deals with the resolution performance of the algorithms described above. For radar applications it is very important to have the capability to detect targets which are quite close together. The advantage of pulse based UWB radar is, that the used subnanosecond pulses ($<$ 330 ps) enable a target resolution of smaller than 10 cm. By using appropriate signal processing algorithms the target resolution can be improved. The used linear and quadratic time-frequency algorithms were analyzed in terms of unique target discrimination in noisy environment. The results show that the Wavelet transform achieve the best performance by using a mother wavelet similar to the receiving pulse, same as described above. If the received signal can be decomposed into a set of single pulses a resolution of 6 cm can be achieved. One problem occurs if the two targets are so close together that the two reflected pulses appear, in fact of superposition, as one pulse at the receiver. We accomplished several measurements where one target was standing still and the other was moving by. In Figure 4 you can see that there is a step in the determined first target position and the dilatation factor. This step stems from the wrong pulse estimation of the wavelet transform, because the receiving pulse is broaden in fact of the superposition of the two single reflection pulses. But the step also indicates that there is a variation in the target properties, which leads to the knowledge that there are two or more targets which can not be discriminated. By estimating the superposed pulse as a sum of shifted single pulses the resolution of the radar can be improved.

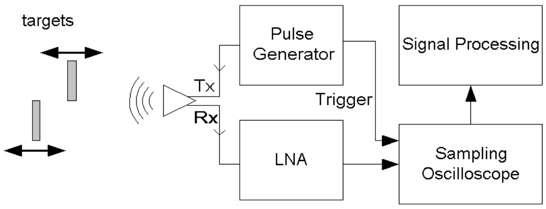

Figure 1: Block diagram of the implemented test set-up

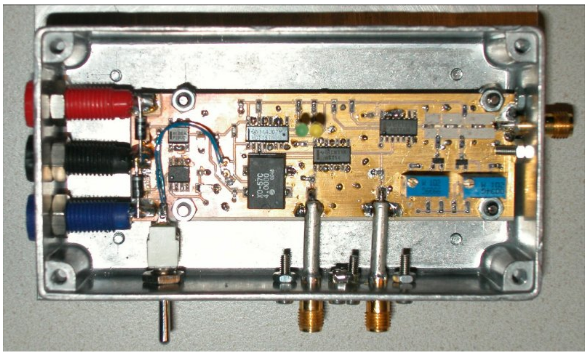

Figure 2: Self developed pulse generator

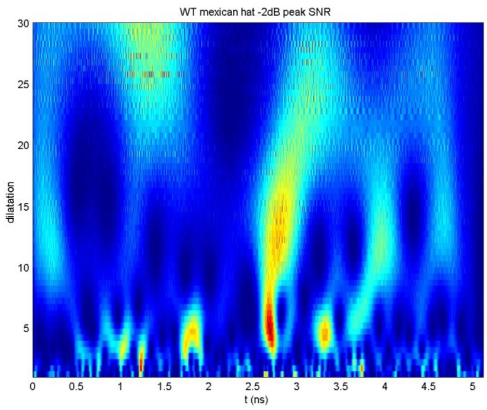

Figure 3: Scalogram mexican hat -2dB peak SNR

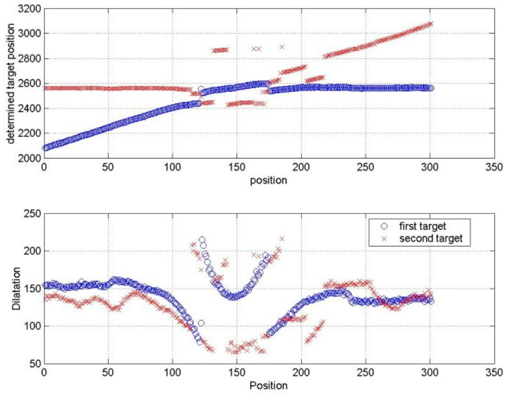

Figure 4: Two target position determination

UWB 9-3: Advances in Ground Penetrating Radar (GPR) For Landmine Detection

R. Weaver
Night Vision and Electronic Sensors Directorate

This presentation discusses down-looking, close-in, vehicular mounted GPR for detection of anti-tank mines buried in roadways and along routes. The talk emphasizes the detection of plastic-cased mines with little metal and discusses the technical trade-off's in GPR for mine detection. The mine detection problem for radar is "clutter" limited not noise limited. If one hopes to achieve a reasonable false alarm rate, the main problem in is not only the detection of buried objects but also obtaining some information on the qualities of the buried objects. In other words, some level of classification of detected objects is indispensable. For mine detecting radars obtaining more information means exploiting higher frequencies than have typically been used in past systems. However, these higher frequencies are subject to severe attenuation, particularly in wet soils. The resulting attenuation can lead to very weak signals from the buried objects. Detecting these weak signals requires a radar system with an extremely clean pulse and a way to deal with the clutter that interferes with these weak signals. The antenna and its interaction with the ground surface (so called "ground bounce") provide the main source of clutter.
The discussion focuses on a wide band, short pulse GPR system developed over many years in Germany that specifically tries to address the mine detection problem of shallow buried targets. This radar incorporates several features designed to improve target signals by reducing unwanted "clutter" signals. These special features are discussed and illustrated. Performance measures are described and signal comparisons with other GPR's are shown over various types of targets. The talk concludes by comparing "blind" tests results from this radar with results from other radars over the same test roads and suggests future directions.

UWB 9-4: UWB Radar System Sensing of Human Being Buried in Rubbles for Earthquake Disaster

I. Akiyama[1], **Y. Araki**[1], **M. Isozaki**[1], **M. Ohki**[1], **A. Ohya**[2]
[1]*Shonan Institute of Technology*; [2]*University of Tsukuba*

A human being sensing system which searches for a living human buried in rubbles from on (or over) the rubbles for earthquake disaster is under developing. This system is characterized in that only a living human is detected by distinguishing a reflection wave from the human from the one from other stationary objects, noticing a sign representing that a human is living, that is, respiratory fluctuation, or "motion" due to breath. We use EVK200 manufactured by Time Domain Corporation. We added the horn antennas to it so that 30 degree beam profile is attained. Figire 1 shows simulated rubbles made of woods and a human being. Figure 2 and 3 show the envelope of received signals as a color map as collecting the every shots of pulses. Horizontal direction indicates distance from the antenna. Vertical direction indicates time. UWB pulses transmites every two seconds. Figure 2 shows tha map when a human being walked backward. Figure 3 shows tha map when a human being stood and moved his hands up and downn. The mark of human being is easily found in the maps. As a result, this system finds a human being by the above mentioned visualization.

This work is supported by Japanese MEXT Special Project for Earthquake Disaster Mitigation in Urban Areas Advanced Disaster Management System.

Figure 1: Simulated rubbles and a human being.

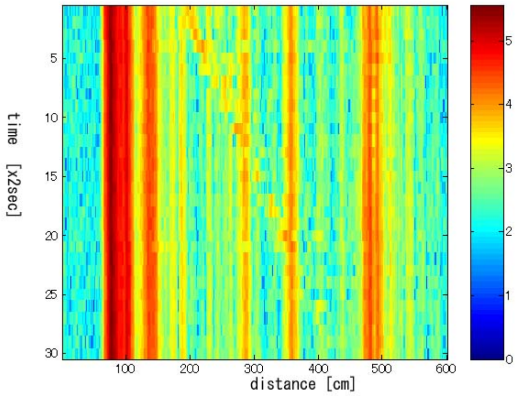

Figure 2: A human being walked backward.

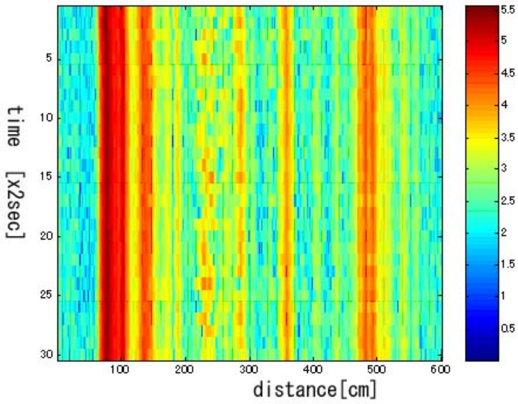

Figure 3: A human being stood and moved his hands up and down.

UWB 9-5: UWB Radar System for ISAR Imaging

B. Levitas, J. Matuzas

ISAR Imaging is used for measurement and modeling the properties of different scattered targets (1.James D. Taylor. Ultra-Wideband radar technology. CRC Press 2001. 2. Roger J. Sullivan. Microwave Radar Imaging and Advanced Concepts. Artech House 2000.). Good quality images can be achieved using Ultra Wide Band (UWB) Radar System. This system works in Time Domain. Using time windowing it is easy to exclude signal from occasional reflections from the walls, ceilings and from signal leakage in bistatic measurement. These advantages let to do measurements indoor without expansive anechoic chambers. ISAR Imaging is done turning the object around with positionier and taking signal at every angle. Our ISAR Imaging measurement was done in ordinary room using UWB Radar System. One of the examples of the results is presented in the figures 1, 2. Working band was 0.8-22 GHz, time window - 3 ns.

UWB Radar System include Pulse Generator (30ps duration), Sampling Converter (DC – 26GHz), Positionier, Transmitting and Receiving Antennas, Personal Computer. In such configuration system bandwidth is limited with antenna bandwidth.

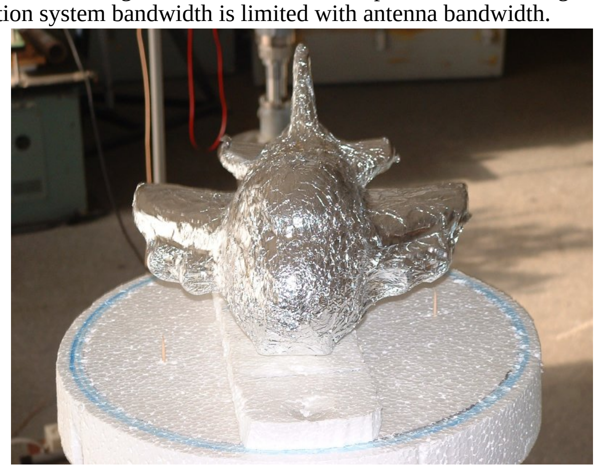

Figure 1: Target photo

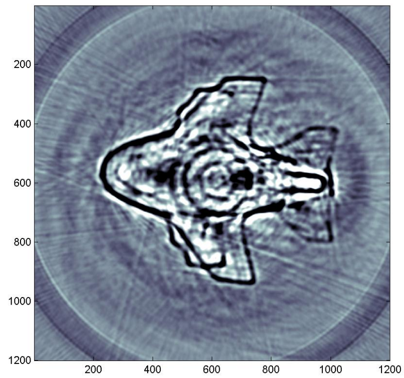

Figure 2: RCS density plot

UWB 9-6: A High-Voltage UWB Directional Coupler for Radar

E. G. Farr[1], L. M. Atchley[1], D. E. Ellibee[1], C. E. Baum[2], D. I. Lawry[2]

[1]*Farr Research, Inc.*; [2]*U.S. Air Force Research Laboratory / DE*

Most UWB radar systems currently use two separate antennas for transmit and receive. If a single antenna could be used for both functions, a more compact and convenient radar system could be realized. We report here on the development of such a directional coupler. The directional coupler developed here is based on two coupled parallel transmission lines. The four ports of the directional coupler are designated the Source, Through, Coupled, and Isolated Ports. When the Source Port is driven by a pulser, the Isolated Port sees, in theory, no signal until the backscattered signal returns. In practice, there is always leakage, so one goal of this design is to minimize the leakage from the Source Port to the Isolated Port. The signal at the Coupled Port is, in theory, a faithful replication of the returned signal for the round-trip transit time of the coupled lines. The bandwidth of the coupler is determined by two factors. At the high end, the bandwidth is determined by the diameter of the coupled lines. At the low end, the bandwidth is determined by the length of the coupled lines. We begin by providing the time domain equations that describe the circuit. We then demonstrate how to optimize the design to obtain the largest voltage into the scope. We then built and tested two prototype designs that should be able to handle a short transient signal of 50 kV. We tested these two devices at low voltage, and found that they operated about as expected. The leakage signal at the Isolated Port was down by about 20 dB from the source signal driving the Source Port. In future designs we would hope to reduce the leakage signal to 40 dB down from the source signal. We then used these one of these couplers in a radar measurement, using a fast low-voltage pulser, an IRA-3 antenna, and a fast sampling oscilloscope. We found that the field scattered from a corner reflector was readily apparent in the received signal. Future work will include smoothing the device response, reducing loss through the device, increasing the bandwidth, and testing at high voltage. We will also work to reduce the coupling to the Isolated Port.

UWB 9-7: UWB Full-Polarimetric Video Impulse Radar for Landmine Detection

A. Yarovoy[1], **A. Schukin**[2], **I. Kaploun**[2], **L. P. Ligthart**[1]
[1]*Int. Research Centre for Telecom and Radar, Delft University of Technology*; [2]*Academician A.L. Mintz Radiotechnical Institute*

Recently considerable efforts are put in development of GPR systems for detection of surface-laid and shallow buried targets such as antipersonnel landmines. Such application requires principally new (in comparison with conventional GPR) design of the system. Together with essential improvements of such hardware specifications as down- and cross-range resolution, sensitivity, stability, etc., this specific application requires a principally new ability to classify and identify detected targets. To meet these requirements we have developed a multi-waveform full-polarimetric system with essentially increased (comparing to conventional GPR) bandwidth.

The design of the radar is based on our analysis of different GPR scenarios. Trying to satisfy technical demands listed in (Yarovoy A.G., Schukin A.D., Kaploun I.V. and Ligthart L.P., 2001, “Multi-channel video impulse radar for landmine detection”, Detection and Remediation Technologies for Mines and Minelike Targets VI, SPIE 4394, 662-670) we developed a GPR system, which comprises a pulse generator section, a multi-static antenna system, a four-channel signal conditioner, a five-channel sampling converter and a remote control PC. The radar operates at the pulse repetition rate of 254kHz (all channels sample simultaneously). The operational bandwidth of the radar (measured via external calibration of the radar) covers an interval from 260MHz till 2220MHz for the 0.8ns generator and an interval from 790MHz till 3040MHz for the 0.5ns generator (on 10dB level). The linear dynamic range of the receiver is of about 69dB (with averaging over 128 signals).

The principal novelty of the radar performance lies in its multi-waveform nature. The radar transmits and receives quasi-simultaneously different waveforms corresponding to different transmitted polarizations and different pulse generators. To implement this multi-waveform feature the stroboscopic nature of the sampling scope is used. It allows toggling of both pulse generators and both transmit polarizations within an A-scan (a single measured waveform). Comparison with the signals measured with a constant operating generator shows a good agreement between both types of the measurements. Polarization and generators toggling prevents a necessity of multiple scans over the same area, which is of large practical value for demining.

The system has been tested at the test facility for landmine detection systems located at TNO-FEL, The Hague. The measurements have been done over the sandy lane (in two conditions: dry and wet) and over the grass lane. Analysis of the recorded data has shown that the dynamic range of the radar is sufficient for detecting all antipersonnel mines laid in the lanes in all tested types of soils. Comparison of the data measured with two different generators over the same lane does not confirm the belief that larger bandwidth of the signal necessarily leads to a better detection of the mines in inhomogeneous soil. Processing of the recorded data resulted in high-resolution full-polarimetric images of the subsurface. These images have been successfully used for classification of detected targets by shape, polarimetric features and dielectric permittivity (more explicitly, by the dielectric permittivity contrast with surrounding soil).

UWB 11 - Short-Pulse Measurement Techniques

UWB 11-1: A Comparison of Two Sensors used to Measure High-voltage, Fast-risetime Signals in Coaxial Cable

E. G. Farr[1], **L. M. Atchley**[1], **D. E. Ellibee**[1], **W. J. Carey**[2], **L. L. Altgilbers**[3]
[1]*Farr Research, Inc.*; [2]*ARC Technology*; [3]*U.S. Army Space and Missile Defense Command*

We consider here two sensors that are commonly used to measure high-voltage fast-risetime signals in coaxial cable. One sensor measures the current in the cable, and is called a Current-Viewing Resistor, or CVR. In this design, the cable jacket is cut, a portion of the cable jacket is removed, and a number of resistors are inserted in parallel across the gap, thereby creating a low resistance in series with the outer cable jacket. The voltage across these resistors is proportional to the current in the coax. The second sensor measures the derivative of the voltage in the coax. It is fabricated from a “sawed-off” SMA connector that is inserted through a small hole in the cable jacket. In this paper we characterize the accuracy of both sensors when used with RG-220 cable, and we discuss the situations when one might prefer one measurement type over the other.

We observe that for driving voltages of around 300 ps, either sensor provides an accurate measurement. However, when we reduce the risetime to 100 ps, the CVR rings badly, resulting in a 50% overshoot of the peak level. On the other hand, the integrated output of the SMA sensor is quite accurate, and it virtually overlays the source function. Despite the observed ringing at very fast risetimes, there are still several reasons why one might prefer using a CVR instead of an SMA. First, many signals of interest are not fast enough for the ringing to become evident. Second, a CVR provides a direct measurement of the signal, without the need for integration. A numerical integration is sometimes inconvenient, while an analog integration may result in either a reduced signal or reduced accuracy of the measured signal. Finally, the SMA sensor has less sensitivity than the CVR, so in some applications with low voltages or long risetimes the SMA sensor may not provide sufficient signal to drive the oscilloscope. There are also many situations where an SMA sensor would be preferred. First, for fast signals, this is the only way to avoid ringing. Second, the SMA sensor introduces only a small hole into the cable, which can easily be repaired. The CVR, on the other hand, is more invasive, and it permanently alters the cable. Finally, and perhaps most importantly, the SMA sensor is much simpler to build.

UWB 11-2: Short Pulse Measurements by Field Sensors with Arbitrary Frequency Response

G. Cerri[1], **H. Herlemann**[2], **V. M. Primiani**[1], **H. Garbe**[2]
[1]*Istituto di Elettromagnetismo e Bioingegneria, Università Politecnica delle Marche, Ancona, Italy;* [2]*Institut für Grundlagen der Elektrotechnik und Messtechnik, Universität Hannover, Germany*

The demand for the measurement of transient electromagnetic fields arises in several EMC and communications applications: Electrical Fast Transient Tests (G. Cerri, R. De Leo, V. Mariani Primiani, "Electrical Fast Transient Test: conducted and radiated disturbance determination by a complete source modelling", IEEE Transaction on EMC, vol. 43 no. 1, February 2001, pp. 37-44), Electrostatic Discharges (D. Pommerenke, "ESD: what has been achieved, what is less well understood?", 13th Int. Zurich Symp. and Technical Exhibition on Electromag. Compat., Zurich, Feb. 16-18, 1999, pp. 77-82) and Ultra Wide Band transmissions (M.Camp, H. Garbe and D. Nitsch, "UWB and EMP susceptibility of modern electronics", 2001 IEEE EMC International Symposium, Aug. 2001, Montreal, pp. 1015-1020). This is not an easy task because it requires sensors having flatness of the amplitude response over a wide frequency range (several GHz), a minimum phase distortion, a proper sensibility and reduced dimensions for minimum field perturbation for point measurements. The realization of such sensors requires an accurate design and a considerable technological effort. In particular, it is possible to use purely derivative sensors, in order to easily recover the relationship between the output voltage and the impinging field. They are typically very small, to maintain their properties within the used frequency range, and therefore suffer for low sensitivity, limiting their use to extremely high intensity field applications. A way to achieve a flat response is to use capacitively loaded dipoles with a preamplifier (active probes): the useful frequency range is upper limited by the resonance of the dipole and can be increased reducing its dimensions and therefore the sensitivity.

In the present contribution, the use of sensors not explicitly designed for transient field measurement is proposed. Their main features are: 1) a fully passive construction 2) dimensions not negligible with respect to the shortest significant wavelength of the measured field, that assure a sensitivity enhancement. They are therefore characterised by an arbitrary transfer function between the incident field and the output voltage: its precise knowledge, in amplitude and phase, allows the measurement of very fast transient field through the application of a deconvolution procedure to the sensor output voltage time history.

A calibration procedure for the characterization of E-field sensors is presented. It is based on the use of a simple structure for the generation of a known field, the TEM-horn cell. It is a very cheap structure, because no cell terminations are used, and the unwanted effects of the cell truncation are removed by a proper time domain gating of the sensor response. The sensor under characterization is placed inside the cell, along the longitudinal axis, and a Network Analyser (HP 8753D in the present case) is used to relate the sensor output voltage to the cell input voltage, by the measurement of the S_{21} parameter, and therefore in the frequency domain. The use of the Time Domain facility of the instrument allows to separate the principal sensor response, produced by the incident pulse, from that one reflected by the cell's open termination, achieving the correct sensor transfer function by turning back in the frequency domain. The calibration field inside the cell is analytically computed applying the conformal mapping method. As an example, Fig. 1 shows the amplitude of the transfer function obtained for a resonant dipole (HZ-13 from Rohde & Schwarz): it does not have a flat response, it is far away from the derivative behaviour and exhibits a deep resonance.

The so calibrated sensor is successively used to measure the transient field radiated by an annular slot realised in the screen of a coaxial cable inside which an ESD pulse propagates, Fig. 2. A coax cable type RG 213 is fed by a 2 kV discharge, performed inside a shielded room to avoid unwanted radiation components, and lies along the z-axis at a height of 1.5 m above the laboratory floor. The cable is matched at its end. The gap width is 3 mm and the dipole is oriented along the cable axis. The measurements are performed at a distance of d = 10, 20, 40 cm from the gap, and a height of 1,5 m above the laboratory floor. The results are reported in Fig. 3, where the dipole measured field is compared to that one measured by a commercially available flat response active sensor (Thomson ET 1052), showing a good agreement for all measurement positions. The obtained results confirm the possibility to use whatever type of receiving structure, even though with a complicated frequency behaviour, to measure a transient field.

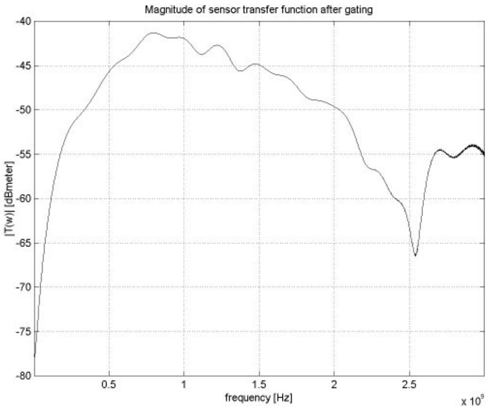

Figure 1: Sensor transfer function.

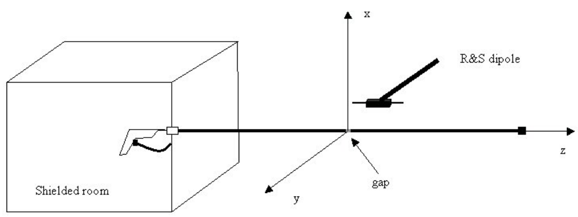

Figure 2: Set-up for the measurement of the aperture radiated field.

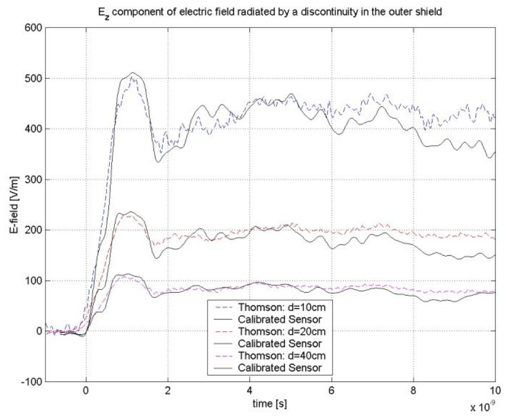

Figure 3: Field radiated by a cable aperture under ESD excitation.

UWB 11-3: Time-domain Measurement of Electric Field Emitted from UWB Device within an Arbitrary Bandwidth by using the Complex Antenna Factor

S. Ishigami, **Y. Yamanaka**
EMC Group, Communications Research Laboratory

This paper mentions the waveform reconstruction method of the electric field by using the complex antenna factor (S.Ishigami, et. al. IEEE Transactions. on EMC, vol.38, pp.424-432, 1996) and observed waveform with an oscilloscope. The electric field radiated from a double-ridged guide horn antenna and a pulse generator is observed with an oscilloscope. The electric-field

waveform is reconstructed from the observed result by using the method. The peak-power measurement of 50 MHz RBW described in the documents of FCC part 15 is also examined by using the method.
Figure 1 shows an example of an apparatus for measuring the electric-field waveform radiated by UWB equipment. The waveform observed with an oscilloscope, $v_m(t)$, is convoluted on the characteristic of the measuring apparatus to the antenna output, $v_a(t)$. The limits of spectrum in FCC are defined in the equivalent isotropic radiation-power (EIRP), and can convert EIRP from the electric-field intensity at measurement distance of 3m. Therefore, the real waveform of the field should be reconstructed from the measured output by using the characteristics of the antenna and the apparatus. In the figure, $S_a(\omega)$ denotes the S-matrix of a pre-amplifier and cable. $S_{21o}(\omega)$ does the transmission S-parameter of an oscilloscope. Γ_a and Γ_o show the reflection coefficients of a receiving antenna and of the input port of the oscilloscope, respectively. Now, S_{12a} is assumed to be zero. When S-parameter analysis of the equivalent circuit is performed under the above-mentioned conditions, the waveform of the electric field, $E(t)$, is expressed as shown in Equation (1). F and F^{-1} denotes the Fourier and the inverse Fourier transform. In the equation, $X(\omega)$ is a frequency response of a receiver for measurements. When we want to obtain the peak power in a case of a resolution bandwidth of 50 MHz which is specified in the FCC part 15 subpart F, $X(\omega)$ is a function of the Gaussian filter.
The reconstructed and evaluated waveforms of the electric field at the distance of 3m are shown in Figure 2. The reconstruction of the waveform was performed by using Equation (1). The equipment for experiments consists of an impulse generator (Picosecond Pulse Labs 4016), antennas (EMCO 3115), cables, and a digital sampling oscilloscope (Tektronix TDS8000B with the sampling head 80E03, 20GHz). The impulse generator is intended to simulate the waveform of an impulse radio of UWB system. The distance between the transmitting and the receiving antennas is 3m. The antenna height is 1.5m. The pulse reputation frequency of the generator is 500 kHz. We can find the good agreement between the evaluated electric-field waveform with the measured waveform in the figure. This result is led that the reconstruction method is appropriate.
When the center frequency, f_c, is set to 5.8 GHz as an example, the peak power in a case of a resolution bandwidth of 50 MHz is calculated as -10.7 dBm. The peak power can be converted by the impulse bandwidth, B_{imp}, defined by CISPR 16-1 as –14.3 dBm. When the BPF is a Gaussian filter, B_{imp} is about 1.5 times the 3dB bandwidth.
In the FCC documents, the peak power, $P_{p(50MHz)}$, can be calculated as shown in Equation (2).
The value P_{pRBW} is the peak power measured by a spectrum analyzer at the RBW of B_s. Since the signal is impulsive, the impulse bandwidth should be used for the value of B_s. The results which are measured by spectrum analyzers (SA) and calculated by Equation (2) are compared with the peak power obtained by the reconstruction method. The spectrum analyzers are set to peak-detector and zero span modes. The value of the RBW, B_s, and the video bandwidth are set to 3 MHz. The impulse bandwidth is measured by the method described in [2]. The results are shown below.
SA1: $P_{p(50MHz)}$=-15.2dBm, B_{imp}=2.73MHz
SA2: $P_{p(50MHz)}$=-14.4dBm, B_{imp}=4.10MHz
When the peak electric power value by the proposed method was compared with the above values, the differences were 0.9 dB (SA1) and 0.1 dB (SA2), respectively. When an impulse signal, such as an UWB signal is measured with a spectrum analyzer, the spectrum analyzer should be converted by the impulse bandwidth.

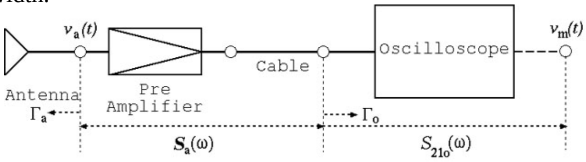

Figure 1: Waveform measuring apparatus.

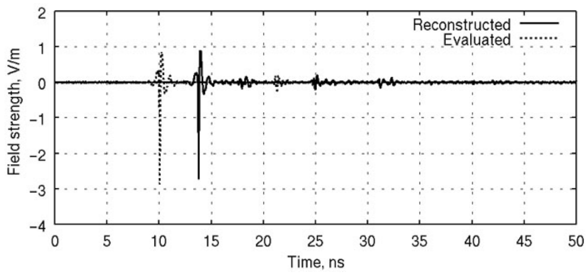

Figure 2: The reconstructed and evaluated electric field waveform.

$$E(t) = \Im^{-1}\left[\frac{(1 - S_{11a}\Gamma_a)(1 - S_{22a}\Gamma_o)}{S_{21}S_{21o}} F_c(\omega) X(\omega) \Im[v_m(t)]\right]$$

Figure 3: Equation 1.

$$P_{p(50MHz)} = P_{pRBW} + 20\log_{10}\left(\frac{50}{B_s}\right)$$

Figure 4: Equation 2.

UWB 11-4: Measurement System for UWB Applications

B. Levitas, **A. Martyanov**, **A. Minin**

UWB measurement system includes Pulse Generator, Sampling Converter and Computer. The generator includes a mainframe and a set of Generator Heads. The mainframe is provided with tunable delay and opportunity of computer control via RS232. Pulse repetition rate may be up to 50 MHz. The main pulse parameters are ensured by Generator Heads. There are 3 types of waveforms:
Step voltage:
Shaping is realized with two cascades on step recovery diodes. Amplitude >20 V, rise time <50 ps. Up to 7 GHz frequency pulse spectrum descends in inverse proportion to a frequency.
Pulses; duration from 30 ps to 20 ns:
The nanosecond pulses include cascades on power amplifiers and avalanche transistors. Amplitude can reach 100-250 V. Duration may be tunable. Pulse shapers with pulse duration a few hundred of picoseconds are made on Step Recovery Diodes with shorting plugs.
The nonlinear shaping transmission lines are used to shape the shortest pulses, 30 ps to 50 ps with amplitude >30 V. In this line 20–30 varactors are connected in parallels. In case of step voltage propagation in the line, the diode capacity decreases, speed of propagation increases for the later points of the front as compared with the earlier points. As a result the rise time decreases. After differentiation we get a short signal. Computer modeling of the signal shaping was executed. The calculated waveforms coincide with the experimental waveforms. Spectrum of the signals with duration 30 ps descends for 10 dB at frequency 18 GHz (as compared with DC) and for 20 dB at frequency 26 GHz.
Monosines are pulses with one period of oscillation. Amplitude 7–25 V, central frequency 0,4–4 GHz. They are shaped with using Step Recovery Diodes and shorting plugs. Sampling Converter with bandwidth DC–26 GHz can operate with sampling rate 25 MHz that ensures high speed of data acquisition. The figures show waveform and spectrum of 30 ps duration pulse.
The system may be applied for UWB radars (for example GPR, ISAR Imaging) and Time Domain Measurement Systems in frequency range up to 26 GHz. S-parameters, Antennas characteristics, RCS are measured.

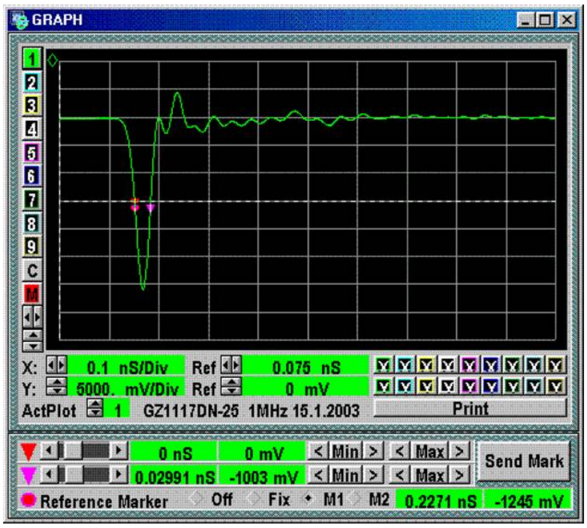

Figure 1: Waveform of 30 ps duration pulse

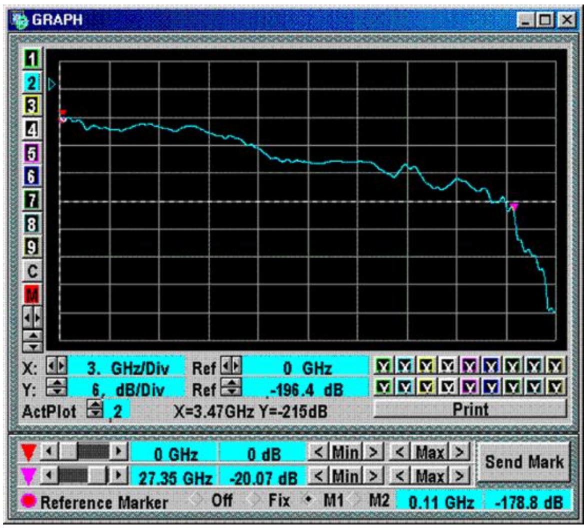

Figure 2: Spectrum of 30 ps duration pulse

UWB 11-5: Time Domain Measurements to Validate Test Site Characteristics

S. Battermann, H. Garbe
Institut für Grundlagen der Elektrotechnik und Messtechnik, Universität Hannover, Germany

The performance check of test sites is very important to achieve a good reproducibility of EMC compliance measurements. The normalised site attenuation (NSA) is the standardised method to detect errors of the test site. This approach has the disadvantage, that it does not give any information about the kind and position of the error. The only information is the deviation of the NSA at special frequencies. To eliminate this problem further investigations have been performed with measurements in time domain, which give the desired error localisation possibility.

Measurements

The measurement equipment consists of a vector network analyser with time domain extension and a pair of antennas. The measurement of the transmission coefficient S_{12} between the antennas is performed in the frequency domain and then transformed to the time domain with the inverse Fourier transform. The excitation signal is a pulse function. Thus it is possible to separate the signal, which arrives via the direct path and the following signal, which arrives temporally delayed via the reflected path. The reflection may occur via the ground plane or via (unwanted) reflecting objects on the test site.

A conical monopole provides a broadband antenna with a nearly omni-directional radiation pattern. Contrary to a logarithmic periodic antenna the problems by dispersion effects are negligible. Dispersion would widen the transmitted pulse, which makes the space localisation worse. Furthermore it is possible to illuminate the whole room to detect errors at all positions.

If a superposition of different errors occurs it is a simple method to disambiguate the measurement by moving a metal plate as a defined reflector on the test site. The place of the error is determined if the strong reflection of the metal plate matches with the site defect reflection in the time domain measurement. Thus it is possible to perform a correction with control of the improvement by observing the magnitude of the reflection coefficient.

Conclusion

The measurement results on different test sites (FAR, OATS) show, that the time domain measurements provide a powerful tool to detect errors. Furthermore it is possible to perform a fast check of the site characteristics during operation by comparing actual measurements with the measurements performed after site construction. This method should be used as an extension of the NSA measurement.

UWB 11-6: Dielectric Constant Measurement by a Free-space Method in Time Domain

A. Ahmadi[1], R. Fallahi[2], M. Okhovvat[3], M. Hakkak[4]
[1]*Iran Telecommunication Research Center and Iran University of Science & Technology;* [2]*Iran Telecommunication Research Center ;* [3]*Iran Telecommunication Research Center and Imam-Hossein University ;* [4]*Iran Telecommunication Research Center and Tarbiat Modarres University*

Knowledge of dielectric properties of materials is of particular importance in various fields such as radome dielectric materials. The computation of complex permittivity from the measured reflection and transmission coefficients is described by various authors in frequency domain (FD) such as Ghodgancar et al. (IEEE Transactions on Instrumentation and Measurement, 1989). In this paper we introduce a free space setup measurement in time domain (TD) for measuring dielectric constant of planar slabs. Measurement in TD offers some advantages over the classical techniques in FD: 1) Reduction of measurement time; Really in TD by doing only one test one can compute dielectric constant for a wide frequency band, 2) All reflected signals from various parts of environments can be distinguished by their different time locations in the received signal due to their different distances to the receiving antenna and one can remove multiple reflections between the horn and the sample by using the time gating technique.

For measurement of reflection, the set-up illustrated in Fig. 1 is used. The pulse generator generates a short picosecond pulse which is transmitted by a double-ridge horn antenna. The reflected signal from the slab is received by the same antenna and transferred through the wide band coupler to the sampling oscilloscope.

This measurement involves three steps. First, the signal reflected from the metal-backed sample is saved as S_{sample}. Second, a metal plate instead of the sample is placed and the reflected signal, S_{metal}, is saved as the reference signal. This would be a calibration signal for our measurement. Third, for removing any undesired environment influence, received signal without any sample, S_{free}, is saved. The Fast Fourier Transform is used for converting signals to the frequency domain. Then the reflected coefficient may be calculated from equation 1. Also from transmission line theory, the reflection coefficient for normal incidence plane wave is related to the complex relative permittivity by following relationship (Ghodgancar et al., IEEE Trans. on IM, 1989)(equation 2). For nonmagnetic materials (equations 3 and 4), d is the thickness of the sample. Then the complex relative permittivity is extracted by solving this equation. Using this measurement system (Fig. 1), the complex permittivity was measured for plexiglass. For comparison, the results obtained from a waveguide method in the frequency range 11-12 GHz and the result from our measurement setup are given in Table 1.

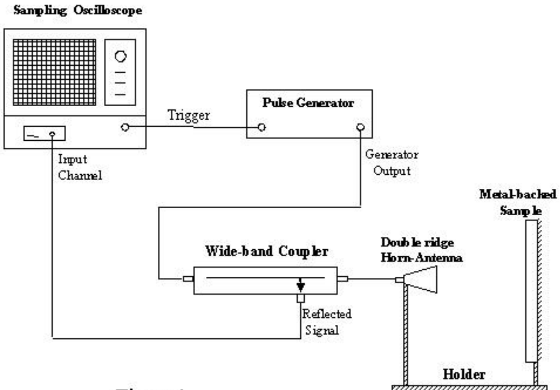

Figure 1

Figure 1: The measurement setup

Eq. 1: $$S_{11} = FFT\left\{S_{sample} - S_{free}\right\} / FFT\left\{S_{metal} - S_{free}\right\}$$

Eq. 2: $$S_{11} = \left(j\,Z\tan(\beta d) - 1\right) / \left(j\,Z\tan(\beta d) + 1\right)$$

Eq. 3: $$Z = 1 \Big/ \sqrt{\varepsilon_r}$$

Eq. 4: $$\beta = 2\pi\sqrt{\varepsilon_r}\,/\lambda_0$$

Figure 2: The Equations

Table I

Frequency (GHz)	ε_r	
	Our measurement setup	*Waveguide method*
11.1	2.77	2.610
11.2	2.70	2.657
11.3	2.69	2.627
11.4	2.73	2.622
11.5	2.71	2.590
11.6	2.58	2.560
11.7	2.46	2.615
11.8	2.45	2.673
11.9	2.54	2.674
12	2.49	2.615

Table 1: The measurement results for plexiglass

UWB 11-7: Realization of All-Pass-Networks for Linearizing Logarithmic-periodic Dipole Antennas

E. Hirschmüller[1], **G. Mönich**[2]
[1]*EADS RACOMS*; [2]*TU Berlin*

Log.-periodic dipole antennas (LPDAs) have been shown to be inapplicable for radiating short impulses (Russegger, "Einschwingvorgänge bei logarithmisch-periodischen Dipolantennen", TU Braunschweig, 1975). The ringing effect occurring when the antenna is fed by an impulse is mainly caused by the nonlinear phase of the LPDA. The nonlinear phase characteristic results from the pole reversals of the antenna's dipole elements. The resulting logarithmic phase characteristic of LPDAs can be modelled by second-order all-pass networks. The 180°-resonance frequencies of the all-passes match with the resonance frequencies of the dipole elements (Hirschmüller, Mönich, Schmidt, "LPD-Antennen für Impulsabstrahlung", EMV Düsseldorf, 2000, and "Phase linearized Log.-Periodic Dipole Antennas for undistorted Pulse Radiation and Reception", EMC Zurich, 2001). This is graphically depicted by pole-zero positions of the all-passes along the frequency axis corresponding with the respecting resonance frequencies. More precise considerations showed that the exact pole-zero positions of the all-passes depend on the antenna's geometry (Hirschmüller, Mönich, "Präzisierung der Phasenlinearisierung von LPD-Antennen", EMV Düsseldorf, 2002). This results in an arrangement, where the correspondig pole-zero pairs lie on a line through the origin, the slope of the line respecting the antenna's geometry. Linearizing the antenna means to compensate the antenna's phase-characteristic with additional all-pass networks. The positions of the poles and zeroes are gained by a mirroring-priciple (Hirschmüller, Mönich, Schmidt, "Phase linearized Log.-Periodic Dipole Antennas for undistorted Pulse Radiation and Reception", EMC Zurich, 2001). However, the realization of the higher-frequent all-pass networks turned out to be impossible with discrete elements. In this paper, a new approach for a phase compensation network for log-periodic dipole antennas is presented. The network consists now of a cascade of five second-order asymmetrical all-pass networks. The realization of assymmetrical networks offers different benefits compared with symmetrical ones: The compensation networks can be placed anywhere in the feed line of the antenna and needs no longer to be part of the antenna itself. Above all, the compensation network can be placed between the impulse generator and the power amplifier in the radiating case. Thus, a long signal with comparatively low magnitude has to be amplified and transported. The high field impulse is composed not until it is radiated by the antenna. Moreover, an unsymmetrical all-pass network does not need balanced elements in order to achieve good matching. Here, it is only important to have corresponding resonance frequencies of the parallel and the serial resonant circuits. The coupling, which is required by asymmetrical all-pass structures, is now realized by a coupled transmission line. The coupled line, as well as the capacitors and inductors with small values are relized in micro-strip technology. The wiring diagram, element dimensions and layout for the realized compensation network will be given as well as simulation results.

UWB 12 - Applications of High-Power, Ultra-Wideband and Short-Pulse Electromagnetics to Homeland, Air & Missile Defence

UWB 12-1: Transient Responses of Short-pulse Signals in Scattering Problems

M. Yuan, **M. C. Taylor**, **T. K. Sarkar**
Department of Electrical Engineering & Computer Science, Syracuse University

The transient responses of short-pulse (ultra-wideband) signals are analyzed in electromagnetic scattering problems. An efficient way to simulate the short-pulse measurements is introduced. In short-pulse measurement, we usually generate some incident wave by a transmitting antenna and radiate the wave toward the target. The scattered wave will be reflected back by the target and observed by a receiving antenna. For narrow band or single frequency scattering problems, we don't need to care about the properties of the transmitting and the receiving antennas. We take the incident wave as the replica of the exciting voltage in transmitting antenna and the induced voltage in the receiving antenna as the far scattered field. However, it's not true for ultra-wide band or time domain analysis. Each antenna in practice will illustrate some non-linear properties trough the broad band, and these properties will distort the input signals (T. K. Sarkar, M. C. Wicks, M. Salazar-Palma, and R. J. Bonneau, Smart Antennas, 2003). If we ignore the properties of antennas, the information we get or observe will be different from the real data.

Each electromagnetic component can be seen as a linear time invariant (LTI) system. The system of measurement can be divided into cascaded subsystems. We take the transmitting antenna as the first system and the input of the subsystem is the exciting voltage and the output is the radiated wave. The target is the second system with the input of the incident wave (wave radiated from the transmitting antenna) and output of the scattered wave. The receiving antenna is the third system. If we replace the second system with the wireless channel, the whole system can be looked as a system of ultra-wideband wireless communications. We can analyze each subsystem by sequence, and get the final output (the induced voltage of the receiving antenna). Examples of both metallic and dielectric targets are simulated and the short-pulse responses are analyzed. The exciting voltage of the transmitting antenna is a short Gaussian pulse. If we put a short wire-like receiving dipole at the observing point, it does the temporal derivative of the scattered wave. This nonlinear property will filter out the low frequency component of the scattered wave and some late-time pulses will be shown in the induced voltage. These late-time pulses are caused by the resonance of the structure and can be used to analyze the target.

UWB 12-2: Radar Signal Polarization Structure Investigation for Object Recognition

V. I. Koshelev, **E. V. Balzovsky**, **Y. I. Buyanov**, **P. A. Konkov**, **V. T. Sarychev**, **S. E. Shipilov**
Institute of High Current Electronics, RAS

A new approach for object recognition at sounding by ultrawideband (UWB) radiation pulses with linear polarization of electromagmetic field is suggested. The approach is based on the change of a polarization structure of the field scattered by an object. Recorded cross-polarized field components are used in the task of recognition jointly with the main polarization component. A discrepancy calculated with the use of the signal scattered by the object as well as signals from the data bank calculated for test objects is used as a recognition criterion. By means of numerical simulation there was created a bank of signals scattered from perfectly conducting test objects disposed at different angles relative to the incident wave front. The objects were round and square plates with dimensions of the order of a spatial pulse length. For the square plate two situations were considered. In the first case, the square plate diagonal was parallel to the incident wave polarization vector and in the second case the angle between the square plate diagonal and the incident wave polarization vector was of 45 degrees. For numerical simulation there was developed a code based on the finite-difference time-domain method allowing calculating a polarization structure of the electromagnetic field scattered from different three-dimensional perfectly conducting objects. The signals obtained by numerical simulation and consisting of the main and cross-polarized components were added by Gaussian noise with zero average one and the level up to 20% of the main signal component maximum. For their amplitudes and phases the discrepancies with amplitides and phases from the data bank were calculated.
It was determined that at the use of only the main signal component the objects are stably recognized (probability of correct recognition is more than 80%) at sounding over the angle range from 0 to 90 degrees at the noise level up to 5%. At the noise level of 20% stable object recognition was observed over the sounding angle ranges from 20 to 70 degrees when the ratio of the cross-polarized and the main components was near maximum. When sounding objects at the opposite angles α and $-\alpha$ it was determined that the main components of such signals were equal to each other while the cross-polarized components were different by sign. Thus, joint use of the main and cross-polarized field components allows distinguishing the objects similar by their shape that are sounded over a wide angle range at high noise levels.
To investigate experimentally the UWB pulse polarization structure, the vector receiving antenna (VRA) with improved characteristics has been developed on the basis of resistive dipoles. The VRA allows making simultaneous and small-distortion measuring of three coordinate components of a nanosecond pulsed electromagnetic field. By the voltages measured in the VRA channels, the godograph of the electric field vector E was plotted during a pulse. The error of determining the angular position of the vector E was no more than 2 degrees. Investigations of UWB pulse scattering at different objects that were carried out experimentally are compared with numerical simulation results.

UWB 12-3: Pole Estimation for Target Recognition via Late-time Transients

K. J. Pascoe[1], **W. D. Wood**[2], **P. S. Maybeck**[2], **A. W. Wood**[2]
[1]*Air Force Research Laboratory*; [2]*Air Force Institute of Technology*

Targets illuminated by ultra-wideband, short pulse radars have predictable properties in their late-time scattering that may be used to identify them. This work attempts to exploit these properties in a practical target recognition algorithm. Singularity Expansion Method theory predicts that the late-time return from a finite, perfectly conducting target is composed of a weighted sum of damped sinusoids whose frequencies of oscillation and damping are independent of target aspect angles (angles from which the target is viewed). However, the weighting coefficients of these terms are aspect-dependent. The focus of this work is to find the oscillation and damping frequencies (treated as imaginary and real components, respectively, of complex frequencies) for significant components of the late-time scattered signal. The complex frequencies correspond to poles in the Laplace domain. Poles are identified for simulated or measured late-time scattering from various targets using a novel variant of the Matrix Pencil Method (MPM), called the Modified Total Least-Squares Matrix Pencil Method (M-TLS-MPM). This method adds the low-rank Hankel approximation to the existing Total Least-Squares MPM (TLS-MPM) algorithm. M-TLS-MPM has less parameter estimation error in the presence of noise than TLS-MPM at the cost of a significant increase in the number of computations. M-TLS-MPM can also be used to suppress noise on a signal consisting of damped sinusoids. Selectively grouping and averaging the poles estimated from single-aspect measurements of a target produces an all-aspect signature. The signatures generated for several targets are used to develop filters for the target recognition algorithm, Maximum A Posteriori Multiple-Model Adaptive Estimation (MMAE-MAP), which is based on Kalman filtering. The MMAE-MAP algorithm was presented at AMEREM 2002. The target recognition technique employing M-TLS-MPM and MMAE-MAP is suited to identification problems where range to the target is short, such as classification of land mines and unexploded ordnance that may be shallowly buried or concealed in foliage. This technique may also be employed on targets that are concealed in baggage or behind walls. The views expressed in this article are those of the author and do not reflect the official policy or position of the United States Air Force, Department of Defense, or United States Government.

UWB 12-4: 100 GHz Broadband High Power Antennas

A. S. Podgorski
ASR Technologirs Inc., Ottawa, Ontario, Canada

The scientific programs conducted by the author in the past, were intended to permit an independent electromagnetic threat assessment, development of new testing methods and facilities and development of new standards. The aim was to establish a strategy that combines the threat estimation, hardening and testing for all naturally occurring and man made electromagnetic threats. Introduction of developed by the author, Composite Electromagnetic Threat concept that encompasses all threats, allowed a single threat definition permitting not only prediction of maximum possible threat in the present and future electromagnetic environment, but as well use of complementary time and frequency domain testing for easy and cost effective verification of hardening. However as a result of following the Composite Electromagnetic Threat concept, development of broadband electromagnetic technology spanning through frequencies extending from few kHz to 100 GHz became a necessity.
The unclassified technical review on HPM published in 1992, resulted in the author initiation of study to identify the limits of peak power levels, coupling mechanism of electromagnetic energies and sensitivities of equipment, so that the future electromagnetic protection requirements can easily be determined. From the experiments conducted it became apparent that to in-

flict a maximum damage with a minimum cost, the pulse excitation rather than continues wave excitation should be used in the microwave frequency region. As a result of our findings, we built the fastest, at the time, testing facility operating with a rise time of 100 ps and field levels of 100 kV/m. Later on, facility operating with a rise time of 10 ps and field levels of 1000 kV/m, was built.
The time and frequency domain electromagnetic measurements in the frequency range up to 100 GHz imposed the need for development of individual high gain, high power, high directivity broadband antennas capable of operating over many decades of frequency at once. Furthermore, the need for development of high power, high gain, high directivity broadband antenna arrays capable of operating up to 100 GHz became evident. The Presentation will demonstrate the latest achievements in the area of broadband antennas and antenna arrays, supported by modelling results obtained using the FDTD code. The emphasis will be directed towards the application of such antennas and arrays for:
- propagation, cross-polarization and scattering testing,
- time domain stealth material testing,
- EMI/EMC/EMP testing.
Furthermore, based on ability to generate and propagate the electromagnetic pulses in the frequency range where the attenuation of the propagated signal is the lowest, the application of 100 GHz broadband technology to development of the newest security/safety equipment, will also be addressed.

UWB 13 - Pulsed Power

UWB 13-1: A Marx-type Electromagnetic Pulse Generator

J. Ahn, **S. Song**, **J. Ryu**, **M. Jung**
Agency for Defense Development

Marx generators have been frequently used in power sources of electromagnetic pulse generators. The power and frequency spectrum of output pulses of pulse generators are closely related with characteristics of power source and antenna. We have investigated the characteristics of output pulses generated by an electromagnetic pulse source consisting of a Marx generator, a peaking gap switch and an antenna. The Marx generator produces pulses with relatively slow rise time of a few ns. The characteristics of output electromagnetic pulses are experimentally determined while changing operation time of the peaking gap switch installed in the antenna. Radiation amplitude and pattern of electromagnetic pulses are calculated by using a 3D simulation program and the results were used in designing antennas. The results of tests and computer simulations will be presented.

UWB 13-2: Fast Volume Breakdown in Argon and Air at Low Pressures

E. Crull, **H. Krompholz**, **A. Neuber**, **L. Hatfield**
Center for Pulsed Power and Power Electronics, Departments of Electrical & Computer Engineering and Physics

Fast volume breakdown with formative times in the few hundreds of picosecond regime is of interest for pulsed power switching and UWB applications. We have chosen a coaxial geometry for delivering fast rising high-voltage pulses to a spark gap that is designed to conserve an impedance of 50 ohms throughout the high-voltage carrying part of the test apparatus. Voltage sensors incorporated into the coaxial transmission line enable measuring the transient signals with $\approx$ 100 ps temporal resolution. We derive the current through and voltage across the spark gap from these transient voltage signals. For small pulse amplitudes, with risetimes of 400 ps, we have used a tip-plane geometry, with radii of curvature of 0.5 mm (tungsten tip). At pulse amplitudes of 5 kV, and macroscopic field enhancements on the order of 1000, delay times between current and applied voltage of less than 200 ps for pressures larger than 100 torr are observed, in both argon and dry air. Corresponding current risetimes $I/(dI/dt)$ are less than 100 ps. Different tip polarities cause a distinct difference in the dependence of the breakdown delay as a function of pressure. This is due to the strongly inhomogeneous field and a combination of gaseous ionization in the volume and explosive field emission from the tip in negative polarity. We achieve fast breakdown under more homogenous fields by utilizing a pulser with higher voltage output (RADAN 303B with pulse slicer SN4, risetime 150 ps at 150 kV amplitude). This enables us to compare the formative times for the tip-plane geometry with those of more homogeneous field distributions in the gap. This work is supported by AFOSR.

UWB 13-3: Modeling the Conductivity of a Subnanosecond Breakdown Gas Switch

J. H. Chen, **C. J. Buchenauer**, **J. S. Tyo**
Electrical and Computer Engineering Department, University of New Mexico

In our previous work (J. H. Chen, C. J. Buchenauer and J. S. Tyo. "Numerical and Experimental Modeling of Subnanosecond Plasma Closing Switches in Gases", 14th Int. Pulsed Power Conference, Dallas, Jun. 2003.), an ideal model is used to describe the dynamic closing plasma channel for a subnanosecond gas switch. The plasma channel current is assumed to be on the surface of a uniform cylinder. Several authors' studies show that the channel conductivity and radius vary dynamically. This variation results in dynamic impedance of the channel, and corresponding current and voltage that vary with time across the gap. All of the above parameters are hard to measure directly because of the small geometry and the high gap voltage and current on a subnanosecond time scale. Therefore, we have to develop a mathematical model to study the switch properties and compare it with experimental result.
In this paper, a Braginskii conduction model is used to describe the nonlinear dynamic plasma channel. Several references show that the resistive collapse of a very fast spark discharge in the gas is governed in large part by the radial expansion of a cylindrical shock wave, which rapidly increase the cross-sectional area of the conducting channel. At an initially very narrow channel joule heats the channel temperature and its pressure rapidly increases, which, in turn, drives a strong cylindrical shock wave into the undisturbed gas. If we assume that the hydrodynamic cooling associated with expansion, together with radiative cooling, is sufficient to keep the temperature of the conducting channel constant. Therefore, the plasma channel electrical conductivity almost keeps constant. The plasma channel radius is proportional to the integration of channel current.
The Braginskii model is simulated in Pspice, and then a switch is driven by the channel current generated by this model. Because of the discontinuous impedance of the switch, the reflected current from the switch, in turn, affects the development of the channel current and radius. An iteration method is used to find the final stable solution of the channel current. In every iteration step, the current drive the switch is simulated by the Finite Element Method in Time Domain (FETD). After that, the channel impedance, the voltage and current across the gap are also studied based on the simulated channel current. This work was supported by AFOSR under the MURI program and by Sandia National Lab under the Sandia University Research Program.

UWB 13-4: Compact Megawatt Pulsed Power Modules with Nano- and Picosecond Pulse Width

V. Efanov, **A. Kricklenko**, **A. Komashko**, **P. Yarin**
FID GmbH

A series of the compact size power modules is developed which allows generating the voltage pulses with the amplitude from 1 to 50 kV and the pulse duration from 100 ps to several nanoseconds. Their dimensions are from 50x25x25 mm to 250x125x60mm.
Power module FPM30-1
- Maximum output voltage: 30-50 kV
- Pulse duration: 0,5-1 ns
- Rise time: 100-150ps

- Power supply: DC/AC 2-2,5 kV
- Delay between the triggering pulse and the output voltage pulse: 150-200 ns
- Jitter: 40 ps
- Dimensions: 220x110x50 mm

A digital control block was designed to control the delays between modules. It allows adjusting delays with accuracy up to 20 ps.

Power modules feature high reliability and are capable to withstand short and open circuit modes. FID GmbH has developed several variants of power modules e.g. FPM20-10 which has maximum PRF of 10 kHz, maximum output of 20-25 kV, rise time of 150-200 ps.

UWB 13-5: High Repetition Rate Nano- and Picosecond Pulse Generators

V. Efanov, **A. Komashko**
FID GmbH

A series of high repetition rate nano- and picosecond pulse generators has been developed. The pulsers have ultra compact size and weight from 1 kg.

Pulse generator FPG 3-500K
Maximum output voltage into 50 Ohm: 3 kV
Rise time: 100-120 ps
Pulse duration: 200-1000 ps
Maximum PRF: 500 kHz
External triggering: 5-20 V, 100 ns

Pulse generator FPG 1-10M
Maximum output voltage into 50 Ohm: 500-700 V
Rise time: 0,2-0,3 ns
Pulse duration: 0,5-1 ns
Maximum PRF: 10 MHz
External triggering: 5-20 V, 100 ns

Pulse generator FPG 05-100M
Maximum output voltage into 50 Ohm: 50 V
Rise time: 100-120 ps
Pulse duration: 150-250 ps
Maximum PRF: 100 MHz
External triggering: 2-5 V, 3-5 ns

The pulsers are capable to operate into high bandwidth antennas. A synchronous operation of several pulsers with stability of 20-30 ps is possible.

UWB 13-6: Development of Ultra-Wideband Pulsers at the University of Texas at Dallas

F. Davanloo[1], **C. B. Collins**[1], **F. J. Agee**[2]
[1]*Center for Quantum Electronics, University of Texas at Dallas*; [2]*Air Force Office of Scientific Research, AFOSR/NE*

In recent years new fields of Bioelectric and Induced Gamma Emission have opened challenging applications for pulsed power research and development. The intracellular electromanipulation are bioelectric processes that require the development of reliable pulsed power sources that produce Ultra-Wideband (UWB) electric fields larger than 50 kV/cm at pulse durations into nanosecond range (K. H. Schoenbach et al., "Bioelectrics-New applications for pulsed power technology," IEEE Trans. Plasma Sciences 30, pp. 293-301, 2002). Such devices are also needed to generate pulses of x-ray of short durations for irradiation of isomeric targets for study of induced gamma reactions (C. B. Collins et al., "Tunable synchrotron radiation used to induce gamma-emission from the 31 year isomer of 178Hf," Europhys. Lett., 57, pp. 677-682, 2002).

The generic concept for ultra-fast pulsers at the University of Texas at Dallas (UTD) employs a Blumlein based pulse forming system commutated by a fast switching device. Characterization studies of these pulsers have been extensively performed at UTD and results indicate that they are capable of producing high power nanosecond waveforms with using a photoconductive switch (F. Davanloo et al., "Photoconductive Switch Enhancements and Lifetime Studies for Use in Stacked Blumlein Pulsers," IEEE Trans. Plasma Sciences 28, pp. 1500-1506, 2000).

The pulser design has been adapted to enable it to reliably produce powers as great as 100 MW, in nanosecond pulses with risetimes on the order of 200 ps. These devices have compact line geometries and are commutated by an avalanche GaAs photoconductive semiconductor switch (PCSS) triggered with a low power laser diode array. Significant lifetime improvements for PCSS have been achieved by advanced switch treatments with amorphic diamond coatings also developed at UTD.

This report presents the progress in the development and use of the ultra-fast pulsers at UTD. We explore the impedance parameter space in our modulator pulse forming lines to develop a reliable low impedance pulser capable of generating intense ultra-fast electric fields with nanosecond durations suitable for UWB applications such as Bioelectric. Emphasis will be placed upon resolution and understanding of the principal issues affecting the low impedance operation, compactness and waveform delivery to low impedance loads.

UWB 13-7: On the Spectral Variability of Ultra-Wideband High-Power Microwave Sources by Generating Pulse Sequences

J. Schmitz, **M. Jung**, **G. Wollman**
Rheinmetall W&M GmbH, Unterluess, Germany

A scalable ultra-wideband system consists of an antenna array and four semiconductor sub-ns sources, each of 1 kHz repetition rate, 30 kV output voltage and about 120 ps rise time. Measurements of one fully synchronized pulse or pulse sequences containing up to four pulses
with predefined delay T, are accomplished and compared to theoretical calculations with regard to spectral distribution of the electrical field strength. As a result it can be shown that pulse sequences optimize the spectral electrical field strength at $1/T$. A basic experiment demonstrates the influence of variable spectral field distributions on electronic circuits.

UWB 13-8: Compact Photoconductive Switches for Ultra-Wideband High Power Microwave Generation

N. E. Islam[1], **W. Nunnally**[1], **G. Tzeremes**[2], **J. A. Gaudet**[2]
[1]*Department of Electrical and Computer Engineering, University of Missouri, Columbia, MO, USA*; [2]*Electrical and Computer Engineering Department, University of New Mexico, Albuquerque, NM, USA*

A photoconductive semiconductor switch (PCSS) can be operated in both linear and non-linear modes in applications ranging from firing sets to drivers for lasers. At high fields and in the non-linear mode the switches have also been used in the generation of ultra wideband high power microwaves (UWB-HPM). These PCSSs largely employ semi-insulating gallium arsenide (GaAs) as the material of choice [J. S. H. Schoenberg, J. W. Burger, J. S. Tyo, M. D. Abdalla and M. C. Skipper and W. R. Buchwald, IEEE Trans. Plasma Sci., vol. 25, p. 327, 1997].

In high-field applications, however, GaAs photoconductive switches have been plagued by premature breakdown and the number of switching operations has been limited to less than 105 shots, before burnout occur. The role played by the intrinsic traps in the breakdown process has been investigated [N.E. Islam, E. Schamloglu, G. M. Loubriel, F. J. Zutavern and A. Mar, Ultra Wideband Short Pulse Electromagnetic V, Plenum Press, 2000] and the use of the trap characteristics for improved device performance have also been discussed [E. Schamiloglu, N. E. Islam, J. Agee, Material Science Vols. 384-385, pp249-252, Trans Tech., Switzerland, 2002]. Problems however still remain and there is a need to find alternative PCSS materials with improved high-field characteristics. Silicon carbide (SiC) is an excellent candidate for high power, high frequency electronic devices that operate at high temperature and radiation environment.

In this paper we discuss a novel PCSS fabricated from semi-insulating SiC that is being tested at the University of Missouri-Columbia for use in a high electric field configuration. High electric field geometry is made possible by employing sub-

bandgap energy photons and inter-bandgap dopants / defects inherent in the switch material. Semi-insulating SiC is compensated in much the same manner as semi-insulating GaAs in that the bandgap structure has a number of intergap energy levels that can be controlled during the growth process and that determine the optical absorption depth for photon energy less than the band gap. In V:SiC, for example, V forms two deep levels, an acceptor at E_C=0.97 eV and a donor at E_C=1.6eV (4H-SiC) [M. Bickermann, D. Hofmann, T. L. Straubinger, R. Weingartner, and A. Winnacker, "On the preparation of Vanadium-Doped Semi-Insulating SiC Bulk Crystals", Mat. Sci. Forum, Vols. 389-393, 2002, pp. 139-142. and J. Grillenberger, N. Achtziger, G. Pasold, and W. Witthuhn, "Polytype Dependence of Transition Metal-Related Deep Levels in 4H-, 6H-, and 15R-SiC", Mat. Sci. Forum, Vols. 389-393, 2002, pp. 573-576].
The high field, long absorption depth package used in experiments at the University reduces the required linear mode, optical closure energy and also reduces the conduction current density through the active material and at the contacts. Thus the probability of breakdown is reduced. The paper also discusses the experiments, the parameters of semi-insulating SiC materials and methods of fabricating such materials into a high power photo-switch.

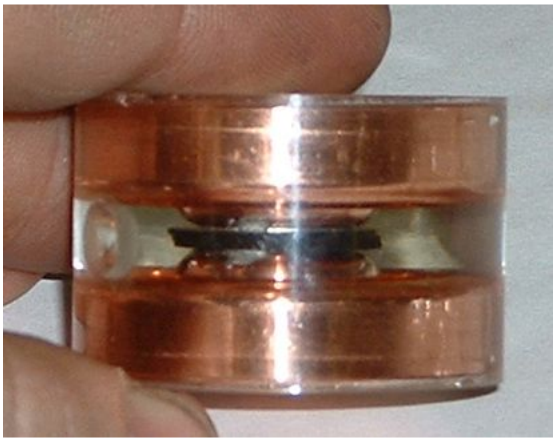

Figure 1: Silicon carbide (SiC) photoconductive switch package for high field applications

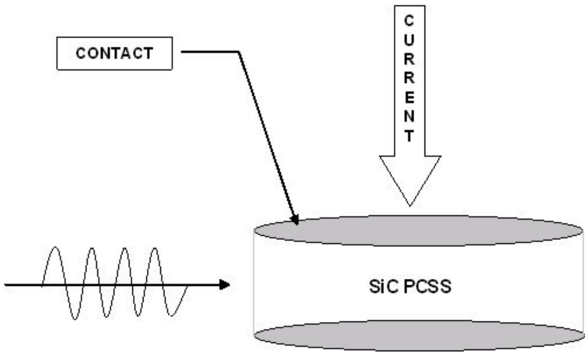

Figure 2: Conduction process in the high-field photoconductive switch

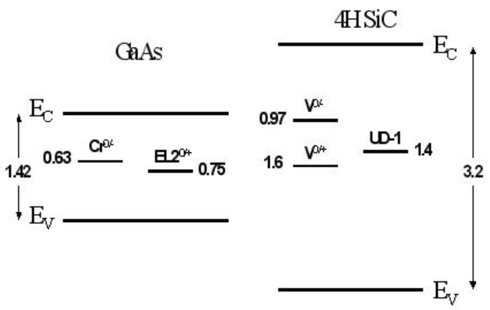

Figure 3: Bandgap structure for GaAs and 4H-SiC

UWB 13-9: Gigawatt All-Solid-State Nano- and Picosecond Pulse Generators for Radar Applications

V. Efanov, A. Kricklenko, A. Komashko, P. Yarin
FID GmbH

A series of all-solid-state multi-channel pulse generators with a pulse duration of about 1 ns and rise time of about 150-200 ps has been developed. A total peak power of the generators reaches 1 GW. The number of channels can vary from two to several tens. Jitter between the channels is not more than 30-40 ps.
The pulsers of the FPG series are capable to withstand short and open circuit mode, as well as operate with any types of antennas. The variants of pulse generators with the pulse repetition frequency higher than 1 kHz and output of up to 100-200 kV are possible.
High voltage pulse generator FPG 50-1MC4
- Maximum output voltage into 50 Ohm: 50-60 kV
- Number of channels: 4
- Rise time: 150-200 ps
- Pulse duration: 1 ns
- Maximum PRF: 1 kHz
- Size: 500x500x200 mm

High voltage pulse generator FPG 10-2MC16
- Maximum output voltage into 50 Ohm: 10 kV
- Number of channels: 16
- Rise time: 150-200 ps
- Pulse duration: 1-1,5 ns
- Maximum PRF: 10 kHz
- Size: 500x500x200 mm

UWB 14 - Electromagnetic Theory

UWB 14-1: Embedding Multiple Wires within a Single TLM Node

P. Sewell, K. Biwojno, Y. Liu, C. Christopoulos
George Green Institute for Electromagnetics Research, The University of Nottingham

Transmission Line Modelling, TLM, is an established technique for simulating electromagnetic fields in a wide variety of application areas. As with any numerical algorithm, the complexity of the problem that can be practically dealt with is determined by the availability of computational resources.
Particularly demanding of resources are simulations that involve a diverse range of physical scales, all of which have a discernable impact on the results of the simulation and which therefore must be adequately modelled. One recurring illustration of this, typical of EMC predictions, is the inclusion of thin wires in simulations of large-scale objects and where a significant volume of empty space must be modelled.
Previously, a specific TLM node has been developed that allows a single thin wire to be analytically embedded with one of the TLM nodes; centrally in 3D and arbitrarily placed in 2D, [P. Sewell, Y. K. Choong and C. Christopoulos, "An Accurate Thin-Wire Model for 3D TLM Simulations," IEEE Trans. Electromag. Compat., vol . 45, pp 207-217, 2003. Y. K. Choong, P. Sewell and C. Christopoulos "Accurate modelling of an arbitrary placed thin wire in a coarse mesh," IEE Proceedings- Science, Measurement and Technolog. ,vol 149, pp250 – 253, 2002]. In this work we extend this formulation to provide a 2D TLM node that can include an arbitrary number of arbitrarily placed thin wires within one cell and which are coupled by their near fields. This is of particular interest for simulating cabling looms as well as for consideration of certain classes of micro-structured materials.
The technique proceeds by identifying a set of local analytical solutions for the fields in the vicinity of the multiple wires and for each determining the relationship between the tangential electric and magnetic fields on the surface of the node. This set is interfaced with the fields from the adjacent TLM nodes, yielding an algorithm that is both explicitly stable and conservative as well as incurring only a minor computational overhead.
Results will be presented for a range of practical configurations

as well as a discussion of the generalisation of the approach to include other small features within the node.

UWB 14-2: Simulation of Nonlinear Integrated Photonics Devices: A Comparison of TLM and Numerical Time Domain Integral Equation Approaches

T. Benson, **A. Al-Jarro**, **P. Sewell**, **V. Janyani**, **J. D. Paul**, **A. Vukovic**
George Greeen institue for Electromagnetics, University of Nottingham

Numerical techniques are essential for the design and simulation of modern integrated photonics devices. Time domain models are becoming more popular as bandwidths increase and with the need to account for complex material properties such as nonlinearities. The Finite Difference Time Domain, FDTD [1] and Transmission Line Modelling, TLM [2], methods are eminently suited to this task in all but one aspect, computationally efficiency. For physically large structures, the need to directly discretise the full problem space inevitably leads to a voracious consumption of memory and prohibitively long run times. Notwithstanding this, the ease with which complex geometries and nonlinear and dispersive materials can be included explains the prosaic use of these techniques.
In addition to FDTD and TLM, it is possible to construct numerical algorithms from a Volterra Integral Equation formulation of the fields in the time domain, TDVIE [3,4]. Such schemes only necessitate direct discretisation of the fields in regions that differ from a known background medium, albeit including sufficient time history. Consequently, it is simple to envisage scenarios where TDVIE will require significantly less memory to perform a simulation. For example, determining the behaviour of small, coupled micro-resonators. One further advantage offered by these schemes is that the kernels of the Volterra equations intrinsically satisfy the radiation conditions at infinity, negating the need to explicitly construct absorbing boundaries.
To date, 1D TDVIE formulations have been demonstrated to be capable of dealing with complex material behaviour as well as with time varying materials, as might be found in switches, modulators and lasers. Recently, a full 3D scheme has also been developed that extends the approach to truly realistic geometries.
The objective of this work is to illustrate the capability of the TDVIE approach and to establish guidelines for its selection in preference to FDTD or TLM.

References

1. A. Taflove and S. Hagness, Computational Electrodynamics: The Finite-Difference Time-Domain Method, Artech House, 2000.
2. C. Christopoulos, The Transmission Line Modelling Method: TLM, IEEE Press, 1995.
3. F.V. Fedotov, A.G. Nerukh, T.M. Benson and P. Sewell, "Investigation of Electromagnetic Field in a Layer with Time Varying Medium by Volterra Integral Equation Method" Journal of Lightwave Technology, Vol. 21, 305-314, 2003.
4. A. Al-Jarro, P. Sewell, T.M. Benson and A. Nerukh, "Effective and flexible analysis for propagation in time varying waveguides", Optical and Quantum Electronics, in press.

UWB 14-3: Circuit Based Full-Wave Models for Non-Uniform Line Structures Created with the Method of Partial Elements

S. V. Kochetov, **G. Wollenberg**
Otto-von-Guericke-University Magdeburg

Increasing operational frequencies, high changing rates of currents and voltages, high packaging densities of electronic devices and components, and an enormously increasing density of electromagnetic noise sources often require advanced modeling of interconnection structures. The required models have to be exact in two basic areas. At first they have to be precise in modeling the electromagnetic phenomena in interconnections, secondly the models have to be able to include the circuit environment of the interconnection system in the simulation process. For precise modeling of interconnections at high operational frequencies one should use full-wave models considering also the skin and proximity effects in conductors as well as losses in their dielectric materials (e. g. multilayer PCBs). As circuit environment of the interconnection system we understand arbitrary circuits composed of linear and non-linear lumped elements. Because non-linear loads can cause distortions and phenomena of intermodulation an exact modeling such objects can be principally important for many problems.
The conventional transmission line theory [1] allows to create very effective numerical procedures on the basis of the Bergeron method. The method of equivalent circuits [2] provides effective models for the skin effect. However, the disadvantage is the limitation to 2D field problems (quasi TEM mode) and, as consequence, the inability to treat radiation effects.
The most widespread differential methods applied to interconnection modeling are the Finite Difference Time Domain Method (FDTD), Transmission Line Matrix Method (TLM), Finite Elements Method (FEM), and Finite Integration Technique (FIT) [3,4]. To all of them several commercial and educational programs have been created. The main characteristics of differential methods are the simplicity of treating inhomogeneous media, the possibility for modeling arbitrary complex configurations of conductor stuctures, and the need to discretize the entire volume for which the electromagnetic problem has to be solved (closed problem). In the case of open EM problems boundary conditions are to be applied and, in this case, the volume which has to be analyzed, can essentially increase. Additionally, not all models created by differential methods can be computed within the non-linear circuit environment.
The best known numerical integral method for simulation of interconnections is the Method of Moments (MoM) [1]. The MoM is the a widespread numerical tool in the traditional EMC practice. Using the MoM is preferable in analysis of open problems with essentially radiating interconnections. The main disadvantage of the MoM is the absence of the possibility for computations in the time domain at a non-linear circuit environment.
The best way for taking into account a non-linear circuit environment is the circuit based full-wave modeling. The modern state of the art shows us four basic directions for doing it: insertion of macromodels derived from from full-wave solutions into the circuit simulator, extraction of equivalent circuits from models provided by any full-wave code, creation of full-wave generalized telegrapher theory [5] and using the Partial Element Equivalent Circuit (PEEC) method [6].
The PEEC method developed by A. Ruehli is a suitable approach for analysis considering the above explained problems. The PEEC method gives a possibility to create full-wave models of interconnection systems in the time and frequency domain so that non-linear elements of the circuit environment can be included.
After a short explaining the PEEC method the report is devoted to using the PEEC method for modeling line structures with both internal and external excitations. Two examples are considered. The first one deals with the coupling an external plane wave into a system of transmission lines with linear and non-linear loads. In the second example the signal delay and distortion caused by printed delay lines of spiral and serpentine types are analyzed on the basis of PEEC full-wave models in the time domain.

[1] M.V.Ianoz, F.M.Tesche, T.Karlsson, EMC analysis method and computational models, J.Wiley&Sons, Inc., New York., NY.,1977, 623 p.
[2] N.V.Korovkin, S.V.Kotchetov, E.E.Selina, M.Ianoz Simulation of frequency characteristics of transmission lines for transient calculations, in Proc. 13th Int. Zurich Symp. On Electromagnetic Compatibility, Zurich, Switzerland, Feb. 16-18, 1999, pp 84M4.
[3] A.F. Peterson, S.L. Ray, R. Mittra, Computational methods for electromagnetics, IEEE Press, New York, NY.,1998, 564 p.
[4] C. Christopoulos, The Transmission-Line Modeling Method TLM, IEEE Press, New York, NY.,1995, 220 p.
[5] Haase, H.; Nitsch, J., Investigation of nonuniform transmission line structures by a generalized transmission-line theory., in Proc. 15th Int. Zurich Symp. On Electromagnetic Compatibil-

ity, Zurich, Switzerland, Feb. 2003, p. 597-602.
[6] A. E. Ruehli, Equivalent circuit models for three-dimensional multiconductor systems, IEEE Trans. Microwave Theory Techn., Vol. 22, March 1974, pp. 216-221

UWB 14-4: On the Non-Uniqueness of the Electric Field Components –Static, Induction or Intermediate, and Radiation - From Extended Source Distributions

R. Thottappillil
Division for Electricity and Lightning Research, Uppsala University, Sweden

The problem of calculating the electric and magnetic fields from a known source distribution is discussed extensively in literature. Usually the fields are calculated by using scalar and vector potentials. These potentials are directly related to the source distribution. Two equivalent approaches to calculating the electric fields produced by a specified source is discussed here. The commonly used first approach, the so-called dipole technique or Lorentz condition (LC) technique, involves the specification of current density, the use of current density to find the vector potential, the use of vector potential and the Lorentz condition to find the scalar potential, and the computation of electric field using vector and scalar potentials. In this technique, the source is described only in terms of current density, and the field equations are expressed only in terms of current. The use of the Lorentz condition eliminates the need for the specification of the charge density along with the current density and assures that the current continuity equation, which is not explicitly used in this technique, is satisfied.
The second approach, the so-called monopole technique or the continuity equation (CE) technique (or the Jefimenko approach), involves the specification of current density (or charge density), the use of current density (or charge density) and the continuity equation to find charge density (or current density), the use of current density to find vector potential and charge density to find scalar potential, and the computation of electric field using both vector and scalar potentials. In this technique, the source is described in terms of both current density and charge density, and the field equations are expressed in terms of both charge density and current density. The current continuity equation is needed to relate the current density and charge density. There is no need for the explicit use of the Lorentz condition in this technique, although properly specified scalar and vector potentials do satisfy the Lorentz condition.
Total electric field is uniquely determined using either of these approaches, but the individual field components, identified as static, induction (or intermediate), and radiation components are not unique between these two approaches. In the LC technique the gradient of the scalar potential completely determines the static and intermediate components and contributes a portion to the radiation component. The time derivative of the vector potential also contributes to the radiation field. In the CE technique the gradient of the scalar potential completely determines the static and intermediate components and do not contributes to the radiation component. The radiation field is completely given by the time derivative of the vector potential. The differences between the field components in the two techniques are discussed in this note. For the clarity of discussions the field components are derived for a line source distribution, in which the line is fixed at one end and the other end may extend with certain speed, as in the model for lightning return stroke. The current and charge on the line are general functions of space and time. The work presented here is the continuation of the work in (R. Thottappillil, V. A. Rakov, On different approaches to calculating lightning electric fields, Journal of Geophysical Research, 106, 14191-14205, 2001.)

UWB 14-5: Hybrid TLM Partial Wave Expansion Method for Time-Domain Modeling of Wideband Antenna Structures

P. Lorenz, P. Russer
Lehrstuhl fuer Hochfrequenztechnik, TU Muenchen

The Transmission Line Matrix (TLM) method is a very powerful numerical technique for the modeling of complex electromagnetic structures with general source distribution. For the wideband antenna simulations, the use of a time-domain method is appropriate since it allows the characterization of the antenna over a broad frequency by a single pulse response simulation.
In the case of antenna simulation we have to consider the radiated field. To do this the problem space is subdivided in two parts, i.e. subspace 1 represented by a sphere surrounding the antenna and subspace 2, which is the space outside the sphere. In subspace 1 the electromagnetic field is modeled via the TLM method, whereas in subspace 2 the electromagnetic field is expanded in orthogonal spherical partial waves. At the spherical boundary between subspaces 1 and 2 the tangential electric and magnetic field components are matched.
With this hybrid approach we can compute all the parameters of the antenna by just one simulation run. The input impedance, radiated power, radiation pattern and gain are obtained in the whole frequency range.
* The input impedance is calculated from the time dependent voltage and current at the input port (terminals) of the antenna. Using the Fourier transform, the time dependent voltage and current are transformed to frequency domain.
* The total radiated power is computed as a sum of all the active powers associated with every radiation mode. Due to the expansion of the electromagnetic field into orthonormal spherical modes in subspace 2 the numerical effort for this part of the computation is low.
* Radiation patterns are calculated directly from the superposition of the spherical modes in subspace 2. Transforming the time dependent modal amplitudes to frequency domain, we obtain the frequency dependence of the radiation pattern and the antenna gain.
Conclusion: A novel hybrid method for time-domain simulation of broadband antennas is presented. The method allows to compute pattern, gain and impedance over the whole band by a single simulation run by simulation and postprocessing of the impulse response.

UWB 14-6: Transient Diffraction by Boundary of Two Lossy Dielectrics in a Waveguide

A. Y. Butrym[1], Y. Zheng[1], O. A. Tretyakov[2]
[1]*Kharkiv National University, Kharkiv, Ukraine*; [2]*Gebze Institute of Technology, Gebze, Turkey*

A basic problem of transient diffraction by a plane boundary between two lossy magnetodielectric media in a waveguide is considered in Time Domain (TD). The solution to this problem in Frequency Domain is well known. However, to consider transient signal propagation it is desirable to know the impulse characteristics for this structure.
The solution can be applied in EMC problems, such as impulse signal penetration via shielding that has a hole with a thick dielectric seal. Moreover, since wave propagation in a waveguide is governed by the same equation that describes wave beam propagation in free space, the obtained solution is also applicable to the problem of 3D impulse wave beam diffraction by a half space of lossy dielectric. This problem is important in modelling ground penetrating radar.
A generalised scattering matrix approach in TD is used to present the solution in the form of convolution type transmission and reflection operators that map an incident wave at the interface into boundary derivatives of the reflected and transmitted waves. The reflected and transmitted waves propagation can be then easily calculated by convolution the obtained boundary derivatives with corresponding propagation operator. In this form the diffraction operators has comparatively simple form be-

ing expressed via bessel functions of the first and zero order and their convolution with sine and exponential function. To obtain more convenient form connecting wave amplitudes (not derivatives) one have additionally to convolve the operators with bessel function of zero order.

Electromagnetic fields in a waveguide can be expanded into mode series with expansion coefficients (mode amplitudes) satisfying the Klein-Gordon equation. A convolution equation for the mode amplitudes of the diffracting waves at the interface can be obtained by imposing boundary conditions. It is solved analytically by Laplace transform thus yielding closed-form expressions for the diffraction operators. These operators consist of singular and regular parts, the former describes a prompt response of the structure, while the latter describes a resonant late-time part of the response. In the case of lossless dielectrics the singular parts coincide with Fresnel's formulae since they can be obtained by reducing the Klein-Gordon equation to the wave equation (by removing the dispersion term).

The special case of iso-impedance media needs separate consideration because the common solution has uncertainty 0/0. It appears that the singular part of the reflection operator vanishes in this case, thus no prompt response occurs. At that, the regular part is non-zero, so resonant reflection still takes place. In another special case of iso-refractive media the field at the boundary are connected algebraically so only prompt response is presented in the diffracted fields and no additional signal distortion occurs.

The solution is illustrated with energy flow space-time diagrams, as used by H. G. Schantz [IEEE AP Magazine, Vol. 43, No. 2, 50-62, April 2001]. In these diagrams both energy density and energy flow speed can be traced in each space-time point.

At the end we would like to notice, that the more common problem of wave diffraction by longitudinal dielectric distribution in a waveguide has been solved with wave-splitting technique by W. Weston [S. He, S. Strom, and W. Weston, Time-Domain Wave-Splitting and Inverse Problems, Oxford Univ. Press, 1998]. A complex non-linear operator equation has been obtained for the reflection operator. In contrast, we consider here a simpler problem, which has analytical closed-form solution. The main result of this contribution is a closed-form presentation of the diffraction operators for the considered problem and their thorough analysis in TD.

UWB 14-7: TEM Field Structure of Electric and Magnetic Fields From a Semi-Infinite Vertical Thin-Wire Antenna Above a Conducting Plane

R. Thottappillil[1], **M. A. Uman**[2]

[1]*Division for Electricity and Lightning Research, Uppsala University, Uppsala, SWEDEN*; [2]*Department of Electrical and Computer Engineering, University of Florida, Gainesville, USA*

The electric and magnetic field structures around a semi-infinite thin-wire antenna vertically placed above a perfectly conducting ground plane are investigated when the antenna is supporting two different types of sources, static sources and time-varying sources. It is shown that when the wire is carrying a uniform line charge, the electrostatic potentials are equal on the surfaces of imaginary cones of fixed cone angles with axis along the wire and apex at the conducting plane. The electrostatic field vectors are shown to be perpendicular to the imaginary cones and tangential to the meridian lines of half-spherical shells centered at the base of the line charge. The vertical components of the electrostatic field on the surface of these imaginary half-spherical shells of a given radius are constant, except at the wire itself. The magnetic field structure associated with a constant current in the semi-infinite antenna is that of an infinite wire. The electric and magnetic fields due to a time-varying point source at the bottom of the antenna have a field structure identical to that for the case of a uniform line charge and a uniform current, and have a spherical transverse electromagnetic (TEM) field structure. Simple, but exact, expressions for electric and magnetic fields are derived, and it is shown that the general expressions for the electric and magnetic fields from time-varying sources on a thin wire semi-infinite antenna reduce to the same simple expressions if the source is assumed to be a current or charge pulse travelling at speed of light and without attenuation. In that case, the Poynting vector is in the r-direction, which indicates energy flow in the radial direction from the source at the bottom of the antenna. That is, in this ideal case the only source of radiation is the point source at the bottom of the antenna and the vertical antenna itself does not radiate. The wave impedance at all distances from this antenna is the free space impedance. Finally, a general discussion on TEM type solutions in different structures containing two perfect conductors is provided.

The work presented in this paper is a continuation and extension of the works listed below.

[1] Uman, M. A., D. K. McLain, and E. P. Krider, The electromagnetic radiation from a finite antenna, Am. J. Phys., 43, 33-38, 1975;

[2] Thottappillil, R., J. Schoene, and M.A. Uman, Return stroke transmission line model for stroke speed near and equal that of light, Geophysical Research Letters, 28, 3593-3596, 2001;

[3] Thottappillil, R., M.A. Uman, Reply to the 'Comment on "Return stroke transmission line model for stroke speed near and equal that of light by R. Thottappillil, J. Schoene, and M.A. Uman' " by G. Kordi, R. Moini, and V.A. Rakov, Geophysical Research Letters, 29, May 2002;

[4] Thottappillil, R., and V.A. Rakov, On different approaches to calculating lightning electric fields, Journal of Geophysical Research, 106, 14191-14205, 2001.

UWB 14-8: Impulse Wave Propagation in Transversely Inhomogeneous Closed Waveguide

A. Y. Butrym[1], **O. A. Tretyakov**[2]

[1]*Kharkiv National University*; [2]*Gebze Institute of Technology, Gebze, Turkey*

An analytical method for solving the problem of transient signal propagation in an inhomogeneous waveguide with factorised medium parameters f(x,y)f'(z,t) is described. The method is based on separation of transversal and longitudinal-time coordinates but without preliminary exploitation of Fourier transform. The framework of the method is as follows. A self-adjoint transversal derivative operator is separated from within Maxwell's equations. Then the sought fields are expanded into series on eigenmodes of this operator. A system of partial differential equations with longitudinal coordinate z and time t as independent variables is obtained for the expansion coefficients. This System of Evolutionary Equations (SEE) describes transient wave excitation and propagation in an inhomogeneous waveguide in the Time Domain (TD). It can be solved either numerically on a 2D mesh in z-t domain, or analytically by restricting the number of equations, applying Laplace transform, solving the resulted system of ordinary differential equations, and transforming the results back into TD.

It should be noted that the separated transversal derivative operator contains transversely dependent factors of permittivity and permeability of the waveguide filling and no frequency parameter (since no Fourier transform has been used). So, the obtained waveguide modes are frequency independent, orthogonal, take into account transverse medium distribution and, hence, they are a natural basis for field expansion. They are actually E- and H-waves. It should be noted as well that conductivity is not included in the operator and may be non-factorised.

For harmonic signals the proposed approach has advantages as well. If harmonic space and time dependence is supposed, the SEE is reduced to a system of linear algebraic equation (SLAU) with complex mode amplitudes as unknowns, while propagation constant and frequency are parameters and appears linearly or quadratically. This SLAU yields characteristic equation and mode configuration in all the frequency range. At that, for lossless medium the characteristic equation is a polynomial in squared frequency and propagation constant. Consequently, this method can be applied for fast FD analysis of waveguides along with recently proposed similar matrix techniques [L. Rozzi et al. IEEE Trans. MTT, vol. 45, p. 345-353], [E. Silvestre et. al. IEEE Trans. MTT, vol.48, p. 589-595].

Turning back to the SEE we note that in the case of transversely uniform distribution of index of refraction all modes are independent and the SSE splits into Klein-Gordon equations. In the general case the SEE can be presented as a Klein-Gordon equation with matrix coefficients and additional term describing mutual transformations of E- and H-waves. The coefficients depends on longitudinally dependent factors of medium parameters.

For numerical study we consider a rectangular waveguide with longitudinal dielectric slab. This structure admits analytical solution for the eigenvalue problem for mode determination. The SEE coefficients also can be presented in a closed-form. Solving the SLAU for harmonic signals case we have obtained the same dispersion curves as can be obtained by familiar LM-LE-wave formulation in FD. In such way the method has been validated. The next step is to consider pulse wave propagation in this waveguide. In contrast to the case of a hollow waveguide there are some problems with splitting waves into incoming and outgoing ones. So, we consider the problem with excitation by modal currents. Some numerical results on mode structure changing with propagation will be presented.

UWB 14-9: Radiation of Oscillating Dipole Moving in Dielectric with Resonance Dispersion

A. V. Tyukhtin
Department of Radiophysics, Saint-Petersburg University. Ul'yanovskaya, 1, Petrodvorets, Saint-Petersburg, 198504, Russia. E-mail: tyukhtin@pobox.ru

This work deals with radiation of oscillating electric dipole that moves in dielectric with resonance frequency dispersion. It is noted that radiation of moving oscillators were analyzed relatively seldom (see, for example, I.M.Frank, Vavilov-Cherenkov Radiation, 1988). Such problems in the case of the medium with resonance dispersion have not been considered previously. We use the Drude-Lorentz model of medium. It is supposed that dielectric has a single resonance frequency and the conductivity is negligible. It is noted that radiation of moving charge in such medium was analyzed extensively in papers (G.N.Afanasiev, V.G.Kartavenko, Journal of Physics D, 1998, vol.31, p.2760; G.N.Afanasiev, V.G.Kartavenko, E.N.Magar, Physica B, 1999, vol.269, p.95). The dipole is supposed to be harmonic; its electric dipole moment is parallel to the motion velocity. We obtained analytical expressions for the components of electromagnetic field. Furthermore, some formulas for the spectral density of radiation power have been found. Special attention has been given to the approximate and numerical analyses of this characteristic and the total radiation power.

Approximate analytical description of main properties of the radiation has been carried out for some particular cases. In the first one the frequency of dipole oscillations is supposed to be essentially greater than the resonance frequency. If it is greater than Langmuir frequency as well, so the radiation spectrum consists of two frequency ranges. One of them lies near the resonance frequency (resonance range). Another range lies near the frequency of oscillators (own range). In described conditions the power of resonance radiation is essentially less than the power of own radiation. However, if the frequency of the oscillator is less than the Langmiur frequency, so own radiation disappears, and resonance radiation exists as before.

In the second case the frequency of oscillator is supposed to be essentially less than the resonance frequency. In this case two alternatives take place as well. For some parameters we have two separate frequency ranges. It is interesting that each of them may be dominant. For alternative parameters of the problem these ranges are combined, and we have a total range of radiation frequencies. In this case the spectral density of radiation power has either single maximum or two maxima. The dominant maximum takes place for resonance frequency.

Some numerical computations were carried out by the use of the obtained exact formulas. Their results illustrate extraordinary phenomena that take place for oscillator moving in the medium with resonance dispersion.

UWB 14-10: Radiation of Moving Charges in Waveguide Structures Containing Dielectric with Resonance Dispersion

A. V. Tyukhtin
Department of Radiophysics, Saint-Petersburg University. Ul'yanovskaya, 1, Petrodvorets, Saint-Petersburg, 198504, Russia. E-mail: tyukhtin@pobox.ru

Problems of radiation of charged particles moving in vacuum channels and waveguide structures were analyzed in many publications (see, for example, B.M.Bolotovskiy, Uspekhi Fizicheskikh Nauk, 1961, vol.75, p.295; A.S.Vardanyan, G.G.Oksuzyan, Technical Physics, 2002, vol.47, p.448). However, the role of the concrete dispersive characteristics of media were not considered. Here we study the situation when the medium is a dielectric possessing resonance dispersion. It is supposed that the dielectric has a single resonance frequency and the conductivity is negligible. It is noted that the radiation of charge moving in unbounded medium with analogous properties was analyzed extensively only in last years (see, for example, G.N.Afanasiev, V.G.Kartavenko, E.N.Magar, Physica B, 1999, vol.269, p.95).

This work deals with three problems.

1. Radiation of the point charged particle that moves along the axis of vacuum channel in the dielectric with resonance frequency dispersion is investigated. In particular, it is shown that the maximum of spectral density of radiation energy is shifted to lower frequencies with increase of the radius of the channel. The obtained results are compared with ones for the case of nondispersive dielectric. It is noted that for ultra-relativistic velocity of charge motion the dispersion influence is small at low frequencies. However, at high frequencies the spectral density of radiation energy is essentially less than in the case of the medium without dispersion. The total radiation energy loss is essentially less than one in the case of nondispersive dielectric if the velocity of charge motion is sufficiently large.
2. Radiation of the charged particle that moves along the axis of the circular waveguide with dispersive dielectric is investigated. It is shown that the resonance dispersion influences significantly on the frequencies of harmonics and radiation energy. For example the dispersion depresses all harmonics, and this effect increases with the number of harmonic. In the case of thin waveguide the maximum energy is expended in radiation of the first harmonic, and the energy loss decreases with increase of harmonic number. In the case of sufficiently thick waveguide the energy maximum falls on the harmonic with the number being not equal to 1. This number increases with the radius of waveguide.
3. Radiation of the charged particle that moves along the axis of the waveguide structure is studied. The structure is a circular waveguide that has the cylindrical layer of dispersive dielectric and the circular vacuum channel. The waveguide axis coincides with the axis of the channel. The special attention has been given to the case of ultrarelativistic motion of the charge. It is noted in particular that the influence of the medium dispersion may be essential even for very thin dielectric layer.

The obtained results show that the resonance dispersion of the medium has a principal influence on Vavilov-Cherenkov radiation in waveguide structures.

UWB 15 - Antennas for UWB Communication

UWB 15-1: Characterisation of UWB Antennas by their Spatio-temporal Transfer Function based on FDTD Simulations

D. Manteuffel, **J. Kunisch**, **W. Simon**, **M. Geissler**
IMST

As any other complex rf-system that has to be brought to the market within a short development process, the design of UWB systems requires numerical simulations in an early stage where no prototypes are yet available and different implementations have to be tested. For UWB systems, the demands for the antenna are not limited to large bandwidths only. Other quality criteria, like low ringing and gain stability over the frequency range, are often requested [1] and are of course affected by the specific implementation of the antenna in the user environment. In this paper a concept for the efficient characterisation of UWB antennas based on an FDTD calculation using EMPIRETM software in combination with signal processing techniques is presented. It is the basic idea to consider the antenna as a LTI (Linear Time-Invariant) system completely characterized by its spatio-temporal transfer function [1, 2]. In order to assess the transmit transfer function it is sufficient to perform the EM simulation of the antenna only in a small nearfield region if the farfield characteristics is calculated by a nearfield-to-farfield-transformation. Using Lorentz' principle of reciprocity, the receive transfer function is calculated from the prior assessed transmit transfer function. Based on the transfer functions all other quality measures can be calculated [1]. In particular it is possible to predict the antenna performance in a realistic user environment by a numerical simulation.

In order to proof the above approach, the transmission between two identical biconical antennas is calculated by two methods. For the first method both antennas are modeled in the computational domain. While the first antenna is excited by a Gaussian pulse (1 GHz $< f <$ 20 GHz) the second is positioned in a distance of 50 cm and receives the field radiated by the first antenna. This allows the calculation of the transmission in terms of s_{21}. For the second method only the farfield characteristics of one antenna is calculated by a FDTD simulation. The transmit and receive transfer functions of the antenna are determined using the above approach [2]. Therefore the transmission between two virtual antennas can be calculated by equation 1.

In equation 1 A_1 is the transmit transfer function of the transmit antenna and h_2 is the receive transfer function of the receive antenna assuming that the antennas are separated by the distance d. The comparison of the results from both methods in Fig. 2 shows a good agreement. This proves the implemented method and allows the calculation of all quality measures of interest based on the transfer function of the antenna.

[1] W. SÖRGEL, CH. WALDSCHMIDT, W. WIESBECK: Transient response of Vivaldi antenna and logarithmic periodical dipole array for ultra wideband communication. In: AP-S – International Symposium on Antennas and Propagation, Proc. on CDROM, Columbus (Ohio) USA, 2003

[2] J. KUNISCH, J. PAMP: UWB radio channel modeling considerations. In: Proc. Of ICEAA'03, Turin, Sep. 2003

$$s_{21}(\omega) = \left.\frac{b_2}{a_1}\right|_{a_2=0} = \vec{A}_1\left(\hat{\vec{k}}_{12},\omega\right)\cdot\vec{h}_2\left(\hat{\vec{k}}_{12},\omega\right)\frac{e^{-jk_0 d}}{d}$$

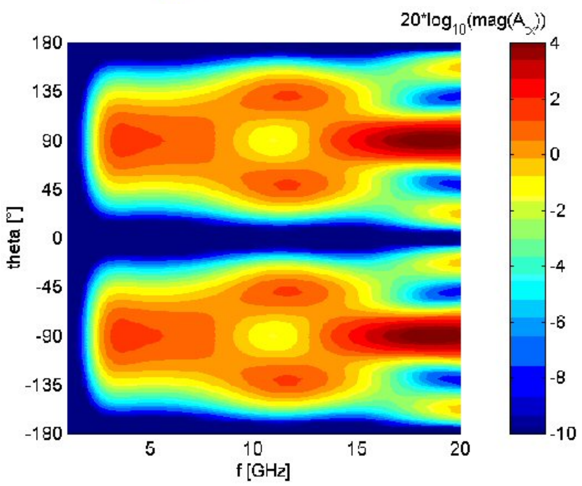

Figure 1: TX transfer function of the biconical antenna in the E-Plane.

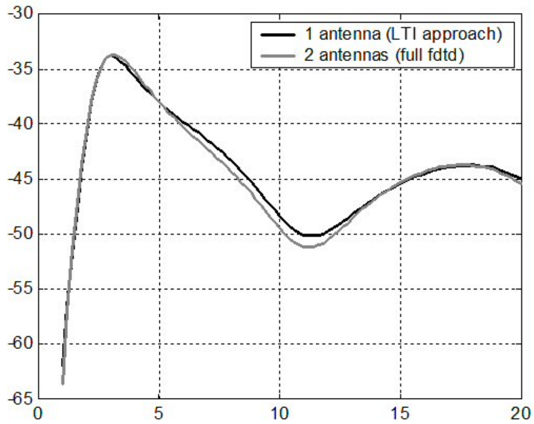

Figure 2: Transmission between two biconical antennas positioned at 50 cm distance. Presented approach vs. full analysis.

UWB 15-2: A Novel Methodology Combining Antennas, Propagation and Non-Linear Switching Circuits in Transient Time-Domain Simulation

S. Zwierzchowski[1], **M. Okoniewski**[2]
[1]*Gnostar Inc./University of Calgary*; [2]*University of Calgary*

For many decades, the conventional methods of characterizing antennas within systems have proven adequate for radio system and circuit design–even though the associated free space path loss has a very counter-intuitive fictional frequency dependency. This has been acceptable for the relatively narrow bandwidths that systems have typically operated in. Today this still holds for multi-band UWB given the bandwidths used. However, for short-pulse UWB communications where the pulse spectrum occupies several giga-hertz, the conventional methods of antenna characterization are inadequate. To address this difficulty, several authors (W. Sörgel, et al; Z.N. Chen, et al; J. D. Kraus, et al; S.J. Zwierzchowski, et al) have proposed various transfer function definitions to associate with an antenna. This paper addresses the usefulness in circuit and system design of one such antenna transfer function definition which was first presented by Zwierzchowski at the International Symposium on Antennas and Propogation 2003 (S.J. Zwierzchowski, et al, "A Systems and Network Analysis Approach to Antenna Design for UWB Communications", 2003). This antenna transfer function (referred to as Hant-ATF in this paper) is defined by the signal flow diagram shown in Figure 1. The Hant-ATF has been shown to be a genuine characteristic of antennas as attested to by Figure 2 (Zwierzchowski, et al, "Derivation and Determination of the Antenna Transfer Function for Use in UWB Communications Analysis", 2003). In Figure 2, the Hant-ATF for a dipole and equivalent monopole antenna is plotted as determined theoretically, empirically, and from computational electromagnetics (CEM) using FDTD simulation.

As introduced in this paper, using the Hant-ATF's for a system's transmit and receive antennas, UWB short pulse systems can be completely and accurately simulated in a highly integrated approach from the transmitter through to the receiver–from end to end–at a circuit design level. Very importantly, this statement holds for transient/Spice simulations of transmitter and receiver circuits that contain non-linear switching elements. Once the Hant-ATF has been determined for a given set of transmit and receive antennas, the Hant-ATF's can be incorporated into a non-linear switching circuit simulation as shown in Fig 3. Figure 3 presents the Agilent ADS simulation schematic for a step recovery diode circuit that generates a fast (50ps) rise-time edge. Applying this sharp edge to a transmit antenna results in the reception of a pulse out of a receive antenna. The antennas in this simulation are represented by 2-port S-parameter-type network blocks which are based on the antenna model given in Figure 1. The data used for the Hant-ATF's contained in the 2-port network blocks can be determined from theory, CEM simulation, or measurement, as shown in Figure 2. The spreading and time delay corresponding to free-space propagation is represented by an additional 2-port S-parameter box. Agilent ADS incorporates S-parameter network blocks in its time domain transient simulation through convolution of the associated impulse responses of the network blocks. The transient time-domain simulation results for the circuit of Figure 3 using ideal dipole antennas and using a monopole (MP) and conical monopole (CM) are shown in Figures 4(a) and 4(b) respectively. Actual measured results for a circuit similar to that of Fig. 3 with the MP and CM antennas are shown in Fig. 4(c).

The simulation methodology presented in this paper can be extended to provide EIRP's and to model multipath channels containing complex frequency dispersive behaviour. EIRP can be determined from a spectral analysis and scaling with frequency of the signal at the output node (labeled EIRP) of the transmit antenna in Fig 3. Multipath channels can be modeled by extending the 2-port models for the antennas to n-port models where the number of direct and reflection paths is n-1. Frequency dispersive propagation can be modeled by an appropriate S-parameter block for a given propagation path. Thus, building on the methodology presented in this paper, very elaborate simulations can be achieved of short-pulse UWB systems that contain many circuit elements, noise effects, complicated antennas, realistic propagation modeling, and signal processing.

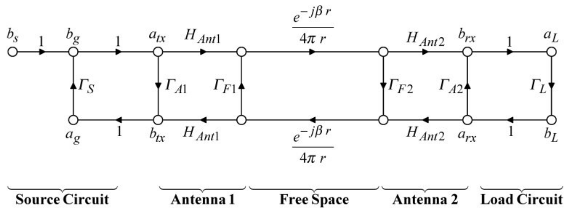

Figure 1: Signal flow diagram defining the Hant antenna transfer function.

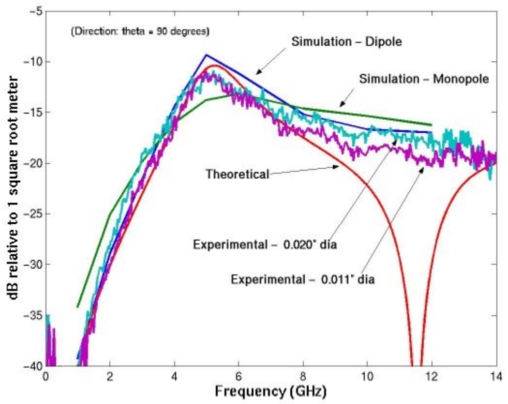

Figure 2: The antenna transfer function Hant for a 26mm dipole/ 13mm monopole as determined analytically, from FDTD simulation, and empirically.

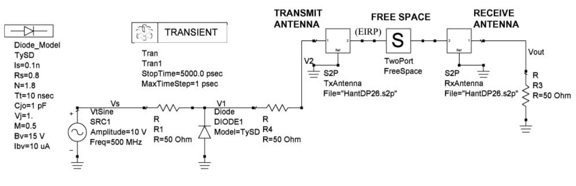

Figure 3: Agilent ADS transient/Spice circuit simulation combining step-recovery diode transmitter circuitry, the Hant antenna transfer function of transmit and receive antennas, and receiver circuitry.

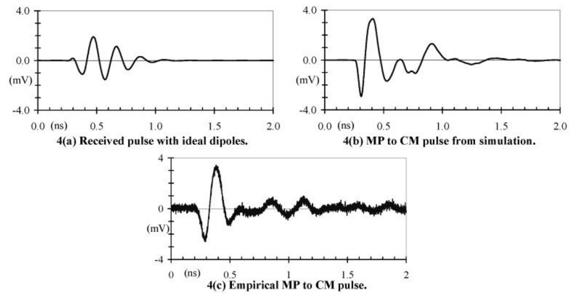

Figure 4: Received pulses (a)(b) as predicted from ADS Spice/transient simulation employing Hant and (c) as measured experimentally.

UWB 15-3: Characterising Impulse Radiating Antennas by an Intuitive Approach

J. Sachs[1], **P. Peyerl**[2], **P. Rauschenbach**[1], **F. Tkac**[1], **R. Zetik**[1]

[1]*TU Ilmenau*; [2]*Meodat GmbH*

The task of an antenna is to transform a guided wave into a free wave and vice versa. By that, antenna characteristics should also describe how the antenna spreads the signal energy over the solid angle and how the temporal shape of the signal (respectively its complex spectrum) is influenced.

Physically, an antenna is a spatially distributed object. In most of the practical applications however such as for communication links, radar or positioning - it is usually modelled as a point object, which is considered as the source of the radiated wave. For simplicity, in most current applications, the radiation is supposed as a spherical wave having constant properties within the antenna beamwidth. However, these assumptions are not acceptable for sophisticated scenarios which require high spatial resolutions.

A complete and exact characterisation of antenna behaviour is given by their spatial impulse response function (sIRF) respectively the (complex valued) spatial frequency response function (sFRF). However, this will result in a considerable computational burden if they are completely respected for SAR- or positioning algorithms. Therefore, it is often desirable to have a computationally less expensive solution available which only refers to specific parameters of the sIRF instead of the complete (multi-dimensional) function.

The paper provides the definitions of some selected parameters of interest such as:

a) Centre of radiation (a global "phase centre" of the antenna)

b) Internal delay

c) Weight pattern (comparable to the classical gain pattern)

d) Coherence pattern

e) Spherical deviation pattern etc.

It will be shown that these parameters depend to a certain extent on the signal processing and the method of signal detections (peak, square root etc.) applied in the receiver. Thus, there is no unique parameter set which characterises the antenna. It is therefore useful to consider the antenna in connection with its "signal processing environment". Within the article some measurement examples will be given with a description of the IRA-test facility. It will be shown, through an example, how the precision of a positioning system can be improved by respecting appropriate antenna parameters.

UWB 15-4: Optimal Antenna and Signal Co-design for UWB Antenna Link

A. O. Boryssenko, **D. H. Schaubert**

Antenna & Propagation Lab, University of Massachusetts at Amherst

UWB link system needs to be designed to send signals of pulsed energy between transmit and receiver antennas under several rigid constraints of: (1) finite energy available for transmitting antenna, (2) maximum energy efficiency of transmitter, (3) max-

imum available signal intensity in receiver, (4) very sharp shape of received voltage, (5) flat broadly spread spectral density of radiated field, (6) matching to several regulations on spectrum using/sharing (the FCC frequency mask etc.). Such demanding and often mutually conflicting requirements need to be implemented through using of (1) antennas of different uncomplicated geometries (dipoles, biconical, horn, patch, tapered-slot etc.) and (2) some simple (preferred digital) circuitries used in both the UWB transmitter and receiver front-end electronics.
We propose a design strategy to UWB antenna link that accounts complexity of analysis for geometry of real antennas with operation on multipart scenes where the antennas are disturbed by nearby bodies and the blockage, multipath, antenna moving and other factors can effect strongly on the UWB link features. To this end, a full-wave Method of Moment simulation is employed in time/frequency domain to compute numerical transfer functions for the radiated field at any spatial points and the received voltage in the receiver load. Such a numerical model can be computed for any antenna geometry and arbitrary location of such antennas and nearby bodies over any UWB link scene. Then, pulse transition between the antennas is explored in post processing mode for different possible pulse shapes. The designer has to choose among the formers such pulses that could satisfy in a compromise manner the above constraints and could be relatively simple for their implementation through a low-cost circuitry.
Thus, co-design of antenna and front-end circuitry for supporting a particular optimal (nearly optimal) UWB signaling schema can be provided. For example, a twofold windowing technique is applicable in frequency and time domain to simplify a pulse shape (A.O. Boryssenko, D.H. Schaubert, Efficient and Practical Pulses for Dipole Antenna UWB Link, submitted to 2004 IEEE Ant. Propagat. Symp.). For such pulses the product of time duration by bandwidth is nearly equal to one. So, processing gain in the receiver can be achieved if the received pulsed is compressed in time, correlated with reference pulse shape and time-gating is employed to the correlated output. Essentially, optimization of the UWB link performance could be based on some criteria (D. Pozar, Waveform Optimization for Ultra-Wideband Radio System, IEEE Trans. on Ant. & Propag., Vol. 51, pp. 2335-2345, September 2003). Also, a combined numerical analysis is possible to simulate in time-domain both the electromagnetic part, viz. antennas, and nonlinear electronics of the transmitter and driving circuitry.
Basically, two simple pulse generating circuitries are required for both the transmitter and receiver and two different and usually complicated pulse shapes are necessary for functioning of the transmitter and receiver. In the case of transmitter, an optimal pulse needs to drive it efficiently in terms of power taken by the transmit antenna from the driver and delivered to the receiver standpoint. Such low complexity drivers need to be in focus with special intent to their digital realization because of low-cost and inherent performance repeatability. It is vital also to support a simple shape of the received pulse for the receiver end of the UWB link. In this case, an impulsive waveform needs to be generated and used as reference in a correlation receiver. On the whole, the waveforms in the receiver differ from a canonical shape like Gaussian monocycle (R. Scholtz, M.Z. Win, Impulse Radio, IEEE PIMRC'97). However, the waveforms can be well localized in time and feasible for their digital generation. In this way, a high signal-to-noise ratio can be achieved and an increased detectable range for the receiver can be provided.
Thus, the optimal pulse transmission through a UWB 2-antenna link is considered and illustrated through simulation. Several key geometries of antennas and operational scenarios are investigated to create the required UWB links. Several effects of geometry of antennas on the achievable UWB link performance are explored. Also, different operational factors like effects in the near field of antennas, applying the FCC spectral mask, antennas' blockage and multipath are simulated and evaluated. A number of cases of near-optimal co-designs of antenna, front-end circuitry and signaling schema are presented and discussed in the full paper version.

UWB 15-5: Antenna Effects and Modelling in UWB Impulse Radio

C. Roblin, **A. Sibille**
ENSTA

Introduction:
This communication intends to tackle several questions raised by the behaviour of the antennas and the propagation channel in the Time Domain (TD) of UWB (Ultra Wide Band) impulse radio:
1. How to model the UWB antennas, and mainly their TD (or FD) response, since unlike in the narrow band case, they operate as multidimensional linear filters (they are represented by a transfer function H for each direction of space $(\hat{r}, f)$). A subsidiary question arises here: how to characterize the antennas efficiency? Although it is not a fundamental theoretical question, it is very important in practice: such a transfer function holds a huge amount of data, is difficult to manage in practice and, moreover, is probably not necessary if we address the overall system from a statistical point of view.
2. What is the relative impact of the antennas behaviour (gain and dispersion/distortion) and the channel characteristics (mainly regarding multipath density) on the overall system performances?
In the transmitting mode, the antenna is fully characterized by the vector transfer function as defined in equation (1). Note that $|H|$ squared is nothing else than the effective (or realized) gain (which takes into account the input mismatch).
In the receiving mode, the reciprocity theorem states that the transfer function H^r defined by equation (2) is related to H by equation (3). Eventually, the transfer function H_{21} for the case of the 2-antennas system in free space is given by equation (4). In the TD, the antenna is characterized by the (vector) impulse responses h (Fig. 1), which are the inverse Fourier transforms of the previous functions [Ch. Roblin, S. Bories, and A. Sibille: Characterization Tools of Antennas in the Time Domain, IWUBS, Oulu, Finland, June 2-5 2003].
Data compression:
From the point of view of data storage and handling, we propose to represent the antenna response with an IIR filter bank, computed from the impulse responses with the classical and simple Steiglitz-McBride algorithm (Fig. 1, Eq. 5). The obtained compression factors range from about 4 to 10 or more, depending on the requested precision and on the impulse response time duration (the longer the spreading the more efficient is the compression). In order to reach even more important compression factors, a statistical approach of the modelling is under progress. This approach is based on the observation that the channel is only known statistically, so that one can seriously cast doubt on the necessity to know the antennas deterministically.
Antenna effects on the system as regards the channel characteristics:
The purpose is here to evaluate how antennas affect the performance of an impulse radio link, evaluated through the signal to noise ratio (SNR) assuming AWGN at the output of the correlator, and in comparison with that of an ideal antenna ($G(f)$=1). In order to isolate the antenna gain and antenna distortion effects, several normalizations of the transfer function w.r.t. the case of an ideal antenna are introduced: none (includes antenna gains), fixed received energy in an ideal channel (removes both gains), and constant EIRP (removes the Tx gain). The chosen impulse waveform has a transmitted spectrum compliant with the FCC mask (for a distortionless antenna), and the reference template used to perform the correlation is either the ideal received signal (ideal antenna & channel) or the signal actually received for a pure LOS case (antenna filtered template).
The cumulative probabilities of the normalized SNR (Fig. 2) are evaluated for various antennas (measured log-periodic & monocone-like antennas, and simulated horn) and various channels (IEEE-CM1 & CM4, measured LOS & NLOS). The observation of the results leads to the following partial conclusions: 1 - the SNR is almost always worse for real than for ideal antennas, 2 - the behaviour depends on the channel multipath density (interplay between antenna dispersion and channel dispersion),

3 - In general, the SNR is degraded when the ideal reference template is used, and less or not degraded when the antenna filtered template is used, 4 - the SNR degradation is smaller for the monocone than for other antennas (lowest distortion), 5 - unexpected SNR improvement can occur as the result of antenna limited bandwidth.

(1) $\mathcal{H}(\hat{\mathbf{r}}, f) = \frac{\mathbf{A}(\hat{\mathbf{r}}, f)}{a_1(f)}$

with : $\mathbf{A}$ the amplitude of the radiated far field $\mathbf{E}(\hat{\mathbf{r}}, f) = \frac{e^{-jkr}}{r}\sqrt{\frac{\eta_0}{4\pi}}\mathbf{A}(\hat{\mathbf{r}}, f)$, $\hat{\mathbf{r}} = \frac{\mathbf{r}}{r} = (\hat{\theta}, \hat{\varphi})$ the unit radial vector, a_1 the complex **incident** partial wave, and $k = \frac{2\pi}{\lambda} = \frac{2\pi f}{c}$ the wave number.

(2) $b_2(\hat{\mathbf{r}}, f) = \mathcal{H}^r(\hat{\mathbf{r}}, f) \cdot \mathbf{A}_{pw}(f)$ with : $\mathbf{A}_{pw}$ the *amplitude density* of the incident plane wave $\mathbf{E}_{pw}(\mathbf{k}) = e^{j\mathbf{k}\cdot\mathbf{r}}\sqrt{\eta_0}\mathbf{A}_{pw}(f)$

(3) $\mathcal{H}^r = -j\frac{\lambda}{\sqrt{4\pi}}\mathcal{H}^t$ with : $\mathcal{H}^t = \mathcal{H}$

(4) $H_{21} = \frac{b_2}{a_1} = \frac{e^{-jkr}}{r}\left(\frac{-j\lambda}{4\pi}\right)\mathcal{H}_{Tx} \cdot \mathcal{H}_{Rx}$ with : $\mathcal{H}_{Tx}$ (resp. $\mathcal{H}_{Rx}$) the transfer functions in the transmitting mode for the Tx (resp. Rx) antenna.

(5) $\mathcal{H}(\theta, z) = \frac{\sum_{n=0}^{N_b} b_{n+1}(\theta) z^{-n}}{\sum_{m=0}^{N_a} a_{m+1}(\theta) z^{-m}}\hat{\theta}$ for the simplified case of omni-directionality and linear polarization.

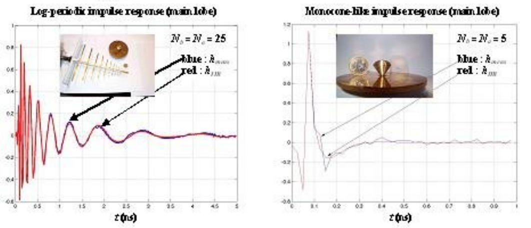

Fig. 1 : (blue) impulse response in the main lobe of a log-periodic antenna (left) and a monocone antenna (right) ; (red) comparison with IIR filter responses.

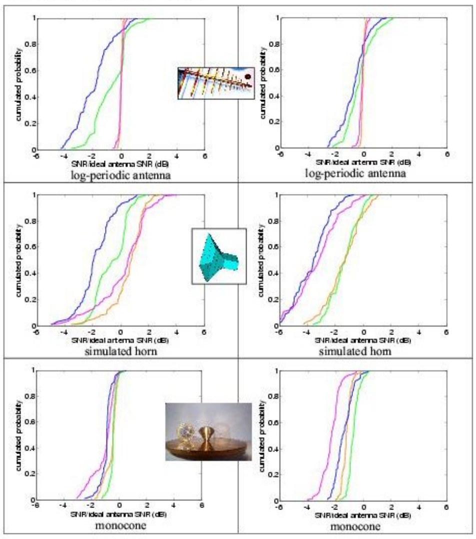

Fig. 2 : distribution of SNR with respect to ideal antennas ; IEEE channels ; left : IEEE-CM1; right : IEEE-CM4 ;

UWB 15-6: UWB Beamforming in Realistic Channel Scenarios

T. Kaiser, **C. Buchholz**, **G. Yang**
University Duisburg-Essen, Bismarckstrasse 81, 47048 Duisburg, Germany

UWB and multi-antenna techniques belong to the few emerging key technologies in wireless communications. Due to their complementary features its wedding seems worth to be investigated. For example, even for a highly frequency-selective UWB-channel the well-known "frequency-flat" equation

$$C = NB\log_2(1 + SNR),$$

where N is the number of transmit and receive antennas, B is the used bandwidth and SNR the signal-to-noise ratio, holds approximately true [1],[2]. Hence, the data rate can be N-fold if N transmit and N receive antennas are used. In this contribution we will focus on one multi-antenna technique, namely beamforming. Beamforming enables range extension due to additional array gain, reduced receiver complexity due to lower delay spread, and allows more users due to interference cancellation. In order to study the principal behaviour of UWB beamforming, previous contributions (e.g. [3]) imply a classical Gaussian monocycle for the received pulse shape. However, this assumption is rather unrealistic, first because of multipath propagation and second because of mismatch to regulated spectral masks. For that reason, we will draw the bow starting with Gaussian monocycles, continuing with impulse shapes satisfying the FCC and the temporary ETSI mask and ending up with taking into account a spatial multipath channel. Note that the current IEEE 802.15.3a UWB multipath channel model does not cover spatial aspects(see [4]), a straightforward extension is based on [5] and given by the angle-variant impulse response

$$h(t,\theta) = \sum_{l=1}^{L}\sum_{k=1}^{K}\alpha_{k,l}\delta(t - T_l - \tau_{k,l}, \theta - \Theta_l - \vartheta_{k,l}), \quad \tau_{1,l} = 0.$$

Here, l enumerates the clusters and k is the ray index within each cluster. $\alpha_{k,l}$ defines the multipath coefficients, T_l denotes the arrival time of the l^{th} cluster and $\tau_{k,l}$ is the delay of the k^{th} ray within the l^{th} cluster. The mean angle of arrival in cluster l is specified by Θ_l, consequently $\vartheta_{k,l}$ is the angle of the k^{th} ray in cluster l relative to Θ_l. The probability densities of all these parameters can be found in [4],[5]. The following figure shows a time and angle of arrival estimator (ToA and AoA, respectively) based on a broadband sum and delay beamformer. The numerous dots on the ground plane indicate the true time and angle of arrival of any incident ray, hence multipath propagation is fully taken into account. The z-axis represents the normalized beamformer output energy averaged over 50ns for arbitray true AoA. It can be cleary seen that not only the ToA but also the AoA can be resolved with satisfactory resolution. Hence, beamforming is feasible even in highly frequency-selective UWB channels. The final presentation of this work will cover a thorough investigation about the impact of the various parameters, e.g. number of antennas, antenna spacing, pulse shapes, etc., on the accuracy of beamforming-based time and angle of arrival estimation.

[1] Zheng Feng, Thomas Kaiser and Andreas Czylwik, "On the Evaluation of Channel Capacity of Multi-Antenna UWB Indoor Wireless Systems - Part I: Frequency Flat Case", submitted to IEEE Transactions on Communications.

[2] Zheng Feng, Thomas Kaiser and Andreas Czylwik, "On the Evaluation of Channel Capacity of Multi-Antenna UWB Indoor Wireless Systems - Part II: Frequency Selective Case", submitted to IEEE Transactions on Communications.

[3] Thomas Kaiser, "On UWB Beamforming", Kleinheubacher Tagung, Session on "Efficient Communication Systems using Smart Antennas", September 29-October 2, 2003, Kleinheubach, Germany.

[4] A. Molisch, J. Foerster, M. Pendergrass, "Channel Models for Ultrawideband Personal Area Networks", IEEE Wireless Communications, December 2003, pp. 14-21.

[5] Q. Spencer, B. Jeffs, M. Jensen, A. Swindlehurst, "Modeling the Statistical Time and Angle of Arrival Characteristics of an Indoor Multipath Channel", IEEE Journal on Selected Areas in Communications, Vol 18., No. 3, March 2000, pp. 347-360.

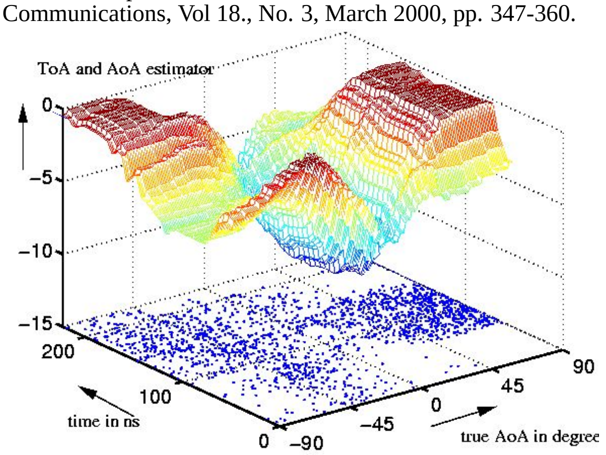

Figure 1: UWB beamforming for ToA and AoA estimation under multipath propagation

UWB 15-7: An Ultra Wideband Aperture Coupled Bow Tie Antenna for Communications

W. Soergel, C. Waldschmidt, W. Wiesbeck
Institut für Hoechstfrequenztechnik und Elektronik, University Karlsruhe (TH), Germany

Spectrum is presently one of the most valuable goods worldwide as the demand is permanently increasing and it can be traded only locally. Since the United States Federal Commission on Communication (FCC) has opened the spectrum from 3.1 GHz to 10.6 GHz, i.e. a bandwidth of 7.5 GHz, for unlicensed use with up to -41.25 dBm/MHz EIRP numerous applications in communications and sensor areas are showing up: the ultra wideband radio technology promises high resolution radar applications, sensor networks with a large number of sensors for industrial or home surveillance as well as high data rate communication over short range for personal area networks (PAN).
For applications like UWB sensor networks and PANs there is a need for small and efficient UWB antennas. The antennas have to be well matched to the signal source since multiple reflections between amplifier and antenna will create a perceptible ringing. The antenna radiation and receiving characteristics ought to be stable over the whole frequency range. The transient radiation characteristic should exhibit as low dispersion as is needed for a good system performance. It is often said, that a UWB antenna should avoid a balun because of its large size and its possible bandwidth limitations. In the following an UWB antenna concept, which is based on a symmetric bowtie structure, is fed by an integrated balun structure with a coaxial SMA port. The antenna consists of two triangular radiating elements of which one serves as ground plane for the tapered feed line that ends with a broadband stub (see fig.1). The feeding structure couples the energy from an asymmetric micro-strip line emerging from the coaxial connector to the radiating elements through the aperture formed by the tips of the triangles. Therefore the antenna is called Aperture Coupled Bow Tie Antenna, ACB. The investigations carried out have shown that this antenna concept can provide a return loss below –9 dB from 3–10 GHz. This has been proven for different realizations with typical over all dimensions of 36x31 mm (ACB36) and 24x20 mm (ACB24). In general the antenna gain, especially for lower frequencies, decreases rapidly for smaller antenna size, therefore realizations of the concept with 19x18mm are possible, but have a very low gain. The antenna gain can be increased by attaching a metal patch in 5 mm distance to the backside of the antenna, however the return loss is strongly affected by this parasitic element. In figure 1 an example realization on DUROID 5880 is shown. The front metallization consists of two triangles, which are not totally symmetric in order to compensate for the influence of the SMA connector. Figure 2 shows the reflection coefficient at the coaxial port for two examples. Figure 3 shows the gain pattern in azimuth and elevation for the ACB36. The antenna impulse response (Baum, "General Properties of Antennas", Sensor and Simulation Notes, Note 330, 1991) is analyzed also in the azimuth and elevation planes. The antenna exhibits very good impulse radiating characteristics with a FWHM of 163 ps in the main beam direction.

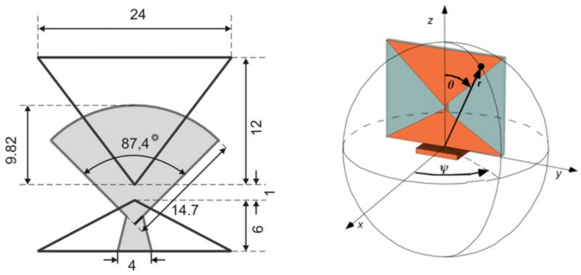

Figure 1: Left side: example for an aperture coupled bow tie antenna (ACB24) on DUROID 5880 substrate. Right side: coordinate system with model of ACB36.

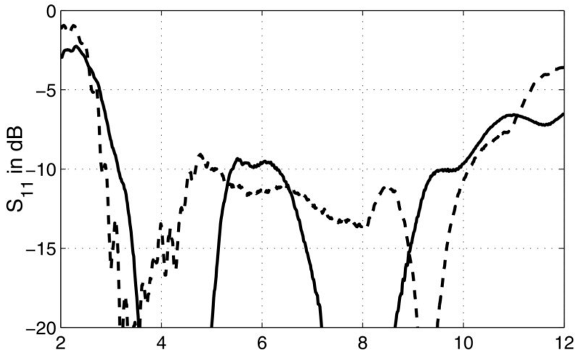

Figure 2: Measured input reflection coefficient S_{11} for ACB24 (solid line) and ACB36 (dashed line).

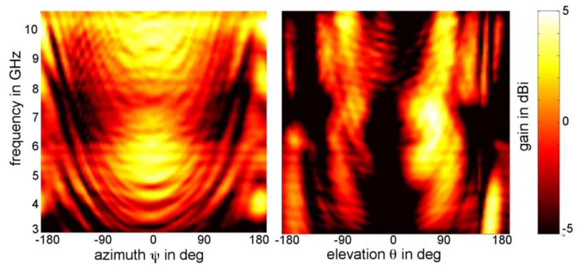

Figure 3: azimuth ($\theta = 90°$). Right side: elevation ($\psi = 0°$). The maximum gain is 5.3 dBi at 7.2 GHz.

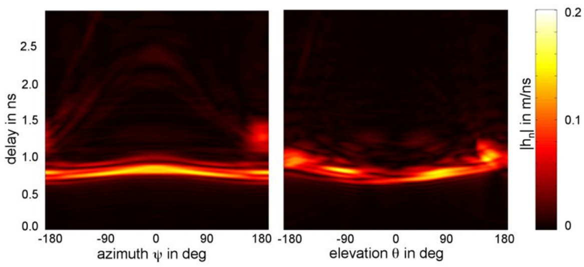

Figure 4: Measured magnitude of antenna impulse response plotted versus delay time and direction. Left side: azimuth ($\theta = 90°$). Right side: elevation ($\psi = 0°$).

UWB 15-8: Small Patch Antennas for Ultra-Wideband Wireless Body Area Network

M. Klemm, G. Tröster
Electronics Laboratory, ETH Zürich

Abstract – This paper presents the transient characteristics of an Aperture-Stacked Patch Antenna (ASPA) and its miniaturized version. These two antennas were designed for Ultra-wideband (UWB) Body Area Network (BAN) applications. They operate within the 3-6 GHz frequency band. The first APSA has planar dimension 32/19 mm, the second one (miniaturized version) 23/16 mm. This gives 40% reduction of the antenna surface. Time- and frequency-domain characteristics of this antenna were calculated for transmission mode (Tx) and for the complete 2-antenna (Tx-Rx) system. We have used 3 different waveforms to drive the antenna: gaussian pulse (duration-250 ps), monocycle pulse (duration-300 ps), defined waveform (duration-650 ps). The received pulses has very similar shapes (fidelity >90%), but they differ in the voltage amplitudes. This shows that constraining the maximum voltage of different input waveforms to the same value, the highest received voltage will be achieved for the pulse, which has the closest spectrum to the antenna's transfer function characteristic. In our case received pulses have maximum voltage of 0.064, 0.091 and 0.158 V for a gausian, monocycle and defined excitation (max. voltage limited to 1 V), respectively.
Taking into account good transient characteristics of our ASPAs,

but also some practical advantages (e.g. small size, possibility of integration into the clothing) we see this antenna as a very good candidate for UWB wireless Body Area Network (T. Zasowski el.al., 'UWB for Noninvasive Wireless Body Area Networks: Channel Measurements and Results', 2003) applications.

1. Introduction

Ultra-wideband (UWB) communication systems have recently received more and more attention in the wireless world. Their envisioned advantages over conventional wireless communication systems are: extremely low power consumption, high data rates and simple hardware configuration. UWB radio is characterised by a wide signal spectrum and low radiated power spectral density. The most interesting approach of the UWB radio system is so-called impulse radio [3]. Its basic concept is to transmit and receive very short electromagnetic pulses (few tens of picoseconds to few nanoseconds in duration).

Antennas play a critical role in UWB communication systems since they influence the complexity of the receiver and transmitter (pulse generator) designs. Its design is even more challenging for UWB wearable devices. The antenna is mounted on the human body and more aspects are of great importance: antenna dimensions, possibilities of integration into the clothing, human body influence on the antenna characteristics and also on the short-pulses propagation.

We aimed our research interests at antennas for non-invasive Wireless Body Area Networks (WBAN). WBAN nodes are usually placed close to the body, on or in everyday clothing. It has some distinct features from other wireless networks, which are also constraints for antenna designs: close proximity of the human body (electromagnetic 'pollution' should be extremely low), low transmitting power, possibly low radiation towards body. From the practical point of view, aperture-stacked patch microstrip antenna is a very attractive candidate for WBAN applications (is small and compact, do not radiate significant power into the human body). Moreover, its wideband matching and radiation characteristics were reported (S.D. Targonski el.al., 'Design of Wide-Band Aperture-Stacked Patch Microstrip Antennas', 1998.). To make sure that ASPA is suitable for UWB (pulsed) WBAN, we have investigated its transient characteristics. We are also interested in a smallest possible antenna in wearable applications, thus we designed the miniaturized version of 'normal' APSA.

2. Antenna design

The geometry of the aperture-stacked patch microstrip antenna is shown in Fig. 1. It differs from typical aperture-coupled patch antennas in that a larger aperture and thicker substrates with low dielectric constants have to be used. Because the aperture in the ASPA is also used as a radiator, dual-offset tuning stubs control the coupling from the feedline. Length and distance between them are one of the important parameters to achieve broadband characteristics.

For our application, we have designed the ASPA for a frequency range from 3 to 6 GHz, considering the input matching. Smaller design of ASPA was done by applying 2 slits into both patches, thus changing the length of current patch for the fundamental mode of the antenna.

Comment: more design details will be written in the full paper

3. Antenna characteristics.

The antenna was designed and analysed with aid of the commercial time-domain simulator CST Microwave Studio (finite integration (FI) method). The simulated return loss (RL) of the ASPA and ASPA with slits is shown in Fig. 2. The RL >10dB is from 3 to 6 GHz for normal ASPA, and from 4 to 5.9 GHz for ASPA with slits. One could claim that smaller ASPA is not an ultra-wideband antenna looking only at S11 characteristic. But actually input matching is not a useful measure to describe antenna transient performance. It can give just an idea about the antenna efficiency. Generally the pulsed antennas are characterized by the set of specific parameters, different from those known from the classical antenna theory. The most important parameters describing transient properties of antennas are: transfer functions (Tx-, Rx- or Tx-Rx- transfer function), fidelity factor (telling how similar are pulses radiated in different directions), and the pulse shapes itself.

From Fig. 3 we can see, that actually both versions of antennas have almost identical impulse responses (as an excitation we have used the gaussian pulse, the same as in Fig. 4a) in 2-antennas mode (Tx and Rx antenna, 20 cm separation distance). 0° indicates the transmission in the perpendicular direction to the patch surface (normal direction for patch antennas), 90° indicates radiation parallel to the patch surface (end-fire-like radiation, usually not considered for patch antennas, but attractive for our application, simulating radiation along the human body). We can also see from Fig. 3 how the impulse responses differ for 0° and 90° directions. The pulse transmitted in the end-fire-like mode has not only the much lower voltage amplitude (what is normal for patch antennas), but what is more important in UWB radio system, the pulse is stretched out with additional late-time ringing effect (in full paper we will present additionally transfer function characteristics where the reasons of this effect will be shown and explained).

Fig. 4 presents the transient characteristics of the ('normal') ASPA for a three different pulses driving the antenna. Fig. 4a shows the case when the gaussian excitation is used (250 ps duration, 90% of the pulse energy within 0-6 GHz), Fig. 4b presents results for the monocycle excitation (300 ps duration, 90% of the pulse energy within 2-9 GHz). Input pulse to the Tx-antenna presented in Fig. 4c was created by method described in [B. Parr el.al., 'A Novel Ultra-Wideband Pulse Design Algorithm', May 2003]. It has the duration of 650 ps and was designed to cover the 3-6.5 GHz frequency range (for 90% of the pulse energy). We can notice that for all excitation used, the received pulses ('normalized received pulse' in Fig. 4) are very similar in shape (fidelity factors >90%). But they have different maximum voltage amplitudes of 0.064, 0.091 and 0.158 V for a gausian, monocycle and defined excitations (max. voltage 1 V), respectively. We can explain this as the effect of band-pass characteristic of the antenna transfer function (which is not shown here due to the limitation in number of figures; will be presented in a full paper). The lowest voltages of the received pulse are for the gaussian input pulse, where its energy is widely spread along the spectrum with the maximal values in the lower frequency band (it has also DC component). Thus the significant amount of the pulse energy is filtered out. This is also the case for the monocycle excitation (Fig. 4b). But this pulse has no DC component and the maximal values of the pulse energy spectrum are within operational bandwidth of the antenna, giving higher received voltages than for the gaussian pulse. The highest received voltages are for the pulse presented in Fig. 4c. Its energy spectrum (on a –10dBi level) is matched very well to the band-pass characteristic of the antenna transfer function (also on a –10dBi level).

One of the characteristic features of UWB communication systems is the fact, that antenna has an impact on the transmitter and receiver circuitry complexity. We can imagine two opposite cases: 1. for a given antenna we have a very simple (low-power) pulse generator (without any pulse shaping elements); but then usually received pulse has the shape which need more sophisticated detection methods (e.g. Rake receiver); this lead to a complex (and usually power consuming) receiver architecture; 2. for the same antenna as in case 1, we have the transfer function given, so we can defined the simplest possible to detect waveform, thus simplifying receiver; but this lead to the completely arbitrary waveform in the transmitter (which is difficult to create). This shows how important antenna in a UWB system is, and also tells that it cannot be designed separately from the rest of the system elements. (results illustrating above issues will be presented in a full paper)

4. Conclusions

In this paper we investigated the aperture-stacked patch microstrip antennas for UWB WBAN applications. Based on the general methodology (using TD simulator), the most important parameters of the pulse antenna were found. Their knowledge is necessary to perform simulations of the UWB radio system, including pulse generator, UWB channel model and receiver front-end. It is very difficult to judge the pulse antenna performance, since it cannot be separated from the entire system. There is a clear call for generator-antenna-receiver co-design in UWB radios. Our results present the possible influence on the system complexity using ASPA. Further investigations will include measurements of these antennas, influence of the human body on the antenna parameters and further trials of antenna miniaturizations.

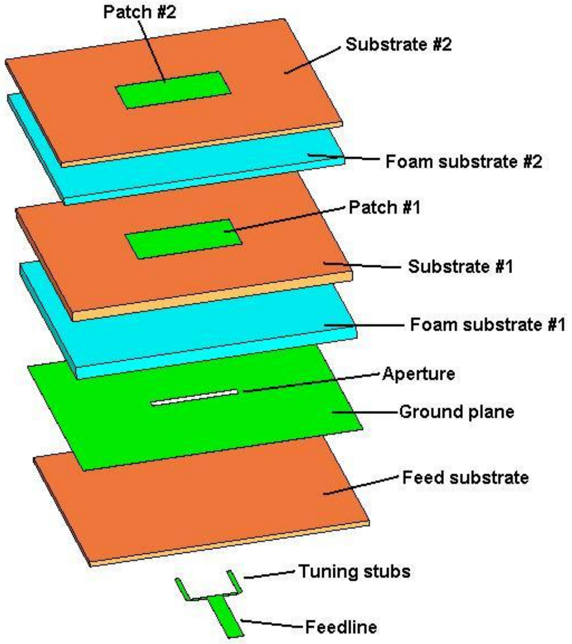

Figure 1: Geometry of ASPA.

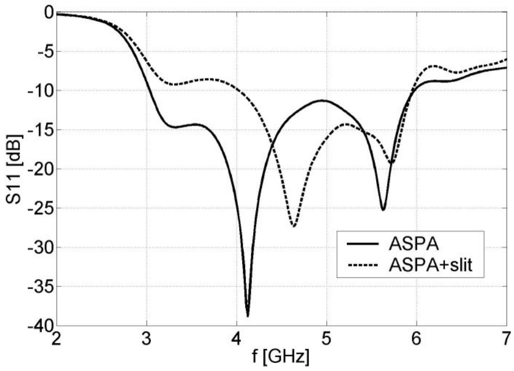

Figure 2: Return loss of ASPA and small ASPA (with slits).

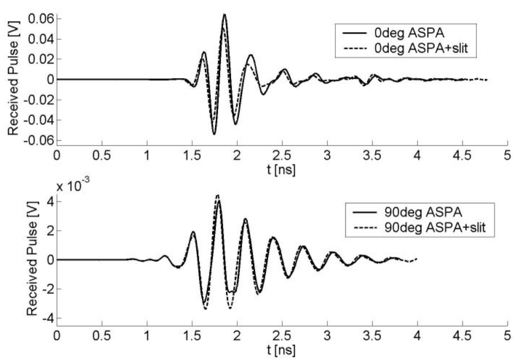

Figure 3: Comparison of received pulses for ASPA and small ASPA for 2 propagation directions.

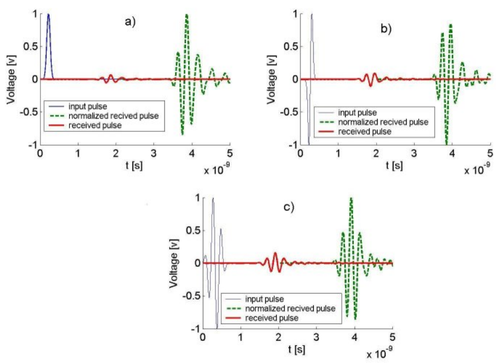

Figure 4: Time-domain characteristics of ASPA for 3 different excitations: a) gaussian pulse, b) monocycle, c) defined excitation.

UWB 16 - Scattering

UWB 16-1: Measurements of Ultra-Wideband Radar Cross Sections of an Automobile at Ka Band

T. Kobayashi[1], **N. Takahashi**[2], **M. Yoshikawa**[2], **K. Tsunoda**[3], **N. Tenno**[3]
[1]*Communications Research Laboratory/Tokyo Denki University*; [2]*NTT Advanced Technology Corp.*; [3]*Murata Manufacturing Co., Ltd.*

An ultra-wide bandwidth from 22 to 29 GHz has been proposed for use for vehicular radar; the Federal Communications Commission of the United States approved an unlicensed use of this bandwidth in 2002. This paper presents ultra-wideband (UWB) radar cross sections (RCS) of an automobile measured within this bandwidth, which are indispensable data to develop such radars. A 4-door sedan, 4.75 m long by 1.75 m wide by 1.39 m high with an engine displacement of 2 liters, was used for the measurements. This automobile was lifted about 0.3 m above a flat-surface turntable in a radio anechoic chamber using jack stands, as shown in Fig. 1. The floor of the chamber was covered with radio absorbers. This setup enabled us to measure the RCS of the automobile itself, excluding the effects of the ground. The transmitting and receiving antennas (double-ridged waveguide horns) were placed parallel and adjacent, and directed horizontally to the automobile. The average distance between the antennas and the automobile was 10 m. The antennas were located close together in order to make monostatic RCS measurements. The height of the antennas was the same as that of the automobile's front bumper. The antenna gain was 22.5 dBi at 25.5 GHz. The antenna footprint (product of transmission and reception) was approximately 10% less than the projected area of the automobile when the radar was directed to the side of the automobile; otherwise it spread over the whole body. The antennas were connected to ports 1 and 2 of a vector network analyzer, and used a low noise amplifier to measure the received power and to derive the UWB RCS by integrating the power from 22 to 29 GHz. The combinations of transmitting and receiving polarizations were vertical-vertical (V-V), horizontal-horizontal (H-H), and +45°- –45°. The automobile was rotated 180° azimuthally from the forefront to the back in 1° intervals. System calibration was carried out by using a dihedral corner reflector with a projected area of 0.3 m by 0.3 m to validate the average error of 1 dB in the RCS measurements.

The results are presented in Fig. 2 for (a) V-V, (b) H-H, and (c) +45°- –45° polarizations. The left half of each radar chart shows the UWB (22 to 29 GHz) RCS in dBm2 (0 dBm^2 = 1 m2) and the right half shows the continuous wave (CW, 25.5 GHz) RCS. It was found that the automobile's UWB RCS varied as follows:

V-V and H-H polarizations: 2 to 20 dBm^2

+45°- –45° polarizations: –4 to 10 dBm^2.

Fluctuations of the RCS were smaller in UWB than in CW for all the polarization combinations. This is because the ultra-wide bandwidth cancels RCS plunges that are caused by frequency-dependent interference among reflected waves from various parts of the target.

This work was carried out by UWB Technology Institute and UWB Research and Development Consortium at Communications Research Laboratory, Japan.

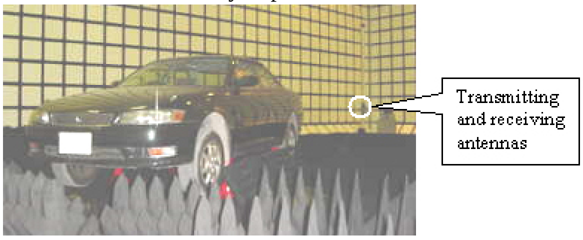

Figure 1: RCS measurement setup.

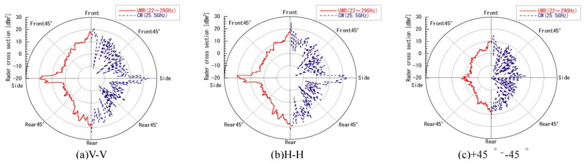

Figure 2: UWB and CW (25.5 GHz) RCS of an automobile.

UWB 16-2: Directly Measuring Ocean Forward Scatter with an UWB Radar

P. Hansen, **K. Scheff**, **E. Mokole**
Radar Division, Naval Research Laboratory

A knowledge of the behavior of radar forward scatter is important for designing naval radar systems and defining their performance. Radar targets physically located close to the ocean surface are often illuminated by radiation coming both directly from the radar and, by reflection, from the ocean surface. Interference at the target and on the reciprocal path causes fluctuations in the amplitude of the detected radar signal and distorts the measured phase front. At low grazing angles, experimental characterization of the forward scatter is challenging since it requires either ultra high resolution in time or angle or must be inferred from the combined signal. Direct resolution by time delay allows the separation of contributions from the multiple radiation paths as well as giving an indication of the true spread of reflection points on the ocean surface. Required radar time resolutions for typical measurement geometries are well below one nanosecond.

This paper describes a dual frequency, ultrawideband (9 GHz, 0.15 ns pulse and 4 GHz, 0.25 ns pulse), dual polarized measurement radar system and a field experiment designed to directly measure ocean forward scatter associated with a test target mounted above a wind disturbed ocean surface. For a grazing angle of 2.9 degrees to the specular point, radar resolution was sufficient to fully resolve both direct and reflected path contributions to the received target signal. Data samples highlight some new results with regard to conventional wisdom concerning radar forward scatter from the ocean. First, there is evidence of a focusing phenomena, where the forward scatter path occasionally presents an equivalent reflection coefficient greater than unity. Second, the measurements show a dependence on both wind speed and orientation with the average forward scatter being significantly greater for a crosswind orientation than for a comparable upwind orientation.

UWB 16-3: Some Broadband Calculated RF Scatter from the Trihedral Corner Reflector

E. Mokole[1], **D. Taylor**[1], **B. Gold**[1], **T. Sarkar**[2]
[1]*Naval Research Laboratory (Radar Division)*; [2]*Syracuse University*

For the last 5 years, trihedral corner reflectors have been used in a series of ultrawideband (UWB) measurements at the Atlantic Underwater Test and Experiment Center (AUTEC) in the Bahamas to investigate the low-elevation (grazing angles less than 4 degrees) scatter of RF signals from the open ocean in an attempt to understand and mitigate the phenomenon known as sea spikes, which introduce undesirable target-like artifacts in radar returns. To extract information about sea scatter from these measurements, the monostatic and bistatic radar cross sections (RCSs) from the trihedral are being computed for selected frequencies between 1 GHz and 12 GHz. Monostatic and bistatic predictions are needed, because collected ultrahigh-resolution UWB data display significant signal returns from four propagation paths: the direct path (monostatic); the two single-bounce specular paths (bistatic); and the double-bounce specular path (monostatic).

Historically, the trihedral has been used for instrumentation purposes, radar calibration, and devices with enhanced RCSs. Until recently, most scattering studies of the trihedral have been understood through optics and empirical evidence, as a result of the excessively large computational burden imposed by this problem. Despite its simple geometric structure, the trihedral is a complex target for computational-electromagnetics solvers. As the frequency and target size increase, the number of unknowns required by these solvers grows significantly. By using advanced application tools (like WIPL-D) and modern computer resources, simulated results of monostatic and bistatic RCSs of a 1-m anodized aluminum trihedral are calculated. Initial results and the associated computational constraints are discussed.

UWB 16-4: Transient Phase-Space Inhomogeneous Green's Function for Modeling High Contrast Scattering

T. Melamed
Dep. of Electrical & Computer Eng., Ben-Gurion University of the Negev, Beer Sheva, Israel.

Inhomogeneous media Green's functions are of fundamental significance for modeling wave propagation, inverse scattering, numerical methods, etc. Green's functions are wave objects that link sources in the configuration space to the configuration observation domain by a convolution integral. These wave objects are global in nature in the sense that each point in the source domain contributes to all points in the observation domain, hence the difficulty in the evaluation, both analytically and numerically, of these wave objects. Since modeling wave propagation directly in the configuration space implies global Green's functions, transferring the fields via transient phase-space (TPS) transform seems to be favorable for the search after localized Green's function which may be easily evaluated both asymptotically and numerically. Furthermore, since wave interactions with scattering media have been found to be local in nature, it is suggested that the evaluation of Green's functions should not be carried out in the configuration space but in the TPS domain, which extracts local radiation properties of the data and by that synthesizes local wave-medium interactions.

Following this strategy, we introduce Inhomogeneous media transient Green's functions in the phase-space domain, by which the TPS spectral distributions of the field scattered by a high contrast object due a genetic transient incidence are evaluated. Two forms of phase-space Green's function are considered: By applying TPS transform to the scattered field over some planar surface, one obtains a TPS Green's function that links induced sources in the configuration space to TPS distributions of the scattered field. A second kind of TPS Green's function is obtained by applying the TPS transform to both incident and scattered field distributions resulting in a Green's function that directly links the TPS distribution of the incident field to TPS distributions of the scattered field. The scattering mechanism is described in terms of local samplings of the object function which are localized in the object domain according to the scattered- and incidence- phase-space processing parameters.

The general formulation is used for the special case of transient Gaussian windows processing yielding closed form analytic expressions for the TPS Green's function propagating in the perturbed media. Applications in the field of inverse scattering are explored yielding fast and efficient algorithms due to the capability to analytically evaluate the (forward) scattering Green's functions.

UWB 16-5: Axial Backscattering from a Wide Angular Sector

C. E. Baum
Air Force Research Laboratory, DEHP; Directed Energy Directorate; Kirtand AFB; NM; USA

A perfectly conducting angular sector is a canonical shape for scattering calculations. A previous paper has calculated the axial backscatter from a thin angular sector, obtaining an asymptotic result in the limit of $\Psi \rightarrow 0$ where Ψ is the half angle of the angular sector. Using a completely different technique the present paper calculates the axial backscatter for a wide angular sector, asymptotic in the limit as $\Psi \rightarrow \pi/2$.
The solution here has some interesting properties. Note the proportionality to $cot(\Psi')$ ($\Psi' = \pi/2 - \Psi$). This can be contrasted to the $cot^2(\Psi')$ dependence for the wide circular cone. The difference between these two can be ascribed to the fact that the angular sector has an integral over the surface current density using only one transverse coordinate, while the circular cone has an integral over two transverse coordinates. As an alternate view consider that for $\Psi' \rightarrow 0$ the angular sector tends to a half plane which scatters field proportional to $r^{-1/2}$, while the circular cone tends to a plane which scatters field proportional to r^0 (which requires a more singular behavior of the r^{-1} term as $\Psi' \rightarrow 0$).
So now we have solutions for the axial backscattering from both this and wide perfectly conducting angular sectors. This leaves the intermediate angles Ψ to be solved. There exists a solution in terms of an infinite series of eigenfunctions. However, this does not give simple analytic insights. Further development of "exact" analytical and numerical results would be helpful.

UWB 17 - UWB Communication

UWB 17-1: Study on the Probability of Error in UWB with Multiuser Interferences

J. Fiorina
Supelec, Service Radioélectricité, 91192 Gif-sur-Yvette, France

I. Introduction
Ultra-Wideband technology has been presented as a promising way to provide very high speed communication with multiple access. It could be a solution for new types of local area network. The basic proposal has been developed by R. A. Scholtz [Multiple Access with Time-Hopping Impulse Modulation, Milcom'93], (TH-PPM UWB). The multiple access has been studied with a single user matched filter (SUMF) receiver which is a simple receiver using correlation which has the advantage to be a relatively easy and low cost receiver [F. Ramirez-Mireles and R. A. Scholtz, Multiple-Access Performance Limits with Time Hopping and Pulse Position Modulation ,ICC 1998], [M. Z. Win and R. A. Scholtz, Impulse Radio: How it works, IEEE Communications Letters, January 98]. But in order to calculate the performances of such a system, the free-space propagation model has been often used and the multiuser interference (MUI) has been supposed to be a mean-zero Gaussian random process. It is known that in many cases this last assumption is untrue [G. Durisi and G. Romano, On the validity of Gaussian Approximation to Characterize the Multiuser Capacity of UWB TH PPM, UWBST, 2002]. Performance studies have also been made in multi-path propagation channel but there is no simple formula for the probability of error when the Gaussian approximation is not valid. It is why we focus here on free space propagation with perfect power control to give a simple formula for error probability. The calculation is made with the signal to noise ratio E_b/N_o tending to infinity, giving thus an inferior bound for the error probability.
II. Signal model and calculation
The received signal is given in (1). w is the received impulse which is the classical second derivative of a Gaussian pulse. The SUMF receiver output is given in (2), the sign of this output gives the received symbol. We show the value of this output for just one impulse received, in function on the time of arrival of this impulse in Fig. A.
There are Nu users unsynchronized, the delay of each is t_k. The receiver is synchronized on user 1, t_1=0. To perform the calculation of the probability of error we approximate the SUMF output by the function in Fig. A, where the two main lobes are modelized by two squares. We note $N0$ the number of impulses sent by interferers and received in $D0$, and $N1$ the number of impulses sent by interferers and received in $D1$ (cf. Fig. A). The impulse sent by transmitter 1 is received in $D0$. The signal to noise ratio E_b/N_o tending to infinity, the error probability is given by (3). Then (4),(5),(6) lead to the final formula (7). Table I shows how this formula fit the simulations. Fig. B shows the difference with the Gaussian approximation. Formula (8) gives also the error probability when the users are synchronized but not orthogonal.
III. Conclusion
This study gives a closed form expression which allows calculating the performance of UWB with Multiuser Interferences, the results better fit the simulations when Gaussian approximation is not valid. This calculation can be adapted to different scenarios as seen in this study with the case of unsynchronized signals and the case of synchronized signals having non-orthogonal hopping code sequences. The study of this last case quantifies also the importance of orthogonality when there is synchronization and the benefit of unsynchronization in the case of non-orthogonality (Table II). The poor performances obtained in free-space propagation underlined in this study show the importance of a rich multi path channel smoothing multiuser interferences and thus increasing performances.

$$y(t) = \sum_{k=1}^{Nu} y_k(t - t_k) + n(t) \qquad (1)$$

With n additive white gaussian noise.

$$y_k(t) = \sum_m w(t - mT_f - c_{k,m}.T_c + \delta.a_{k,m})$$

The symbols $\{a_{k,m}\}$ have their values in {0,1}, δ is the time shift used for position modulation.
$(c_{k,m})$ is the sequence representing the time hopping code. Tf is the frame period, Tc the slot period.

$$x = \int y(t)p(t - c_{1,0}.Tc)dt \qquad (2)$$

x is the SUMF output for symbol $a_{1,0}$.

$$p(t) = w(t) - w(t + \delta)$$

The decided symbol is $\hat{a}_{1,0}$.

$$\hat{a}_{1,0} = (1 - sign(x))/2$$

Figure 1: Equations, part I

$$P_e = P(N1 > NO+1) + (1/2)P(N1 = NO+1) \quad (3)$$

$$P(N1 = N0+1) = \sum_{k=0}^{n/2}\binom{n}{k}.p^{k}.\binom{n-k}{k+1}.p^{k+1}.(1-2p)^{n-2k-1}$$
$$= \frac{1}{2\pi}\int_0^{2\pi}(1-2.p+p.e^{i\theta}+p.e^{-i\theta})^{Nu-1}.e^{i\theta}d\theta \quad (4)$$

with p=D0/Tf=D1/Tf and n=Nu-1.

$$P(N1 = NO) = \frac{1}{2\pi}\int_0^{2\pi}(1-2.p+p.e^{i\theta}+pe^{-i\theta})^{Nu-1}d\theta \quad (5)$$

$$\frac{1}{2\pi}\int_0^{2\pi}(1-2p+pe^{i\theta}+pe^{-i\theta})^{n}d\theta = (1-4p)^{n/2}P_n\left(\frac{1-2p}{\sqrt{1-4p}}\right) \quad (6)$$

with P_n the Legendre polygon of degree n.

$$\begin{cases} Pe = 1/2 - W_n - (1/4p)(W_{n+1} - W_n) \\ W_n = (1-4.p)^{n/2}\, P_n\left(\dfrac{1-2p}{\sqrt{1-4p}}\right) \end{cases} \quad (7)$$

with n=Nu-1.

$$Pe = 1/2 - W_n - (1/4p')(W_{n+1} - W_n) \quad (8)$$

with p'=1/(2.Ns) and Ns=T_f / T_c

Figure 2: Equations, part II

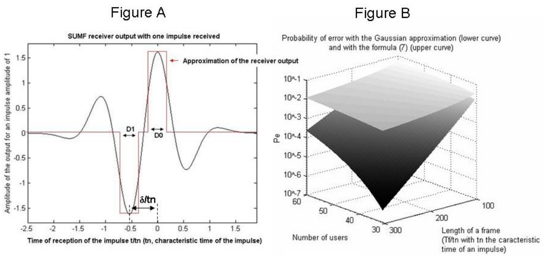

Figure 3: Figures A and B

TABLE I
COMPARISON OF THE RESULTS OF SIMULATIONS AND FORMULA

Length of Tf	BER by simulation	BER with the formula (7)	BER with Gaussian approximation
356*tn	8.5.10^-3	8.56.10^-3	2.5.10^-5
178*tn	1.7.10^-2	1.68.10^-2	2.10^-3
100*tn	3.10^-2	2.92.10^-2	1.5.10^-2

Simulations are made with tn=0.2877 ns, δ=0.156 ns.
The formula is calculated with (length of D0)=(length of D1)=0.2*tn
Number of users is 32.

TABLE II
COMPARISON OF SYNCHRONISATION AND UNSYNCHRONIZATION

Length of Tf	Number of slots Ns in a frame	BER with the synchronisation but non orthogonality	BER with unsynchronisation
356*tn	114	5.99.10^-2	8.56.10^-3
178*tn	57	1.07.10^-1	1.68.10^-2
100*tn	32	1.61.10^-1	2.92.10^-2

Simulations are made with tn=0.2877 ns, δ=0.156 ns.
The formula is calculated with (length of D0)=(length of D1)=0.2*tn
Number of users is 32.

Figure 4: Tables I and II

UWB 17-2: Contribution to the Study of the Dynamics and Synchronization of Chaotic Modulation in UWB Communication and Positioning Systems

J. C. Chedjou, S. A. Kamanou, K. Kyamakya
International Centre for Theoretical Physics (ICTP) Trieste (Italy) and University of Dschang (Cameroon), University of Yaounde I (Cameroon), and University of Hannover (Germany)

The last years have witnessed intensive studies of Ultra Wide Band (UWB) communication systems. The interest devoted to such systems is motivated by the various potential advantages the UWB technology can bring to the wireless industry. Indeed, the UWB technology can solve the RF spectrum availability problem, can improve security, and can provide less expensive and less power consuming equipment for a variety of wireless applications [1].

Synchronization of chaos [2, 3] has aroused much interest in light of its potential applications. In particular, the use of chaotic synchronization in communication systems has been investigated intensively [4 – 10]. The principle consists of the transmission of an information signal containing a message, using chaotic signal as a broadband carrier. The synchronization process is achieved to recover the information at the receiver. Due to the broadband feature of the chaotic signal, it can be used in ultra-wideband and communications systems in chaotic pulse position modulation [11].

We present in this report some effects of phase synchronization of coupled self-sustained non-identical chaotic Rössler oscillators. To characterize these phenomena, we use both numerical and analog simulation techniques. We consider the synchronization as the ability of coupled self-sustained oscillators with different frequencies to switch their behavior from the regime of independent oscillations characterized by beats to the regime of cooperative oscillations (stable periodic or unstable oscillations), as the strength of the coupling is monitored. The experimental observation of chaotic oscillations in coupled nonlinear circuits is used to discuss some unknown forms of cooperative behavior that are related to the regimes of synchronized chaos. One of the most important contributions of this work is to list some important and new problems when synchronizing non-identical chaotic Rössler oscillators. Such a synchronization process can be achieved through the use of an auxiliary system (a third oscillator of the Rössler type), which is considered as the ideal predictor that is able to indicate the current state of the response system by processing the driving signal. A similar approach was carried out by Rulkov [12]. He considered simplified cases of non-identical synchronized chaotic oscillations that were observed in directionally coupled circuits with different parameter values. He also generalized the definition of chaos synchronization as the ability to predict the current state of the response system from the chaotic data measured from the driving system.

The general goal of this work is to adapt the study carried out by Rulkov [12] to the more complex case of UWB Rössler generators. We use a class of synchronizing systems, which are unidirectionally coupled non-identical Rössler systems (master-slave or drive-response configurations). The interest devoted to the Rössler system is motivated by their capability to behave chaotically at very high frequencies. Chaotically modulated oscillations and chaotic pulses are obtained and are shown as characteristic features of the oscillators. These oscillators are of great interest in UWB applications and communications [13, 14]. The analog simulation in this work has the advantage that it offers the possibility to simulate the behavior of the system at very high frequencies by performing and appropriate time scaling. A technique of synchronization in case of chaotic modulation is presented. Numerical solutions are compared with the experimental results and a very good agreement is obtained between both methods. One of the interests of this work is, amongst others, to show that analog computation is also suitable, similar to its numerical counterpart, for the understanding the real physical behavior of chaotic systems.

References:

[1]- A. Volkovskii, and I. Langmore, “Ultra Wide Band Communication Device with Chaotic Frequency Modulation,” AIP Conference Proceedings, Vol. 676, pp. 364-, August, 2003.
[2]- L. Pecora, and T. L. Carroll, Phys. Rev. Lett. 64, 821-823, 1990.
[3]- T. L. Carroll, and L. Pecora, IEEE Trans. Circuits Syst. 38, 453-456, 1991.
[4]- K. M. Cuomo and A. V. Oppenheim, Phys. Pev. Lett. 71, 65-68, 1993.
[5]- L. Kocarev, K. S. Halle, K. Eckert, L. O. Chua, and U. Parlitz, Int. J. Bifurcation Chaos 2, 709-713, 1992.
[6]- R. Lozi, and L. O. Chua, Int. J. Bifurcation Chaos 3, 1319-1325, 1993.
[7]- K. M. Cuomo, A. V. Oppenheim, and S. H. Strogatz, Int. J. Bifurcation Chaos 3, 1629-1638, 1993
[8]- U. Parlitz, L. O. Chua, L. Kocarev, K. S. Halle, and A. Shang, Int. J. Bifurcation Chaos 2, 973-977, 1992.
[9]- K. S. Halle, C. W. Wu, M. Itoh, and L. O. Chua, Int. J. Bifurcation Chaos 3, 469-477, 1993.

UWB 17-3: Differential Modulation in UWB Range Estimation

J. Schröder, **S. Galler**, **K. Kyamakya**
Institute of Communications Engineering, University of Hannover, Germany

Ultra-Wideband communication and positioning has received great interest in the industry and the research community. This is due to the inherent robust multipath performance and material-penetration properties, promising very high datarates and excellent ranging capabilities in coexistence with already used spectrum. Further encouragement has been generated by the FCC’s allocation of frequency bands for the unlicensed use of UWB devices und ETSI’s planning to deliver harmonised standards in December 2004.
Precise range estimation between mobile terminals and reference stations with UWB pulses has been developed using two different approaches in the receiver architecture: The first one is based on threshold detection, where fast tunnel diodes detect the peak of the received signal (e.g. Multispectral’s PAL). The second one uses very fast A/D converters, which sample received signals with high resolution and then detect the arrival time via correlation (e.g. Ultra-Wideband for Navigation and Communications, John Carl Adams, 2001). The latter approach outperforms the former one in terms of SNR, on the cost of higher computational demand.
Recently, a simple UWB-pulse radio communication system has been proposed using differential modulation with low complexity (timederivative.com/pubs.htm). The transmitter simply modulates the data stream as a differential encoded pulse train, which is reconstructed at the receiver via multiplication of successive pulses followed by integration.
Systems have been developed combining communication and positioning using UWB pulses. In exploiting the advantages of the differential communication architecture and additionally obtaining high resolution positioning with the correlation method, this paper studies the influence of differential modulation on UWB range estimation.

UWB 17-4: A Low-Complexity Receiver for Ultra Wide Band Communications

R. Alesii, **M. D. Renzo**, **F. Graziosi**, **F. Santucci**, **A. Scarano**, **P. Tognolatti**
DEWS - University of L’Aquila, Italy

Ultra Wide Bandwidth (UWB) spread-spectrum techniques have recently attracted growing interest in scientific, commercial, and military sectors (see for example M. Z. Win and R. A. Scholtz, “Impulse radio: How it works,” IEEE Commun. Lett., vol. 2, pp. 36–38, Feb. 1998). Recent results indicate that UWB radio is a viable candidate for short-range single-user and/or multiple-access communications in dense multipath environments. Due to the very large bandwidth of impulse signals, the radio channel exhibits frequency selective fading; however, through the use of Rake receivers, fading effects can be significantly mitigated (M. Z. Win and R. A. Scholtz, “On the robustness of ultra-wide bandwidth signals in dense multipath environments,” IEEE Commun. Lett., vol. 2, pp. 51–53, Feb. 1998). This abstract describes some activities carried on at DEWS research center of the University of L’Aquila, Italy. These activities refer to the design of a new architecture for a low-complexity receiver and to an experimental validation of a simple UWB antenna.
Despite its potentialities, UWB technology is not yet fully developed, and the efficient design of such communication systems requires new experimental and theoretical activities. Recent efforts in reducing the receiver complexity (i.e. selective Rake receiver architectures) have been devoted to encourage a wide diffusion of the UWB-radio technology. Nevertheless, the Rake receiver, even if designed with a reduced number of fingers, presents an intrinsic complexity due to the need of a channel estimation and template matching algorithms which are crucial for the system to guarantee good performances. The design of digital receivers presents other important problems besides channel estimation and template matching: 1) the extremely wide signal bandwidth requires the received signal to be sampled through a bank of interleaved Analog-to-Digital (A/D) converter with sustainable sampling frequencies, thus increasing the receiver complexity; 2) the samples at the output of the above A/D bank require a large memory to be stored and processed.
It is reasonable to suppose that such receiver complexity can be justified only for high data rate applications in certain contexts, where costs and power consumption are not crucial concerns. On the contrary, for some kinds of applications like ad-hoc wireless sensors networks, some studies are in progress to develop alternative UWB receiver architectures, where the design goal is to keep complexity at reasonable levels, even if the price to pay is a drop of receiver performances. In particular, sub-optimal solutions are being explored, that circumvent the problem of template estimation while operating with template matching. More in particular, in (R. Fleming, C. Kushner, “Low-Power, Miniature, Distribuited Position Location and Communication Devices Using Ultra-Wideband, Nonsinusoidal Communication Technology” Aether Wire 1995) the locally generated pulse waveform is a very simplified version of the received pulse (i.e. a rectangular pulse). This solution seems to give good performances when the received pulse is strictly a base-band signal (i.e. the pulse energy is mainly carried by a main lobe), while much more attention must be paid when the transmitted pulse waveform has a pass-band spectrum (i.e. the pulse waveform appears as an high frequency oscillation with a pulse-like envelope). The latter case is likely to occur given the FCC rules which actually permit UWB transmissions in the 3.1-10.6 GHz frequency range (a lower band is also accessible for UWB but with limited spectral resources – i.e. Up to 1 GHz). In order to avoid these two problems, a differential detection approach has been proposed in (M. Ho, V.S. Somayazulu, J. Foerster, S. Roy, “A differential detector for an ultra-wideband communications system”, IEEE 55th Vehicular Technology Conference, 6-9 May 2002, vol. 4, pp. 1896-1900) and (Liang Li, Yafei Tian, Chenyang Yang, ”A Low-complexity UWB modulation and Demodulation Method for Low Data-Rate WPAN”, submitted to IEEE P802.15 Working Group for Wireless Personal Area Networks (WPANs) (doc.: 802-15-03/170)): the receiver correlates the received signal with a delayed version of itself, which provides a (noisy) template of the received waveform at the receiver input, including any multipath effect. The transmitted bits are differentially encoded, and the sampled output of the mixer is used to recover the transmitted data.
A possible limitation of the setup proposed in the above papers is that Pseudo Noise (PN) coding is not included in the transmission chain: in fact, only a single pulse per bit is transmitted. Instead, in this abstract an enhanced version of such family of detectors, developed at DEWS, is proposed. Firstly, PN-coded transmission is considered (for each bit a codeword is transmitted), and Pulse Position Modulation (PPM) and Pulse Amplitude Modulation (PAM) are explored. Encoding is essential for achieving acceptable performance of symbol acquisition, which is even more important in the asynchronous communication con-

text of our interest. Another important novelty of this work is that we propose a simplified but accurate analytical model, which can provide a consistent base for Bit Error Rate (BER) assessment. In this frame we demonstrate that a Gaussian approximation can be reasonably adopted for the noise term at the detector input. On the contrary, all the above papers characterize the receiver performances only by simulation results.

On the experimental point of view, one of the antennas which are currently under test at DEWS research center, for UWB applications, is a travelling-wave type. It is made by an exponentially tapered transmission line terminated by two series-connected lumped resistors. It operates over a ground plane and exhibits a good impedance matching to pulse generator. It has an endfire directive radiation pattern that seems suited for some applications as automotive UWB systems. Fig. 1 shows the antenna structure. Fig. 2 reports VSWR obtained by frequency-domain measurements made by a network analyser. Measured performances are in good agreement with simulation results obtained by a MOM code (NEC-2).

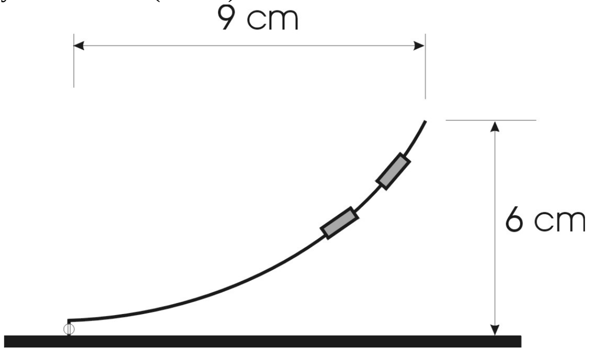

Figure 1: Tapered wire antenna with lumped terminating resistors

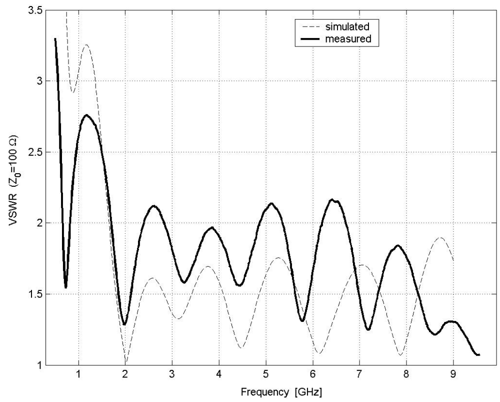

Figure 2: Measured and simulated VSWR, showing a good impedance matching

UWB 17-5: Performance of a Modified Early-Late Gate Synchronizer for UWB Impulse Radio

L. Reggiani[1], **G. M. Maggio**[2]

[1]*Dip. di Elettronica ed Informazione, Politecnico di Milano, Italy*; [2]*STMicroelectronics, Inc. & Center for Wireless Communications, University of California, San Diego, CA, USA*

Introduction

UWB (ultra-wideband) impulse radio makes use of ultra-short duration pulses which yield ultra-wideband signals characterized by extremely low-power spectral densities, thus by a low probability of detection (LPD). One of the key technical aspects that will influence the successful development of UWB impulse radio is timing acquisition. In this work, we present performance results of a synchronization strategy comprising a coarse acquisition phase, followed by fine tuning / tracking. The tracking phase of the synchronization is characterized by a peculiar processing of the received signal; furthermore, the proposed modified early-late gate algorithm provides finer time resolution and an estimate of the temporal window where most of the pulse(s) energy is concentrated.

System Model

We envisage here a base station transmitting, synchronously, several data streams towards M users. Each user is typically assigned a pseudo-noise (PN) sequence, which is mapped to a pulse sequence through a time-hopping scheme. An unmodulated pulse sequence (preamble) is utilized for the time acquisition of new connections. The channel impulse response can be modelled by a tapped delay line expression, according to the model proposed in [2]. In our analysis, the interference sources of the channel are additive white Gaussian noise (AWGN) and the other active users.

Synchronizer Architecture

In general, the synchronizer includes a pulse detector which prefilters and then samples the received signal, realizing a filter matched to the pulse waveform. This pulse detector is followed by a digital block implementing the synchronization algorithm, as sketched in Fig. 1. The digital section performs the actual coarse acquisition and fine tracking operations. This is achieved through an acquisition block and the modified early-late gate algorithm, respectively. In this work, since we cannot assume any knowledge of the channel and the received pulse waveform, we consider the implementation of the pulse detector as an energy detector, as it is usual in the context of non-coherent detection [3].

Acquisition Algorithm

The acquisition block detects the presence of the synchronization sequences by computing the correlations with the expected PN sequence, for each position in the frame, and comparing the maximum value with a threshold. If the correlation output is greater than this threshold, the acquisition is declared successful. The threshold is adjusted in order to find a trade-off between the probabilities of detection and false alarm. Hence, the algorithm realizes a coarse estimation of a parameter (position) of the expected PN sequence based on the success of a detection test. In this work, we will also exploit the simplified search procedure presented in [4]. The concept of n-scaled acquisition relies on the synchronization algorithm operating on different quantizations of the time frame.

Modified Early-Late Gate Algorithm

Following the correlation with the expected PN sequences, we implement an early-late gate discrete algorithm for estimating the time window, T_W, in which a relevant fraction of the pulses energy is concentrated. The early-late algorithm is preceded by a block, i.e. pulse coherent re-alignment, which subdivides the observation window into time frames and aligns all the received pulses belonging to the expected PN sequence. These (fragmented) frames are then combined together providing a single time frame reference, by superpositions of all the received pulses. This re-folding operation is carried out according to the initial timing estimate, provided by the acquisition block, and to the (known) PN sequence. Re-folding is useful in order to decrease the number of operations in the early-late gate algorithm and for increasing performance when a coherent sum is realized among the pulses. In addition, this block is able to detect more efficiently false alarms caused by the acquisition block. So, the modified early-late algorithm receives the re-aligned expected pulses within a single time frame and refines their timing and duration. In a standard early-late gate algorithm, the timing acquisition is refined by comparing the correlation with two replicas of the expected signal, one delayed (with correlation denoted by C^+ and the other anticipated (resp. C^-) by a time offset. In this work, we modified the algorithm by adding the possibility of increasing the integration period, with the aim of capturing the greatest fraction of signal energy. The algorithm, for each iteration, consists of two steps, reported in (1). In the first step, the two correlations C^- and C^+ are compared, within a threshold, and the center and the width variations D_C and D_W of the correlation window are modified by the fixed amount D. In the second step, at each iteration k, the new center T_C and width T_W of the correlation window are computed according to a comparison (again within a threshold) between the shifted correlations C^- and C^+ and the current correlation C, computed at the current location without time offsets (1). We reiterate that in the proposed algorithm, for avoiding difficulties with the received pulse estimation, the correlations are performed on the squared signal by means of rectangular pulses, thus reducing to simple integrations (i.e. energy detection). Fig. 2 reports an example of the probability of detecting at least a certain percentage of the signal energy in case of successful acquisition before and after the modified early-late algorithm; note that there are not significant performance differences among the receivers that use an n-scaled acquisition.

References
[1] M. Z. Win and R. A. Scholtz, “Ultra-wide bandwidth time-hopping spread-spectrum impulse radio for wireless multiple access communications”, IEEE Trans. on Communications, April 2000.
[2] J. Foerster and Q. Li, “UWB channel modeling contribution from Intel”, IEEE P802.15 Wireless Personal Area Networks, IEEE P802.15-02/279r0-SG3a, June 2002.
[3] S. M. Kay, “Fundamentals of Statistical Signal Processing: Detection Theory” Vol. II, Prentice Hall, New Jersey, 1998.
[4] L. Reggiani, G.M. Maggio, “A Reduced-Complexity Acquisition Algorithm for UWB Impulse Radio” Proc. UWBST’03, Reston (Virginia, USA) Nov. 2003.

Step 1
- If $C^+ > C^- + C_{TH} \rightarrow D_C = +D, D_W = +D.$
- If $C^+ < C^- - C_{TH} \rightarrow D_C = -D, D_W = +D.$
- If $|C^+ - C^-| \leq C_{TH} \rightarrow D_C = 0, D_W = +2D.$

Step 2
- Define $C_N = \max\{C^+, C^-\}.$
- If $C_N > C + C_{TH} \rightarrow T_C^{(k)} = T_C^{(k-1)} + D_C,\ T_W^{(k)} = T_W^{(k-1)}.$
- If $C_N < C - C_{TH} \rightarrow T_C^{(k)} = T_C^{(k-1)},\ T_W^{(k)} = T_W^{(k-1)}.$
- If $|C_N - C| \leq C_{TH} \rightarrow T_C^{(k)} = T_C^{(k-1)} + D_C/2,\ T_W^{(k)} = T_W^{(k-1)} + D_W.$

Figure 1: Equation 1

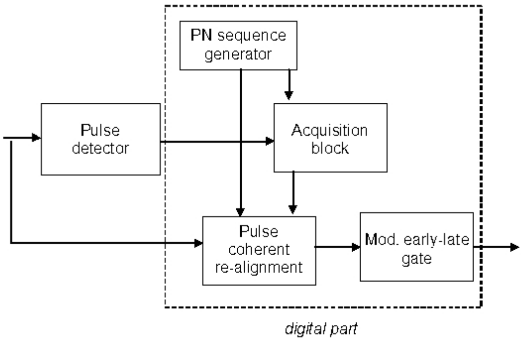

Figure 2: Synchronizer architecture.

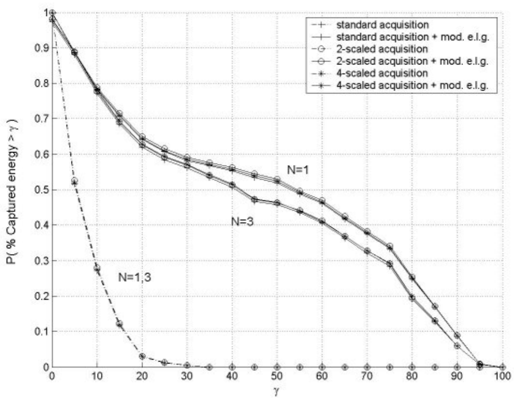

Figure 3: Cumulative probability of captured energy in case of N=1,3 users, false alarm probability equal to 0.1 before (dashed lines) and after (continuous lines) the modified early-late gate (mod. e.l.g.).

UXO - UneXploded Ordnances

UXO 1 - Defining UXO - Sites, Problems

UXO 1-1: Mined and UXO Areas from Around the World

H. E. Bertrand
Institute for Defense Analyses

The world of demining and UXO clean-up is often envisioned as taking place in an after-battle environment that is relatively benign. This presentation is intended to give all who see it a better idea of what deminers and EOD personnel, and the equipment they use, are up against. All areas presented in this briefing were either mined or contaminated with UXO as the result of hostilities. No areas shown were contaminated as the result of training exercises.

UXO 1-2: Project Network HuMin/MD - Advanced Data Analysis Methods for Metal Detectors

H. Eigenbrod
Fraunhofer-Institut IPA, Stuttgart, Germany

The BMBF-funded German research project on Humanitarian Demining (HuMin/MD) aims to reduce the number of false alarms produced by metal detectors. To achieve this, the project network will primarily develop the potential of secondary mathematical methods for analyzing data obtained from commercial off-the-shelf metal detectors. Two approaches will be considered in parallel: (1) local 3-D imaging and (2) signal analysis. In addition, work associated with soil influences and the optimization of metrological methods will also be carried out (see Figure 1).
Local 3-D imaging is made up of two areas: First, new inversion methods will be developed and tested by the project network enabling inverse problems to be calculated in real time and thus be implemented directly at the demining site. Methods which will be applied include the linear sampling method, the factorization method, the point source method and the approximative inverse. Second, in the field of forward calculation, the aim is to carry out a real-time analysis of detector signals using rapid forward calculation methods. Based on a model assumption for the metal distribution in the ground, the resulting ‘virtual’ detector signals can be calculated and then compared with the real detector signals. The model assumptions are then altered iteratively to enable the best possible match between the data calculated and the data measured to be achieved.
The metal detector signals are also analyzed using signal analysis methods. On one hand, modern feature extraction and classification concepts are used such as support vector machines, neuronal networks and Bayes classifiers. On the other hand, phenomenological or physical correlations are also taken into account in the implementation. Additionally, work concerned with pre-processing data (e.g. noise removal) will be carried out.
In total, ten institutes working in the fields of applied and numerical mathematics, electrical engineering, geophysics and non-destructive testing are participating in the project network. A list of the participating institutes is shown in Figure 2. The project network will run over a total of three years; the individual projects started in October 2003.

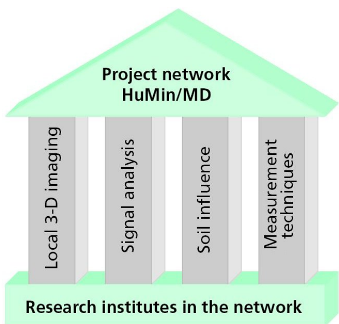

Figure 1: Main topics.

CUTEC Institute, Clausthal-Zellerfeld
Fraunhofer Institute for Manufacturing Engineering and Automation IPA, Stuttgart
Fraunhofer Institute for Non-Destructive Testing IZFP, Saarbrücken
Leibniz Institute for Applied Geosciences (GGA), Hannover
Göttingen University, Institute for Numerical and Applied Mathematics
Karlsruhe University, Mathematical Institute II
Köln University, Institute for Geophysics and Meteorology (together with Bonn University, Department of Geodynamics and Geophysics, Habourdom GmbH, Köln)
Mainz University, Mathematics & Computer Science
Rostock University, Institute for General Electrical Engineering
Saarland University, Institute for Applied Mathematics

Figure 2: Participating institutes. Contact partners for each individual institute are listed in the project network Web pages: www.humin-md.de.

UXO 1-3: easyMine: A Comprehensive Approach in UXO/Land Mine Detection Research

U. Böttger, **K. Beier**, **B. Biering**, **M. Peichl**, **U. van Rienen**, **S. Schulze**, **W. Spyra**
DLR Zentrum, Germany

Mine detection is to date mainly performed with metal detectors, although new methods for UXO detection are explored worldwide. The main problem for the mine detection to date is, that there exist some ideas of which sensor combinations could yield a high score, but until now there is no systematic analysis of mine detection methods together with realistic environmental conditions to conclude on a physically and technically optimised sensor combination. This gap will be removed by a project "easyMine" (Realistic and systematic Mine Detection Simulation Tool) which will result in a simulation tool for optimising land mine detection in a realistic mine field.
The project idea for this software tool is presented, that will simulate the closed chain of mine detection, including the mine in its natural environment, the sensor, the evaluation and application of the measurements by an user. The tool will be modularly designed. Each chain link will be an independent, exchangeable sub module and will describe a stand alone part of the whole mine detection procedure. The advantage of the tool will be the evaluation of very different kinds of sensor combinations in relation of their real potential for mine detection. Three detection methods (metal detector, GPR and IR-Polarimetry) will be explained to be introduced into the easyMine software tool in a first step. An actual example for land mine detection problem will be presented, and approaches for solutions with easyMine will be shown.

UXO 2 - Soil, Clutter, and Discrimination

UXO 2-1: Developmental Test Design to Evaluate System Performance

A. Dean
Joint UXO Coordination Office

A grid-based (as opposed to a lane-based) developmental test facility was designed and constructed by the DoD JUXOCO. Background clutter was removed from the site. Site maintenance and international use continue to the present at this Fort AP Hill, Virginia, test site. In the center of each 1m x 1m cell there is a 'detection opportunity' – thereby removing position from the test. The tester must declare the probability (within a range of his choice) of there being a target in the cell. Both ordnance and landmine detection technologies and system developers begin by working on a calibration grid (140-224 cells), where the groundtruth is known. In this way they familiarize themselves with the response of their sensor system (which often includes the operator as a system component) to various target-filled, clutter-filled, and blank cells. The user then performs blind testing (with no knowledge of the cell content) in the blind grid (910-1008 cells). The UXO set at the 71A site are buried at realistic depths, and represent the current set of ordnance and landmine threats. Each landmine in the landmine calibration and blind grids is fully operational, with the exception that all detonators are demilled. In this way, an authentic system evaluation is provided to the developer. Technologies sensitive to the primary characteristics (e.g., molecular, nuclear, biological) of landmines may be evaluated, as well as those sensing secondary characteristics (e.g., metal detectors, GPR).
JUXOCO scores the results using three ROC standard curves relating the probability of detection (P_d) of the targets with the probability of false alarms (P_{fa}), for clutter, for blanks, and for the grouping of clutter and blanks. Each user is the sole recipient of his performance scoring but each user must provide his raw data (where applicable) to the JUXOCO for inclusion in the database on the JUXOCO web site. Software developers may access the website database, request scoring of the JUXOCO, and assess the performance of their automatic target recognition (ATR) algorithms, as applied to the technologies of interest.
The UXO test site provides an example to the international community for the standardization of both developmental and operational testing, is an exceptional source of lessons-learned for the testing community, and submits a consistent prototype for the testing and ROC curve evaluation of all current sensor technologies. The facility also provides a validation of new systems, technologies and developer claims.

UXO 2-2: Discrimination of UXO in a Clutter-rich Environment using EMI Data

L. Collins, **W. Hu**, **D. Schofield**, **L. Carin**
Duke University

Detection and remediation of unexploded ordnance (UXO) represents a major challenge on closed, closing, and transferred military ranges as well as on active installations. The detection problem is exacerbated by the fact that on sites contaminated with UXO, extensive surface and sub-surface clutter and shrapnel is also present. Recently, statistically-based processing algorithms have been shown to out-perform traditional methods used for UXO remediation that have difficulty distinguishing buried UXO from anthropic clutter items as well as from naturally occurring magnetic geologic noise. However, most of the research in the UXO identification area assumes that objects are well isolated from each other and thus that a single signature is measured by the sensing system. In the scenario where multiple closely-spaced subsurface objects are present within the field of view of the sensor, the signals measured using electromagnetic induction sensors are mixed, and the mixed measurements cannot be used to determine the identity of each of the individual objects using conventional techniques. Since only the mixed observations are available, and these are usually available at multiple target/sensor orientations, separating individual signals from the set of mixtures can be posed as a Blind Source Separation (BSS) problem. In this work, we present two approaches to source separation, one based on the second order statistics and the other based on the fourth order statistics of the data. Following the source separation, UXO classification performance is obtained using the separated sources and a Bayesian classifier. We analyze the strengths and weaknesses of each BSS approach and compare their performance. We first present a simulation study in which pairs of UXO objects are presented to the separation and classification algorithms. Our next study extends these simulations to consider the case where there are more than two objects present, and addresses issues involving determining the number of objects present. Finally, we present results from a series of experimental studies. The first mimics the two-object simulation study and we consider classification of pairs of UXO that are present simultaneously in the field of view of the sensor. The second considers experimental data in which a UXO item is present concurrently with several clutter objects. Results indicate that discrimination can still be achieved when multiple objects are present within the field of view of the sensor provided enough high quality data is available, and that the appropriate BSS algorithm is selected.
This work supported by SERDP.

UXO 2-3: Soil Ground Reference Height and Frequency-dependent Magnetic Susceptibility of Soil

A. Gregorovic, **A. M. Lewis**, **T. J. Bloodworth**
Joint Research Centre (IPSC), Ispra, Italy

A well-known problem with metal detectors is that certain minerals in the soil can provoke a response by the detector even in the absence of metal. ”Noisy” or ”uncooperative” soil causes significant difficulties in demining operations. Evidence from reliability trials confirms that false alarm rate is increased in noisy soils and also indicates that probability of detection is reduced, because the operators may not be able to distinguish a weak signal from a mine against the background from the noisy soil. The effect can occur even for detectors with phase or time discrimination that are insensitive to purely real, frequency independent, soil magnetic susceptibility. Metal detector circuits incorporating soil compensation based on multiple frequencies and/or more sophisticated time-domain processing are able to reduce the problem. This phenomenon has been attributed to the frequency-dependence of magnetic susceptibility, also known as magnetic viscosity, which occurs in soil with magnetic grains of sizes below the superparamagnetic limit.

An empirical method, suitable for field-use by demining organisations, has previously been proposed to assess how noisy the soil is, when surveying an area prior to the demining. A static-mode detector without soil compensation is calibrated to an agreed sensitivity and then slowly lowered onto the soil. The distance above the soil at which it begins to alarm is termed the ground reference height and is used as the measure of the soil properties. However, ground reference height is not simply related to the two commonly measured properties of magnetic soils: low field magnetic susceptibility at low and high frequency. In this contribution we propose a model of frequency dependent susceptibility which is first calibrated to the two-frequency susceptibility measurements and then used to predict the ground reference height. We compare thus obtained values of ground reference heights and the ones measured on the field. The agreement is very good for almost all of the samples considered. This susceptibility model could eventually allow predicting or comparing the performance of other metal detectors on problematic magnetic grounds.

UXO 2-4: The Possibility of the Determination of Complex Permittivity of Early Age Loss Samples for Industrial Based Applications by using Microwave Free-space Method

U. C. Hasar[2], **S. Dover**[1], **S. N. Kharkovsky**[3]
[1]*Department of Electrical and Electronics Engineering, University of Cukurova, Adana, Turkey*; [2]*Department of Electrical and Electronics Engineering, University of Ataturk, Erzurum, Turkey*; [3]*Department of Electrical and Computer Engineering, University of Missouri-Rolla, Rolla, MO, USA*

The possibility of the determination of complex permittivity of cement-based materials at their early ages inserted in a low loss container by using free-space method for microcontroller based applications is shown. In the proposed approach, only are the amplitudes of reflection and transmission properties of materials are used for calculation. A special and unique function that characterises one of the complex permittivity parameters (real or imaginary part) of materials allowing the easily implementation of the determination of complex permittivity from high level (computer based systems) to low level (microcontroller based systems) is found.

The proposed approach can be used in industrial based applications because of its promising features. These are low cost, easy measurement, simple.

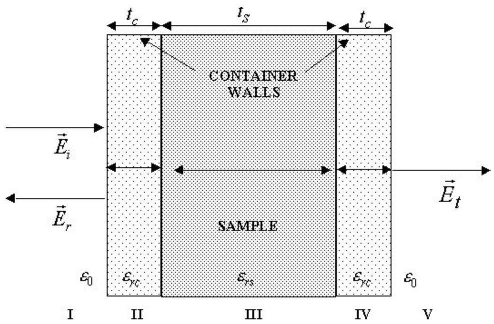

Figure 1: A five-layered structure for theoretical investigation.

$$r = \left(\frac{r_{12} + r_{23} e^{-2\gamma_c t_c}}{1 + r_{12} r_{23} e^{-2\gamma_c t_c}} \right) \quad t = \left(\frac{\left(1 - r_{12}{}^2\right)\left(1 - r_{23}{}^2\right) e^{-2\gamma_c t_c}}{\left(1 + r_{12} r_{23} e^{-2\gamma_c t_c}\right)^2} \right) e^{-\gamma_s t_s}$$

Figure 2: The expressions for reflection and transmission coefficients of overall system.

$$\begin{array}{ll}
e^{j2k_c t_c} = A - jB & \left(|r|^2 \left(E^2 + F^2\right) - 1\right) = K_1 \\
\left(1 - r_{12}^2\right) e^{j2k_c t_c} = C - jD & 2\left(|r|^2 \left(EA + BF\right) - G\right) = K_2 \\
r_{12} = E - jF & 2\left(|r|^2 \left(EA + BF\right) - H\right) = K_3 \\
r_{12} \cdot e^{j2k_c t_c} = G - jH & \left(G^2 + H^2\right) - |r|^2 \left(A^2 + B^2\right) = K_4 \\
r_{23} = X - jY & \\
\sqrt{\varepsilon_{rs}} = a - jb & \\
\sqrt{\varepsilon_{rc}} = c - jd &
\end{array}$$

Figure 3: Mathematical notations for simplification of calculations.

$$f(Y) = |t| - \left(\frac{\left(\sqrt{C^2 + D^2}\right) \sqrt{\left(1 + Y^2 - \left\{\frac{-K_2 + \sqrt{K_2^2 - 4K_1K}}{2K_1}\right\}^2\right)^2 + 4\left\{\frac{-K_2 + \sqrt{K_2^2 - 4K_1K}}{2K_1}\right\}^2 Y^2}}{\left(A + E\left\{\frac{-K_2 + \sqrt{K_2^2 - 4K_1K}}{2K_1}\right\} - FY\right)^2 + \left(B + EY + F\left\{\frac{-K_2 + \sqrt{K_2^2 - 4K_1K}}{2K_1}\right\}\right)^2} \right) e^{-bK_0 t_s}$$

Figure 4: Expression of special function.

UXO 3 - UXO & Landmines: Detection, Identification, and Neutralization

UXO 3-1: Quadrupole Terms in Magnetic Singularity Identification, Part 2

C. E. Baum
Air Force Research Laboratory, DEHP; Directed Energy Directorate; Kirtland AFB; NM, USA

This paper continues the treatment of the quadrupole terms in magnetic singularity identification (MSI) in [C. E. Baum “Quadrupole Terms in Magnetic Singularity Identification”, Interaction Note 569, 2001] which we can conveniently reference as Part 1. In that paper the magnetic-dipole formulae were extended to magnetic-quadrupole terms as certain integrals over the magnetization vector, particularly in the form of natural modes. Then questions were addressed concerning optimal choice of coordinate origin to “minimize” the quadrupole term associated with modes having a magnetic-dipole moment. The present paper (Part 2) further extends this development, including the use of norms and the point symmetry groups.

This paper (Part 2) extends the basic properties of magnetic quadrupoles in MSI. For minimizing such terms associated with natural modes with nonzero magnetic dipoles, the 2-norm over the unit sphere is formed. This leads to the definition of the optimal coordinate center (or center of the natural mode) for minimizing the quadrupole term. The case of two displaced magnetic dipole is generalized for zero quadrupole. The symmetry considerations are extended to discrete two-dimensional rotation with a transverse symmetry plane.

There may be other cases to consider, but this should help in optimal employment of MSI.

UXO 3-2: EMI Sensor Optimized for UXO Discrimination

L. Riggs[1], **S. Chilaka**[1], **D. Faircloth**[1], **H. Nelson**[3], **T. Bell**[2], **J. Kingdon**[2], **L. Collins**[4]
[1]*Auburn University*; [2]*AETC Inc.*; [3]*Naval Research Laboratory*; [4]*Duke University*

This paper addresses extremely low frequency measurements, below 30Hz, of UXO-Like Objects. Specifically, measurements of thin, medium, and thick walled magnetic cylinders with length-to-diameter ratios of approximately 4 have been measured using a conventional EMI test setup consisting of a 60cm x 100 cm transmitting coil and a 30cm x 60 cm figure-eight (bucked) receiving coil. Measurements were carried out in the frequency domain using an HP 89410A vector signal analyzer along with appropriate transmitter and receiver coil amplifiers. All cylinders were measured with the predominant component of the excitatory magnetic field both parallel and perpendicular (two distinct measurements) to the axis of the cylinder and measurements were made with and without a copper ring centered on the cylinder. The copper ring simulates the presence of rotating bands on actual UXO.
Not surprisingly, we have observed that the quadrature peak of the response shifts down in frequency much more when the axis of the ringed cylinder is aligned with the excitatory magnetic field then when perpendicular to it. We have also observed that real part of the response of the smallest cylinders measured flattens out and asymptotically approaches its DC value around 1Hz while the largest of the cylinders measured doesn't flatten out until well below 1Hz.
It appears that target information that may be crucial for discrimination purposes, especially for larger UXO targets, exists at frequencies well below 30Hz. The figure below compares the response of a thin, medium, and thick walled steel cylinder and in each case the excitatory magnetic field is aligned with the cylinder's axis. Notice that the responses are practically identical above 30Hz making it difficult or impossible to discriminate among the cylinders based on their response unless very low frequencies are utilized.
Although we have successfully measured the very low frequency response (below 30Hz) in a laboratory setting it is not at all clear that such measurements can be carried out from a moving platform. For example at 0.1Hz a complete cycle of one sinusoid takes 10 seconds and for high signal-to-noise ratios one hundred averages at this frequency would require 1000 seconds or 16.66 minutes. Alternatively, it may be reasonable to scan a large area at higher frequencies and then based on the results of this preliminary investigation return to locations of interest for a more complete, and necessarily more time consuming, interrogation. This and other practical issues shall be addressed in the presentation.

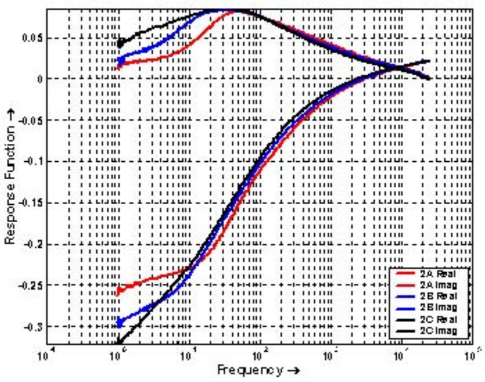

Figure 1: Response of thin, medium, and thick walled steel cylinders. The incident magnetic field is parallel to the axis of the cylinders.

UXO 3-3: SAR-GPR System for Landmine Detection and its Evaluation

T. Kobayashi, **X. Feng**, **T. Savelyev**, **M. Sato**
JST/Tohoku University

A UWB synthetic aperture type SAR-GPR system for landmine detection was developed. The model is a demonstration model that has been developed based on formerly developed experimental model (M. Sato et al., GPR using an array antenna for landmine detection, Near Surface Geophysics, 2004). The GPR system is a stepped frequency imaging radar system whose operation frequency range is 40kHz to 4GHz. The maximum detection depth is supposed to be deeper than 30cm under dry condition. The antenna is a bipodal Vivaldi antenna of which dimension is 20cm x 20cm. The system is equipped with an array antenna which consists of 3 pairs of transmission and receiving antennas. These antenna pairs are arranged in a CMP configuration: corresponding transmission and receiving antennas are arranged symmetrical to the mid point of the array base line so that the point makes the Common Mid Point of the antenna pairs. The antenna scans two dimensionally over the mine field keeping the standoff distance off the ground surface at a constant level. GPR measurement is carried out as the antenna array scans. Acquired data is processed to produce 3D image data of subsurface objects. CMP stacking is employed to suppress the ground surface clutters before the diffraction stacking method is applied to produce subsurface images.
Laboratory experiments were conducted to evaluate the performance of the SAR-GPR system. The laboratory test site of Tohoku University has a sand pool which is as big as 4m x 4m x 1m and is filled with sand as deep as 75cm. On the sand pool is placed an XY positioner which control the antenna scan and determines the position with the accuracy of 1mm.
Along with hardware development, an FDTD simulation model of the SAR-GPR system was developed in order to evaluate the SAR-GPR performance under wet conditions. The model can simulate a space of 1.5m x 1.5m x 1.5m large with full array antenna system installed. Preliminary experiments were carried out for the antenna spacing of 4cm, 6cm and 8cm under a flat surface condition. The target was a mock model of Type-72 AP mine which was horizontally put at the depth of 3cm. The standoff distance was 5cm. The experiments revealed that the smallest antenna spacing condition gives the highest contrast target image, i.e. the best performance. However, on the other hand, the FDTD simulations revealed that the largest spacing antenna transmitted the radar pulse most efficiently. Considering the narrow beam width of the Vivaldi antenna, those results imply at least two factors, antenna spacing and standoff distance, play important roles in determining the SAR-GPR performance. Further investigation on the SAR-GPR performance is currently being carried out.

UXO 3-4: Adaptive Feature-based GPR Signal Processing for Landmine Detection

C. Throckmorton[1], **P. Torrione**[1], **L. Collins**[1], **W.-H. Lee**[2], **R. Grandhi**[2], **J. Wilson**[2], **P. Gader**[2], **I. Starnes**[3], **S. Frasier**[3], **F. Clodfelter**[3]
[1]*Duke University*; [2]*University of Florida*; [3]*NIITEK Corporation*

Recently, the application of adaptive statistical signal processing methodologies to the high quality data measured using the Wichmann/NIITEK ground penetrating radar (GPR) have shown dramatic performance improvement for landmine detection over other radar and processing systems. This performance, which included two orders of magnitude reduction in false alarm rates over other systems operated on the same sites, has been achieved on data collected from several government-prepared test sites in the Eastern and Western USA. Such test sites primarily consist of prepared road beds that are relatively flat with few sources of clutter. Ultimately, the radar and algorithms will be deployed on less pristine roads and on off-road areas. To begin to assess performance in these more realistic scenarios, GPR data was collected for several diverse, off-road, unprepared locations. These sites varied in composition, including gravel roads and field-like conditions. They provided more frequent and variable natural clutter in the form of grass, rocks, tree roots, etc. This study focuses on the performance of the current prescreener, a 2-D lattice LMS algorithm developed at Duke University, on these off-road test sites as well as performance enhancements achieved through algorithm fusion and feature-based statistical processing. The performance of LMS under these challenging conditions is considered first, followed by the possible performance increases gained by fusing this algorithm with the FROSAW and FOWA algorithms designed by the University of Florida. Performance gains are also investigated for a two-step, feature processing method developed by Duke University. First, LMS, the fusion of LMS and FROSAW, or the fusion of LMS and FOWA is used as a prescreener to discard much of the uninteresting radar anomalies. Second, a more computationally-intense discrimination algorithm based on the fusion of multiple features is applied to the reduced data set. The results of the off-road data analysis indicate that LMS is a robust algorithm with regard to variable testing conditions. Further, off-road testing demonstrates that the two-part feature processing method as well as algorithm fusion can provide significant benefits, especially in challenging environments. In particular, while LMS performance was quite good across environments, absolute performance varied as a function of environment. Algorithm fusion reduced this variability while improving performance slightly, and the two-step feature processing method reduced the variability further and improved performance markedly. These trends are demonstrated on several data sets, including one measured in snowy conditions.

This work supported by NVESD through a contract with ARO.

UXO 3-5: Buried Landmine Detection using Spectral Radiometric Microwave Signatures

M. von Chiari, **S. Dill**, **M. Peichl**, **H. Süß**
DLR, Institute of Radiofrequency Technology and Radar Systems, Oberpfaffenhofen, Germany

At present many million anti-personnel mines are polluting our environment in many countries. They cause a considerable limitation of the living space and make the land unuseable for agricultural purposes. Because the mine clearance procedures are much slower than the mine laying operations the number of polluting mines and the related contaminated areas are nowadays still increasing. For the current mine detection technologies and for the most modern mines, which become continuously smaller and have less metal content, a high false alarm rate of up to 1000 to 1 is very likely.

Classical mine detection procedures like using metal detectors or dogs, or brute-force methods like mechanical plowing through the soil by tank-like vehicles are not able to solve satisfactorily the mine contamination problem. They suffer mainly from many drawbacks like a high false alarm rate, unclear reliability, high costs, and a destroying mode of operation, which cannot be tolerated in each situation. Thus an advanced mine detection system consists of multiple sensors based on different physical phenomena and principles and benefits from fusing their data. By doing this the different advantages of each sensor can be isolated from its shortcomings and merged to match as comprehensive as possible the specific mine detection requirements.

In the past we developed a broadband microwave radiometer operating in the frequency range of about 1-7 GHz. The radiometer was designed as a part of a three-sensor system within the HOPE project using additionally a metal detector and a ground penetrating radar. Using a common search head, the system was intended to be hand-held operated as the conventional metal detector, but allowing the application of imaging for all three sensors in conjunction with an optical position monitoring system. The capability of measuring at multiple low-bandwidth channels by sweeping the center frequency for the radiometer allows the collection of frequency signatures.

In an additional mode the sensor system should work in a stationary non-moving operation above an area of interest, where an unvisible and conspicious object was detected by the information of the imaging mode or by other sensors. By analysing this frequency signature together with the specific layer profile, this fingerprint information can help to discriminate landmines from other objects. This paper describes the modeling of the whole measurement process including the sensor and the observed ground volume. The purpose of this work is to get a simulation tool, which allows in combination with models of other sensors to find an adequate and optimal sensor set for effective landmine detection. Additionally this simulation tool can be part of a possible future DLR project called EasyMine. First comparison results of simulated and measured signatures are presented.

UXO 3-6: Standoff Mine Neutralization Technologies and Techniques

K. Sherbondy
U.S. Army, RDECOM-CERDEC, NVESD

The U.S. Army's Night Vision and Electronic Sensors Directorate (NVESD) have been pursuing the development, evaluation and demonstration of several standoff mine neutralization technologies and techniques for ground vehicular platforms. One of these has been a magnetron phased array to perform High Power Microwave (HPM) mine neutralization of electronically fuzed devices. A second has been the development of a remotely controlled launched projectile payload concept. The third has been a pyro-technique. These technologies and techniques have been and are currently being field demonstrated and evaluated against a variety of electronically fuzed anti-vehicle mines. A summary of the technical progress that has been made and the future work and direction will be given.

UXO 3-7: Active EM System for Detection of UXO in Urban Area

F. Dudkin, **V. Korepanov**
Lviv Centre of Institute of Space Research

Electrical, magnetic and electromagnetic (EM) methods are widely used at study of a subsurface ground area for detection of utilities and unexploded ordnance (UXO). These methods can be divided on passive and active. Passive methods use the EM field of the Earth or radio stations. In active methods the own source of EM field, so called controlled, is applied. The main merit of passive methods is the low power consumption, but at low signal-to-noise (S/N) ratio. This drawback excludes the application of these methods in urban area. The main merit of active methods is a gained S/N ratio because of controlled source of artificial EM field.

A portable system ELISMA was designed for active EM sounding of the subsurface ground layer up to 4 m in depth. System has an improved S/N ratio because it works at fixed crystal-controlled monochromatic frequency unlike systems that use a transient EM field for detection of UXO. The ELISMA instrument can detect both metallic targets and dielectric ones in city area.

The system can be used both for continuous induction profiling and for stationary EM sounding at gained S/N ratio in specific points of the profile. The ELISMA consists of the radiating and receiving units mounted in a rigid boom about 3 m length. The operating frequency is about 100 kHz. The power consumption is a few Watts from battery supply unit. An embedded radio modem transmits the digital data to a basic portable computer for a distance about 100 - 300 m. The application of an autonomous transporting device is available.

UXO 4 - Modeling & Simulation

UXO 4-1: Electromagnetic Detection and Identification of Automobiles

T. Hubing, **D. Beetner**, **X. Dong**, **H. Weng**, **M. Noll**, **H. Goksu**, **B. Moss**, **D. Wunsch**
Department of Electrical and Computer Engineering, University of Missouri-Rolla, Rolla, MO, USA

A typical automobile has dozens of intentional and unintentional sources of electromagnetic emissions. Microprocessor circuits, power circuits, communication circuits, electronic ignitions, sensors, motors and actuators are all capable of becoming significant sources of electromagnetic interference. Over the years, electromagnetic compatibility (EMC) engineers have developed a number of tools and techniques to help identify and characterize various sources of electromagnetic emissions. These techniques include time-domain waveform analysis, spectrum analysis, short-term FFTs, zero-span measurements, and AM/FM demodulation. With experience using these techniques, EMC engineers learn to recognize the electromagnetic signatures of various sources. These techniques can also be applied to the automatic identification of electronic systems. For example, two automobiles made by different companies or with different components will generally produce different electromagnetic emissions. Using the tools mentioned above to process EM emissions data, it is possible to record EM emissions information in a form that highlights the differences. These differences can be used to recognize the presence of an automobile or to identify a particular type of automobile.

Figure 1 shows a short-term FFT plot of the ambient fields in the Automotive EMC Laboratory at the University of Missouri-Rolla. The horizontal axis is time (0 – 0.1 ms) and the vertical axis is frequency (0 – 250 MHz). The three horizontal lines near 100 MHz are FM radio stations. The dark band near 10 MHz was due to an unidentified intermittent noise source. It appears in some ambient measurements, but not all of them. Fainter horizontal lines at other frequencies and the series of dashes at 10 MHz are due to electronic equipment in the room and other unidentified noise sources.

Figure 2 shows a short-term FFT plot of the fields in the same location with a 2003 Cadillac idling nearby. The vertical streak in the plot is due to an ignition pulse. Several automobiles were evaluated and the spectrum and duration of the ignition pulse varied significantly from one automobile to another.

Measurements of the fields in the lab with and without the automobile idling were made at various times over a period of several days. 80 data sets were collected and the data in each set was reduced to 155 parameters. These parameters were converted to 40 inputs using Principle Component Analysis (PCA) and analyzed using a Multilayer Perceptron (MLP) Neural Network. Approximately 2/3 of the data sets were used to train the network and the remaining 1/3 to test the network. It is perhaps not surprising that the neural network had no trouble recognizing the measurements that included an ignition spark. However, the time window of the measurement was only 0.1 ms, while ignition sparks occurred approximately every 12 ms. Therefore most of the data collected with the engine running did not include an ignition spark.

Figure 3 shows a short-term FFT plot taken while the engine was running that does not include an ignition spark. Although this plot looks very similar to a measurement of the ambient noise in the room, the neural network was able to tell the difference between ambient noise and noise from the automobile with 100% accuracy. This was true even though there were significant variations in the ambient noise and the noise from the automobile in the measurements taken at different times.

Additional results and information describing the neural network analysis will be included in the presentation. The preliminary results show that this is a promising technique for identifying different types of automobiles based on their EM emissions. A similar procedure could be used to identify the presence of other types of EM sources, even when they are located in a noisy environment.

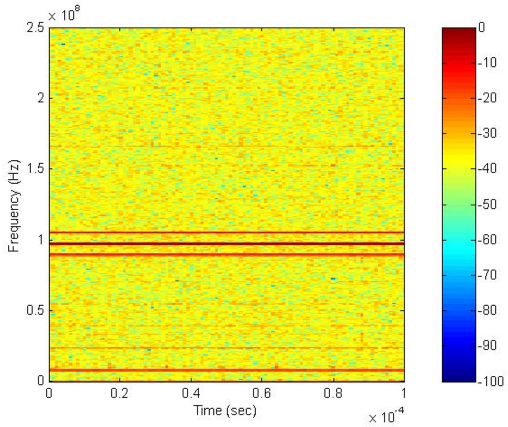

Figure 1: Short-term FFT plot of the ambient in the automotive EMC lab.

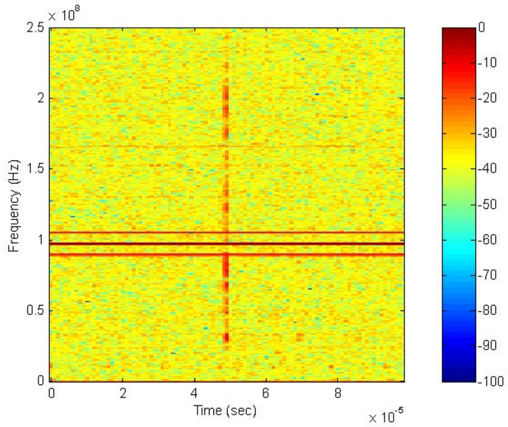

Figure 2: Short-term FFT plot of ambient with the automobile idling.

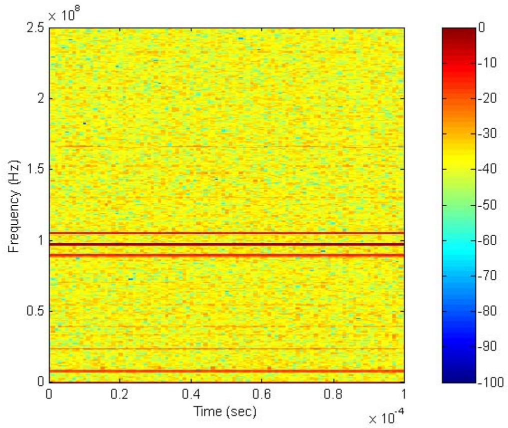

Figure 3: Short-term FFT plot with automobile idling (no ignition spark).

UXO 4-2: Solving Ill-posed Linear Inverse Problems without Regularization

H. G. Krauthäuser, **J. Nitsch**
IGET, Otto-von-Guericke-University Magdeburg, Germany

In an inverse scattering problem one has to predict some parameters (e.g. the spacial distribution of the complex permittivity) from measured data of an other quantity (e.g. scattered field) where the physical relationship is known. The knowledge of the physical relationship means, that the forward problem can be solved in an unique manner (scattered field can be calculated from the incident field and the spacial distribution of the permittivity). Unfortunately, most real inverse scattering problems

tend to be ill-posed, i.e. direct inversion is impossible. Most often, this is due to the fact, that the solution of the inverse problem is not unique within the measurement errors. There are well established mathematical procedures, e.g. regularization or maximum-entropy method, that transform the ill-posed problem to a regular problem. Within the constrained (reduced) solution space, the solution becomes unique.
In the presented work, we propose a method for solving linear ill-posed inverse problems without any regularization and without any prior knowledge. The method was introduced 10 years ago in the field of small-angle x-ray (SAXS) and small-angle neutron scattering (SANS) (Krauthäuser, H. G.: Deducing Material Properties from Indirect Measurements. Physica A, 211:317 326, 1994; Krauthäuser, H. G., Nimtz, G.: Real Space Distributions from SAS Data using the Novel Structure Interference Method. Journal of Molecular Structure, 383:315-318, 1996). There it has been used to calculate particle-size distributions from scattered intensities. Now, the method has be adapted to the problem of the reconstruction of the so called "Ipswich Data" (http://ece.caeds.eng.uml.edu/RCs/CEMOS/Ipswich_Data.html). The results will be shown and compared to results presented in the literature.

UXO 4-3: Eddy Current Computation for Small Metal Objects under a Coil

S. Schulze, **H. W. Glock**, **U. van Rienen**, **H. Ewald**
Institut für Allgemeine Elektrotechnik, Fachbereich Elektrotechnik und Informationstechnik, Universität Rostock, Germany

In order to reduce the rate of false alarms of metal detectors used for humanitarian demining a precise knowledge of the electromagnetic fields is mandatory. The comparison of measured data with calculated fields is going to be a criterion to distinct between mines and other metal objects detected. The calculation of electromagnetic fields excited by the metal detector's coil and influenced by a mine object embedded in soil has to be done numerically with programs based on the Finite Element Method (FEM) or Finite Integration Technique (FIT), e.g.. Due to the weak electromagnetic influence of buried mines such simulations have to be undertaken very precisely. Then, often a trade-off between field accuracy and numerical efforts in terms of memory and cpu time requirements has to be found. We are going to present such calculations for simplified mine-like objects in comparison between FEM- and FIT-based programs illustrating their capabilities and limits.

UXO 4-4: Artificial Neural Networks for Correction of Microwave Images

G. Krell, **B. Michaelis**
IESK, Otto-von-Guericke-University Magdeburg, Germany

Generally speaking, classical procedures for image restoration, such as Wiener or Inverse Filtering, can be applied to correction of microwave images in an analogous manner as to classical gray-level images (F. Daniel, G. Krell, O. Schnelting, . Schünemann, Elektronische Bildkorrektur für Rückprojektionsdisplays zur Qualitätsverbesserung und Kostenoptimierung. Electronic Displays, Wiesbaden September 24/25 (2003), proceedings, pp. 140-146). However, measurement of the system point spread function and assessment of the statistical parameters regarding disturbances are prerequisites for these solutions. Furthermore, geometrical distortions, space-variant parameters and unknown errors with the known solutions are very difficult to handle.
Models and algorithms in artificial neural networks offer a number of benefits for processing image signals. Important considerations are extensive investigations on biological models, where visual information is preprocessed by neural layers directly after the photoreceptors in the eye. A critical advantage of this "softcomputing" solution is that the model of the system to be corrected does not have to be described explicitly, rather the parameters are adapted in a learning phase.
The imaging system is calibrated by a training procedure in the correcting neural network (Fig. 1). Test patterns are input to the image acquisition or display system and compared with the "ideal" data (training pattern). When an image display is corrected the displayed test pattern must be rescanned.
A suitable error criterion is required for calibration. When the image source is restored, the mean quadratic deviation between target pattern and current output of the correcting network can be minimized. Superimposed noise thus impacts automatically on the adjustment criterion. Geometrical distortions are taken into consideration in the quality criterion, as no geometrical errors occur in the target pattern. Other quality criteria can be useful: for example - when a particular contrast enhancement or increase in image sharpness with respect to the image source is desired. The network is trained using a gradient technique, or - assuming linear behavior of the sensor - with the help of the calculus of observations. The system must be recalibrated if the behavior of the image producing system changes.
Generating the training pattern
The learning template is an important aid in training the correction filter. The geometry and intensity of objects in this learning template have to meet certain specifications. Geometrical objects on the learning template that are easy to describe have proven to be practical with the gray level correction procedure. Rectangles arranged as a chessboard or circles on the learning template are well suited for generating the ideal learning template from the input image of the template. Assuming linear activation functions of the neurons, the approaches for parameter estimation by test functions known from systems theory yield. The ideal template is obtained from the input image of the learning template during the learning phase. This procedure is executed using knowledge of the geometry and topology of the geometric forms in the template. If it is not possible to capture real test patterns or bodies an alternative approach must be chosen. One approach could be to generate synthetic patterns and to process them by a model of the microwave sensor (M. Magg, J. Nitsch, Mine Detecton with Microwaves RTO Lecture Series 214, pp. 8-1 ... 8-12, 1998). This way input and target patterns can be defined. The patterns can be additionally modified by noise superposition and/or blurring to meet the requirements. This approach corresponds to an electronic focussing of the imager until the output of the correction is considered as optimal.
Learning procedure for calculating the compensation parameters
The product of the filter coefficients and image section in the input learning template to be filtered is calculated to train the compensation parameters. The resulting pixel is compared with the ideal learning template, and the filter coefficients are adapted according to the size and value of the difference. This procedure is performed for every pixel in the learning template to ensure stable filter operation. Upon completion of the training procedure the filter coefficients are set so that the difference between the chosen image section and the target pixel is minimized. During the training process the filter is produced from subareas in the learning template. When generating a space-invariant filter a cut-out in the middle of the template is used in the learning process. The space-variant filter is applied across the entire image during recall. This procedure is only suited for images containing no significant space-variant disturbances. Space-variant parameters in the image are not taken into consideration when the image is corrected. This is particularly true of out of focus blur at the margin. Space-variant disturbances usually render errors at the boundaries of images more distinctive. In order to be better able to take such effects into account during correction, space-variant filters must be calculated. During the training process subfilters are generated for defined areas of the learning template The number of space-variant subfilters trained is a measure of the space variance of the disturbances. These subfilters can be calculated for each pixel as well as for large sections of the image. A disadvantage of space-variant filtering is the very laborious learning phase and the large filter matrix comprising submatrices for spatial filters.

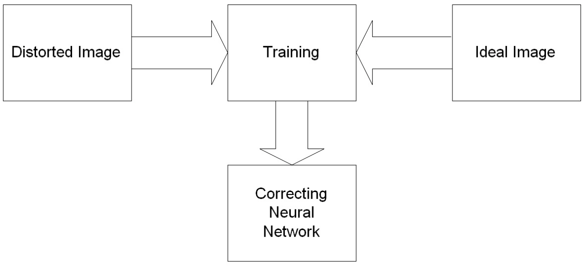

Figure 1: Training the correction of image data with an artificial neural network (ANN).

Author Index

Werner von Siemens
(1816-1892)

ISBN 3-929757-73-7